ANALYTICAL AND APPROXIMATE SOLUTIONS OF SELECTED CHEMICAL ENGINEERING MODELS

A THESIS

*Submitted in partial fulfilment of the
requirements for the award of the degree
of*

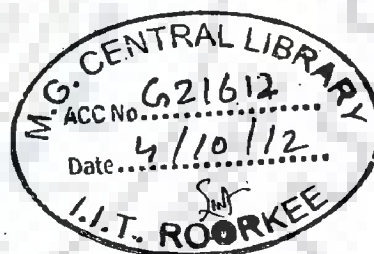DOCTOR OF PHILOSOPHY

in

CHEMICAL ENGINEERING

by

MOHD. DANISH

DEPARTMENT OF CHEMICAL ENGINEERING
INDIAN INSTITUTE OF TECHNOLOGY ROORKEE
ROORKEE-247 667 (INDIA)
DECEMBER, 2011
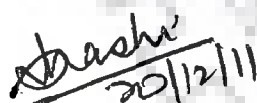
INDIAN INSTITUTE OF TECHNOLOGY ROORKEE
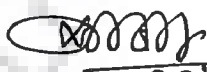## ROORKEE

CANDIDATE'S DECLARATION

I hereby certify that the work which is being presented in the thesis entitled **"Analytical and Approximate Solutions of Selected Chemical Engineering Models"** in partial fulfilment of the requirement for the award of the Degree of Doctor of Philosophy and submitted in the Department of Chemical Engineering of the Indian Institute of Technology Roorkee, Roorkee is an authentic record of my own work carried out during a period from August 2008 to December 2011 under the supervision of Dr. Surendra Kumar, Professor, and Dr. (Mrs.) Shashi Kumar, Associate Professor, Department of Chemical Engineering, Indian Institute of Technology Roorkee, Roorkee, India.

The matter presented in this thesis has not been submitted by me for the award of any other degree of this or any other Institute.

(MOHD. DANISH)

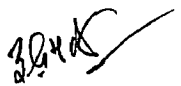This is to certify that the above statement made by the candidate is correct to the best of our knowledge.
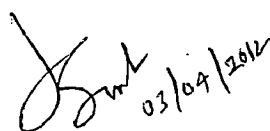
(Shashi)
Supervisor

(Surendra Kumar)
Supervisor

Date: 22·12·11

The Ph.D. Viva - Voce Examination of **Mr. Mohd. Danish**, Research Scholar, has been held on 3.4.2012 at 9.30 A.M

Signature of Supervisors   Chairman SRC   Signature of External Examiner

Head of the Department/Chairman ODC

ABSTRACT

In chemical engineering, mathematical models of various processes/systems often appear in the guise of different types of equations, e.g. algebraic equations [AEs], ordinary differential equations [ODEs] and partial differential equations [PDEs]. For instance, AEs arise in the steady state modeling of lumped parameter systems, such as CSTR, tray in a separation column and evaporators. Several constitutive models are also represented by AEs, e.g. thermodynamic equations of state and friction factor equations. ODEs are ensued in the unsteady state modeling of lumped parameter systems, e.g. CSTR or series of CSTRs, or in the steady state modeling of distributed parameter systems, e.g. PFR, packed bed columns/reactors. Also, steady state modeling of various processes, such as reaction-diffusion process inside a porous catalyst and heat transfer process from a fin, give rise to the formation of ODEs. PDEs may appear in the steady or unsteady state modeling of various processes/systems, such as unsteady reaction-convection-diffusion process, unsteady reaction-diffusion process, unsteady operation of a PFR, steady or unsteady operation of packed bed columns and steady state boundary layer flows. In general, these model equations are nonlinear and since analytical/approximate solutions of these nonlinear equations are difficult and sometimes even impossible to obtain, numerical methods are used to solve them. However, due to their obvious advantages over numerical solutions, analytical/approximate solutions are preferred and thus are explored first.

The present research work is basically an attempt in this direction and is concerned with the analytical/approximate solutions of several selected nonlinear model equations, which arise in the modeling of various chemical engineering processes and systems, e.g. heat transfer processes, fluid flow process, reaction-diffusion processes, rotary kiln and tubular chemical reactor. Besides, two constitutive equations, i.e. thermodynamic equation of state and friction factor equation, have also been considered for obtaining their approximate solutions. These selected model equations are mathematically represented by nonlinear AEs and nonlinear ODEs, and from the critical survey of the literature pertaining to the solutions of these equations, it is revealed that the analytical solutions exist for a few of them only. Moreover, these analytical solutions are merely applicable to a few specific situations. Similarly, the approximate

solutions existing for some of the processes/systems are valid in a restricted range only. Besides, use of some recently developed efficient approximate methods, e.g. Adomian Decomposition Method [ADM], Homotopy Analysis Method [HAM] and their variants, for obtaining the approximate solutions of some of the processes/systems has not been fully explored. Due to the nonlinear nature of the model equations, only some of them could be solved analytically, and for obtaining the analytical solutions, several well known methods, e.g. separation of variables in combination with the partial fraction decomposition method and derivative substitution method, have been used. On the other hand, model equations, which could not be solved analytically, have been solved in an approximate manner by using ADM, HAM, and/or their variants.

In particular, the selected heat transfer processes include transient convective cooling of a lumped spherical body, transient convective-radiative cooling of a lumped spherical body, steady state heat conduction in a metallic rod, radiative heat transfer from a rectangular fin and convective heat transfer from a rectangular fin. The model equations of these processes are represented by nonlinear first and second order ODEs constituting IVPs and BVPs, respectively, and have been solved by using the well known separation of variables method in conjunction with the partial fraction decomposition method and derivative substitution method. For all of these model equations, the obtained analytical solutions have been verified with the corresponding numerical solutions. Besides, the limitations of existing approximate solutions, which have been found to be valid in a restricted range of parameters' values, have also been highlighted by comparing them with the respective analytical solutions. For one of the processes, i.e. the transient convective-radiative cooling of a lumped spherical body, an available experimental study has also been successfully simulated. Likewise, due to the general nature of the model equation of convective heat transfer from a rectangular fin, the criteria of existence, uniqueness/multiplicity and stability of the solutions have also been studied.

The model equation of rotary kiln, considered in this work, describes the bed depth profile of solids flowing in the kiln and is represented by a nonlinear first order ODE constituting an IVP. This equation has been solved by using the separation of variables method in conjunction with the partial fraction decomposition method and the obtained analytical solution has been successfully validated with the numerical solution. Effects of various parameters have been studied in detail and it is shown that the present

analytical solution is accurate in the entire range of ε [local fill angle of the solids] unlike the existing approximate solution, which is accurate only in the range, 20.05 deg $\leq \varepsilon \leq$ 65.89 deg. Usefulness of the derived analytical solution has been shown by successfully simulating some of the existing experimental results pertaining to the solid bed depth profile.

The model equation selected from the area of fluid flow describes the Poiseuille and Couette-Poiseuille flow of a third grade fluid between two parallel plates, and is given by a nonlinear second order ODE constituting a BVP. This model equation has been solved by using the derivative substitution method, and the analytical solutions of velocity profiles and flow rate have been obtained. Beside the successful validation of analytical solutions, a discussion regarding the effects of various parameters has also been presented. Limitations of the available approximate solutions have also been highlighted by comparing them with the analytical and numerical solutions. It is shown that the velocity profiles obtained by using the existing approximate solutions depict an opposite trend and starts deviating from the true profiles even for moderately higher values of β a dimensionless parameter dependent on the material moduli.

Thermodynamic equation of state is represented by a nonlinear AE and is concerned with the estimation of gas volume at a given pressure and temperature. Approximate solutions of this equation have been obtained for finding the gas volume by using ADM and one of its variants, i.e. Restarted Adomian Decomposition Method [RADM]. Advantages and limitations of these two methods have been highlighted and the limitations can be avoided by following the proposed guiding principles.

The friction factor equation is also expressed by AE and is used to find the friction factor for the laminar and turbulent flow of fluids in smooth pipes. In this work, the fluid considered is a Bingham fluid. This equation has also been solved by using ADM and RADM, and several explicit approximate solutions of friction factor with reasonable accuracy have been derived. These solutions have been successfully compared with the corresponding numerical solution as well as with the available explicit correlations. For turbulent regime, the derived RADM solution of friction factor exhibit an error less than 0.005%, which is smaller than that exhibited by the available correlations. Similarly for laminar regime, the error in RADM solution of friction factor

is found to be within ± 5.2 % error, which can further be reduced by considering more terms in the RADM solution.

The model equations of reaction-diffusion processes inside a porous catalyst slab and sphere describe the concentration profile of reactant, and are used in evaluating the effectiveness factor. These equations are represented by second order ODEs constituting BVPs, and have been solved by using ADM and RADM. It is revealed that the ADM solutions yield erroneous results for reaction order $n < 1$ [$n \neq 0$] and for higher Thiele modulus [$\phi \geq 2$]. These limitations can be avoided by using RADM, which not only yields accurate results but is also applicable to other forms of reaction kinetics. The model equation of reaction-diffusion process inside a porous catalyst sphere has also been successfully solved by using another efficient approximate method based on HAM, i.e. Optimal Homotopy Analysis Method [OHAM]. It is shown that due to the presence of convergence control parameter, the error in OHAM solutions can be minimized, which renders the OHAM solutions better than the other existing approximate solutions. Moreover, the approximate solutions obtained by using ADM or its variants can also be obtained by using OHAM as a special case.

The axial dispersion model equation of a tubular chemical reactor describes the concentration profile existing in the reactor and is represented by a second order ODE constituting BVP. This equation has also been solved in an approximate manner by using OHAM and the obtained OHAM solutions have been verified with the corresponding numerical solutions. Besides, utility of OHAM has been depicted by trapping multiple solutions which exist for the non-monotonic reaction kinetics.

It is our view that the analytical and approximate solutions of selected process models, obtained in the present thesis, will be useful in many ways, i.e. for simulating experimental studies and for the estimation of parameters. Use of techniques and methods adopted for solving AEs and ODEs can also be made to other process models. We feel that if such an attempt is made it would certainly prove to be advantageous in terms of better understanding of the process and also in ease of obtaining solutions.

ACKNOWLEDGEMENTS

Acknowledging gratitude or any thanksgiving is indeed the most cherished moment of a task as it comes to its successful completion, especially a task as big and important as a Ph.D. in the academia. I am pleased to thank to all those who helped me during my research in their own special ways.

First and foremost, I express my heartiest gratitude towards my esteemed research supervisors, **Dr. Surendra Kumar, Professor & Dean Academic Research,** and **Dr. (Mrs.) Shashi, Associate Professor**, Department of Chemical Engineering, I.I.T. Roorkee, Roorkee, for their valuable guidance, refreshing ideas, consistent advice and help during the completion of my thesis work. Their encouraging remarks, crucial and rational analyses, and belief in my capabilities have always raised my enthusiasm and confidence level. Moreover, the exceptional liberty given to me for accomplishing this task is unforgettable. Their painstaking efforts in perusal of this manuscript are fully acknowledged. I humbly acknowledge a lifetime's gratitude to them. Thank you very much, Sir and Madam.

I would like to thank my SRC members: Dr. I.M. Mishra, Professor & DRC Chairman, Department of Chemical Engineering, I.I.T. Roorkee, Dr. Satya Prakash, Professor, Department of Metallurgical and Materials Engineering, I.I.T. Roorkee, and Dr. Shishir Sinha, Associate Professor, Department of Chemical Engineering, I.I.T. Roorkee, for their comments and cooperation.

I am also thankful to Dr. I.D. Mall, Professor & Head, Department of Chemical Engineering, I.I.T. Roorkee, for providing me necessary facilities to carry out this research work. I am also grateful to all the members of the Department of Chemical Engineering, I.I.T. Roorkee, for their help and cooperation in many ways.

I am also thankful to the staff members of Reaction Engineering Laboratory, Mr. Mange Ram and Mr. Rahman, for their needful help and cooperation. I am also gratified for staff members of CAD Center, Department of Chemical Engineering, I.I.T. Roorkee, Mr. Akhilesh Sharma, Mr. Raj Kumar and Mr. Narendra, for their well-timed help, especially for taking a plenty of printouts.

CONTENTS

CHAPTER IV: ROTARY KILN AND FLUID FLOW PROCESS
– ANALYTICAL SOLUTIONS   **129-186**

LIST OF TABLES

LIST OF FIGURES

LIST OF PUBLICATIONS

[A]   **Research Papers Published in Peer Reviewed Journals:**

1.   Danish, M., Kumar, Shashi, Kumar, S., 2010. Analytical solution of reaction-diffusion process in a permeable spherical catalyst. **Chemical Engineering & Technology**, 33 (4), 664-675.

2.   Danish, M., Kumar, Shashi, Kumar, S., 2010. Revisiting reaction-diffusion process in a porous catalyst: improving the Adomian solution. **Chemical Product and Process Modeling**, 5 (1), Article 10, 1-34.

3.   Danish, M., Kumar, Shashi, Kumar, S., 2010. Approximate explicit analytical expressions of friction factor for flow of Bingham fluids in smooth pipes using Adomian decomposition method. **Communications in Nonlinear Science and Numerical Simulation**, 16, 239-251.

4.   Danish, M., Kumar, Shashi, Kumar, S., 2012. Exact analytical solutions for the Poiseuille and Couette-Poiseuille flow of third grade fluid between parallel plates. **Communications in Nonlinear Science and Numerical Simulation**, 17, 1089–1097.

5.   Danish, M., Kumar, Shashi, Kumar, S., 2012. A note on the solution of singular boundary value problems arising in engineering and applied sciences: Use of OHAM. **Computers & Chemical Engineering**, 36, 57–67.

6.   Danish, M., Kumar, Shashi, Kumar, S., 2011. OHAM solution of a singular BVP of reaction cum diffusion in a biocatalyst. **IAENG International Journal of Applied Mathematics**, 41 (3), 223-227.

7.   Danish, M., Kumar, Shashi, Kumar, S., 2011. Exact solutions of three nonlinear heat transfer problems. **Engineering Letters**, 19 (3), 255-260.

[B]   Research Papers to be Submitted after First Review:

8.   Danish, M., Kumar, Shashi, Kumar, S., 2011. Exact analytical solution of a lumped model of the transient convective-radiative cooling of a hot spherical body in an environment. **Chemical Engineering Communications**, *revised version to be submitted.*

[C]   Research Papers to be Communicated:

9.   Danish, M., Kumar, Shashi, Kumar, S. An optimal homotopy based numerical method for the solution of process models represented by axial dispersion model, *to be submitted.*

10.   Danish, M., Kumar, Shashi, Kumar, S. Exact solutions of a nonlinear model of heat transfer through a rectangular fin and analysis of multiplicity of solutions, *to be submitted.*

11.   Danish, M., Kumar, Shashi, Kumar, S. Exact analytical solution for the axial transport of solids in a rotary kiln, *to be submitted.*

[D]   Research Papers Published in International Conferences:

12.   Danish, M., Kumar, S., Kumar, S., 2011. Exact analytical solutions of three nonlinear heat transfer models. **Lecture notes in Engineering and Computer Science: Proceedings of the World Congress on Engineering 2011**, WCE 2011, 6-8 July, 2011, London, U.K., 2550-2555.

13.   Danish, M., Kumar, S., Kumar, S., 2011. Solution of a singular BVP of reaction-diffusion in a biocatalyst by optimal homotopy analysis method. **Lecture notes in Engineering and Computer Science: Proceedings of the World Congress on Engineering 2011**, WCE 2011, 6-8 July, 2011, London, U.K., 24-28.

INTRODUCTION

Chemical engineering is one of the broad and versatile branches of engineering, and with the passage of time many allied disciplines have emerged from it. In chemical engineering, one frequently encounters processing of chemicals in process equipments, e.g. reactors. The operations occurring there in may be one or more of numerous unit operations and processes, e.g. separation, reaction, mixing, heating/cooling, which when modelled with the help of physico-chemical principles and phenomenological relations, give rise to different types of equations (Mickley et al., 1957; Himmelblau and Bischoff, 1967; Rice and Do, 1995; Varma and Morbidelli, 1997; Pushpavanam, 1998; Bird et al., 2002; Babu, 2004). In fact many important mathematical equations of varied complexity levels have originated from the modelling of various chemical process equipments.

In general, mathematical modelling of a chemical engineering system or equipment is carried out by applying the fundamental laws of science [conservation of mass, momentum and energy] and also by searching the appropriate constitutive relations pertaining to these systems (Himmelblau and Bischoff, 1967; Rice and Do, 1995; Pushpavanam, 1998; Bird et al., 2002; Babu, 2004). Depending on the degree of details and the level of complexity required, these resulting models can be mathematically represented by algebraic equations [AEs], ordinary differential equations [ODEs] and partial differential equations [PDEs]. Table 1.1 highlights the instances in which these equations appear while modelling various chemical engineering systems or equipments.

The methods which may be used to solve these model equations can be classified into three types, namely analytical methods, approximate methods and numerical methods, each having its own merits and demerits. Generally, analytical methods are desirable as these yield accurate solutions and provide better insight of the process. Moreover, these can also serve as benchmarks for the future testing of

Table 1.1:   Chemical Process Equipments/Systems, and their Model Equations

S. No.	Process Equipment/System or Component	Operating Condition	Process Model Consists of		
			AEs	ODEs	PDEs
1	Ideal CSTR (Fogler, 1992)	Steady state	✓	-	-
		Unsteady state	-	✓	-
2	Series of ideal CSTRs (Fogler, 1992)	Steady state	✓	-	-
		Unsteady state	-	✓	-
3	Ideal batch reactor (Fogler, 1992)	Unsteady state	-	✓	-
4	Ideal tubular reactor [PFR] (Fogler, 1992)	Steady state	-	✓	-
		Unsteady state	-	-	✓
5	Tubular reactor with axial dispersion (Villadsen and Michelsen, 1978; Fogler, 1992)	Steady state	-	✓	-
		Unsteady state	-	-	✓
6	Tubular reactor with axial and radial dispersion (Finlayson, 1980)	Steady state	-	-	✓
		Unsteady state	-	-	✓
7	Reaction-diffusion process in a porous catalyst slab or sphere (Villadsen and Michelsen, 1978)	Steady state	-	✓	-
		Unsteady state	-	-	✓
8	Falling film reactor (Gupta et al., 1986; Rice and Do, 1995; Bird et al., 2002)	Steady state	-	-	✓
		Unsteady state	-	-	✓
9	Transient cooling of a spherical body [lumped parameter model] (Campo and Blotter, 2000)	Unsteady state	-	✓	-

Table 1.1 Contd.

S. No.	Process Equipment/System or Component	Operating Condition	Process Model Consists of		
			AEs	ODEs	PDEs
10	Transient cooling of a spherical body [distributed parameter model] (Liao et al., 2006)	Unsteady state	-	-	✓
11	Heat conduction in a metallic rod (Rice and Do, 1995)	Steady state	-	✓	-
		Unsteady state	-	-	✓
12	Heat transfer from a rectangular or cylindrical fin (Bird et al., 2002)	Steady state	-	✓	-
		Unsteady state	-	-	✓
13	Double pipe heat exchanger (Pushpavanam, 1998)	Steady state	-	✓	-
		Unsteady state	-	-	✓
14	Multiple effect evaporators (Zain and Kumar, 1995)	Steady state	✓	-	-
		Unsteady state	-	✓	-
15	Single tray of a separation column (Himmelblau and Bischoff, 1967)	Steady state	✓	-	-
		Unsteady state	-	✓	-
16	Flash drum (Gupta, 1995)	Steady state	✓	-	-
17	Separation columns (Himmelblau and Bischoff, 1967; Gupta, 1995)	Steady state	✓	-	-
		Unsteady state	-	✓	-
18	Falling film absorber (Rice and Do, 1995; Bird et al., 2002)	Steady state	-	-	✓
		Unsteady state	-	-	✓
19	Batch adsorption column (Rice and Do, 1995)	Unsteady state	-	-	✓

Contd...

Table 1.1 Contd.

S. No.	Process Equipment/System or Component	Operating Condition	Process Model Consists of		
			AEs	ODEs	PDEs
20	Boundary layer flow over a flat plate (Bird et al., 2002)	Steady state	-	-	✓
		Unsteady state	-	-	✓
21	Couette and Poiseuille flow of Newtonian and non-Newtonian fluids (Bird et al., 2002; Siddiqui et al., 2008b)	Steady state	-	✓	-
		Unsteady state	-	-	✓
22	Fully developed laminar and turbulent flow in a pipe (Bird et al., 2002)	Steady state	-	✓	-
		Unsteady state	-	-	✓
23	Transport of solids in a rotary kiln (Liu et al., 2009)	Steady state	-	✓	-
		Unsteady state	-	-	✓
	Other Type of Models				
24	Thermodynamic equation of state (Smith et al. 2003; Annamalai and Puri, 2002)	-	✓	-	-
25	Frictional factor equation (Bird et al., 2002)	-	✓	-	-

various approximate and numerical solutions. However, it is not possible to obtain the solutions of most of the model equations analytically. On the other hand, approximate methods such as perturbation methods and δ-decomposition methods are applicable to a relatively large number of nonlinear model equations (Nayfeh, 1981; Liao, 2003). But, these methods require the presence of small or large parameters' values and are sometimes problem specific (Raina and Wanchoo, 1984; Haswani et al., 1995). Likewise, the weighted residual based approximate methods are specific to a model equation (Villadsen and Michelsen, 1978; Finlayson, 1980). Being approximate in nature, the question of accuracy and convergence of these approximate methods arise, which is normally addressed by using various theorems. While numerical methods constitute a powerful class of methods and are equally applicable to all types of model equations (Dennis and Schnabel, 1983; Gupta, 1995), these suffer from two limitations: (i) results are obtained in discrete form with truncation errors present in the solution, and (ii) generally, an entirely new computation is required for each set of parameters' values and/or auxiliary quantities (Pushpavanam, 1998; Liao, 2003). In order to solve the model equations, one generally first opts for analytical or approximate method, and if these do not work or are cumbersome, then the numerical methods are adopted.

The present research work is focused on obtaining the analytical or approximate solutions of some of the selected model equations which arise in the modelling of various chemical engineering processes and systems, such as heat transfer processes, fluid flow process, rotary kiln, reaction-diffusion processes and the real tubular chemical reactor. In particular, the selected heat transfer processes include transient convective and/or radiative cooling of a lumped spherical body, steady state heat conduction in a metallic rod, and steady state radiative/convective heat transfer from a rectangular fin. In a rotary kiln, the selected model equation is concerned with the axial transport of solids along the kiln length. Similarly, the model equation selected from the area of fluid flow describes the Poiseuille and Couette-Poiseuille flow of a third grade fluid. Likewise, the model equations selected from the area of reaction engineering describe the reaction-diffusion process inside a porous catalyst slab and sphere, and the axial dispersion model of a tubular chemical reactor. Beside these model equations, two constitutive correlations, i.e. thermodynamic equation of state and the friction factor equation, have also been considered for obtaining their approximate solutions.

The following section presents discussion about the above mentioned processes and systems, and their model equations along with the critical review of solution methods employed in the past.

1.1 SELECTED CHEMICAL ENGINEERING PROCESSES/SYSTEMS: MODEL EQUATIONS AND THEIR SOLUTION METHODS

For convenience, the discussion presented in this section has been divided into the following four categories.

1.1.1 Heat Transfer Processes

(i) Transient convective cooling of a lumped body

The process of transient convective cooling of a lumped body is encountered in several instances of heat transfer operations, e.g. cooling of stirred jacketed vessels, smaller metallic bodies and electronic components etc. This process is modelled by a first order ODE constituting an initial value problem [IVP]. In recent past, this model equation has been solved by several researchers by using various approximate methods, e.g. homotopy perturbation method [HPM], homotopy analysis method [HAM], variational iteration method [VIM] and optimal homotopy analysis method [OHAM] (Ganji, 2006; Abbasbandy, 2006a; Tari et al., 2007; Marinca and Herişanu, 2008), and the approximate solutions for the transient temperature profiles have been obtained. However, these approximate solutions are found to have a limited validity for a certain range of parameters' values.

(ii) Transient convective-radiative cooling of a lumped body

The process of transient convective-radiative cooling of a lumped body is also encountered in various heat transfer operations, e.g. gas burners, bulb filament, metallic bodies etc. The model equation of this process is given by a first order ODE constituting an IVP. Recently, a similar process, i.e. the transient convective-radiative cooling of a spherical body [metal ball bearings], has been experimentally studied by Campo and

Blotter (2000). These researchers have also successfully simulated the obtained experimental results [transient temperature profiles] by numerically solving the model equation. A simpler model equation, depicting the specific case of this process, i.e. the transient cooling of a lumped body in an environment of absolute zero temperature, has been solved by Ganji et al. (2007), Rajabi et al. (2007), and Domairry and Nadim (2008) by using different approximate methods, e.g. HPM, HAM, VIM and PM [perturbation method], and the approximate solution for the transient temperature profile have been obtained. However, the approximate solutions derived by these researchers have been found to work in a limited range of parameters' values.

(iii)   Steady state heat conduction in a metallic rod

The process of steady state heat conduction in a metallic rod arises in several instruments/processes, e.g. in heat flow meters, heat conduction through walls (Bejan and Kraus, 2003). This process is modelled by a second order ODE constituting a boundary value problem [BVP]. The allied boundary conditions [BCs] are of Dirichlet type. Recently, several researchers have solved this model equation by using various approximate methods, e.g. HPM and HAM (Rajabi et al., 2007; Sajid and Hayat, 2008a; Domairry and Nadim, 2008), and the approximate solutions for the temperature profiles along the rod length have been obtained. Here too, these approximate solutions are found to be suitable for a certain range of parameters' values only.

(iv)   Steady state radiative heat transfer from a rectangular fin

The process of radiative heat transfer from a rectangular fin occurs in the heat transfer operations in outer space. This process is modelled by a second order ODE constituting a BVP. The associated BCs are given by a Dirichlet BC at the fin base and a Neumann BC at the fin tip. Recently, this model equation has been solved in an approximate manner by Ganji (2006) and Abbasbandy (2006a) with the help of HPM and HAM, respectively, and the approximate solutions for the temperature profiles along the fin length have been obtained. Similarly, Tari et al. (2007) and Marinca and Herişanu (2008) have used VIM and OHAM, respectively, to obtain the approximate

7

solutions [temperature profiles] of this model equation. Due to their approximate forms these approximate solutions are also susceptible to errors.

(v)   Steady state convective heat transfer from a rectangular fin

The process of convective heat transfer from a rectangular fin is widely encountered in various heat transfer operations, e.g. refrigerators, air conditioners, CPU of a computer, electrical transformers etc. The model equation of this process is represented by a second order ODE which constitutes a BVP. The BCs are same as those used in the model equation of the previous process, i.e. a Dirichlet BC at the fin base and a Neumann BC at the fin tip. Recently, a similar but a more general type of model equation, incorporating the temperature dependent thermal conductivity and heat transfer coefficient, has been solved analytically by Moitsheki et al. (2010b). These researchers have employed the symmetry methods to obtain the analytical solutions of the temperature profile and the fin efficiency. However, only a few specific cases of this model equation have been solved by these researchers.

1.1.2   Rotary Kiln and Fluid Flow Process

(i)   Rotary kiln

Rotary kilns are widely used in the chemical industries for performing different operations on granular solids, e.g. mixing, drying, roasting, and gas-solid reactions etc (Liu et al., 2009). Some of the solid materials produced in rotary kilns are: cement, lime and alumina etc. An important problem related to the design of rotary kiln is to estimate the solid bed depth profile along the kiln length (Liu et al., 2009), for which the model equation proposed by Saeman (1951) is invariably employed. This model equation is represented by a first order ODE constituting an IVP. In literature, several researchers have solved this model equation by using various specific approximations and obtained the approximate solutions for the solid bed depth profile (Kramers and Croockewit, 1952; Liu et al., 2009). The approximate solution derived by Liu et al. (2009) is the most recent one and is found to be more accurate as compared to those of Kramers and Croockewit (1952). Although, Liu et al. (2009) have successfully simulated several

available experimental studies (Sai et al., 1990; Spurling, 2000) by using their approximate solution, yet, due to approximation used, their approximate solution has also been found to be prone to errors in some situations.

(ii)   Fluid flow process

Many engineering fluids, e.g. slurries, pastes, lubricants, different polymer solutions etc are characterized as non-Newtonian fluids (Siddiqui et al., 2010). One such type of fluid is the third grade fluid (Oldroyd, 1950; Rivlin and Ericksen, 1955; Bird et al., 1987) and due to its engineering importance, different studies pertaining to various flow situations of these fluids have been carried out. One such study is related to the flow process describing Poiseuille and Couette-Poiseuille flow of a third grade fluid between the two parallel plates. This fluid flow process is modelled by a second order ODE which constitutes a BVP with Dirichlet BCs. This model equation has recently been solved by Siddiqui et al. (2008b, 2010) in an approximate manner by using two approximate methods, namely HPM and Adomian decomposition method [ADM]. In both these studies, however, these researchers have obtained the approximate solutions for the velocity profiles and no solution expression was obtained for the flow rate. Moreover, these approximate solutions also suffer from a limited range of applicability.

1.1.3   Thermodynamic Equation of State and Friction Factor Equation

(i)   Thermodynamic equation of state

Thermodynamic equation of state is generally employed to estimate the volume of a non-ideal gas at a given temperature and pressure. One of the popular thermodynamic equation of state is the Beattie-Bridgeman equation of state, which is basically a quartic equation in volume. Since analytical solution of this quartic equation is cumbersome and the approximate solution of this equation is not available, it is generally solved by using numerical methods, e.g. Newton-Raphson method (Gupta, 1995). Use of some of the newly developed approximate method, e.g. ADM, to solve this equation is unavailable.

9

(ii)   Friction factor equation

For the flow of fluids through pipes and conduits, friction factor equation is used to evaluate the friction factor which in turn is used for finding pressure drop. Depending upon the type of fluid [Newtonian, non-Newtonian etc], the flow regime [turbulent and laminar] and the geometry of the system [circular pipe, rectangular channel], properties of the contacting surface [smooth, rough], different friction factor equations exist. In the present work, the friction factor equations for the laminar and turbulent flow of Bingham fluids through smooth circular pipes have been selected. For the laminar flow of Bingham fluids, the friction factor equation is given by a quartic equation. Whereas, for the turbulent flow of Bingham fluids in smooth pipes, the implicit Nikuradse-Prandtl-Karman [NPK] equation is applicable; NPK equation is also valid for the flow of Newtonian fluids in smooth pipes. Hence, the various approximate explicit expressions of friction factor for the turbulent flow of Newtonian fluids, given in literature (Serghides, 1984; Manadilli, 1997; Romeo et al., 2002), may also be used for the Bingham fluids. However, no approximate explicit expression of friction factor is available for the laminar flow of Bingham fluids.

1.1.4   Reaction-Diffusion Processes and Tubular Chemical Reactor Model

(i)   Reaction-diffusion processes

The well known reaction-diffusion process occurring inside a porous catalyst is widely encountered in many heterogeneous catalytic reactions. Due to its importance in the design of heterogeneous catalytic reactors, this process has been the subject of great interest to chemical engineers and an enormous amount of research work is available in the literature (Thiele, 1939; Wheeler, 1955; Aris, 1975; Finalyson, 1980; Kubicek and Hlavacek, 1983; Mehta and Aris, 1971; Magyari, 2008; Moitsheki et al., 2010a). At steady state, this process is modelled by a second order ODE, which constitutes a BVP with Dirichlet and Neumann BCs at the catalyst surface and the catalyst center, respectively. For a porous catalyst with slab geometry, the model equation of this process gives rise to a non-singular BVP, whereas it results into a singular BVP for the porous spherical catalyst.

10

Recently, several researchers have approximately solved the model equation of this process for a porous catalyst slab by using various approximate methods, e.g. ADM and HAM (Sun et al., 2004; Abbasbandy, 2008), and obtained the approximate solutions for the reactant concentration profile and catalyst effectiveness factor. However, these solutions are limited to the power-law kinetics only. Moreover, it has been observed that the solutions obtained by Sun et al. (2004) by using ADM break down in those cases, where reaction order is smaller than unity $[n < 1,\ n \neq 0]$ and Thiele modulus is high $[\phi \geq 2]$. In another work, Gottifredi and Gonzo (2005) have applied the perturbation and matching procedure to solve the model equation of this process for a porous catalyst slab and obtained the approximate solutions for the reactant concentration profile and catalyst effectiveness factor. It is found that the approximate solution for effectiveness factor is fairly accurate in its prediction and is valid for any type of kinetics. However, the approximate solution for concentration profile shows deviations near the pore center. Besides, like the ADM solution of Sun et al. (2004) and the HAM solution of Abbasbandy (2008), the approximate solution of Gottifredi and Gonzo (2005) is only valid for the catalyst slab. Several other researchers have also obtained the approximate and analytical solutions of the same model equation of a porous catalyst slab (Mehta and Aris, 1971; Magyari, 2008; Moitsheki et al., 2010a). However, these solutions are valid for the power-law kinetics only.

The model equation of reaction-diffusion process for a porous spherical catalyst has also been solved by many researchers. Recently, Shi-Bin et al. (2003) have approximately solved this model equation by using ADM and obtained the approximate solutions for the concentration profile of reactant and the catalyst effectiveness factor. However, these approximate solutions are applicable for power-law kinetics only, and here too, the ADM solutions fail for the reaction order smaller than unity $[n < 1,\ n \neq 0]$ and higher Thiele modulus $[\phi \geq 2]$. In another work, Li et al. (2004) have approximately solved the same model equation for a bio-catalyst with the help of series expansion method and obtained the approximate solutions for the reactant concentration profile and catalyst effectiveness factor. In this case, biochemical reaction follows the Michaelis-Menten kinetics. In a few situations, however, approximate solution of Li et al. (2004) has also been found to be prone to errors. In yet another study, Kumar and Singh (2010) have approximately solved similar types of singular BVPs by using a modified Adomian decomposition method [MADM].

(ii)   Tubular chemical reactor model

The flow patterns existing in real tubular chemical reactor are by and large represented by using axial dispersion model (Fogler, 1992). Under steady state, the axial dispersion model of a tubular chemical reactor results in a second order ODE which constitutes a BVP. The associated BCs are expressed by a non-homogeneous Robin BC at the reactor inlet, whereas homogeneous Neumann BC at the reactor outlet. These BCs are collectively known as the famous Danckwerts boundary conditions. For a tubular chemical reactor sustaining nonlinear kinetics, this model equation has been solved by many researchers by using different methods, e.g. approximate methods have been used by Freeman and Houghton (1966), Burghardt and Zaleski (1968), Wissler (1969), Fan et al. (1971), Ray et al. (1972), Marek and Stuchl (1975), Shah and Paraskos (1975) etc and numerical methods have been employed by Fan and Bailie (1960), Lee (1966), Wan and Ziegler (1970), Rao et al. (1981) etc, and obtained the approximate solutions for the reactant concentration profiles. However, the recently developed approximate methods, e.g. ADM, HAM, or their variants, have not yet been applied to solve this model equation.

1.1.5   Remarks

From the above discussion about the selected model equations and their available solutions, the following observations can be made:

(i)   Analytical solutions exist only for the model equations of convective heat transfer from a rectangular fin and reaction-diffusion process inside a porous catalyst slab. However, these analytical solutions are valid for a few specific situations only.

(ii)   Approximate solutions, existing for the model equations of convective and/or radiative cooling of a lumped body, heat conduction in a metallic rod, radiative heat transfer from a rectangular fin, Poiseuille and Couette-Poiseuille flow of a third grade fluid and the reaction-diffusion processes inside a porous catalyst slab/sphere, are applicable in a limited range only.

(iii)   Approximate solutions for the thermodynamic equation of state, friction factor equation, and axial dispersion model of a tubular chemical reactor, have not yet been found by using some of the recently developed approximate methods, e.g. ADM, HAM and their variants.

Keeping the above observations in view, the present research work has been planned with the main aim of finding the analytical and approximate solutions of the above discussed model equations along with the validation and discussion of the obtained results. It should, however, be noted that due to the nonlinear nature of these model equations, only some of them may be solved analytically. Whereas, those model equations, which may not be solved analytically, are proposed to be solved in an approximate manner by using two recently developed approximate methods, namely ADM, HAM, and/or their variants. These two techniques have been proved to be quite efficient and promising for solving nonlinear equations of different kind, and have been successfully applied in various branches of engineering and allied sciences. Since, the main concern of this research work is to obtain the analytical/approximate solutions of the model equations of selected chemical engineering processes/systems, the development of model equations has been omitted. Nevertheless, the derivations of these model equations can be found in any of the standard texts available on modelling and simulation of chemical engineering systems (Himmelblau and Bischoff, 1967; Rice and Do, 1995; Bird et al., 2002; Babu, 2004).

1.2   OBJECTIVES

On the basis of review presented in the previous sections, objectives of the research work in the thesis have been formulated as follows:

[A]   **To Obtain Analytical / Approximate Solutions of Models of the following Processes/Systems.**

(a)   **Heat Transfer Processes**

Transient convective cooling of a lumped body; Transient convective-radiative cooling of a lumped body; Steady state heat conduction in a

metallic rod; Steady state radiative heat transfer from a rectangular fin; Steady state convective heat transfer from a rectangular fin

(b)   Rotary Kiln and Fluid Flow Process

Rotary kiln; Fluid flow process

(c)   Thermodynamic Equation of State and Friction Factor Equation

Thermodynamic equation of state; Friction factor equation

(d)   Reaction-Diffusion Processes and Tubular Chemical Reactor Model

Reaction-diffusion process in a porous catalyst slab and sphere; Tubular chemical reactor model

[B]   To Compare the Obtained Analytical/Approximate Solutions with the Numerically Obtained Solutions as well as with the Approximate Solutions Available in Literature. Table 1.2 provides their essential details.

1.3   ORGANIZATION OF THE THESIS

The thesis has been organized into six chapters as discussed below.

Chapter II covers the detailed literature review of the solution methodologies employed by different researchers for solving the selected chemical engineering processes and systems along with their brief description. **Chapters III** to **VI** are the main contributions of the thesis, and pertain to the development of the analytical/approximate solutions of the selected model equations. In **Chapter III** analytical solutions of the selected heat transfer processes have been presented, whereas, in **Chapter IV** analytical solutions of the rotary kiln and the fluid flow process

Table 1.2:   **Essential details of the Objectives**

S. No.	Chemical Engineering Process/System	Method(s) proposed to be used	Comparison of the obtained analytical/approximate solution, proposed to be made with	Additional aspects proposed to be studied / Remarks
(a)	**Heat Transfer Processes**			
(i)	Transient convective cooling of a lumped system	Analytical method	- Numerical solution - Approximate solutions (Ganji, 2006; Abbasbandy, 2006a)	–
				To simulate the existing experimental results of cooling of metal ball bearing by the combined mechanisms of convection and radiation (Campo and Blotter, 2000).
(ii)	Transient convective-radiative cooling of a lumped system	Analytical method	Numerical solution	To obtain the analytical solution of a specific case of this process and to compare the analytical results with the numerically obtained results as well as with the available approximate results (Ganji et al., 2007; Rajabi et al., 2007).

Table 1.2 Contd.

S. No.	Chemical Engineering Process/System	Method(s) proposed to be used	Comparison of the obtained analytical/approximate solution, proposed to be made with	Additional aspects proposed to be studied / Remarks
(iii)	Steady state heat conduction in a metallic rod	Analytical method	- Numerical solution - Approximate solutions (Rajabi et al., 2007; Sajid and Hayat, 2008a)	-
(iv)	Steady state radiative heat transfer from a rectangular fin	Analytical method	- Numerical solution - Approximate solutions (Ganji, 2006; Abbasbandy, 2006a)	-
(v)	Steady state convective heat transfer from a rectangular fin	Analytical method	- Numerical solution - Analytical solution (Moitsheki et al., 2010b)	To analyse the multiplicity and stability of the obtained analytical solutions
(b)	**Rotary Kiln and Fluid Flow Process**			
(i)	Rotary kiln	Analytical method	- Numerical solution - Approximate solution (Liu et al., 2009)	To simulate the available experimental results (Lebas et al., 1995; Spurling et al., 2001; Scott et al., 2008; Liu et al., 2009)

Contd…

16

Table 1.2 Contd.

S. No.	Chemical Engineering Process/System	Method(s) proposed to be used	Comparison of the obtained analytical/approximate solution, proposed to be made with	Additional aspects proposed to be studied / Remarks
(ii)	Fluid flow process	Analytical method	- Numerical solution - Approximate solution (Siddiqui et al., 2008b)	-
(c)	**Thermodynamic Equation of State and Friction Factor Equation**			
(i)	Thermodynamic equation of state	ADM and RADM [approximate methods]	Numerical solution	-
(ii)	Friction factor equation	ADM and RADM [approximate methods]	- Numerical solution - Approximate solutions for turbulent flow (Serghides, 1984; Manadilli, 1997; Romeo et al., 2002)	-
(d)	**Reaction-Diffusion Processes and Tubular Chemical Reactor Model**			
(i)	Reaction-diffusion process in a porous catalyst slab	ADM and RADM [approximate methods]	- Numerical solution - Approximate solutions (Sun et al., 2004; Gottifredi and Gonzo, 2005)	To highlight the limitations of the approximate solution obtained by using ADM

Contd...

17

Table 1.2 Contd.

S. No.	Chemical Engineering Process/System	Method(s) proposed to be used	Comparison of the obtained analytical/approximate solution, proposed to be made with	Additional aspects proposed to be studied / Remarks
(ii)	Reaction-diffusion process in a porous catalyst sphere	ADM, RADM and OHAM [approximate methods]	- Numerical solution - Approximate solutions (Shi-Bin et al., 2003; Kumar and Singh, 2010; Li et al., 2004)	To highlight the limitations of the approximate solution obtained by using ADM
(iii)	Tubular chemical reactor model	OHAM [approximate methods]	- Numerical solution - Approximate solutions (Burghardt and Zaleski, 1968; Wan and Ziegler, 1970; Fan et al., 1971; Ray, et al., 1972; Marek and Stuchl, 1975; Shah and Paraskos, 1975; Rao, et al., 1981)	To obtain the dual solutions existing for the non-monotonous reaction kinetics

18

have been given. In **Chapter V** the approximate solutions of the thermodynamic equation of state, the friction factor equation and the model equations of reaction-diffusion processes have been obtained by using ADM and RADM. In **Chapter VI** the approximate solutions of the reaction-diffusion process and the tubular chemical reactor model have been obtained by using OHAM. Finally, the **Chapter VII** presents the conclusions of the thesis and the recommendations for future research work.

Due to the mathematical nature of this thesis, the mathematical symbols have been used in abundance. Hence, to avoid any ambiguity, the symbols have been defined at the end of each chapter. Similarly, to avoid the discontinuity in the text, the detailed mathematical steps used in obtaining the solutions of some of the model equations have been given in appendices.

LITERATURE REVIEW

2.0   INTRODUCTION

In this chapter, the literature pertaining to the solution methodologies adopted by several researchers to solve the model equations of selected chemical engineering processes/systems has been reviewed in detail. Besides, the literature relating to the presently employed approximate methods, namely ADM, HAM, and their variants, has also been described. For convenience, the literature review of similar processes/systems has been combined and presented at the same place. It should, however, be noted that the cited literature is in no way an exhaustive review, but just represents a part of the abundant literature available on the selected processes/systems, which is relevant to the present study.

2.1   SELECTED HEAT TRANSFER PROCESSES

In this section, the review of previously adopted methods to solve the model equations of five selected heat transfer processes has been presented. The selected heat transfer processes are: transient convective cooling of a lumped body, transient radiative-convective cooling of a lumped body, steady state heat conduction in a metallic rod, steady state radiative heat transfer from a rectangular fin and the convective heat transfer from a rectangular fin.

2.1.1   Transient Convective and/or Radiative Cooling of a Lumped Body

The process of transient cooling of a body by the individual or combined mechanisms of convection and radiation is widely encountered in different areas of heat transfer operations. Some of the specific examples are: cooling of gas burners, broiler, automobile radiators, bulb filament, industrial furnaces, combustion chambers, building walls, cooling of metals in various metallurgical processes, rocket nozzles, radiation

devices in outer space applications (Parang et al., 1990; Siegel and Howell, 1992; Modest, 2003; Bejan and Kraus, 2003; Tan et al., 2009). There also exists a different class of moderate temperature operations in which radiative fluxes are small, however, in conjunction with the free convective heat transfer, the radiative part may be comparable to the convective part; some of the examples include cooling of electronic components and heat removal by convecting-radiating fins and spines, cooling of hot metallic bodies (Bejan and Kraus, 2003; Campo and Blotter, 2000).

In literature, several mathematical modelling approaches have been applied to portray the above unsteady convective-radiative heat transfer processes, starting from the simple lumped parameter model to the more complex distributed parameter model (Siegel and Howell, 1992; Bejan and Kraus, 2003; Cortés et al., 2003; Modest, 2003; Su, 2004; Liao et al., 2006; Tan et al., 2009; Kupiec and Komorowicz, 2010). For example, the distributed parameter model has been employed to simulate some of the similar heat transfer processes, e.g. the process of groundwater freezing and metal solidification (Parang et al., 1990), thermal chemical vapour deposition (Theodoropoulou et al., 1998), and cooling of a spherical body (Liao et al., 2006). Likewise, the lumped parameter model has been applied to represent various heat transfer processes, e.g. the freezing of water in the night sky in deserted areas (Bird et al., 2002), cooling of metal ball bearing (Campo and Blotter, 2000), baking process in an oven (Sakin et al., 2009; Tan et al., 2009) and dielectric barrier discharge reactor (Sadat et al., 2010).

The distributed parameter models of these processes are represented by PDEs, and provide the spatial and temporal details of the temperature of the concerned body. However, numerical solution of the so derived PDEs is cumbersome and time consuming especially in repeated calculations. To overcome this difficulty, various attempts have been made to propose different improved lumped models so as to obtain the sufficiently accurate information with minimum efforts (Cortés et al., 2003; Su, 2004; Kupiec and Komorowicz, 2010). The equations characterizing the lumped model of a system are derived after performing some spatial averaging over the distributed parameter model and the governing PDE is rendered into a nonlinear ODE. In contrast to the distributed model equation, the so derived lumped model equation of a system is mathematically tractable and is generally preferred. However, it only provides the temporal details of the temperature of the body. The choice between the lumped and

distributed parameter approaches basically depends on the degree of accuracy and the level of details required, and should only be made by properly evaluating the concerned Biot number, Bi. It should be noted that the lumped model approach is valid if $Bi < 0.3$ (Liao et al., 2006; Campo and Blotter, 2000).

Recently, the model equation of transient convective cooling of a lumped body, a nonlinear first order ODE constituting an IVP, has been solved by several researchers by using some newly developed approximate methods, e.g HPM (Ganji, 2006), HAM (Abbasbandy, 2006a), VIM (Tari et al., 2007) and OHAM (Marinca and Herişanu, 2008), and different approximate solutions of transient temperature profile were obtained in terms of some finite series. It should also be noted that in some of these studies (Ganji, 2006; Abbasbandy, 2006a), analytical solution of this model equation has also been found, however, the form of analytical solution is implicit and to the best of our knowledge, explicit analytical solution for this process has not yet been found.

A similar process of transient convective-radiative cooling of a lumped spherical body [metal ball bearing] has been experimentally studied by Campo and Blotter (2000). The model equation of this process was described by a nonlinear first order ODE constituting an IVP and was numerically solved by these researchers by using RK-Fehlberg method. The obtained numerical results for transient temperature profiles were successfully crosschecked against the experimentally obtained results. However, no attempt was made for obtaining the analytical/approximate solution of the concerned model equation.

In another recent study, a simplified model equation of this process, represented by a nonlinear first order ODE constituting an IVP and depicting the transient cooling of a lumped body in an environment of absolute zero temperature, has been solved by several researchers by using various approximate methods. Rajabi et al. (2007) have employed HPM to solve the same model equation and obtained the approximate solution of transient temperature profile. Ganji et al. (2007) have applied PM, HPM and VIM to obtain the approximate solution of transient temperature profiles and compared the obtained results so as to judge effectiveness of these methods. Domairry and Nadim (2008) have applied HPM and HAM and compared the obtained results to prove the superiority of HAM. However, to the best of our knowledge, analytical solution of this model equation is also unreported till date.

2.1.2 Steady State Heat Conduction in a Metallic Rod

The process of steady state heat conduction in a metallic rod arises while measuring the thermal conductivity of metals by using flow meters (Bejan and Kraus, 2003). The model equation of this process is represented by a linear second order ODE constituting a BVP, and in case of temperature dependent thermal conductivity, this model equation becomes nonlinear. Recently, one such nonlinear model equation in which the thermal conductivity is assumed to vary linearly with temperature has been solved by several researchers by using various approximate methods. For example, Rajabi et al. (2007) and Sajid and Hayat (2008a) have solved the resultant model equation by using HPM and HAM, respectively, and obtained the approximate solution of temperature profile in the form of some finite series. Domairry and Nadim (2008) have shown the superiority of HAM over HPM by solving the same model equation by both the methods. However, none of these studies have reported the analytical solution of this model equation, and to the best of our knowledge, it is also not available elsewhere.

2.1.3 Steady State Radiative/Convective Heat Transfer from a Rectangular Fin

Extended surfaces also called fins play a vital role in removing the heat energy from any system, and are frequently encountered in many heat transfer applications, e.g. radiators in space vehicle, refrigerators, air conditioners, CPU of a computer, electrical transformers, heat exchangers, engines and electrical motors etc. A lot of theoretical and experimental studies have been carried out to analyze different types of fins and an excellent account of work can be found in the books by Sunden and Heggs (2000) and Kraus et al. (2001).

In real situations, fins with familiar geometries, e.g. rectangular or cylindrical, are quite common. The steady state process of heat transfer through these fins is, in general, represented by a second order ODE constituting BVP. On the basis of the heat transfer conditions [transient boiling, laminar film boiling/condensation, turbulent convection, nucleate boiling], these model equations, can be linear and nonlinear. Linear model equations, depicting the constant thermal conductivity and heat transfer coefficient, are solvable analytically. However, in applications where large temperature

gradients exist, the model equations become nonlinear due to the variation of thermal conductivity and heat transfer coefficient with temperature. These nonlinear model equations are normally difficult and sometimes impossible to solve analytically. Despite this difficulty, numerous attempts have been made by several investigators to get the approximate and/or analytical solutions of these nonlinear model equations. Nonlinear model equation with constant thermal conductivity but power-law temperature dependent heat transfer coefficient [a nonlinear second order ODE constituting a BVP] has been approximately solved by Aziz and Benzines (1976) by using perturbation method. Dul'kin and Garas'ko (2002) have exercised some fitting procedure to get the approximate solution of the same model equation. In some recent works, several researchers have also employed various approximate methods for solving the same model equation, e.g. Lesnic and Heggs (2004), and Chang (2005) have employed ADM, whereas Chowdhary and Hashim (2008) have used HPM. On the other hand, analytical solutions of the same model equation have also been obtained by different workers (Sen and Trinh, 1986; Yeh and Liaw, 1990; Abbasbandy and Shivanian, 2010).

Recently, a similar type of model equation represented by a nonlinear second order ODE constituting a BVP and depicting the process of radiative heat transfer from a rectangular fin to the free space has been solved by several researchers by using different approximate methods. For example, Ganji (2006) and Abbasbandy (2006a) have, respectively, employed HPM and HAM to solve this model equation, and obtained the approximate solution of temperature profile. Similarly, Tari et al. (2007) and Marinca and Herişanu (2008) have employed VIM and OHAM, respectively, to solve the same model equation, and obtained the approximate solution of temperature profile. However, in all these studies no attempts have been made to obtain the analytical solution of this model equation.

In another recent study, a more general model equation depicting the process of convective heat transfer from a rectangular fin has been analytically solved by Moitsheki et al. (2010b). These researchers have applied symmetry methods to solve this general model equation and obtained the analytical solutions of temperature profiles and fin efficiency. Although, this equation is also represented by a nonlinear second order ODE constituting a BVP, but it now incorporates the different power-law functions of temperature for thermal conductivity and heat transfer coefficient. However, neither all of the cases appearing in this model equation have been solved by

these researchers, nor any discussion regarding the existence, uniqueness/multiplicity and stability/instability of the obtained solutions is presented.

It should be noted that the model equations of the following processes are the specific cases of this general model equation:

- The convective heat transfer process from a rectangular fin with the assumption of constant thermal conductivity but power-law temperature dependent heat transfer coefficient (Aziz and Benzies, 1976; Sen and Trinh, 1986; Yeh and Liaw, 1990; Dul'kin and Garas'ko, 2002; Lesnic and Heggs, 2004; Chang, 2005; Chowdhury and Hashim, 2008; Abbasbandy and Shivanian, 2010).

- The radiative heat transfer process from a rectangular fin with the assumption of constant thermal conductivity (Ganji, 2006; Abbasbandy, 2006a; Tari et al., 2007; Marinca and Herişanu, 2008).

- The reaction-diffusion process taking place in a porous catalyst slab with the assumption of power-law kinetics and constant diffusivity (Mehta and Aris, 1971; Sun et al., 2004; Abbasbandy, 2008; Abbasbandy et al., 2009; Magyari, 2008; Moitsheki et al., 2010a).

Hence, the solutions obtained for the above more general model equation may also be applied to the above mentioned processes.

2.2 ROTARY KILN AND FLUID FLOW PROCESS

In this section, the literature related to the solution methodologies adopted by various researchers to solve the model equations of rotary kiln and fluid flow process has been presented. The model equation of rotary kiln describes the axial transport of solids, whereas the model equation of fluid flow process concerns with the flow of a third grade fluid between two parallel plates.

26

2.2.1 Rotary Kiln

Rotary kilns are widely used in the chemical and allied industries for performing various operations on the granular solids, e.g. mixing, heating and gas-solid reactions. Some of the processes in which these operations occur are calcination and sintering. Rotary kilns are basically a type of reactor in which solids travel down the cylinder with the hot gas flowing co-currently or counter-currently. The heat transfer takes place from the hot gas to the solid particles and the above different operations take place simultaneously. Because of the industrial importance of rotary kiln, a lot of theoretical and experimental studies are available in the literature.

An important problem in the design of rotary kiln is to estimate the solid bed depth profile along the kiln length (Liu et al., 2009). The heat transferred to the solids in a kiln strongly depends on their residence time and hold-up, which are basically dependent on the bed depth profile. Once the bed depth profile is known, these quantities can easily be found thereafter.

The process of axial transport of solids in a rotary kiln was first studied experimentally by Sullivan et al. (1927). Based on the obtained experimental results, these researchers derived empirical relations for the time of passage of solids through the rotary kiln. However, it was Saeman (1951) who initially established a sound theoretical background for the flow of granular solids in a rotary kiln and presented a nonlinear model equation for finding the bed depth profile. Due to the simplicity of the Saeman's model equation and its close agreement with the experimental data, it is widely used in literature. This model equation is represented by a nonlinear first order ODE constituting an IVP, and to the best of our knowledge, its analytical solution is not available. However, in some studies approximate solutions of this model equation have been reported. For example, Kramers and Croockewit (1952) derived the approximate solution for finding the bed depth profile and fractional hold-up. But, due to higher error in its prediction in certain cases, it is generally not preferred (Liu et al. 2009).

Recently, Liu et al. (2009) have derived a more accurate approximate solution of the bed depth profile by simplifying the nonlinearity in the Saeman's model equation. These researchers have also successfully simulated the experimental data taken from two different sources (Sai et al., 1990; Spurling, 2000), and shown that their approximate solution is superior to the one derived by Kramers and Croockewit (1952).

However, the approximate solution of Liu et al. (2009) has also been found to be susceptible to errors and in some cases, it develops deviations in its predictions. In their work, Liu et al. (2009) have also pointed out this shortcoming.

There have been several other experimental and simulation studies to investigate different aspects of the rotary kiln. For instance, Lebas et al. (1995) have performed experimental and simulation studies for finding the bed depth profile and residence time, whereas Spurling et al. (2001) have developed the dynamic mechanistic model for studying the transient response to large step changes in various operating variables. The experimental and theoretical studies to investigate the residence time distributions of solids inside the rotary kiln and the effect of different dam configurations have been carried out by Sai et al. (1990) and Scott et al. (2008), respectively. However, none of these studies have reported the analytical solution of the Saeman's nonlinear model equation.

2.2.2 Fluid Flow Process

In general, many engineering fluids and fluid-solid mixtures, e.g. slurries, emulsions, pastes, lubricants, different polymer solutions, and various biological and pharmaceutical fluids, e.g. ketchups, honey, blood, are characterized by non-Newtonian fluids (Hillier et al., 2002; Ali et al., 2009a; Siddiqui et al., 2010; Mehdizadeh and Oberlack, 2010; Wang et al., 2011). Most of these non-Newtonian fluids exhibit numerous strange features unlike their Newtonian counterparts, and thus, the classical Navier-Stokes equations become redundant in describing their rheological behaviour properly (Wanchoo et al., 1996; Wanchoo et al., 2007a; Wanchoo et al., 2008). Some of the attributes of these non-Newtonian fluids are the strong dependence of fluid viscosities on the velocity gradients, display of elastic effects and presence of nonzero and unequal normal stresses. Due to this reason, various rheological models have been proposed to correctly portray the non-Newtonian flow behaviour (Oldroyd, 1950; Rivlin and Ericksen, 1955; Bird et al., 1987; Bird et al., 2002). One such type of rheological model is the differential type fluid model and the third grade fluid is one of the subclass of these differential type fluid models. Due to the ability of the third grade fluid in successfully capturing various non-Newtonian effects, viz. shear thinning, shear thickening as well as normal stresses, it has been the subject of many investigations

28

ranging from fundamental studies to the practical flow situations. For example, thermodynamical aspects of these fluids have been investigated by some of the researchers (Fosdick and Rajagopal, 1980; Rajagopal, 1980; Patria, 1989). Studies, related to the existence and uniqueness of solutions of the concerned model equations, have been carried out by Bellout et al. (1999), Passerini and Patria (2000), and Vajravelu et al. (2002). Besides, some basic flow situations arising in the flow of a third grade fluid have also been tackled by several investigators, e.g. the model equations describing the pulsating Poiseuille flow of third grade fluid have been numerically solved by Rajagopal and Sciubba (1984), the process of pulsatile flow of blood [an important example of third grade fluid] due to body acceleration has been studied by Majhi and Nair (1994). Similarly, the flow of third grade fluid in a single rotating cylinder and between two rotating cylinders has been examined by Vajravelu et al. (2002) and by Akyildiz et al. (2004), respectively. The model equations representing the flow of a third grade fluid over flat plate has been solved by several researchers by using various approximate methods, e.g. HAM (Ayub et al., 2003; Sajid and Hayat, 2008b) and HPM (Siddiqui et al., 2008a). The model equation of a similar flow process has been analytically solved by Hayat et al. (2008). Slip effects for the peristaltic flow of third grade fluid in tubes have been studied by Ali et al. (2009b). Model equations of heat and mass transfer processes with chemical reaction in unsteady flow of a third grade fluid have been solved approximately by Hayat et al. (2010) by using HAM.

Recently, the model equations of similar flow processes, i.e. the Poiseuille flow and Couette-Poiseuille flow of a third grade fluid between the two parallel plates, have been solved by several researchers with the help of two approximate methods, namely HPM (Siddiqui et al., 2008b) and ADM (Siddiqui et al., 2010). These flow processes are described by nonlinear second order ODEs constituting BVPs. In both these studies, these researchers have obtained the approximate solutions of the velocity profile, however, no solutions were found for the flow rate. It should be noted that in many fluid flow processes, it is the flow rate that is conveniently measured, whereas the measurement of velocity profile is generally not done. Nevertheless, in our knowledge, the analytical solutions of velocity profile and flow rate have not yet been found for these flow processes.

2.3 EQUATION OF STATE AND FRICTION FACTOR EQUATION

In this section the appraisal of literature pertaining to the solution methods used for solving the thermodynamic equation of state and friction factor equation has been presented.

2.3.1 Thermodynamic Equation of State

The thermodynamic equation of state basically describes the relationship between two or more state functions, e.g. temperature, pressure and volume. There exist many equations of state, e.g. Beattie-Bridgeman equation, Peng-Robison equation, Redlich-Kwong equation, BWR [Benedict–Webb–Rubin] equation, each having its own advantages and disadvantages (Annamalai and Puri, 2002). In chemical engineering, these equations of states are used in predicting the properties of gases, liquids, solids and mixtures of gases and mixtures of liquids. Mathematically, these equations are represented by nonlinear AEs and are, in general, solved by using numerical methods.

One such equation of state is the Beattie-Bridgeman equation of state, which is widely used in estimating the volume of a gas at a given pressure and temperature. This equation of state is given by a quartic equation in volume. However, due to the cumbrous analytical solution of this equation, it is normally solved by using numerical methods, and use of some recent approximate methods, e.g. ADM and RADM, to solve this equation is unavailable.

2.3.2 Friction Factor Equation

The prediction of frictional losses is a vital issue in various pipe-flow problems, viz. pressure drop evaluation for estimating the pump size or to find the flow-rate in a piping network for a given pressure drop. Frictional losses are computed with the help of friction factor, which is normally given by implicit algebraic equations. In a huge piping network involving different pipe elements, a large number of implicit algebraic equations have to be solved for evaluating the friction factor (Bralts et al., 1993). This task becomes tedious as the network size increases and to gain a computational efficiency, a good initial guess of friction factor has to be specified for each pipe

element. Therefore, to avoid these cumbersome numerical iterative processes, explicit expressions of friction factor are needed.

Since many industrially important non-Newtonian fluids, e.g. pastes, gels, plastics, are represented by Bingham fluids (Bird et al., 2002), it becomes essential to express the friction factor equation in explicit form in order to evaluate friction factor conveniently. The friction factor for the laminar flow of Bingham fluids in smooth pipes depends upon Bingham Reynolds number [$Re = \dfrac{\rho \hat{v} D}{\mu_B}$] and Hedstrom number [$He = \dfrac{\tau_0 \rho D^2}{\mu_B^2}$], and is given by an implicit quartic equation whose closed form analytical solution is possible (Govier and Aziz, 1972; Sablani et al., 2003). However, due to its complexity this analytical solution is rarely employed, and as per our knowledge, no approximate explicit solution is available. Therefore, other approaches, e.g. numerical method, artificial neural network [ANN], are employed to find the friction factor (Sablani et al., 2003). Similarly, for turbulent flow of Bingham fluids in smooth pipe, the famous implicit NPK [Nikuradse-Prandtl-Karman] equation is applicable (Sablani et al., 2003), which can be deduced from the well-known Colebrook-White equation (Colebrook, 1939) under smooth pipe condition (Romeo et al., 2002). It should be mentioned that the NPK equation is the same equation as the one used for Newtonian fluids in turbulent flow in smooth pipes. Therefore, corresponding explicit correlations can also be used for these fluids. Some of the explicit correlations used in place of implicit NPK equation are those proposed by Churchill (1977), Chen (1979), Zigrang and Sylvester (1982), Serghides (1984), Manadilli (1997) and Romeo et al. (2002). Out of these, the correlations proposed by Serghides (1984), Manadilli (1997) and Romeo et al. (2002) yield reasonably close results to those of NPK equation. The friction factor correlation proposed by Serghides (1984) is valid for $Re > 2100$ and for any value of relative roughness [ε/D], whereas the correlation proposed by Manadilli (1997) is applicable for $5000 < Re < 10^8$ and for any value of ε/D. The correlation given by Romeo et al. (2002) is valid for $3000 < Re < 1.5 \times 10^8$ and $0 < \varepsilon/D < 0.05$. Beside these, some other studies have also been carried out for evaluating the friction factor.

For example, Sablani et al. (2003) have developed an explicit procedure for finding the friction factor for Bingham fluids in smooth pipes using an empirical soft computing tool, i.e. artificial neural network [ANN], but no explicit correlation was provided. Goudar and Sonnad (2003), and More (2006) have obtained explicit expressions of friction factor for turbulent flow of Newtonian fluids by solving the NPK and Colebrook-White equations, respectively, by using Lambert W function (Keady, 1998).

However, use of ADM and RADM to obtain the explicit expressions of friction factor has not yet been reported in any of the above studies.

2.4   REACTION-DIFFUSION PROCESSES AND TUBULAR CHEMICAL REACTOR MODEL

2.4.1   Reaction-Diffusion Process in a Porous Catalyst Slab

The reaction-diffusion process inside a porous catalyst plays an important role in the design of gas-solid heterogeneous reactors and has been a subject of great interest for chemical engineers (Thiele, 1939; Wheeler, 1955; Pushpavanam and Narayanan, 1988; Fogler, 1992; Levenspiel, 1999). In these processes, the reactant diffuses and reacts inside the catalyst pores to give the desired product. The amount of costly catalysts to be used in the reactor and the proper design of the reactor are primarily dictated by the prediction of diffusion and reaction rates inside the catalyst. Therefore, it becomes an essential task to obtain the accurate solution of the model equation of reaction-diffusion process.

Under steady-state and isothermal conditions, the model equation of reaction-diffusion process is represented by a second order ODE constituting a BVP. However, the presence of frequently encountered complicated kinetics terms render this model equation nonlinear, and to obtain the analytical solution for such cases becomes almost infeasible except in very special cases, e.g. for first order kinetics (Thiele, 1939). Many workers have studied this process in detail and obtained the solution of its model equation for several important situations. However, because of the nonlinear nature of

the model equation, these approaches have been limited to various linearization or numerical techniques. For example, the finite difference techniques have been employed by Kubicek and Hlavacek (1983), whereas weighted residual techniques have been applied by Villadsen and Michelsen (1978), and Finalyson (1980). For power-law kinetics, the asymptotic and analytical solutions of this model equation have been given by Mehta and Aris (1971). Recently, Magyari (2008) and Moitsheki et al. (2010a) have also obtained the analytical solution of this model equation by using derivative substitution method and symmetry methods, respectively. However, the analytical solutions obtained by these researchers are limited to the catalyst slab sustaining power-law kinetics. In some other studies, several approximate methods, e.g. ADM and VIM, have also been applied by different researchers to solve the same model equation (Lesnic, 2007; Mo, 2007; Wang and He, 2008). A good account of work related to the multiplicity and stability of solutions of this model equation can be found in voluminous books by Aris (1975).

Recently, Sun et al. (2004) and Abbasbandy (2008) have employed ADM and HAM, respectively, to solve the model equation of this process, and obtained the approximate solutions of concentration profile and effectiveness factor. However, the approximate solutions obtained by these researchers are restricted to catalyst slab and power law kinetics only. Moreover, the ADM solution obtained by Sun et al. (2004) breaks down in those cases where reaction order is smaller than unity [$n < 1, n \neq 0$] and Thiele modulus is high [$\phi \geq 2$]. In another study, Gottifredi and Gonzo (2005) have obtained the approximate solutions of concentration profile and effectiveness factor with the help of perturbation and matching procedure. These solutions are applicable to any types of kinetics but are valid for slab geometry only. Moreover, unlike the approximate solution of effectiveness factor which is found to be good enough in accurately predicting its value, the approximate solution of concentration profile shows significant deviations near the pore end for high Thiele modulus. These limitations have also been pointed out by Gottifredi and Gonzo (2005).

However, in our knowledge, the above restrictions present in the ADM solution of Sun et al. (2004) and the approximate solution of Gottifredi and Gonzo (2005) have not yet been rectified.

2.4.2 Reaction-Diffusion Process in a Porous Catalyst Sphere

Like the previously discussed reaction-diffusion process inside a porous catalyst slab, the reaction-diffusion process inside a catalyst sphere is also equally important in the design of heterogeneous catalytic reactors. Under steady state and isothermal conditions, the model equation of this process is described by a second order ODE constituting a singular BVP (Fogler, 1992), which poses difficulty in obtaining its solution as the solution may blow up near the singularity. In literature, this model equation has also been studied by many researchers in different contexts. For example, aspects related to the multiplicity and stability of solutions have been discussed by Aris (1975). Approximate solutions of this model equation have been obtained by numerous researchers by using several specific approximate methods, e.g. asymptotic methods (Kim .and Lee, 2004, 2006) and Taylor series method (Li et al., 2004). Similarly, different numerical methods, e.g. finite difference method, weighted residual method, have been applied by several researchers (Ferguson and Finlayson, 1970; Villadsen and Michelsen, 1978; Finlayson, 1980; Kubicek and Hlavacek, 1983). Valdes-Parada et al. (2008) have applied the Green's function approach to improve the finite-difference scheme for solving the model equation of this process for the spherical catalysts as well as the catalysts of other geometries. Recently, Magyari (2010) has applied symmetry method to obtain the analytical solution of this equation for a particular value of reaction order.

One should also note that the model equation of this process resembles with the well known Lane-Emden equation, which has also been solved by various researchers by using different approximate methods. For example, ADM and its modified versions have been employed by various researchers (Wazwaz, 2002; Wazwaz, 2005; Inc et al., 2005; Mittal and Nigam, 2008). Similarly, HPM (Ramos, 2008; Chowdhury and Hashim, 2009), HAM (Liao, 2003; Bataineh et al., 2009), VIM (Lu, 2007) and collocation method (Parand et al., 2010), have also been successfully used to solve the Lane-Emden equation. A small survey of the solution techniques used for solving similar types of singular BVPs has been given by Kumar and Singh (2009).

Recently, the model equation of this process has been solved by Shi-Bin et al. (2003) by using ADM and the approximate solutions of concentration profile and effectiveness factor have been obtained. In fact, ADM was introduced for the first time

in chemical engineering by these researchers. However, the obtained ADM solution is applicable to power-law kinetics only and breaks down in case of $n < 1$ [$n \neq 0$] and $\phi \geq 2$. To the best of our knowledge, no remedial measures have yet been taken for this limitation.

2.4.3 Tubular Chemical Reactor Model

The flow pattern existing in a real tubular chemical reactor as well as in many other chemical engineering systems is generally represented by axial dispersion model. In axial dispersion model, the non-ideal flow pattern is basically assumed as a combination of two types of flows, namely convective flow and dispersive flow. The dispersive flow is governed by a law analogous to the Fick's law of diffusion and takes into account all the non idealities caused by the radial mixing or other non flat velocity profiles. In this way, the departure from ideal plug flow is taken care of. Moreover, it has the advantage of reducing to two ideal flow patterns, viz. the plug flow and the completely mixed flow, by substituting the dispersion coefficient equal to zero or infinity respectively; these are the flow patterns that are used to analyze and design the ideal reactors. Due to these merits, it has been the subject of great interest for chemical engineers for more than half a century, especially in the field of tubular chemical reactors (Taylor, 1953; Danckwerts, 1953; Aris, 1956; Wehner and Wilhelm, 1956; Zwietering, 1959; Bischoff and Levenspiel, 1962a and 1962b; Deckwer and Mählmann, 1976; Hsu and Dranoff, 1986; Gunn, 1993, 2004; Wanchoo et al., 2007b; Babu et al., 2007). Besides, it has also been very effective in correctly portraying the flow pattern existing in various other types of reactor and systems, for example: fluidized bed reactor (Fan and Fan, 1979), fixed bed reactor (Rodrigues et al., 1994), membrane reactor (Tan and Li, 2000), rotary kiln (Abouzeid et al., 1980; Sudah et al., 2002), double pipe and plate heat exchangers (Roetzel et al., 1994; Roetzel and Balzereit, 1997), shell and tube heat exchanger (Roetzel and Lee, 1993; Roetzel and Balzereit, 2000), and fixed bed adsorber (Liao and Shiau, 2000). Once flow pattern / mixing level is quantified, other issues, e.g. optimization and control, can be studied (Babu and Angira, 2005; Babu et al., 2005; Gujarathi and Babu, 2009; Gujarathi and Babu, 2010).

Under steady state, the axial dispersion model is represented by a second order ODE, which constitutes a two point BVP. The associated BCs are known as the famous

Danckwerts BCs. In fact, the model equation is similar to the convection-diffusion equation. Different methods have been used to solve the axial dispersion model of various chemical engineering systems. In case of linear model equations, analytical methods, e.g. Laplace transform and Fourier transform, have been employed by several researchers (Rodrigues et al., 1994; Sudah et al., 2002; Roetzel et al., 1994; Roetzel and Balzerite, 1997), whereas nonlinear model equations have been tackled by using different approximate analytical/numerical methods, e.g. perturbation methods (Freeman and Houghton, 1966; Burghardt and Zaleski, 1968; Wissler, 1969; Ray et al., 1972; Turian, 1973; Rahman, 1974; Marek and Stuchl, 1975), finite difference methods (Fan and Bailie, 1960; Wan and Ziegler, 1970), collocation methods (Fan et al., 1971; Shah and Paraskos, 1975), quasi-linearization with finite difference (Lee, 1966), quasi-linearization with collocation method (Rao et al., 1981), spectral element method (Sporleder, 2010), inbuilt solvers in commercial mathematical softwares such as "MATLAB" (Tan and Li, 2000; Finlayson, 2006). Books by Villadsen and Michelsen (1978), Finlayson (1980), and Kubicek and Hlavacek (1983) are the excellent treatises on this subject.

However, the application of some of the newly developed approximate methods, e.g. HAM, OHAM, has not yet been carried out to solve the axial dispersion model equation of a tubular chemical reactor sustaining nonlinear kinetics.

2.5 DECOMPOSITION METHODS

In this section, the literature pertaining to the applications of ADM and its modified versions for solving AEs and ODEs has been reviewed. Various studies concerning the convergence of ADM and its modified versions have also been presented.

2.5.1 Adomian Decomposition Method

Adomian decomposition method, developed by George Adomian in early 1980s, has proved to be an efficient approximate method for solving different types of linear and nonlinear equations (Adomian, 1986, 1994). Due to its versatile and effective

36

nature, it has attracted the attention of many researchers and a lot of literature is available ranging from theoretical investigations to the applied studies.

The basic idea utilized in ADM is to decompose the nonlinear equation into a set of infinite but simpler linear equations by incorporating a hypothetical parameter λ $\in [0,1]$. The so formed linear equations are solved in a sequential manner and the obtained solutions of these linear equations are then combined to give the ADM solution of the original nonlinear equation. In this process, the nonlinearities present in the original nonlinear equations are expressed in terms of Adomian polynomials, which can conveniently be generated for any type of nonlinearity (Adomian, 1986, 1994). These polynomials are an integral part of the ADM and play a significant role in finding the solutions of different types of equations. The classical way of generating the Adomian polynomials has been given by Adomian (1986), however, there also exist various other algorithms for generating these polynomials (Adomian, 1994; Seng et al., 1996; Wazwaz, 2000b; Abdelwahid, 2003; Biazar et al., 2003a; Choi and Shin, 2003; Rach, 2008). It should, however, be noted that the Adomian polynomials are not unique and some other improved definitions of these polynomials [also called accelerated Adomian polynomials] have also been proposed (Nigam, 2009).

The ADM solution, found by combining the individual solutions of linear equations, is generally obtained in the form of a series called Adomian series. In most of the cases, this series is found to have better convergence as compared to the Mclaurine and Taylor series. A comparison between the Adomian series, Maclaurine series and Taylor series has been carried out by Rach et al. (1992) and Wazwaz (1998). Despite effectiveness, the limitations of ADM have also been reported by some researchers (Nelson, 1988; Golberg, 1999). The convergence related issues for the ADM have also been studied by several researchers (Gabet, 1994; Abboui, and Cherruault, 1994; Abboui and Cherruault, 1995; Abboui et al., 1995; Babolain, and Biazar, 2002a; Allan, 2007).

In the following two subsections, the literature concerning the application of ADM to solve AEs and ODEs, have been presented.

2.5.1.1 Algebraic equations

The first application of ADM to solve AEs has been presented by Adomian himself in his book (Adomian, 1986). Thereafter, several attempts have been made by various researchers to solve systems of AEs. For instance, Babolian et al. (2004a) and Kaya and El-Sayed (2004) have successfully employed ADM to solve AEs, whereas Li (2009) has not only employed ADM to solve AEs but also shown that the working of ADM is equivalent to that of another approximate method, i.e. HPM.

In addition to these, ADM has also been employed to improve some of the existing numerical schemes used for solving AEs, e.g. Abbasbandy (2003, 2006b), Chun (2006) and Basto et al. (2006) have separately devised Newton-Raphson like approximate numerical schemes for solving AEs. The convergence related aspects of ADM for solving AEs have been discussed by Abbaoui and Cherruault (1994, 1995), Cherruault et al. (1995), Babolian and Biazar (2002a) and Babolian et al. (2004a).

2.5.1.2 Ordinary differential equations

In literature, one of the important applications of ADM has been to solve the nonlinear ODEs, and numerous research studies are available in this respect. Nonlinear first order ODEs constituting IVPs, which arise in various engineering applications, have been solved by several researchers by using ADM. For example, the model equations of various chemical and biochemical reaction engineering processes [coupled first order ODEs constituting IVPs] have been successfully solved by using ADM (Sen, 1988; Biazar et al., 2003b; Kaya, 2004). Nonlinear first order ODE constituting an IVP, arising in the optics problem, has been solved by Sanchez et al. (2000). Similar sets of coupled ODEs have also been solved by other investigators (Abboui et al., 1995; Biazar et al., 2004).

On similar lines, nonlinear second order ODEs constituting BVPs have also been successfully solved by many researchers by using ADM. For example, the model equation of well known reaction-diffusion process occurring inside a porous catalyst slab, represented by a second order ODE [BVP], has been solved by Sun et al. (2004) by using ADM. Similarly, model equation of the same reaction-diffusion process but occurring inside a porous catalyst sphere [a second order ODE constituting a singular

BVP], has also been solved by Shi-Bin et al. (2003) by using ADM. The famous Lane-Emden and Emden-Fowler equations, also expressed by the similar types of singular BVPs, have also been solved by various researchers with the help of ADM (Wazwaz, 2002, 2005; Inc et al., 2005; Mittal and Nigam, 2008).

BVPs arising in various heat transfer, mass transfer and fluid flow operations have also been successfully solved by using ADM. For example, the model equation for the process of heat transfer from a rectangular fin [nonlinear second order ODE constituting a BVP] has been solved by Lesnic and Heggs (2004) and Chang (2005) by using ADM. Sun and Scott (2004) have solved the model equation of mass transfer process in a porous electrode by using ADM; the modelling equations are coupled second order ODEs constituting BVPs. Kechil and Hashim (2007) have solved the convective boundary layer equations by using the ADM, whereas Alizadeh et al. (2009) have applied ADM to solve Falkner-Skan equation. Holmquist (2007) has applied ADM to solve fluid dynamics problems. The original model equations in these studies were a set of nonlinear PDEs, which were first transformed into a set of nonlinear ODEs by using symmetry methods and solved subsequently by using ADM.

The convergence and stability related issues of ADM for solving ODEs have been presented by Repaci (1990), Abbaoui and Cherruault (1994), Cherruault et al. (1995), Hosseini and Nasabzadeh (2006), Aminataei and Hosseini (2007).

2.5.2 Restarted Adomian Decomposition Method

While applying ADM to solve various types of equations, it has been observed that ADM exhibits slow convergence and sometimes, it diverges too (Nelson, 1988). In such cases, several modifications have been proposed in ADM by various researchers for solving different types of equations. Review of some of the related modifications in ADM to solve AEs and ODEs have been presented in the following two subsections, respectively.

2.5.2.1 Algebraic equations

For AEs, Babolian and Biazar (2002b) have proposed an efficient iterative scheme of ADM called Restarted ADM. Later, Babolian and Javadi (2003) applied the same RADM to successfully solve several examples of AEs. Basto et al. (2006) have shown that in spite of its faster convergence, the RADM, as proposed by Babolian and Biazar (2002b), may also diverge. In such situations, Basto et al. (2006) have given certain guidelines to avoid the divergence of RADM. Beside RADM, some other modified versions of ADM have also been proposed by other researchers to effectively solve AEs (El-Sayed, 2002; Jafari and Daftardar-Gejji, 2006; Jiao et al., 2008). For some of these modified versions of ADM, the convergence characteristics have also been discussed by some researchers (El-Sayed, 2002; Chun, 2006; Basto et al., 2006).

2.5.2.2 Ordinary differential equations

There have also been many attempts to modify ADM so as to efficiently solve the ODEs (Venkatarangan and Rajalakshmi, 1995; Andrianov, 1998; Wazwaz, 2000a; Jiao et al., 2002; Casasús and Al-Hayani, 2002; Mahmood et al., 2005; Hasan and Zhu, 2009). For solving ODEs, the use of orthogonal polynomials in conjunction with ADM have been presented by several researchers (Hosseini, 2006; Layeni, 2008; Tien and Chen, 2009; Liu, 2009). Different numerical adaptations of ADM for solving ODEs have been presented by Adomian et al. (1991), Ghosh et al. (2007) and Ramos (2009). Various other modified versions of ADM for solving ODEs constituting singular and non-singular BVPs have also been proposed by different researchers (Adomian and Rach, 1994; Wazwaz, 2005; Inc et al., 2005; Hosseini and Nasabzadeh, 2007; Aslanov and Abu-Alshaikh, 2008; Jang, 2008; Hasan and Zhu, 2009; Kumar and Singh, 2010).

Like in the case of AEs, Babolian et al. (2004b) and Babolian et al. (2005) have also devised RADM for IEs [integral equations] and ODEs, respectively. However, in the latter case merely IVPs in first order ODEs have been considered.

2.6   HOMOTOPY METHODS

This section reviews the literature available on another approximate method, namely HAM and one of its effective variants, i.e. OHAM. Various studies, concerning the theoretical and application aspects of these two methods have also been assessed. However, the main emphasis has been given to those studies, in which ODE models of various processes/systems have been solved by using HAM or its variants.

2.6.1   Homotopy Analysis Method

Homotopy analysis method, first developed by Liao in early nineties is an efficient approximate method for solving different types of nonlinear equations (Liao, 1995, 2003, 2009a). Like ADM, HAM is also a hypothetical parameter based method and its working is somewhat similar to that of ADM. However, as compared to ADM, HAM is a more general and effective method, since it involves several auxiliary quantities, which render it more flexible for solving nonlinear equations. The detailed methodology of HAM to solve different types of equations has been given in a monograph by Liao (2003). Selection of auxiliary quantities required in HAM has also been given in this monograph as well as in a recent paper by Gorder and Vajravelu (2009).

Due to its versatile and robust nature, profuse literature on HAM is available and is still increasing. For instance, model equations of various heat transfer processes have been effectively solved by many researchers by using HAM (Liao et al., 2006; Abbasbandy, 2006a; Domairry and Nadim, 2008; Sajid and Hayat, 2008a; Sweet, 2009; Abbas et al., 2010). Similarly, model equations of several fluid flow processes have also been solved by many researchers by using HAM (Hayat et al., 2007; Abbas et al., 2008; Sajid and Hayat, 2008b; Sweet, 2009; Dinarvand and Rashidi, 2010). Besides, model equations of some of the boundary layer problems have also been successfully tackled by a number of researchers (Liao and Pop, 2004; Cheng et al., 2008; Shateyi et al., 2010). One should note that these boundary layer problems are represented by coupled PDEs, however, by using symmetry methods these PDEs were converted into coupled ODEs, which were subsequently solved by using HAM. In some other applications, PDEs were directly solved without converting them into ODEs (Liao et al., 2006; Liao,

2009b). The model equation of reaction-diffusion process inside a porous catalyst slab has been solved by Abbasbandy (2008). The Lane-Emden equation which resembles with the model equation of reaction-diffusion process in a porous spherical catalyst [a second order ODE constituting a singular BVP] has also been solved by several workers (Liao, 2003; Bataineh et al., 2009).

In addition to the above applications, HAM has also been applied to solve different types of nonlinear equations numerically, e.g. numerical application of HAM to solve AEs and ODEs has been demonstrated by Abbasbandy et al. (2007) and Motsa et al. (2010), respectively. Similarly, PDEs have also been solved by using the numerical scheme of HAM (Liao, 1997; Zhu et al., 2010). Besides, multiple solutions arising in various ODEs [BVPs] and PDEs have also been successfully found by several investigators (Abbasbandy et al., 2009; Abbasbandy and Shivanian, 2010; Xu and Liao, 2008).

Some other mathematical aspects of HAM have also been studied by various workers. For example, comparison of HAM with other methods has been performed by He (2004), Liao (2005) and Allan (2007). Convergence related issues of HAM have been discussed by Liao (2009a), Odidat (2010) and Turkyilmazoglu (2010, 2011). Recently, Liu (2010, 2011) and Abbasbandy et al. (2011) have discussed the mathematical significance of the convergence control parameter, which is a vital component of HAM. Liu (2010, 2011) has also analyzed the relation between the HAM and the generalized Taylor series method.

2.6.2 Optimal Homotopy Analysis Method

OHAM is an efficient variant of HAM and has also been proposed by Liao (2010). Its working is almost similar to that of HAM, however, in OHAM, the convergence control parameter is selected by minimizing the sum of square of residual errors instead of the so called h-curve (Liao, 2003).

Since OHAM has been developed recently, only a few studies are available depicting its successful application (Wang, 2011). There exist some other versions of OHAM, however, these are somewhat different than the one proposed by Liao (2010). These modified versions have been applied to solve different equations including those

encountered in various flow and heat transfer processes (Marinca et al., 2008; Marinca and Herişanu, 2008; Idrees et al., 2010; Niu and Wang, 2010; Iqbal and Javed, 2011).

2.7   MOTIVATION FOR THE PRESENT RESEARCH WORK

By critically analyzing the reviews of selected processes/systems presented in the above sections, one concludes that still there are ample possibilities of further research work in each case. These possible areas of research have been indicated in corresponding sections in this chapter.

2.8   CONCLUDING REMARKS

In this chapter, the literature pertaining to the methodologies adopted by previous researchers for solving the model equations of selected processes/systems as well as the solutions obtained by using these methods have been reviewed and critically evaluated for identifying the research gaps. The selected processes/systems arise in different areas of chemical engineering, namely heat transfer, fluid mechanics, thermodynamics and reaction engineering. These research gaps may possibly be addressed with a view to obtain the analytical/approximate solutions of the model equations of these selected processes/systems. Based upon this, the motivation for the proposed study has been outlined.

CHAPTER III

SELECTED HEAT TRANSFER PROCESSES – ANALYTICAL SOLUTIONS

3.0   INTRODUCTION

This chapter concerns with the development of analytical solutions of the model equations of five selected heat transfer processes, namely the transient convective cooling of a lumped body, the convective-radiative cooling of a lumped body, the steady state heat conduction in a metallic rod, the radiative heat transfer from a rectangular fin and the convective heat transfer from a rectangular fin. These processes are frequently encountered in various heat transfer operations, e.g. broiler, automobile radiators, metallurgical processes, radiation devices in outer space applications, heat flow meters, engines and electric motors etc.

In literature, many researchers have obtained the approximate solutions of these processes by using various approximate methods, e.g. HPM, HAM and OHAM etc. For some of these processes, analytical solutions have also been found by several researchers. However, these are valid for a few special cases, and to the best of our knowledge, analytical solutions of these processes, which cover all the situations arising therein, have not yet been found.

For obtaining analytical solutions, analytical methods, namely separation of variables method, partial fraction decomposition method, and derivative substitution method, have been used individually or in a combination of two of them. These analytical solutions have been validated with the numerical solutions of model equation and with the available solutions. Besides, an existing experimental study, pertaining to the process of transient convective and radiative cooling of a metal ball bearing, has been simulated by using the derived analytical solution. Special attention has been paid to the process of convective heat transfer from a rectangular fin, as the model equation is quite general and the results obtained show a variety of features, e.g. multiplicity.

3.1 TRANSIENT CONVECTIVE COOLING OF A LUMPED BODY

In this section, we have shown that the model equation of this process is amenable to an explicit analytical solution, which can be obtained by using the separation of variables and partial fraction decomposition methods.

3.1.1 Model Equation

A body with density ρ, volume V and heat transfer area A, is considered. This body is initially at a temperature T_i. At time $t = 0$, it is exposed to an environment at a lower temperature T_a and thus starts loosing heat energy to the surroundings by convection. Following assumptions have been made:

(i)   The specific heat of body varies linearly with temperature.

(ii)   The convective heat transfer coefficient remains constant.

(iii)   The body satisfies the condition of lumped model, i.e. $Bi_c < 0.3$, (Campo and Blotter, 2000).

The model equation of this process can be derived by applying the unsteady energy balance over the body, and the following nonlinear first order ODE constituting an IVP is obtained (Ganji, 2006; Abbasbandy, 2006a; Tari et al., 2007; Marinca and Herişanu, 2008):

$$\rho V c_p(T)\frac{dT}{dt} + hA(T - T_a) = 0 \qquad (3.1a)$$

$$\text{IC: } T(0) = T_i \qquad (3.1b)$$

where $c_p(T) = c_a\left(1 + \beta\frac{T - T_a}{T_i - T_a}\right)$ is the heat capacity of the body showing linear dependency on the temperature, and h is the constant heat transfer coefficient. For simplicity, we have considered the transient convective cooling of a spherical body, however, the presented methodology to obtain the analytical solution is also applicable

to a lumped body with any geometry. For a spherical body, the Eq. (3.1a) reduces to the following equation, however, the associated IC will remain the same.

$$\rho c_a \left(1 + \beta \frac{T - T_a}{T_i - T_a}\right) \frac{dT}{dt} + \frac{3h}{R}(T - T_a) = 0 \tag{3.2}$$

3.1.2 Solution and Discussion: Temperature Profile

Before solving Eq. (3.2), we first define the following dimensionless quantities (Liao et al., 2006):

$$\theta = \frac{T - T_a}{T_i - T_a}, \quad \alpha = \frac{k}{\rho c_a}, \quad \tau = \frac{\alpha t}{R^2}, \quad Bi_c = \frac{hR}{k}$$

where α is the thermal diffusivity and Bi_c is the Biot number for convection. In fact, there exists another definition of Biot number for convection, i.e. $\frac{hR}{3k}$ (Campo and Blotter, 2000), however, we have followed the definitions as used by Liao et al. (2006).

Now, with the assistance of the above dimensionless variables, Eqs. (3.2) and (3.1b) attain the following dimensionless forms, respectively:

$$(1 + \beta\theta)\theta' + 3Bi_c\theta = 0 \tag{3.3a}$$

$$\text{IC:} \quad \theta(0) = 1 \tag{3.3b}$$

where θ' denotes $\frac{d\theta}{d\tau}$. A simple rearrangement of the Eq. (3.3a) yields:

$$\frac{\theta'}{\theta} + \beta\theta' = -3Bi_c \tag{3.4}$$

Integration of the Eq. (3.4) with respect to τ results in the following solution:

$$ln[\theta] + \beta\theta = -3Bi_c\tau + C_1 \tag{3.5}$$

where C_1 is the constant of integration, and is found to be $C_1 = \beta$ by using the IC. Substituting back the so found value of C_1 in Eq. (3.5), one obtains the following

analytical solution:

$$ln[\theta] + \beta\theta = \beta - 3Bi_c\tau \qquad (3.6)$$

It can be noted that the above analytical solution is in implicit form and match well with the analytical solution obtained by Ganji (2006) and Abbasbandy (2006a). Here we show that by a slight rearrangement it can be expressed in an explicit form. For doing this, a constant term $ln[\beta]$ is added and subtracted in Eq. (3.6), and after a little modification the following equation is obtained:

$$ln\left[\beta\theta e^{\beta\theta}\right] = \beta - 3Bi_c\tau + ln[\beta] \qquad (3.7)$$

The Eq. (3.7) can be further expressed as:

$$(\beta\theta)e^{(\beta\theta)} = \beta e^{\beta - 3Bi_c\tau} \qquad (3.8)$$

The L.H.S. of Eq. (3.8) can be replaced by the Lambert W function, which is implemented as "ProductLog" function in some mathematical softwares, e.g. MATHEMATICA. A Lambert W function is basically the inverse function of $x = ye^y$, i.e. $y = Lambert(x)$, and is given by $y = W(x)$. In general, the domain and range of the function is the set of complex values, however, for $x \in [0, \infty)$ the Lambert W function yields single real value. For $x \in (-\infty, -\frac{1}{e})$, the Lambert W function does not evaluate to any real value, whereas, for $x \in [-\frac{1}{e}, 0)$ it yields two real values. Now, with this function, the transient dimensionless temperature profile is given by:

$$\theta = \frac{1}{\beta} ProductLog\left[\beta e^{\beta - 3Bi_c\tau}\right] \qquad (3.9)$$

(i)   Comparison between the analytical, numerical and approximate solutions

To validate the above analytical solution [AS], i.e. Eq. (3.9), the dimensionless temperature profiles obtained by it as well as by numerical method [NS] are plotted in Fig. 3.1 for various values of β. It is clear from this figure that both the profiles match well and thus validate the present analytical solution.

48
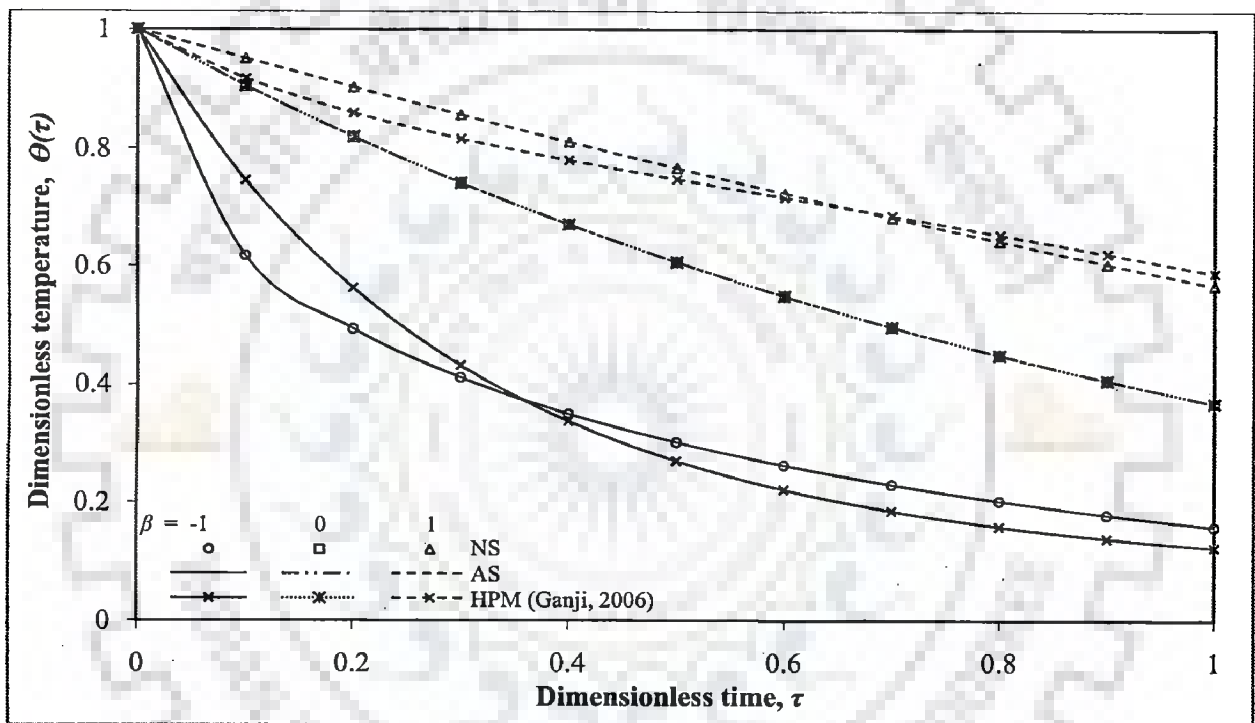
Figure 3.1: Transient profiles of dimensionless temperature at $Bi_c = 1/3$ for various values of β

The obtained analytical results have also been compared with those obtained by using the two approximate methods, i.e. HPM (Ganji, 2006) and HAM (Abbasbandy, 2006a). In these two studies, the approximate solutions [transient temperature profiles] were obtained for the transient convective cooling of an irregular shaped body with characteristic length $l\left[=\dfrac{V}{A}\right]$. The two approximate solutions are reproduced below:

$$\theta_{Ganji} \approx e^{-\tau_1} + \beta\left(e^{-\tau_1} - e^{-2\tau_1}\right) + \frac{\beta^2}{2}\left(e^{-\tau_1} - 4e^{-2\tau_1} + 3e^{-3\tau_1}\right) \tag{3.10a}$$

$$\theta_{Abbasbandy} \approx e^{-\tau_1} - \beta h_1 e^{-\tau_1} + \beta h e^{-2\tau_1} + \left(-\beta h_1(1+h_1) + \frac{\beta^2 h_1^2}{2}\right)$$

$$+\left(\beta h_1(1+h_1) - 2\beta^2 h_1^2\right)e^{-2\tau_1} + \frac{3\beta^2 h_1^2}{2}e^{-2\tau_1} \tag{3.10b}$$
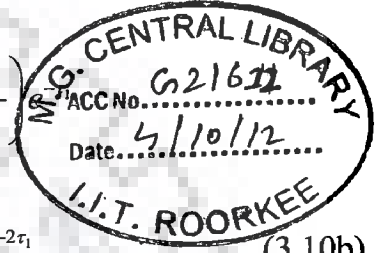
where τ_1 is the dimensionless time considered by Ganji (2006) and Abbasbandy (2006a), and is equal to $\dfrac{hAt}{\rho c_a V}\left[=\dfrac{ht}{\rho c_a}\dfrac{1}{l}\right]$, and h_1 is the convergence control parameter in HAM solution (Abbasbandy, 2006a).

For a spherical body, $l = R / 3$, hence, $\tau_1 = 3\,Bi_c\tau$. Now by taking $Bi_c = 1/3$, the two dimensionless times become equal, i.e. $\tau_1 = \tau$. Moreover, for this value of Bi_c [= 1/3], the present model equations for a spherical body, i.e. Eqs. (3.3a) and (3.3b), and the one considered by Ganji (2006) and Abbasbandy (2006a) for an irregular shaped body become identical, and thus, allows the comparison between the present analytical solution [Eq. (3.9)] and the above mentioned approximate solutions. This value of Bi_c [= 1/3] has been selected only for the comparison of the analytical results with the available approximate results (Ganji, 2006; Abbasbandy, 2006a), though it is slightly more than the prescribed upper limit for the lumped model.

For the comparison of these solutions, the dimensionless temperature θ, given by Eq. (3.9), is expanded around $\beta = 0$ by using the Taylor series method, and the following expansion is obtained for $Bi_c = 1/3$:

$$\theta \approx e^{-\tau} + \beta\left(e^{-\tau} - e^{-2\tau}\right) + \frac{\beta^2}{2}\left(e^{-\tau} - 4e^{-2\tau} + 3e^{-3\tau}\right) + \dots \tag{3.10c}$$

On comparing one finds that Eq. (3.10c) harmonizes well with the Eq. (3.10a) of Ganji (2006) as well as with the Eq. (3.10b) of Abbasbandy (2006a) for convergence parameter $h = -1$. This comparison has also been shown in Fig. 3.1, where analytical results [dimensionless temperature profiles] have been compared with the numerical results as well as with the approximate results obtained by using HPM (Ganji, 2006). This figure clearly shows that the analytically obtained results are in close agreement with the numerical results. However, the results obtained by using Eq. (3.10a), being approximate, exhibit considerable discrepancies except for $\beta = 0$, where the Eq. (3.3a) becomes linear.

A comparison of the initial rate of change of temperature $\theta'(0)$ [at $Bi_c = 1/3$], predicted by the analytical solution [Eq. (3.9)] and the approximate solution of Abbasbandy (2006a), has also been made. Analytical solution yields the following expression of $\theta'(0)$:

$$\theta'(0) = \frac{-1}{1+\beta} \tag{3.11}$$

Fig. 3.2 compares the profiles of $\theta'(0)$ as obtained by the Eq. (3.11) and the one obtained by Abbasbandy (2006a). Accuracy is evident by these overlapping profiles. Fig. 3.2 also supports the fact that with the increase in β, the specific heat increases, which in turn decreases the rate of change of temperature.

Similar comparisons with the OHAM solution of Marinca and Herişanu (2008) could not been made because of their more involved solution expression. However, it is obvious that the present solution, being analytical in form, is superior to the approximate solution of Marinca and Herişanu (2008).

3.2 TRANSIENT CONVECTIVE-RADIATIVE COOLING OF A LUMPED BODY

In the following subsections, we have analytically solved the model equation of

52
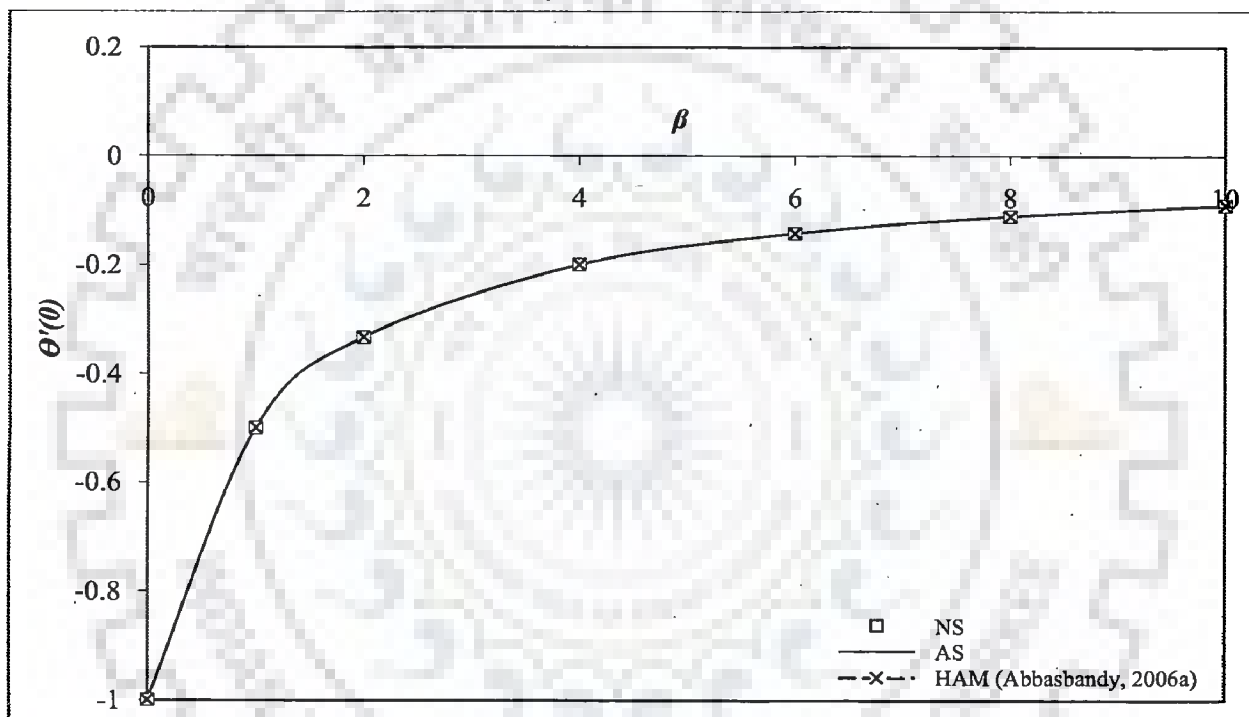
Figure 3.2: Variation of initial rate of change of dimensionless temperature with β at $Bi_c = 1/3$

this process by using the separation of variables method and the partial fraction decomposition method. Besides, the simplified model equation, depicting the transient cooling of a lumped body in an environment of absolute zero temperature and earlier solved by several researchers by using different approximate methods, namely PM, HPM and HAM (Ganji et al., 2007; Rajabi et al., 2007; Domairry and Nadim, 2008), has also been solved analytically by using the same methods, i.e. the separation of variables method and the partial fraction decomposition method.

3.2.1 Model Equation

Consider a spherical body with radius R, density ρ, thermal conductivity k and heat capacity c_p, respectively. Initially this body is at a higher temperature T_i, and at the start of the process it looses heat to the surroundings [the temperature of surroundings is T_f and the average radiation sink temperature is T_s] by convection and radiation. It is also assumed that the body is isotropic and opaque. By applying the energy balance over a thin spherical shell in this body, the following equation, along with the associated IC and BCs, is obtained (Su, 2004; Liao et al., 2006).

$$\rho c_p \frac{\partial T}{\partial t} = \frac{1}{r^2} \frac{\partial}{\partial r}\left(kr^2 \frac{\partial T}{\partial r}\right) \tag{3.12a}$$

The initial and boundary conditions are given as follows:

IC: $T = T_i$ at $t = 0$ $\forall\, r \le R$ (3.12b)

BC I: $-k\dfrac{\partial T}{\partial r} = h(T - T_f) + \sigma \in (T^4 - T_s^4)$ at $r = R$ $\forall\, t > 0$ (3.12c)

BC II: $\dfrac{\partial T}{\partial r} = 0$ at $r = 0$ $\forall\, t > 0$ (3.12d)

where h is the convective heat transfer coefficient, $\in$ is the emissivity of the spherical body and σ is the well-known Stephan-Boltzmann constant. Generally, T_f and T_s are equal, however, in case of different environment and sink temperatures, it is appropriate

55

to introduce the adiabatic surface temperature defined by the following equation (Liao et al., 2006):

$$h(T_a - T_f) + \sigma \in (T_a^4 - T_s^4) = 0 \tag{3.13}$$

With the help of adiabatic surface temperature $[T_a]$, the BC I attains the following form, which, as shown later, eases the computational work.

$$\text{BC I:} \quad -k\frac{\partial T}{\partial r} = h(T - T_a) + \sigma \in (T^4 - T_a^4) \text{ at } r = R \quad \forall \, t > 0 \tag{3.14}$$

With the assistance of the following dimensionless variables (Liao et al., 2006),

$$\theta = \frac{T}{T_i}, \; \eta = \frac{r}{R}, \; \theta_a = \frac{T_a}{T_i}, \; \alpha = \frac{k}{\rho c_p}, \; \tau = \frac{\alpha t}{R^2}, \; Bi_c = \frac{hR}{k}, \; N_{rc} = \frac{\sigma \in RT_i^3}{k},$$

where α is the thermal diffusivity, Bi_c is the Biot number for convection and N_{rc} is the conduction-radiation parameter, the Eqs. (3.12a), (3.12b), (3.12d) and (3.14) are transformed into the following dimensionless forms:

$$\frac{\partial \theta}{\partial \tau} = \frac{1}{\eta^2} \frac{\partial}{\partial \eta}\left(\eta^2 \frac{\partial \theta}{\partial \eta}\right) \tag{3.15a}$$

$$\text{IC:} \quad \theta = 1 \quad \text{at } \tau = 0 \quad \forall \, \eta \leq 1 \tag{3.15b}$$

$$\text{BC I:} \quad -\frac{\partial \theta}{\partial \eta} = Bi_c(\theta - \theta_a) + N_{rc}(\theta^4 - \theta_a^4) \text{ at } \eta = 1 \quad \forall \, \tau > 0 \tag{3.15c}$$

$$\text{BC II:} \quad \frac{\partial \theta}{\partial \eta} = 0 \text{ at } \eta = 0 \quad \forall \, \tau > 0 \tag{3.15d}$$

3.2.1.1 Lumped Parameter Model

For a spherical body with smaller dimensions and higher thermal conductivity, the spatial temperature variation can be neglected and the lumped model approach can be adopted. However, this should be supported by the criteria $Bi_T < 0.3$, where

$Bi_T \left(= \dfrac{(h + h_r)R}{k} \right)$ is the overall Biot number and takes into account the Biot numbers for convection and radiation (Campo and Blotter, 2000; Liao et al., 2006; Tan et al., 2009). Here, it should be noted that the definition of Bi_T is based on the one proposed by Liao et al. (2006).

For a spherical body, the equation for lumped parameter model is obtained by using the following definition of the spatially averaged dimensionless temperature (Su, 2004).

$$\theta_{av} = 3 \int_0^1 \theta \eta^2 d\eta \qquad (3.16)$$

The above definition renders the earlier obtained PDE into a first order nonlinear ODE constituting an IVP. Thus from Eqs. (3.15a)-(3.15d) and (3.16), one finally finds the following dimensionless equation to describe the transient convective-radiative cooling of a lumped spherical body:

$$\frac{d\theta_{av}}{d\tau} = -3Bi_c(\theta_{av} - \theta_a) - 3N_{rc}(\theta_{av}^4 - \theta_a^4) \qquad (3.17)$$

Similarly, the associated IC, i.e. Eq. (3.15b), with the use of Eq. (3.16), is expressed in terms of the spatially averaged temperature and attains the following form:

$$\text{IC:} \qquad \theta_{av} = 1 \qquad \text{at } \tau = 0 \ \forall \ \eta \leq 1 \qquad (3.18)$$

3.2.2 Solutions and Discussion: Temperature Profile

In this section, analytical solutions for the three cases, i.e. (i) $\theta_a \neq 0$, $Bi_T < 0.3$, (ii) $\theta_a = 0$, $Bi_c = 1/3$ and (iii) $\theta_a = 0$, $Bi_c = 0$, have been obtained below, individually. The value of $Bi_c = 1/3$ in case (ii) is chosen solely for the comparison purposes with the available results (Ganji et al., 2007; Rajabi et al., 2007; Domairry and Nadim, 2008). The obtained results of these three cases have been compared with the corresponding numerical results as well as with the available results.

3.2.2.1 General Case: $\theta_a \neq 0$, $Bi_T < 0.3$

After rearranging Eq. (3.17) and integrating it with the help of Eq. (3.18), one finds:

$$\frac{1}{N_{rc}} \int_1^{\theta_{av}} \frac{d\theta_{av}}{\dfrac{Bi_c}{N_{rc}}(\theta_{av}-\theta_a)+(\theta_{av}^4-\theta_a^4)} = -3\int_0^{\tau} d\tau \tag{3.19}$$

The partial fraction decomposition of the integrand in Eq. (3.19) yields the following simplified form:

$$\frac{1}{N_{rc}}\left[\int_1^{\theta_{av}} \frac{A_1 d\theta_{av}}{(\theta_{av}-r_1)} + \int_1^{\theta_{av}} \frac{B_1 d\theta_{av}}{(\theta_{av}-r_2)} + \int_1^{\theta_{av}} \frac{(C_1\theta_{av}+D_1)d\theta_{av}}{(\theta_{av}^2-(r_3+r_4)\theta_{av}+r_3r_4)} \right] = -3\int_0^{\tau} d\tau \tag{3.20}$$

where r_1, r_2, r_3 and r_4 are the roots of the quartic equation $\frac{Bi_c}{N_{rc}}(\theta_{av}-\theta_a)+(\theta_{av}^4-\theta_a^4)=0$; the explicit expressions of these roots are given in Appendix A1, where, it is also revealed that r_1 is real and positive, r_2 is real and negative, and r_3 and r_4 are complex conjugates. A_1, B_1, C_1 and D_1 are the constants appeared during the process of partial fraction decomposition, and their expressions are given in Appendix A2.

Now, expressing the complex conjugate pair r_3 and r_4 as $r_3 = a+ib$ and $r_4 = a-ib$, and integrating the Eq. (3.20), we obtain the following equation:

$$\frac{1}{N_{rc}}\left[\frac{(D_1+C_1a)}{b}\tan^{-1}\left[\frac{\theta_{av}-a}{b}\right] + \frac{1}{2}C_1 ln\left[(\theta_{av}-a)^2+b^2\right] + A_1 ln\left[\theta_{av}-r_1\right] + B_1 ln\left[\theta_{av}-r_2\right] \right]_1^{\theta_{av}}$$

$$= -3\int_0^{\tau} d\tau \tag{3.21}$$

After substituting the limits in the above equation, the following analytical solution is found:

$$\frac{1}{N_{rc}}\left[\frac{(D_1+C_1a)}{b}\left(\tan^{-1}\left[\frac{\theta_{av}-a}{b}\right] - \tan^{-1}\left[\frac{1-a}{b}\right]\right) + \frac{1}{2}C_1 ln\left[\frac{(\theta_{av}-a)^2+b^2}{(1-a)^2+b^2}\right]\right.$$

58

$$+ A_1 ln \left[\frac{\theta_{av} - r_1}{1 - r_1} \right] + B_1 ln \left[\frac{\theta_{av} - r_2}{\theta_{av} - r_2} \right] \right] = -3\tau \qquad (3.22)$$

(i)   Comparison between the analytical, numerical and approximate solutions

For various values of Bi_c, N_{rc} and θ_a, Fig. 3.3 shows the transient profiles of the spatially averaged dimensionless temperature θ_{av} obtained by using the above analytical solution [Eq. (3.22)] and the numerical method. A close agreement is observed between these profiles, which validates the analytical solution.

3.2.2.2 Simplified Case I: $\theta_a = 0$, $Bi_c = 1/3$

This particular situation is characterized by the fact that both the surroundings and the sink temperatures are assumed to be the same and are equal to zero, i.e. $T_s = T_f = 0$, and this implies that [from Eq. (3.13)] $T_a = \theta_a = 0$. This situation may arise in the outer space or in a vacuum. The model equation of this specific situation has been solved by several researchers by using various approximate methods, e.g. PM, HPM and HAM (Ganji et al., 2007; Rajabi et al., 2007; Domairry and Nadim, 2008). Although, this model equation, as considered by these researchers, becomes invalid, since at $\theta_a = 0$ [absolute zero temperature of the surroundings], there will be no convective heat transfer, i.e. $Bi_c = 0$. Moreover, for the chosen value of convection Biot number [$Bi_c = 1/3$] the assumption of lumped body becomes invalid [as $Bi_c >$ 0.3] and the same is true for the model equation and its solution. However, we have considered this situation just for the sake of comparison, and the realistic model equation for this situation has been considered in the next subsection.

As a consequence of the above assumption, the Eq. (3.17) assumes the following form, which is same as the one considered by the above researchers (Ganji et al., 2007; Rajabi et al., 2007; Domairry and Nadim, 2008). However, the associated IC remains the same, i.e. $\theta_{av}(0) = 1$.

$$\theta'_{av} + \theta_{av} + \varepsilon\theta^4_{av} \;=\; 0 \tag{3.23}$$

where ε $[= 3N_{rc}]$ is a parameter considered by these researchers. After minor rearrangements of terms in Eq. (3.23) and the subsequent partial fraction decomposition of the resulting equation, the following equation has been obtained:

$$\frac{d\theta_{av}}{\theta_{av}} - \frac{\varepsilon\theta^2_{av}d\theta}{1+\varepsilon\theta^3_{av}} \;=\; -d\tau \tag{3.24}$$

Integrating the above equation with the associated IC, the following explicit solution expression is found:

$$\theta_{av} \;=\; \frac{e^{-\tau}}{(1+\varepsilon-\varepsilon e^{-3\tau})^{1/3}} \tag{3.25}$$

As expected, the above analytical solution reveals: $\theta_{av} \to 0$ as $\tau \to \infty$ $\forall\varepsilon$.

(i) *Comparison between the analytical, numerical and approximate solutions*

Now, if one expands the θ_{av} [Eq. (3.25)] around $\varepsilon = 0$ by using the Taylor series method, the following series is obtained:

$$\theta_{av} \;\approx\; e^{-\tau} - \frac{1}{3}\varepsilon e^{-4\tau}(-1+e^{3\tau}) + \frac{2}{9}\varepsilon^2 e^{-7\tau}(1+e^{6\tau}-2e^{3\tau}) \tag{3.26}$$

On comparing, it is observed that Eq. (3.26) is exactly the same as the approximate solutions obtained by using PM and HPM (Rajabi et al., 2007; Ganji et al., 2007). Similarly, Eq. (3.26) also matches well with the approximate solution obtained by Domairry and Nadim (2008) by using HAM for the convergence control parameter equal to "-1", considered therein [it should be noted that there are some typographical errors in the work of Domairry and Nadim (2008)].

However, being approximate in form, the solutions obtained by these researchers have a limited applicability. This fact is also revealed in Fig. 3.4, where the results [transient temperature profiles] obtained by using the analytical solution, have been compared with those obtained by using the numerical method as well as with those obtained by the available approximate solution of Rajabi et al. (2007) and Ganji et al.
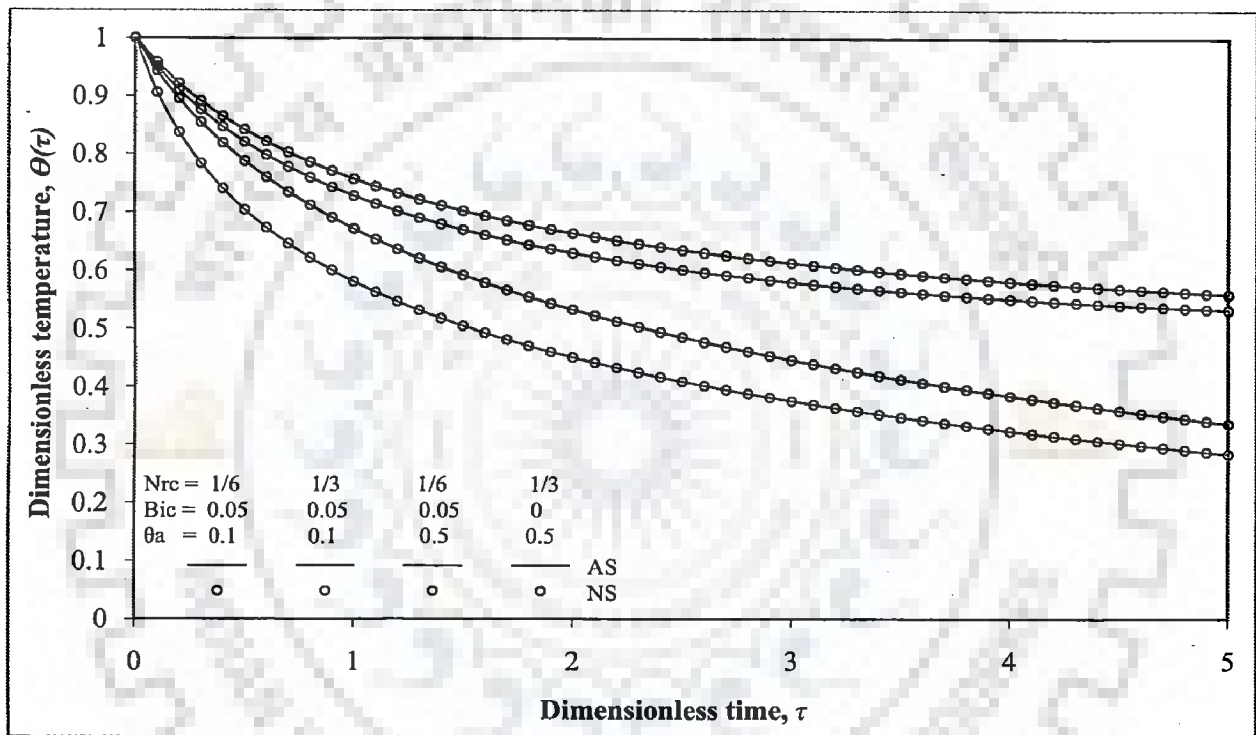
Figure 3.3: Transient profiles of dimensionless temperature for various values of N_{rc}, Bi_c and θ_a
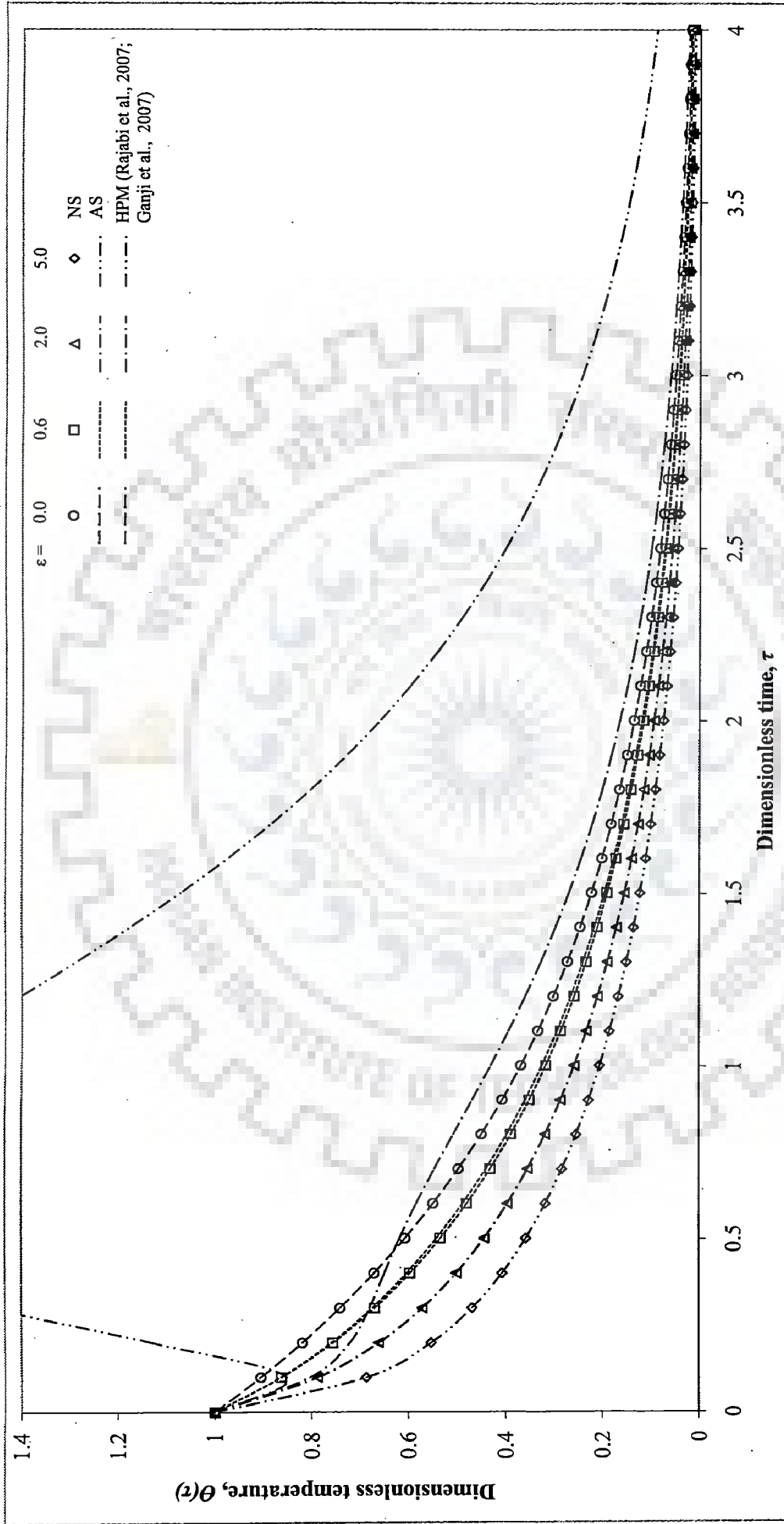
Figure 3.4: Transient profiles of dimensionless temperature at $Bi_c = 1/3$ and $\theta_a = 0$ for various values of ε [$= 3N_{rc}$]

(2007). It is clear from this figure that the results obtained by using the analytical solution, i.e. Eq. (3.25), matches well with the numerical results for all values of ε [= 0, 0.6, 2, 5]. On the contrary, the results obtained by using the approximate solutions of Rajabi et al. (2007) and Ganji et al. (2007), i.e. the above Eq. (3.26), deviate appreciably even for moderate values of ε and become superfluous for larger values of ε

3.2.2.3 Simplified Case II: $\theta_a = 0$, $Bi_c = 0$

In this subsection, we have presented the appropriate model equation for the previous case I, i.e. when the surroundings temperature is absolute zero [$\theta_a = 0$]. This model equation is given below in dimensionless form along with the associated IC [it should be noted that the convective heat transfer term is absent in this equation, because $Bi_c = 0$]:

$$\frac{d\theta_{av}}{d\tau} + 3N_{rc}\theta_{av}^4 = 0 \qquad (3.27a)$$

$$\text{IC:} \quad \theta_{av}(\tau = 0) = 1 \qquad (3.27b)$$

Integrating the above equation after separating the variables and using IC, one finds the following analytical solution:

$$\theta_{av} = \frac{1}{(1+9N_{rc}\tau)^{1/3}} \qquad (3.28)$$

(i) Comparison between the analytical and numerical solutions

For the several values of parameter N_{rc} [$= \varepsilon/3 = 0$, 0.3, 0.6, 0.9], the dimensionless temperature profiles obtained by using the analytical solution and the numerical solution are plotted in Fig. 3.5. These values of N_{rc} satisfy the lumped model criteria. The Fig. 3.5 shows an agreement between these profiles, which validates the presently obtained analytical solution.

3.2.3 A Case Study

In this subsection, the practical applicability of the presently obtained analytical solution, i.e. Eq. (3.22), has been demonstrated by simulating an existing experimental study of cooling of metal ball bearing by the mode of convection and radiation (Campo and Blotter, 2000). The lumped model approach for this experimental study was shown to be justified by these researchers, i.e. $Bi_T < 0.3$. Where $Bi_T \left[= \dfrac{(h + h_r)R}{k} \right]$ is the overall Biot number and $h_r \left[= \dfrac{\sigma \in (T^4 - T_a^4)}{(T - T_a)} \right]$ is the radiative heat transfer coefficient. Later, we have also verified this condition. Therefore, this process can conveniently be represented by a lumped model and thus the application of the presently derived analytical solution is justified.

Out of the two tests carried out by Campo and Blotter (2000), the data of test 1 have been selected in this study, although, the experimental results of test 2 can also be simulated in a similar fashion. Necessary details of the test 1 are summarized in Table 3.1 and the complete details can be found in the original work (Campo and Blotter, 2000). The parameters, ρ, c_p and k were not given by Campo and Blotter (2000), hence, in the present study, their values have been taken from Bejan and Kraus (2003); these values do not affect the results in any significant way and the results almost remain intact.

This heat transfer process is governed by the same model equations, i.e. Eqs. (3.17) and (3.18), however, the convective heat transfer coefficient is now a weak nonlinear function of temperature and is given by the following relation (Campo and Blotter, 2000):

$$h(T) = 9.03 + 2.95(T - 302)^{0.25} \ (\text{W/m}^2\,\text{K}) \tag{3.29}$$

With the introduction of the above expression for convective heat transfer coefficient, the lumped model equation attains the following dimensional form:

$$\rho c_p \frac{R}{3} \frac{dT}{dt} = -\left[9.03 + 2.95(T - 302)^{0.25} \right](T - T_a) - \sigma \in (T^4 - T_a^4) \tag{3.30}$$

IC: $\quad T(0) = T_i = 823K \tag{3.31}$
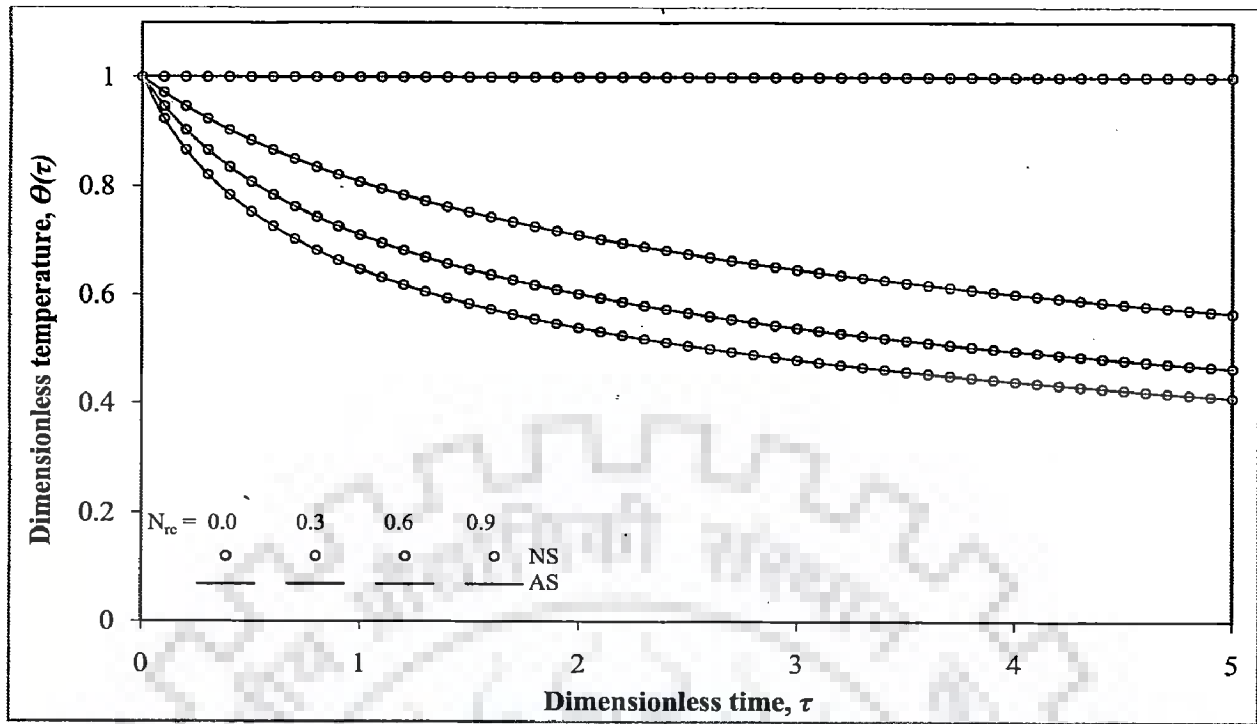
Figure 3.5: Transient profiles of dimensionless temperature at $Bi_c = 0$ and $\theta_a = 0$ for various values of N_{rc}

Table 3.1: Experimental data used for simulation

Variables/Parameters		Value
Source: Campo and Blotter (2000)		
Initial temperature of ball bearing	T_i	823 K
Constant room air temperature	T_f	302 K
Radiation sink temperature	T_s	302 K
Diameter of ball bearing	D	0.953×10^{-2} m
Emissivity of ball bearing	$\in$	0.7
Source: Bejan and Kraus (2003)		
Density of ball bearing	ρ	7865 kg.m^{-3}
Specific heat of ball bearing	c_p	460 J.kg^{-1}.K^{-1}
Thermal conductivity of ball bearing	k	47 W.m^{-1}.K^{-1}

67

Now, to show the applicability of the derived analytical solution [Eq. (3.22)], the average value of the convective heat transfer coefficient, h_{av} over the concerned temperature range $[T_i - T_a]$ is used in place of its temperature dependent form [Eq. (3.29)]. The average value of the convective heat transfer coefficient is found to be 20.3051 W/m²K and has been evaluated by using the following relation:

$$h_{av} = \frac{1}{(T_i - T_a)} \int_{T_a}^{T_i} h(T) dT \tag{3.32}$$

By replacing the temperature dependent $h(T)$ with its average value h_{av} in Eq. (3.30), one gets the following equation:

$$\rho c_p \frac{R}{3} \frac{dT}{dt} = -h_{av}(T - T_a) - \sigma \in (T^4 - T_a^4) \tag{3.33}$$

The Eq. (3.33) is now forced to attain the dimensionless form similar to the Eq. (3.17) by using the previously defined dimensionless variables. In doing so, the values of θ_a, Bi_c and N_{rc} are found to be 0.366950, 0.002059 and 0.002243, respectively. One should note that the value of Bi_c is based on h_{av}. Besides, the maximum values of h and h_r, i.e. at the beginning of the cooling of bearing, are 23.1239 W/m² K and 34.3099 W/m² K, respectively, and corresponding to these values, the maximum value of the total Biot number $[Bi_T]$ is 0.005823, which satisfies the lumped model criteria $[Bi_T < 0.3]$. Hence, the assumption of lumped model is valid for whole of the duration of this experimental study.

Now, corresponding to the above values of θ_a, Bi_c and N_{rc}, the four roots are found to be: $r_1(= \theta_a) = 0.366950$, $r_2 = -1.076538$, $r_3 = a + bi$ and $r_4 = a - bi$; $a = 0.354794$, $b = 0.879018$. Substituting these values in Eq. (3.22), one obtains the following equation:

$$404.24805 + 183.80592 \tan^{-1}[0.40362 - 1.13763\theta_{av}] + 399.70488 \ln[\theta_{av} - 0.36695]$$

$$- 145.10981 \ln[0.77267 + (\theta_{av} - 0.35479)^2] - 109.48525 \ln[\theta_{av} + 1.07654]$$

$$= -3\tau \tag{3.34}$$

(i) ***Comparison between the analytical, numerical and experimental results***

A comparison between the analytical, numerical and experimental results has been made by plotting the respective temperature profiles in Fig. 3.6. The numerical results have been found by numerically solving the Eqs. (3.30) and (3.31) with the help of an inbuilt command "NDSolve" of MATHEMATICA. As evident from Fig. 3.6, these numerical results depict a close agreement with the experimental results of Campo and Blotter (2000) [one should note that some of the experimental readings in our work have been read from the Fig. 2 of Campo and Blotter (2000) with the help of user-friendly software "Plot Digitizer", available online for free, as only a few values have been tabulated in Table 1 of Campo and Blotter (2000)].

Beside these two temperature profiles, Fig. 3.6 also shows the temperature profiles obtained by using the analytical and numerical solutions of the modified equation, i.e. Eq. (3.33). From the figure, it is clear that a close match exists between these two solutions, and thus it signifies the correctness of the analytical solution. Moreover, like the numerical results of Eq. (3.30), the results of Eq. (3.33) obtained either by the analytical solution [Eq. (3.34)] or by the numerical method, also match well with the experimental data. This validates the use of analytical solution and the average convective heat transfer coefficient, h_{av}. Hence, it can be concluded that no appreciable change in the results is observed if one models the above heat transfer process using Eq. (3.33) instead of Eq. (3.30).

3.3 STEADY STATE HEAT CONDUCTION IN A METALLIC ROD

Here, the explicit analytical solution of the model equation of this process has been obtained in two different ways, i.e. by simplifying the equation and by using the derivative substitution method. For brevity the application of derivative substitution method to obtain the analytical solution has been given in Appendix A3.

3.3.1   Model Equation

Consider a metallic rod of length L and uniform cross sectional area A_c. The two
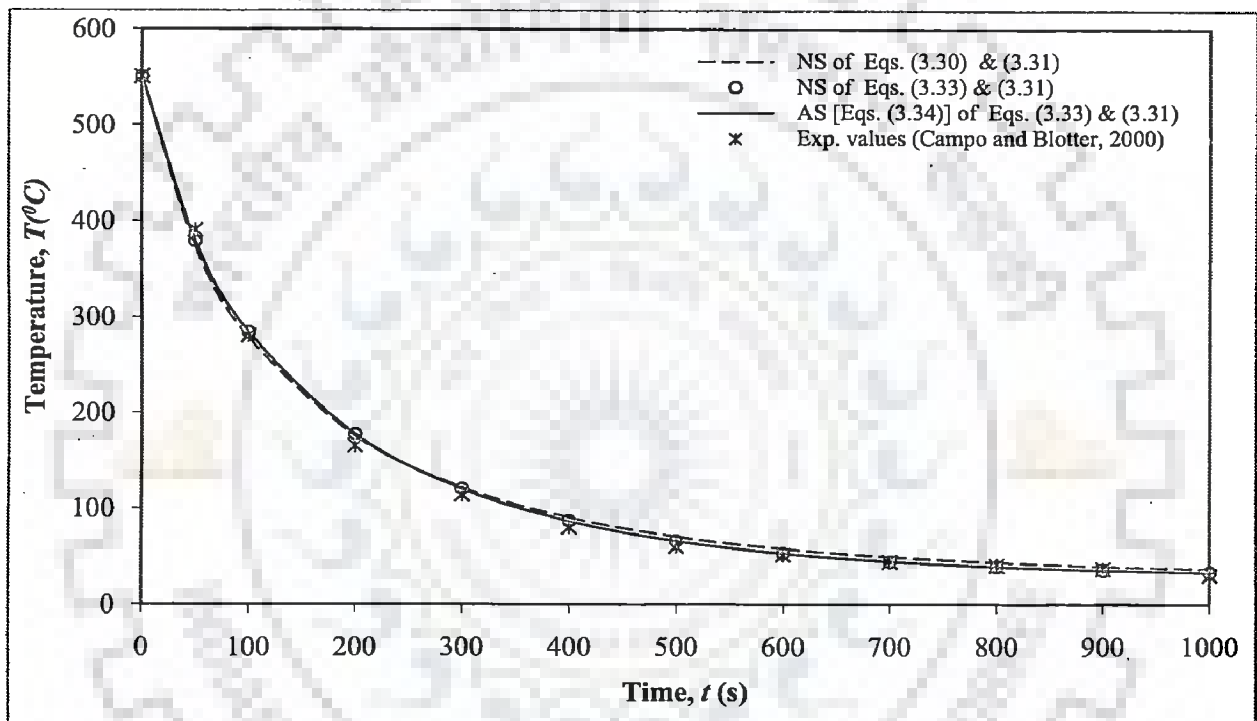
Figure 3.6: Transient temperature profiles for the cooling of a metal ball bearing by convection and radiation mechanisms [θ_a = 0.366950, N_{rc} = 0.002243, Bi_c = 0.002059]

ends of this rod are kept at different but fixed temperatures and the heat transfer takes place by conduction. It is assumed that the thermal conductivity of the rod varies linearly with temperature and there is no heat loss to the surroundings from the curved surface of the rod. The model equation of this process is derived by applying the steady state energy balance over a control element of the rod, and the following second order ODE along with the allied BCs is obtained (Rajabi et al., 2007; Domairry and Nadim, 2008; Sajid and Hayat, 2008a):

$$\frac{d}{dx}\left(A_c k(T)\frac{dT}{dx}\right) = 0 \tag{3.35a}$$

BC I: $T = T_a$ at $x = 0$ $\tag{3.35b}$

BC II: $T = T_b$ at $x = L$; $\qquad T_a \neq T_b$ $\tag{3.35c}$

where $k(T) = k_a\left(1 + \beta\dfrac{T - T_a}{T_b - T_a}\right)$ is the temperature dependent thermal conductivity of the rod.

3.3.2   Solutions and Discussion: Temperature Profile

With the introduction of the following dimensionless variables,

$$\xi = \frac{x}{L}, \ \theta = \frac{T - T_a}{T_b - T_a},$$

the model equation and the associated BCs, i.e. Eqs. (3.35a)-(3.35c), are transformed into the following dimensionless equations:

$$(1 + \beta\theta)\theta'' + \beta(\theta')^2 = 0 \tag{3.36a}$$

BC I: $\theta(0) = 0$ $\tag{3.36b}$

BC II: $\theta(1) = 1$ $\tag{3.36c}$

where θ' and θ'' represents the first and second order derivatives of θ with respect to ξ, respectively.

A careful examination of Eq. (3.36a) shows that it can be conveniently expressed into the following form:

$$((1+\beta\theta)\theta')' = 0 \qquad (3.37)$$

Integrating the above equation two times with respect to ξ, we obtain the following quadratic equation in θ:

$$\left(\theta + \beta\frac{\theta^2}{2}\right) = C_1\xi + C_2 \qquad (3.38)$$

where $C_1\left[=1+\beta/2\right]$ and $C_2\left[=0\right]$ are the constants of integration and have been found from the associated BCs. Substituting these values in Eq. (3.38) and solving for θ, the following two different explicit solutions are found; two solutions appear because of the nonlinear nature of the model equation.

$$\theta = \frac{-1+\sqrt{1+2\beta\xi+\beta^2\xi}}{\beta} \qquad (3.39a)$$

$$\theta = \frac{-1-\sqrt{1+2\beta\xi+\beta^2\xi}}{\beta} \qquad (3.39b)$$

It should be noted that the second solution gives negative temperature values and is therefore unrealistic. Moreover, this second solution does not satisfy the concerned BCs, and is therefore discarded.

(i) *Comparison between the analytical, numerical and approximate solutions*

If one expands θ [Eq. (3.39a)] around $\beta = 0$ by using the Taylor series method, the following approximate solution is obtained:

$$\theta \approx \xi + \frac{1}{2}\beta\left(\xi-\xi^2\right) + \frac{1}{2}\beta^2\left(\xi^3-\xi^2\right) + \dots \qquad (3.40)$$

On comparing the above approximate solution with the approximate solution

obtained by Rajabi et al. (2007) by using HPM and the approximate solution obtained by Domairry and Nadim (2008) by using HAM for the convergence control parameter $h_1 = -1$ used therein, we observe an exact conformity. However, due to their approximate forms, these solutions have a limited applicability. This fact is also revealed in Fig. 3.7, where the temperature profiles, obtained by using the analytical solution [Eq. (3.39a)], the approximate solution (Rajabi et al., 2007) and the numerical method, have been plotted for several values of β [= 0.5, 2, 5]. This figure clearly illustrates that the approximate temperature profiles obtained by Rajabi e. al. (2007) deviates appreciably even for moderate values of β and becomes redundant for larger values of β. Although not shown, the same characteristics can also be attributed to the approximate solution obtained by Domairry and Nadim (2008) by using HAM for the convergence control parameter $h_1 = -1$. On the other hand, no deviation is observed in analytical solution, even for higher values of β. It is also clear from Fig. 3.7 that as β varies from 0 to ∞, the temperature of the rod tends to reach the higher temperature [$\theta = 1$] and thus establishes the fact that with the increase in thermal conductivity the rate of heat transfer increases and so the temperature of the rod.

However, we could not compare our results with those of Sajid and Hayat (2008a), as no such solution expression was given by them. Nevertheless, in this case the results have been judged against those of Sajid and Hayat (2008a) by tabulating the values of temperature gradients at $\xi = 0$ and $\xi = 1$ in Table 3.2. This table also shows the corresponding numerically obtained values of temperature gradients. It is observed that our results match perfectly well with the numerical results and those obtained by Sajid and Hayat (2008a) by using HAM.

3.4 STEADY STATE RADIATIVE HEAT TRANSFER FROM A RECTANGULAR FIN

This section uses the derivative substitution method to solve the model equation analytically.

3.4.1 Model Equation

Consider a rectangular fin having cross sectional area A_c, perimeter P, length L and the constant thermal conductivity k, and emissivity $\in$. The fin base is maintained at a higher temperature T_b and the fin is transmitting the heat energy into space by the radiation. It is assumed that the steady state is prevailing and negligible heat transfer takes place from fin tip. Keeping these assumptions in view, the model equation can be derived by applying the steady state energy balance over a control volume in the fin and is given by the following nonlinear second order ODE along with the allied BCs (Ganji, 2006; Abbasbandy, 2006a; Tari et al., 2007; Marinca and Herişanu, 2008):

$$\frac{d}{dx}\left(A_c k \frac{dT}{dx} \right) = P\sigma \in (T^4 - T_s^4) \tag{3.41a}$$

BC I: $\quad T = T_b$ at $x = L$ (at fin base) $\tag{3.41b}$

BC II: $\quad \dfrac{dT}{dx} = 0$ at $x = 0$ (at fin end) $\tag{3.41c}$

where T_s is the space temperature and σ is the Stephan-Boltzmann constant.

3.4.2 Solution and Discussion: Temperature Profile

It is worthwhile to note that the space temperature can very well be replaced by the absolute zero temperature, i.e. $T_s = 0$ (Ganji, 2006; Abbasbandy, 2006a; Marinca and Herişanu, 2008). Taking this fact into account and by defining the following dimensionless variables,

$$\theta = \frac{T}{T_b}, \quad \xi = \frac{x}{L}, \quad \varepsilon = \frac{\sigma \in P T_b^3 L^2}{k A_c},$$

we obtain the following dimensionless forms of Eqs. (3.41a)-(3.41c):

$$\frac{d^2\theta}{d\xi^2} = \varepsilon\theta^4 \tag{3.42a}$$

Table 3.2: Comparison of the slopes of dimensionless temperature profile at both ends of the rod

β	$\theta'(1)$			$\theta'(0)$	
	Numerical solution	Sajid and Hayat, (2008a)	Analytical solution [Eq. (3.39a)]	Numerical solution	Analytical solution [Eq. (3.39a)]
0.5	0.833333	0.833333	0.833333	1.250000	1.250000
2	0.666667	0.666667	0.666667	2.000000	2.000000
5	0.583333	0.583333	0.583333	3.500000	3.500000
50	26/51	26/51	26/51	26.000000	26.000000
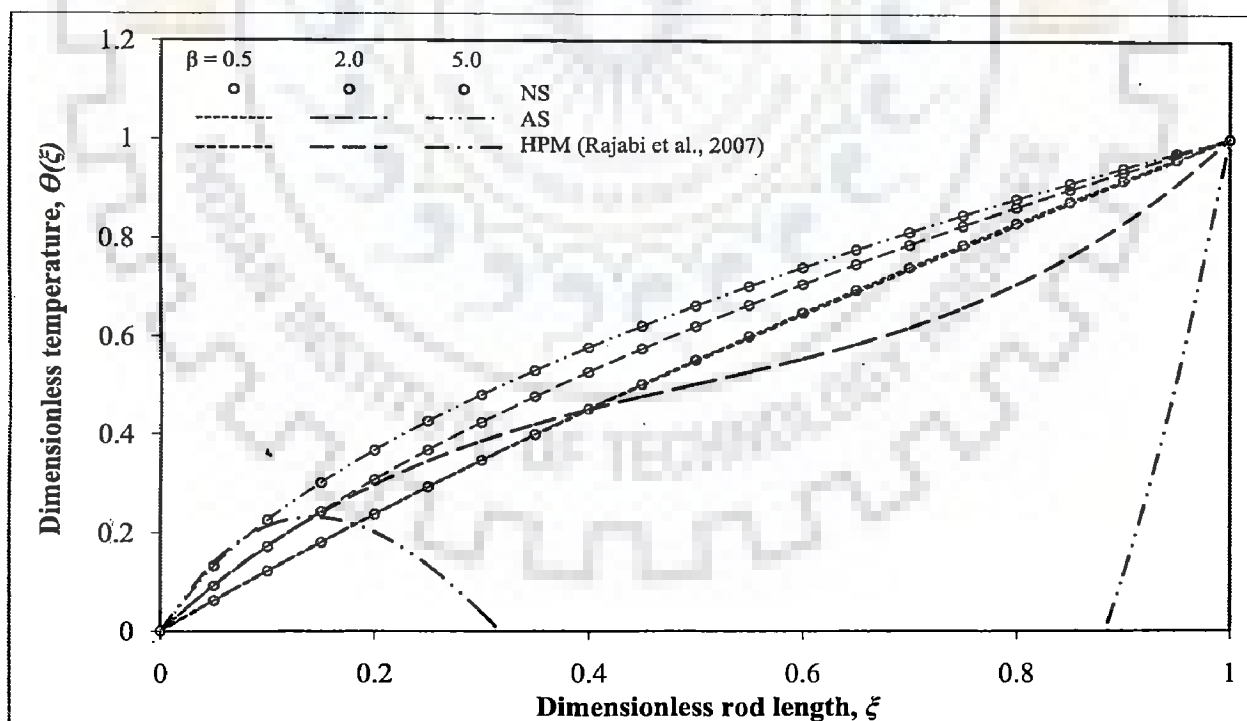
Figure 3.7: Dimensionless temperature profiles along the rod length for various values of β

77

BC I: $\theta = 1$ at $\xi = 1$ (at fin base)   (3.42b)

BC II: $\dfrac{d\theta}{d\xi} = 0$ at $\xi = 0$ (at fin tip)   (3.42c)

To solve the above equation, we have adopted the same approach as was followed for the model equation of steady state heat conduction in a metallic rod. In other words, here too the derivative $\dfrac{d\theta}{d\xi}$ is assumed to be a function of θ only, i.e.

$\dfrac{d\theta}{d\xi} = p(\theta)$; where $p(\theta)$ is yet to be found. This assumption leads to $\theta'' = \dfrac{1}{2}\dfrac{d\left(p(\theta)^2\right)}{d\theta}$.

Replacing θ'' in Eq. (3.42a) by this relation, one obtains:

$$\frac{d\left(p(\theta)^2\right)}{d\theta} = 2\varepsilon\theta^4 \tag{3.43}$$

Now, replacing $p(\theta)^2$ with y, the Eq. (3.43) attains the following linear first order ODE:

$$\frac{dy}{d\theta} = 2\varepsilon\theta^4 \tag{3.44}$$

Integration of the above equation yields the following result:

$$y = \frac{2}{5}\varepsilon\theta^5 + C_1 \tag{3.45}$$

where $C_1\left[= -\dfrac{2}{5}\varepsilon\theta_0^5\right]$ is the constant of integration and has been evaluated with the help of BC II. θ_0 is the unknown dimensionless temperature at the fin tip and can be found by using BC I. Substituting this value of C_1 in Eq. (3.45), one gets:

$$y = \left(\frac{d\theta}{d\xi}\right)^2 = \frac{2}{5}\varepsilon\left(\theta^5 - \theta_0^5\right) \tag{3.46}$$

A minor rearrangement of the above equation yields the following equation. It should, however, be noted that for this situation, $\dfrac{d\theta}{d\xi} > 0$, and therefore, positive sign before the

79

radical should be considered.

$$\frac{d\theta}{\sqrt{\frac{2}{5}\varepsilon\left(\theta^5-\theta_0^5\right)}}=d\xi \tag{3.47}$$

Integrating the above equation between the limits prescribed by BC I and BC II, we get:

$$\int_{\theta_0}^{\theta}\frac{d\theta}{\sqrt{\frac{2}{5}\varepsilon\left(\theta^5-\theta_0^5\right)}}=\int_0^{\xi}d\xi \tag{3.48}$$

Evaluation of the above integration results in the following analytical solution:

$$\sqrt{\frac{5}{2\varepsilon\left(\theta^5-\theta_0^5\right)}}\theta\sqrt{1-\frac{\theta^5}{\theta_0^5}}Hypergeometric2F1\left[\frac{1}{5},\frac{1}{2},\frac{6}{5},\frac{\theta^5}{\theta_0^5}\right]-i\sqrt{\frac{5\pi}{2\varepsilon}}\frac{1}{\theta_0^{3/2}}\frac{\Gamma\left[\frac{6}{5}\right]}{\Gamma\left[\frac{7}{10}\right]}=\xi \tag{3.49}$$

The unknown θ_0 is computed by solving the following nonlinear equation, which has been obtained by forcing the Eq. (3.49) to satisfy the unutilized BC I, i.e. $\theta=1$ at $\xi=1$.

$$\sqrt{\frac{5}{2\varepsilon\left(1-\theta_0^5\right)}}\sqrt{1-\frac{1}{\theta_0^5}}Hypergeometric2F1\left[\frac{1}{5},\frac{1}{2},\frac{6}{5},\frac{1}{\theta_0^5}\right]-i\sqrt{\frac{5\pi}{2\varepsilon}}\frac{1}{\theta_0^{3/2}}\frac{\Gamma\left[\frac{6}{5}\right]}{\Gamma\left[\frac{7}{10}\right]}=1 \tag{3.50}$$

where $\Gamma[z]$ and $HG_2F_1[a,b,c,z]$ are the well known Gamma and the Gauss' Hypergeometric functions, respectively and are defined as follows (Abramowitz and Stegun, 1964):

$$\Gamma[z]=\int_0^{\infty}t^{z-1}e^{-t}dt \tag{3.51a}$$

$$HG_2F_1[a,b,c,z]=\frac{\Gamma[c]}{\Gamma[b]\,\Gamma[c-b]}\int_0^1 t^{b-1}(1-t)^{c-b-1}(1-tz)^{-a}dt \tag{3.51b}$$

80

With the help of Eqs. (3.49) and (3.50), one can find the dimensionless temperature profile.

(i)   *Comparison between the analytical, numerical and approximate solutions*

For several values of the parameter ε [= 0.09, 0.7] the temperature profiles obtained by using the analytical and numerical solutions have been shown in Figs. 3.8 and 3.9. These overlapping profiles show a close agreement and thus verify the analytical solution. On comparing the two profiles drawn in these figures, it is observed that as the parameter ε increases, the temperature profile shows a sharp decrease, and signifies the increase in heat transfer rate. This observation is in compliance with the physics of the problem.

The obtained analytical results have also been compared with the approximate results obtained by Ganji (2006) and Abbasbandy (2006a) by using HPM and HAM, respectively. It should be noted that Ganji (2006) has obtained the approximate solution up to the second order approximation in HPM, whereas, Abbasbandy (2006a) has obtained the approximate solutions for both the second and fifth order approximation in HAM. However, the expression for the approximate solution of fifth order approximation was not given by Abbasbandy (2006a). Here, based on his approach [HAM] (Abbasbandy, 2006a), we have developed the fifth order approximate solution and obtained the results from it.

We below reproduce the approximate solutions [second order approximation in HPM and HAM], as obtained by these researchers (Ganji, 2006; Abbasbandy, 2006a).

$$\theta_{Ganji} \cong 1 + \varepsilon \left(\frac{x^2 - 1}{2} \right) + \varepsilon^2 \left(\frac{x^4 - 6x^2 + 5}{6} \right) \tag{3.52a}$$

$$\theta_{Abbasbandy} \cong 1 - \varepsilon h_1 \left(\frac{x^2 - 1}{2} \right) - \varepsilon h_1 (1 + h_1) \left(\frac{x^2 - 1}{2} \right) + \varepsilon^2 h_1^2 \left(\frac{x^4 - 6x^2 + 5}{6} \right) \tag{3.52b}$$

where h_1 is convergence control parameter in HAM and is evaluated from h-curve (Abbasbandy, 2006a). The dimensionless temperature profiles obtained by the above approximate solutions have also been shown in Figs. 3.8 and 3.9 for the same values of

81

the parameter ε [= 0.09, 0.7] as those considered by Ganji (2006) and Abbasbandy (2006a), respectively. It is clear from Fig. 3.8 that the profile obtained by Ganji (2006) slightly deviates with the numerically obtained profile, whereas, the profile obtained by the analytical solution shows a close matching with the numerically obtained profile.

Similarly, in Fig. 3.9 the approximate solution of Ganji (2006) yields divergent results, whereas, the approximate solution of Abbasbandy (2006a) [second order approximation in HAM] shows minor deviation with the numerically obtained profile. However, the approximate solution of Abbasbandy (2006a) [fifth order approximation in HAM] matches well with the numerically obtained profile. In contrast to this, the profile obtained by using the analytical solution is in complete agreement with the numerically obtained profile. It can be verified that the deviations in the approximate solutions of Ganji (2006) and Abbasbandy (2006a) will increase with the increase in the value of ε, however, this is not true for the analytical solution. Hence, the analytical solution derived here is better than these approximate solutions. Because of complexity in the approximate solution obtained by Marinca and Herişanu (2008) by using OHAM, we have not considered it.

3.5 STEADY STATE CONVECTIVE HEAT TRANSFER FROM A RECTANGULAR FIN

The derivative substitution method has been used to solve the model equation of this process, and the analytical solutions of the temperature profile and fin efficiency have been obtained in terms of the familiar algebraic and non-algebraic functions (Abramowitz and Stegun, 1964) for all the cases arising in this model equation. Moreover, the discussions of the obtained analytical solutions with regard to the existence, uniqueness/multiplicity and stability/instability have also been presented.

3.5.1 Model Equation

The model equation of this process can be derived by applying the steady state energy balance over the fin element, and the following dimensional equation along with the related BCs is obtained (Moitsheki et al., 2010b). In this equation, it has been

82
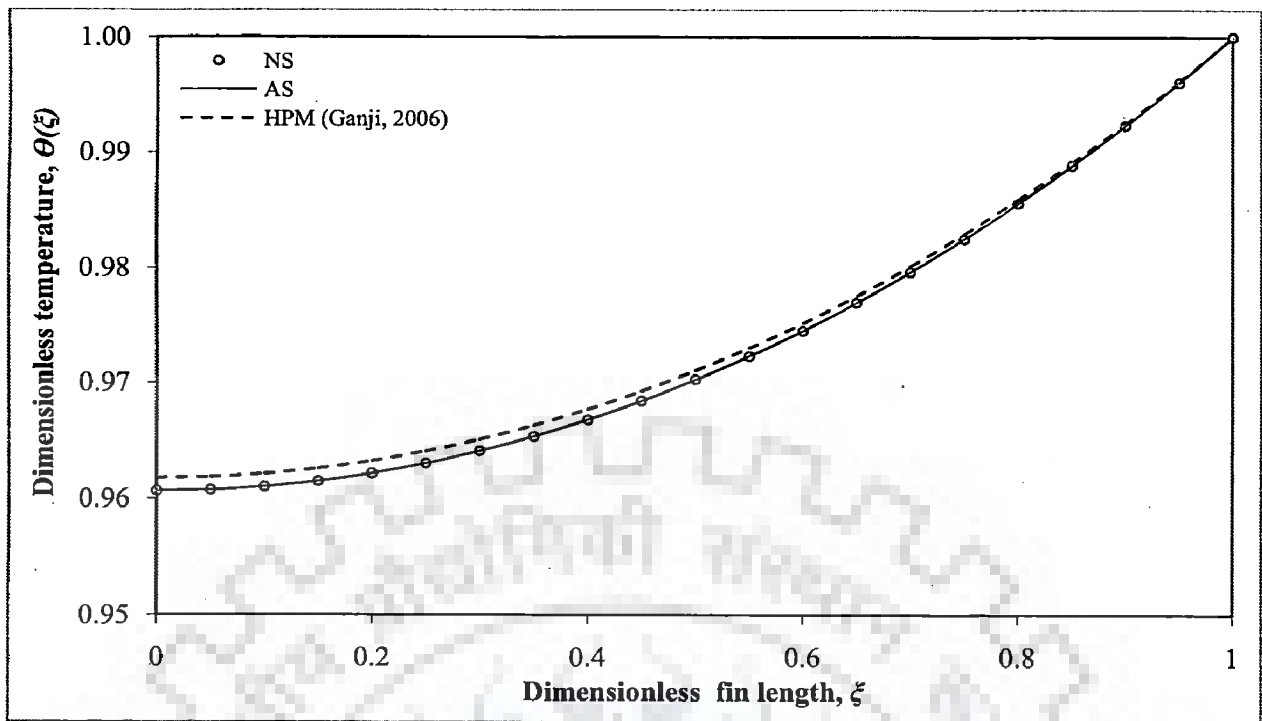
Figure 3.8: Dimensionless temperature profiles along the fin length at $\varepsilon = 0.09$
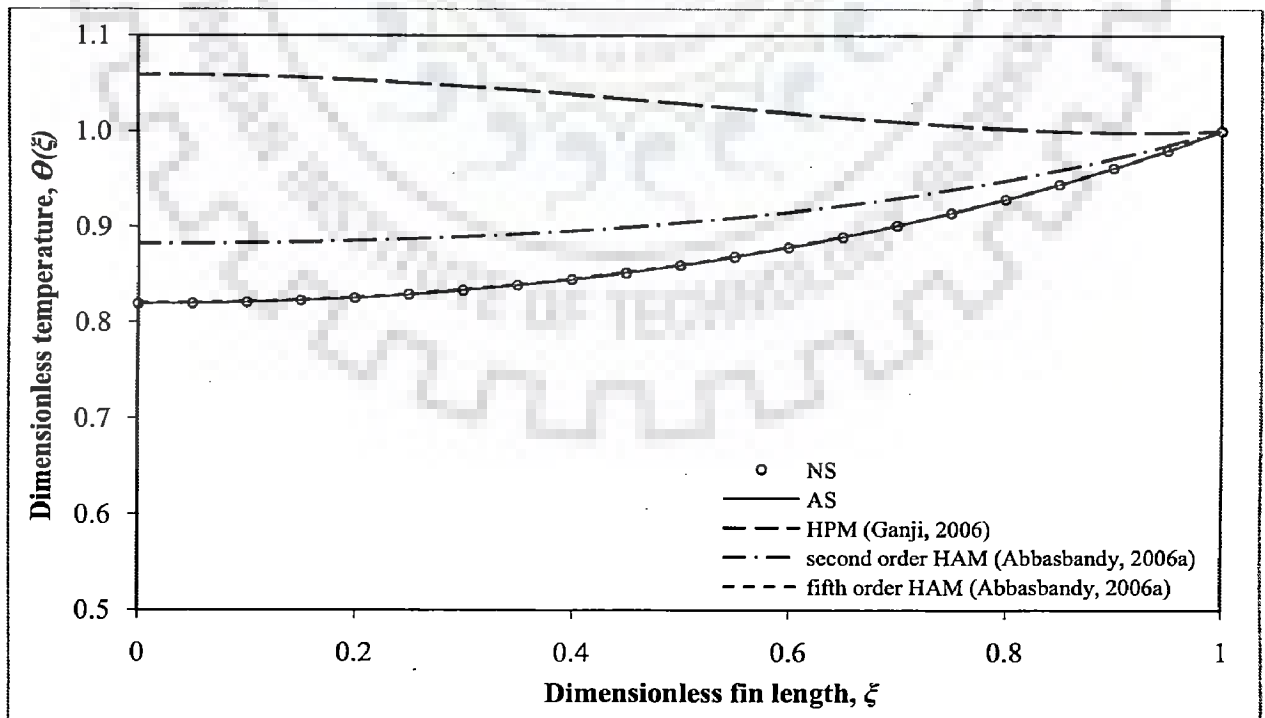
Figure 3.9: Dimensionless temperature profiles along the fin length at $\varepsilon = 0.7$

assumed that the fin tip is insulated.

$$A_c \frac{d}{dx}\left(k(T)\frac{dT}{dx} \right) - Ph(T)(T - T_a) = 0 \qquad\qquad (3.53a)$$

BC I: $\dfrac{dT}{dx} = 0$ at $x = 0$ (at fin tip) $\qquad\qquad (3.53b)$

BC II: $T = T_b$ at $x = L$ (at fin base) $\qquad\qquad (3.53c)$

where L, P and A_c denote the length, perimeter and cross sectional area of the rectangular fin, respectively. T_b is the temperature of the fin base, and T_a is the temperature of the surroundings fluid. $k(T)$ and $h(T)$ are the thermal conductivity of the fin and the heat transfer coefficient, respectively. In case of large temperature gradients, the assumption of constant heat transfer coefficient and thermal conductivity does not hold true, and this situation is normally addressed by introducing various types of nonlinear fin models in which the thermal conductivity and/or heat transfer coefficient are assumed to be temperature dependent. In this section, we have dealt with one such nonlinear fin model, in which the heat transfer coefficient and thermal conductivity are assumed to vary as distinct power-law functions of temperature, and are given by: $k(T) = k_b \left(\dfrac{T - T_a}{T_b - T_a} \right)^{\beta}$ and $h(T) = h_b \left(\dfrac{T - T_a}{T_b - T_a} \right)^{n}$, respectively (Moitsheki et al., 2010b). It can be noticed that for different values of n, $h(T)$ can represent the heat transfer coefficient for various heat transfer phenomena, i.e. $n = -4$ for transition boiling, $n = -\frac{1}{4}$ for laminar film boiling/condensation, $n = 0$ for forced convection, $n = \frac{1}{4}$ for laminar free/natural convection, $n = \frac{1}{3}$ for turbulent free/natural convection, $n = 2$ for nucleate boiling, $n = 3$ for radiation (Yeh and Liaw, 1990; Moitsheki et al., 2010b).

It should also be noted that the similar types of model equations also arise in various other processes: (i) the previously considered process of radiative heat transfer from a rectangular fin to the outer space, (ii) the process of convective heat transfer from a rectangular fin with power-law dependent heat transfer coefficient, and (iii) the reaction-diffusion process inside a porous catalyst slab sustaining power-law kinetics.

The performance of a fin is measured by the fin efficiency [η], which is defined as the ratio of the actual heat transfer rate to the heat transfer rate had it been evaluated at the base temperature (Sunden and Heggs, 2000; Kraus and Aziz, 2001). For a rectangular fin, it is mathematically expressed as follows (Moitsheki et al., 2010b):

$$\eta = \frac{A_c}{PL} \frac{k(T_b)\dfrac{dT}{dx}\Big|_{x=L}}{h(T_b)(T_b - T_a)} \tag{3.54a}$$

or

$$\eta = \frac{\displaystyle\int_0^L h(T)(T - T_a)dx}{h(T_b)(T_b - T_a)L} \tag{3.54b}$$

3.5.2 Solutions and Discussion: Temperature Profile and Fin Efficiency

Before finding the analytical solution of Eqs. (3.53a)-(3.53c), it is convenient to introduce the following dimensionless variables (Moitsheki et al., 2010b):

$$\theta = \frac{T - T_a}{T_b - T_a}, \quad \xi = \frac{x}{L}, \quad N^2 = \frac{h_b P L^2}{k_b A_c}$$

With the incorporation of the above dimensionless variables, the Eqs. (3.53a)-(3.53c) become:

$$(\theta^\beta \theta')' - N^2 \theta^{1+n} = 0 \tag{3.55a}$$

BC I: $\theta'(0) = 0$ $\tag{3.55b}$

BC II: $\theta(1) = 1$ $\tag{3.55c}$

where θ' denotes the first order derivative of θ with respect to ξ. By expanding the Eq. (3.55a), one obtains the following equation:

$$\theta^\beta \theta'' + \beta \theta^{\beta-1} (\theta')^2 - N^2 \theta^{1+n} = 0 \tag{3.56}$$

Similarly, by using the above dimensionless variables, the fin efficiency is also expressed in terms of the following relations:

$$\eta = \frac{\theta'(1)}{N^2}$$ (3.57a)

or

$$\eta = \int_0^1 \theta^{1+n} d\xi$$ (3.57b)

Once the analytical solution of θ is available, the fin efficiency η can easily be found by substituting the analytical solution of θ in any of the above equations. We now apply the derivative substitution method to obtain the analytical solution of the Eq. (3.56) for the associated BCs [Eqs. (3.55b) and (3.55c)]. For this we assume that $\theta' = p(\theta)$, where $p(\theta)$ is some unknown function of θ. With this postulation, one finds $\theta'' = \frac{1}{2} \frac{d(p^2)}{d\theta}$, and by substituting these relations into the Eq. (3.56) and slightly rearranging the resultant equation, the following first order ODE is obtained:

$$\frac{d(p^2)}{d\theta} + 2\beta\theta^{-1}p^2 - 2N^2\theta^{1+n-\beta} = 0$$ (3.58)

Replacing $p^2 \left(= (\theta')^2\right)$ with y, the above equation can further be reduced into the following first order linear ODE:

$$y' + 2\beta\theta^{-1}y - 2N^2\theta^{1+n-\beta} = 0$$ (3.59)

where y' denotes $\frac{dy}{d\theta}$. The above equation can be solved by using the integrating factor method and the particular solution is obtained by employing BC I. An equivalent condition corresponding to BC I is: $y(\theta_0) = 0$, where θ_0 is the unknown temperature at $\xi = 0$, i.e. $\theta_0 = \theta(\xi = 0)$. In this way, the expression of y can be found in terms of θ and θ_0, which will subsequently be used to obtain the expression of θ by integrating the previously defined relation, i.e. $(\theta')^2 = y$ between the limits $\theta = \theta_0$ at $\xi = 0$ to θ at ξ. After getting the expression of θ, the unknown θ_0 can automatically be found by

using the prescribed BC II.

Before proceeding further, it is worthwhile to mention that for different combinations of β and n, the Eq. (3.59) reveals various forms of solutions, each having its own peculiar characteristics. Because of this reason, these solutions have been divided into different cases and are tackled separately. However, the above general procedure is applicable to these cases, as demonstrated below.

3.5.2.1 Case 1(a): $\beta + n = -2$ & $\beta \neq n$

(i) Temperature profile

For the above set of parameters, the Eq. (3.59) reduces to

$$y' - (4 + 2n)\theta^{-1}y - 2N^2\theta^{3+2n} = 0 \tag{3.60}$$

Solution of the above linear equation can be obtained by using the integrating factor method and is given by:

$$y = p(\theta)^2 = \left(\frac{d\theta}{d\xi}\right)^2 = \theta^{4+2n}\left(C_1 + 2N^2 ln[\theta]\right) \tag{3.61}$$

where $C_1 \ [= -2N^2 ln[\theta_0]]$ is the constant of integration and has been found by satisfying the homogeneous BC I, i.e. $\theta'(0) = 0$ or $y(\theta_0) = 0$. Substituting the value of C_1 in Eq. (3.61), one obtains the following expression of y:

$$y = p(\theta)^2 = \left(\frac{d\theta}{d\xi}\right)^2 = \theta^{4+2n}\left(2N^2 ln\left[\frac{\theta}{\theta_0}\right]\right) \tag{3.62}$$

Integrating the above Eq. (3.62) between the limits $\theta = \theta_0$ at $\xi = 0$ to θ at ξ, the following integral is resulted:

$$\int_{\theta_0}^{\theta} \frac{d\theta}{\theta^{2+n}\sqrt{\left(2N^2 ln\left[\frac{\theta}{\theta_0}\right]\right)}} = \int_0^{\xi} d\xi \tag{3.63}$$

Solution of the above integral between the specified limits yields the following analytical solution of the dimensionless temperature θ.

$$\sqrt{\frac{\pi}{2(1+n)N^2}} \frac{1}{\theta_0^{1+n}} Erf\left[\sqrt{(1+n)ln\left[\frac{\theta}{\theta_0}\right]}\right] = \xi \tag{3.64}$$

where $Erf[z]$ is the well known error function, i.e. $Erf[z] = \frac{2}{\sqrt{\pi}} \int\limits_0^z e^{-t^2} dt$. It can be noted that θ_0 in Eq. (3.64), is still unknown and can be computed by the following equation, which has been obtained by forcing the Eq. (3.64) to satisfy the remaining BC II, i.e. $\theta(1) = 1$.

$$\sqrt{\frac{\pi}{2(1+n)N^2}} \frac{1}{\theta_0^{1+n}} Erf\left[\sqrt{(1+n)ln\left[\frac{1}{\theta_0}\right]}\right] = 1 \tag{3.65}$$

For a given n and N, θ_0 is obtained from Eq. (3.65), and thus obtained value of θ_0 is substituted back in Eq. (3.64) to get the complete profile of dimensionless temperature, $\theta(\xi)$.

(ii) Fin efficiency

Fin efficiency is found either by using the Eq. (3.57a) or Eq. (3.57b). To find η from the Eq. (3.57a), one can resort to Eq. (3.62) from which $\left.\frac{d\theta}{d\xi}\right|_{\xi=1}$ can directly be found, and the following analytical solution of η is obtained:

$$\eta = \frac{\theta'(1)}{N^2} = \frac{1}{N}\theta^{2+n}\left.\sqrt{2ln\left[\theta/\theta_0\right]}\right|_{\xi=1} = \frac{1}{N}\sqrt{-2ln\left[\theta_0\right]} \tag{3.66}$$

However, if one prefers to find η from the Eq. (3.57b), then one may straightforwardly proceed by integrating the Eq. (3.55a) with respect to ξ from 0 to 1 and again obtain the same analytical solution of η.

(iii) Solution properties and discussion of results

Since, the original Eqs. (3.55a)-(3.55c) form a nonlinear BVP, hence, there exists a possibility of more than one solutions. In the present case [$\beta + n = -2$ & $\beta \neq n$], this fact is supported by the nonlinear implicit form of the Eq. (3.65), which can yield more than one feasible value of $\theta_0 \in (0,1)$ for a particular value of N, and corresponding to each θ_0 one can have a different solution. For verifying this supposition, the dimensionless temperature of the fin tip [θ_0] has been drawn in Fig. 3.10 against the fin parameter N for various combinations of n and β. Eq. (3.65) is used to evaluate θ_0 for different values of N.

The solution properties can also be found in a non-graphical way by making use of the quantity $\dfrac{dN}{d\theta_0}$, which is the inverse of the slope of θ_0 curves plotted against N. $\dfrac{dN}{d\theta_0}$ is an important quantity in analyzing the characteristics of these solutions and can be obtained by differentiating Eq. (3.65) with respect to θ_0. For this case, $\dfrac{dN}{d\theta_0}$ is given by the following Eq. (3.67). It is clear from Fig. 3.10 that if there exist more than one solutions then the inverse of the slope of θ_0 curve will be zero $\left[\dfrac{dN}{d\theta_0} = 0 \right]$ atleast once for $\theta_0 \in (0,1)$. The value of θ_0, where the inverse of the slope becomes zero, can be found by substituting $\dfrac{dN}{d\theta_0} = 0$ in Eq. (3.67) and solving the resultant equation for θ_0. This value of θ_0 is denoted by θ_{0crit} and the corresponding value of N is denoted by N_{max}.

$$\frac{dN}{d\theta_0} = -\sqrt{\frac{\pi(1+n)}{2}} \frac{1}{\theta_0^{2+n}} Erf \left[\sqrt{(1+n)ln \frac{1}{\theta_0}} \right] - \frac{1}{\theta_0 \sqrt{2ln \frac{1}{\theta_0}}} \tag{3.67}$$
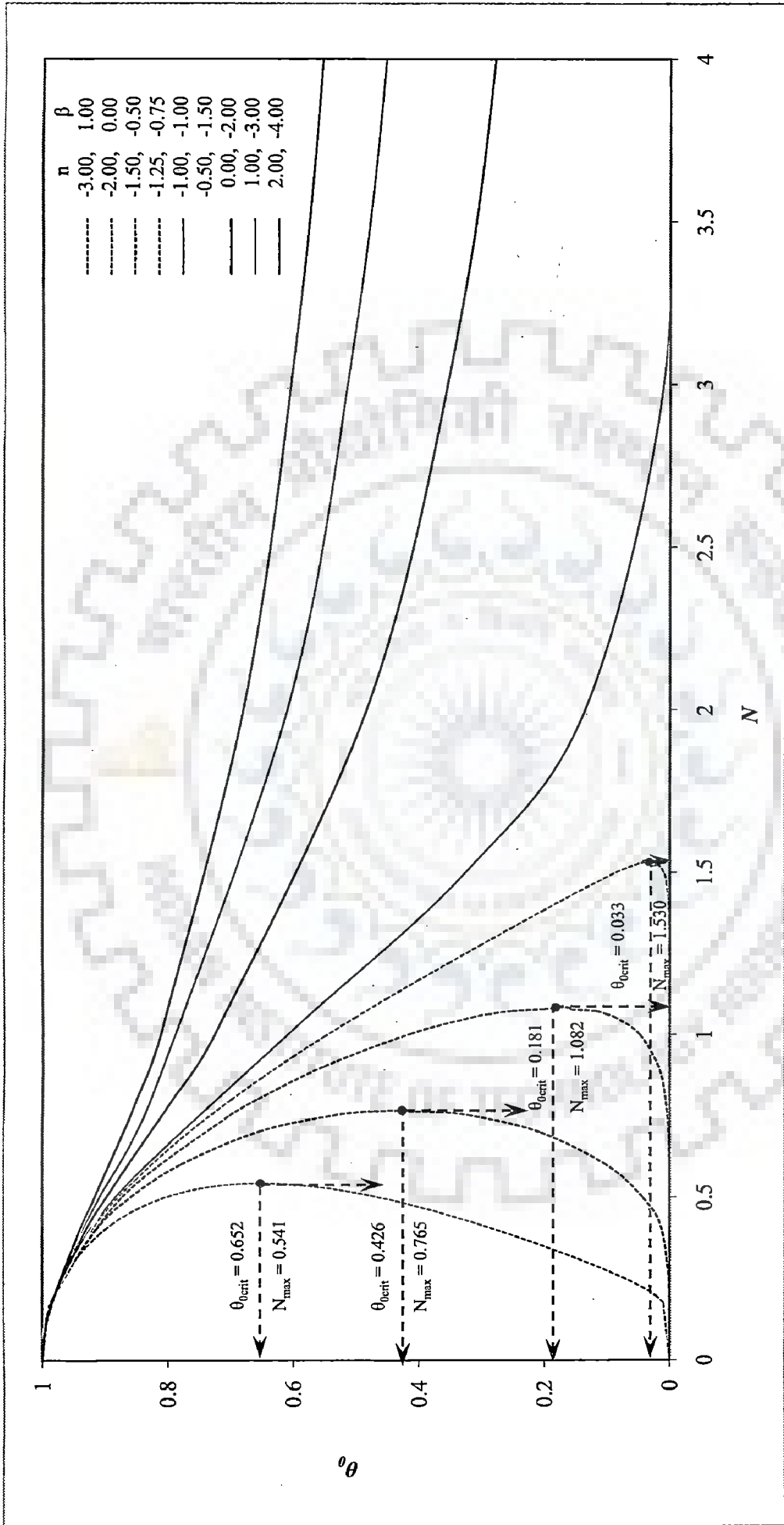
Figure 3.10: Variation of θ_0 with N for case 1(a) and case 1(b)

The legend of the figure:

n	β
-3.00,	1.00
-2.00,	0.00
-1.50,	-0.50
-1.25,	-0.75
-1.00,	-1.00
-0.50,	-1.50
0.00,	-2.00
1.00,	-3.00
2.00,	-4.00

$\theta_{0crit} = 0.652$
$N_{max} = 0.541$

$\theta_{0crit} = 0.426$
$N_{max} = 0.765$

$\theta_{0crit} = 0.181$
$N_{max} = 1.082$

$\theta_{0crit} = 0.033$
$N_{max} = 1.530$

From the inspection of the Fig. 3.10 and by analysing the numerical value of $\frac{dN}{d\theta_0}$, we observe that for several combinations of the parameters [N, n, β], no solution, single solution and even dual solutions may be present. The following points decide their existence:

(i)   For $n > -1$, θ_0 decreases monotonically from $\theta_0 = 1$ at $N = 0$ and approaches $\theta_0 \to 0$ as $N \to \infty$. In other words, $\frac{d\theta_0}{dN} < 0$ [or $\frac{dN}{d\theta_0} < 0$], for $N \in [0, \infty)$. This entails that only single value of θ_0 and thus only single solution can exist for $N \in [0, \infty)$. $\frac{dN}{d\theta_0} < 0$ implies that the so found single solution is stable. For such cases [$n = -0.5$, $\beta = -1.5$; $n = 0$, $\beta = -2$; $n = 1$, $\beta = -3$; $n = 2$, $\beta = -4$], the plots of θ_0 against N have been shown in Fig. 3.10, whereas, Fig. 3.11 displays the single dimensionless temperature profiles for one such case [$n = 0$, $\beta = -2$].

It is also important to pay attention on the variation of η with N. Although not shown, η for this case [Eqs. (3.66)] will start decreasing from its maximum value, i.e. unity [$\eta_{max} = 1$], to its minimum value, i.e. zero [$\eta_{min} \to 0$], as N is increased from its minimum value, i.e. zero [$N_{min} = 0$], to the maximum value, i.e. infinity [$N_{max} \to \infty$].

(ii)   For $n < -1$, an altogether different situation, also shown in Fig. 3.10, appears: dual θ_0 exist for $N \in (0, N_{max})$, and $\frac{dN}{d\theta_0}$ can be > 0, $= 0$, < 0 in this range. This signifies that two solutions exist for $N \in (0, N_{max})$, and at $N = N_{max}$ these two solutions merge to give a single solution, whereas, at $N_{min} = 0$, single solution exists. Moreover, for $N > N_{max}$ no solution can be found. θ_{0crit} can be found by equating Eq. (3.67) to zero and solving for θ_0. The corresponding value of N, i.e. N_{max}, can be found by evaluating N at $\theta_0 = \theta_{0crit}$ with the help of Eq. (3.65). The plots of θ_0 against N have also been depicted in Fig. 3.10 for such situations [$n = -3$, $\beta = 1$; $n = -2$, $\beta = 0$; $n = -1.5$, $\beta = -0.5$; $n = -1.25$, $\beta =$

-0.75], and for some of them [$n = -2$, $\beta = 0$; $n = -1.5$, $\beta = -0.5$] the dual temperature profiles have been plotted in Fig. 3.11. Although not shown, it can be verified that the solution corresponding to the larger temperature gradient [$\frac{dN}{d\theta_0} > 0$] is unstable.

Unlike the situation for $n > -1$, η increases from $\eta_{min} = 1$ to $\eta_{max} = \frac{1}{N_{max}}\sqrt{-2ln(\theta_{0crit})}$, as N increases from $N_{min} = 0$ to N_{max}. It can be seen that η is greater than unity, because for $n < -1$, the heat removal terms in Eq. (3.55a), i.e. $N^2\theta^{n+1}$, will be higher for smaller temperature. This fact can also be substantiated from Eq. (3.57b).

For the following cases, analytical solutions of the temperature profile and fin efficiency have been obtained in the same way as described above. Hence, for brevity only solutions and their discussions are presented here; the details of their derivation have been deferred to the Appendix A4.

3.5.2.2 Case 1(b): $\beta + n = -2$ & $\beta = n = -1$

(i)   Temperature profile

$$\theta = \theta_0 Exp\left(\frac{N^2\xi^2}{2}\right) \tag{3.68}$$

where θ_0 is given by:

$$\theta_0 = Exp\left(-N^2/2\right) \tag{3.69}$$

This case has also been tackled by Moitsheki et al. (2010b), and the present analytical solution [Eq. (3.68)] matches well with the one obtained by these researchers.

(ii)   Fin efficiency

For this case: $\eta = 1$ $\forall$ N. This is because the heat transfer from the fin is independent of temperature for $n = -1$, i.e. $N^2\theta^{n+1} = N^2$ [see Eqs. (3.55a) or (3.57b)].

94
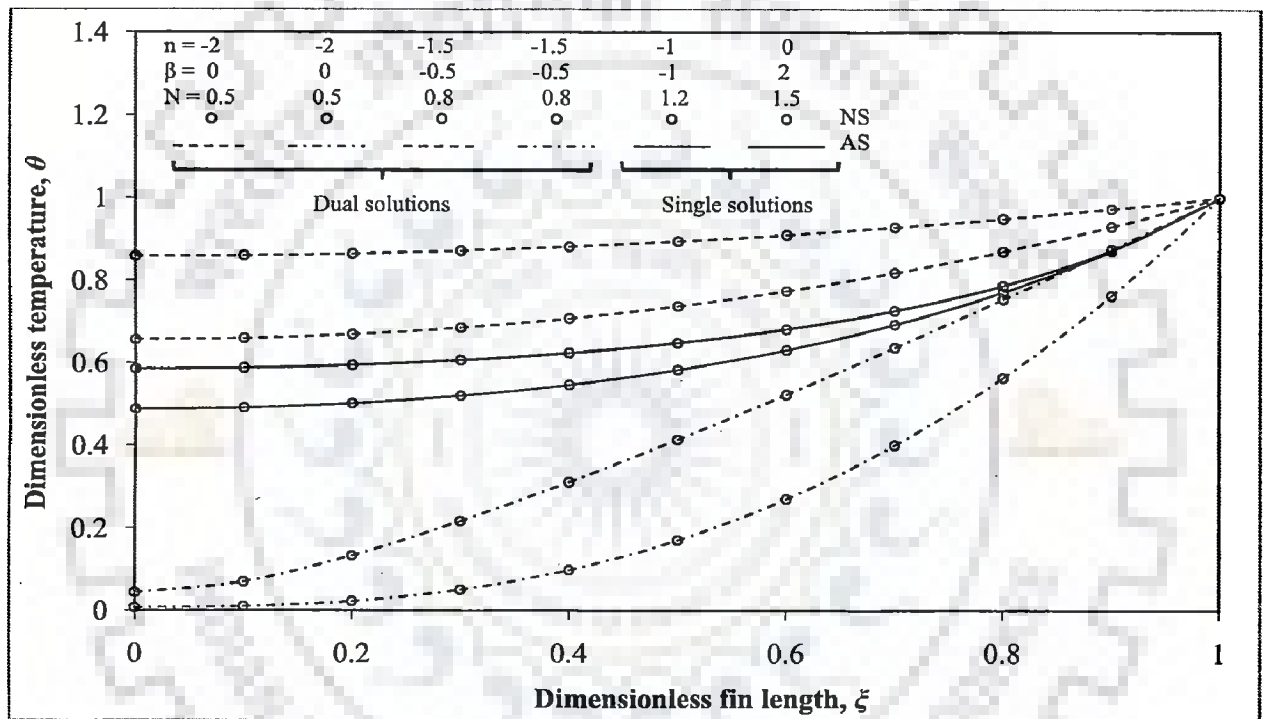
Figure 3.11: Dimensionless temperature profiles along the fin length for case 1(a) and case 1(b)

(iii)   *Solution properties and discussion of results*

For this case [$n = -1$, $\beta = -1$], the variation of θ_0 with N is shown in Fig. 3.10 and the expression for $\dfrac{dN}{d\theta_0}$ is given below:

$$\frac{dN}{d\theta_0} = -\frac{1}{\theta_0\sqrt{-2ln[\theta_0]}}$$

(3.70)

The Fig. 3.10 reveals the same features as described in the point (i) of case 1 (a), i.e. $\dfrac{dN}{d\theta_0} < 0$ $\forall$ $N \in [0,\infty)$, and $\theta_0 = 1$ at $N = 0$ and $\theta_0 \to 0$ as $N \to \infty$. Hence, only single value of θ_0, and consequently, only single and stable solution can be found for $N \in [0,\infty)$. The dimensionless temperature profile corresponding to this case [$n = -1$, $\beta = -1$] for $N = 1.2$ have been displayed in Fig. 3.11.

3.5.2.3 Case 2(a): $\beta + n \neq -2$ & $\beta = n \neq -1$

(i)   *Temperature profile*

$$\theta = \theta_0\left(cosh[N\sqrt{1+n}\xi]\right)^{\frac{1}{1+n}}$$

(3.71)

where θ_0 is given by:

$$\theta_0 = \left(cosh[N\sqrt{1+n}]\right)^{\frac{-1}{1+n}}$$

(3.72)

One should note that Moitsheki et al. (2010b) have obtained two different analytical solutions for this case by using symmetry method. The first solution was valid for $n \in (-\infty,-1)\cup(-1,\infty)$, whereas, the second solution was valid for $n \in (-1,0)$ $-1 < n < 0$. However, here, we have directly obtained the first solution, i.e. Eq. (3.71), which is valid for all $n \in (-\infty,-1)\cup(-1,\infty)$.

(ii) ***Fin efficiency***

$$\eta = \frac{1}{N}\sqrt{\frac{\left(1-\theta_0^{2n+2}\right)}{(1+n)}}$$ (3.73)

With the help of Eqs. (3.72) and (3.73), the following expression of η is obtained for $n=0$, which also matches with that of Moitsheki et al. (2010b).

$$\eta = \frac{1}{N}\sqrt{1-\theta_0^2} = \frac{tanh[N]}{N}$$

(iii) ***Solution properties and discussion of results***

Using Eq. (3.72), the variation of θ_0 with N' [Fig. 3.12] and the following expression of $\dfrac{dN}{d\theta_0}$ [Eq. (3.74)] have been obtained.

$$\frac{dN}{d\theta_0} = -\frac{\sqrt{1+n}\ \theta_0^{-2-n}}{\sqrt{\theta_0^{-2-n}-1}\sqrt{\theta_0^{-2-n}+1}}$$ (3.74)

A close look on the plots of θ_0, shown in the Fig. 3.12, reveals the following facts:

(i)   For $n<-1$, θ_0 varies periodically with N, hence, innumerous values of N can have the same fin tip temperature, θ_0. However, there can be no realistic solution for $N \geq N_{max}$, i.e. after the first positive zero of the θ_0 curve [marked with the bold circles in Fig. 3.12]. N_{max} can be found by substituting $\theta_0 = 0$ in Eq. (3.72) and solving the resultant equation for the minimum positive value of N. $\dfrac{dN}{d\theta_0} < 0$ for $0 \leq N < N_{max}$, which signifies the existence of single and stable solution in this range. Fig. 3.12 shows the variation of θ_0 with N for $n = \beta = -2$ and $n = \beta = -3/2$, and the Fig. 3.13 shows the corresponding dimensionless temperature profiles [single solution] for $N = 1$.
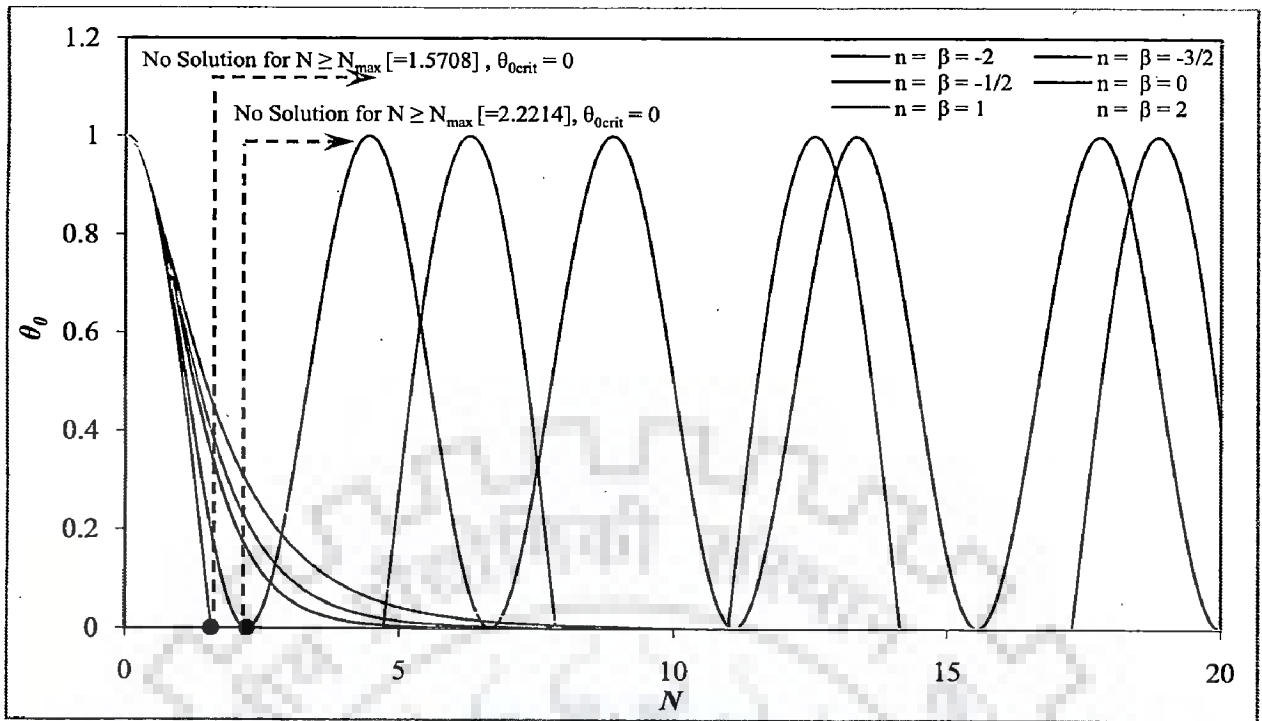
Figure 3.12: Variation of θ_0 with N for case 2(a)
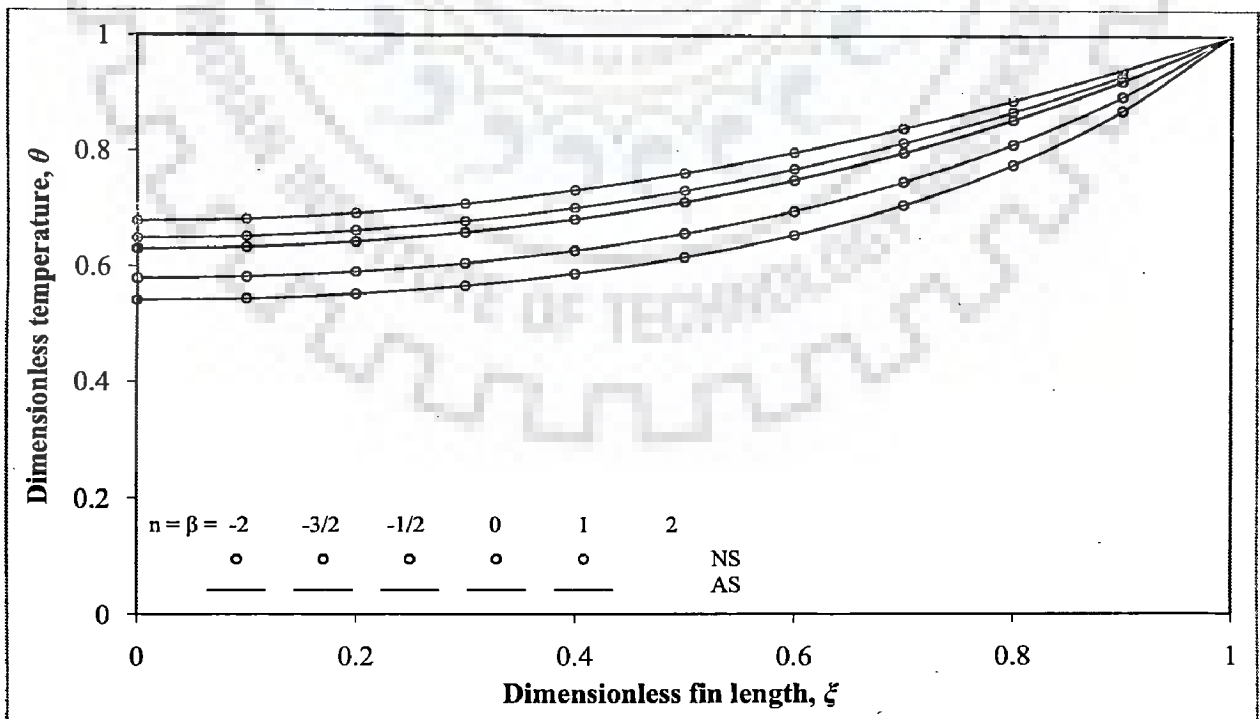
Figure 3.13: Dimensionless temperature profiles along the fin length at $N = 1$ for case 2(a)

99

For this situation, η increases from $\eta_{min} = 1$ to $\eta_{max} = \dfrac{1}{N_{max}} \sqrt{\dfrac{\left(1 - \theta_{0crit}^{2n+2}\right)}{(1+n)}}$ when

N increases from $N_{min} = 0$ to N_{max}. It can be noted that $\eta \geq 1$ [for the same reason as mentioned in the point (ii) of case 1(a)].

(ii)   For $n > -1$, $\dfrac{dN}{d\theta_0} < 0$ $\forall$ $N \in [0, \infty)$. Thus, only single solutions exist for $N \in [0, \infty)$. For some of these situations [$n = \beta = -1/2$; $n = \beta = 0$; $n = \beta = 1$; $n = \beta = 2$], the variation of θ_0 with N and the corresponding dimensionless temperature profiles have also been depicted in Fig. 3.12 and Fig. 3.13, respectively.

For this condition, η decreases from $\eta_{max} = 1$ to $\eta_{min} \to 0$ as N increases from $N = 0$ to $N \to \infty$.

For the sake of comparison, the dimensionless temperature profiles for the same values of n as considered by Moitsheki et al. (2010b), i.e. $n = -\frac{1}{4}$ [laminar film boiling/condensation], $n = 0$ [forced convection], $n = \frac{1}{4}$ [laminar free/natural convection], $n = \frac{1}{3}$ [turbulent free/natural convection], $n = 2$ [nucleate boiling], $n = 3$ [radiation], have also been drawn by using the analytical solution and are shown in Fig. 3.14. It can be seen that a close agreement exists between these profiles and those drawn by Moitsheki et al. (2010b). Similarly, the variation of η with N [$n = \beta = 0$] has been shown in Fig. 3.15, which also matches with the one given by Moitsheki et al. (2010b).

3.5.2.4 Case 2(b): $\beta + n \neq -2$ & $\beta \neq n$ & $2\beta + n \neq -3$

(i)   Temperature profile

The following implicit analytical solution of θ is obtained:

$$\frac{\theta^{1+\beta}\sqrt{1-\dfrac{\theta^{2+n+\beta}}{\theta_0^{2+n+\beta}}}HG_2F_1\left[\dfrac{1+\beta}{2+n+\beta},\dfrac{1}{2},\dfrac{3+n+2\beta}{2+n+\beta},\dfrac{\theta^{2+n+\beta}}{\theta_0^{2+n+\beta}}\right]}{(1+\beta)\sqrt{\dfrac{2N^2(\theta^{2+n+\beta}-\theta_0^{2+n+\beta})}{2+n+\beta}}}$$

$$-\frac{\sqrt{-\pi(2+n+\beta)}\,\theta_0^{1+\beta}\,\Gamma\left[\dfrac{3+n+2\beta}{2+n+\beta}\right]}{(1+\beta)\sqrt{2N^2\theta_0^{2+n+\beta}}\,\Gamma\left[\dfrac{4+n+3\beta}{4+2n+2\beta}\right]}=\xi \qquad (3.75)$$

where $\Gamma[z]$ and $HG_2F_1[a,b,c,z]$ are the well known Gamma and the Gauss' Hypergeometric functions, respectively, and have been defined earlier in Eqs. (3.51a) and (3.51b), respectively. The unknown θ_0, in Eq. (3.75), is obtained by solving the following equation.

$$\frac{\sqrt{1-\dfrac{1}{\theta_0^{2+n+\beta}}}HG_2F_1\left[\dfrac{1+\beta}{2+n+\beta},\dfrac{1}{2},\dfrac{3+n+2\beta}{2+n+\beta},\dfrac{1}{\theta_0^{2+n+\beta}}\right]}{(1+\beta)\sqrt{\dfrac{2N^2(1-\theta_0^{2+n+\beta})}{2+n+\beta}}}$$

$$-\frac{\sqrt{-\pi(2+n+\beta)}\,\theta_0^{1+\beta}\,\Gamma\left[\dfrac{3+n+2\beta}{2+n+\beta}\right]}{(1+\beta)\sqrt{2N^2\theta_0^{2+n+\beta}}\,\Gamma\left[\dfrac{4+n+3\beta}{4+2n+2\beta}\right]}=1 \qquad (3.76)$$

(ii) **Fin efficiency**

$$\eta=\frac{1}{N}\sqrt{\frac{2}{(2+n+\beta)}\left(1-\theta_0^{2+n+\beta}\right)} \qquad (3.77)$$

Form Eq. (3.57b) it can be deduced that $\eta=1$ for $n=-1$ and for any value of β and N.
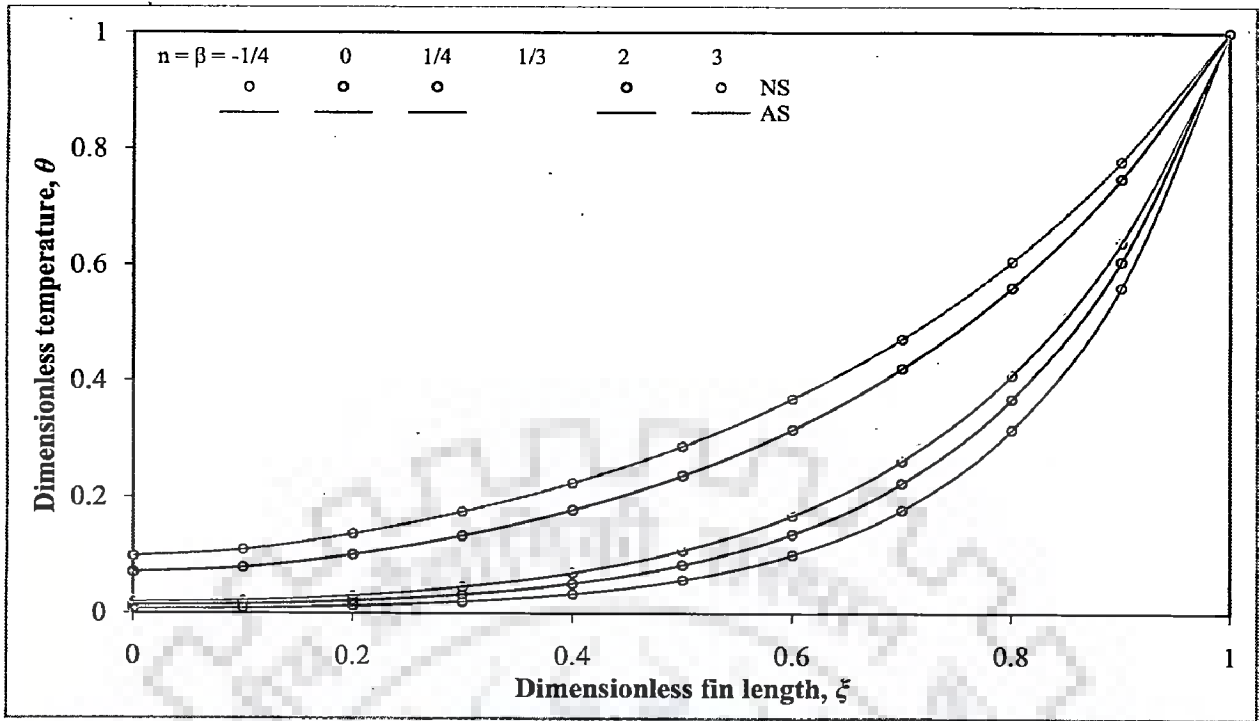
Figure 3.14: Dimensionless temperature profiles along the fin length at $N = 5$ for case 2(a) for the same values of parameters as those considered by Moitsheki et al. (2010b)
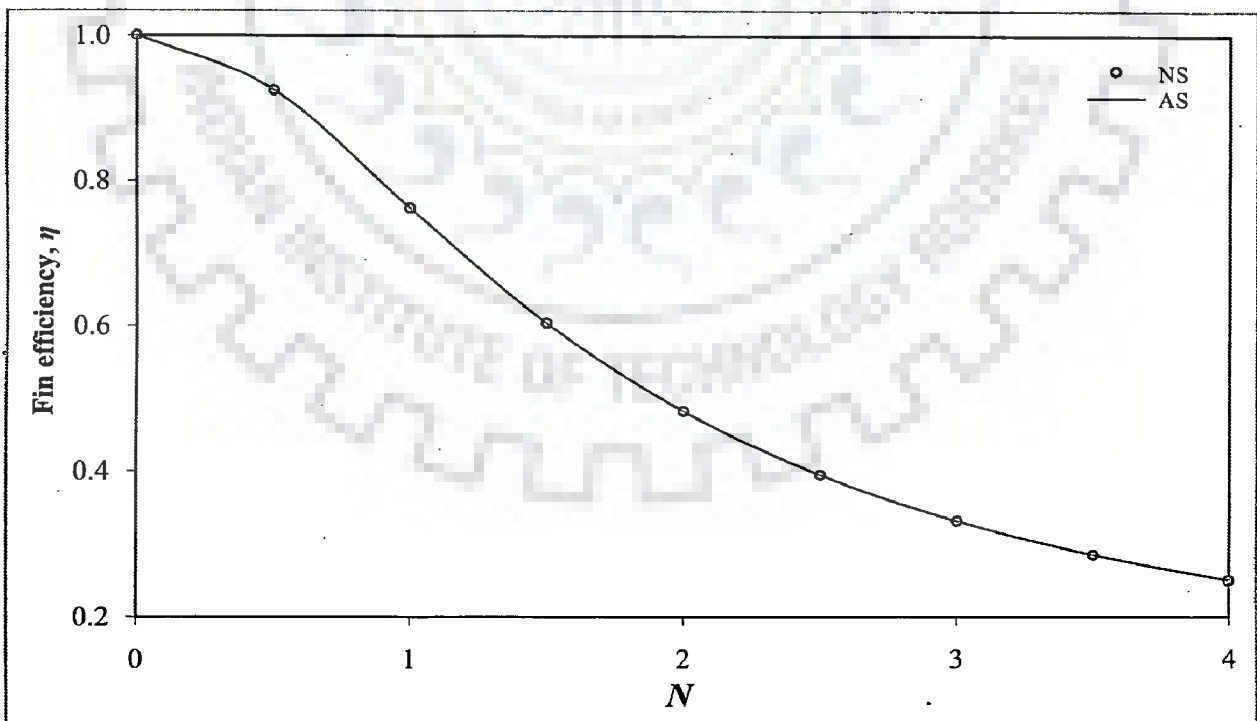
Figure 3.15: Variation of fin efficiency with N for case 2(a) for the same values of parameters [$n = \beta = 0$] as those considered by Moitsheki et al. (2010b)

(iii) Solution properties and discussion of results

The variation of θ_0 with N, and the respective temperature profiles are have been shown in Figs. 3.16-3.19. $\dfrac{dN}{d\theta_0}$ is given by the following equation:

$$\frac{dN}{d\theta_0} = \frac{\left(-2(1+\beta)\sqrt{-\dfrac{(2+n+\beta)\pi}{\theta_0}}\sqrt{\theta_0^{5+n+3\beta}}\left(1-\theta_0^{-2-n-\beta}\right)\Gamma\left[\dfrac{1+\beta}{2+n+\beta}\right]\right)}{2\sqrt{2}(1+\beta)\theta_0\left(-1+\theta_0^{2+n+\beta}\right)\Gamma\left[\dfrac{-n+\beta}{4+2n+2\beta}\right]}$$

$$+\frac{(2+n+\beta)\sqrt{\dfrac{1-\theta_0^{2+n+\beta}}{2+n+\beta}}}{2\sqrt{2}(1+\beta)\theta_0\left(-1+\theta_0^{2+n+\beta}\right)}\times$$

$$\left(2(1+\beta)+(n-\beta)\sqrt{1-\theta_0^{-2-n-\beta}}\,HG_2F_1\left[\frac{1}{2},\frac{1+\beta}{2+n+\beta},1+\frac{1+\beta}{2+n+\beta},\frac{1}{\theta_0^{2+n+\beta}}\right]\right)$$

$$(3.78)$$

A careful assessment of the Figs. 3.16 and 3.18 showing the variation of θ_0 with N, discloses the following three situations:

(i) Fig. 3.16 reveals that $\dfrac{dN}{d\theta_0}<0$ for $N\in[0,N_{max})$. Hence, only single and stable solutions exist for $N\in[0,N_{max})$, and no solution exists for $N\geq N_{max}$. N_{max} can be found from Eq. (3.76) by substituting $\theta_0=0$. For some of the parameters' values pertaining to this case [$n=-1$, $\beta=1/2$; $n=-1$, $\beta=1$; $n=-1$, $\beta=2$; $n=-1$, $\beta=4$], these plots have been shown in Fig. 3.16 and the corresponding single temperature profiles are shown in Fig. 3.17.

η increases from $\eta_{min}=1$ to $\eta_{max}=\dfrac{1}{N_{max}}\sqrt{\dfrac{2}{(2+n+\beta)}}\left(1-\theta_{0\,crit}^{2+n+\beta}\right)$ when N increases from $N=0$ to N_{max}. However, $\eta=1$ for $n=-1$ and for any value of β and N.

(ii)   As shown in Fig. 3.18 for $n = -1.5$ and $\beta = -2$, $\dfrac{dN}{d\theta_0} < 0$ for $N \in [0,\infty)$. Thus,

single and stable solutions can be found for $N \in [0,\infty)$. The respective temperature profile is shown in Fig. 3.19. η increases from $\eta_{min} = 1$ to

$$\eta_{max} \to \frac{1}{N_{max}}\sqrt{\frac{2}{(2+n+\beta)}\left(1-\theta_{0crit}^{2+n+\beta}\right)}$$ [since $n < -1$] when N increases

from $N = 0$ to $N_{max} \to \infty$.

(iii)   For other situations [$n = -1.5$, $\beta = 1$; $n = -1.5$, $\beta = 2$; $n = -1.5$, $\beta = -0.25$; $n = -1.5$, $\beta = 0.5$] also shown in Fig. 3.18, θ_0 exists for $0 \le N \le N_{max}$. For $N \in [0, N_T)$, θ_0 is single valued and $\dfrac{dN}{d\theta_0} < 0$, therefore single and stable solution can be obtained. N_T can be computed from Eq. (3.76) by substituting $\theta_0 = 0$. For $N \in [N_T, N_{max})$, θ_0 is double valued and $\dfrac{dN}{d\theta_0}$ can be negative or positive, therefore dual solutions [one stable and the other unstable] can be obtained. At $N = N_{max}\left[\dfrac{dN}{d\theta_0} = 0\right]$ the dual solutions merge into a single solution. For $N > N_{max}$, no solution can be found. This situation has been portrayed in Fig. 3.18 and the corresponding dual temperature profiles [for $n = -1.5$, $\beta = -0.25$ and $n = -1.5$, $\beta = 0.5$] are shown in Fig. 3.19.

Here also, η increases from $\eta_{min} = 1$ to $\eta_{max} = \dfrac{1}{N_{max}}\sqrt{\dfrac{2}{(2+n+\beta)}\left(1-\theta_{0crit}^{2+n+\beta}\right)}$

when N increases from $N = 0$ to N_{max}.

It should also be noted that the previously considered model equation of radiative heat transfer from a rectangular fin is a special case of case 2(b), and therefore, the results and discussions of this case are also applicable to it.

106
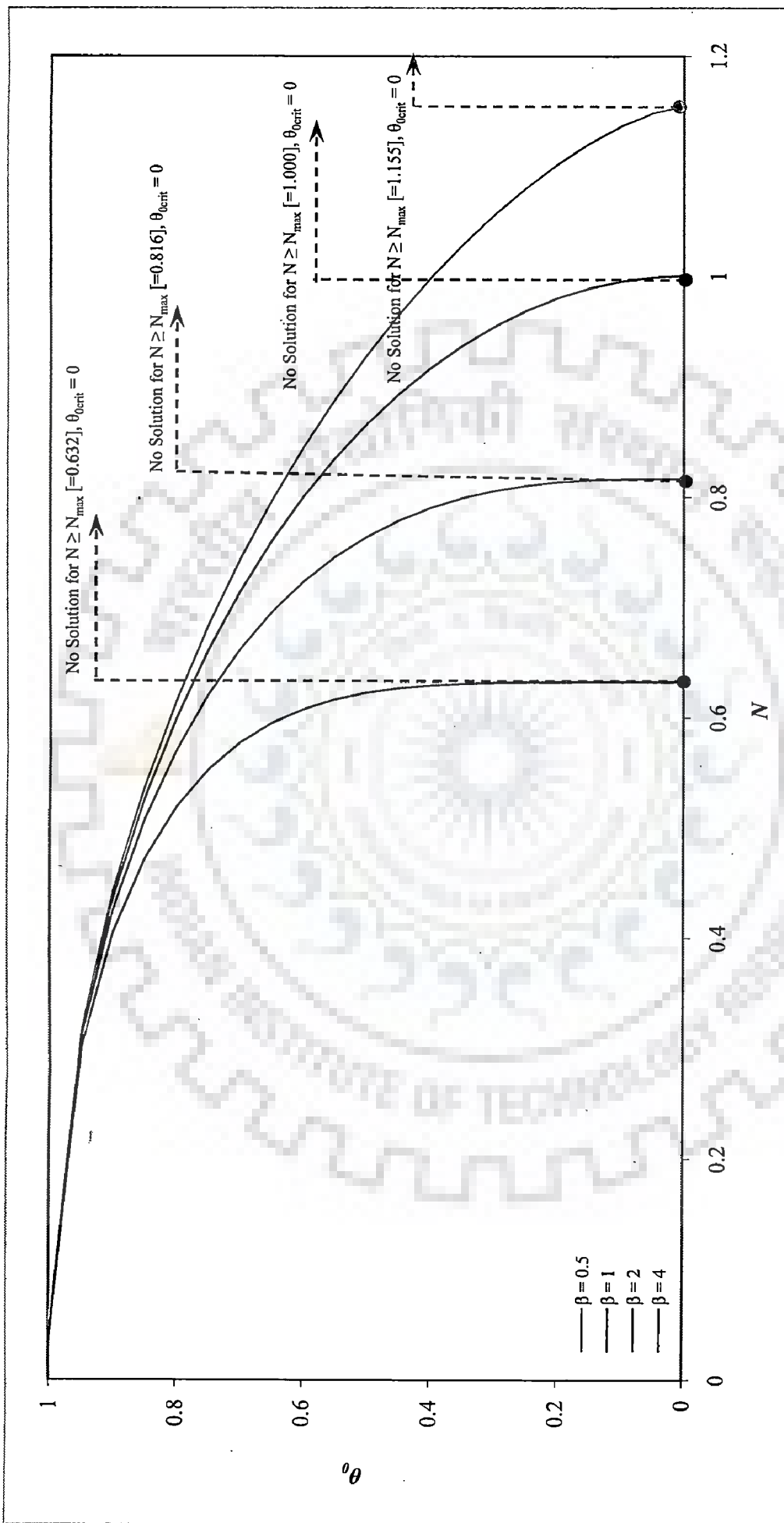
Figure 3.16: Variation of θ_0 with N at $n = -1$ for case 2(b)

Curves labeled:
- $\beta = 0.5$
- $\beta = 1$
- $\beta = 2$
- $\beta = 4$

No Solution for $N \geq N_{max}$ [=0.632], $\theta_{0crit} = 0$

No Solution for $N \geq N_{max}$ [=0.816], $\theta_{0crit} = 0$

No Solution for $N \geq N_{max}$ [=1.000], $\theta_{0crit} = 0$

No Solution for $N \geq N_{max}$ [=1.155], $\theta_{0crit} = 0$

107
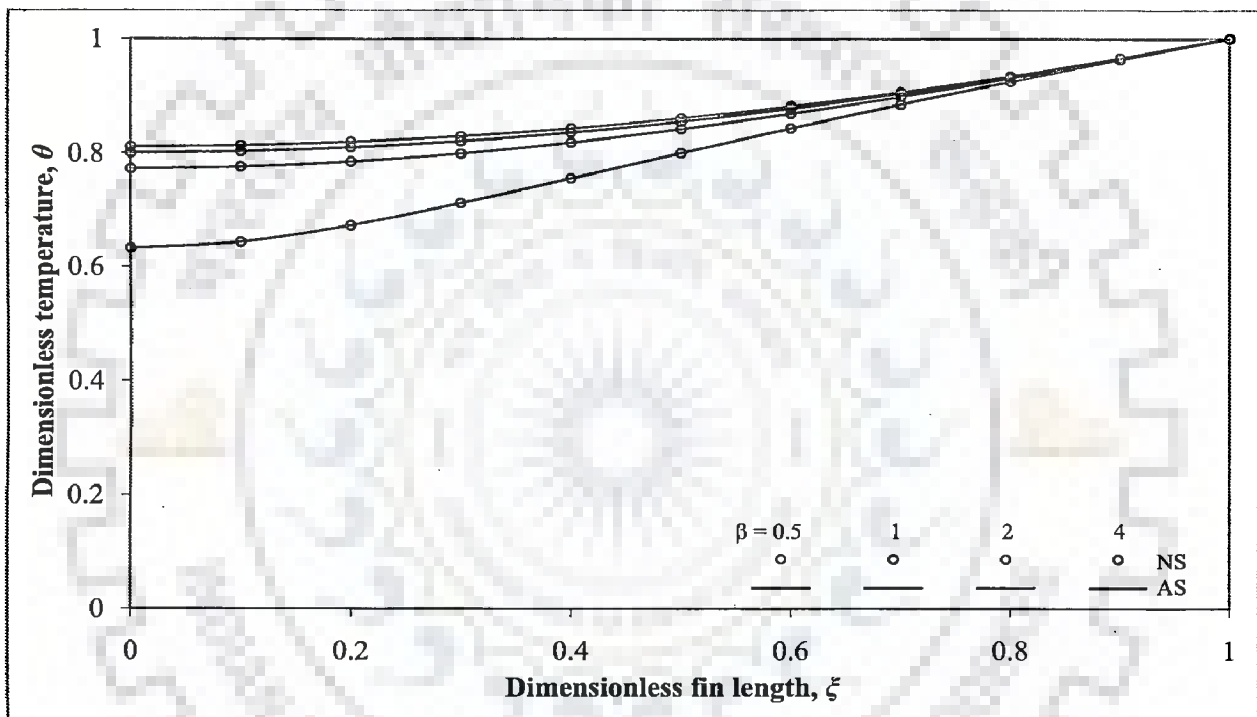
Figure 3.17: Dimensionless temperature profiles along the fin length at $n = -1$ and $N = 0.6$ for case 2(b)
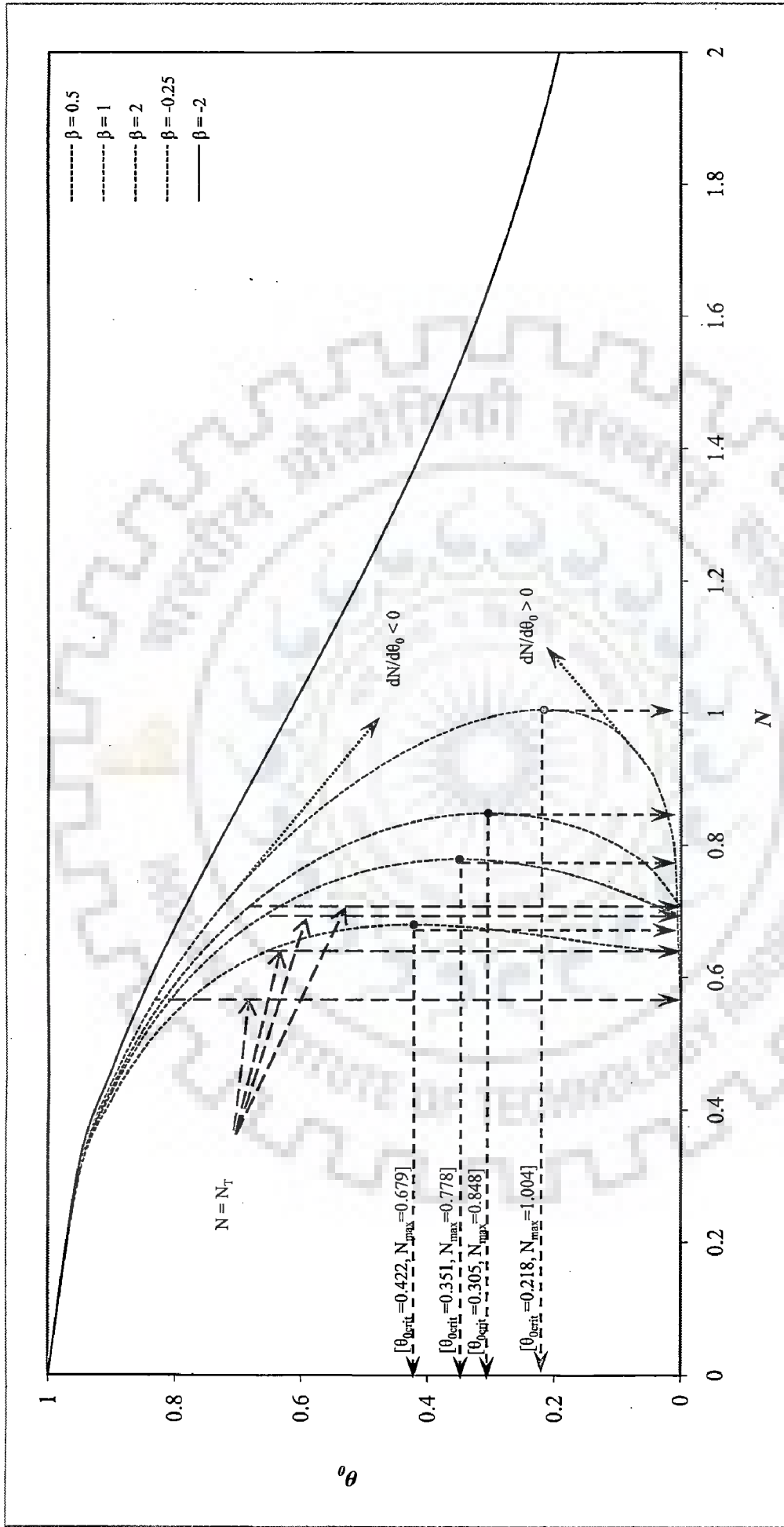
Figure 3.18: Variation of θ_0 with N at $n = -1.5$ for case 2(b)

111
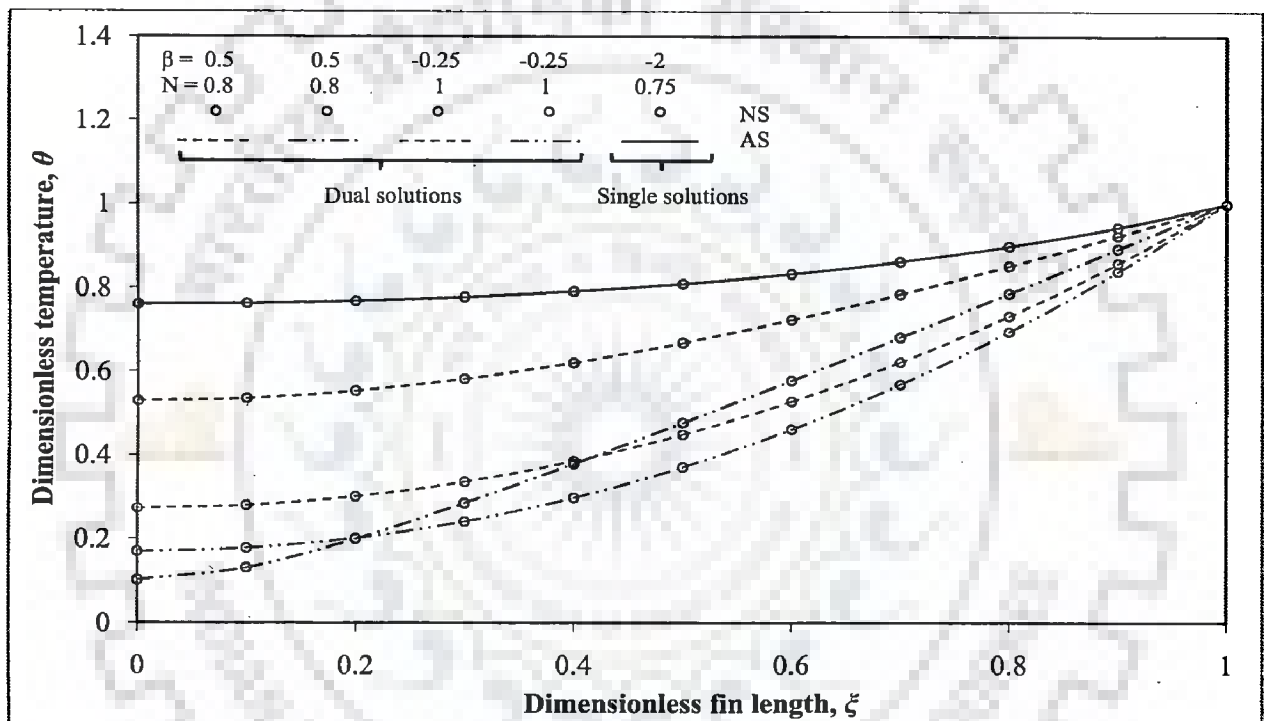
Figure 3.19: Dimensionless temperature profiles along the fin length at $n = -1.5$ for case 2(b)

3.5.2.5 Case 2(c): $\beta + n \neq -2$ & $\beta \neq n$ & $2\beta + n = -3$

(i) Temperature profile

It can be noted that the analytical solution of the previous case 2(b), i.e. Eq. (3.75), fails whenever $2\beta + n = -3$. This is because both the Hypergeometric function and the Gamma function become indeterminate for $2\beta + n = -3$. Hence, in such situations, the whole steps starting from Eq. (3.55a) have to be worked out again as shown in Appendix A4. Finally, the following implicit analytical solution of θ is obtained for this case:

$$\frac{\sqrt{\left(\dfrac{\theta^{\frac{(1+n)}{2}} - \theta_0^{\frac{(1+n)}{2}}}{1+n}\right)}\left(-\sqrt{1-\left(\dfrac{\theta_0}{\theta}\right)^{\frac{(1+n)}{2}}} + \sin^{-1}\left[\left(\dfrac{\theta_0}{\theta}\right)^{\frac{(1+n)}{4}}\right]\right)}{N(\theta\theta_0)^{\frac{(1+n)}{2}}\sqrt{\left(1-\left(\dfrac{\theta_0}{\theta}\right)^{\frac{(1+n)}{2}}\right)}} + \frac{\pi\theta_0^{-(1+n)}\sqrt{\theta_0^{\frac{(-1+n)}{2}}}}{2N\sqrt{\dfrac{(1+n)}{\theta_0}}} = \xi \tag{3.79}$$

where θ_0 is evaluated by the following equation.

$$\frac{\sqrt{\left(\dfrac{1-\theta_0^{\frac{(1+n)}{2}}}{1+n}\right)}\left(-\sqrt{1-\theta_0^{\frac{(1+n)}{2}}} + \sin^{-1}\left[\theta_0^{\frac{(1+n)}{4}}\right]\right)}{N\theta_0^{\frac{(1+n)}{2}}\sqrt{\left(1-\theta_0^{\frac{(1+n)}{2}}\right)}} + \frac{\pi\theta_0^{-(1+n)}\sqrt{\theta_0^{\frac{(-1+n)}{2}}}}{2N\sqrt{\dfrac{(1+n)}{\theta_0}}} = 1 \tag{3.80}$$

(ii) Fin efficiency

$$\eta = \frac{2}{N}\sqrt{\frac{1}{n+1}\left(1-\theta_0^{\frac{n+1}{2}}\right)} \tag{3.81}$$

(iii) *Solution properties and discussion of results*

The variation of θ_0 with N is shown in Fig. 3.20. For this case, the dimensionless temperature profiles have been drawn in Fig. 3.21. The expression of $\dfrac{dN}{d\theta_0}$ is given by the following Eq. (3.82):

$$\frac{dN}{d\theta_0} = \frac{\theta_0^{\frac{-(7+4n)}{4}}}{8\left(1-\theta_0^{\frac{1+n}{2}}\right)^{\frac{5}{2}}}\left(\sqrt{1-\theta_0^{\frac{1+n}{2}}}\left(2(1+n)\theta_0^{\frac{1+2n}{4}}\sqrt{\frac{1-\theta_0^{\frac{1+n}{2}}}{1+n}}\left(-3+4\theta_0^{\frac{1+n}{2}}-\theta_0^{1+n}\right)\right.\right.$$
$$\left.\left.-3\pi\sqrt{\frac{1+n}{\theta_0}}\theta_0^{\frac{3}{4}}\sqrt{\theta_0^{\frac{-1+n}{2}}}\left(1-2\theta_0^{\frac{1+n}{2}}+\theta_0^{1+n}\right)\right)\right)$$

$$+\frac{\theta_0^{\frac{-(7+4n)}{4}}}{8\left(1-\theta_0^{\frac{1+n}{2}}\right)^{\frac{5}{2}}}\left(-6(1+n)\theta_0^{\frac{n}{4}}\sqrt{\frac{1-\theta_0^{\frac{1+n}{2}}}{1+n}}\left(1-2\theta_0^{\frac{1+n}{2}}+\theta_0^{1+n}\right)\sin^{-1}\left[\theta_0^{\frac{1+n}{4}}\right]\right)$$

$$(3.82)$$

By examining the Fig. 3.20, the following two observations have been made:

(i)   For $n < -1$, θ_0 exist for $N \in [0, N_{max}]$ in which $\dfrac{dN}{d\theta_0} < 0, > 0, = 0$, in other words $N_T = 0$. Therefore, only dual solutions will exist for $N \in (0, N_{max})$. At $N = N_{max}$ these two solutions merge into a single solution. For $N > N_{max}$, no solution is possible. For some of the parameters' values pertaining to this case [$n = -3$, $\beta = 0$; $n = -2$, $\beta = -1/2$], the variation of θ_0 with N has been shown in Fig. 3.20, and for $n = -3$, $\beta = 0$ and $N = 0.4$, the obtained dual temperature profiles are shown in Fig. 3.21. It can also be observed that for $n = -3$ and $\beta = 0$, results [Figs. 3.20 and 3.21] match well with those of Abbasbandy and Sivanian (2010).

η increases from $\eta_{min} = 1$ to $\eta_{max} = \dfrac{2}{N_{max}}\sqrt{\dfrac{1}{n+1}\left(1-\theta_{0crit}^{\frac{n+1}{2}}\right)}$ when N increases from $N_{min} = 0$ to N_{max}, [same observations as in point (ii) of case 1(a)].
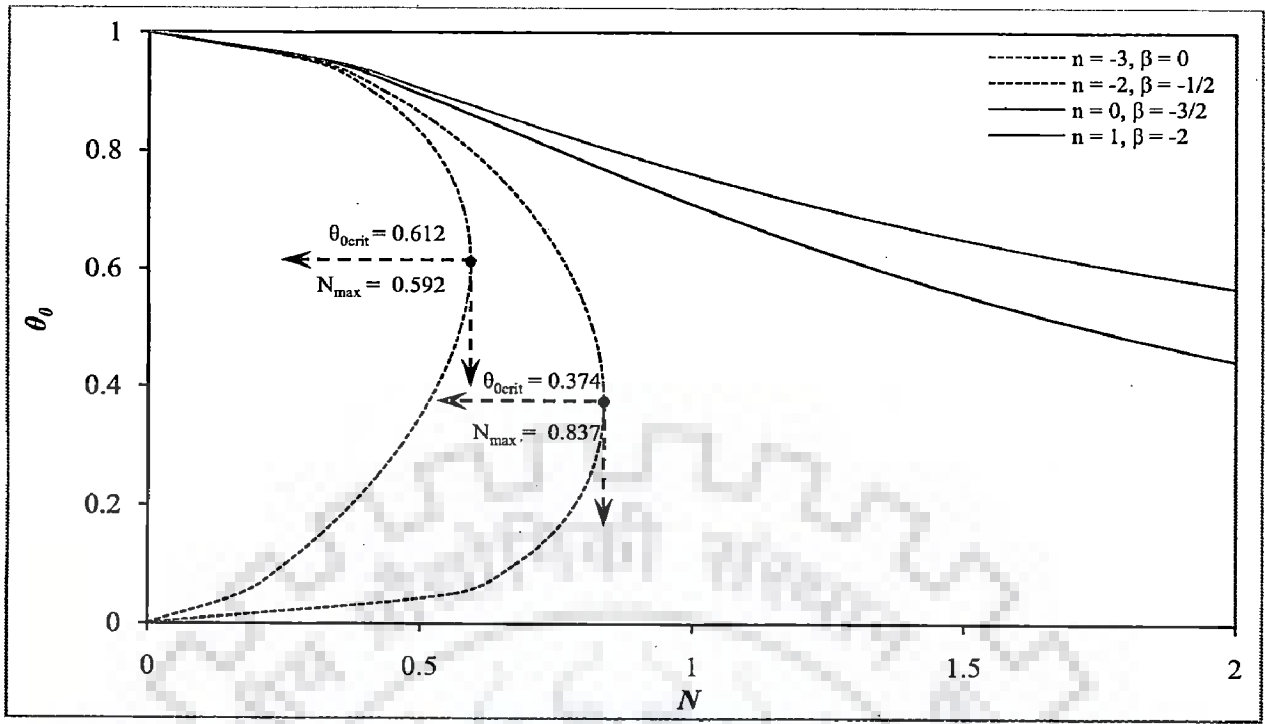
Figure 3.20: Variation of θ_0 with N for case 2(c)
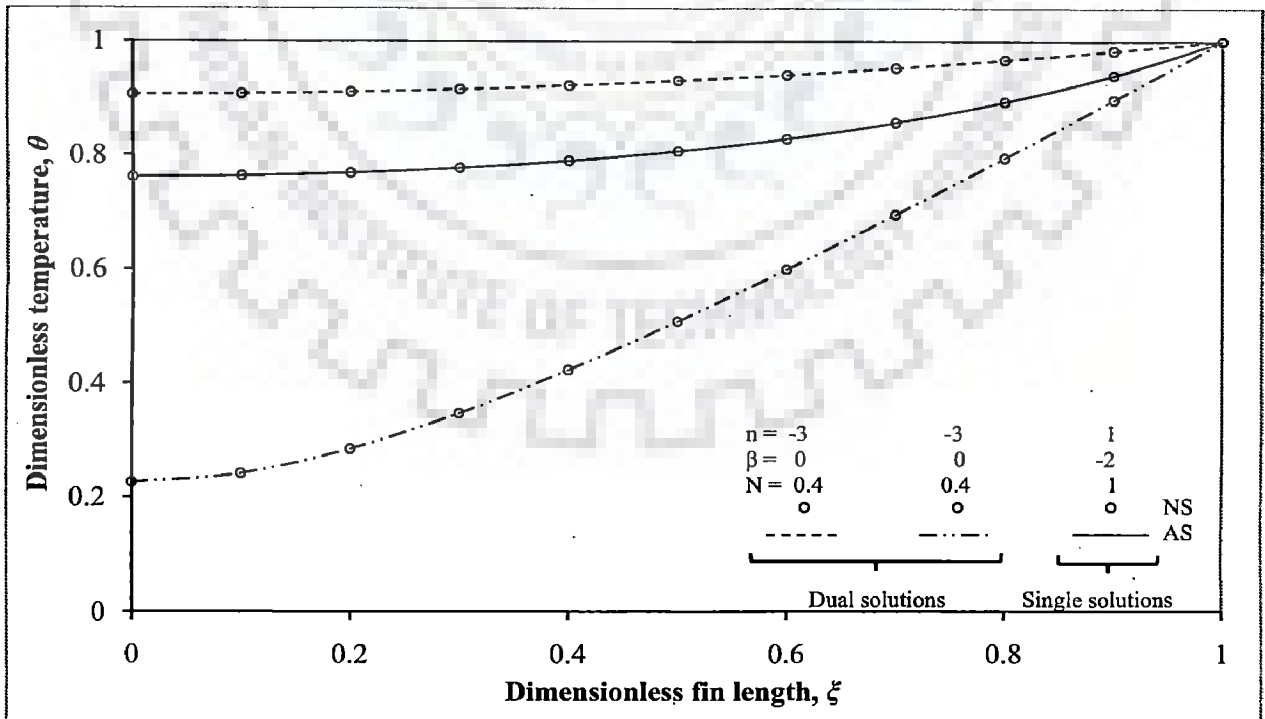
Figure 3.21: Dimensionless temperature profiles along the fin length for case 2(c)

(ii)   For $n > -1$, Fig. 3.20 shows that $\dfrac{dN}{d\theta_0} < 0$ $\forall$ $N \in [0,\infty)$. Therefore, only single stable solutions will be present for $N \in [0,\infty)$. Fig. 3.20 also draws the plot of θ_0 against N [$n = 0$, $\beta = -3/2$; $n = 1$, $\beta = -2$], and Fig. 3.21 shows the temperature profile corresponding to $n = 1$ and $\beta = -2$ for $N = 1$.

η decreases from $\eta_{max} = 1$ to $\eta_{min} \to 0$ when N increases from $N = 0$ to $N_{max} \to \infty$ [same as in point (ii) of case 2(a)].

For all the above cases, the temperature profiles have also been obtained by using numerical method and are shown in various figures [Figs. 3.11, 3.13 - 3.15, 3.17, 3.19, 3.21] along with the presently obtained analytical profiles; a close match between these profiles validates all the derived analytical solutions.

3.5.2.6 Resemblance with Previous Works

(i)   For $\beta \neq 0$, Moitsheki et al. (2010b) have obtained the analytical solutions of the same model equation for cases 1(b) and 2(a) only. On the contrary, in the present study we have successfully simulated all the cases including those considered by Moitsheki et al. (2010b).

(ii)   For $\beta = 0$, the original Eqs. (3.55a)-(3.55c) reduce to the well known equations of heat conduction-convection and reaction-diffusion processes, which were earlier tackled by various investigators for obtaining the approximate and analytical solutions. It can be easily examined that the presently obtained analytical solutions cover all the previously found analytical solutions of these processes (Sen and Trinh, 1986; Yeh and Liaw, 1990; Abbasbandy and Shivanian, 2010; Magyari, 2008; Moitsheki et al., 2010a; Moitsheki et al., 2010b).

3.6   CONCLUDING REMARKS

In this chapter, model equations of the following selected heat transfer processes

have been solved analytically and the conclusions pertaining to these processes are summarized below.

(i) Transient Convective Cooling of a Lumped Body

Explicit analytical solution of the transient temperature profile has been obtained in terms of Lambert W function by using the separation of variables method followed by partial fraction decomposition method. The obtained analytical solution has been successfully verified with the numerical solution, and a comparison between the analytical and the available approximate solutions (Ganji, 2006; Abbasbandy, 2006a; Marinca and Herişanu, 2008) reveals that the analytical solution is better than the approximate solutions.

(ii) Transient Convective-Radiative Cooling of a Lumped Body

Implicit analytical solution of the transient temperature profile has been obtained by using the separation of variables method and the partial fraction decomposition method. The analytical solution has been validated with the numerical solution, and the practical utility of the analytical solution has been shown by successfully simulating an existing experimental study of the cooling of metal ball bearing (Campo and Blotter, 2000). While simulating this experimental study, it is shown that the temperature dependent heat transfer coefficient can effectively be replaced by its average value.

Besides, explicit analytical solution of the transient temperature profile for the specific case of transient cooling of a lumped body in an absolute zero temperature has also been obtained. Limitations of an existing model equation of this specific situation and its available approximate solutions (Rajabi et al., 2007; Ganji et al., 2007; Domairry and Nadim, 2008) have also been discussed and rectified.

(iii) Steady State Heat Conduction in a Metallic Rod

Explicit analytical solution of the temperature profile has been obtained by using two different methods, i.e. by simplifying the model equation and by using the

120

derivative substitution method. By comparing the results obtained by using the analytical, numerical and the available approximate solutions (Rajabi et al., 2007; Domairry and Nadim, 2008; Sajid and Hayat, 2008a), the validity of analytical solution has been established and it is shown that the analytical solution is better than the available approximate solutions.

(iv) Steady State Radiative Heat Transfer from a Rectangular Fin

Analytical solution of the temperature profile has been obtained in terms of an implicit hypergeometric function by using the derivative substitution method. The so obtained analytical solution has been successfully verified with the numerical solution and is found to be better than the approximate solutions available in literature (Ganji, 2006; Abbasbandy, 2006a; Marinca and Herişanu, 2008).

(v) Steady State Convective Heat Transfer from a Rectangular Fin

Analytical solutions of the temperature profile and fin efficiency have been obtained in implicit/explicit forms of the well known algebraic/non-algebraic functions by using the derivative substitution method. These analytical solutions have been found for all the possible values of parameters [N, β and n] and also include the analytical solutions earlier obtained by Moitsheki et al. (2010b). These analytical solutions have been effectively validated with their numerical counterparts and may also be employed for other similar processes, e.g. reaction-diffusion process in a catalyst slab.

It is observed that for some sets of parameters' values the model equation exhibited no solution, single solution and dual solutions. All the single solutions so found are stable, whereas in case of dual solutions, the one corresponding to higher heat transfer rate [or the one for which $\frac{dN}{d\theta_0} > 0$], is unstable. For some cases, it is shown that the fin efficiency does not exceed a certain maximum value, which is determined by the value of the parameter N prevailing at the boundary of the region of solution existence.

NOMENCLATURE

Abbreviations

AS	analytical solution
NS	numerical solution
HPM	homotopy perturbation method
HAM	homotopy analysis method
Exp.	Experimental

Notations

A	[m^2]	heat transfer area of the body
A_c	[m^2]	cross-sectional area of the rod / rectangular fin
Bi_c	[-]	Biot number for convection for a spherical body $\left(=\dfrac{hR}{k}\right)$
Bi_T	[-]	overall Biot number for convective and radiative heat transfer for a spherical body $\left(=\dfrac{(h+h_r)R}{k}\right)$
c_a	[kJ.kg^{-1}.K^{-1}]	specific heat of the body at temperature T_a
c_p	[kJ.kg^{-1}.K^{-1}]	constant specific heat of the body
$c_p(T)$	[kJ.kg^{-1}.K^{-1}]	specific heat of the body at temperature T $\left(=c_a\left(1+\beta\dfrac{(T-T_a)}{(T_i-T_a)}\right)\right)$
C_1, C_2	[-]	constants of integration
D	[m]	diameter of the ball bearing $[=2R]$
e	[-]	exponential function
h	[W.m^{-2}.K^{-1}]	convective heat transfer coefficient
h_1	[-]	convergence control parameter in HAM solution given in the present Eqs. (3.10b) and (3.52b) as used by Abbasbandy (2006a)
h_{av}	[W.m^{-2}.K^{-1}]	average convective heat transfer coefficient [Eq.

$(3.32)]$

h_b	$[W.m^{-2}.K^{-1}]$	convective heat transfer coefficient at temperature T_b
h_r	$[W.m^{-2}.K^{-1}]$	radiative heat transfer coefficient $\left(= \dfrac{\sigma \in (T^4 - T_a^4)}{(T - T_a)} \right)$
$h(T)$	$[W.m^{-2}.K^{-1}]$	convective heat transfer coefficient at temperature T
i	$[-]$	imaginary unit $[= \sqrt{-1}]$; index variable
k	$[W.m^{-1}.K^{-1}]$	constant thermal conductivity of the body / rectangular fin
k_a	$[W.m^{-1}.K^{-1}]$	thermal conductivity of the rod at temperature T_a
k_b	$[W.m^{-1}.K^{-1}]$	thermal conductivity of the rectangular fin at temperature T_b
l	$[m]$	characteristic length of the body
L	$[m]$	length of the rod / rectangular fin
n	$[-]$	dimensionless parameter in convective heat transfer coefficient
N	$[-]$	dimensionless fin parameter $\left(= \left(\dfrac{h_b P L^2}{k_b A} \right)^{1/2} \right)$
N_{max}	$[-]$	maximum possible value of dimensionless fin parameter
N_{min}	$[-]$	minimum possible value of dimensionless fin parameter
N_T	$[-]$	value of dimensionless fin parameter at $\theta_0 = 0$
N_{rc}	$[-]$	dimensionless conduction-radiation parameter $\left(= \dfrac{\sigma \in R T_i^3}{k} \right)$
$p(\theta)$	$[-]$	function of θ $\left(= \dfrac{d\theta}{d\xi} \right)$
P	$[m]$	perimeter of the rectangular fin
r	$[m]$	radial coordinate
r_i	$[-]$	i^{th} root [Appendix A1]

123

R	[m]	radius of the spherical body
T	[K]	temperature of the body / rod / rectangular fin
T_i	[K]	initial temperature of the body
T_s	[K]	radiation sink temperature
V	[m³]	volume of the body

Greek letters

α	[m².s⁻¹]	thermal diffusivity of the body $\left(=\dfrac{k}{\rho c_a}\right)$
β	[-]	dimensionless parameter in specific heat
$\in$	[-]	emissivity of the body
ρ	[kg.m⁻³]	density of the body
τ	[-]	dimensionless time $\left(=\dfrac{\alpha t}{R^2}\right)$
τ_1	[-]	dimensionless time considered by Ganji (2006) and Abbasbandy (2006a) $\left(=\dfrac{h A t}{\rho c_a V}\right)$
σ	[W.m⁻².K⁻⁴]	Stephan-Boltzmann constant [= 5.669 × 10⁻⁸]
ξ	[-]	dimensionless distance $\left(=\dfrac{x}{L}\right)$

Section 3.1

Notations

t	[s]	time
T_a	[K]	ambient temperature
x	[-]	dimensionless independent variable
y	[-]	dimensionless dependent variable

Greek letters

θ	[-]	dimensionless temperature $\left(=\dfrac{T-T_a}{T_i-T_a}\right)$

124

Section 3.2

Notations

a, b	[-]	real and imaginary parts of the complex roots [r_3 and r_4]
A_1, B_1, C_1, D_1	[-]	constants appearing in the partial fraction decomposition
t	[s]	time
T_a	[K]	adiabatic surface temperature [Eq. (3.13)]
T_f	[K]	ambient temperature of the surroundings [ambient temperature]

Greek letters

ε	[-]	dimensionless parameter defined in Ganji et al. (2007), Rajabi et al. (2007), Domairry and Nadim (2008) [$=3N_{rc}$]
η	[-]	dimensionless radial coordinate $\left(=\dfrac{r}{R}\right)$
θ	[-]	dimensionless temperature $\left(=\dfrac{T}{T_i}\right)$
θ_a	[-]	dimensionless adiabatic surface temperature $\left(=\dfrac{T_a}{T_i}\right)$
θ_{av}	[-]	spatially averaged dimensionless temperature [Eq. (3.16)]

Section 3.3

Notations

$k(T)$	[W.m^{-1}.K^{-1}]	thermal conductivity of the rod [$=k_a(1+\beta\theta)$]
T_a	[K]	temperature of the rod at the $x = 0$
T_b	[K]	temperature of the rod at the $x = L$
x	[m]	distance along the length of the rod

125

| y | [-] | function of θ $\left(= p(\theta)^2 = \left(\dfrac{d\theta}{d\xi}\right)^2 \right)$ |

Greek letters

| θ | [-] | dimensionless temperature $\left(= \dfrac{T-T_a}{T_b - T_a} \right)$ |

Section 3.4

Notations

a,b,c	[-]	constants in Eq. (3.51b)
t	[-]	dummy variable in Eqs. (3.51a)-(3.51b)
T_b	[K]	temperature at the base of rectangular fin
x	[m]	distance from the tip of rectangular fin
y	[-]	function of θ $\left(= p^2 = \left(\dfrac{d\theta}{d\xi}\right)^2 \right)$
z	[-]	dummy variable in Eqs. (3.51a)-(3.51b)

Greek letters

ε	[-]	conduction radiation parameter for the rectangular fin $\left(= \dfrac{\sigma \in P T_b^3 L^2}{kA_c} \right)$
θ	[-]	dimensionless temperature $\left(= \dfrac{T}{T_b} \right)$
θ_0	[-]	dimensionless temperature at the fin tip

Section 3.5

Notations

$k(T)$	[W.m^{-1}.K^{-1}]	thermal conductivity of the rectangular fin at temperature T
t	[-]	dummy variable
T_a	[K]	temperature of the surroundings

T_b	[K]	temperature at the base of the rectangular fin
x	[m]	distance from the tip of the rectangular fin
y	[-]	function of θ $\left(= p^2 = \left(\dfrac{d\theta}{d\xi}\right)^2\right)$
z	[-]	dummy variable

Greek letters

η	[-]	fin efficiency
η_{max}	[-]	maximum possible value of the fin efficiency
η_{min}	[-]	minimum possible value of the fin efficiency
θ	[-]	dimensionless temperature $\left(= \dfrac{T - T_a}{T_b - T_a}\right)$
θ_0	[-]	dimensionless temperature at the tip of the rectangular fin
θ_{0crit}	[-]	dimensionless temperature at fin tip corresponding to N_{max}

ROTARY KILN AND FLUID FLOW PROCESS
– ANALYTICAL SOLUTIONS

4.0   INTRODUCTION

This chapter is concerned with the development of analytical solutions of the model equations of rotary kiln and fluid flow process. The model equation of rotary kiln is used to determine the bed depth profile of solids flowing in it, whereas the model equation of fluid flow process describes the Poiseuille and Couette-Poiseuille flow of the third grade fluid between two parallel plates, and may be used to compute the velocity profile.

In literature, several researchers have obtained the approximate solutions of these model equations by using various approximate methods. However, to the best of our knowledge, analytical solutions of these model equations have not yet been found.

For obtaining analytical solutions, analytical methods, namely separation of variables method, partial fraction decomposition method, and derivative substitution method, have been used independently or in a combination of two of them. The obtained analytical solutions have been validated with the numerical solutions as well as with the approximate solutions available in literature. Besides, an existing experimental study, pertaining to the axial transport of solids in a rotary kiln, has been simulated by using the derived analytical solution.

4.1   ROTARY KILN

In this section, the model equation of a rotary kiln, also referred to as Saeman's nonlinear ODE model (Liu et al., 2009), has been solved analytically by using separation of variables and partial fraction decomposition methods.

4.1.1 Model Equation

The mechanistic model equation of Saeman considers that the bed depth profile is influenced by several factors: the dimensions of the kiln [L, R and h_0], the operating conditions [$\dot{m}$, n and β] and the properties of the flowing solids [ρ and θ]. Mathematically, this model equation is represented by a nonlinear first order ODE constituting an IVP and has been presented below. For brevity, the details of the derivation of this model equation have been omitted and the reader is referred to the original work (Saeman, 1951).

Consider a rotary kiln with radius R and length L, inclined with the horizontal at an angle β and spinning at an angular speed n, as shown in Fig. 4.1. The granular material having density ρ, particle diameter d and dynamic angle of repose θ, is being fed to the upper end of the kiln with a mass flow rate $\dot{m}$. Due to the inclination and rotation, the solids move downward spiralling. Based on the geometry and the mechanism involved in the movement of the particles, the profile of solid bed depth along the kiln length is represented by the following equation (Saeman, 1951; Kramers and Croockewit, 1952; Liu et al, 2009).

$$\frac{dh}{dx} = \frac{3\tan(\theta)}{4\pi n}\frac{\dot{m}}{\rho}[R^2 - (h-R)^2]^{-3/2} - \frac{\tan(\beta)}{\cos(\theta)} \tag{4.1a}$$

where h is the solid bed depth at the axial distance x from the discharge end [$x = 0$]. The associated initial condition is given by the solid bed depth at the discharge end [$x = 0$], and is equal to the height of the dam if present, i.e.

IC: $h(0) = h_0$ [height of the dam] \hfill (4.1b)

In case of the absence of dam, the solid bed depth at the discharge end is taken equal to the particle diameter d, i.e.

IC: $h(0) = d$ \hfill (4.1b')

The solid bed depth h can also be expressed in terms of the fill angle ε and the radius of kiln R, as shown below (Liu et al., 2009):

$$h = R[1 - \cos(\varepsilon)] \tag{4.2}$$
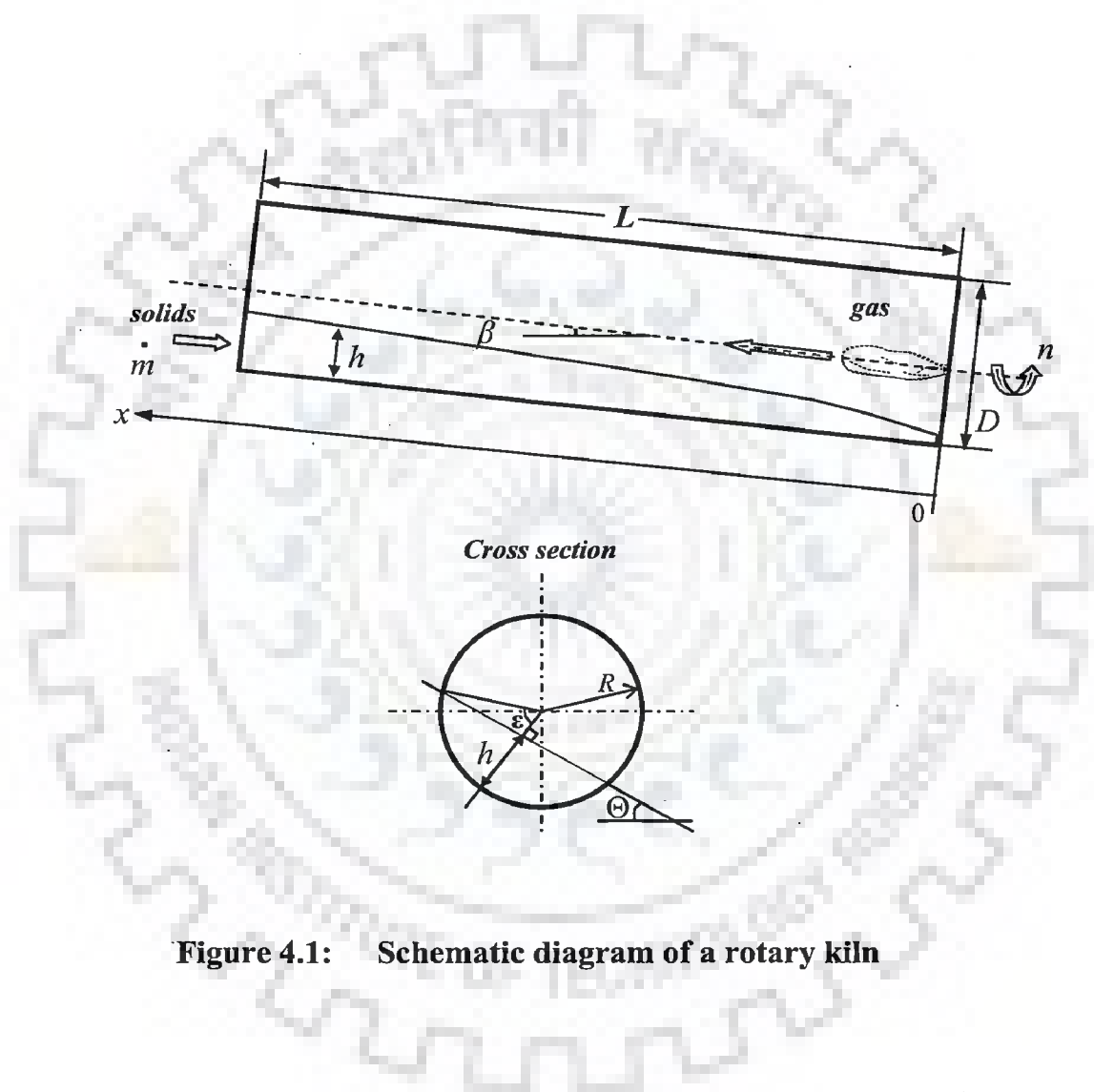
Figure 4.1: Schematic diagram of a rotary kiln

Substitution of this relation in Eq. (4.1a) yields the following equation (Liu et al., 2009):

$$\frac{d\varepsilon}{dx} = \frac{3\tan(\theta)}{4\pi nR^4}\frac{\dot{m}}{\rho}\frac{1}{\sin^4(\varepsilon)} - \frac{\tan(\beta)}{R\cos(\theta)}\frac{1}{\sin(\varepsilon)}$$ (4.3a)

and the allied IC becomes:

IC: $\quad \varepsilon = \varepsilon_0 = cos^{-1}[1 - \frac{h(0)}{R}] = cos^{-1}[1 - \frac{h_0}{R}]$, if dam is present, (4.3b)

otherwise

IC: $\quad \varepsilon = \varepsilon_0 = cos^{-1}[1 - \frac{h(0)}{R}] = cos^{-1}[1 - \frac{d}{R}]$, if dam is not present. (4.3b')

4.1.2 Solution and Discussion: Bed Depth Profile

Before finding the analytical solution of Eq. (4.3a), it is convenient to express it into the following dimensionless form:

$$\frac{d\varepsilon}{dX} = \frac{a}{\sin^4(\varepsilon)} - \frac{b}{\sin(\varepsilon)}$$ (4.4)

where a and b are the dimensionless constants, and are given by $a = \dfrac{3\tan(\theta)L}{4\pi nR^4}\dfrac{\dot{m}}{\rho}$

and $b = \dfrac{L\tan(\beta)}{R\cos(\theta)}$, respectively. $X = \dfrac{x}{L}$ is the dimensionless axial distance from the discharge end.

Eq. (4.4) can be rearranged into the following form:

$$\left(\frac{\sin^4(\varepsilon)}{a - b\sin^3(\varepsilon)}\right)d\varepsilon = dX$$ (4.5)

After performing the polynomial division of the bracketed term, one obtains:

$$\frac{-\sin(\varepsilon)}{b}d\varepsilon - \frac{a}{b^2}\left(\frac{\sin(\varepsilon)}{\sin^3(\varepsilon) - \dfrac{a}{b}}\right)d\varepsilon = dX$$ (4.6)

By decomposing the bracketed term, the Eq. (4.6) can further be represented as follows:

$$\frac{-\sin(\varepsilon)}{b}d\varepsilon - \frac{a}{b^2}\left(\frac{\sin(\varepsilon)}{(\sin(\varepsilon)-r_1)(\sin(\varepsilon)-r_2)(\sin(\varepsilon)-r_3)}\right)d\varepsilon = dX \qquad (4.7)$$

where r_1, r_2 and r_3 are the roots of the cubic equation: $\sin^3(\varepsilon)-\frac{a}{b}=0$, or $r^3-\frac{a}{b}=0$,

and are given by the following expressions:

$$r_1=\left(\frac{a}{b}\right)^{\frac{1}{3}}, \quad r_2=-(-1)^{\frac{1}{3}}\left(\frac{a}{b}\right)^{\frac{1}{3}}, \quad r_3=(-1)^{\frac{2}{3}}\left(\frac{a}{b}\right)^{\frac{1}{3}} \qquad (4.8)$$

Since $a>0$ and $b>0$, it is clear that one of the roots will be real and positive [say r_1], whereas, the remaining two roots will be imaginary [say r_2 and r_3]. This means all the three roots are distinct, and thereby render the process of partial fraction decomposition very simple. Now, the partial fraction decomposition of the bracketed term in Eq. (4.7) is carried out and the following equation is obtained:

$$\frac{-\sin(\varepsilon)}{b}d\varepsilon - \frac{a}{b^2}\left(\frac{r_1}{(r_1-r_2)(r_1-r_3)(\sin(\varepsilon)-r_1)}\right)d\varepsilon - \frac{a}{b^2}\left(\frac{r_2}{(r_2-r_1)(r_2-r_3)(\sin(\varepsilon)-r_2)}\right)d\varepsilon$$

$$-\frac{a}{b^2}\left(\frac{r_3}{(r_3-r_1)(r_3-r_2)(\sin(\varepsilon)-r_3)}\right)d\varepsilon = dX \qquad (4.9)$$

Eq. (4.9) is integrated with respect to X between the limits: ε_0 at $X=0$ and ε at X, i.e.

$$\int_{\varepsilon_0}^{\varepsilon}\frac{-\sin(\varepsilon)}{b}d\varepsilon - \frac{a}{b^2}\frac{r_1}{(r_1-r_2)(r_1-r_3)}\int_{\varepsilon_0}^{\varepsilon}\frac{d\varepsilon}{(\sin(\varepsilon)-r_1)} - \frac{a}{b^2}\frac{r_2}{(r_2-r_1)(r_2-r_3)}\int_{\varepsilon_0}^{\varepsilon}\frac{d\varepsilon}{(\sin(\varepsilon)-r_2)}$$

$$-\frac{a}{b^2}\frac{r_3}{(r_3-r_1)(r_3-r_2)}\int_{\varepsilon_0}^{\varepsilon}\frac{d\varepsilon}{(\sin(\varepsilon)-r_3)} = \int_{0}^{X}dX$$

Integration of the above equation is straightforward and the following results are obtained:

$$\left.\frac{b\cos(\varepsilon)}{2a}\right|_{\varepsilon_0}^{\varepsilon} - \frac{r_1}{(r_1-r_2)(r_1-r_3)}\frac{1}{\sqrt{r_1^2-1}}\tan^{-1}\left[\frac{1-r_1\tan\left(\dfrac{\varepsilon}{2}\right)}{\sqrt{r_1^2-1}}\right]\Biggr|_{\varepsilon_0}^{\varepsilon}$$

$$-\frac{r_2}{(r_2-r_1)(r_2-r_3)}\frac{1}{\sqrt{r_2^2-1}}\tan^{-1}\left[\frac{1-r_2\tan\left(\dfrac{\varepsilon}{2}\right)}{\sqrt{r_2^2-1}}\right]\Biggr|_{\varepsilon_0}^{\varepsilon}$$

$$-\frac{r_3}{(r_3-r_1)(r_3-r_2)}\frac{1}{\sqrt{r_3^2-1}}\tan^{-1}\left[\frac{1-r_3\tan\left(\dfrac{\varepsilon}{2}\right)}{\sqrt{r_3^2-1}}\right]\Biggr|_{\varepsilon_0}^{\varepsilon} = \frac{b^2 X}{2a}$$

After substituting the limits, one gets the following implicit analytical solution of ε:

$$\frac{b(\cos(\varepsilon)-\cos(\varepsilon_0))}{2a} - \frac{r_1}{(r_1-r_2)(r_1-r_3)}\frac{1}{\sqrt{r_1^2-1}}\left(\tan^{-1}\left[\frac{1-r_1\tan(\varepsilon/2)}{\sqrt{r_1^2-1}}\right] - \tan^{-1}\left[\frac{1-r_1\tan(\varepsilon_0/2)}{\sqrt{r_1^2-1}}\right]\right)$$

$$-\frac{r_2}{(r_2-r_1)(r_2-r_3)}\frac{1}{\sqrt{r_2^2-1}}\left(\tan^{-1}\left[\frac{1-r_2\tan(\varepsilon/2)}{\sqrt{r_2^2-1}}\right] - \tan^{-1}\left[\frac{1-r_2\tan(\varepsilon_0/2)}{\sqrt{r_2^2-1}}\right]\right)$$

$$-\frac{r_3}{(r_3-r_1)(r_3-r_2)}\frac{1}{\sqrt{r_3^2-1}}\left(\tan^{-1}\left[\frac{1-r_3\tan(\varepsilon/2)}{\sqrt{r_3^2-1}}\right] - \tan^{-1}\left[\frac{1-r_3\tan(\varepsilon_0/2)}{\sqrt{r_3^2-1}}\right]\right)$$

$$= \frac{b^2 X}{2a} \tag{4.10}$$

For the evaluation of ε for each X, the above Eq. (4.10) can easily be solved numerically by using any of the available soft computing tools, e.g. MATLAB, MATHEMATICA and MAPLE. Once ε is known, the solid bed depth can be found by using the Eq. (4.2).

(i) Comparison between the analytical, numerical and experimental results

For the comparison of analytical results [AS] with the numerical results [NS] and with the existing experimental results, several experimental conditions have been selected from various sources (Lebas et al., 1995; Spurling et al., 2001; Scott et al., 2008; Liu et al., 2009). These experimental conditions have been presented in Table 4.1 and the corresponding experimental bed depth profiles have been shown [by symbols] in Figs. 4.2 - 4.8. These experimental values of bed depth profiles have been read from various figures plotted in the respective references with the help of a user-friendly software "Plot Digitizer" available online for free. Moreover, these figures have been shown in the same format in which these appeared in the concerned reference. This is because: (i) visual comparison of the figures may be easy and (ii) the experimental values read with the help of "Plot Digitizer" remains intact. For the same experimental conditions, the bed depth profiles have been calculated by using the analytical solution [Eq. (4.10)], and the obtained results are also plotted in Figs. 4.2 - 4.8. Numerical results have also been obtained by solving the original Eqs. (4.3a), (4.3b) or (4.3b') with the help of a soft computing tool, i.e. MATHEMATICA. For this we have written a computer code in the programming language of MATHEMATICA, in which the inbuilt command "NDSolve" has been used. The numerical values thus obtained have also been shown in Figs. 4.2 - 4.8. These figures clearly show that the results obtained by using the analytical solution match well with the numerically obtained results as well as with the experimental results, and thus validate the analytical solution.

(ii) Comparison between the analytical solution and the approximate solution of Liu et al. (2009)

The Eq. (4.4) has recently been solved by Liu et al. (2009) in an approximate manner to yield the approximate implicit solution of the solid bed depth profile. In their work, Liu et al. (2009) have approximated ε [in Eq. (4.4)] by "$0.39\sin^2(\varepsilon)+0.86\sin(\varepsilon)$" and obtained the following form of Eq. (4.4).

$$(0.78\sin(\varepsilon)+0.86)\frac{d\sin(\varepsilon)}{dX} = \frac{a}{\sin^4(\varepsilon)} - \frac{b}{\sin(\varepsilon)} \tag{4.11}$$

Table 4.1: Experimental data used for simulation

Data No.	Source		Mass feed rate $\dot{m}$ (kg/s)	Bulk density of solids ρ (kg/m³)	Dynamic angle of repose of solids θ (deg)	Radius of kiln R (m)	Length of rotary kiln L (m)	Inclination of kiln β (deg)	Dam height h_0 (m)	Rotation speed n (rps)	$\mu = r_1 = \left(\dfrac{a}{h}\right)^{1/3}$	Present Fig. No.
	Reference	Fig. No.										
1	Spurling et al. (2001)	3	2.45×10⁻³	1600	32	0.0515	1	1	0	0.0855	0.9831	4.2
2	Spurling et al. (2001)	4	0.65×10⁻³	1600	32	0.0515	1	1	0	0.0855	0.6317	4.2
3	Spurling et al. (2001)	5	3.1×10⁻³	1600	32	0.0515	1	1	0	0.119	0.7559	4.2
4	Spurling et al. (2001)	6	3.15×10⁻³	1600	32	0.0515	1	2	0	0.0595	0.9574	4.3
5	Spurling et al. (2001)	7	3×10⁻³	1600	32	0.0515	1	4	0	0.0862	0.6605	4.3
6	Spurling et al. (2001)	8	3.05×10⁻³	1600	32	0.0515	1	2	0	0.0842	0.8436	4.3
7	Scott et al. (2008)	3	1.5×10⁻³	1600	32	0.0515	1	1	0.0115	0.097	0.8004	4.4
8	Scott et al. (2008)	3	1×10⁻³	1600	32	0.0515	1	1	0.0115	0.097	0.6992	4.4
9	Scott et al. (2008)	3	0.56×10⁻³	1600	32	0.0515	1	1	0.0115	0.097	0.5764	4.4
10	Scott et al. (2008)	3	0.1×10⁻³	1600	32	0.0515	1	1	0.0115	0.097	0.3246	4.4
11	Lebas et al. (1995)	11	80.556×10⁻³	750	37	0.3	6	1	0	0.0333	0.9941	4.5
12	Lebas et al. (1995)	11	80.556×10⁻³	750	37	0.3	6	1	0	0.05	0.8684	4.5
13	Lebas et al. (1995)	11	80.556×10⁻³	750	37	0.3	6	1	0	0.0667	0.7890	4.5
14	Lebas et al. (1995)	12	68.333×10⁻³	750	37	0.3	6	1	0	0.05	0.8220	4.6
15	Lebas et al. (1995)	12	97.222×10⁻³	750	37	0.3	6	1	0	0.05	0.9246	4.6
16	Lebas et al. (1995)	12	133.333×10⁻³	750	37	0.3	6	1	0	0.05	1.0272	4.6
17	Liu et al. (2009)	3	1.5×10⁻³	1600	32	0.0525	1	1	0.0125	0.097	0.7852	4.7
18	Liu et al. (2009)	3	1.0×10⁻³	1600	32	0.0525	1	1	0.0125	0.097	0.6859	4.7
19	Liu et al. (2009)	3	0.56×10⁻³	1600	32	0.0525	1	1	0.0125	0.097	0.5654	4.7
20	Liu et al. (2009)	3	0.1×10⁻³	1600	32	0.0525	1	1	0.0125	0.097	0.3184	4.8
21	Liu et al. (2009)	4	3.69×10⁻³	2500	27.4	0.0525	5.9	1.37	0.015	0.0167	1.0081	4.8
22	Liu et al. (2009)	4	3.69×10⁻³	2500	27.4	0.0735	5.9	1.37	0.015	0.05	0.6990	4.8

137
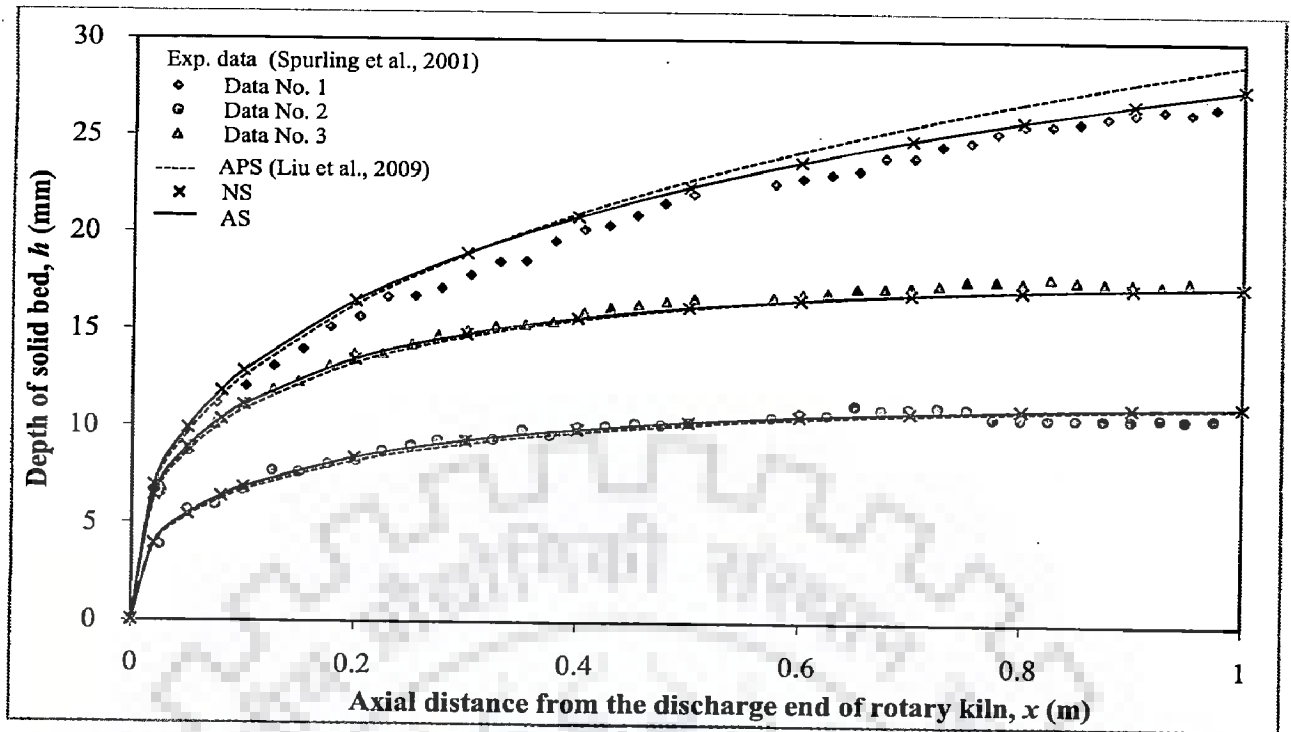
Figure 4.2: Solid bed depth profiles along the length of the rotary kiln
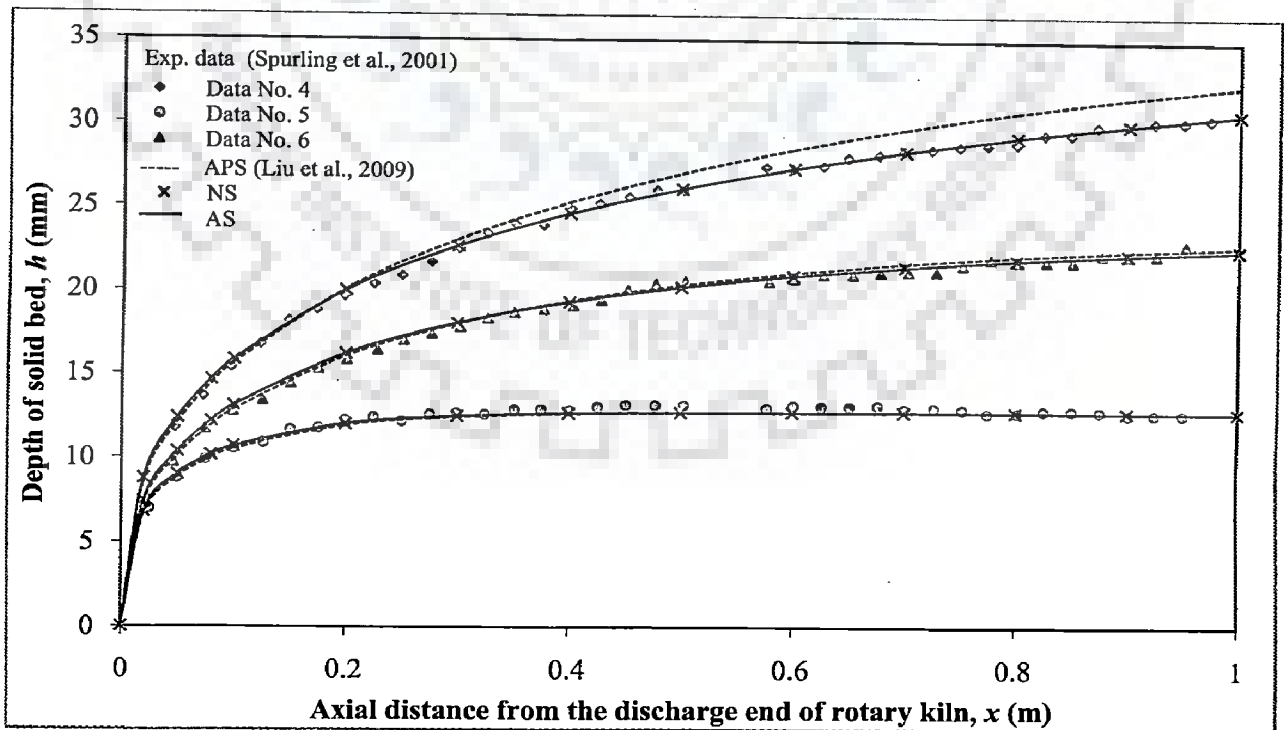
Figure 4.3: Solid bed depth profiles along the length of the rotary kiln
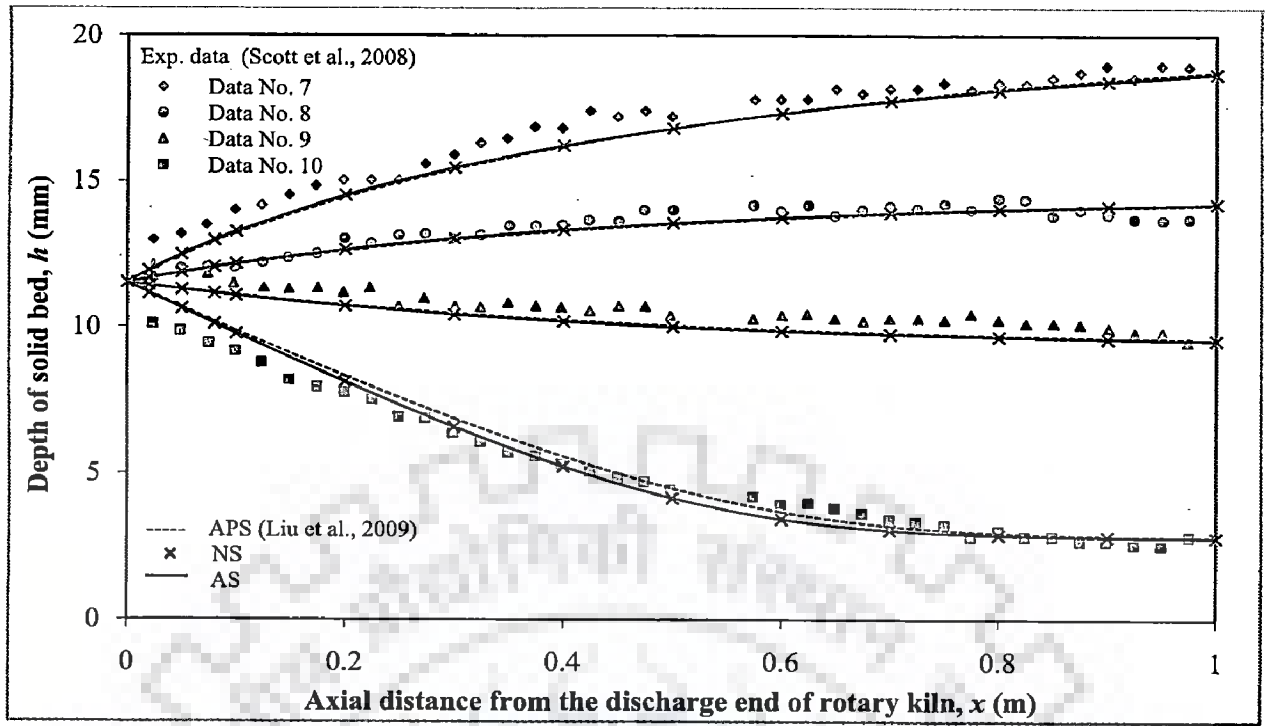
Figure 4.4: Solid bed depth profiles along the length of the rotary kiln
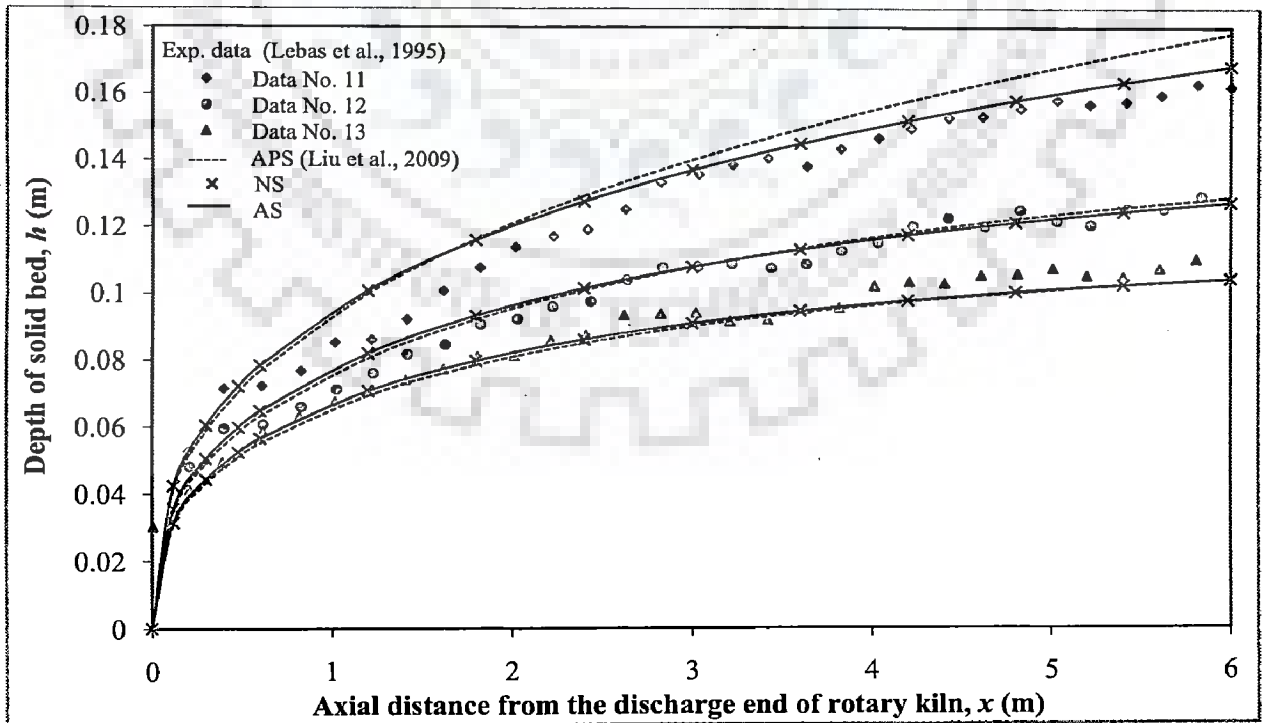
Figure 4.5: Solid bed depth profiles along the length of the rotary kiln
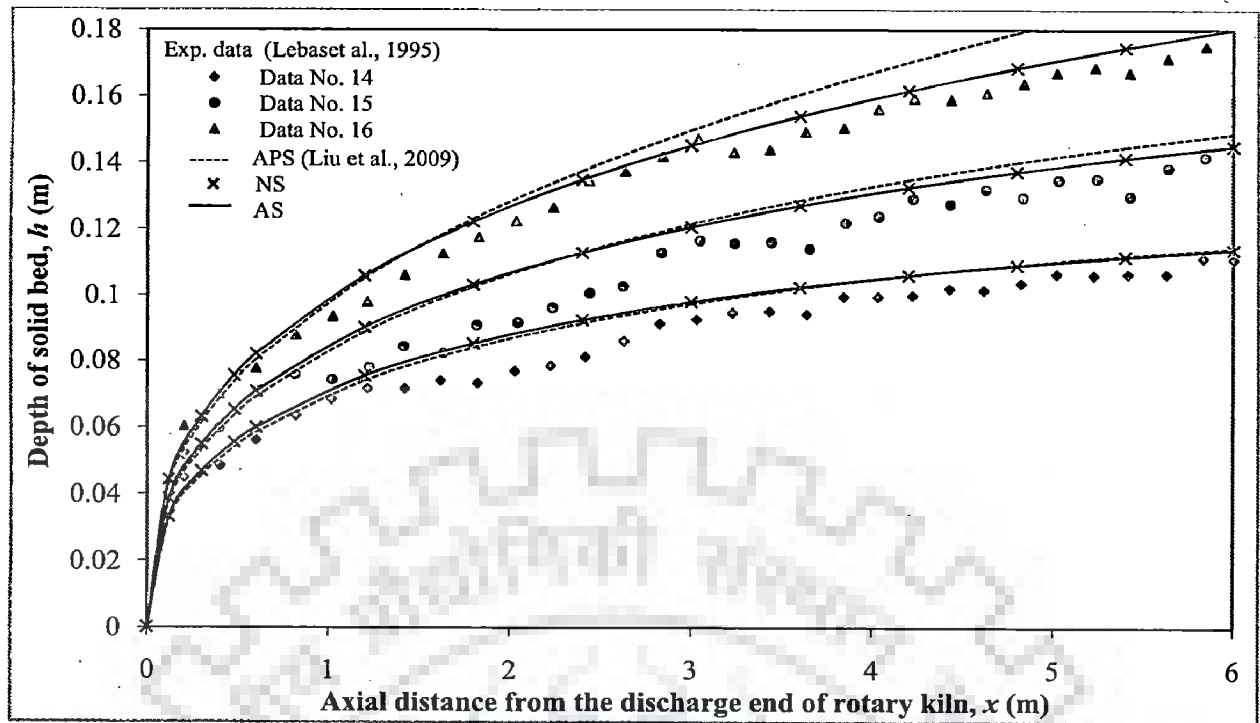
Figure 4.6: Solid bed depth profiles along the length of the rotary kiln
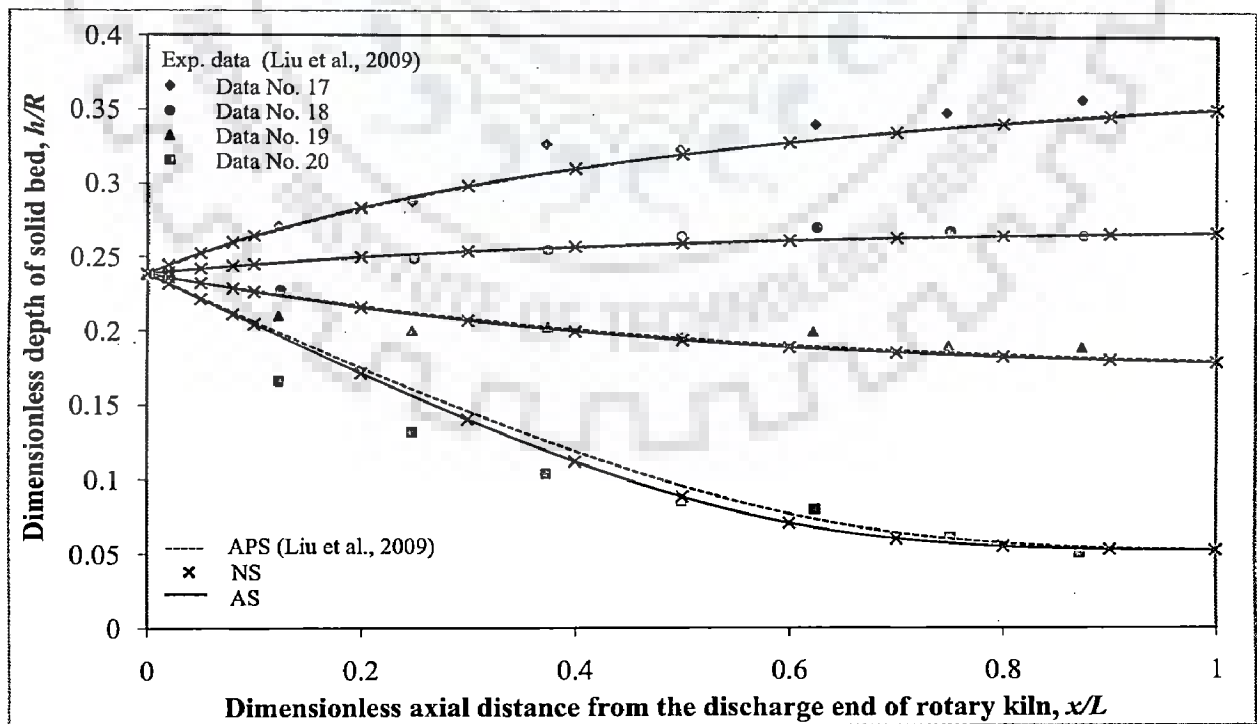
Figure 4.7: Dimensionless solid bed depth profiles along the dimensionless length of the rotary kiln
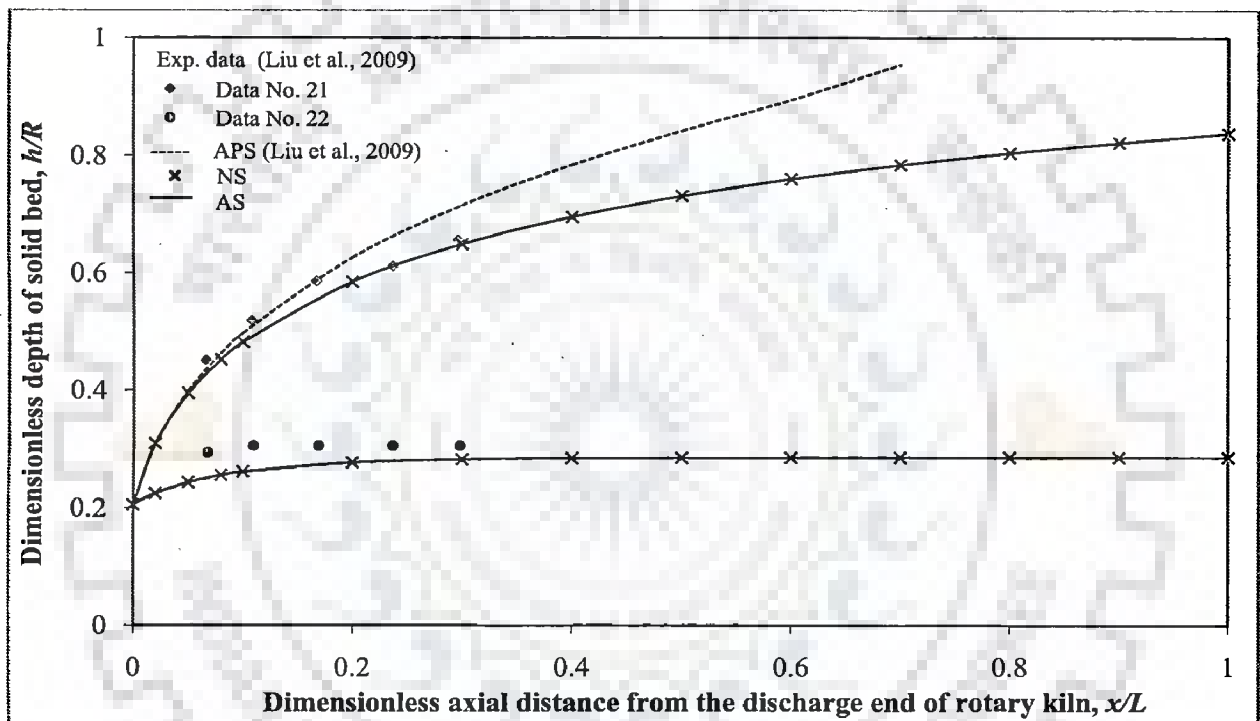
Figure 4.8: Dimensionless solid bed depth profiles along the dimensionless length of the rotary kiln

It can be observed that by using the above approximation for ε, these researchers were successful in retaining the dependent variable in the form of "$\sin(\varepsilon)$" only, instead of both ε and $\sin(\varepsilon)$. Due to this modification, the original Eq. (4.4) got transformed into the above easily solvable form. For convenience, we reproduce below the solution of Eq. (4.11) as obtained by Liu et al. (2009).

$$0.14\frac{a}{b^2\mu}ln\left[\frac{(Y^2+\mu Y+\mu^2)(\mu-Y_0)^2}{(Y_0^2+\mu Y_0+\mu^2)(\mu-Y)^2}\right]+0.26\frac{(Y_0^3-Y^3)}{b}+0.43\frac{(Y_0^2-Y^2)}{b}+0.26ln\left(\left|\frac{(bY_0^3-a)}{bY^3-a}\right|\right)$$

$$+0.5\frac{a}{b^2\mu}\left[\tan^{-1}\left(1.15\frac{Y_0}{\mu}+0.58\right)-\tan^{-1}\left(1.15\frac{Y}{\mu}+0.58\right)\right]=X \qquad (4.12)$$

where $Y=\sin(\varepsilon)$, $Y_0=\sin(\varepsilon_0)$ and $\mu=\left(\frac{a}{b}\right)^{1/3}$.

For the purpose of comparison, we have found the bed depth profile by using the above approximate solution for the same experimental data as listed in Table 4.1. The obtained approximate results [APS] have also been shown in Figs. 4.2 - 4.8. It is clearly visible from these figures that in most of the cases, the results obtained by using the approximate solution of Liu et al. (2009), i.e. Eq. (4.12), successfully match with the analytical results, the numerical results as well as with the experimental results. These cases are present in all of the Figs. 4.2 - 4.8, i.e. bed depth profiles for data numbers 2 and 3 in Fig. 4.2; for data numbers 5 and 6 in Fig. 4.3; for data numbers 7-9 in Fig. 4.4; for data numbers 12 and 13 in Fig. 4.5; for data numbers 14 and 15 in Fig. 4.6; for data numbers 17-19 in Fig. 4.7 and for data number 22 in Fig. 4.8. However, in some cases the bed depth profiles show some deviation from the true values, e.g. profiles corresponding to the data number 1 in Fig. 4.2, data number 4 in Fig. 4.3, data number 10 in Fig. 4.4, data number 11 in Fig. 4.5, data number 16 in Fig. 4.6, data number 20 in Fig. 4.7 and data number 21 in Fig. 4.8. Such discrepancies in the predictions of approximate solution appear in case of (i) higher filling ratio [25% corresponding to $\varepsilon\geq65.89$ deg or $\mu\geq0.91$] or (ii) lower filling ratio [0.9% corresponding to $\varepsilon\leq20.05$ deg or $\mu\leq0.4$]. This fact can also be observed from the corresponding values of μ shown in Table 4.1. The former situation emerges when the bed depth profile is increasing, whilst the latter one occurs when the bed depth profile is decreasing. These

deviations in the prediction of approximate solution are due to the restricted validity of the approximated form of the nonlinearity as assumed by Liu et al. (2009), i.e. $\varepsilon \approx 0.39\sin^2(\varepsilon) + 0.86\sin(\varepsilon)$. It can be noted that the percentage error in this approximation decreases monotonically from 12 % at $\varepsilon = 2.86$ deg to -0.35% at $\varepsilon = 28.65$ deg and then increases continuously to 17% at $\varepsilon = 85.94$ deg. These errors in the approximation of ε are quite significant from the view point of accuracy, as the subsequent operation, e.g. integration, may further enhance the errors in some cases. Nevertheless, the optimum range, for this approximation to be valid, is found to be lying between $\varepsilon = 20.05$ deg [$\mu \approx 0.4$] to $\varepsilon = 65.89$ deg [$\mu \approx 0.91$].

It is noteworthy that Liu et al. (2009) have also pointed out the first type of the discrepancy, i.e. the one arising due to the higher filling ratio, and reported that their approximate solution deviates from the numerical solution in the case of higher filling ratio [25% corresponding to $\varepsilon \geq 65.89$ deg or $\mu \geq 0.91$]. On the contrary, the results obtained by using the analytical solution are found to be in good harmony with the numerical results as well as with the experimental values for all the cases considered herein. Therefore, the analytical solution, being valid for the entire range, has wider applicability as compared to the approximate solution of Liu et al. (2009), especially in those cases where ε [or μ] may lie outside the optimum range set for the approximate solution. Moreover, since the rotary kiln may also operate outside this optimum range [as also revealed from the data shown in Table 4.1], the use of analytical solution becomes essential, and this establishes the usefulness of the analytical solution.

Since both the present analytical solution and the approximate solution of Liu et al. (2009), are implicit in forms, therefore, these have to be solved numerically with the help of some mathematical soft tools, e.g. MATHEMATICA, MAPLE, MATLAB. However, it should be noted that these soft computing tools require the initial estimate of the unknown variable(s), while solving the nonlinear algebraic equation(s), and care should be taken in selecting the initial guess before solving the nonlinear algebraic equation(s). Otherwise, the solution may either give imaginary or even unrealistic multiple roots. Unfortunately, this fact is true for both the solutions, i.e. the analytical solution [Eq. (4.10)], and the approximate solution [Eq. (4.12)].

Here it is important to mention that we have not considered the approximate solution of Kramers and Croockewit (1952) to find the bed depth profile, since it is

reported in the literature that under certain circumstances it can exhibit up to 50% error in its prediction (Liu et al. 2009).

(iii) Analysis of the effect of various parameters

Several independent numerical experiments have also been carried out to study the effect of various parameters on the bed depth profile, and a careful analysis of the obtained results is summarized below:

- The dimensionless bed depth $\left[h/R\right]$ is found to be dependent on three dimensionless variables, namely a, b and ε_0.

- For a fixed value of ε_0 [or $h(0)$], the dimensionless bed depth $\left[h/R\right]$ increases with the increase in a and vice-versa, and the reverse is true for b, i.e. h/R decreases with the increase in b and vice-versa. This also means that by properly manipulating these two variables, their effect can be neutralized, and one can achieve a constant bed depth. These facts can also be verified from the following Eqs. (4.14a)-(4.14c).

- Whether the bed depth first increases or decreases, it eventually reaches a constant value after certain length of the kiln and that minimum length in dimensionless form is given by the following Eq. (4.15).

Along with the bed depth profile, other useful information are:

- Maximum/minimum depth reached by the bed

- Increasing/decreasing trend of the bed depth profile

- Minimum kiln length after which the bed depth remains static.

The maximum/minimum depth reached by the bed is easily obtained by forcing the $\frac{dh}{dx} = 0$ in Eq. (4.1a) and simplifying the resultant equation. The maximum/minimum bed depth is given by:

$$h_{\text{max/min}} = R(1-\sqrt{1-r_1^2}) = R(1-\sqrt{1-\mu^2})$$ (4.13)

In a similar fashion, the following inequalities, deciding the increasing or decreasing trend of the bed depth profile, can also be obtained.

- Bed depth will be higher than the dam height, i.e. $\dfrac{dh}{dx} > 0$, if

$$\sin(\varepsilon_0) < \mu^{1/3} \quad \text{or} \quad \sqrt{1-\left(1-\frac{h(0)}{R}\right)^2} < \mu$$ (4.14a)

- Bed depth will be lower than the dam height, i.e. $\dfrac{dh}{dx} < 0$, if

$$\sin(\varepsilon_0) > \mu^{1/3} \quad \text{or} \quad \sqrt{1-\left(1-\frac{h(0)}{R}\right)^2} > \mu$$ (4.14b)

- Bed depth will be same throughout the kiln length as that of the end constriction [dam height], i.e. $\dfrac{dh}{dx} = 0$, if

$$\sin(\varepsilon_0) = \mu^{1/3} \quad \text{or} \quad \sqrt{1-\left(1-\frac{h(0)}{R}\right)^2} = \mu$$ (4.14c)

These observations and equations are in agreement with those reported by Liu et al. (2009). As far as the minimum kiln length corresponding to $h_{\text{max/min}}$ is concerned, it is found by substituting $h_{\text{max/min}}$ [Eq. (4.13)] along with the use of Eq. (4.2) into Eq. (4.10), and simplifying the resultant equation. The following expression for minimum kiln length is found:

$$X_{\text{min}} = \frac{\cos(\varepsilon_{\text{max/min}}) - \cos(\varepsilon_0)}{b}$$

$$+ \frac{2\mu^3 r_1}{b(r_1-r_2)(r_1-r_3)\sqrt{r_1^2-1}}\left(\tan^{-1}\left[\frac{1-r_1\tan\left[\frac{\varepsilon_0}{2}\right]}{\sqrt{r_1^2-1}}\right] - \tan^{-1}\left[\frac{1-r_1\tan\left[\frac{\varepsilon_{\text{max/min}}}{2}\right]}{\sqrt{r_1^2-1}}\right]\right)$$

$$+\frac{2\mu^3 r_2}{b(r_1-r_2)(r_2-r_3)\sqrt{r_2^2-1}}\left(\tan^{-1}\left[\frac{1-r_2\tan\left[\frac{\varepsilon_0}{2}\right]}{\sqrt{r_2^2-1}}\right]-\tan^{-1}\left[\frac{1-r_2\tan\left[\frac{\varepsilon_{max/min}}{2}\right]}{\sqrt{r_2^2-1}}\right]\right)$$

$$+\frac{2\mu^3 r_3}{b(r_1-r_3)(r_2-r_3)\sqrt{r_3^2-1}}\left(\tan^{-1}\left[\frac{1-r_3\tan\left[\frac{\varepsilon_0}{2}\right]}{\sqrt{r_3^2-1}}\right]-\tan^{-1}\left[\frac{1-r_3\tan\left[\frac{\varepsilon_{max/min}}{2}\right]}{\sqrt{r_3^2-1}}\right]\right)$$

$$(4.15)$$

where $\varepsilon_{max/min}=\cos^{-1}(\sqrt{1-\mu^2})$.

4.1.3 A Case Study

In this subsection, we illustrate the use of the presently derived analytical solution to find the bed depth profile for one of the experimental runs [for data no. 7 in Table 4.1]. Corresponding to this experimental condition, the experimentally obtained bed depth profile has been shown in Fig. 4.4. The procedure starts with the evaluation of ε_0, which is obtained by using Eq. (4.3b), and for the selected experimental condition [data number 7 in Table 4.1], it is found that: $\varepsilon_0=39.04$ deg. Thereafter, the dimensionless constants a [=0.204961] and b [=0.399663] are evaluated. Once the values of a and b are available, the roots of the cubic equation $r^3-\frac{a}{b}=0$ are found with the help of Eq. (4.8), and are given below.

$$r_1=0.800435$$

$$r_2=-0.400217-0.693197i$$

$$r_3=-0.400217+0.693197i$$

Substituting these values in the Eq. (4.10), one obtains the following nonlinear algebraic equation:

151

$$-(0.669902-0.590535i)\tan^{-1}[(0.165119+0.819124i)+(0.633898+0.213367i)\tan(\varepsilon/2)]$$

$$-(0.590535-0.669902i)\tanh^{-1}[(0.819124+0.165119i)+\tan(\varepsilon/2)]+2.50211\cos[\varepsilon]$$

$$+1.78293\tanh^{-1}[1.668828(1-0.800435\tan(\varepsilon/2))]+(-2.16534+2.80063i)=X$$

$$(4.16)$$

In Eq. (4.16), the value of ε for a given X can be found numerically. For example, for $X = 0.3$ the value of ε is found to be 45.59 deg, which corresponds to the bed depth $h = 0.0154601\,\mathrm{m}$. It can be verified that exactly the same value of h is found from the numerical method for the same value of X. This is also evident from Fig. 4.4 for data number 7. In a similar way the whole profile for the bed depth can be obtained.

4.2 FLUID FLOW PROCESS

In this section, the model equations describing the Poiseuille and the Couette-Poiseuille flow of a third grade fluid between two parallel plates have been solved analytically by using the derivative substitution method. The explicit analytical solutions of the velocity profile and the flow rate have been obtained for all the flow situations arising herein. The pure Couette flow of third grade fluid has not been considered, since the analytical solution for this flow process has already been given by Siddiqui et al. (2008b).

4.2.1 Model Equation

Consider the Fig. 4.9, in which the flow of a third grade fluid between two parallel plates separated by a distance $2h$, is shown. The fluid movement is caused by (i) the pressure gradient resulting in the Poiseuille flow, and/or (ii) the movement of one of the plates [say upper plate], resulting in the Couette flow. It is assumed that the steady state and the isothermal conditions are prevailing, and the fluid properties [density, viscosity] are constant. With these assumptions, the application of mass and momentum balances along with the constitutive equations of third grade fluid results in the following model equation. For briefness, the details of derivation have been avoided here and are given in Appendix B1.
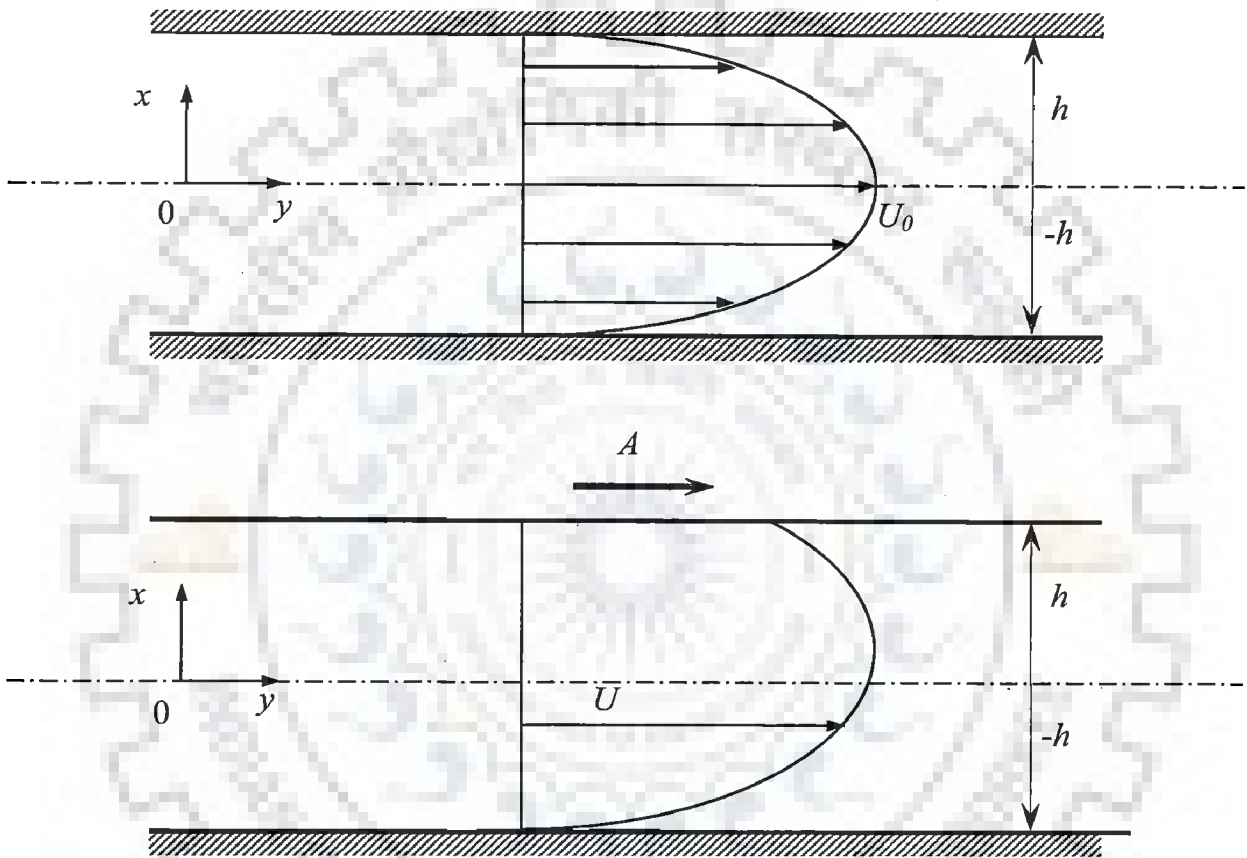
Figure 4.9:   Pure Poiseuille Flow and Couette-Poiseuille Flow

$$\frac{d\hat{p}}{dy} = \mu\frac{d^2u}{dx^2} + 6(\beta_2 + \beta_3)\left(\frac{du}{dx}\right)^2\frac{d^2u}{dx^2} \qquad (4.17)$$

where $\hat{p}$ is the generalized pressure, β_2 and β_3 are the material moduli, μ is the coefficient of viscosity, and u is the nonzero velocity component in the y direction (Rajagopal and Sciubba, 1984; Siddiqui et al., 2008b). It should be noted that the Eq. (4.17) will remain unchanged while portraying the different flow situations arising in the current flow process. However, the allied BCs will differ from one situation to the other, and thus give rise to different analytical solutions for each of the situations. In the following subsection, these situations have been discussed in detail and the corresponding analytical solutions have been obtained.

4.2.2 Solutions and Discussion: Velocity Profile and Flow Rate

Basically, two main situations arise in the current flow process, i.e. the pure Poiseuille flow and the Couette-Poiseuille flow. These two situations have been divided into case 1 and case 2, respectively. In case 2, three situations appear, which have further been divided into three sub-cases, i.e. case 2(a) - case 2(c). For each of these situations, the corresponding analytical solutions [velocity profile and flow rate] as well as the discussion and comparison of the obtained analytical results, have been presented below.

4.2.2.1 Case 1: Pure Poiseuille Flow

In this situation, the movement of fluid is solely due to the pressure gradient and the flow is governed by the Eq. (4.17) along with the following BCs:

BC I: $u = 0$ at $x = h$ [upper stationary plate] $\qquad (4.18a)$

BC II: $u = 0$ at $x = -h$ [lower stationary plate] $\qquad (4.18b)$

The solution of Eq. (4.17) in conjunction with the above BCs yields the velocity profile for this case. It is convenient to nondimensionalize the Eqs. (4.17), (4.18a) and (4.18b) by defining the following dimensionless variables:

$$X = \frac{x}{h}, \quad \beta = (\beta_2 + \beta_3)\left(-\frac{d\hat{p}}{dy}\right)^2 \frac{h^2}{\mu^3}, \quad U = u \Big/ \left(-\frac{d\hat{p}}{dy}\frac{h^2}{\mu}\right)$$

Eventually, the following dimensionless forms of the Eqs. (4.17), (4.18a) and (4.18b) are obtained:

$$\frac{d^2U}{dX^2} + 6\beta\left(\frac{dU}{dX}\right)^2 \frac{d^2U}{dX^2} = -1 \qquad (4.19\text{a})$$

BC I: $U = 0$ at $X = 1$ [upper stationary plate] $\qquad (4.19\text{b})$

BC II: $U = 0$ at $X = -1$ [lower stationary plate] $\qquad (4.19\text{c})$

From the above BCs, it can be observed that the resultant velocity profile will be symmetric around $X = 0$, hence, one of the BCs [say BC II] can easily be replaced by the following equivalent BCII', i.e.

BC II': $\dfrac{dU}{dX} = 0$ at $X = 0$ [middle of the two plates] $\qquad (4.19\text{c}')$

Now, by using the transformation $\dfrac{dU}{dX} = f(U)$, where $f(U)$ is some unknown function of U, one finds $\dfrac{d^2U}{dX^2} = \dfrac{1}{2}\dfrac{d(f^2)}{dU}$. With these derivatives, the Eq. (4.19a), after slight rearrangement, is rendered into the following first order nonlinear ODE.

$$w'(1 + 6\beta w) = -2 \qquad (4.20)$$

where $w = f^2(U)$ and $w' = \dfrac{dw}{dU}$. Eq. (4.20) is easily amenable to the following analytical solution:

$$w + 3\beta w^2 = 2U + C_1 \qquad (4.21)$$

where C_1 is the constant of integration and by using the modified BCII', it is found to be $C_1 = 2U_0$. U_0 is the unknown dimensionless velocity at the centreline [$X = 0$]. Substituting C_1 in Eq. (4.21) and solving the quadratic equation for w, one obtains the following equation:

$$w = f^2 = (U')^2 = \frac{-1 \pm \sqrt{1 + 24\beta(U_0 - U)}}{6\beta} \tag{4.22}$$

In the above equation, the negative sign of the radical is dropped so as to avoid the imaginary value of the velocity gradient $[U']$, and the following expression is obtained for U':

$$U' = \frac{dU}{dX} = \pm\sqrt{\frac{-1 + \sqrt{1 + 24\beta(U_0 - U)}}{6\beta}} \tag{4.23}$$

The sign of U' is determined by the form of the velocity profile. For this case, the physically feasible velocity profile suggests that U' is positive for $-1 \le X < 0$, negative for $0 < X \le 1$ and zero at $X = 0$ [see Fig. 4.10]. Since velocity profile is symmetric about $X = 0$, hence, without any loss of generality one can select the region $0 \le X \le 1$, for which the Eq. (4.23) becomes:

$$U' = \frac{dU}{dX} = -\sqrt{\frac{-1 + \sqrt{1 + 24\beta(U_0 - U)}}{6\beta}} \qquad \text{for } 0 \le X \le 1 \tag{4.24}$$

The above equation is integrated between 0 to X, and the following integral is obtained:

$$\int_{U_0}^{U} \frac{-\sqrt{6\beta}\,dU}{\sqrt{-1 + \sqrt{1 + 24\beta(U_0 - U)}}} = \int_0^X dX \tag{4.25}$$

Solution of the above integral yields the following implicit analytical solution of U:

$$\frac{\sqrt{-1 + \sqrt{1 + 24\beta(U_0 - U)}}\left(2 + \sqrt{1 + 24\beta(U_0 - U)}\right)}{3\sqrt{6\beta}} = X \tag{4.26}$$

The unknown U_0 is found by forcing the above equation to satisfy the yet unutilized BC I, and one obtains the following implicit expression of U_0:

$$\frac{\sqrt{-1 + \sqrt{1 + 24\beta U_0}}\left(2 + \sqrt{1 + 24\beta U_0}\right)}{3\sqrt{6\beta}} = 1 \tag{4.27}$$

Fortunately, U_0 in the above equation can be represented explicitly. However, it is observed that three explicit solutions exist for U_0 and only one of them is real. The remaining two solutions are complex conjugates and have been ignored.

Considering only the real solution, the following explicit expression is obtained for U_0:

$$U_0 = \frac{1}{12\beta} - \frac{-1+108\beta}{24\beta\left(-1-270\beta +1458\beta^2 +6\sqrt{3}\sqrt{8\beta +324\beta^2 +4374\beta^3 +19683\beta^4}\right)^{1/3}}$$

$$+ \frac{\left(-1-270\beta +1458\beta^2 +6\sqrt{3}\sqrt{8\beta +324\beta^2 +4374\beta^3 +19683\beta^4}\right)^{1/3}}{24\beta}$$

$$(4.28)$$

In a similar manner, the implicit analytical solution of U [Eq. (4.26)] can also be expressed explicitly and the following explicit analytical solution of U is obtained. Like in the case of U_0, here too, the two complex conjugates relations appear for U. However, due to the complex nature, these two have been discarded.

$$U = \frac{1-T^2 +24U_0\beta}{24\beta} \qquad (4.29)$$

where $T = -1 + \dfrac{2^{1/3}}{\left(2+K_1^2X^2 +\sqrt{4K_1^2X^2 + K_1^4X^4}\right)^{1/3}} + \dfrac{\left(2+K_1^2X^2 +\sqrt{4K_1^2X^2 + K_1^4X^4}\right)^{1/3}}{2^{1/3}}$

and $K_1 = -3\sqrt{6\beta}$.

Now, for a given value of β, one can directly find U_0 and U with the help of Eqs. (4.28) and (4.29), respectively.

Another important quantity, from the viewpoint of pumps and piping design, is the flow rate. The flow rate per unit width of the plates is given by the following equation:

$$q = \int_{-h}^{h} u\,dx \qquad (4.30)$$

In nondimensionalized form, it can be expressed as follows:
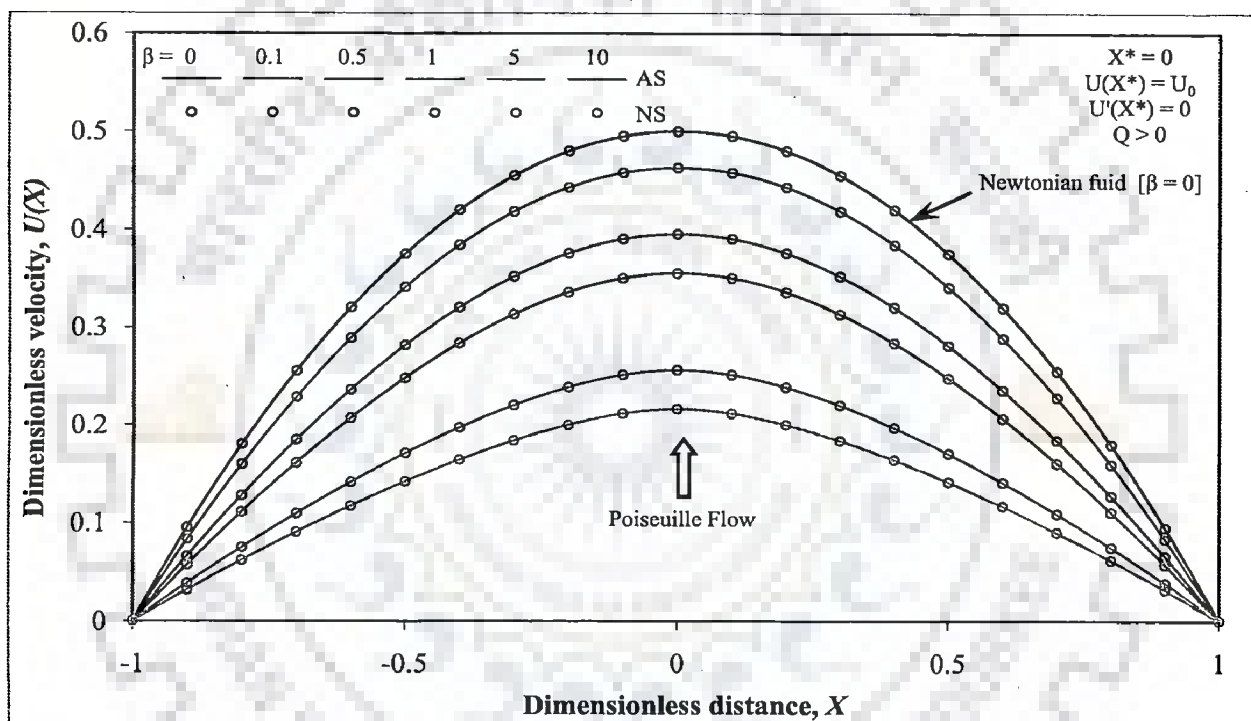
Figure 4.10: **Dimensionless velocity profiles for the Poiseuille flow**

159

$$Q = \int_{-1}^{1} U dX \qquad (4.31)$$

where $Q = q \bigg/ \left(-\dfrac{d\hat{p}}{dy} \dfrac{h^3}{\mu} \right)$, and U and X are the earlier defined dimensionless

velocity and dimensionless distance, respectively. Due to the symmetrical velocity profile, the above Eq. (4.31) reduces to:

$$Q = 2 \int_{0}^{1} U dX \qquad (4.32)$$

However, because of the complicated form of U [Eq. (4.29)], the analytical integration in the above equation is not practically possible, hence, the following different approach has been adopted to find the explicit analytical solution of Q.

$$Q = 2 \int_{0}^{1} U dX = 2 \int_{U_0}^{0} U \frac{1}{\left(\dfrac{dU}{dX} \right)} dU \qquad (4.33)$$

Using Eq. (4.24), the Eq. (4.33) yields the following integral:

$$Q = 2 \int_{U_0}^{0} \frac{-\sqrt{6\beta U}}{\sqrt{-1 + \sqrt{1 + 24\beta(U_0 - U)}}} dU \qquad (4.34)$$

Solving the above integral, one finally obtains the following explicit analytical solution of Q:

$$Q = \frac{\sqrt{-1 + \sqrt{1 + 24\beta U_0}} \left(1 - \sqrt{1 + 24\beta U_0} + 24 U_0 \beta \left(13 + 5\sqrt{1 + 24\beta U_0} \right) \right)}{315\sqrt{6}\beta^{3/2}} \qquad (4.35)$$

The above expression yields the positive value of Q, which signifies that the flow is in positive y direction.

(i)   Comparison between the analytical and numerical solutions

For this case, the velocity profiles obtained by using the analytical solution and the numerical solution have been shown in Figs. 4.10 and 4.11 for various values of β. Numerical solution has been obtained by solving the Eqs. (4.19a)-(4.19c) using the inbuilt ODE solver of MATHEMATICA, i.e. "NDSolve". It is clear that the velocity profiles obtained by these two solutions overlap with each other and thus validate the analytical solution.

The values of flowrate per unit width of the plates obtained by using the analytical solution and the numerical solution have been shown in Table 4.2. Here also, we observe a close agreement between the values of Q obtained by using the analytical solution and numerical solution.

(ii)   Effect of parameters

Here, the effect of parameter β on U and Q have been analysed. For a limiting case of $\beta = 0$, the fluid behaves as a Newtonian fluid and the Eq. (4.19a) reduces to $U'' = -1$. Solution of this resultant equation for the allied BCs gives the following analytical solutions of U and Q, which match well with the established results (Bird et al., 2002).

$$U = \frac{1}{2}(1 - X^2) \tag{4.36a}$$

$$U_0 = \frac{1}{2} \tag{4.36b}$$

$$Q = \frac{2}{3} \tag{4.36c}$$

In another limiting case of $\beta = \infty$, the Eq. (4.19a) becomes $U'' = 0$. By solving this resultant equation along with the concerned BCs, one finds: $U = 0$ and $Q = 0$. Hence, one can conclude that with the increase in β, U decreases and so as Q. This fact is also evident from the Fig. 4.10, which shows that with the increase in β, the velocity profile tends to be flat and signifies the decrease in flow rate.

162
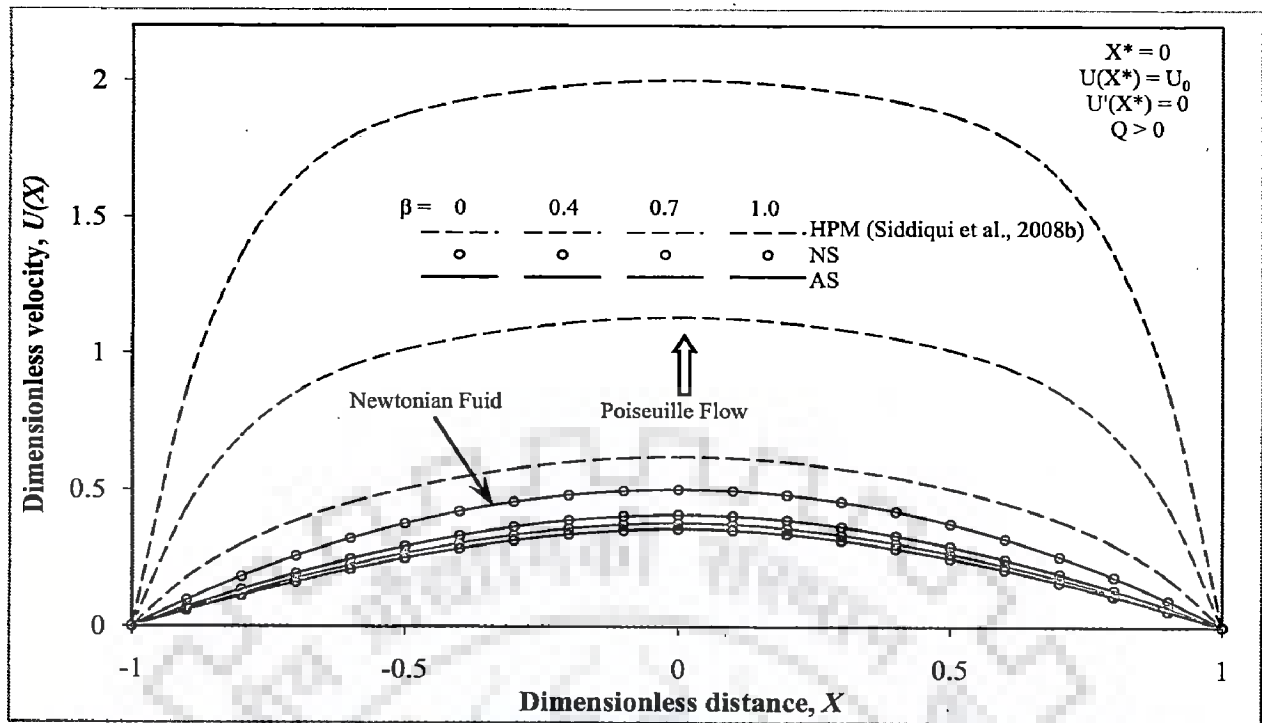
Figure 4.11: **Dimensionless velocity profiles for the Poiseuille flow**

Table 4.2: **Comparison of the values of flow rate per unit width of the plate for the Poiseuille flow: Case 1**

β	Q			% Error	
	HPM solution Siddiqui et al. (2008b) [Eq. (4.38)]	Analytical solution [Eq. (4.35)]	Numerical solution	HPM solution Siddiqui et al. (2008b) [Eq. (4.38)]	Analytical solution [Eq. (4.35)]
			$A = 0$		
0	0.66667	0.66667	0.66667	0	0
0.4	0.89524	0.52465	0.52465	-70.635	0
0.7	1.78667	0.48019	0.48019	-272.073	0
1	3.29524	0.45013	0.45013	-632.071	0

163

(iii)   *Comparison between the analytical solution and the approximate solution of Siddiqui et al. (2008b)*

We have also compared analytical results with those available in literature. For this purpose, the approximate solution obtained by Siddiqui et al. (2008b) by using HPM, has been chosen. It is worthwhile to mention that the dimensionless variables defined by these researchers are slightly different, however, for $B = 1$ [a dimensionless parameter considered by these researchers], the governing model equation and the associated BCs employed by Siddiqui et al. (2008b), become identical to those used in the present study. In this way, the analytical solution and the approximate solution obtained by Siddiqui et al. (2008b) can be compared in an unbiased manner. Moreover, these investigators have considered the presence of heat transfer effects in flow process, whereas, in this work we have considered the isothermal situations. However, despite this difference, the present comparison is justified, since in their work Siddiqui et al. (2008b) have assumed that the equation of momentum is independent of temperature and can be solved independently. This results into the same velocity profiles whether the heat transfer effects are considered or not. These facts are also true for all other cases tackled later on. It can, however, be noted that the assumption of independent momentum equation, as considered by Siddiqui et al. (2008b), is only true for small temperature differences, while for large temperature gradients this assumption will no longer be valid as the density and viscosity will not be constant, especially for non-Newtonian fluids, and the momentum equation cannot be solved independently. Therefore, the approximate solution found by these researchers is either applicable to isothermal situations or where smaller temperature effects are prevailing. The approximate solution of velocity profile $[U_{HPM}]$, as obtained by Siddiqui et al. (2008b) by using HPM, is reproduced below.

$$U_{HPM} = \frac{1}{2}(1 - X^2) - \frac{1}{2}\beta(1 - X^4) + 2\beta^2(1 - X^6) \tag{4.37}$$

For comparison, the velocity profiles obtained by using the analytical solution, the numerical solution and the above approximate solution, have been drawn in Fig. 4.11 for the same values of β as those considered by Siddiqui et al. (2008b). It is clear that the velocity profiles obtained by using the analytical solution and the numerical solution match very well for all the values of β, whereas, the velocity profiles obtained by

using the approximate solution match only for $\beta = 0$ and deviate significantly for other values of β. Moreover, the approximate solution depicts an opposite trend in the velocity profiles as β increases, which is not valid as discussed earlier. With these observations it can be concluded that the approximate solution obtained by Siddiqui et al. (2008b) by using HPM are valid only for $\beta = 0$.

In addition to the above, a comparison between the values of Q predicted by the analytical solution, the numerical solution and the above approximate solution has also been made. The approximate solution of velocity profile yields the following expression of Q.

$$Q_{HPM} = \int_{-1}^{1} U_{HPM}\, dX = \frac{2}{3} - \frac{4}{5}\beta + \frac{24}{7}\beta^2 \qquad (4.38)$$

For various values of β, Table 4.2 compares the values of Q obtained by using these three solutions, and it is clear that except for $\beta = 0$, the predictions of approximate solution deviate with the numerical values and the percentage error increases with the increase in β. On the other hand, Q predicted by the analytical solution matches well with its numerical counterpart for all values of β.

4.2.2.2 Case 2: Couette-Poiseuille flow

In this situation, the fluid movement is due to the two effects superimposed over each other: (i) due to the movement of one of the plates [say upper plate], which moves with certain velocity [say a] resulting in the Couette flow and (ii) due to the pressure gradient on the fluid resulting in the Poiseuille flow. The model equation for this situation will remain same as that of the previous case, i.e. Eq. (4.17), however, the allied BCs will be slightly different incorporating the plate movement. These BCs are given below:

BC I: $u = a$ at $x = h$ [upper moving plate] $\qquad$ (4.39a)

BC II: $u = 0$ at $x = -h$ [lower stationary plate] $\qquad$ (4.39b)

166

Positive value of a denotes that the upper plate moves in the positive y direction, whereas, the negative value of a indicates that the upper plate moves in the negative y direction. Considering the previously introduced dimensionless variables in addition to the following dimensionless plate velocity

$$A = \frac{a}{\left(-\frac{dp}{dy}\right)\frac{h^2}{\mu}},$$

the Eq. (4.17) and the related BCs, i.e. Eqs. (4.39a) and (4.39b), are transformed into the following dimensionless forms:

$$\frac{d^2U}{dX^2} + 6\beta\left(\frac{dU}{dX}\right)^2\frac{d^2U}{dX^2} = -1 \tag{4.40a}$$

$$\text{BC I:} \quad U = A \text{ at } X = 1 \text{ [upper moving plate]} \tag{4.40b}$$

$$\text{BC II:} \quad U = 0 \text{ at } X = -1 \text{ [lower stationary plate]} \tag{4.40c}$$

For solving the above Eqs. (4.40a)-(4.40c), the same steps of derivative substitution method, as adopted in case 1, have also been followed here, and the following expression is obtained for U':

$$U' = \frac{dU}{dX} = \pm\sqrt{\frac{-1+\sqrt{1+12\beta(C_1-2U)}}{6\beta}} \tag{4.41}$$

where C_1 is the constant of integration. The integration of Eq. (4.41) with the help of appropriate BCs yields the expression for velocity profile. However, unlike the previous case, the resultant velocity profile for this configuration will not be symmetric around $X = 0$. Hence, $U'(0) \neq 0$. Instead $U' = 0$ at some unknown position $X = X^*$, and at this position the fluid velocity will be maximum and is denoted by U_0. In fact, the location of X^* depends on the magnitude of the plate velocity and can lie inside or outside the region of interest $[-1 \leq X \leq 1]$. Owing to this, one needs to consider the whole region, i.e. $-1 \leq X \leq 1$. Following three situations may arise in the present case:

(i)   Upper plate moves in the positive y direction [same direction as that of the flow due to the pressure gradient], but with a velocity smaller than the maximum

167

velocity of the moving fluid $[A < U_0]$. In this situation, the location of the maximum velocity will be near to the moving plate [upper plate], i.e. $0 < X^* < 1$. Figs. 4.12 and 4.13 depict this state. On the contrary, if the upper plate moves in the negative y direction [opposite to the flow due to the pressure gradient], but with a velocity smaller enough such that the maximum velocity of the fluid is still in the positive y direction $[U_0 > 0]$, then the location of the maximum velocity will be near to the stationary plate [lower plate], i.e. $-1 < X^* < 0$. Fig. 4.14 shows this situation. In both these situations, $U'(X^*) = 0$.

(ii)   Upper plate moves in the positive y direction, but with a velocity higher enough such that the maximum fluid velocity equals to that of the moving plate $[U_0 = A]$. Thus the location of the maximum velocity will lie on the moving plate $[X^* = 1]$. However, $U'(X^* = 1) > 0$. This situation is presented in Fig. 4.15.

(iii) Upper plate moves in the negative y direction, but with a velocity higher enough such that the maximum positive velocity of the fluid equals to that of the stationary plate $[U_0 = 0]$. Hence, $X^* = -1$ and $U'(X^* = -1) < 0$. Fig. 4.16 exemplifies this situation.

For each of the above cited situations, the analytical solutions of Eqs. (4.40a)-(4.40c) assume different forms, i.e. the solutions depend upon the direction as well as the magnitude of the plate velocity. In other words, the location of X^* dictates the form of the solution. It can also be noted that the maximum fluid velocity and its location, i.e. U_0 and X^*, are unknown for the conditions mentioned in point (i), and can be evaluated by using the corresponding BCs. However, for the situations mentioned in points (ii) and (iii), these two are known a priori. The analytical solutions of these cases are obtained below, however, for each of them the procedure remains same as followed in the previous case.
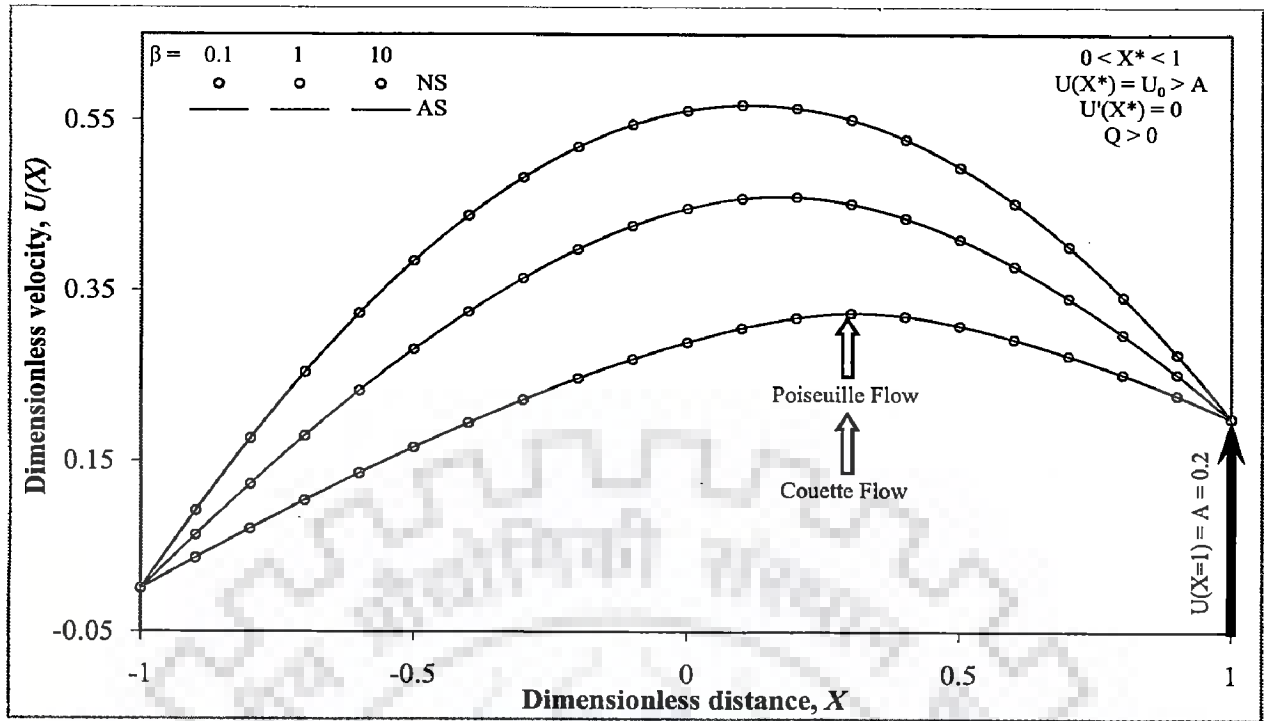
Figure 4.12: Dimensionless velocity profiles for the Couette-Poiseuille flow [upper plate is moving slowly in the positive y direction]
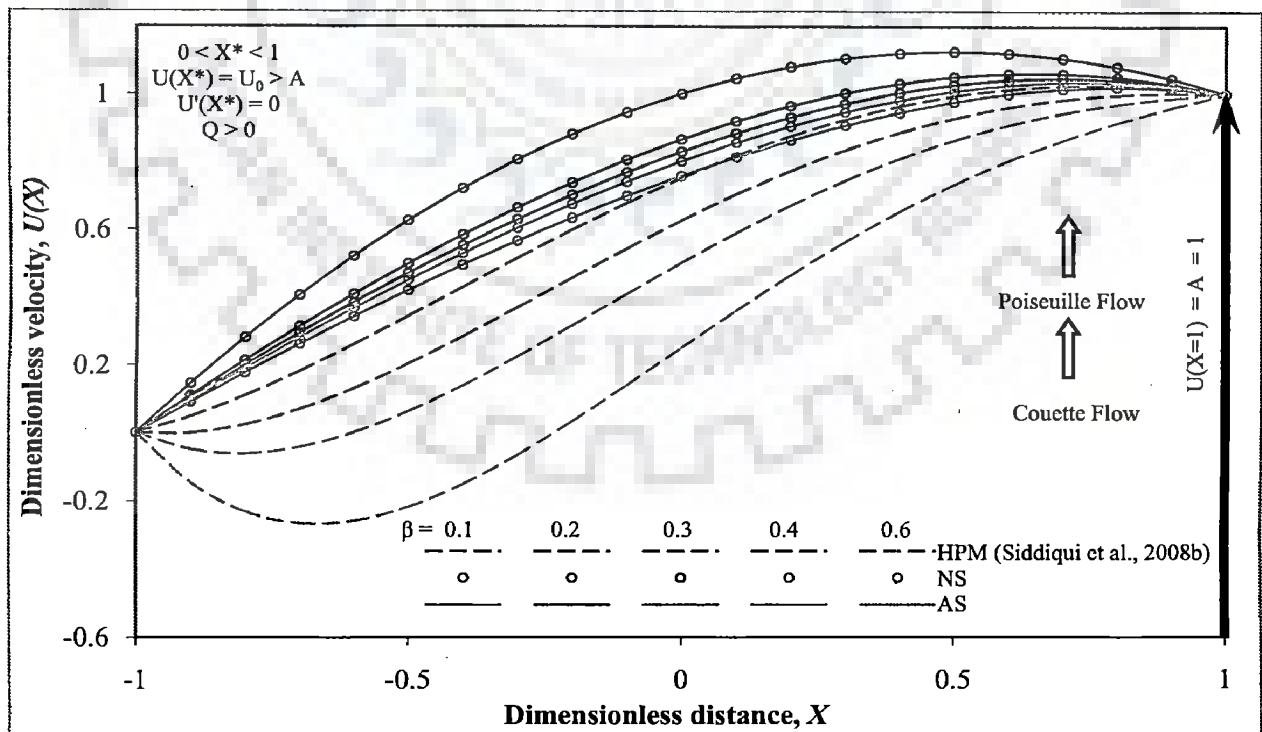
Figure 4.13: Dimensionless velocity profiles for the Couette-Poiseuille flow [upper plate is moving slowly in the positive y direction]
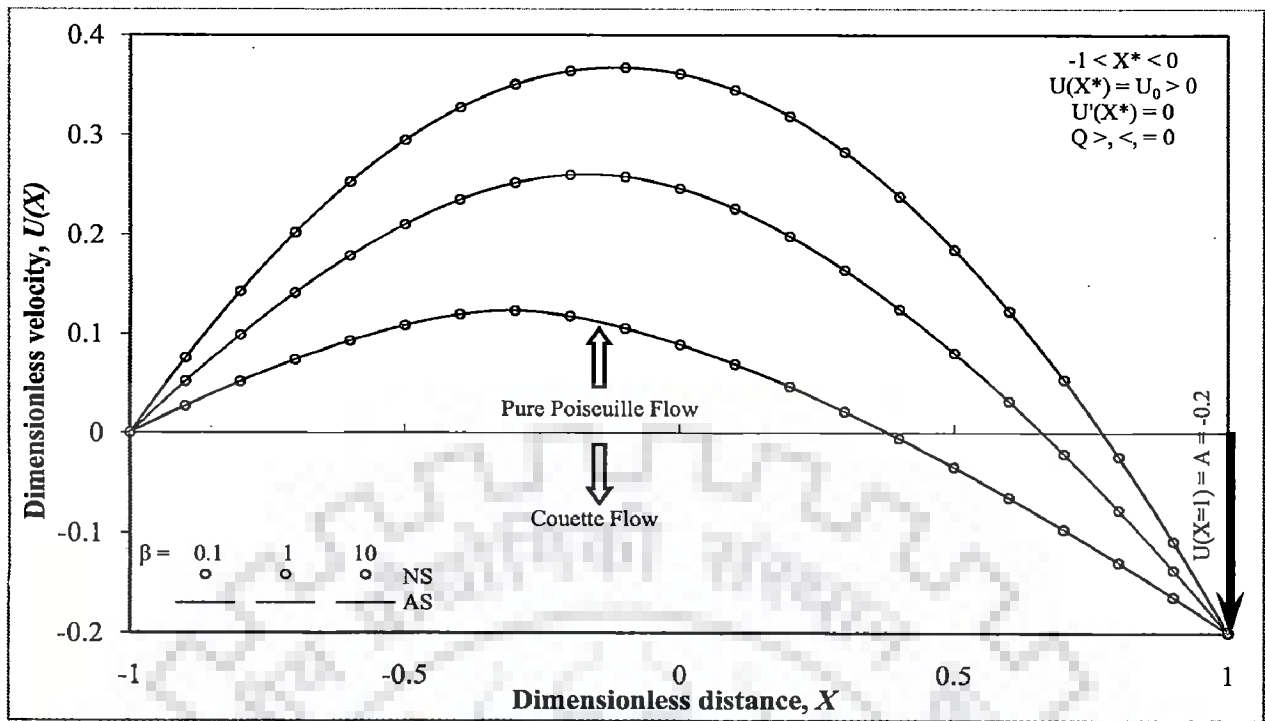
Figure 4.14: Dimensionless velocity profiles for the Couette-Poiseuille flow [upper plate is moving slowly in the negative y direction]
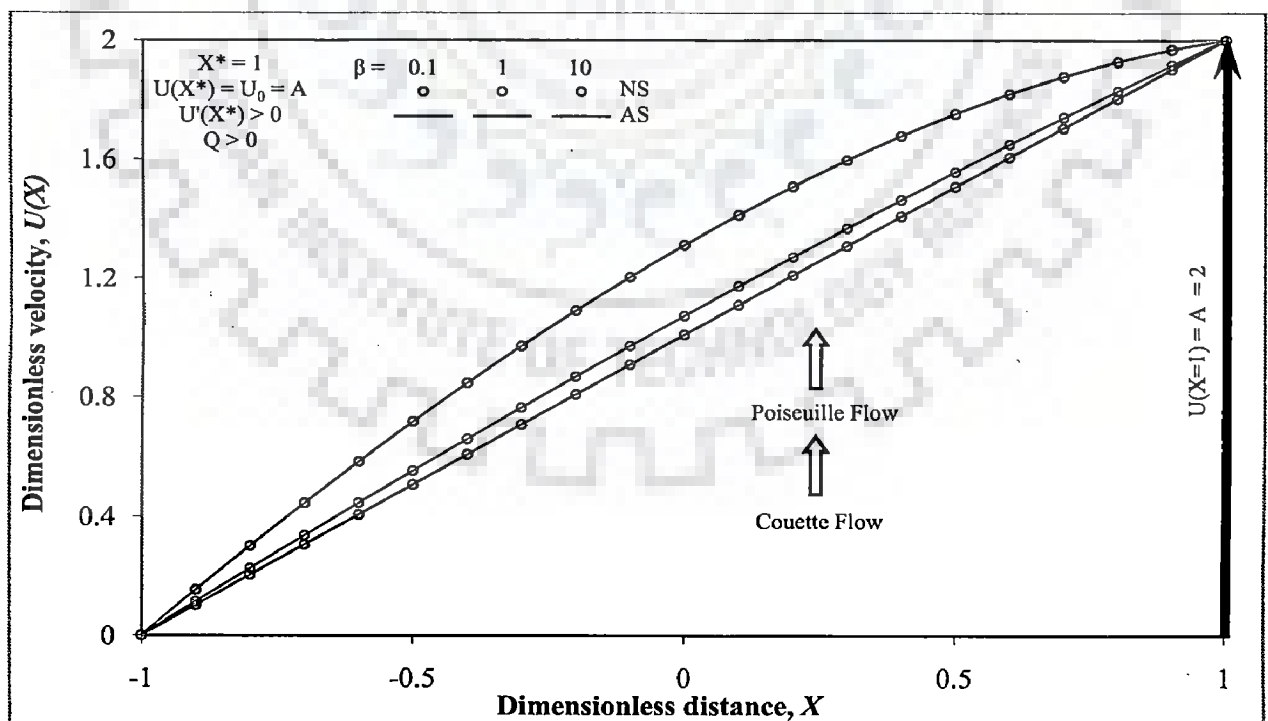
Figure 4.15: Dimensionless velocity profiles for the Couette-Poiseuille flow [upper plate is moving quickly in the positive y direction]

171
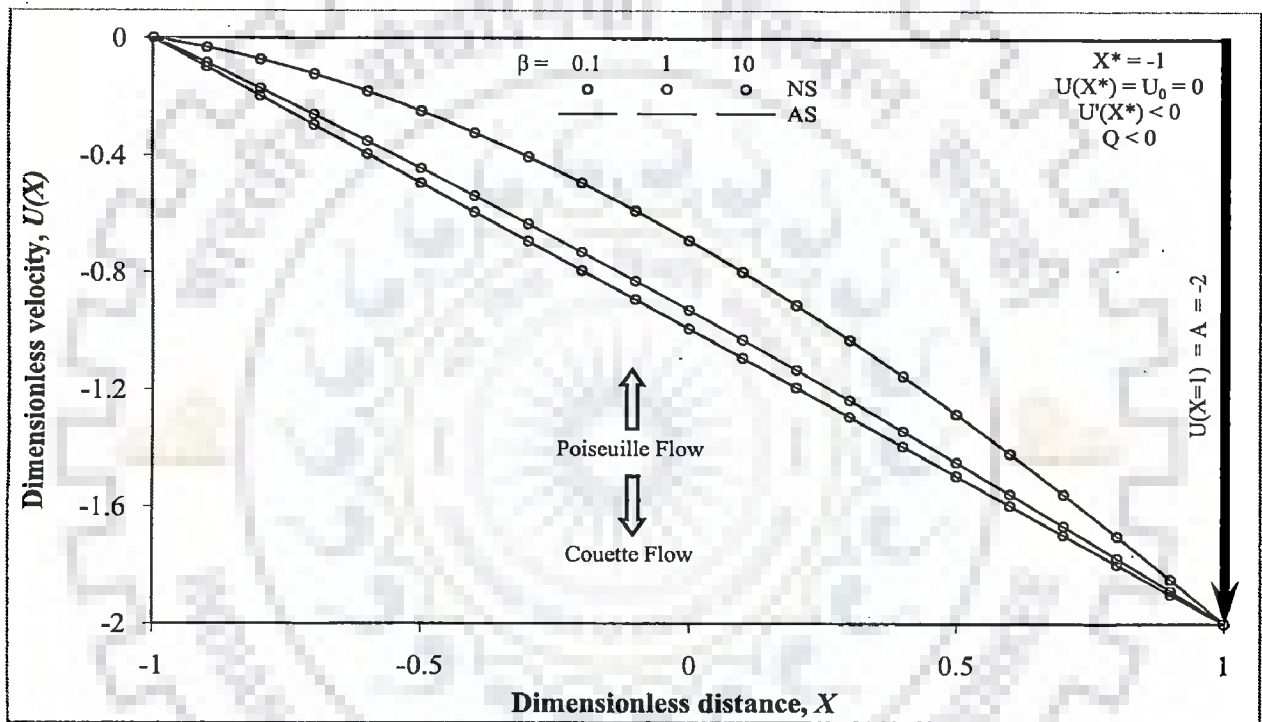
Figure 4.16: Dimensionless velocity profiles for the Couette-Poiseuille flow [upper plate is moving quickly in the negative *y* direction]

(a) ***Case 2(a): Couette-Poiseuille Flow with Upper Plate Moving Slowly in Any Direction ($|A|$ is Small)***

For this situation, X^* will be positioned between the two plates, and therefore, indicates that $U' > 0$ for $-1 \leq X < X^*$, $U' < 0$ for $X^* < X \leq 1$ and $U' = 0$ at X^*. Since, $U' = 0$ at $X = X^*$ [$\neq 0$], one only needs to consider the region $X^* \leq X \leq 1$ for the integration of Eq. (4.41). However, now the negative sign before the radical in Eq. (4.41) should be considered. The unknown C_1 in Eq. (4.41) is found by using the condition $U' = 0$ at $X = X^*$ and is given by: $C_1 = 2U_0$. Substituting this value of C_1 in Eq. (4.41), and considering the region $X^* \leq X \leq 1$ only, one obtains:

$$\frac{dU}{dX} = -\sqrt{\frac{-1 + \sqrt{1 + 24\beta(U_0 - U)}}{6\beta}} \quad \text{for } X^* \leq X \leq 1 \tag{4.42}$$

Integration of the above equation from X^* to X gives the following implicit analytical solution of U :

$$\frac{\sqrt{-1 + \sqrt{1 + 24\beta(U_0 - U)}}\left(2 + \sqrt{1 + 24\beta(U_0 - U)}\right)}{3\sqrt{6\beta}} = X - X^* \tag{4.43}$$

From the above equation, U can be expressed explicitly and is given below [here also, three explicit solutions of U appear, however, two of them are complex conjugates, and are therefore neglected].

$$U = \frac{1 - T^2 + 24U_0\beta}{24\beta} \tag{4.44}$$

where $T = -1 + \dfrac{2^{1/3}}{\left(2 + K_1^2(X - X^*)^2 + \sqrt{4K_1^2(X - X^*)^2 + K_1^4(X - X^*)^4}\right)^{1/3}}$

$+ \dfrac{\left(2 + K_1^2(X - X^*)^2 + \sqrt{4K_1^2(X - X^*)^2 + K_1^4(X - X^*)^4}\right)^{1/3}}{2^{1/3}}$ and $K_1 = -3\sqrt{6\beta}$

The above analytical solution of U gives $U' = 0$ at $X = X^*$ [$\neq 0$], and is valid for whole of the region $-1 \leq X \leq 1$. For the particular values of β and A, the unknown

U_0 and X^* are found by solving the following coupled equations. These equations have been found by solving the equation of U', i.e. Eq. (4.41), for both the regions, respectively, and satisfying the relevant BCs, i.e. Eqs. (4.40b) and (4.40c).

$$\frac{\sqrt{-1+\sqrt{1+24\beta(U_0-A)}}\left(2+\sqrt{1+24\beta(U_0-A)}\right)}{3\sqrt{6\beta}}=1-X^* \tag{4.45a}$$

$$\frac{\sqrt{-1+\sqrt{1+24\beta U_0}}\left(2+\sqrt{1+24\beta U_0}\right)}{3\sqrt{6\beta}}=1+X^* \tag{4.45b}$$

With the help of Eqs. (4.44), (4.45a) and (4.45b), one can explicitly find U. Once the analytical solution of U is available, Q can easily be found by using Eq. (4.31). However, due to the complicated form of U [Eq. (4.44)], one has to follow the same approach as was followed in case 1, i.e.

$$Q = \int_{-1}^{1} U dX = \underbrace{\int_{0}^{U_0} U \frac{1}{\left(\dfrac{dU}{dX}\right)} dU}_{for\ -1\leq X\leq X^*} + \underbrace{\int_{U_0}^{A} U \frac{1}{\left(\dfrac{dU}{dX}\right)} dU}_{for\ X^*\leq X\leq1} \tag{4.46}$$

Substituting the expressions of U' for both the regions in the above equation, and evaluating the above integrals between the specified limits, one obtains the following explicit analytical solution of Q.

$$Q=-\frac{\sqrt{-1+\sqrt{1+24\beta U_0}}\left(-1+\sqrt{1+24\beta U_0}-24U_0\beta\left(13+5\sqrt{1+24\beta U_0}\right)\right)}{630\sqrt{6}\beta^{3/2}}$$

$$+\frac{\sqrt{-1+\sqrt{1+24\beta(U_0-A)}}}{630\sqrt{6}\beta^{3/2}}\left[\right.$$

$$\left(1-\sqrt{1+24\beta(U_0-A)}+18A\beta\left(6+5\sqrt{1+24\beta(U_0-A)}\right)+24\beta U_0\left(13+5\sqrt{1+24\beta(U_0-A)}\right)\right)\left.\right] \tag{4.47}$$

Depending on the value of A, Q obtained from the above equation can be positive or negative, which corresponds to the net flow in the positive and negative y directions, respectively.

(i) *Comparison between the analytical and numerical solutions*

For this subcase, we have validated the analytical solution with the numerical solution by plotting the respective velocity profiles in Figs. 4.12-4.14 for various values of β. These figures depict both the co-current and counter-current movements of the plate, and a close look on these plots reveals an agreement between the analytical and numerical results. Besides, for $A = 1$, the Table 4.3 compares the values of Q obtained by using the analytical solution and the numerical solution, and a close match is observed between these values. Although not shown, the same is also true for $A = -1$.

(ii) *Effect of parameters*

For this subcase, the limiting value of $\beta = \infty$ gives: $U = \dfrac{A}{2}(1+X)$ and $Q = A$,

whereas, for $\beta = 0$ (Newtonian fluid) one finds: $U = \dfrac{1}{2}(1+A+AX-X^2)$ and

$Q = \dfrac{2}{3} + A$. This means that with the increase in β, the flow tends to be a Couette flow and results in the decrease in Q. Since, for this subcase $A > 0$, Q will be maximum for Newtonian fluid. This fact is also supported by Figs. 4.12-4.14.

Table 4.3: **Comparison of the values of flow rate per unit width of the plate for the Couette-Poiseuille flow: Case 2(a)**

β	Q			% Error	
	HPM solution Siddiqui et al. (2008b) [Eq. (4.49)]	Analytical solution [Eq. (4.47)]	Numerical solution	HPM solution Siddiqui et al. (2008b) [Eq. (4.49)]	Analytical solution [Eq. (4.47)]
			$A = 1$		
0	1.66667	1.66667	1.66667	0	0
0.2	1.30667	1.4866	1.4866	12.10346	0
0.3	1.12667	1.44032	1.44032	21.77641	0
0.4	0.946667	1.40413	1.40413	32.57982	0
0.6	0.586667	1.34904	1.34904	56.51226	0

(iii)   *Comparison between the analytical solution and the approximate solution of Siddiqui et al. (2008b)*

The approximate solution for velocity profile [U_{HPM}], as obtained by Siddiqui et al. (2008b), is reporduced below for the purpose of comparison.

$$U_{HPM} = \frac{(1+X)}{2} + \frac{1}{2}(1-X^2) + \frac{\beta}{4}\left(3(-1+X^2) + 4(X-X^3) + 2(-1+X^4)\right)$$

(4.48)

Fig. 4.13 portrays the velocity profiles obtained by using the above approximate solution [Eq. (4.48)] along with those obtained by using the analytical solution and the numerical solution. It can be observed that except for $\beta = 0$, the velocity profiles obtained by using the approximate solution diverge significantly with the numerically obtained velocity profiles, and the deviation in these profiles increases with the increase in β. Moreover, for higher values of β, the approximate solution predicts the negative [opposite] velocity in the vicinity of stationary plate, which is not physically viable, as discussed above. Furthermore, consideration of higher terms in the approximate solution will rather enhance this discrepancy instead of rectifying it. Therefore, for this case too, the approximate solution obtained by Siddiqui et al. (2008b) has limited applicability.

Similar conclusions can also be drawn by comparing the values of Q obtained by using the analytical solution, the numerical solution and the approximate solution. The above presented approximate solution of velocity profile, i.e. Eq. (4.48), gives the following approximate solution for Q.

$$Q_{HPM} = \frac{5}{3} - \frac{9}{5}\beta$$

(4.49)

For various values of β, the values of Q predicted by the analytical solution, i.e. Eq. (4.47), the approximate solution, i.e. Eq. (4.49), and the numerical method, have been tabulated in Table 4.3. It is noticeable that except for $\beta = 0$, the values of Q predicted by the approximate solution deviate with the numerically obtained values and the error increases with the increase in β. In contrast, the flow rates, predicted by the analytical solution, match exactly with their numerical counterparts. This confirms the accuracy of

the presently obtained analytical solution and highlights the limitations of the approximate solution of Siddiqui et al. (2008b).

(b)   Case 2(b): Couette-Poiseuille Flow With Upper Plate Moving in Positive y Direction with a High Velocity (A>0 and Large)

By following the same steps as were adopted in the previous subcase, one obtains the following explicit analytical solution of U [details of the derivation have been given in Appendix B2].

$$U = \frac{1 - T^2 + 12C_1\beta}{24\beta} \tag{4.50}$$

where $T = -1 + \dfrac{3(2)^{1/3}}{\left(K_3 + \sqrt{-2916 + K_3^2}\right)^{1/3}} + \dfrac{\left(K_3 + \sqrt{-2916 + K_3^2}\right)^{1/3}}{3(2)^{1/3}}$,

$K_1 = -3\sqrt{6\beta}$, $K_2 = \sqrt{-1 + \sqrt{1 + 12C_1\beta}}\left(2 + \sqrt{1 + 12C_1\beta}\right)$ and

$K_3 = 54 + 27K_1^2 + 54K_1K_2 + 27K_2^2 + 54K_1^2 X + 54K_1 K_2 X + 27K_1^2 X^2$.

The unknown C_1 is found by solving the following equation:

$$-\sqrt{-1 + \sqrt{1 + 12\beta(C_1 - 2A)}}\left(2 + \sqrt{1 + 12\beta(C_1 - 2A)}\right)$$

$$+\sqrt{-1 + \sqrt{1 + 12\beta C_1}}\left(2 + \sqrt{1 + 12\beta C_1}\right) = 6\sqrt{6\beta} \tag{4.51}$$

Similarly, by proceeding as in the previous subcase, the following explicit analytical solution of Q can be obtained:

$$Q = -\frac{\sqrt{-1 + \sqrt{1 + 12C_1\beta}}\left(-1 + \sqrt{1 + 12C_1\beta} - 12C_1\beta\left(13 + 5\sqrt{1 + 12C_1\beta}\right)\right)}{630\sqrt{6}\beta^{3/2}}$$

$$+\frac{\sqrt{-1 + \sqrt{1 + 12C_1\beta - 24A\beta}}}{630\sqrt{6}\beta^{3/2}}\left[-1 + \sqrt{1 + 12C_1\beta - 24A\beta}\right.$$

179

$$-12C_1\beta\left(13+5\sqrt{1+12C_1\beta-24A\beta}\right)-18A\beta\left(6+5\sqrt{1+12C_1\beta-24A\beta}\right)\Big] \qquad (4.52)$$

Since, $A>0$, Q is always positive, and corresponds to the net flow in the positive y direction.

(i)   *Comparison between the analytical and numerical solutions*

For this subcase, the velocity profiles obtained by using the analytical solution have been plotted in Fig. 4.15 along with the numerically obtained velocity profiles. This figure reveals that a close harmony exists between the velocity profiles obtained by using the analytical solution and the numerical solution. Although not shown, the similar conclusions can also be drawn by comparing the values of Q obtained by using the analytical and numerical solutions. However, we could not compare these solutions with the solutions of Siddiqui et al. (2008b), as these researchers did not explore this situation.

(ii)   *Effect of parameters*

For this subcase, the same expressions of U and Q are obtained for the limiting values of $\beta=\infty$ and $\beta=0$, as those obtained in the previous subcase.

(c)   *Case 2(c): Couette-Poiseuille Flow with Upper Plate Moving in Negative y Direction with a High Velocity ($A<0$ and $|A|$ is Large)*

The following explicit analytical solution of U is obtained [Appendix B2]:

$$U=\frac{1-T^2+12C_1\beta}{24\beta} \qquad (4.53)$$

where $T=-1+\dfrac{3(2)^{1/3}}{\left(K_3+\sqrt{-2916+K_3^2}\right)^{1/3}}+\dfrac{\left(K_3+\sqrt{-2916+K_3^2}\right)^{1/3}}{3(2)^{1/3}}$,

$$K_1 = -3\sqrt{6\beta}, \quad K_2 = \sqrt{-1+\sqrt{1+12C_1\beta}}\left(2+\sqrt{1+12C_1\beta}\right) \text{ and}$$

$$K_3 = 54 + 27K_1^2 - 54K_1K_2 + 27K_2^2 + 54K_1^2X - 54K_1K_2X + 27K_1^2X^2$$

The unknown C_1 can be found from the following equation:

$$\sqrt{-1+\sqrt{1+12\beta(C_1-2A)}}\left(2+\sqrt{1+12\beta(C_1-2A)}\right)$$

$$-\sqrt{-1+\sqrt{1+12\beta C_1}}\left(2+\sqrt{1+12\beta C_1}\right) = 6\sqrt{6\beta} \tag{4.54}$$

On comparison with the case 2(b), one finds that the equation used for finding C_1, i.e. Eq. (4.54), only differ in sign with that of the previous subcase, i.e. Eq. (4.51). Moreover, except K_3, all the other expressions $[U, T, K_1, K_2]$ are same as that of the previous case.

The following explicit analytical solution of Q is found:

$$Q = \frac{\sqrt{-1+\sqrt{1+12C_1\beta}}\left(-1+\sqrt{1+12C_1\beta}-12C_1\beta\left(13+5\sqrt{1+12C_1\beta}\right)\right)}{630\sqrt{6}\beta^{3/2}}$$

$$-\frac{\sqrt{-1+\sqrt{1+12C_1\beta-24A\beta}}}{630\sqrt{6}\beta^{3/2}}\left[-1+\sqrt{1+12C_1\beta-24A\beta}\right.$$

$$\left.-12C_1\beta\left(13+5\sqrt{1+12C_1\beta-24A\beta}\right)-18A\beta\left(6+5\sqrt{1+12C_1\beta-24A\beta}\right)\right] \tag{4.55}$$

Here also, we observe that the above analytical solution just differ in sign with that of the previous case 2(b), i.e. Eq. (4.52), and gives negative values of Q, which implies that the net flow is in the negative y direction.

(i) ***Comparison between the analytical and numerical solutions***

For this subcase, velocity profiles obtained by using the analytical and numerical solutions are depicted in Fig. 4.16. It is apparent from this figure that a close agreement exists between the predictions of these two solutions. Here also, we have not shown the

comparison between the analytical and numerical values of Q. However, it can be verified that the values of Q obtained by using both the solutions match exactly. We have not compared our results with those of Siddiqui et al. (2008b) as this situation was not dealt with by them.

(ii) Effect of parameters

The limiting values of β [$=\infty, 0$] gives the same expressions of U and Q as those obtained in the case 2(a). Since, $A < 0$ for this subcase, Q is always negative. Negative Q signifies the flow in negative y direction. However, since $A < 0$, $|Q|$ $\left(=\left|\frac{2}{3}+A\right|\right)$ will be minimum for Newtonian fluid.

4.3 CONCLUDING REMARKS

In this chapter analytical solutions of the model equation of rotary kiln and fluid flow process have been obtained and the conclusions pertaining to them are presented below.

(i) Rotary Kiln

Implicit analytical solution for estimating the solid bed depth profile has been obtained by using the separation of variables and partial fraction decomposition methods. It is revealed that the present analytical solution is accurate and covers the entire range of ε unlike the implicit approximate solution of Liu et al. (2009), which is accurate only in its optimum range [20.05deg $\leq \varepsilon \leq$ 65.89deg or 0.4 $\leq \mu \leq$ 0.91]. Several available experimental results have also been successfully simulated by using the derived analytical solution, which proves its practical utility.

(ii)   Fluid Flow Process

Explicit analytical solutions of the velocity profile and the flow rate have been obtained with the help of derivative substitution method for all the possible configurations of plate's movement which also include the flow situations previously considered by Siddiqui et al. (2008b). All these analytical solutions show an excellent agreement when crosschecked against their numerical counterparts and are found to be superior to the approximate solutions obtained by Siddiqui et al. (2008b).

It is found that the Couette flow features start dominating as β and/or $|A|$ are increased, and for a given plate velocity, the effects of Poiseuille flow are more pronounced in the Newtonian fluid [$\beta = 0$].
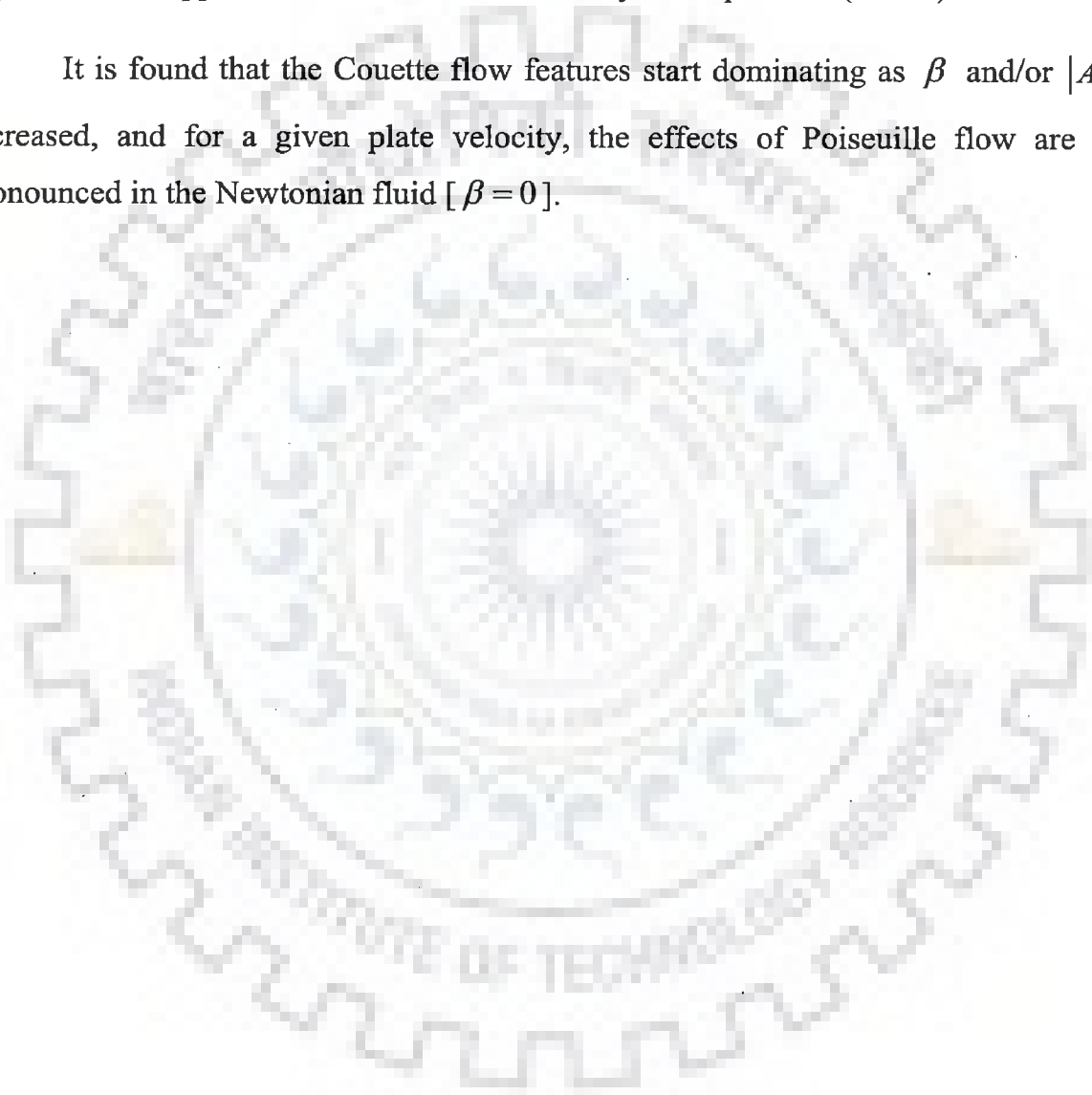
NOMENCLATURE

Abbreviations

AS   analytical solution

NS   numerical solution

APS   approximate solution

Exp.   experimental

HPM   homotopy perturbation method

Notations

A [-]   dimensionless velocity of the plate

$$\left(= \frac{a\mu}{h^2} \left(-\frac{d\hat{p}}{dy} \right)^{-1} \right)$$

B [-]   dimensionless parameter considered by Siddiqui et

al. (2008b) $\left(= -\frac{h^2}{\mu U} \frac{d\hat{p}}{dx} \right)$

C_1, C_2 [-]   constants of integration

d [m]   diameter of solid particle

D [m]   diameter of the rotary kiln

$f(U)$ [-]   function of U $\left(= \frac{dU}{dX} \right)$

K_1, K_2 [-]   constant terms

K_3 [-]   function of X

L [m]   length of the rotary kiln

$\dot{m}$ [kg.s^{-1}]   mass flow rate of the solids

n [revolution.s^{-1}]   rotational speed of the kiln

$\hat{p}$ [N.m^{-2}]   generalized pressure

q [m^2.s^{-1}]   fluid flow rate per unit width of the plate

Q [-]   dimensionless fluid flow rate per unit width of the

plate $\left(= \frac{q\mu}{h^3} \left(-\frac{d\hat{p}}{dy} \right)^{-1} \right)$

Q_{HPM}	[-]	Q obtained by using HPM
r_i	[-]	i^{th} root given by the Eq. (4.8)
R	[m]	radius of the rotary kiln
T	[-]	function of X
u	[m.s^{-1}]	fluid velocity in the direction of y coordinate
U	[-]	dimensionless fluid velocity $\left(= \dfrac{u\mu}{h^2}\left(-\dfrac{dp}{dy}\right)^{-1}\right)$
U_{HPM}	[-]	U obtained by using HPM
U_0	[-]	dimensionless maximum fluid velocity
w	[-]	function of U $[= f(U)^2]$
Y	[-]	$sin(\varepsilon)$ in Eq. (4.12)
Y_0	[-]	$sin(\varepsilon_0)$ in Eq. (4.12)

Greek letters

β_2	[kg.m^{-1}.s]	material moduli
β_3	[kg.m^{-1}.s]	material moduli
ε	[degree]	local fill angle of the solids
ε_0	[degree]	local fill angle of the solids at the exit of the kiln
$\varepsilon_{max/min}$	[degree]	local fill angle of the solids corresponding to $h_{max/min}$
θ	[degree]	dynamic angle of repose of the solids
ρ	[kg.m^{-3}]	bulk density of the solids

Section 4.1

Notations

a	[-]	dimensionless parameter $\left(= \dfrac{3\tan(\theta)L\dot{m}}{4\pi nR^4\rho}\right)$
b	[-]	dimensionless parameter $\left(= \dfrac{L\tan(\beta)}{R\cos(\theta)}\right)$
h	[m]	depth of the solid bed

h_0	[m]	height of the dam at the discharge end
$h_{max/min}$	[m]	maximum/minimum depth finally attained by the solid bed
x	[m]	axial distance from the discharge end along the kiln length
X	[-]	dimensionless axial distance from the discharge end along the kiln length $\left(=\dfrac{x}{L}\right)$
X_{min}	[-]	minimum value of X corresponding to $h_{max/min}$

Greek letters

β	[degree]	inclination of the kiln to the horizontal
μ	[-]	dimensionless parameter $\left(=\left(\dfrac{a}{b}\right)^{1/3}\right)$

Section 4.2

Notations

a	[m.s^{-1}]	velocity of the plate
$2h$	[m]	separation between the two plates
X	[-]	dimensionless distance in x direction $\left(=\dfrac{x}{h}\right)$
X^*	[-]	dimensionless distance where maximum fluid velocity occurs
x, y, z	[m]	distances in x, y and z directions, respectively

Greek letters

β	[-]	dimensionless parameter $\left(=(\beta_2+\beta_3)\left(-\dfrac{dp}{dy}\right)^2\dfrac{h^2}{\mu^3}\right)$
μ	[kg.m^{-1}.s^{-1}]	fluid viscosity

EQUATION OF STATE, FRICTION FACTOR EQUATION AND REACTION–DIFFUSION PROCESSES – APPROXIMATE SOLUTIONS BY ADM

5.0 INTRODUCTION

This chapter describes the development of approximate solutions of thermodynamic equation of state, friction factor equation, and the model equations of reaction-diffusion processes occurring inside a porous catalyst slab and sphere. Thermodynamic equation of state is concerned with the estimation of gas volume at a given pressure and temperature, whereas, the friction factor equation is used to find the friction factor for the laminar and turbulent flow of fluids in smooth pipes. The fluid considered in the present study is Bingham fluid. The model equation of reaction-diffusion process is used in evaluating the concentration profile and effectiveness factor. The thermodynamic equation of state and friction factor equation are nonlinear algebraic equations, whereas, the reaction-diffusion process in a catalyst is represented by a second order ODE.

In the literature, the thermodynamic equation of state and the friction factor equation have been solved by using various numerical methods. Besides, for the friction factor equation, several explicit correlations used as a substitute for this equation have also been developed. However, to the best of our knowledge, use of some recent approximate methods, e.g. ADM and RADM, for obtaining the solutions of these equations are unavailable. On the other hand, the model equations of reaction-diffusion process have been solved by several researchers by using various approximate methods, namely ADM, and perturbation and matching procedure. However, it is observed that these approximate solutions become invalid in some situations.

For obtaining the approximate solutions of these equations, two approximate methods, namely ADM and RADM have been employed. For judging the effectiveness of these two methods the obtained results have been compared with the numerical results as well as those obtained by using the available approximate solutions. For the

sake of completeness, ADM and RADM have, respectively, been described in sections 5.1 and 5.2, along with their methodologies. In order to demonstrate their use in solving AEs and ODEs, two simple illustrations have also been presented.

5.1   ADOMIAN DECOMPOSITION METHOD [ADM]

Developed by George Adomian in 1980s, ADM has proved to be an effective approximate method for solving various kinds of nonlinear equations, e.g. AEs, ODEs, PDEs and IEs [integral equations] (Adomian, 1986 and 1994). This parameter based method is attractive since it can deal with all types of nonlinearities and does not require the presence of any small or large parameter unlike other approximate methods, e.g. perturbation method or δ- decomposition method (Adomian, 1986, 1994). Because of this, it has been widely applied by many researchers to solve a variety of nonlinear equations and a vast amount of published literature is available. Chapter II presents some of the relevant studies.

The basic idea of ADM, while solving a nonlinear equation, is to break it into a set of infinite but simpler linear equations. This is done by expanding the linear and nonlinear terms of the given equation in the Taylor series of a hypothetical parameter, $\lambda \in [0,1]$. Thereafter, a homotopy equation from the original equation is formed. The terms having same powers of λ in the so formed homotopy equation are equated to obtain the infinite set of linear but simpler equations. While linear terms are decomposed easily, the nonlinear terms are decomposed into components called Adomian polynomials, A_i. These polynomials can easily be generated for any type of nonlinearity with the help of several effective algorithms (Seng et al., 1996; Wazwaz, 2000b; Biazar et al., 2003a; Abdelwahid, 2003; Choi and Shin, 2003; Rach, 2008). The obtained linear equations are solved sequentially and the ADM solution [solution obtained by using ADM] is found by adding the individual solutions [also called decomposed parts of the ADM solution] of these linear equations (Adomian, 1986, 1994). Ultimately, the ADM solution is obtained in the form of a series called Adomian series. This series is basically a generalized Taylor series around a function rather than around a point and in general, converges more rapidly than the Taylor series (Rach et

al., 1992; Cherruault et al., 1995; Wazwaz, 1998). Hence, in general, smaller numbers of terms are sufficient to represent the solutions as compared to the Taylor series.

5.1.1 Adomian Polynomials

In this section, the procedure of generating the Adomian polynomials for any type of nonlinearity has been described. The procedure presented below has been adopted from Adomian (1986, 1994) in which a detailed course of action is given for generating these polynomials for different types of nonlinearities, viz. y'', e^{y^2}, $\sin y^2$. Besides, the stepwise procedure for finding the solutions of different types of equations have also been given in it.

For generating the Adomian polynomials, we consider a nonlinear function $N(y)$ of unknown variable y. y is assumed to be dependent on a hypothetical parameter $\lambda \in [0,1]$, i.e. $y = y(\lambda)$. Using Taylor series y is expanded around $\lambda = 0$ and the following equation is obtained (Adomian, 1986, 1994):

$$y(\lambda) = \sum_{i=0}^{\infty} \lambda^i y_i = y_0 + \lambda y_1 + \lambda^2 y_2 + \ldots \tag{5.1}$$

where $y_i = \dfrac{1}{i!} \dfrac{\partial^i y}{\partial \lambda^i}\bigg|_{\lambda=0}$. Similarly, $N(y(\lambda))$ is expanded around $\lambda = 0$ and one obtains:

$$N(y) = \sum_{i=0}^{\infty} \lambda^i A_i = A_0 + \lambda A_1 + \lambda^2 A_2 + \ldots \tag{5.2}$$

where $A_i \left[= \dfrac{1}{i!} \dfrac{\partial^i N(y)}{\partial \lambda^i}\bigg|_{\lambda=0} \right]$ is the ith Adomian polynomial for nonlinearity $N(y)$, and can be found by substituting the expanded form of y [Eq. (5.1)] into Eq. (5.2) and collecting the terms having same powers of λ. For example, Adomian polynomials for $N(y) = y^2$ are obtained as follows:

(i) From Eq. (5.1), one assumes

$$y(\lambda) = y_0 + \lambda y_1 + \lambda^2 y_2 + \ldots$$

(ii) Substituting the above expression in the concerned nonlinearity, i.e. $N(y) = y^2$

$$N(y) = y^2 = \left(y_0 + \lambda y_1 + \lambda^2 y_2 + \dots \right)^2$$

or

$$N(y) = y_0^2 + 2\lambda y_0 y_1 + \lambda^2 \left(y_0 y_2 + y_1^2 \right) + \dots$$

(iii) On comparing the above expanded form of nonlinearity $N(y) = y^2$ with Eq. (5.2), one finds:

$$A_0 = y_0^2$$

$$A_1 = 2y_0 y_1$$

$$A_2 = \left(y_0 y_2 + y_1^2 \right)$$

...

In this way, one can obtain the expressions of A_is for a given $N(y)$. One should note that there also exist some other algorithms to generate these polynomials more efficiently (Seng et al., 1996; Wazwaz, 2000b; Biazar et al., 2003a; Abdelwahid, 2003; Choi and Shin, 2003).

Once the expressions of A_is are known, they are properly substituted into the concerned equations [AEs, ODEs, PDEs]. Thereafter, each type of equation is solved in their respective manner. It should be noted that the above steps of generating the A_is and the subsequent steps to solve the concerned equations [described later] can easily be implemented in the programming language of robust symbolic computational tools like MATHEMATICA and MAPLE.

5.1.2 Algebraic Equation: Solution by ADM

In this subsection, the application of ADM has been demonstrated for solving a nonlinear AE. For this we consider a nonlinear equation in a single variable $N(y) = 0$,

and express it in the following canonical form (Adomian, 1986; Babolian and Biazar, 2002a, 2002b):

$$y = C_0 + F_0(y) \tag{5.3}$$

where $N(y) = C_0 + F_0(y) - y$, C_0 is a constant and $F_0(y)$ is some function of y. Now, corresponding to Eq. (5.3), the following homotopy is constructed (Li, 2009):

$$y = C_0 + \lambda F_0(y) \tag{5.4}$$

where λ is the same embedding parameter considered in the previous subsection. Using Eqs. (5.1) and (5.2), y and $F_0(y)$ in Eq. (5.4) can be replaced by their respective decomposed parts, as shown below:

$$y_0 + \lambda y_1 + \lambda^2 y_2 + \ldots = C_0 + \lambda(A_0 + \lambda A_1 + \lambda^2 A_2 + \ldots) \tag{5.5}$$

where $y_i \left(= \left. \dfrac{1}{i!} \dfrac{\partial^i y}{\partial \lambda^i} \right|_{\lambda=0} \right)$ is the ith decomposed part of the ADM solution and A_i

$\left(= \left. \dfrac{1}{i!} \dfrac{\partial^i F_0(y)}{\partial \lambda^i} \right|_{\lambda=0} = \left. \dfrac{1}{i!} \dfrac{\partial^i}{\partial \lambda^i} F_0\left(\sum\limits_{i=0}^{\infty} y_i\right) \right|_{\lambda=0} \right)$ is the ith Adomian polynomial corresponding

to the nonlinearity $F_0(y)$.

On comparing the terms in Eq. (5.5) having same power of λ, one finds $y_0 = C_0$, $y_1 = A_0(y_0)$, $y_2 = A_1(y_0, y_1), \ldots, y_i = A_{i-1}(y_0, y_1, \ldots, y_{i-1})$. It is clear that as $\lambda \to 0$, $y = y_0 = C_0$, whereas, if $\lambda \to 1$, $y = y_0 + y_1 + y_2 + \ldots = C_0 + A_0 + A_1 + A_2 + \ldots = F(y)$. This means as λ tends from 0 to 1, the initial guess $[y = y_0 = C_0]$ approaches to the solution of Eq. (5.3), i.e. $y = \sum\limits_{i=0}^{\infty} y_i = C_0 + \sum\limits_{i=0}^{\infty} A_i$. Obviously, there are many ways in which the above canonical form, i.e. Eq. (5.3), can be formed, and therefore, the convergence of the resultant solution strongly depends on the chosen canonical form of the equation. Besides, the final solution form will be different for each of the equation forms. However, if the solution is convergent it will converge to the smallest magnitude root as proved by Adomian (1986); other roots can be found by the repeated application of

191

ADM in conjunction with the deflation method. It can be noted that the above procedure can also be extended, in a similar way, to obtain the solutions of coupled AEs (Babolian et al., 2004a; Kaya and El-Sayed, 2004).

5.1.2.1 Illustration 5.1

In this subsection, ADM has been applied to solve a polynomial equation of third degree, however, for more examples the reader is referred to the literature (Adomian, 1986; Babolian et al., 2004a; Kaya and El-Sayed, 2004).

Consider the following third degree polynomial equation:

$$N(y) = a_3 y^3 + a_2 y^2 + a_1 y + a_0 = 0 \tag{5.6a}$$

where it is assumed that a_is are real and $a_0, a_1 \neq 0$. For finding the ADM solution $[y_{ADM}]$ of Eq. (5.6a), it is first expressed in the following canonical form:

$$\underbrace{y}_{\sum\limits_{i=0}^{\infty} y_i} = \underbrace{-\frac{a_0}{a_1}}_{C_0} - \underbrace{\left(\frac{a_2}{a_1} y^2 + \frac{a_3}{a_1} y^3 \right)}_{F_0(y) = \sum\limits_{i=0}^{\infty} A_i} \tag{5.6b}$$

Thereafter, the Adomian polynomials are found for the nonlinearity $F_0(y)$ as described in subsection 5.1.1, provided $a_0 \neq 0$. In case $a_0 = 0$, a constant may be added in place of C_0 and subtracted from $F_0(y)$. Now, using Eqs. (5.3)-(5.5), one has:

$$y_0 = C_0$$

$$y_1 = A_0(y_0)$$

$$y_2 = A_1(y_0, y_1)$$

...

$$y_i = A_{i-1}(y_0, y_1, ..., y_{i-1})$$

Finally, the ADM solution for a finite number of terms [say n_T] is given by:

$$y_{ADM} = \sum_{i=0}^{n_T-1} y_i = C_0 + \sum_{i=0}^{n_T-1} A_i \qquad (5.6c)$$

For a better understanding, we below obtain the five terms [$n_T = 5$] ADM solution of Eq. (5.6b) for the following values of a_is:

$$a_3 = 1, \ a_2 = 11/6, \ a_1 = 1 \text{ and } a_0 = 1/6$$

For the above values of a_is, the following components of the canonical equation are obtained:

$$C_0 = -\frac{a_0}{a_1} = -\frac{1}{6} \qquad (5.7a)$$

$$F_0(y) = -\frac{a_2}{a_1}y^2 - \frac{a_3}{a_1}y^3 = -\frac{11}{6}y^2 - y^3 \qquad (5.7b)$$

After obtaining the Adomian polynomials for $F_0(y)$, the following values of y_is are obtained:

$$y_0 = C_0 = -1/6$$

$$y_1 = A_0 = -0.0462963$$

$$y_2 = A_1 = -0.0244342$$

$$y_3 = A_2 = -0.0157536$$

$$y_4 = A_3 = -0.0112317$$

Finally, the value of five terms ADM solution is found to be:

$$y_{ADM} = \sum_{i=0}^{4} y_i = -0.264382 \qquad (5.8)$$

Continuing the above steps, the ADM solution can also be found for higher number of terms. Table 5.1 shows the results obtained from the ADM solutions [$n_T = 5$ and 50] and numerical method for several other values of a_3, a_2, a_1, a_0.

Table 5.1: Solutions of cubic equation obtained by using different methods

S. No.	a_3, a_2, a_1, a_0	Solutions [smallest magnitude root]		
		Numerical method	ADM	RADM $[n_T = 5]$
1	1, -6, 11, -6	1	0.849439 [$n_T = 5$], 0.997553 [$n_T = 50$]	0.918895 [$m = 1$] 0.998406 [2] 1.00 [3]
2	1, -11/6, 1, -1/6	1/3	0.264382 [$n_T = 5$], 0.328324 [$n_T = 50$]	0.289849 [1] 0.329913 [2] 0.333329 [3] 0.333333 [4]
3	1, 6, 11, 6	-1	-0.849439 [$n_T = 5$], -0.997553 [$n_T = 50$]	-0.918895 [1] -0.998406 [2] -0.999999 [3] -1.00 [4]
4	1, 11/6, 1, 1/6	-1/3	-0.264382 [$n_T = 5$], -0.328324 [$n_T = 50$]	-0.289849 [1] -0.329913 [2] -0.333329 [3] -0.333333 [4]
5	1, 4, 1, -6	1	ADM failed as the solution diverged.	3.04703 [1] 1.56364 [2] 1.04731 [3] 1.00007 [4] 1.00000 [5]
6	1, -1/6, -2/3, -1/6	-1/3	-0.318742 [$n_T = 5$], -0.333321 [$n_T = 50$]	-0.326532 [1] -0.333318 [2] -0.333333 [3]
7	1, 0, -7, 6	1	0.993045 [$n_T = 5$], 0.999999 [$n_T = 50$]	0.998166 [1] 0.999999 [2] 1.00 [3]
8	1, -7/6, 0, 1/6	-1/3	ADM cannot be used as the canonical form cannot be formed [$a_1 = 0$].	RADM cannot be used as the canonical form cannot be formed [$a_1 = 0$].
9	1, -5/4, 1/8, 1/8	-1/4	ADM failed as the solution diverged.	-0.490489 [1] -0.283132 [2] -0.250259 [3] -0.250000 [4]

It is clear from this table that in some cases, ADM may either fail or exhibit slow convergence. These observations limit the scope of ADM for such cases. To overcome these limitations, some other modified versions of ADM have also been proposed (El-Sayed, 2002; Abbasbandy, 2003; Abbasbandy, 2006b; Jafari and Daftardar-Gejji, 2006; Chun, 2006; Jiao et al., 2008; Li, 2009; Babolian and Biazar, 2002b; Babolian and

Javadi, 2003; Basto et al., 2006). Out of these, we have selected an effective variant of ADM, i.e. Restarted Adomian decomposition method [RADM], which has been described in a later subsection 5.2.1.

5.1.3 Ordinary Differential Equation: Solution by ADM

In this subsection, the methodology of ADM for solving a single ODE has been presented. However, with slight modifications, this methodology can easily be extended to solve the coupled ODEs (Adomian, 1986, 1994). Here, we start by representing the ODE in the following operator form (Adomian, 1986, 1994):

$$F[y(x)] = g(x) \tag{5.9}$$

where $F[y(x)]$ contains various differential operators [with the assumption that the highest differential operator is linear] and the linear/nonlinear terms [functions and operators] of $y(x)$. $g(x)$ is the non-homogeneous term. Eq. (5.9) is further expressed as follows (Adomian, 1986, 1994; Sun et al., 2004; Lesnic, 2007):

$$L[y(x)] - R[y(x)] - N(y(x)) = g(x)$$

or

$$L[y(x)] = g(x) + R[y(x)] + N(y(x)) \tag{5.10}$$

where $F[y(x)] = L[y(x)] - R[y(x)] - N(y(x))$. $L[.]$ is a linear, easily invertible operator of highest differential and $R[.]$ is the remainder of the linear operator. $N(y(x))$ contains the linear/nonlinear terms of $y(x)$.

Now beside x, y is also assumed to be a function of a hypothetical parameter $\lambda \in [0,1]$, i.e. $y = y(x,\lambda)$, and is expanded in the following Taylor series of λ (Adomian, 1986 and 1994):

$$y(x,\lambda) = y(x,\lambda)\big|_{\lambda=0} + \lambda \frac{\partial y(x,\lambda)}{\partial \lambda}\bigg|_{\lambda=0} + \frac{\lambda^2}{2!} \frac{\partial^2 y(x,\lambda)}{\partial \lambda^2}\bigg|_{\lambda=0} + \dots$$

$$= \sum_{i=0}^{\infty} \lambda^i y_i(x,\lambda) \tag{5.11}$$

Like in the case of AEs, here too, $y_i(x)$ $\left[= \dfrac{1}{i!}\dfrac{\partial^i y(x,\lambda)}{\partial \lambda^i}\bigg|_{\lambda=0}\right]$ is the ith decomposed part

of the ADM solution. In a similar fashion, the nonlinearity $N(y(x,\lambda))$ is also

decomposed by expanding it in the following Taylor series of λ :

$$N(y(x,\lambda)) = N(y(x,\lambda))\big|_{\lambda=0} + \lambda\frac{\partial N(y(x,\lambda))}{\partial \lambda}\bigg|_{\lambda=0} + \frac{\lambda^2}{2!}\frac{\partial^2 N(y(x,\lambda))}{\partial \lambda^2}\bigg|_{\lambda=0} + \ldots$$

$$= \sum_{i=0}^{\infty} \lambda^i A_i(y_0(x), y_1(x), \ldots, y_{i-1}(x)) \tag{5.12}$$

where $A_i = \left[= \dfrac{1}{i!}\dfrac{\partial^i N(y(x,\lambda))}{\partial \lambda^i}\bigg|_{\lambda=0}\right]$ is the ith Adomian polynomial corresponding to the

nonlinearity $N(y(x))$. For simplicity, now onwards $y(x,\lambda)$ and $N(y(x,\lambda))$ are denoted

by y and $N(y)$, respectively.

Using Eq. (5.10) the following homotopy is constructed (Li, 2009) [other homotopy equations may also be constructed and the convergence of the obtained solution depends on the form of homotopy equation].

$$L[y] = g(x) + \lambda(R[y] + N(y)) \tag{5.13}$$

Using Eqs. (5.11)-(5.13) one obtains:

$$L[\sum_{i=0}^{\infty} \lambda^i y_i] = g(x) + R[\sum_{i=0}^{\infty} \lambda^{i+1} y_i] + \sum_{i=0}^{\infty} \lambda^{i+1} A_i(y_0, y_1, \ldots, y_i) \tag{5.14}$$

It is clear from Eq. (5.14) that as λ tends from 0 to 1, the solution varies from the

initial guess $y = y_0$ [solution of $L[y] = g(x)$] to $y = \sum_{i=0}^{\infty} y_i$ [solution of

$L[y] = g(x) + R[y] + N(y)$]. Applying the inverse operator L^{-1} to the both side of Eq.

(5.14), one obtains the following equation [L^{-1} actually denotes n times integration for

an nth order differential operator L. However, depending on the problem other

definitions of L^{-1} can also be used. But, L^{-1} should have the same number of integral

operators as the number of orders in the highest order derivative term and should be

dimensionally consistent].

$$\sum_{i=0}^{\infty} \lambda^i y_i = C_n + C_{n-1}x + \ldots + C_2 x^{n-2} + C_1 x^{n-1} + L^{-1}[g(x)] + L^{-1}[R[\sum_{i=0}^{\infty} \lambda^{i+1} y_i]]$$

$$+ L^{-1}[\sum_{i=0}^{\infty} \lambda^{i+1} A_i] \tag{5.15}$$

where $L^{-1}[0] = C_n + C_{n-1}x + \ldots + C_2 x^{n-2} + C_1 x^{n-1}$. C_is $[i = 1, 2 \ldots, n]$ are the n constants of integration. At this instant, the terms having same exponents of λ are compared to give the following relations:

$$y_0 = C_n + C_{n-1}x + \ldots + C_2 x^{n-2} + C_1 x^{n-1} + L^{-1}[g(x)]$$

$$y_1 = L^{-1}[R[y_0]] + L^{-1}[A_0(y_0)]$$

$$y_2 = L^{-1}[R[y_1]] + L^{-1}[A_1(y_0, y_1)]$$

$$y_3 = L^{-1}[R[y_2]] + L^{-1}[A_2(y_0, y_1, y_2)]$$

$$\ldots$$

Finally, the following ADM solution is obtained by adding the above decomposed parts:

$$y|_{\lambda=1} = \sum_{i=0}^{\infty} y_i$$

$$= C_n + \ldots + C_1 x^{n-1} + L^{-1}[g(x)] + L^{-1}[R[y_0]] + L^{-1}[A_0(y_0)] + L^{-1}[R[y_1]]$$

$$+ L^{-1}[A_1(y_0, y_1)] + \ldots \tag{5.16}$$

C_i's are evaluated by using the corresponding ICs and BCs. An illustration for the application of ADM has been presented next.

5.1.3.1 Illustration 5.2

The following linear second order ODE constituting a BVP has been solved by applying ADM. This type of equation frequently appears in the modelling of heat transfer and reaction-diffusion processes (Fogler, 1992; Bird et al., 2002).

197

$$\frac{d^2y}{dx^2} - y = 0 \qquad\qquad (5.17a)$$

BC I: $\quad \dfrac{dy}{dx} = 0$ at $x = 0$ $\qquad\qquad (5.17b)$

BC II: $\quad y = 1$ at $x = 1$ $\qquad\qquad (5.17c)$

The analytical solution of Eqs. (5.17a)-(5.17c) is available in many texts (Bird et al., 2002) and is given by:

$$y = \frac{cosh[x]}{cosh[1]} \qquad\qquad (5.18)$$

For finding the ADM solution, the Eq. (5.17a) is compared with Eq. (5.10), and one obtains: $\quad L[.] = \dfrac{d^2}{dx^2}[.]$, $\quad g(x) = 0$, $\quad R[y] = 0 \quad$ and $\quad N(y) = y$. Therefore,

$L^{-1}[.] = \displaystyle\int_0^x\int [.]dxdx \quad$ and $\quad L^{-1}(0) = C_2 + C_1 x$, where C_1 and C_2 are the constants of integration and are found from the above BCs. Using Eqs. (5.11) and (5.12), y and $N(y)$ are decomposed into their respective parts, i.e. $y = \displaystyle\sum_{i=0}^{\infty} \lambda^i y_i$ and $N(y) = \displaystyle\sum_{i=0}^{\infty} \lambda^i A_i$. It can be verified that for $N(y) = y$ the Adomian polynomials are same as the decomposed parts of the ADM solution, i.e. $A_i = y_i$. Now, with the help of the Eqs. (5.14) and (5.15), one obtains the following relations:

$$y_0 = C_2 + C_1 x$$

$$y_1 = L^{-1}[A_0] = L^{-1}[y_0]$$

$$y_2 = L^{-1}[A_1] = L^{-1}[y_1]$$

$$y_3 = L^{-1}[A_2] = L^{-1}[y_2]$$

$$\cdots$$

However, $C_1 = 0$ from BC I, and the above relations reduce to:

$$y_0 = C_2$$

198

$$y_1 = L^{-1}[A_0] = L^{-1}[y_0] = C_2 \frac{x^2}{2}$$

$$y_2 = L^{-1}[A_1] = L^{-1}[y_1] = C_2 \frac{x^4}{24}$$

$$y_3 = L^{-1}[A_2] = L^{-1}[y_2] = C_2 \frac{x^6}{720}$$

$$y_4 = L^{-1}[A_3] = L^{-1}[y_3] = C_2 \frac{x^8}{40320}$$

$$\cdots$$

Eventually, the five terms [$n_T = 5$] ADM solution is found to be:

$$y_{ADM} = \sum_{i=0}^{4} y_i = C_2 + C_2 \frac{x^2}{2} + C_2 \frac{x^4}{24} + C_2 \frac{x^6}{720} + C_2 \frac{x^8}{40320} \qquad (5.19)$$

C_2 can be found from BC II and is given by:

$$C_2 = \frac{4480}{6913} \qquad (5.20)$$

Substituting this value of C_2 in Eq. (5.19), the following ADM solution is obtained:

$$y_{ADM} = 0.648054 + 0.324027x^2 + 0.027002x^4 + 0.0009x^6 + 0.000016x^8 \qquad (5.21)$$

Taylor series expansion of the analytical solution [Eq. (5.18)], around $x = 0$ and up to the eight power of x, yields the following series solution:

$$y \approx 0.648054 + 0.324027x^2 + 0.027002x^4 + 0.0009x^6 + 0.000016x^8 \qquad (5.22)$$

It can be seen that both the solutions [Eqs. (5.21) and (5.22)] match well, and thus the validity of the ADM solution is established. We have also compared the ADM solutions [for different n_T] with analytical solution by plotting them in Fig. 5.1. This figure clearly shows that with the increase in number of terms [n_T], the ADM solution approaches to the analytical solution.

199

5.2 RESTARTED ADOMIAN DECOMPOSITION METHOD [RADM]

Sometimes due to the poor selection of various quantities, e.g. initial guess, linear operator, canonical form of the equation, the solutions of AEs, ODEs, PDEs obtained by using ADM may diverge. In such circumstances, various modifications in ADM have been proposed. In the following subsections, one such modified version of ADM, namely RADM has been presented for finding the solutions of AEs and ODEs.

5.2.1 Algebraic Equation: Solution by RADM

As shown earlier in the subsection 5.1.2.1, the ADM solution of an AE may converge slowly or may even diverge. This may happen either due to the poor selection of canonical form or due to the presence of complex roots (Adomian, 1986). To overcome this problem as well as to get the results more accurately and quickly, several researchers (Babolian and Biazar, 2002a, 2002b; Babolian and Javadi, 2003) modified the ADM by devising an iterative procedure for updating the Eq. (5.3). The updated equation was then solved by using ADM and this modified ADM was named as Restarted Adomian decomposition method [RADM]. Although, RADM is also not fool proof but many a times it performed better than ADM. The steps involved are summarized below and the details of these modifications can be found in the original works of Babolian and Biazar (2002a, 2002b), and Babolian and Javadi (2003).

Following updating procedure is adopted for Eq. (5.3):

Step 1: $\qquad C_m = C_0 \qquad$ for $m = 1 \qquad$ and

$$C_m = y^{(m-1)} \quad \text{for } m > 1 \tag{5.23a}$$

Step 2: $\qquad F_m(y) = \dfrac{F_0(y) - yF_0'(C_m) + C_0}{1 - F_0'(C_m)} - C_m \quad \text{for } m \geq 1$

$$\text{and } F_0'(C_m) \neq 1 \tag{5.23b}$$

Step 3: $\qquad y^{(m)} = C_m + F_m(y) \qquad \text{for } m \geq 1 \tag{5.23c}$
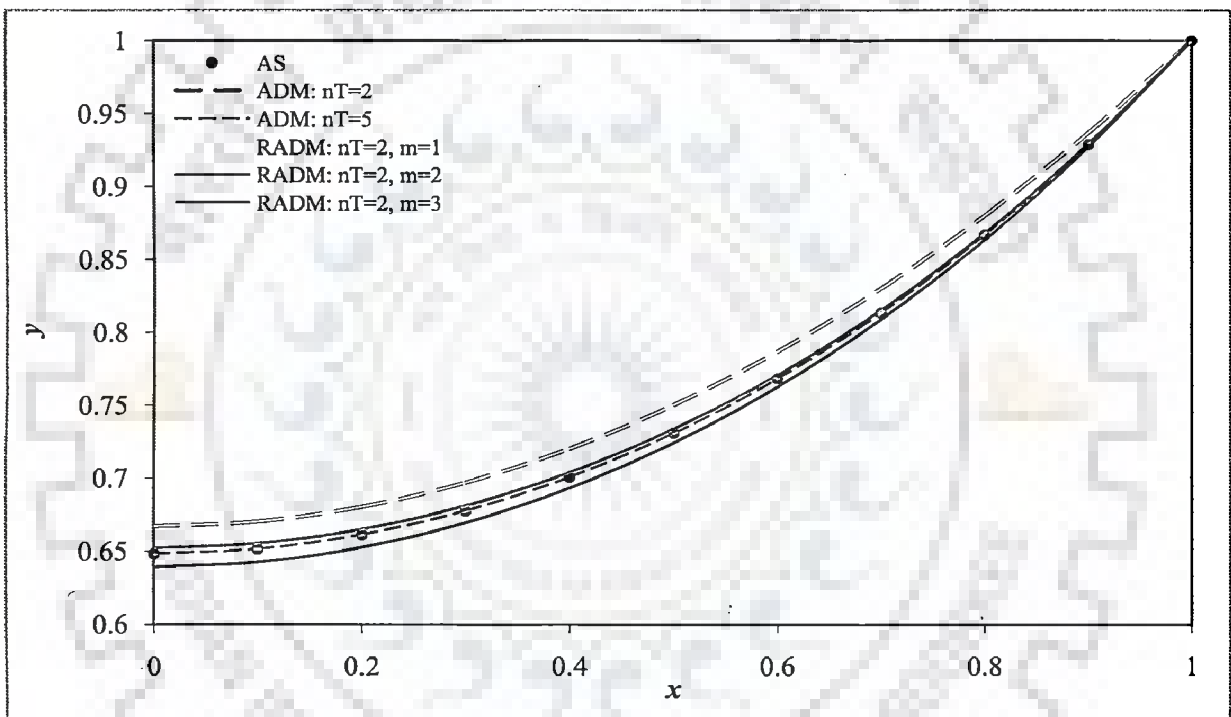
Figure 5.1: Comparison of the solutions of illustration 5.2 obtained by using different methods

where $y^{(m)}$ denotes the solution obtained after the mth iteration of RADM and F_0' denotes $\dfrac{dF_0}{dy}$. C_0 and $F_0(y)$ in Eq. (5.3) are updated using the steps 1 and 2 [one should note that at $m = 1$, C_1 is taken equal to C_0]; thereafter, the solution is obtained for each iteration by applying ADM to the updated equation, i.e. Eq. (5.23c). In the next iteration, the value of the so found solution is used to update C_m and $F_m(y)$ through Eqs. (5.23a) and (5.23b), respectively. With the updated C_m and $F_m(y)$, the newer canonical form, i.e. Eq. (5.23c), is formed and solved by using ADM. This procedure is repeated until one gets the result of desired accuracy.

Using the above step wise procedure of RADM, we have solved all the examples mentioned in Babolian and Javadi (2003) and the results matched up to the last digit. The following illustration explains the procedure of RADM for solving AEs.

5.2.1.1 Illustration 5.3

The application of RADM has been demonstrated by solving the previously treated third degree polynomial equation, i.e. Eq. (5.6a), for the same values of a_i s as those given in Table 5.1. For demonstration, we have considered the values of a_i s given at serial number 5 in Table 5.1, i.e. $a_3 = 1$, $a_2 = 4$, $a_1 = 1$, $a_0 = -6$. This is because, ADM failed to get the solution for this set of values. Here also, five terms [$n_T = 5$] have been considered in the RADM solution.

Following canonical form is selected, before the first iteration [$m = 1$] of RADM is executed:

$$y = C_0 + F_0(y) \tag{5.24a}$$

$$C_0 = -\frac{a_0}{a_1} = 6 \text{ and } F_0(y) = -\frac{a_2}{a_1}y^2 - \frac{a_3}{a_1}y^3 = -4y^2 - y^3 \tag{5.24b}$$

In the first iteration, the corresponding values of updated equation, evaluated from Eqs. (5.23a)-(5.23c), are:

$$C_1 = C_0 = 6 \text{ and}$$

$$F_1(y) = -5.96178 + 0.993631y - 0.0254777y^2 - 0.00636943y^3 \qquad (5.25a)$$

The updated canonical form is given by:

$$y = C_1 + F_1(y) \qquad (5.25b)$$

By solving the Eq. (5.25b) with the help of ADM, one finds the following solution for the first iteration of RADM:

$$y^{(1)} = 3.04703$$

In the second iteration $[m = 2]$, one has:

$$C_2 = y^{(1)} = 3.04703$$

and

$$F_2(y) = -2.93431 + 0.981213y - 0.0751463y^2 - 0.0187866y^3 \qquad (5.26a)$$

$$y = C_2 + F_2(y) \qquad (5.26b)$$

Solving the Eq. (5.26b) by using ADM, one obtains the following solution for this iteration:

$$y^{(2)} = 1.56364$$

Similarly, in the third iteration $[m = 3]$, one finds:

$$C_3 = y^{(2)} = 1.56364$$

and

$$F_3(y) = -1.27579 + 0.952025y - 0.191901y^2 - 0.0479752y^3 \qquad (5.27a)$$

$$y = C_3 + F_3(y) \qquad (5.27b)$$

Applying ADM to Eq. (5.27b), the following solution is obtained for the third iteration:

$$y^{(3)} = 1.04731$$

In this way, one solves the Eq. (5.24b) by using RADM. For several values of a_i s, the RADM solutions of this equation have also been presented in Table 5.1. It is observed that RADM successfully found the solutions in a few iterations, except where canonical form cannot be formed. In few cases, this method may also diverge and for such a situation, Basto et al. (2006) have given a remedy. However, in the present illustration, this situation did not arise.

5.2.2 Ordinary Differential Equation: Solution by RADM

As stated in the case of AEs, the ADM solutions of ODEs may also diverge in some cases, discussed later in last two problems. In such situations, a modified version of ADM, namely RADM can be adopted. RADM was first developed by Babolian et al. (2004b) for solving the IEs, however, we have found that this method works well for many ODEs, and here, the same methodology has been adopted for solving ODEs as was followed by these researchers to solve IEs.

The RADM for ODEs is basically a type of iterative ADM and is somewhat similar to the RADM for AEs. In this subsection, we describe the working of RADM by focussing on the Eq. (5.10), which was earlier solved by using ADM in subsection 5.1.3. The key steps of RADM are as follows:

(i) The first iteration $[m = 1]$ is same as that of finding the ADM solution. In other words, first the ADM solution of Eq. (5.10) [given by Eq. (5.16)] is found. Let this solution be denoted by:

$$y_{RADM,m=1} = y_{ADM} \tag{5.28a}$$

(ii) In the second iteration $[m = 2]$, the same iterative steps are followed for finding the y_is, which were followed in ADM. However, now the following modified relations of y_0 and y_1 are used, whereas, the definitions of rest of the y_is remain the same.

$$y_0 = y_{RADM,m=1}$$

$$y_1 = L^{-1}[R[y_0]] + L^{-1}[A_0(y_0)] + C_n + C_{n-1}x + \ldots + C_2 x^{n-2} + C_1 x^{n-1} + L^{-1}[g(x)] - y_{RADM,m=1}$$

$$y_2 = L^{-1}[R[y_1]] + L^{-1}[A_1(y_0, y_1)]$$

$$y_3 = L^{-1}[R[y_2]] + L^{-1}[A_2(y_0, y_1, y_2)]$$

...

For this iteration $[m = 2]$ and for n_T number of terms, the solution obtained by using RADM is given by:

$$y_{RADM, m=2} = \sum_{i=0}^{n_T-1} y_i \tag{5.28b}$$

C_i s are found by using the associated ICs and BCs.

(iii) For higher iterations $[m = 3, 4...]$, the step (ii) is repeated for a specified number of times, i.e.

$$y_0 = y_{RADM, m=2}$$

$$y_1 = L^{-1}[R[y_0]] + L^{-1}[A_0(y_0)] + C_n + C_{n-1}x + ... + C_2 x^{n-2} + C_1 x^{n-1} + L^{-1}[g(x)] - y_{RADM, m=2}$$

$$y_2 = L^{-1}[R[y_1]] + L^{-1}[A_1(y_0, y_1)]$$

$$y_3 = L^{-1}[R[y_2]] + L^{-1}[A_2(y_0, y_1, y_2)]$$

...

And the solution for this iteration of RADM is given by:

$$y_{RADM, m=3} = \sum_{i=0}^{n_T-1} y_i \tag{5.28c}$$

C_i s are again found by using the associated ICs and BCs. This step may be repeated as many times as required. For a better understanding of RADM, an illustration is presented in the next subsection.

5.2.2.1 Illustration 5.4

For the purpose of comparison, the same ODE, earlier solved in illustration 5.2 by using ADM [Eqs. (5.17a)-(5.17c)], has been solved here by using RADM. However, to show the efficacy of RADM over ADM, only two terms [$n_T = 2$] have been considered in RADM solution. Moreover, the same definitions of $L[.]$, $L^{-1}[.]$, $g(x)$, $R[.]$ and $N(y)$ have been used in RADM, which were used in ADM.

As described in step (i), the following two terms ADM solution is found in the first iteration [$m = 1$].

$$y_{RADM,m=1} = y_{ADM} = \frac{2}{3} + \frac{1}{3}x^2 \qquad (5.29)$$

By pursuing the step (ii), the following relations of y_0 and y_1 are obtained in the second iteration [$m = 2$]. It should be noted that, here too, C_1 will be zero [due to BC I] for all the iterations of RADM.

$$y_0 = y_{RADM,m=1} = y_{ADM} = \frac{2}{3} + \frac{1}{3}x^2$$

$$y_1 = L^{-1}[A_0] + C_2 - y_{RADM,m=1}$$

$$= L^{-1}[y_0] + C_2 - y_{RADM,m=1}$$

$$= C_2 - \frac{2}{3} + \frac{1}{36}x^4$$

Finally, the following two terms solution is obtained after the second iteration of RADM:

$$y_{RADM,m=2} = y_0 + y_1$$

$$= C_2 + \frac{1}{3}x^2 + \frac{1}{36}x^4$$

$$= 0.638889 + 0.333333x^2 + 0.0277778x^4 \qquad (5.30)$$

where C_2 [= 0.638889] has been found from BC II. Similarly, in the third iteration [$m = 3$], one has:

$$y_0 = y_{RADM,m=2} = 0.638889 + 0.333333x^2 + 0.0277778x^4$$

$$y_1 = L^{-1}[y_0] + C_2 - y_{RADM,m=2}$$

Adding y_0 and y_1 yields the following two terms solution after the third iteration of RADM:

$$y_{RADM,m=3} = y_0 + y_1$$

$$= 0.651852 + 0.319444x^2 + 0.0277778x^4 + 0.0009259x^6 \qquad (5.31)$$

where C_2 [= 0.651852] has again been found from BC II. In this way, RADM solutions can be found for higher number of iterations. The above obtained RADM solutions have been plotted in Fig. 5.1 along with the earlier obtained analytical and ADM solutions. It is clear from this figure that the accuracy of the approximate solutions obtained by using RADM increases with each iteration [m]. This fact is also evident from Eq. (5.31), which is approximately same as the Taylor series expansion of the analytical solution, i.e. Eq. (5.22). In contrast to this, the two terms ADM solution shows deviation from the analytical solution.

It is also noteworthy that the above iterative procedure works only for polynomial nonlinearities. Since, for other complicated forms of nonlinearities, e.g. non-integer power of y or some polynomial fractions of y, the above procedure gives rise to some un-integrable terms. However, in such cases the nonlinearity can be expressed as a polynomial nonlinearity by approximating it with the help of some appropriate orthogonal polynomials [OPs]. Moreover, after each iteration of RADM, the terms in solution expression, which when used in the next iteration, may yield even larger expression. Hence, these solutions may also be approximated after each iteration of RADM by using some suitable OPs. Use of OPs with RADM has been shown later in this chapter, while solving the model equations of reaction-diffusion processes.

5.3 THERMODYNAMIC EQUATION OF STATE

In this section, we have solved the Beattie-Bridgeman equation of state, by using ADM and RADM. This equation has been chosen since ADM and RADM exemplify some important characteristics and one can get a better insight for the usefulness or limitations of these methods.

5.3.1 Beattie-Bridgeman Equation of State

The Beattie-Bridgeman equation of state is a well known relation and is widely used to predict the gas volume at a given pressure and temperature. It is basically a fourth degree polynomial equation [quartic equation] in volume. In standard form this equation of state is written as (Annamalai and Puri, 2002):

$$PV = RT + \frac{\beta}{V} + \frac{\gamma}{V^2} + \frac{\delta}{V^3} \qquad (5.32)$$

where $\beta = RTB_0 - A_0 - \frac{Rc}{T^2}$, $\gamma = -RTB_0 b + \alpha A_0 - \frac{RB_0 c}{T^2}$ and $\delta = \frac{RB_0 bc}{T^2}$

5.3.2 Solutions and Discussion: Gas Volume

Here, the Eq. (5.32) has been solved by taking n-butane as an example, and the volume of this gas, corresponding to different pressures but at a fixed temperature $T = 425K$, has been found. Three different canonical forms of Eq. (5.32) are considered and the effects of these canonical forms on the convergence of ADM and RADM solutions have been studied. The constants for n-butane have been taken from Annamalai and Puri (2002) and are given below. It should be noted that for the following set of values, the volume of n-butane has been computed in litre (l).

$A_0 = 17.794 \ atm.l^2$, $B_0 = 0.2462 \ mol.l$, $b = 0.09423 \ l$, $c = 350 \times 10^4 \ l.K.mol$,

$R = 0.08206 \ atm.l.K^{-1}.mol^{-1}$, $\alpha = 0.12161 \ l$

5.3.2.1 Solution by ADM

(i) Canonical Form - I

The following canonical form of Eq. (5.32) has been considered:

$$V = \underbrace{\frac{RT}{P}}_{C_0} + \underbrace{\frac{\beta}{PV} + \frac{\gamma}{PV^2} + \frac{\delta}{PV^3}}_{F_0(V)} \qquad (5.33)$$

Proceeding as described in subsection 5.1.2., the following two decomposed pats of the ADM solution are obtained:

$$y_0 = \frac{RT}{P}$$

$$y_1 = \frac{RT(RT\beta + P\gamma) + P^2\delta}{R^3T^3}$$

Hence, the two terms [$n_T = 2$] ADM solution of Eq. (5.33) is given by:

$$V_{ADM} = y_0 + y_1$$

$$= \frac{RT}{P} + \frac{RT(RT\beta + P\gamma) + P^2\delta}{R^3T^3} \qquad (5.34)$$

In a similar fashion, the ADM solutions for higher number of terms [$n_T = 5, 15$] have also been obtained and the results obtained by using them have been tabulated in Table 5.2. As shown in this table, the above obtained two terms ADM solution [Eq. (5.34)] gives rise to $\pm 1\%$ error up to 10 *atm.* pressure. It is also observed that as the terms in ADM solution are increased, the error decreases, whereas, for a fixed number of terms the error increases at higher pressures; even 15 terms do not give sufficiently accurate results and higher terms are needed for pressures above 30 *atm.*

(ii) Canonical Form - II

After little manipulation the following canonical form of the Eq. (5.32) is obtained:

210

$$V = -\underbrace{\frac{\delta}{\gamma}}_{C_0} + \underbrace{\left(\frac{P}{\gamma}V^4 - \frac{RT}{\gamma}V^3 - \frac{\beta}{\gamma}V^2 \right)}_{F_0(V)}$$ (5.35)

After solving the Eq. (5.35) by using ADM, the following two decomposed parts of the ADM solution are found:

$$y_0 = -\frac{\delta}{\gamma}$$

$$y_1 = \frac{\delta^2 \left(-\beta\gamma^2 + \delta(RT\gamma + P\delta) \right)}{\gamma^5}$$

Table 5.2: **Results of Beattie-Bridgeman equation of state obtained by using numerical method and ADM**

P (atm)	$V_{Numerical}$ (l)	V_{ADM} (l)		
		$n_T = 2$	$n_T = 5$	$n_T = 15$
		Canonical Form - I		
1	34.563900	34.566700	34.563900	34.563900
10	3.155120	3.185950	3.155400	3.155120
20	1.378070	1.450360	1.383170	1.378090
30	0.735711	0.877452	0.769839	0.738326
40	0.229100	0.595352	0.447926	0.323752
		Canonical Form - II		
1	34.563900	-0.019822	-0.049966	-7.704420
10	3.155120	-0.019802	-0.050172	-8.030790
20	1.378070	-0.019780	-0.050402	-8.407540
30	0.735711	-0.019758	-0.050633	-8.799670
40	0.229169	-0.019735	-0.050866	-9.207700
		Canonical Form - III		
1	34.563900	34.569400	34.563900	34.563900
10	3.155120	3.209960	3.155850	3.155120
20	1.378070	1.492620	1.388910	1.378100
30	0.735711	0.933588	0.791929	0.740605
40	0.229169	0.661941	0.498316	0.367304

Thus, the two terms $[n_T = 2]$ ADM solution is obtained as follows:

$$V_{ADM} = y_0 + y_1$$

$$= -\frac{\delta}{\gamma} + \frac{\delta^2\left(-\beta\gamma^2 + \delta\left(RT\gamma + P\delta\right)\right)}{\gamma^5} \qquad (5.36)$$

In a similar pattern, the ADM solutions for higher number of terms have been found and the results obtained from the so found ADM solutions are also given in Table 5.2. This table clearly shows that the ADM solutions failed to yield the correct results for this canonical form. It is even noted that the consideration of more terms in ADM solution increases the divergence as can be verified by the ratio test of the generated solution. This divergence of ADM can be attributed to the fact that the initial guess for this canonical form, i.e. $y_0 \; [= C_0] = -\dfrac{\delta}{\gamma}$, is poor.

(iii) Canonical Form - III

After defining $y = V^{-1}$, the Eq. (5.32) attains the following canonical form:

$$y = \underbrace{\frac{P}{RT}}_{C_0} + \underbrace{\left(-\frac{\beta}{RT}y^2 - \frac{\gamma}{RT}y^3 - \frac{\delta}{RT}y^4\right)}_{F_0(y)} \qquad (5.37)$$

Subjecting the above equation to ADM, the following two decomposed parts of the ADM solution are obtained:

$$y_0 = \frac{P}{RT}$$

$$y_1 = -\frac{P^2RT\left(RT\beta + P\gamma\right) + P^4\delta}{R^5T^5}$$

And the two terms ADM solution is found to be:

$$y_{ADM} = y_0 + y_1$$

$$y_{ADM} = \frac{P}{RT} - \frac{P^2RT(RT\beta + P\gamma) + P^4\delta}{R^5T^5}$$

Therefore, the two terms ADM solution of volume [$y = V^{-1}$] is given by:

$$V_{ADM} = \frac{1}{y_{ADM}} = \frac{R^5T^5}{PRT(R^3T^3 - PRT\beta - P^2\gamma) - P^4\delta} \qquad (5.38)$$

On the same lines, ADM solutions have been found for higher values of n_T, and the results obtained from thus derived solutions are presented in Table 5.2. Here also, it is observed that the error in ADM solution [Eq. (5.38)] decreases with the increase in number of terms. While no divergence occurred in the ADM solution, yet the error increases with the increase in pressure.

5.3.2.2 Solution by RADM

Following the steps described in subsection 5.2.1, the solutions of the above three canonical forms [Eqs. (5.33), (5.35) and (5.37)] have also been obtained below by using RADM.

(i)   Canonical Form - I

By solving the Eq. (5.33) with the help of RADM, one obtains the following two decomposed parts [$n_T = 2$] of the RADM solution after the first iteration [$m = 1$]:

$$y_0 = \frac{RT}{P}$$

$$y_1 = \frac{RT\left(RT\left(RT\beta + P\gamma\right) + P^2\delta\right)}{RT\left(R^3T^3 + PRT\beta + 2P^2\gamma\right) + 3P^3\delta}$$

Hence, the two terms RADM solution after the first iteration is given by:

$$V_{RADM} = y_{RADM} = y_0 + y_1$$

$$= \frac{RT}{P} + \frac{RT\left(RT\left(RT\beta + P\gamma\right) + P^2\delta\right)}{RT\left(R^3T^3 + PRT\beta + 2P^2\gamma\right) + 3P^3\delta} \tag{5.39}$$

On the same lines, one can obtain the RADM solutions for higher values of n_T and m. For some of the values of n_T and m, the results of this canonical form obtained by using RADM have been presented in Table 5.3. As illustrated in this table, the RADM yields satisfactory results, yet increasing the terms doesn't always guarantee the quick and convergent solution, e.g. the results obtained for $P = 40$ *atm* by considering $n_T = 15$ in RADM solution. A comparison between the results of this canonical form, obtained by using ADM [Tables 5.2] and RADM [Tables 5.3], suggest that the results obtained by using ADM do not diverge, whereas, those obtained by using RADM may converge/diverge or may even fluctuate as n_T is increased up to some particular value, and only after considering more terms in RADM, the correct results can be obtained.

For $P = 40$ *atm*, the results of this canonical form obtained after each iteration of RADM, have also been shown in Figs. 5.2 - 5.4. Fig. 5.2 shows that the results obtained for $n_T = 2$ and 5 converge smoothly to the correct value. Although not shown, yet this is also found to be true for $n_T = 4$ and 20; for $n_T = 20$ the convergence was very fast. Similarly, Fig. 5.3 depicts that the results obtained for $n_T = 18$ finally converge to the true value, but one or more peaks are observed; again not shown, yet this is also true for $n_T = 8$ and 16. Fig. 5.4 presents an interesting characteristic of the obtained results and it is noted that for $n_T = 6$, 10, 12 and 15, the results are quite oscillating, and various numerical runs have shown that these oscillations are present even after 500 iterations. This phenomenon was also observed by Basto et al. (2006) while solving the AEs by using RADM, and to get the correct results for these numbers of terms, C_0 in Eq. (5.33) was recommended to change keeping it close to the correct value.

The above observations reveal that between the converging limits, i.e. $n_T = 5$ and 20, the results obtained by using RADM may not necessarily converge, rather these may exhibit divergence, fluctuations or even continued oscillations. Despite these observations, it has been found that if the result converges for several values of n_T, then

214

for larger n_T the routine needs lesser number of iterations to get the correct value and vice versa.

Table 5.3: Results of Beattie-Bridgeman equation of state obtained by using RADM and numerical method for its different canonical forms

P (atm)	$V_{Numerical}$ (l)	V_{RADM} (l)			
		$n_T = 2$	$n_T = 5$	$n_T = 15$	$n_T = 18$
		Canonical Form - I			
1	34.563900	34.563900 [m=1]	34.563900	34.563900	-
10	3.155120	3.158230 [1] 3.155120 [2]	3.155200	3.155200	-
30	0.735711	0.795437 [1] 0.738723 [2] ... 0.735711 [4]	0.757059 0.735730 0.735711	0.736738 0.735711	-
40	0.229169	0.489065 [1] 0.306399 [2] ... 0.229169 [12]	0.414231 [1] 0.044825 [2] ... 0.229169 [10]	0.284262 [1] 8777.080000 [2] ... 8463.370000[14]	0.257108 [1] 2.146280 [2] ... 0.229169 [8]
		Canonical Form - II			
1	34.563900	-0.029139 [m=1] ... -0.028413 [4]	-0.028515 [1] -0.028413 [2]	-0.028413 -0.028413	-
10	3.155120	-0.029139 [1] -0.028414 [2] -0.028409 [3]	-0.028512 -0.028409	-0.028409	-
30	0.735711	-0.029138 -0.028406 -0.028402	-0.028506 -0.028402	-0.028402	-
40	0.229169	-0.029137 -0.028402 -0.028398	-0.028503 -0.028398	-0.028398	-
		Canonical Form - III			
1	34.563900	34.563900 [m=1]	34.563900 34.563900	34.563900 34.563900	-
10	3.155120	3.158230 [1] 3.155120 [2] 3.155120 [3]	3.155180 3.155120	3.155120	-
30	0.735711	0.795437 [1] ... 0.735711 [4]	0.755985 0.735727 0.735711	0.736276 0.735711	-
40	0.229169	0.489065 [1] 0.306399 [2] ... 0.229169 [12]	0.417202 [1] 0.282288 [2] ... -0.028398 [8]	0.352443 [1] 0.000000 [2] ... 0.000000 [5]	0.153795 [1] 0.226123 [2] ... 0.229169 [4]

- Results not computed

215

(ii)   Canonical Form - II

By applying RADM to this canonical form [Eq. (5.35)], the following two decomposed parts of the solution are found after the first iteration:

$$y_0 = -\frac{\delta}{\gamma}$$

$$y_1 = \frac{\delta^2\left(-\beta\gamma^2 + \delta\left(RT\gamma + P\delta\right)\right)}{\gamma\left(\gamma^4 - 2\beta\gamma^2\delta + 3RT\gamma\delta^2 + 4P\delta^3\right)}$$

And the two terms RADM solution is given by:

$$V_{RADM} = y_{RADM} = y_0 + y_1$$

$$= -\frac{\delta}{\gamma} + \frac{\delta^2\left(-\beta\gamma^2 + \delta\left(RT\gamma + P\delta\right)\right)}{\gamma\left(\gamma^4 - 2\beta\gamma^2\delta + 3RT\gamma\delta^2 + 4P\delta^3\right)} \qquad (5.40)$$

In the same way, one can obtain the solutions of this canonical form for higher values of n_T and m. The results obtained by these solutions are also presented in Table 5.3, which shows that the RADM failed to deliver the correct results of Eq. (5.35). This is due to the poor choice of the initial guess, i.e. $y_0 = C_0 = -\frac{\delta}{\gamma}$. Unlike the results of this canonical form obtained by using ADM [Table 5.2], the results obtained by using RADM converged to another negative real root, and increasing the terms in RADM decreases the number of iterations required for arriving at this negative root. Moreover, unlike the results of canonical form-I obtained by using RADM [Table 5.3], no oscillations are present in the results of this canonical form as n_T is increased.

(iii)   Canonical Form - III

For this canonical form [Eq. (5.37)], the following two decomposed terms are obtained after the first iteration of RADM:

$$y_0 = \frac{P}{RT}$$

216
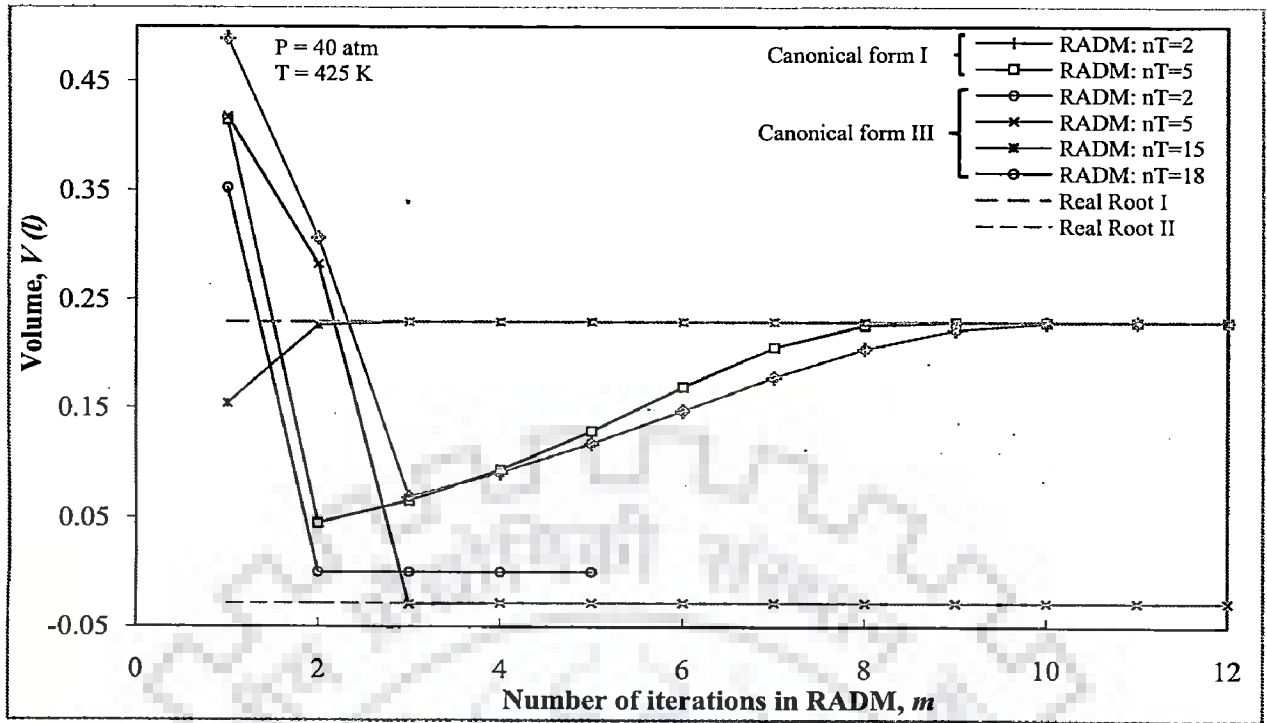
Figure 5.2: Variation of volume with number of iterations in RADM for different number of terms [n_T]
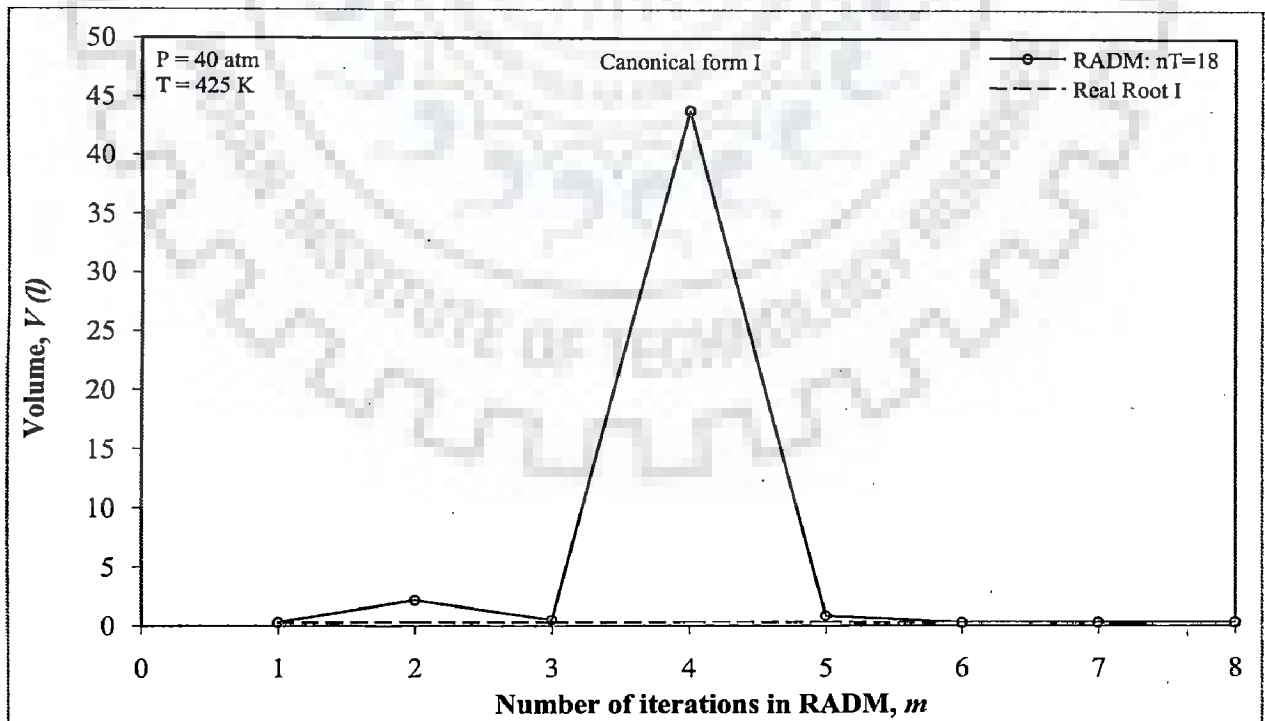
Figure 5.3: Variation of volume with number of iterations in RADM [real root I is same as that of Fig. 5.2]
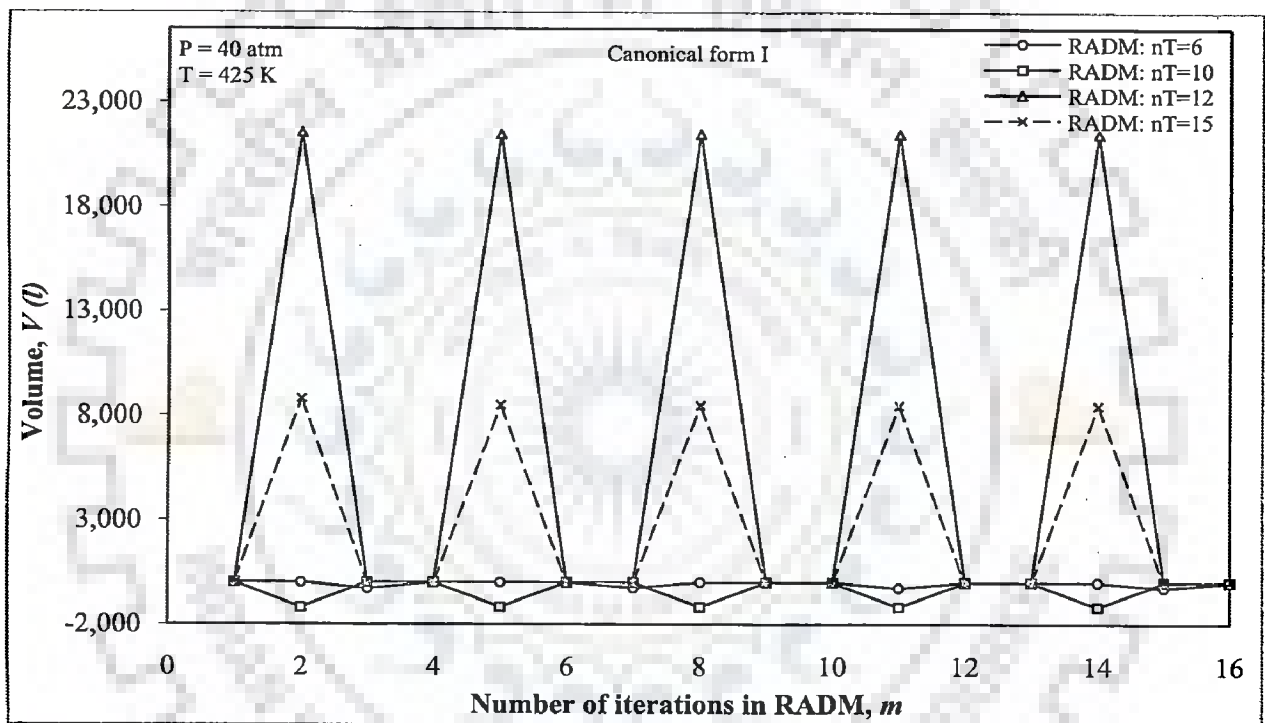
Figure 5.4: **Variation of volume with number of iteration in RADM**

$$y_1 = -\frac{P^2 RT \left(RT\beta + P\gamma \right) + P^4\delta}{RT \left(RT \left(R^3 T^3 + 2PRT\beta + 3P^2\gamma \right) + 4P^3\delta \right)}$$

Consequently, the two terms RADM solution of volume is found to be:

$$V_{RADM} = \frac{1}{y_{RADM}} = \frac{1}{y_0 + y_1}$$

$$= \frac{R^5 T^5 + 2PR^3 T^3 \beta + 3P^2 R^2 T^2 \gamma + 4P^3 RT\delta}{PR^4 T^4 + P^2 R^2 T^2 \beta + 2P^3 RT\gamma + 3P^4\delta} \tag{5.41}$$

Results of this canonical form are illustrated in Fig. 5.2 and Table 5.3. These results show some peculiar features: at lower pressures, the results converge to the correct value for all values of n_T requiring fewer numbers of iterations. Whereas, at higher pressures [30 *atm*], more iterations are required to reach at the correct value. At further higher pressures [40 *atm*], consideration of higher terms in RADM do not ensure the convergence of the solution, e.g. at $P = 40$ *atm*, the results obtained for $n_T = 2$ converge to the correct value after twelve iterations [$m = 12$], however, the results obtained for $n_T = 5$ leads to another correct value [negative real root] as apparent in Fig. 5.2 and Table 5.3. Further increase in the number of terms in RADM, i.e. $n_T = 15$, leads to divergence and still increasing the terms in RADM, i.e. $n_T = 18$, gives the correct result with comparatively lesser number of iterations. This is also illustrated in Fig. 5.2 and Table 5.3.

Analysis of the above ADM/RADM results, obtained for different canonical forms, can be summarized as follows:

(i)   Both the methods are sensitive towards the canonical form of an equation.

(ii)   Increasing the terms in both the methods does not always ensure the convergence.

(iii)   In general, RADM is superior to ADM and in case of breakdown of ADM/RADM, different canonical forms of equation may be employed or a constant may be added and subtracted in Eq. (5.3) so as to modify C_0 and $F_0(y)$ as advised in Basto et al. (2006).

221

It is worth noting that the above two approaches [ADM and RADM] are also applicable to other nonlinear AEs and not just limited to polynomial equations.

5.4   FRICTION FACTOR EQUATION

In this section, the friction factor equations used for the laminar and turbulent flow of Bingham fluids in smooth pipes have been solved by using ADM and RADM, and different solutions [explicit expressions] of friction factor have been obtained. Besides, a comparison between the obtained results, the numerical results and those obtained by using the available correlations (Serghides, 1984; Manadilli, 1997; Romeo et al., 2002) have been carried out. Computational aspects of the obtained solutions have also been discussed in some detail.

5.4.1   Friction Factor Equations for Bingham Fluids

For Bingham fluids, the friction factor correlations for the turbulent and laminar regime are given below.

5.4.1.1 Turbulent Regime

For the turbulent flow of Bingham fluids in smooth pipe, the following famous implicit Nikuradse-Prandtl-Karman [NPK] equation is applicable (Sablani et al., 2003). This equation can be deduced from the Colebrook-White equation (Colebrook, 1939) under smooth pipe condition (Romeo et al., 2002).

$$\frac{1}{\sqrt{f}} = 4.0 Log_{10}(Re\sqrt{f}) - 0.40 \tag{5.42a}$$

where f is the Fanning friction factor and Re is the Bingham Reynolds number

$[Re = \dfrac{\rho \hat{v} D}{\mu_B}]$. It should be noted that the Eq. (5.42a) is the same equation as the one used for Newtonian fluids in turbulent flow in smooth pipes. Therefore, explicit correlations corresponding to Newtonian fluids can also be used for these fluids. Some

of the existing correlations, whose predictions are reasonably close to those of Eq. (5.42a), are presented below:

(i) Serghides (1984) proposed the following friction factor correlation valid for Re >2100 and for any value of ε/D.

$$\frac{1}{\sqrt{f_D}} = \left(A - \left(\frac{(B-A)^2}{(C-2B+A)^2}\right)\right) \tag{5.42b}$$

where f_D [Darcy/Moody friction factor] $= 4f$ [Fanning friction factor],

$$A = -2.0Log\left(-\frac{\varepsilon/D}{3.70} + \frac{12}{Re}\right), \quad B = -2.0Log\left(\frac{\varepsilon/D}{3.70} + \frac{2.51A}{Re}\right) \quad \text{and}$$

$$C = -2.0Log\left(\frac{\varepsilon/D}{3.70} + \frac{2.51B}{Re}\right)$$

(ii) Manadilli (1997) proposed the following correlation for f_D by using his so-called sigmoidal equation. This relation is applicable for $5235 < Re < 10^8$ and for any value of ε/D.

$$\frac{1}{\sqrt{f_D}} = -2.0Log\left(\frac{\varepsilon/D}{3.70} + \frac{95}{Re^{0.983}} - \frac{96.82}{Re}\right) \tag{5.42c}$$

(iii) Romeo et al. (2002), after developing different expressions on the lines of various available models, have given an explicit relation for friction factor using multivariable nonlinear regression for turbulent flow of Newtonian fluids. The relevant range for Re and ε/D lies in $3000 - 1.5 \times 10^8$ and $0 - 0.05$, respectively.

$$\frac{1}{\sqrt{f_D}} = -2.0Log\left(\frac{\varepsilon/D}{3.7065} - \frac{5.0272}{Re}Log\left(\frac{\varepsilon/D}{3.827} - \frac{4.567}{Re} \times Log(A)\right)\right) \tag{5.42d}$$

where $A = \left(\frac{\varepsilon/D}{3.7065}\right)^{0.9924} + \left(\frac{5.3326}{208.815 + Re}\right)^{0.9345}$

Beside the above correlations, there exist some other correlations (Churchill, 1977; Chen, 1979; Zigrang and Sylvester, 1982). However, the error in their predictions is relatively more (not shown here), and hence, these have not been considered in the

present work. Similarly, the explicit ANN based procedure developed by Sablani et al. (2003) has not been considered, since no explicit correlation was provided.

5.4.1.2 Laminar Regime

Friction factor for the laminar flow of Bingham fluids in smooth pipes depends on the Bingham Reynolds number [$Re = \dfrac{\rho \hat{v} D}{\mu_B}$] and the Hedstrom number [$He = \dfrac{\tau_0 \rho D^2}{\mu_B^2}$], and is given by the following implicit [quartic] equation (Govier and Aziz, 1972; Sablani et al., 2003):

$$\frac{f}{16} = \frac{1}{Re} + \frac{He}{6Re^2} - \frac{He^4}{3Re^8 f^3} \tag{5.43}$$

Since, Eq. (5.43) is a quartic equation, a closed form analytical solution is possible. However, due to complexity it is rarely employed and as per our knowledge, no approximate solution of Eq. (5.43) is available and numerical methods are used for obtaining the solution.

5.4.2 Solutions and Discussion: Friction Factor for Turbulent Regime

In this subsection, the Eq. (5.42a) has been solved by using ADM and RADM, and the approximate solutions of friction factor have been obtained for the turbulent regime.

5.4.2.1 Solution by ADM

By letting $y = \dfrac{1}{\sqrt{f}}$, the Eq. (5.42a) is transformed into the following canonical form [similar to the Eq. (5.3)]:

$$y = \underbrace{4.0 Log_{10}(Re) - 0.40}_{C_0} + \underbrace{\left(-4.0 Log_{10}(y)\right)}_{F_0(y)} \tag{5.44}$$

After applying ADM to the above equation, one obtains the following decomposed parts of the ADM solution:

$$y_0 = C_0$$

$$y_1 = A_0 = -\frac{4ln(C_0)}{ln(10)}$$

$$y_2 = A_1 = \frac{16ln(C_0)}{C_0 ln^2(10)}$$

$$y_3 = A_2 = \frac{32ln(C_0)(-2+ln(C_0))}{C_0^2 ln^3(10)}$$

$$y_4 = A_3 = \frac{128ln(C_0)(6-9ln(C_0)+2ln^2(C_0))}{3C_0^3 ln^4(10)}$$

where $C_0 = 4.0Log_{10}(Re) - 0.4$ and $Log_{10}(C_0) = ln(C_0)/ln(10)$. From the above parts, the two terms $[n_T = 2]$ ADM solution can be found as follows:

$$\frac{1}{\sqrt{f}} = y = y_0 + y_1$$

or

$$\frac{1}{\sqrt{f}} = C_0 - 1.73718ln(C_0) \tag{5.45a}$$

Similarly, the five terms $[n_T = 5]$ ADM solution is given by:

$$\frac{1}{\sqrt{f}} = y = y_0 + y_1 + y_2 + y_3 + y_4$$

or

$$\frac{1}{\sqrt{f}} = \frac{(C_0^4 - 1.73718(C_0-1.73718)(3.01779+C_0^2)ln(C_0)}{C_0^3} +$$

$$\frac{(2.62122C_0 - 13.6606)ln^2 C_0 + 3.03568ln^3 C_0)}{C_0^3} \tag{5.45b}$$

225

For convenience, the discussion of results obtained by using the above ADM solutions [Eqs. (5.45a) and (5.45b)] has been presented along with those of RADM. Application of RADM for obtaining the approximate solutions of turbulent regime friction factor has been shown in the following subsection.

5.4.2.2 Solution by RADM

For solving the Eq. (5.44) by using RADM, first the following updated canonical form, similar to Eq. (5.23c), is obtained for the first iteration $[m = 1]$:

$$y = C_1 + F_1(y) \tag{5.46}$$

where $C_0 = C_1 = 4.0Log_{10}(Re) - 0.4$ and $F_1(y) = -\dfrac{4(C_0 - y + C_0 ln(y))}{4 + C_0 ln(10)}$.

Afterward, ADM is applied to solve the Eq. (5.46) and the following decomposed parts are obtained for the first iteration of RADM.

$$y_0 = C_0$$

$$y_1 = A_0 = -\frac{4C_0 ln(C_0)}{4 + C_0 ln(10)}$$

$$y_2 = A_1 = 0$$

$$y_3 = A_2 = \frac{32C_0 ln^2(C_0)}{(4 + C_0 ln(10))^3}$$

$$y_4 = A_3 = \frac{256C_0 ln^3(C_0)}{3(4 + C_0 ln(10))^4}$$

Hence, the two terms $[n_T = 2]$ RADM solution after the first iteration is found to be:

$$\frac{1}{\sqrt{f}} = y = y_0 + y_1$$

or

$$\frac{1}{\sqrt{f}} = C_0 - \frac{1.73718 C_0 ln(C_0)}{1.73718 + C_0} \tag{5.47a}$$

Similarly, the five terms $[n_T = 5]$ RADM solution after the first iteration is found to be:

$$\frac{1}{\sqrt{f}} = y = y_0 + y_1 + y_2 + y_3 + y_4$$

or

$$\frac{1}{\sqrt{f}} = C_0 - \frac{1.73718 C_0 ln(C_0)}{1.73718 + C_0} + \frac{2.62122 C_0 ln^2(C_0)}{(1.73718 + C_0)^3} + \frac{3.03568 C_0 ln^3(C_0)}{(1.73718 + C_0)^4}$$

$$\tag{5.47b}$$

In a similar fashion, the RADM solutions for higher number of iterations can be obtained, and for several values of Re pertaining to the turbulent regime, the results obtained by using the so derived solutions have been tabulated in Tables 5.4 and 5.5 along with those obtained by using the known correlations as well as the numerical method. From Table 5.4, it is evident that the accuracy in the ADM and RADM results increases with the increase in number of terms, however, the convergence in the ADM results is lesser as compared to the RADM results. On comparing these results with the numerical results, it is found that the RADM results matched well even with two terms

and two iterations. Besides, by comparing the number of iterations required by RADM and Newton-Raphson method to achieve the same values, it is revealed that the two terms RADM solution outperformed the latter one; the starting guesses for both the methods are taken to be the same and are equal to $1/C_0^2$ [since, initial guess $y_0 \left[= C_0' \right]$

$= \frac{1}{\sqrt{f}}$]. This can be attributed to the faster convergence properties of Adomian series as compared to the Taylor series (Abbaoui and Cherrault, 1994; Rach et al., 1992; Wazwaz, 1998). Table 5.4 also depicts that in case of RADM, the effect of number of iterations $[m]$ has a more pronounced effect on the result quality as compared to the number of terms $[n_T]$.

Table 5.5 compares the values of turbulent regime friction factor obtained by using different correlations used as alternatives of NPK equation. Fig. 5.5 shows the

Table 5.4: Comparison between the values of turbulent regime friction factor obtained by using different methods

Re	f_{NPK} Numerical solution	Iterations required in Newton-Raphson	Method	Iterations required in RADM [m]	f	
					$n_T = 2$	$n_T = 5$
4000	0.00998597	4	ADM	-	0.01126290	0.00998333
			RADM	1	0.01014430	0.00998623
				2	0.00998606	0.00998597
				3	0.00998597	...
5000	0.00935658	4	ADM	-	0.01049160	0.00935432
			RADM	1	0.00949628	0.00935688
				2	0.00935666	0.00935658
				3	0.00935658	...
10000	0.00772713	4	ADM	-	0.00852989	0.00772571
			RADM	1	0.00782357	0.00772745
				2	0.00772717	0.00772713
				3	0.00772713	...
50,000	0.00522650	4	ADM	-	0.00562191	0.00522598
			RADM	1	0.00527122	0.00522673
				2	0.00522651	0.00522650
				3	0.00522650	...
100,000	0.00450038	4	ADM	-	0.00480185	0.00450003
			RADM	1	0.00453358	0.00450055
				2	0.00450038	0.00450038
1,000,000	0.00291282	4	ADM	-	0.00304959	0.00291271
			RADM	1	0.00292662	0.00291290
				2	0.00291282	0.00291282

corresponding profiles of percentage errors for these correlations [percentage errors have been evaluated with respect to the results obtained from NPK equation]. It is clear from this figure that the RADM solution with $n_T = 5$, $m = 1$, i.e. Eq. (5.47b), outperformed all other correlations, and throughout exhibits an error of less than 0.005%. Sablani et al. (2003) have reported that the friction factor values predicted by

228

Table 5.5: Comparison between the values of turbulent regime friction factor obtained by using different correlations

Re	NPK [Numerical solution]	Serghides (1984)	Manadilli (1997)	Romeo et al. (2002)	RADM $n_T = 2, m = 1$	RADM $n_T = 5, m = 1$
4000	0.00998597	0.00997674	0.00997692	0.00999134	0.01014430	0.00998623
5000	0.00935658	0.00934814	0.00934837	0.00936171	0.00949628	0.00935688
10000	0.00772713	0.00772063	0.00772067	0.00773112	0.00782357	0.00772745
50000	0.00522650	0.00522271	0.00522276	0.00522863	0.00527122	0.00522673
100000	0.00450038	0.00449730	0.00449766	0.00450207	0.00453358	0.00450055
1000000	0.00291282	0.00291118	0.00291291	0.00291373	0.00292662	0.00291290
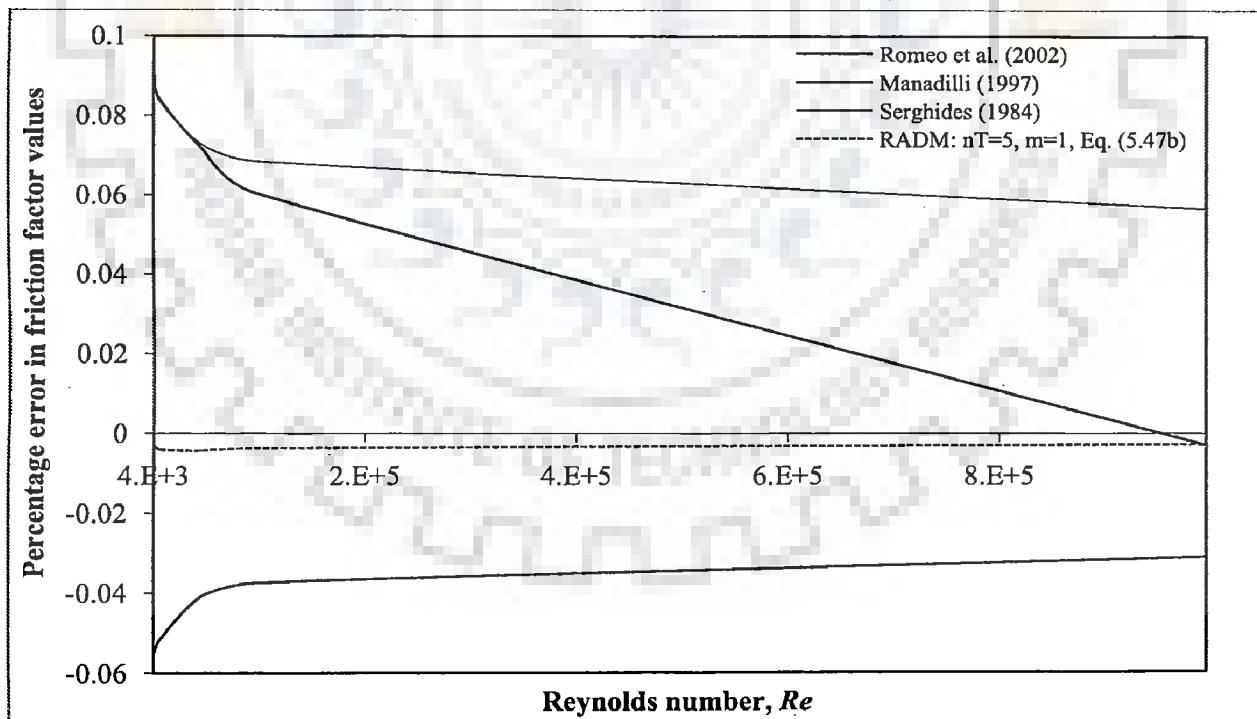
Figure 5.5: Variation of percentage error in friction factor values with Reynolds number [turbulent flow]

229

their optimal ANN configuration had mean relative error of 1.32%, whereas, the best model of Romeo et al. (2002) exhibits errors between 0.02 - 0.05%. Therefore, it is resolved that the RADM solution with $n_T = 5$ and $m = 1$ [Eq. (5.47b)], having very small error, is better as far as the explicit correlations are concerned.

Beside measuring the accuracy of these correlations, we have also measured the computational efforts. For achieving this objective, a computer program was developed in the programming language of MATHEMATICA for evaluating the friction factor from different correlations. This code was run on a machine with the following configuration: Intel Core 2 Duo processor with clock rate equal to 2.2GHz and physical memory [RAM] equal to 4 GB. Two approaches were adopted for this purpose: (i) Measuring the absolute CPU time and (ii) measuring the relative CPU time. For the first approach, most of the mathematical softwares have several inbuilt commands, e.g. "Timing" command is implemented in MATHEMATICA. Using this command, the approximate absolute timings [CPU time] in evaluating the friction factor by using various correlations, have been recorded and are shown in Table 5.6. However, no concrete conclusions can be drawn from these results as almost equal CPU time was spent in evaluating friction factor from all the mentioned correlations. This is because: as compared to the available powerful machine configuration and the robust software [MATHEMATICA], the efforts made by the computer to solve this equation are insignificant. Moreover, many a times the program resulted in zero CPU time. This is also true for other smaller operations, because after the first session of the program, the variables and the data get stored in the system cache, and recalling and reprocessing the data requires negligibly small time. Because of the above disadvantages, this approach was dropped.

In the second approach, the program was instructed to run for many iterations for each correlation for the same value of Re. The overall time consumed by CPU, now a much higher value, is then reported. Dividing it by the number of iterations yields the average CPU time spent in a single iteration for each correlation. Though, in this case the system would be using data stored in system cache and thus would not give a true picture of the time consumed by CPU. However, it definitely provides a relative estimate of the duration spent in the processing of each correlation. The results obtained from this approach have been depicted in Fig. 5.6. One notes that the CPU time per

231

Table 5.6: Comparison of the absolute time consumed by CPU for evaluating the turbulent regime friction factor by using different correlations

Re	Sessions	Approximate absolute time consumed by CPU (s)			
		NPK	Manadilli (1997)	RADM	
				$n_T = 2, m = 1$	$n_T = 5, m = 1$
4×10^3	1	0.016	0.015	0.015	0.016
	2	0.016	0.015	0.016	0.015
	3	0.015	0.015	0.015	0.015
	4	0.016	0.016	0.016	0.016
	5	0.016	0.015	0.015	0.016
10^6	1	0.016	0.015	0.015	0.016
	2	0.015	0.015	0.016	0.015
	3	0.016	0.016	0.015	0.016
	4	0.015	0.015	0.015	0.016
	5	0.016	0.015	0.016	0.015

iteration becomes constant as the number of iteration increases. From this figure, it is clearly visible that the Colebrook–White correlation (Colebrook, 1939) and the Serghides' correlation (Serghides, 1984) consumed much greater CPU time per iteration as compared to the other correlations. The CPU times spent in evaluating the friction factor from the correlation proposed by Romeo et al. (2002) and from the RADM solution $[n_T = 5, m = 1]$, i.e. Eq. (5.47b), are approximately same. Similarly, the correlation proposed by Manadilli (1997) and the RADM solution $[n_T = 2, m = 1]$, i.e. Eq. (5.47a), took approximately the same amount of time in their processing. Moreover, the time spent in evaluating the friction factor from the solution obtained by using RADM $[n_T = 5, m = 1]$ is slightly greater than that needed by the Manadilli's correlation (Manadilli, 1997). However, as evident in Fig. 5.5, the accuracy obtained by the former one [Eq. (5.47b)] is much higher than the latter one, and offsets the price paid in terms of marginally higher CPU time. Although not shown, it is noteworthy that the same observations have also been made while using another mathematical tool, i.e. MATLAB.
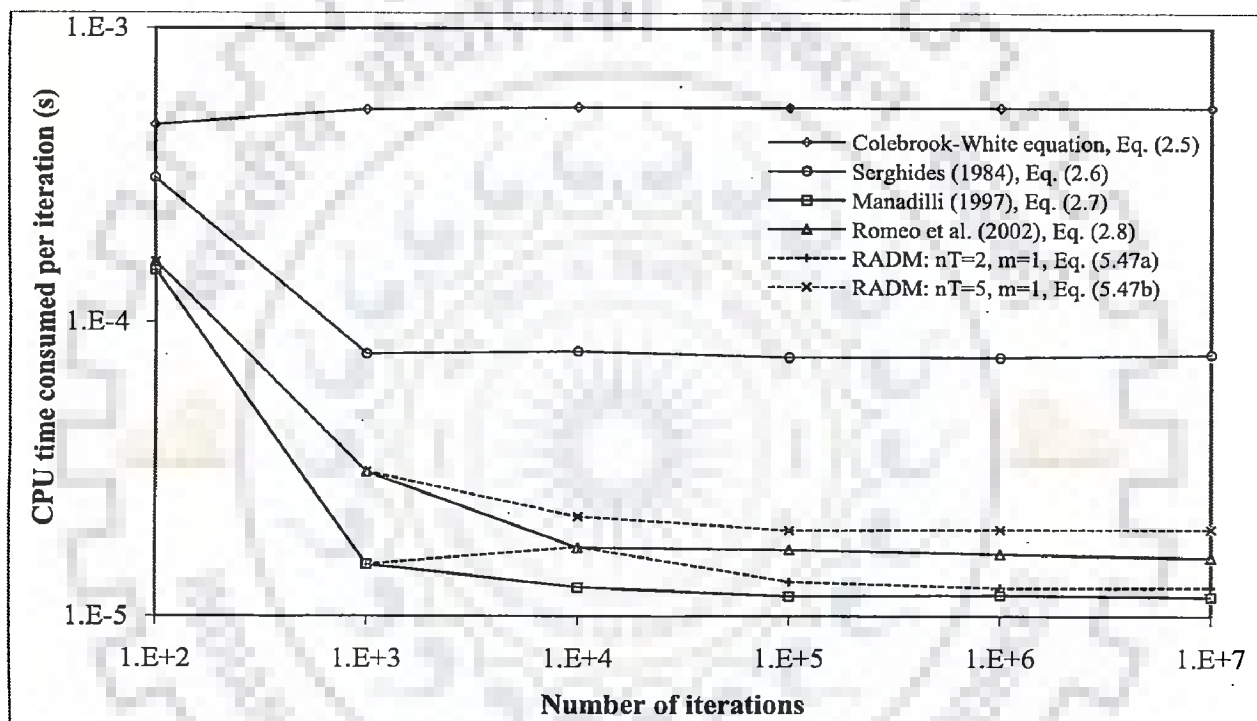
Figure 5.6: CPU time consumed per iteration for evaluating the friction factor by using different correlations [turbulent flow: $Re = 10^6$]

233

5.4.3 Solutions and Discussion: Friction Factor for Laminar Regime

In this subsection, the Eq. (5.43) has been solved by using ADM and RADM, and the approximate solutions of laminar regime friction factor have been obtained.

5.4.3.1 Solution by ADM

To solve Eq. (5.43) by using ADM, it is transformed into the following canonical form by taking $y = f$:

$$y = \underbrace{\frac{16}{Re} + \frac{16He}{6Re^2}}_{C_0} + \underbrace{\left(-\frac{16He^4}{3Re^8 y^3}\right)}_{F_0(y)} \tag{5.48}$$

After solving the above equation with the help of ADM, the following decomposed parts of the ADM solution are obtained:

$$y_0 = C_0 = K_1$$

$$y_1 = A_0 = \frac{K_2}{K_1^3}$$

$$y_2 = A_1 = -\frac{3K_2^2}{K_1^7}$$

$$y_3 = A_2 = \frac{15K_2^3}{K_1^{11}}$$

$$y_4 = A_3 = -\frac{91K_2^4}{K_1^{15}}$$

where $K_1 = \frac{16}{Re} + \frac{16He}{6Re^2}$ and $K_2 = -\frac{16He^4}{3Re^8}$. Now with the decomposed parts available, the two terms [$n_T = 2$] ADM solution is given by:

$$f = y = y_0 + y_1$$

235

$$f = K_1 + \frac{K_2}{K_1^3} \tag{5.49a}$$

Likewise, the five terms $[n_T = 5]$ ADM solution cab also be obtained and is given by:

$$f = y = y_0 + y_1 + y_2 + y_3 + y_4$$

$$f = K_1 + \frac{K_2}{K_1^3} - \frac{3K_2^2}{K_1^7} + \frac{15K_2^3}{K_1^{11}} - \frac{91K_2^4}{K_1^{15}} \tag{5.49b}$$

Here also, the discussions of the results obtained by using the above ADM solutions [Eqs. (5.49a) and (5.49b)] have been combined with those of the RADM. Solutions by RADM have been obtained in the next subsection.

5.4.3.2 Solution by RADM

For the first iteration $[m = 1]$ of RADM, the following updated canonical form of Eq. (5.48) is obtained. For convenience, here also f is denoted by y.

$$y = C_1 + F_1(y) \tag{5.50}$$

where $C_1 = C_0 = K_1$ and $F_1(y) = \dfrac{K_2(K_1^4 - 3K_1 y^3 + 3y^4)}{(K_1^4 + 3K_2)y^3}$.

By solving the Eq. (5.50) with the help of ADM, the following decomposed parts of the RADM solution are obtained:

$$y_0 = C_0 = K_1$$

$$y_1 = A_0 = \frac{K_1 K_2}{K_1^4 + 3K_2}$$

Therefore, the two terms RADM solution after the first iteration attains the following form:

$$f = y = y_0 + y_1$$

236

$$f = K_1 + \frac{K_1 K_2}{K_1^4 + 3K_2} \tag{5.51}$$

In the next iteration of RADM [$m = 2$], the following canonical form is obtained:

$$y = C_2 + F_2(y) \tag{5.52}$$

where $C_0 = K_1$, $C_2 = K_1 + \dfrac{K_1 K_2}{(K_1^4 + 3K_2)}$ and $F_2(y) = -C_2 + \dfrac{K_1 + K_2(y^{-3} + 3yC_2^{-4})}{1 + 3K_2 C_2^{-4}}$

Applying ADM to the above revised canonical form [Eq. (5.52)], one obtains the following two decomposed parts:

$$y_0 = C_2 = K_1 + \frac{K_1 K_2}{K_1^4 + 3K_2}$$

$$y_1 = A_0 = -C_2 + \frac{K_1}{1 + \dfrac{3K_2}{C_2^4}} + \frac{4K_2}{C_2^3\left(1 + \dfrac{3K_2}{C_2^4}\right)}$$

Therefore, the two terms RADM solution after the second iteration is given as:

$$f = y = y_0 + y_1$$

or

$$f = \left(K_1 + \frac{4K_2}{\left(K_1 + \dfrac{K_1 K_2}{K_1^4 + 3K_2}\right)^3} \right) \Bigg/ \left(1 + \frac{3K_2}{\left(K_1 + \dfrac{K_1 K_2}{K_1^4 + 3K_2}\right)^4} \right) \tag{5.53}$$

In the same way, the five terms [$n_T = 5$] solution is obtained by using RADM. For this, one again starts with the following canonical form for the first iteration of RADM [$m = 1$]:

$$y = C_1 + F_1(y) \tag{5.54}$$

where $C_0 = C_1 = K_1$ and $F_1 = \dfrac{K_2(K_1^4 - 3K_1 y^3 + 3y^4)}{(K_1^4 + 3K_2)y^3}$

The following decomposed terms are obtained after solving the above equation by using ADM.

$$y_0 = C_0 = K_1$$

$$y_1 = A_0 = \frac{K_1 K_2}{K_1^4 + 3K_2}$$

$$y_2 = A_1 = 0$$

$$y_3 = A_2 = \frac{6K_1 K_2^3}{\left(K_1^4 + 3K_2\right)^3}$$

$$y_4 = A_3 = -\frac{10K_1 K_2^4}{\left(K_1^4 + 3K_2\right)^4}$$

The five terms RADM solution after the first iteration is given by:

$$f = y = y_0 + y_1 + y_2 + y_3 + y_4$$

or

$$f = K_1 \left(1 - \frac{10K_2^4}{\left(K_1^4 + 3K_2\right)^4} + \frac{6K_2^3}{\left(K_1^4 + 3K_2\right)^3} + \frac{K_2}{\left(K_1^4 + 3K_2\right)} \right) \qquad (5.55)$$

Similarly, for the next iteration of RADM [$m = 2$], the following canonical form is obtained.

$$y = C_2 + F_2(y) \qquad (5.56)$$

where $C_0 = K_1$, $C_2 = T$, $F_2 = -T + \dfrac{K_1 + K_2(y^{-3} + 3yT^{-4})}{1 + 3K_2 T^{-4}}$ and

$$T = K_1 \left(1 - \frac{10K_2^4}{\left(K_1^4 + 3K_2\right)^4} + \frac{6K_2^3}{\left(K_1^4 + 3K_2\right)^3} + \frac{K_2}{\left(K_1^4 + 3K_2\right)} \right)$$

Applying the ADM to solve Eq. (5.56) one gets

$$y_0 = C_2 = T$$

$$y_1 = \frac{T(K_2 + (K_1 - T)T^3)}{3K_2 + T^4}$$

$$y_2 = 0$$

$$y_3 = \frac{6K_2 T(K_2 + (K_1 - T)T^3)^2}{(3K_2 + T^4)^3}$$

$$y_4 = -\frac{10K_2 T(K_2 + (K_1 - T)T^3)^3}{(3K_2 + T^4)^4}$$

Hence, the five terms RADM solution after second iteration is given by:

$$f = y = y_0 + y_1 + y_2 + y_3 + y_4$$

$$f = \frac{1}{(3K_2 + T^4)^4} \left(\begin{array}{l} T(116K_2^4 + K_1 T^{15} + 3K_2^3 T^3 (11K_1 + 36T) + 3K_2^2 T^6 (-4K_1^2 + 21K_1 T + 4T^2) \\ + K_2 T^9 (-10K_1^3 + 36K_1^2 T - 33K_1 T^2 + 20T^3)) \end{array} \right)$$

$$(5.57)$$

In a similar way, the RADM solutions can be obtained for higher number of iterations. However, before finding the friction factor values from these solutions as well as those derived by using ADM, one should note that for the flow of Bingham fluids to be in laminar regime, the Reynolds number for a given Hedstrom number should be less than the corresponding critical Reynolds number [Re_c]. For a given Hedstrom number, the critical Reynolds number can be found by using the method described by Hanks and Pratt (1967). Using this method, the plot of critical Reynolds number versus Hedstrom number has been reproduced in Fig. 5.7. With the help of this figure, several possible combinations of Re and He for laminar flow, have been selected. Subsequently, the friction factor values for these sets of Re and He have been obtained by using the ADM and RADM solutions, and are shown in Tables 5.7 and 5.8. These

two tables clearly show that the friction factor values obtained from the ADM and RADM solutions match closely with their numerical counterparts.

In Fig. 5.8, the effect of number of terms on the accuracy of the friction factor values has also been shown. It is observed that the accuracy of friction factor values increases with the increase in number of terms irrespective of the type of flow, i.e. laminar or turbulent. Though, this effect is more pronounced in the latter case. For the same number of terms, the results obtained by using RADM are better than those of ADM and the accuracy increases with increase in number of iterations. Here too, the number of iterations in RADM has a more significant effect on the result quality than the number of terms.

Table 5.7: **Comparison between the values of laminar regime friction factor obtained by using different methods**

He	Method	n_T	f	
			$Re = 10^2$	$Re = 10^3$
10^2	Numerical	-	0.186658	0.0162667
	ADM	2	0.186658	0.0162667
		5	0.186658	0.0162667
	RADM	2	0.186658 [$m = 1$]	0.0162667 [1]
		5	0.186658 [1]	0.0162667 [1]
10^4	Numerical	-	2.47480	0.0419439
	ADM	2	2.59052	0.0419800
		5	2.49409	0.0419439
	RADM	2	2.51155 [1] 2.47554 [2] 2.4748 [3]	0.0419452 [1] 0.0419439 [2]
		5	2.48368 [1] 2.4748 [2]	0.0419439 [1]

240
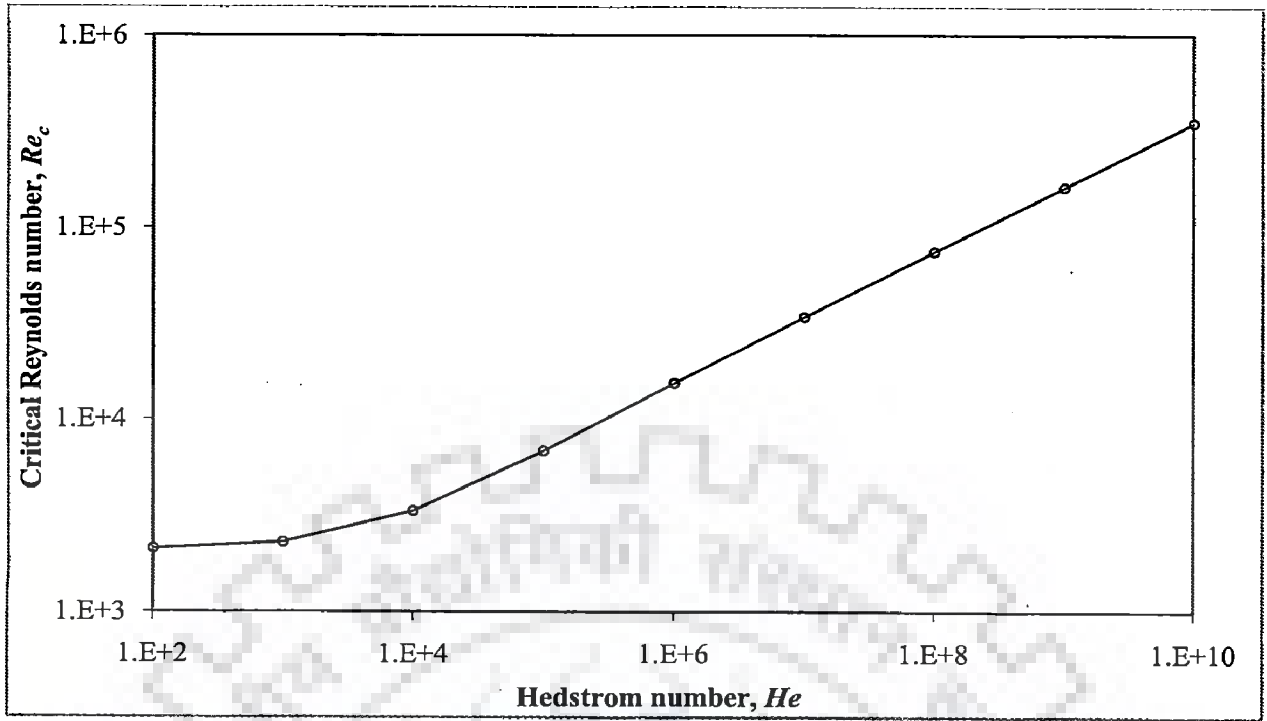
Figure 5.7: Variation in critical Reynolds number with Hedstrom number for Bingham fluids
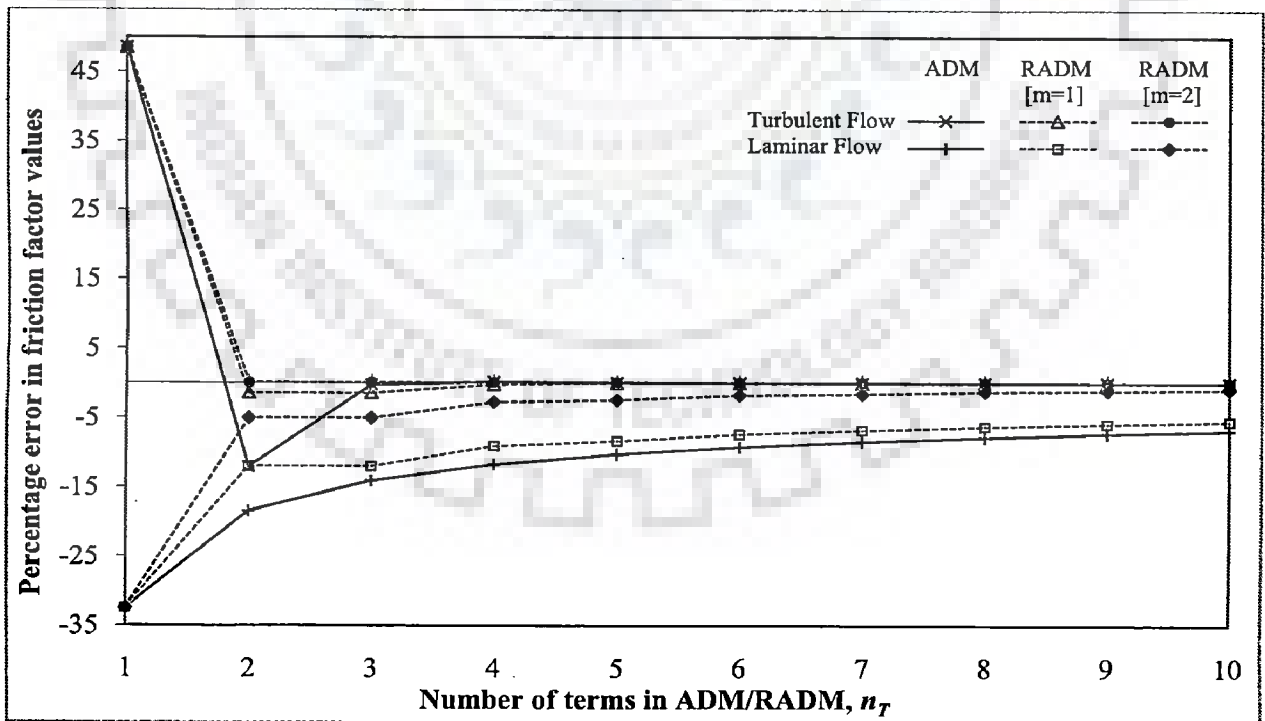
Figure 5.8: Variation of percentage error in friction factor values with number of terms in ADM and RADM [laminar flow: $Re = 10^5$, $He = 10^{10}$; turbulent flow: $Re = 5 \times 10^3$]

241

Table 5.8: Comparison between the values of laminar regime friction factor obtained by using different methods

He	Method	n_T	f		
			$Re = 10^4$	$Re = 5 \times 10^4$	$Re = 10^5$
10^6	Numerical.	-	0.02474800	-	-
	ADM	2	0.02590520	-	-
		5	0.02494090	-	-
	RADM	2	0.0251155 [$m=1$] 0.0247554 [2] 0.024748 [3]	-	-
		5	0.0248368 [1] 0.024748 [2]	-	-
10^8	Numerical	-	–	0.0837146	-
	ADM	2	-	0.0958373	-
		5	-	0.089387	-
	RADM	2	-	0.0907662 [1] 0.0856263 [2] ... 0.0837146 [5]	-
		5	-	0.0879638 [1] 0.0841171 [2] ... 0.0837146 [4]	-
10^{10}	Numerical	-	-	-	2.012720
	ADM	2	-	-	2.385630
		5	-	-	2.219780
	RADM	2	-	-	2.25552 [1] 2.11543 [2] ... 2.01272 [8]
		5	-	-	2.18172 [1] 2.06262 [2] ... 2.01272 [5]

-   Combination not possible

5.5 REACTION-DIFFUSION PROCESS IN A POROUS CATALYST SLAB

In this section, the model equation of reaction-diffusion process has been solved by using ADM and RADM, and the approximate solutions of the concentration profile and effectiveness factor have been obtained for different reaction rates. The obtained results have been compared with the numerical and available results (Sun et al., 2004; Gottifredi and Gonzo, 2005).

5.5.1 Model Equation

Consider a heterogeneous catalytic reaction-diffusion process in which a gaseous reactant A diffuses into the pores of a catalyst slab and simultaneously reacts on the active sites available on the walls of the pores, as portrayed in Fig. 5.9. It is assumed that an isothermal uni-molecular reaction is taking place inside the pores of catalyst with the following stoichiometry:

$$A \longrightarrow \text{Products}$$

Material balance over species A yields the following general continuity equation (Sun et al., 2004). For brevity, the derivation of this equation has been omitted and can be found in many texts (Levenspiel, 1999; Bird et al., 2002):

$$\frac{\partial C_A}{\partial t} = \nabla . D_e . \nabla C_A - (-r_A) \tag{5.58}$$

where D_e is the effective diffusivity of A, and is assumed to be constant along the pore length L. C_A is the concentration of A inside the catalyst pore and $(-r_A)$ is the reaction rate. Under steady-state conditions, the Eq. (5.58) reduces to the following second order ODE constituting a BVP (Sun et al., 2004; Gottifredi and Gonzo, 2005; Abbasbandy, 2008):

$$D_e \frac{d^2 C_A}{dx'^2} = (-r_A) \tag{5.59a}$$

The associated boundary conditions are:

BC I: $\quad C_A = C_{AS}$ at $x' = L$ [pore mouth] $\tag{5.59b}$

BC II: $\quad \dfrac{dC_A}{dx'} = 0$ at $x' = 0$ [pore end] $\tag{5.59c}$

With the following definitions of dimensionless variables (Gottifredi and Gonzo, 2005),

$$x = \frac{x'}{L}, \ y = \frac{C_A}{C_{AS}}, \ (-r_y) = \frac{(-r_A)}{(-r_{AS})} \ \text{and} \ \phi = \sqrt{\frac{(-r_{AS})L^2}{D_e C_{AS}}}$$

the Eqs. (5.59a)-(5.59c) are reduced into the following dimensionless forms:
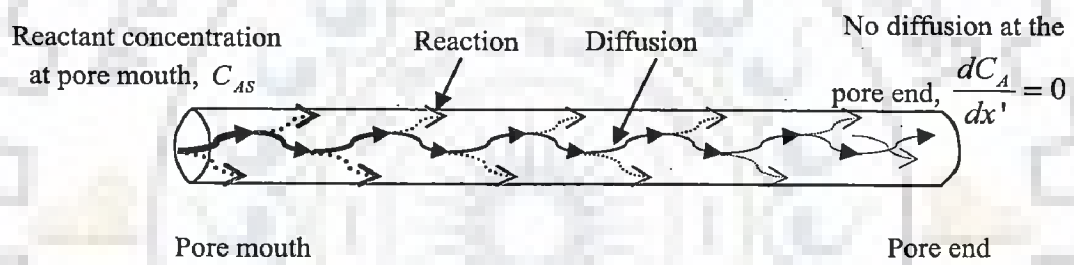
Figure 5.9: Catalytic reaction-diffusion process in a cylindrical pore of catalyst slab

$$\frac{d^2 y}{dx^2} = \phi^2 (-r_y)$$
(5.60a)

BC I: $y = 1$ at $x = 1$ [pore mouth]
(5.60b)

BC II: $\frac{dy}{dx} = 0$ at $x = 0$ [pore end]
(5.60c)

where ϕ is the Thiele modulus and ϕ^2 signifies the ratio of intrinsic chemical reaction rate in the absence of mass transfer limitation to the rate of diffusion through the catalyst (Fogler, 1992):

$$\phi^2 = \frac{reaction\ rate\ at\ the\ catalyst\ surface}{diffusion\ rate\ through\ the\ catalyst\ pores}$$

For the purpose of comparison, the expressions of dimensionless reaction rate for the power-law and Langmuir-Hinshelwood kinetics have been taken from Gottifredi and Gonzo (2005), and are given by: $(-r_y) = y^n$ and $(-r_y) = \frac{y}{1 + Ky}$, respectively. Using these dimensionless reaction rates, the Eq. (5.60a) acquires the following dimensionless forms. However, the BCs I and II remain the same.

$$\frac{d^2 y}{dx^2} - \phi^2 y^n = 0$$

$$\frac{d^2 y}{dx^2} - \phi^2 \frac{y}{1 + Ky} = 0$$

In addition to the dimensionless concentration [y], there is another quantity called effectiveness factor [η], which is defined as the ratio of the total reaction rate with diffusion to the reaction rate had it been evaluated at the pore mouth (Finalyson, 1980; Fogler, 1992; Levenspiel, 1999). This is an important quantity, since the design of a catalytic reactor is directly linked to it. For a catalyst slab, it is mathematically expressed by the following equation (Sun et al., 2004; Gottifredi and Gonzo, 2005):

$$\eta = \frac{1}{\phi^2} \frac{dy}{dx}\bigg|_{x=1}$$
(5.61)

5.5.2 Solutions and Discussion: Concentration Profile and Effectiveness Factor

In this subsection, the approximate solutions of dimensionless concentration profile and effectiveness factor have been obtained for power-law kinetics and Langmuir-Hinshelwood kinetics by solving the Eqs. (5.60a)-(5.60c) and (5.61) with the help of ADM and RADM.

5.5.2.1 Solution by ADM

(i)   Power-law kinetics

By following the procedure outlined in the subsection 5.1.3, one finds the following relations for Eq. (5.60a) for power law kinetics:

$$L[.] = \frac{d^2[.]}{dx^2} \text{ or } L^{-1}[.] = \int_0^x \int [.]dxdx, \; R[y] = 0, \; g(x) = 0 \text{ and } N(y) = (-r_y) = y^n.$$

Thus, Eq. (5.60a) acquires the following operator form:

$$L[y] = \phi^2 N(y) \tag{5.62}$$

Using Eqs. (5.11)-(5.14), the above equation becomes:

$$L[\sum_{i=0}^{\infty} \lambda^i y_i] = \phi^2 \sum_{i=0}^{\infty} \lambda^{i+1} A_i \tag{5.63}$$

Operating on both sides of the Eq. (5.63) by $L^{-1}[.]$, i.e. $\int_0^x \int [.]dxdx$, the following equation is obtained:

$$\sum_{i=0}^{\infty} \lambda^i y_i = C_1 x + C_2 + \phi^2 L^{-1} \sum_{i=0}^{\infty} \lambda^{i+1} A_i \tag{5.64}$$

where y_is are the decomposed parts of the so called ADM solution $[y_{ADM}]$ and A_is are the Adomian polynomials for the nonlinearity $N(y) = y^n$ and $L^{-1}[0] = C_1 x + C_2$. C_1 and C_2 are the unknown constants of integration, and can be found from the associated BCs [Eqs. (5.60b) and (5.60c)]. It is easy to verify that BC II requires C_1 to be zero,

since $\dfrac{dy}{dx} = 0$ at $x = 0$. Now comparing the terms having same powers of λ in Eq. (5.64), one finds:

$$y_0 = C_2$$

$$A_0(y_0) = y_0^n = C_2^n$$

$$y_1 = L^{-1}\left[\phi^2 A_0\right] = \frac{1}{2}C_2^n \phi^2 x^2$$

$$A_1(y_0, y_1) = n y_0^{n-1} y_1 = \frac{1}{2} n C_2^{2n-1} \phi^2 x^2$$

$$y_2 = L^{-1}\left[\phi^2 A_1\right] = \frac{1}{24} n C_2^{2n-1} \phi^4 x^4$$

$$A_2(y_0, y_1, y_2) = \frac{1}{2}n(n-1)y_0^{n-2}y_1^2 + n y_0^{n-1} y_2 = \frac{1}{24} n(4n-3) C_2^{-2+3n} \phi^4 x^4$$

$$y_3 = L^{-1}\left[\phi^2 A_2\right] = \frac{1}{720} n(4n-3) C_2^{3n-2} \phi^6 x^6$$

$$A_3(y_0, y_1, y_2, y_3) = \frac{1}{6}(n-2)(n-1)n y_0^{n-3} y_1^3 + (n-1)n y_0^{n-2} y_1 y_2 + n y_0^{n-1} y_3$$

$$= \frac{1}{720} n(30 - 63n + 34n^2) C_2^{4n-3} \phi^6 x^6$$

$$\ldots$$

Finally, the following ADM solution for some finite number of terms $[n_T]$ is found:

$$y_{ADM} = \sum_{i=0}^{n_T - 1} y_i$$

$$= C_2 + \frac{1}{2}C_2^n x^2 \phi^2 + \frac{1}{24} n C_2^{2n-1} x^4 \phi^4 + \frac{1}{720} n(4n-3) C_2^{3n-2} x^6 \phi^6 + \ldots \quad (5.65)$$

For the particular values of n and ϕ, C_2 is found by solving the following equation, which has been obtained by satisfying the above equation with BC I.

$$y_{ADM}(1) = 1 = C_2 + \frac{1}{2}C_2{}^n\phi^2 + \frac{1}{24}nC_2{}^{2n-1}\phi^4 + \frac{1}{720}n(4n-3)C_2{}^{3n-2}\phi^6 + \dots \qquad (5.66)$$

By substituting the so found value of C_2 in Eq. (5.65), one obtains the desired ADM solution. From Eq. (5.65) it can also be noted that C_2 signifies the dimensionless concentration of reactant A at the pore end [$x = 0$], i.e. $y_{ADM}(0) = C_2$.

Now, by using Eqs. (5.61) and (5.65), the following expression of effectiveness factor is obtained:

$$\eta = \frac{1}{\phi^2} \frac{dy_{ADM}}{dx}\bigg|_{x=1}$$

$$= C_2{}^n + \frac{n}{6}C_2{}^{2n-1}\phi^2 - \frac{n(3+4n)}{120}C_2{}^{3n-2}\phi^4 + \frac{n(30-63n+34n^2)}{5040}C_2{}^{4n-3}\phi^6 + \dots$$

$$(5.67)$$

Although not shown, it can easily be verified that for first order reaction [$n=1$], the Taylor series expansion of the above ADM solution [Eq. (5.65)] around $x = 0$ and $\phi = 0$, match well with the Taylor series expansion of the analytical solution [$y = cosh[\phi x]/cosh[\phi]$] around $x = 0$ and $\phi = 0$. It can also be confirmed that the presently obtained ADM solutions of y and η [Eqs. (5.65) and (5.67)] match well with the ADM solutions of Sun et al. (2004).

For several values of n and ϕ [$n = 0.5$, $\phi = 2$; $n = 0.67$, $\phi = 2$; $n = 1$, $\phi = 10$; $n = 1.73$, $\phi = 10$], the values of C_2 and η obtained by using the ADM solutions [Eqs. (5.66) and (5.67)] have been shown in Table 5.9 along with those obtained by using the numerical method and the approximate solution of Gottifredi and Gonzo (2005). Higher values of Thiele modulus [$\phi \geq 2$] have been considered, since the deviation in the ADM solutions is found to be more for higher values of ϕ; for smaller values of ϕ the ADM solutions do not bear any significant error. It is clear from this table that for reaction orders greater than or equal to unity [$n \geq 1$], the values of C_2 and η obtained by using the ADM solutions converge to those obtained by using the numerical method, and the accuracy increases with the increase in number of terms in ADM solution. However, for reaction orders less than unity [$n < 1, n \neq 0$], the values of C_2 and η deviate

significantly with the increase in number of terms in ADM solution.

Although not shown, similar types of errors have also been observed in the ADM solutions of Sun et al. (2004). For example, η values obtained from the ADM solution of Sun et al. (2004) for $n = 0.5$ and $\phi = 2$ [corresponding to $n_T = 4$, 6 and 10] are found to be 0.4782, 0.1418 and - 2.4431, respectively. However, the exact value of η is 0.5682 [shown in Table 5.9], and thereby the percentage errors in η values [defined as $(1 - \eta_{ADM}/\eta_{Numerical}) \times 100\%$] come out to be 15.8%, 75.0% and 530.0% respectively. These errors in η, as obtained from the ADM solution of Sun et al. (2004), are incongruously high and can grow as high as 1000% if more terms in ADM are

Table 5.9: **Comparison between the values of C_2 and η obtained by using ADM, approximate solution of Gottifredi and Gonzo (2005) and numerical method**

Method	n_T	Diverging ← Converging → C_2 [Concentration at the center of pore]			
		$n = 0.5, \phi = 2$	$n = 0.67, \phi = 2$	$n = 1, \phi = 10$	$n = 1.73, \phi = 10$
ADM	4	0.1160	0.1685	0.0005	0.0433
	5	×	0.1626	0.0002	0.0382
	6	0.1467	0.1698	0.0001	0.0356
	7	×	0.1588	0.0001	0.0342
	10	0.3068	0.1966	0.0001	0.0325
	12	0.4056	0.2408	0.0001	0.0322
Gottifredi and Gonzo (2005)	-	0.2183	0.2395	0.0002	0.0007
Numerical	-	0.0995	0.1658	0.0001	0.0320
Method	n_T	η [Effectiveness factor]			
ADM	4	0.4782	0.5189	0.0544	0.0423
	5	×	0.5553	0.0690	0.0514
	6	0.1418	0.4969	0.0811	0.0591
	7	×	0.6074	0.0899	0.0652
	10	-2.4431	0.0322	0.0995	0.0774
	12	-4.5833	-0.9263	0.1000	0.0820
Gottifredi and Gonzo (2005)	-	0.5600	0.5306	0.1000	0.0856
Numerical	-	0.5682	0.5336	0.1000	0.0857

× Imaginary or no root

considered. This is because, for $n < 1$ [$n \neq 0$] and for higher Thiele modulus, the ratio test for the ADM solution shows divergence. These limitations have also been mentioned by Gottifredi and Gonzo (2005), however, no explicit comparison of the results was performed by them. The present comparison clearly indicates that the ADM solutions, obtained by us and by Sun et al. (2004), diverge and yield erroneous results for $n < 1$ [$n \neq 0$] and large ϕ. It is to be noted that in the work of Sun et al. (2004), η values are not directly shown; rather these have been computed here by using their ADM solution for the purpose of comparison.

It is also noticeable in Table 5.9 that the value of η, predicted by Gottifredi and Gonzo method (2005), matches well with the exact numerical value, however, the prediction of C_2 shows appreciable discrepancy, which increases with ϕ.

For one set of the parameters' values [$n = 0.5$, $\phi = 2$], the dimensionless concentration profiles [y] obtained by using different methods have been shown in Fig. 5.10, and the corresponding residual error profiles are shown in Fig. 5.11; residual error for any solution is obtained by substituting the solution in Eq. (5.60a). It is clear from Fig. 5.10 that the deviation in the ADM solution increases with increase in number of terms. This is also clear from the corresponding residual error profiles drawn in Fig. 5.11. The concentration profile obtained by using the approximate solution of Gottifredi and Gonzo (2005) is also depicted in Fig. 5.10, and it is observed that this profile matches well only near the catalyst surface and starts deviating as one moves towards the pore end. This is also evident from the corresponding residual error profile shown in Fig. 5.11.

(ii)   Langmuir-Hinshelwood kinetics

For Langmuir-Hinshelwood kinetics, the choices of various operators and functions, i.e. $L[.]$, $L^{-1}[.]$, $R[y]$ and $g(x)$, remain the same, however, the nonlinear function now incorporates the Langmuir-Hinshelwood kinetics. These choices are given below:

$$L[.] = \frac{d^2[.]}{dx^2} \text{ or } L^{-1} = \int_0^x \int [.]dxdx \,, \ R[y] = 0 \,, \ g(x) = 0 \,, \ N(y) = (-r_y) = \frac{y}{(1 + Ky)}$$
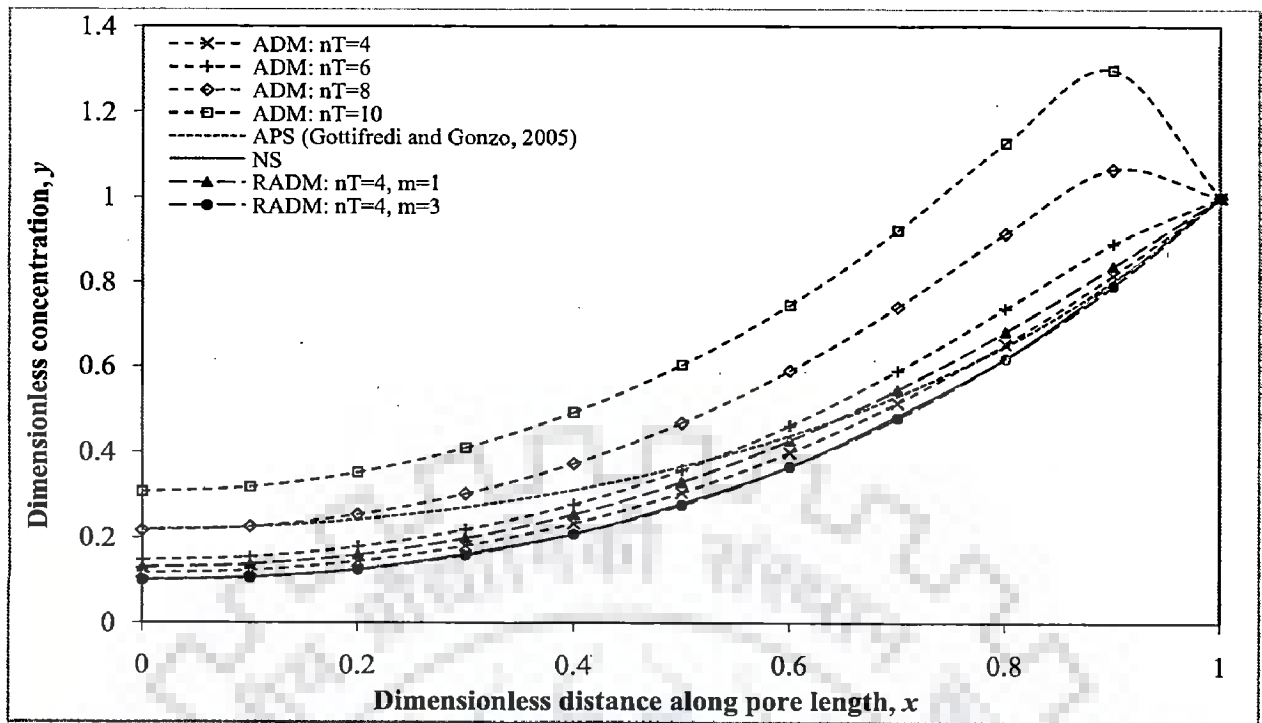
Figure 5.10: Dimensionless concentration profiles [power-law kinetics: n = 0.5, ϕ = 2; x = 0: pore end; x = 1: pore mouth]
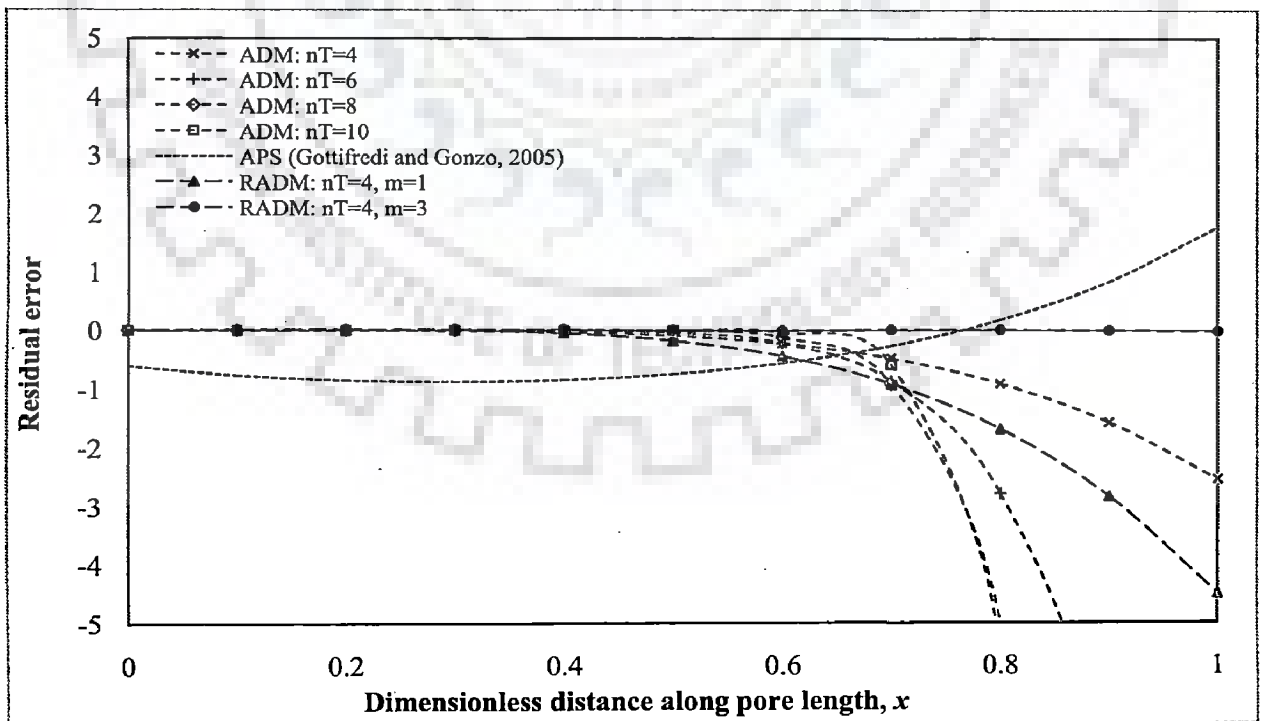
Figure 5.11: Residual error profiles [power-law kinetics: n = 0.5, ϕ = 2; x = 0: pore end; x = 1: pore mouth]

For the above definitions of operators and functions, the application of ADM yields the following relations for y_i and A_i:

$$y_0 = C_2$$

$$A_0(y_0) = \frac{y_0}{(1+Ky_0)} = \frac{C_2}{(1+KC_2)}$$

$$y_1 = L^{-1}\left[\phi^2 A_0\right] = \frac{C_2\phi^2 x^2}{2(1+KC_2)}$$

$$A_1(y_0, y_1) = \frac{y_1}{(1+Ky_0)^2} = \frac{C_2\phi^2 x^2}{2(1+KC_2)^3}$$

$$y_2 = L^{-1}\left[\phi^2 A_1\right] = \frac{C_2\phi^4 x^4}{24(1+KC_2)^3}$$

$$A_2(y_0, y_1, y_2) = \frac{(-Ky_1^2 + y_2 + Ky_0 y_2)}{(1+Ky_0)^3} = \frac{C_2(1-6KC_2)\phi^4 x^4}{24(1+KC_2)^5}$$

$$y_3 = L^{-1}\left[\phi^2 A_2\right] = \frac{C_2(1-6KC_2)\phi^6 x^6}{720(1+KC_2)^5}$$

$$A_3(y_0, y_1, y_2, y_3) = \frac{(K^2 y_1^3 - 2Ky_1 y_2 - 2K^2 y_0 y_1 y_2 + y_3 + 2Ky_0 y_3 + K^2 y_0^2 y_3)}{(1+K y_0)^4}$$

$$= \frac{C_2(1 - 36C_2 K + 90\, C_2^2 K^2)\phi^6 x^6}{720\,(1+KC_2)^7}$$

... and so on.

Finally, the ADM solution is found to be:

$$y_{ADM} = \sum_{i=0}^{n_T-1} y_i = C_2 + \frac{C_2\phi^2 x^2}{2(1+KC_2)} + \frac{C_2\phi^4 x^4}{24(1+KC_2)^3} + \frac{C_2(1-6KC_2)\phi^6 x^6}{720(1+KC_2)^5} + \dots \quad (5.68)$$

For the selected values of K and ϕ, C_2 is found by solving the following equation, which has been obtained by satisfying the Eq. (5.68) with BC I.

$$y_{ADM}(1) = 1 = C_2 + \frac{C_2\phi^2}{2(1+KC_2)} + \frac{C_2\phi^4}{24(1+KC_2)^3} + \frac{C_2(1-6KC_2)\phi^6}{720(1+KC_2)^5} + \dots \qquad (5.69)$$

The so found value of C_2 is substituted back into Eq. (5.68) to get the desired ADM solution. Using Eqs. (5.61) and (5.68), the expression of η is found to be:

$$\eta_{ADM} = \frac{C_2}{(1+KC_2)} + \frac{C_2\phi^2}{6(1+KC_2)^3} + \frac{C_2(1-6\,KC_2)\phi^4}{120(1+KC_2)^5} + \frac{C_2(1-36KC_2+90K^2C_2{}^2)\phi^6}{5040(1+KC_2)^7} + \dots$$

$$(5.70)$$

For $K = 2$ and for different values of ϕ [= 4, 5, 6], the values of C_2 and η have been obtained from Eqs. (5.69) and (5.70), respectively, and are shown in Table 5.10 along with those obtained by using the approximate solution of Gottifredi and Gonzo (2005) and numerical method. This table shows that with the increase in ϕ, the values

Table 5.10: **Comparison between the values of C_2 and η obtained by using ADM, approximate solution of Gottifredi and Gonzo (2005) and numerical method for Langmuir-Hinshelwood kinetics $y/(1+Ky)$ with $K = 2$**

Method	n_T	C_2 [Concentration at the center of pore]		
		$\phi = 4$	$\phi = 5$	$\phi = 6$
ADM	4	0.0602	0.0201	0.0080
	6	0.0678	0.0279	0.0081
	8	0.0670	0.0225	0.0100
	10	0.0659	0.0262	0.0076
Gottifredi and Gonzo (2005)	-	0.1523	0.0868	0.0486
Numerical	-	0.0667	0.0240	0.0087
Method	n_T	η [Effectiveness factor]		
		$\phi = 4$	$\phi = 5$	$\phi = 6$
ADM	4	0.1880	0.1592	0.1265
	6	0.1617	0.0963	0.1180
	8	0.1634	0.1563	0.0862
	10	0.1750	0.0929	0.1509
Gottifredi and Gonzo (2005)	-	0.1678	0.1343	0.1119
Numerical	-	0.1671	0.1341	0.1118

of C_2 and η obtained by using the ADM solutions start diverging from the numerically obtained values. These results also substantiate the observations made in Table 5.9 and indicate that the higher the value of ϕ the higher is the inconsistency in the predictions of ADM solution.

For one of these parameters' values [$K = 2$, $\phi = 6$], the dimensionless concentration profiles obtained by using different methods are depicted in Fig. 5.12. The corresponding residual errors profiles have been shown in Fig. 5.13. Fig. 5.12 shows that the ADM solutions [$n_T = 4, 10$] match approximately with the numerical solution and show slight deviation near the pore mouth. Besides, ADM solution corresponding to $n_T = 4$ is closer to the numerical solution as compared to the one corresponding to $n_T = 10$. This is also apparent in Fig. 5.13, which shows that the residual errors at the pore mouth are larger for $n_T = 10$ than for $n_T = 4$. This observation signifies that for higher ϕ, the ADM solutions diverge and the error increases with the increase in number of terms.

The dimensionless concentration profile obtained by using the approximate solution of Gottifredi and Gonzo (2005), is also shown in Fig. 5.12. It is clear that this profile matches with the numerical solution only near to the mouth. This fact is also observable in the Fig. 5.13, where small residual errors are present at the pore mouth for the approximate solution of Gottifredi and Gonzo as compared to the ADM solutions. However, this trend is reversed at the pore end.

5.5.2.2 Solution by RADM

In this subsection, we have solved Eqs. (5.60a)-(5.60c) by using RADM. The methodology of RADM for solving ODEs has already been explained in subsection 5.2.2. However, here use of orthogonal polynomials [OPs] has also been incorporated in RADM so as to serve the following two purposes:

(i)   In RADM, the solution obtained in an iteration is utilized in the next iteration. In case of complicated nonlinearity, it is observed that the iterative scheme of RADM gives rise to the appearance of some un-integrable terms, e.g.

$\int_0^x \left(a_0 + a_1 x + a_2 x^2 + ... \right)^{0.5} dx$ or $\int_0^x e^{e^x} dx$. It is important to note that these terms are not

nonlinear terms [do not contain nonlinear terms of y], rather these can't be integrated in some closed form. On the other hand, if the complicated nonlinearity is expressed in some polynomial form, then the appearance of such unintegrable terms can be avoided. Since, polynomial nonlinearities do not create such problems, RADM can straight forwardly be used for polynomial nonlinearities without using OPs. The polynomial approximation of a nonlinearity is done as follows:

$$N(y) \approx \sum_{i=0}^{n_1} a_i P_i(y) \tag{5.71}$$

where a_i's are the constants, P_i is i^{th} order orthogonal polynomial and n_1 is the numbers of these polynomials considered for approximation. a_i's are evaluated using the orthogonal property of the OPs. For example: approximation of $N(y) = y^{0.5}$ is given by the following first three Shifted-Legendre polynomials (Abramowitz and Stegun, 1964; Gupta, 1995).

$$y^{0.5} \approx \underbrace{(0.6667)}_{a_0} \underbrace{(1)}_{P_0(y)} + \underbrace{(0.4)}_{a_1} \underbrace{(-1+2y)}_{P_1(y)} + \underbrace{(-0.0952)}_{a_2} \underbrace{(1-6y+6y^2)}_{P_2(y)}$$

(ii) As shown in the illustration 5.4, the RADM solution obtained after each iteration has some additional terms, hence the multiple iterations in RADM will obviously result in a comparatively bigger series. Therefore, it is advantageous to approximate the solution by OPs after each iteration of RADM. This will ease the computation many folds, and at the same time will not affect the quality of results. The RADM solution [y_{RADM}] is approximated as follows:

$$y_{RADM}(x) \approx \sum_{i=0}^{n_2} b_i P_i(x) \tag{5.72}$$

where b_i's are again evaluated using the orthogonal property of the OPs. n_2 is the numbers of these polynomials considered for approximation. Since, in the beginning, the only available solution is the ADM solution, hence, y_{ADM} is
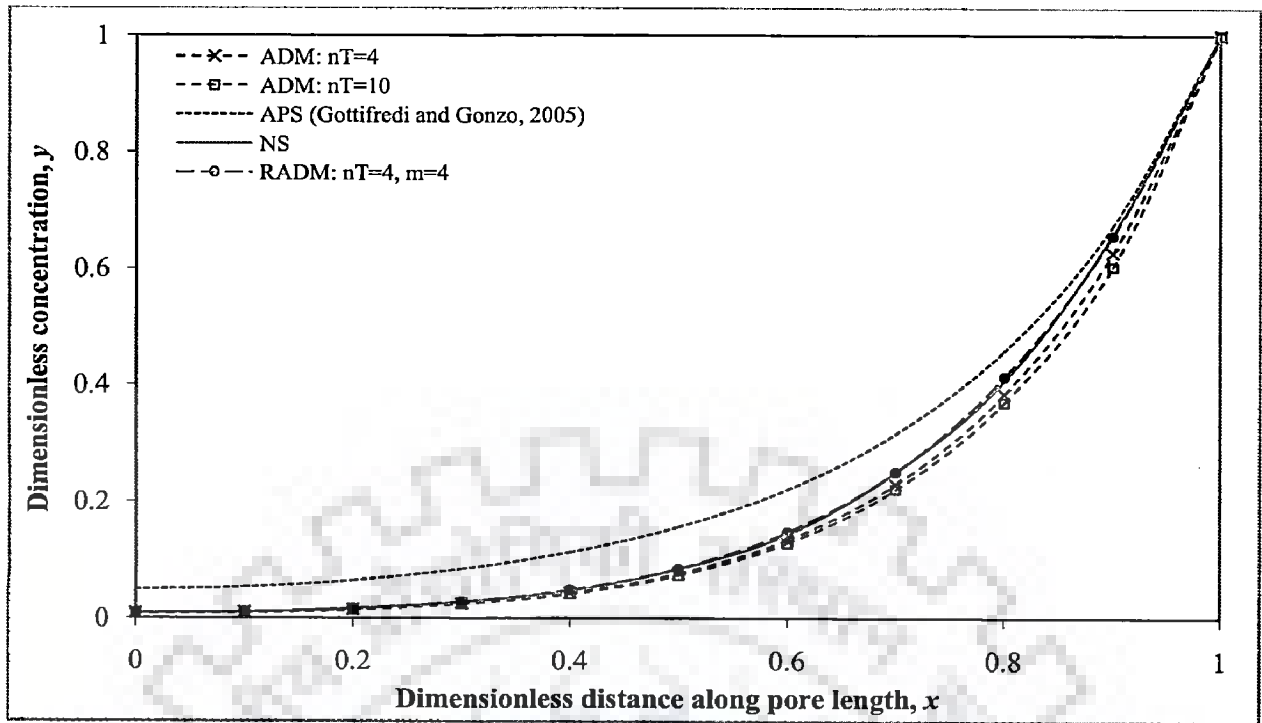
Figure 5.12: Dimensionless concentration profiles [Langmuir-Hinshelwood kinetics: $K = 2$, $\phi = 6$; $x = 0$: pore end; $x = 1$: pore mouth]
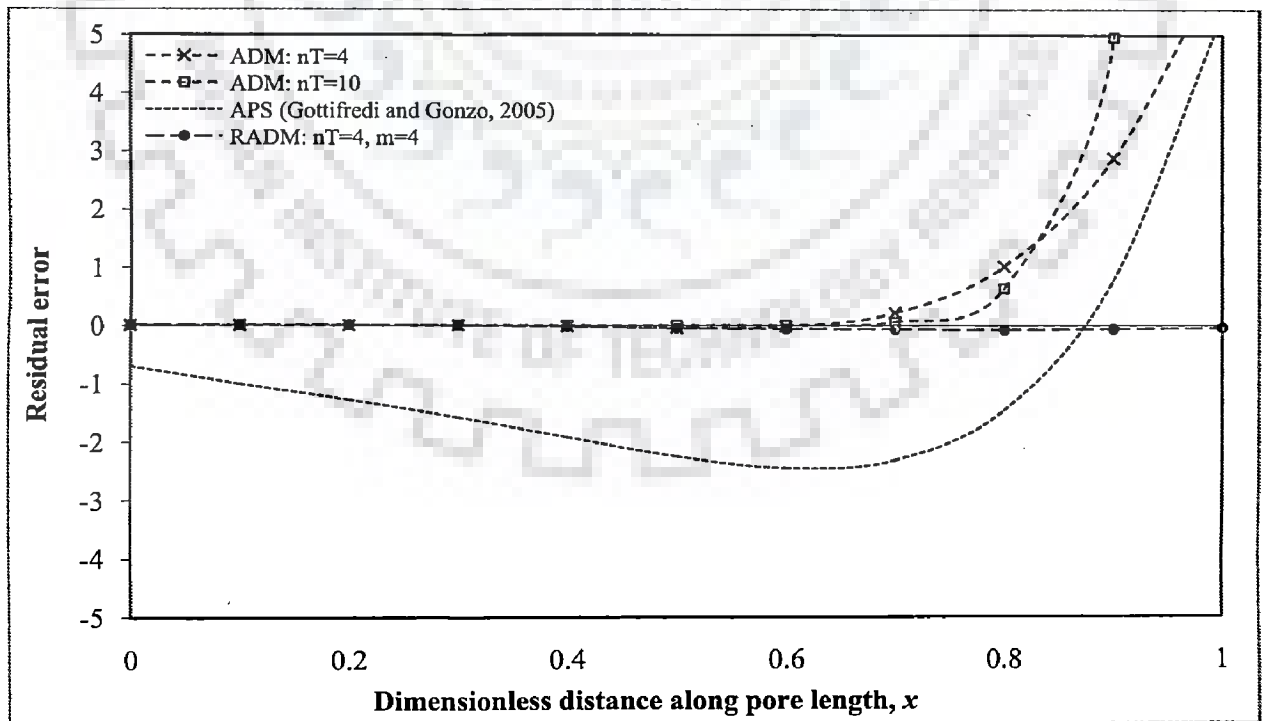
Figure 5.13: Residual error profiles [Langmuir-Hinshelwood kinetics: $K = 2$, $\phi = 6$; $x = 0$: pore end; $x = 1$: pore mouth]

approximated by using Eq. (5.72).

With these two modifications, the applicability as well as the effectiveness of RADM is increased, and short and accurate solutions are obtained within 2 to 3 iterations without generating higher Adomian polynomials. While approximating the nonlinearity, in both the approximations, care should be taken in selecting the types and numbers of OPs so that these polynomials sufficiently represent the approximated function, at least in the interested domain and the accuracy of the resultant approximations is ensured. In the present model equation, the variables [x and y] vary between 0 and 1, hence, Shifted-Legendre's polynomials have been chosen, which are orthogonal in this domain with unity as weighing function. As far as the number of OPs are concerned, generally 4 to 8 initial OPs are found to be sufficient for approximation; lesser number of OPs will give poor and sometimes divergent results, whereas higher number of OPs will offer better results but at the cost of higher computational time.

The step by step procedure to implement the above concept is described below and a flowchart has been shown in Fig. 5.14.

1. Any complicated nonlinearity is first approximated by OPs using Eq. (5.71), thereafter, the numbers of terms [n_T] in ADM are chosen and the ADM solution is found. To obtain a simpler form of the solution and to quickly perform the operations in the next iteration, this ADM solution is approximated by suitable numbers of OPs by using Eq. (5.72); let this be denoted by y_{RADM}. This constitutes first iteration of RADM. After obtaining this approximate solution, ADM is again employed but with the following modifications.

2. Before re-applying ADM, y_0 is set equal to y_{RADM} as a replacement for its previous expression, i.e. $y_0 = C_1 x + C_2$ [note that $C_1 = 0$ for the present reaction-diffusion process].

3. Instead of the earlier relation of y_1, i.e. $y_1 = \phi^2 L^{-1}[A_0]$, y_1 now contains the unknown C_2 for this iteration, i.e. $y_1 = C_2 + \phi^2 L^{-1}[A_0] - y_0$, however, the definitions of remaining y_is remain the same.

4. Although, the solution is again expressed by the relation: $y_{RADM} \approx y_0 + y_1 + \ldots y_m = C_2 + L^{-1}A_0 + \ldots + L^{-1}A_{m-1}$, but due to the appearance of C_2 in y_1 instead of y_0, its value changes when found from BC I. Substituting back the so found value of C_2 into the expression gives the updated solution for this iteration. This solution is again simplified by proper number of OPs as shown in Eq. (5.72) and the approximated solution $[y_{RADM}]$ is obtained. With this, the second iteration of RADM is finished.

5. To continue the third and higher iterations, the approximated solution $[y_{RADM}]$, obtained from step 4, is equated to y_0. Steps 2 onwards are repeated until one finds the solution of desired accuracy.

Since, the initial guess $[y_0]$ gets better with each iteration, it is expected that the solution obtained in the next iteration of RADM will also improve. To get a more clear picture of the above procedure, the solution of Eqs. (5.60a)-(5.60c) has been obtained below for power law kinetics with $n = 0.5$ and $\phi = 2$.

As described in step 1, the nonlinearity $N(y) = y^{0.5}$ is approximated with the help of OPs as shown in Eq. (5.71); seven initial OPs are found to be sufficient.

$$y^{0.5} \approx \sum_{i=0}^{6} a_i P_i(y) \tag{5.73}$$

Computed values of a_0, a_1,... and a_6 are respectively 0.6667, 0.4, -0.0952, 0.0444, -0.0260, 0.0171, -0.0121, and $y^{0.5}$ is expressed by the following polynomial equation:

$$y^{0.5} \approx 0.0718 + 3.4462y - 12.9231y^2 + 34.4615y^3 - 50.7692y^4 + 37.9077y^5$$

$$-11.2y^6$$

After getting the above approximate expression of the nonlinearity, the ADM solution is obtained. For this problem $n_T = 4$ is selected. The values of C_1 and C_2 are computed by forcing the obtained ADM solution to satisfy the concerned BCs and are
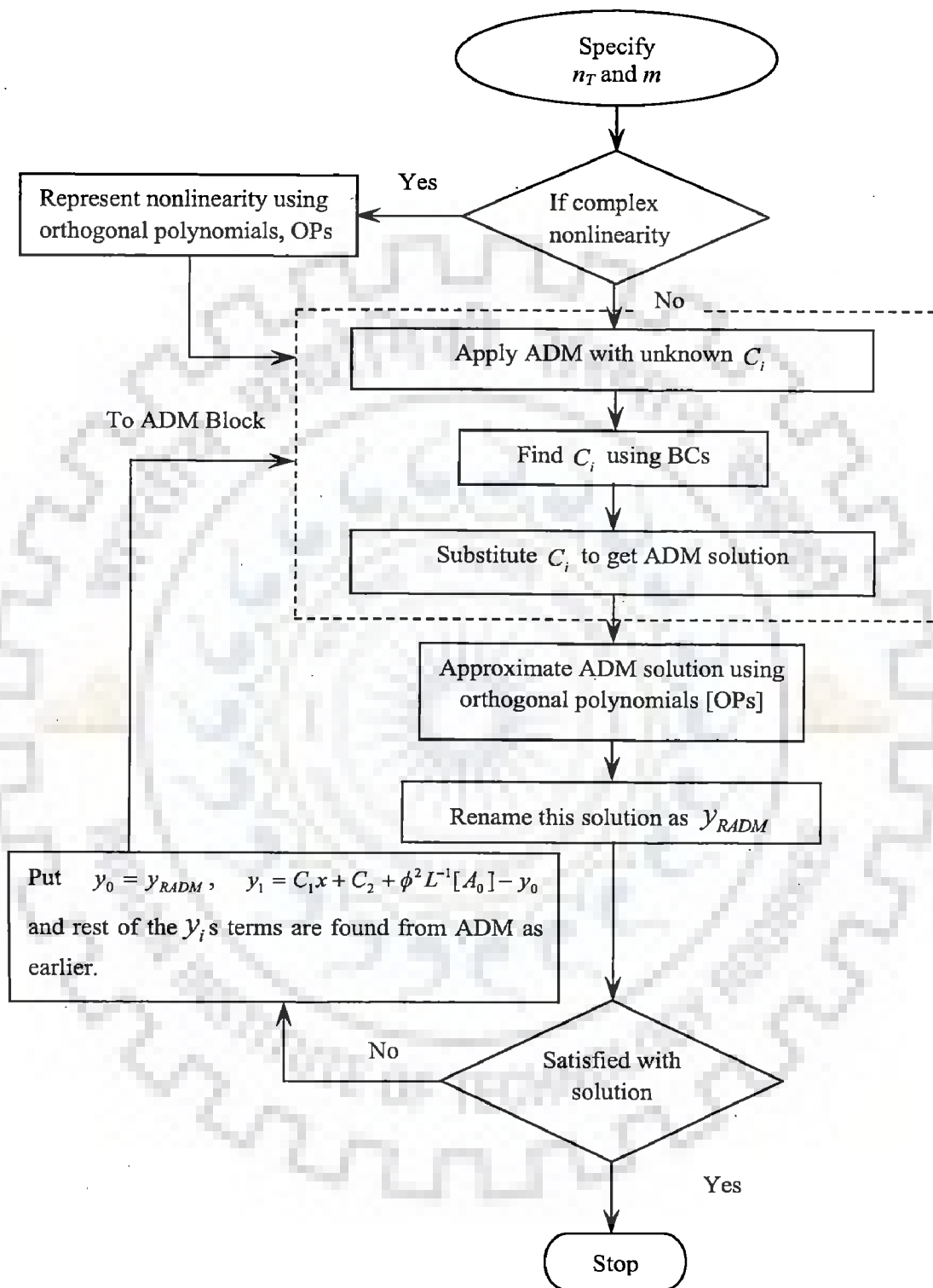
Figure 5.14:   Flow chart of RADM

The flow chart contains the following elements:

Specify n_T and m

If complex nonlinearity

Yes → Represent nonlinearity using orthogonal polynomials, OPs

To ADM Block

No

Apply ADM with unknown C_i

Find C_i using BCs

Substitute C_i to get ADM solution

Approximate ADM solution using orthogonal polynomials [OPs]

Rename this solution as y_{RADM}

Put $y_0 = y_{RADM}$, $\quad y_1 = C_1 x + C_2 + \phi^2 L^{-1}[A_0] - y_0$ and rest of the y_i s terms are found from ADM as earlier.

Satisfied with solution

No

Yes

Stop

263

found to be 0 and 0.1294, respectively. Substituting these values of C_1 and C_2 into the ADM solution, one obtains the following ADM solution.

$$y_{ADM} = 0.1294 + 0.7262x^2 + 0.3494x^4 - 0.2050x^6 \qquad (5.74)$$

As per step 1, this solution should be approximated by using OPs. However, the solution expression is not large and we can continue to the next step without approximating it by using OPs, and the results will not be affected.

Now, as stated in steps 2 and 3, y_0 and y_1 are updated as $y_0 = y_{ADM}$ and $y_1 = C_1x + C_2 + \phi^2 L^{-1}[A_0] - y_0$, respectively, while the definitions of higher y_is remain unchanged. Adding these y_is yields the RADM solution. The improved values of C_1 [= 0] and C_2 [= 0.0970] in RADM solution are obtained after following the step 4. Once, C_1 and C_2 are known, the expression of y_{RADM} is obtained for this iteration, which is then approximated by using OPs as shown in Eq. (5.72). The following polynomial representation of y_{RADM} is obtained for the present iteration; for this case too, seven initial OPs are found to be good enough.

$$y_{RADM} \approx \sum_{i=0}^{6} b_i P_i(x)$$

$$y_{RADM} \approx 0.0969 + 0.0027x + 0.5908x^2 + 0.1573x^3 + 0.0811x^4 + 0.1224x^5 - 0.0511x^6$$

$$(5.75)$$

As stated in step 5, one may continue until the solution with desired accuracy is achieved. It is worthwhile to note that the above methodology is equally applicable for $n \geq 1$.

The results obtained from the above solutions have been displayed in Figs. 5.10 and 5.11, and in Table 5.11. Fig. 5.10 shows that with the increase in iterations, the dimensionless concentration profile obtained by using RADM approaches to the numerically obtained profile, and in contrast to the profile obtained by using ADM, the profile obtained by using RADM after three iterations matches exactly with the numerical profile. This is also evident from Fig. 5.11, which shows that zero residual error exists throughout the pore length for the RADM solution after the third iteration.

Table 5.11: Approximate solutions obtained by using ADM and RADM for power law kinetics with $n = 0.5$, $\phi = 2$ [numbers of Shifted-Legendre's Polynomials considered for approximating $y^{0.5}$ and y_{RADM} are seven]

Method	n_T	m	C_2	η	y
ADM	4	-	0.1160	0.4782	$0.115997 + 0.681165x^2 + 0.333333x^4 -0.130495x^6$
RADM	4	1	0.1294	0.4050	$0.129391 + 0.726165x^2 + 0.349414x^4 - 0.204971x^6$
		2	0.0970	0.5711	$0.0969028 + 0.00268857x + 0.590765x^2 + 0.157331x^3 +0.0810689x^4 + 0.1224x^5 - 0.0511493x^6$
		3	0.0987	0.5683	$0.0986293 + 0.00220913x + 0.602107x^2 + 0.124676x^3 +0.138105x^4 + 0.065856x^5 - 0.0315863x^6$
Numerical	-	-	0.0995	0.5682	-

Besides, these RADM profiles are also better than the one obtained from the approximate solution of Gottifredi and Gonzo (2005).

Table 5.11 depicts the values of C_2 and η obtained by using ADM and RADM solutions [$n_T = 4$]. This table also shows the ADM and RADM solutions of dimensionless concentration profile. It is clear from this table that the values of C_2 and η obtained after the three iterations of RADM are quite close to the numerically obtained values [percentage error: -0.8 % for C_2 and -0.02 % for η]. On the other hand, the values of C_2 and η obtained by using ADM solution are having reasonable error [16.5829 % for C_2 and -15.8395 % for η].

For power-law kinetics [$n = 0.5$, $\phi = 2$], the typical improvement in the values of C_2 and η with number of iterations in RADM have been shown in Figs. 5.15 and 5.16. It can be observed that for lesser number of terms more iterations are required to reach at the correct value and vice-versa.

In a similar fashion, the results for Langmuir-Hinshelwood kinetics [$K = 2$, $\phi = 6$] have also been obtained by using ADM and RADM solutions, and are depicted

266
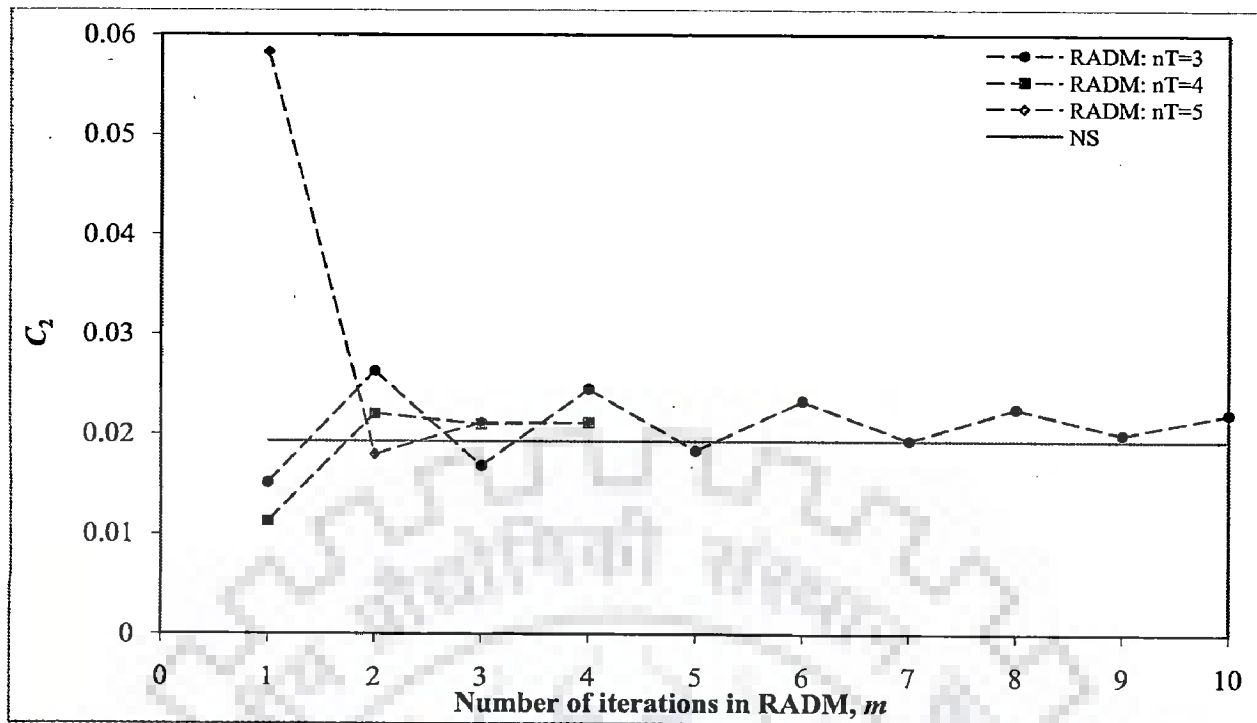
Figure 5.15: Variation in C_2 with number of iterations in RADM [power-law kinetics: $n = 0.5$, $\phi = 2$]
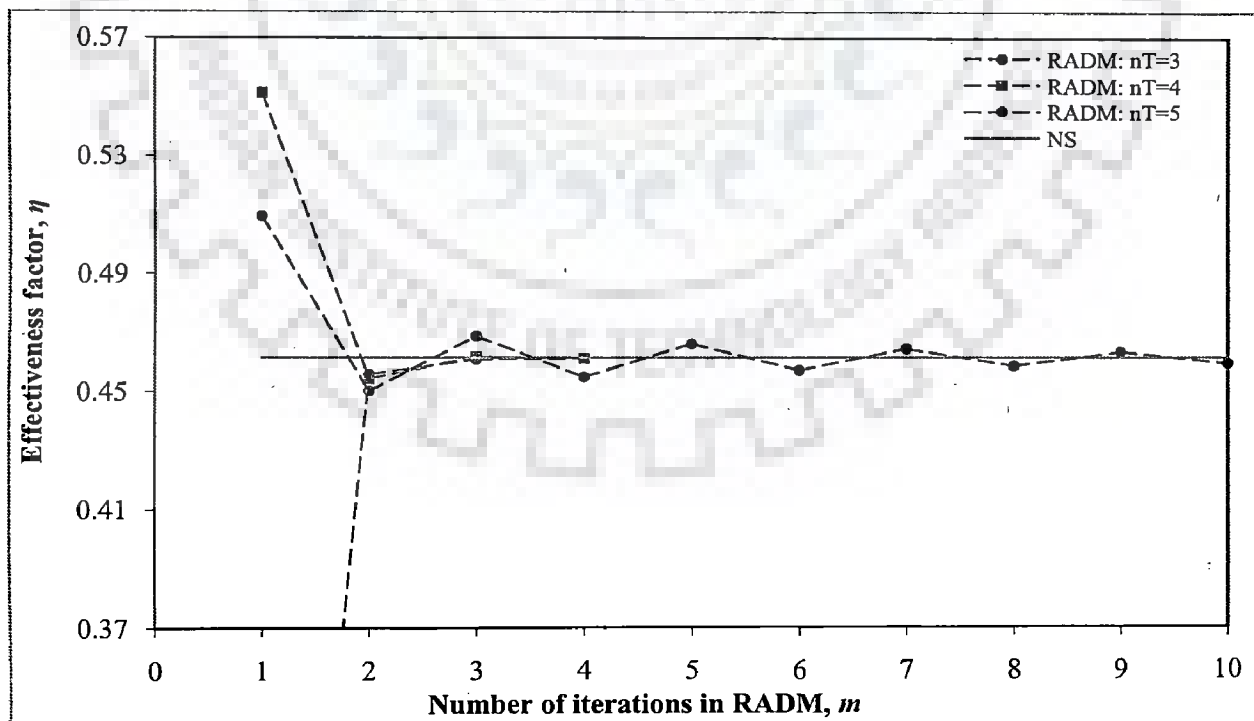
Figure 5.16: Variation in effectiveness factor with number of iterations in RADM [power law kinetics: $n = 0.5$, $\phi = 2$]

Table 5.12: Approximate solutions obtained by using ADM and RADM for $K = 2$, $\phi = 6$ [numbers of Shifted-Legendre's polynomials considered for approximating $y/(1+Ky)$ and y_{RADM} are six and eight, respectively]

Method	n_T	m	C_2	η	y
ADM	4	-	0.0080	0.1265	$0.00804914 + 0.142589x^2 + 0.41432x^4 + 0.435042x^6$
RADM	4	1	0.0079	0.1260	$0.00785021 + 0.146688x^2 + 0.415505x^4 + 0.429957x^6$
		2	0.0089	0.1109	$0.008858 + 0.002992x + 0.123613x^2 + 0.205272x^3 + 0.09399x^4 - 0.09408x^5 + 1.40153x^6 - 0.742286x^7$
		3	0.0082	0.1125	$0.0080854 + 0.00432094x + 0.0897236x^2 + 0.339938x^3 - 0.348954x^4 + 0.503699x^5 + 1.10698x^6 - 0.703916x^7$
		4	0.0087	0.1114	$0.008629 + 0.0032917x + 0.115114x^2 + 0.234571x^3 - 0.002464x^4 + 0.024002x^5 + 1.36102x^6 - 0.744276x^7$
Numerical	-	-	0.0087	0.1118	-

in Figs. 5.12, 5.13 and Table 5.12. Figs. 5.12 and 5.13 show the dimensionless concentration profiles and the corresponding residual error profiles obtained by using RADM, respectively. It is clear from these figures that the accuracy in the RADM solution increases with the number of iterations. These figures again manifest that the RADM solution [$n_T = 4$, $m = 4$] is the closest one to the numerical solution, and yields almost zero residual error as compared to those obtained by using the ADM solutions or the approximate solution of Gottifredi and Gonzo (2005). Table 5.12 depicts the results obtained by using ADM and RADM [$n_T = 4$] for Langmuir-Hinshelwood kinetics [$K = 2$, $\phi = 6$]. Here also, one sees that the values of C_2 and η approach towards the numerical values as the iterations in RADM is increased.

5.6 REACTION-DIFFUSION PROCESS IN A POROUS SPHERICAL CATALYST

In this section, the model equation of reaction-diffusion process occurring inside a porous spherical catalyst has been solved by using ADM and RADM, and the

approximate solutions of concentration profile and effectiveness factor have been obtained.

5.6.1 Model Equation

Consider a porous spherical catalyst of radius R, in which a gaseous reactant A is diffusing and simultaneously reacting on the active sites of the walls of pore. The reaction is assumed to be unimolecular and follows power-law kinetics. It is also assumed that the effective diffusivity of A inside the pore $[D_e]$ is constant, and the steady state and isothermal conditions are prevailing. With these assumptions, the model equation of this process can be derived by applying the material balance of reactant A over the control element of the catalyst, and the following second order ODE constituting a singular BVP is obtained (Shi-Bin et al., 2003). The details of the derivation of this model equation can be found elsewhere (Fogler, 1992).

$$D_e \left(\frac{d^2 C_A}{dr^2} + \frac{2}{r} \frac{dC_A}{dr} \right) = k_n C_A^n \tag{5.76a}$$

BC I: $C_A = C_{AS}$ at $r = R$ [pore mouth] $\tag{5.76b}$

BC II: $\dfrac{dC_A}{dr} = 0$ at $r = 0$ [pore end] $\tag{5.76c}$

where C_A and C_{AS} are the concentration of reactant A inside the catalyst pore and at the catalyst surface [pore mouth], respectively. k_n is the rate constant and n is the reaction order. With the help of the following dimensionless variables (Shi-Bin et al., 2003),

$$y = \frac{C_A}{C_{AS}}, \quad x = \frac{r}{R}, \quad \phi = \sqrt{\frac{(-r_{AS})R^2}{D_e C_{AS}}} = \sqrt{\frac{R^2 k_n C_{AS}^{n-1}}{D_e}} \quad [= \text{Thiele modulus}],$$

the Eqs. (5.76a)-(5.76c) are now reduced into the following dimensionless form:

$$\frac{d^2 y}{dx^2} + \frac{2}{x} \frac{dy}{dx} = \phi^2 y^n \tag{5.77a}$$

BC I: $y = 1$ at $x = 1$ [pore mouth] $\tag{5.77b}$

BC II: $\dfrac{dy}{dx} = 0$ at $x = 0$ [pore end]   (5.77c)

With slight modifications, the Eq. (5.77a) can be represented in the following form. However, the concerned BCs remain the same.

$$\frac{d^2(xy)}{dx^2} = \phi^2 xy^n$$ (5.78)

For a spherical catalyst, the effectiveness factor $[\eta]$, is mathematically given by the following relation (Fogler, 1992):

$$\eta = \frac{3}{\phi^2} \frac{dy}{dx}\bigg|_{x=1}$$ (5.79)

5.6.2 Solutions and Discussion: Concentration Profile and Effectiveness Factor

In this subsection, approximate solutions of the concerned model equation [Eqs. (5.78), (5.77b) and (5.77c)] have been obtained by using ADM and RADM. The obtained results have been compared with the numerical results and the available results (Shi-Bin et al., 2003).

5.6.2.1 Solution by ADM

For convenience, the ADM solutions have been obtained for the first order kinetics $[n = 1]$ and the nth order kinetics $[n \neq 1]$, separately.

(i)   First order kinetics (n = 1)

Following the procedure outlined in subsection 5.1.3, one recognizes that in Eq. (5.78), $L[.] = \dfrac{d^2[.]}{dx^2}$ or $L^{-1}[.] = \displaystyle\int_0^x \int [.]dxdx$, $R(y) = 0$, $g(x) = 0$, and $N(y) = y$. Hence, using Eq. (5.10), the Eq. (5.78) can be expressed in the following operator form:

$$L[x\,y] = \phi^2 x N[y] \tag{5.80}$$

Now, using Eq. (5.11), one can express y in the following form:

$$y = \sum_{i=0}^{\infty} \lambda^i y_i \tag{5.81}$$

where y_is are the decomposed parts of the so called ADM solution y_{ADM}. Similarly, by using Eq. (5.12), the nonlinearity $N(y)$ is expressed in the following series of Adomian polynomials.

$$N(y) = \sum_{i=0}^{\infty} \lambda^i A_i \tag{5.82}$$

Now using Eq. (5.13), the following homotopy is constructed:

$$L[xy] = \lambda \phi^2 x N(y) \tag{5.83}$$

By using Eqs. (5.81) and (5.82), y and $N(y)$ in Eq. (5.83) are replaced with their decomposed parts, and one obtains:

$$L[x \sum_{i=0}^{\infty} \lambda^i y_i] = \phi^2 x \sum_{i=0}^{\infty} \lambda^{i+1} A_i \tag{5.84}$$

Operating by $L^{-1}[.]$, i.e. $\int_0^x \int [.] dx\, dx$, on both the sides of Eq. (5.84), the following equation is obtained:

$$x \sum_{i=0}^{\infty} \lambda^i y_i = C_1 + C_2 x + L^{-1} \left[\phi^2 x \sum_{i=0}^{\infty} \lambda^{i+1} A_i \right] \tag{5.85a}$$

or

$$\sum_{i=0}^{\infty} \lambda^i y_i = C_1 x^{-1} + C_2 + x^{-1} L^{-1} \left[\phi^2 x \sum_{i=0}^{\infty} \lambda^{i+1} A_i \right] \tag{5.85b}$$

where $L^{-1}[0] = C_1 + C_2 x$. C_1 and C_2 are the constants of integration and can be found from the associated BCs. BC II yields $C_1 = 0$, since y is finite at $x = 0$ [Eq. (5.77c)]. It

should be noted that for $N(y) = y$, $A_i = y_i$. Now, on comparing the terms having same exponent of λ and simultaneously evaluating the Adomian polynomials, one finds:

$$y_0 = C_2$$

$$A_0 = y_0 = C_2$$

$$y_1 = x^{-1}L^{-1}\left[\phi^2 x A_0\right] = \frac{C_2\phi^2 x^2}{6}$$

$$A_1 = y_1 = \frac{C_2\phi^2 x^2}{6}$$

$$y_2 = x^{-1}L^{-1}\left[\phi^2 x A_1\right] = \frac{C_2\phi^4 x^4}{120}$$

$$A_2 = y_2 = \frac{C_2\phi^4 x^4}{120}$$

...

Substituting the above expressions for y_is in Eq. (5.81) and setting $\lambda = 1$, one obtains the following ADM solution:

$$y_{ADM} = C_2 + \frac{1}{6}C_2\phi^2 x^2 + \frac{1}{120}C_2\phi^4 x^4 + \frac{1}{5040}C_2\phi^6 x^6 + \frac{1}{362880}C_2\phi^8 x^8 + ... \quad (5.86)$$

For a particular ϕ, the integration constant C_2 is evaluated from the remaining BC I. This is done as follows:

$$y_{ADM}(1) = 1 = C_2 + \frac{1}{6}C_2\phi^2 + \frac{1}{120}C_2\phi^4 + \frac{1}{5040}C_2\phi^6 + \frac{1}{362880}C_2\phi^8 + ...$$

or

$$C_2 = \frac{1}{1 + \frac{1}{6}\phi^2 + \frac{1}{120}\phi^4 + \frac{1}{5040}\phi^6 + \frac{1}{362880}\phi^8 + ...} \quad (5.87)$$

The so found value of C_2 is substituted back into Eq. (5.86) to get the ADM solution of the dimensionless concentration profile. Likewise, by using Eq. (5.79), the ADM solution of effectiveness factor can also be obtained as follows:

$$\eta_{ADM} = \frac{3}{\phi^2} \frac{dy_{ADM}}{dx}\bigg|_{x=1}$$

$$= C_2 + \frac{C_2\phi^2}{10} + \frac{C_2\phi^4}{280} + \frac{C_2\phi^6}{15120} + \frac{C_2\phi^8}{1330560} + \dots \tag{5.88}$$

It is also important to compare the above derived ADM solutions [y_{ADM} and η_{ADM}] with the following analytical solutions [y and η], which fortunately exist for the first order kinetics (Fogler, 1992):

$$y = \frac{sinh\,(\phi x)}{x\,sinh\,(\phi)} \tag{5.89}$$

$$\eta = \frac{3\,[\,\phi\,coth\,(\phi) - 1\,]}{\phi^2} \tag{5.90}$$

For the purpose of comparison, the above analytical solutions [Eqs. (5.89) and (5.90)] are expanded around $x = 0$ and $\phi = 0$ by using Taylor series method and the following expansions of y and η, up to the sixth power of x and ϕ, are obtained, respectively:

$$y \approx 1 + \left(-\frac{1}{6} + \frac{x^2}{6}\right)\phi^2 + \left(\frac{7}{360} - \frac{x^2}{36} + \frac{x^4}{120}\right)\phi^4 + \left(-\frac{31}{15120} + \frac{7x^2}{2160} - \frac{x^4}{720} + \frac{x^6}{5040}\right)\phi^6$$
$$\tag{5.91}$$

$$\eta \approx 1 - \frac{\phi^2}{15} + \frac{2\phi^4}{315} - \frac{\phi^6}{1575} \tag{5.92}$$

Similarly, after substituting C_2 [Eq. (5.87)] in y_{ADM} [Eq. (5.86)] and η_{ADM} [Eq. (5.88)], the following Taylor series expansions of y_{ADM} and η_{ADM} around $x = 0$ and $\phi = 0$ [up to the six power of x and ϕ], are obtained, respectively:

$$y_{ADM} \approx 1 + \left(-\frac{1}{6} + \frac{x^2}{6} \right)\phi^2 + \left(\frac{7}{360} - \frac{x^2}{36} + \frac{x^4}{120} \right)\phi^4 + \left(-\frac{31}{15120} + \frac{7x^2}{2160} - \frac{x^4}{720} + \frac{x^6}{5040} \right)\phi^6$$

$$(5.93)$$

$$\eta_{ADM} \approx 1 - \frac{\phi^2}{15} + \frac{2\phi^4}{315} - \frac{\phi^6}{1575} \qquad (5.94)$$

On comparing, it is found that the above series expansions [Eqs. (5.93) and (5.94)] match very well with those of analytical solutions [Eqs. (5.91) and (5.92)], and thus validate the above ADM solutions [y_{ADM} and η_{ADM}] obtained for the first order kinetics.

(ii)   *n^{th} order kinetics (n ≠ 1)*

Proceeding as described above, the approximate solution for the nth order power-law kinetics [$N(y) = y^n$], has also been obtained by using the ADM, and the following expressions of y_is and A_is are obtained:

$$y_0 = C_2$$

$$A_0 = y_0^n = C_2^{\,n}$$

$$y_1 = x^{-1}L^{-1}\left[\phi^2 x A_0 \right] = \frac{C_2^{\,n}\phi^2 x^2}{6}$$

$$A_1 = ny_0^{n-1}y_1 = \frac{nC_2^{\,2n-1}\phi^2 x^2}{6}$$

$$y_2 = x^{-1}L^{-1}\left[\phi^2 x A_1 \right] = \frac{nC_2^{\,2n-1}\phi^4 x^4}{120}$$

$$A_2 = \frac{1}{2}n(n-1)y_0^{n-2}y_1^2 + ny_0^{n-1}y_2 = \frac{n(8n-5)C_2^{\,3n-2}\phi^4 x^4}{360}$$

$$y_3 = x^{-1}L^{-1}\left[\phi^2 x A_2 \right] = \frac{n(8n-5)C_2^{\,3n-2}\phi^6 x^6}{15120}$$

$$A_3 = \frac{1}{6}(n-2)(n-1)ny_0^{n-3}y_1^3 + (n-1)ny_0^{n-2}y_1y_2 + ny_0^{n-1}y_3$$

$$= \frac{n(122n^2 - 183n + 70)C_2^{4n-3}\phi^6 x^6}{45360}$$

...

Finally, the ADM solution is found to be:

$$y_{ADM} = C_2 + \frac{1}{6}C_2^n x^2\phi^2 + \frac{n}{120}C_2^{-1+2\,n}x^4\phi^4 - \frac{n(8n-5)}{15120}C_2^{-2+3\,n}x^6\phi^6 +$$

$$\frac{n(122n^2 - 183n + 70)}{3265920}C_2^{-3+4\,n}x^8\phi^8 + \dots \tag{5.95}$$

Here also, the value of C_2 is found by forcing Eq. (5.95) to satisfy the BC I, and in doing so the following equation is obtained. By solving this equation, one obtains the value of C_2. Substituting back the so found value of C_2 in Eq. (5.95) gives the desired ADM solution of dimensionless concentration profile. It should also be noted that C_2 represents the dimensionless concentration at the pore end [$y_{ADM}(0) = C_2$].

$$y_{ADM}(1) = 1 = C_2 + \frac{1}{6}C_2^n \phi^2 + \frac{n}{120}C_2^{-1+2\,n}\phi^4 - \frac{n(8n-5)}{15120}C_2^{-2+3\,n}\phi^6 +$$

$$\frac{n(122n^2 - 183n + 70)}{3265920}C_2^{-3+4\,n}\phi^8 + \dots \tag{5.96}$$

The expression for effectiveness factor has been obtained with the help of Eqs. (5.79) and (5.95), and is given by the following equation:

$$\eta_{ADM} = C_2^n + \frac{n}{10}C_2^{2n-1}\phi^2 + \frac{n(8n-5)}{840}C_2^{3n-2}\phi^4 + \frac{n(122n^2 - 183n + 70)}{136080}C_2^{4n-3}\phi^6 + \dots$$

$$\tag{5.97}$$

As expected, the above Eqs. (5.95)-(5.97) reduces to the earlier derived equations for the first order kinetics, i.e. Eqs. (5.86)-(5.88), respectively.

With the help of the above obtained ADM solutions, i.e. Eqs. (5.87), (5.88), (5.96) and (5.97), values of C_2 and η have been obtained for several values of n and ϕ

$[n = 0.23, \phi = 2.6; n = 0.5, \phi = 3.4; n = 0.78, \phi = 5; n = 1, \phi = 10; n = 1.44, \phi = 10; n = 2, \phi = 10]$, respectively, and are displayed in Table 5.13. This table shows that with the increase in number of terms in the ADM solution, the accuracy in C_2 and η increases for $n \geq 1$, whereas, it decreases for $n < 1$ [$n \neq 0$].

For $n = 1$ and $\phi = 10$, the concentration profiles obtained by using the ADM solutions and the respective error profiles [$= y_{Analytical} - y_{ADM}$], have been shown in Figs. 5.17 and 5.18, respectively. Fig. 5.17 depicts that with the increase in number of terms in the ADM solution, the dimensionless concentration profile obtained by it approaches towards the analytically obtained profile [Eq. (5.89)], and for $n_T = 12$ the profile obtained by using ADM matches exactly with the analytically obtained profile. This is also evident from the error profiles drawn in Fig. 5.18.

Similarly for $n = 0.23$ and $\phi = 2.6$, the concentration profiles and the error

Table 5.13: **Variation in C_2 and η with different numbers of terms in ADM solution**

Method	n_T	← Diverging			Converging →		
		$n = 0.23,$ $\phi = 2.6$	$n = 0.5,$ $\phi = 3.4$	$n = .78,$ $\phi = 5$	$n = 1,$ $\phi = 10$	$n = 1.44,$ $\phi = 10$	$n = 2,$ $\phi = 10$
		C_2 [Concentration at the center of pore]					
ADM	2	0.21168	0.18079	0.13353	0.05660	0.12880	0.21678
	4	0.17152	0.07979	0.02254	0.00334	0.04378	0.12221
	6	0.20465	0.11788	0.02533	0.00121	0.03342	0.10719
	8	0.25074	0.18347	0.06503	0.00094	0.03075	0.10258
	10	0.29725	0.26012	0.21476	0.00091	0.02993	0.10083
	12	0.34026	0.33882	0.52802	0.00091	0.02967	0.10010
Numerical	-	0.12700	0.0589	0.0205	0.00091	0.029554	0.09955
Method	n_T	η [Effectiveness factor]					
		0.69969	0.42520	0.20795	0.05660	0.05227	0.04699
	4	0.67131	0.57889	0.48333	0.15602	0.12993	0.10987
	6	0.29227	0.09501	0.40984	0.22775	0.18239	0.15191
	8	-0.39983	-0.98912	-0.67399	0.26157	0.21437	0.17958
	10	-1.33652	-2.58911	-4.73029	0.26924	0.23151	0.19712
	12	-2.45452	-4.59550	-13.07500	0.26997	0.23956	0.20777
Numerical	-	0.87979	0.71401	0.50099	0.27000	0.23650	0.22157

profiles obtained by using ADM solutions have been shown in Figs. 5.19 and 5.20, respectively. However, in contrast to the Fig. 5.17, the Fig. 5.19 shows that with the increase in n_T, the dimensionless concentration profile obtained by using the ADM solution diverges from the numerically obtained profile. This is also supported from the corresponding error profiles depicted in Fig. 5.20. Although not shown, yet the above observations are found to be true [for higher Thiele modulus] for $n \geq 1$ and $n < 1$ [$n \neq 0$], respectively. Therefore, from any of these findings it can easily be judged that the ADM solutions are valid only for $n \geq 1$, and become redundant for $n < 1$ [$n \neq 0$] for higher values of ϕ. One should also note that these errors are also present in the ADM solutions of Shi-bin et al. (2003). For example, the values of η calculated from the ADM solution of Shi-bin et al. (2003) for $n = 0.23$ and $\phi = 2.6$ corresponding to $n_T = $ 4, 6 and 8 are found to be 0.67131, 0.29227 and - 0.39983, respectively. However, the correct value of η is 0.87979 [shown in Table 5.14], and thereby the percentage errors in the values of η come out to be 23.7%, 66.8% and 145.4%, respectively. These errors are unacceptably high and can grow with the increase in number of terms in ADM solution. This clearly indicates that the present ADM solutions and those obtained by Shi-bin et al. (2003) diverge for $n < 1$ [$n \neq 0$] and large ϕ, and yield erroneous results. It is to be noted that in Shi-bin et al. (2003), η values are not explicitly shown, rather these have been evaluated here by using their ADM solutions for the above comparison.

Table 5.14: Solutions obtained by using ADM and RADM for $n = 0.23$, $\phi = 2.6$ [numbers of Shifted-Legendre's polynomials considered for approximating $y^{0.23}$ and y_{RADM} are eight and six, respectively]

Method	n_T	m	C_2	η	y
ADM	4	-	0.17152	0.67131	$0.171518 + 0.751081x^2 + 0.2269411x^4 - 0.14954x^6$
RADM	4	1	0.18046	0.66552	$0.180604 - 0.00592468x + 0.821126x^2 - 0.236987x^3 + 0.632352x^4 - 0.391029x^5$
		2	0.12593	0.88316	$0.125964 - 0.0019004x + 0.733081x^2 - 0.0748365x^3 + 0.337355x^4 - 0.119822x^5$
		3	0.12700	0.88230	$0.12703 - 0.00144715x + 0.725064x^2 - 0.0509388x^3 + 0.308567x^4 - 0.108402x^5$
Numerical	-	-	0.12700	0.87979	-

278

Figure 5.17: Dimensionless concentration profiles [power-law kinetics: $n = 1$, $\phi = 10$; $x = 0$: pore end; $x = 1$: pore mouth]

Figure 5.18: Error profiles [power-law kinetics: $n = 1$, $\phi = 10$; $x = 0$: pore end; $x = 1$: pore mouth]

Figure 5.19: Dimensionless concentration profiles [power-law kinetics: $n = 0.23$, $\phi = 2.6$; $x = 0$: pore end; $x = 1$: pore mouth]

Figure 5.20: Error profiles [power-law kinetics: $n = 0.23$, $\phi = 2.6$; $x = 0$: pore end; $x = 1$: pore mouth]

5.6.2.2 Solution by RADM

In this subsection, the model equation [Eqs. (5.78)] along with the allied BCs [Eqs. (5.77b) and (5.77c)] has been solved by using RADM, and for demonstration the values of n and ϕ have been taken as: $n = 0.23$ and $\phi = 2.6$, since ADM solution failed for this set of parameters' values. Here too, OPs have been coupled with the RADM for the same reason as described in subsection 5.5.2.2, and for convenience, we briefly reiterate them here.

(i)   To approximate the complex nonlinearity $N(y)$ into polynomial form as shown in Eq. (5.71).

(ii) To approximate the solution obtained by using RADM [y_{RADM}] as shown in Eq. (5.72).

As described in the step 1 of the RADM in subsection 5.5.2.2, the nonlinearity $N(y) = y^{0.23}$ is approximated with the help of OPs [shifted Legendre's polynomials]; eight initial OPs are found to be sufficient.

$$y^{0.23} \approx \sum_{i=0}^{7} a_i P_i(y)$$

Computed values of a_0, a_1,... and a_7 are found to be 0.813008, 0.251559, -0.099949, 0.058551, -0.039871, 0.029489, and -0.022993, respectively, and the nonlinearity $N(y) = y^{0.23}$ attains the following polynomial form:

$$y^{0.23} \approx$$

$$0.291996 + 5.49484y - 35.8561y^2 + 140.016y^3 - 308.629y^4 + 380.526y^5$$

$$-244.671y^6 + 63.8359y^7$$

After getting the above approximation for the nonlinearity $N(y) = y^{0.23}$, the ADM solution is obtained; for the present situation $n_T = 4$ has been chosen. The unknown constants [$C_1 = 0$ and $C_2 = 0.180463$], present in the so found ADM solution,

have been found from BCs I and II. Substituting back these values of C_1 and C_2 yields the following ADM solution:

$$y_{ADM} = 0.180463 + 0.761879x^2 + 0.188001x^4 - 0.130343x^6 \qquad (5.98)$$

To avoid large expressions in the next iteration, the above ADM solution is approximated by appropriate number of OPs and the following expression [y_{RADM}] is obtained; for this case, six initial OPs are found to be good enough [it should be noted that the Eq. (5.98) contains fewer terms, hence, one may also proceed to the next step with out approximating y_{ADM} by OPs].

$$y_{RADM} \approx \sum_{i=0}^{5} b_i P_i(x)$$

$$y_{RADM} = 0.180604 - 0.005925x + 0.821126x^2 - 0.236987x^3 + 0.632352x^4$$

$$-0.391029x^5 \qquad (5.99)$$

This completes step 1. Now, as stated in steps 2 and 3, y_0 and y_1 are updated as follows, whereas the rest of the y_is remain the same. With these modifications, the solution is again obtained by applying ADM as explained earlier, and one obtains the following decomposed parts:

$$y_0 = y_{RADM}$$

$$= 0.180604 - 0.00592468x + 0.821126x^2 - 0.236987x^3 + 0.632352x^4$$

$$-0.391029x^5 \qquad (5.100)$$

$$y_1 = C_2 + \phi^2 x^{-1} L^{-1}[xA_0] - y_0$$

$$= C_2 + \phi^2 x^{-1} L^{-1}[xA_0] - (0.180604 - 0.00592468x + 0.821126x^2$$

$$-0.236987x^3 + 0.632352x^4 - 0.391029x^5) \qquad (5.101)$$

$$y_2 = x^{-1} L^{-1} \left[\phi^2 x A_1 \right]$$

$$y_3 = x^{-1} L^{-1} \left[\phi^2 x A_2 \right]$$

...

As per step 4 the solution for this iteration is obtained by adding the above decomposed parts and subsequently, the improved value of C_2 [= 0.12593] is found from BC I. Once, C_2 is known, the expression for y_{RADM} is obtained for this iteration, which is then approximated by using OPs as done in Eq. (5.99) and the following form of y_{RADM} is obtained for the present iteration.

$$y_{RADM} \approx \sum_{i=0}^{5} b_i P_i(x)$$

$$y_{RADM} \approx 0.125964 - 0.0019004x + 0.7330811x^2 - 0.0748365x^3 + 0.337355x^4$$

$$-0.119822x^5 \tag{5.102}$$

As stated in step 5, one may continue the above procedure for higher iterations until the solution with desired accuracy is achieved.

In an analogous way, the solution for another set of parameters' values [$n = 0.78$, $\phi = 5$] has also been obtained by using RADM. The results for these two sets of parameters' values [$n = 0.23$, $\phi = 2.6$; $n = 0.78$, $\phi = 5$] have been shown in Tables 5.14 and 5.15, and Figs. 5.21-5.24. The obtained ADM and RADM solutions have also been shown in these two tables. Table 5.14 shows the values of C_2 and η obtained by using the ADM and RADM solutions for $n = 0.23$, $\phi = 2.6$. Similarly, Table 5.15 shows the values of C_2 and η for $n = 0.78$, $\phi = 5$. Unlike Table 5.13, now the values of C_2 and η obtained by using the RADM solution show convergence towards numerical values and their accuracy increases with the increase in iteration.

Fig. 5.21 shows the dimensionless concentration profiles obtained by using the RADM, for $n = 0.23$ and $\phi = 2.6$. It can be observed that the dimensionless concentration profiles obtained after the first iteration of RADM does not match with the numerically obtained profile as we move inside the pore, whereas, the dimensionless concentration profiles obtained after second and third iterations of RADM show a good agreement with the numerically obtained profile. This fact can also be verified from the corresponding decreasing error profiles shown in Fig. 5.22.

285

In contrast to Fig. 5.21, the deviations in dimensionless concentration profiles are not apparent in Fig. 5.23 since, the profiles obtained after each iteration of RADM appear to be close to the numerical profiles. This is because, very little error is present [of the order of 10^{-3} at any x between 0 and 1] in all the three profiles as shown in Fig. 5.24.

Although not shown, yet it is worthwhile to mention that the results for $n \geq 1$ and for other forms of kinetics, e.g. Langmuir-Hinshelwood kinetics, can also be obtained successfully in a similar fashion. With the above discussion, it is clear that RADM is an effective and versatile method and can successfully be employed where ADM fails.

Table 5.15: Solutions obtained by using ADM and RADM for n = 0.78, ϕ = 5 [numbers of Shifted-Legendre's polynomials considered for approximating y^{078} and y_{RADM} are seven]

Method	n_T	m	C_2	η	y
ADM	4	-	0.02254	0.48333	$0.0225426 + 0.216337x^2 + 0.48582x^4 + 0.2753x^6$
RADM	4	1	0.02093	0.50704	$0.0209294 + 0.19979x^2 + 0.424978x^4 + 0.354303x^6$
		2	0.02143	0.50676	$0.0215362 - 0.00558527x + 0.274917x^2 - 0.36075x^3 + 1.2659x^4 - 0.873713x^5 + 0.677659x^6$
		3	0.02109	0.50866	$0.0211894 - 0.0056015x + 0.272554x^2 - 0.360189x^3 + 1.2555x^4 - 0.858819x^5 + 0.675328x^6$
Numerical	-	-	0.02053	0.50809	-

5.7   CONCLUDING REMARKS

ADM and RADM have been used to solve the thermodynamic equation of state, friction factor equation and the model equations of reaction-diffusion processes, and the conclusions pertaining to them are given below.

(i)   Thermodynamic Equation of State

Approximate solutions for computing the volume of a gas, which are valid for a
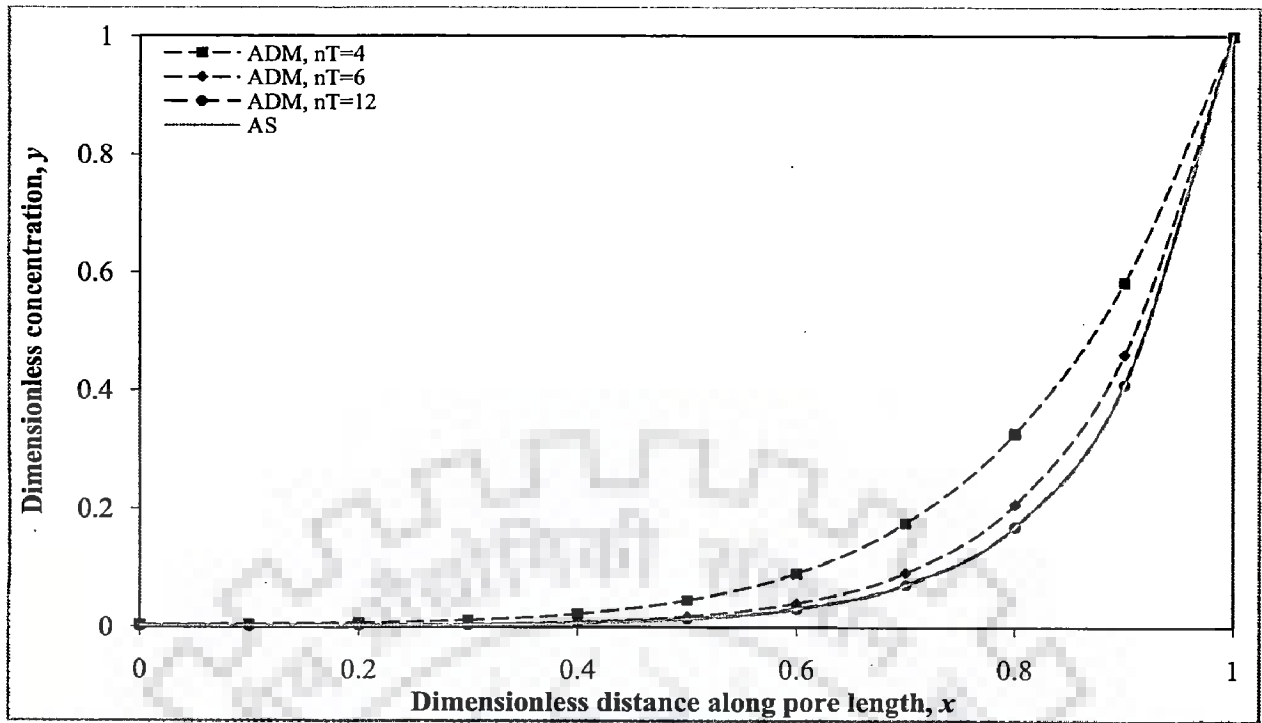
286
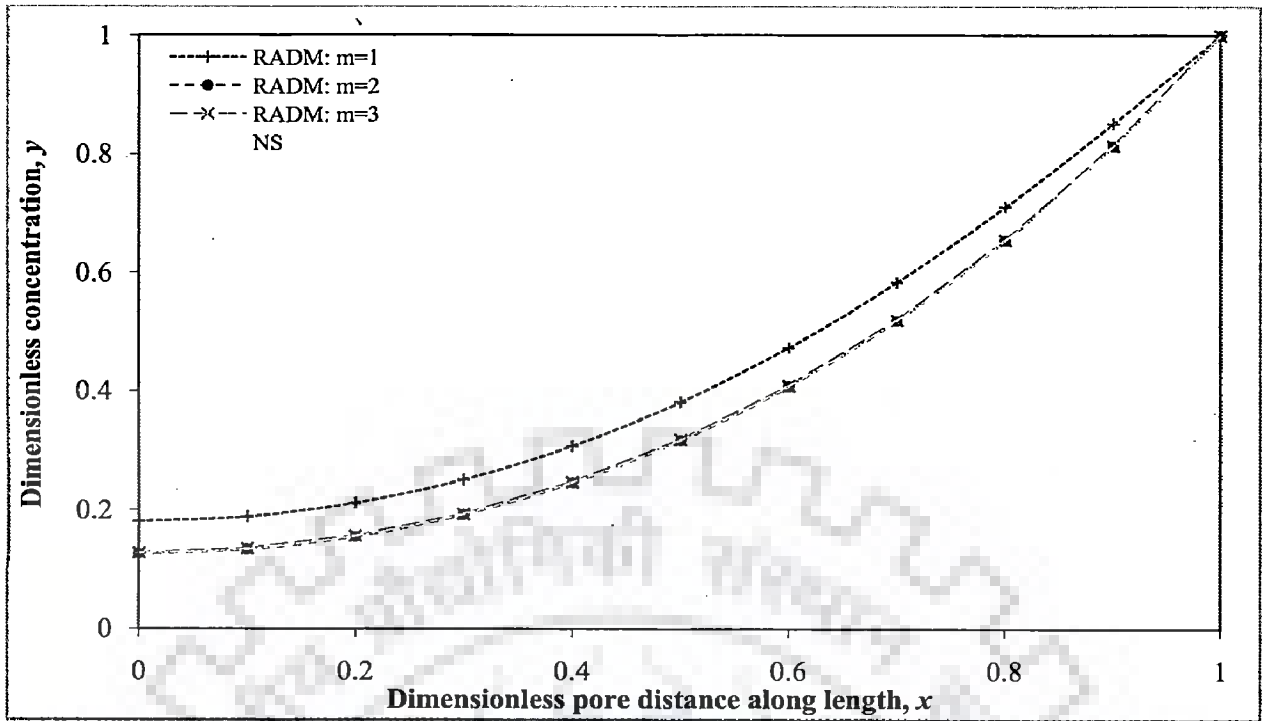
Figure 5.21: Dimensionless concentration profiles [power-law kinetics: $n = 0.23$, $\phi = 2.6$; $x = 0$: pore end; $x = 1$: pore mouth]
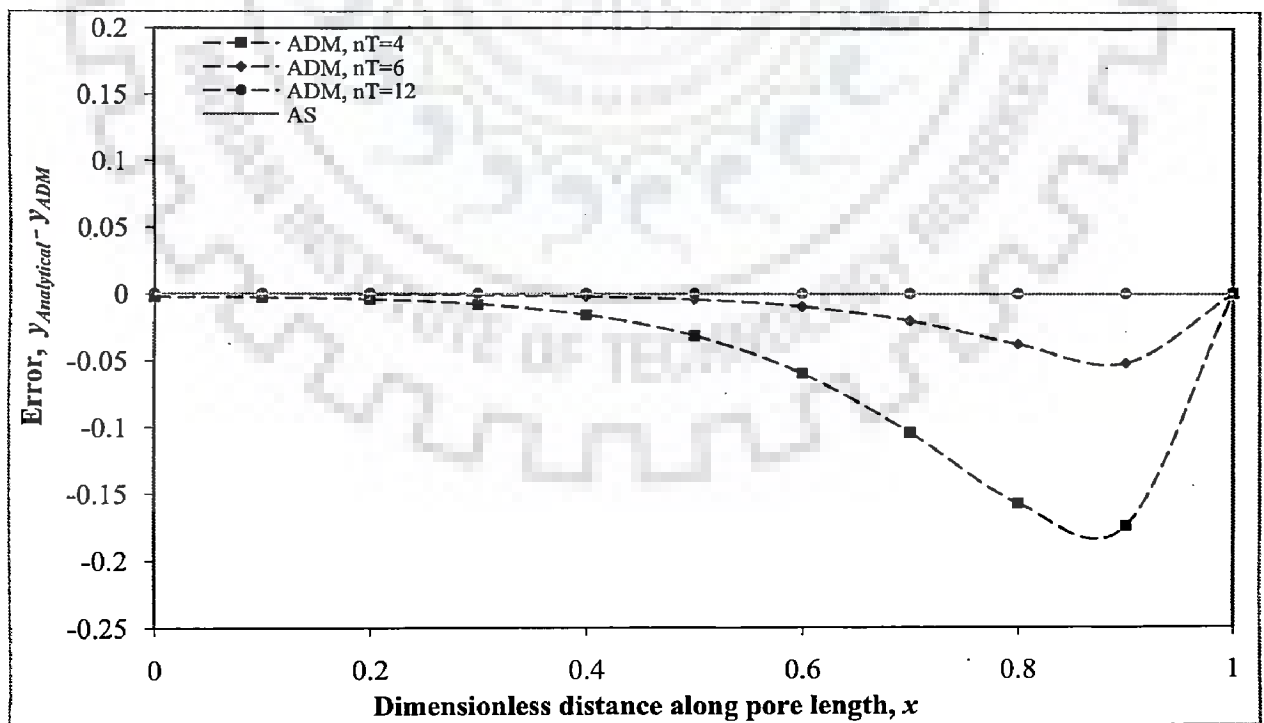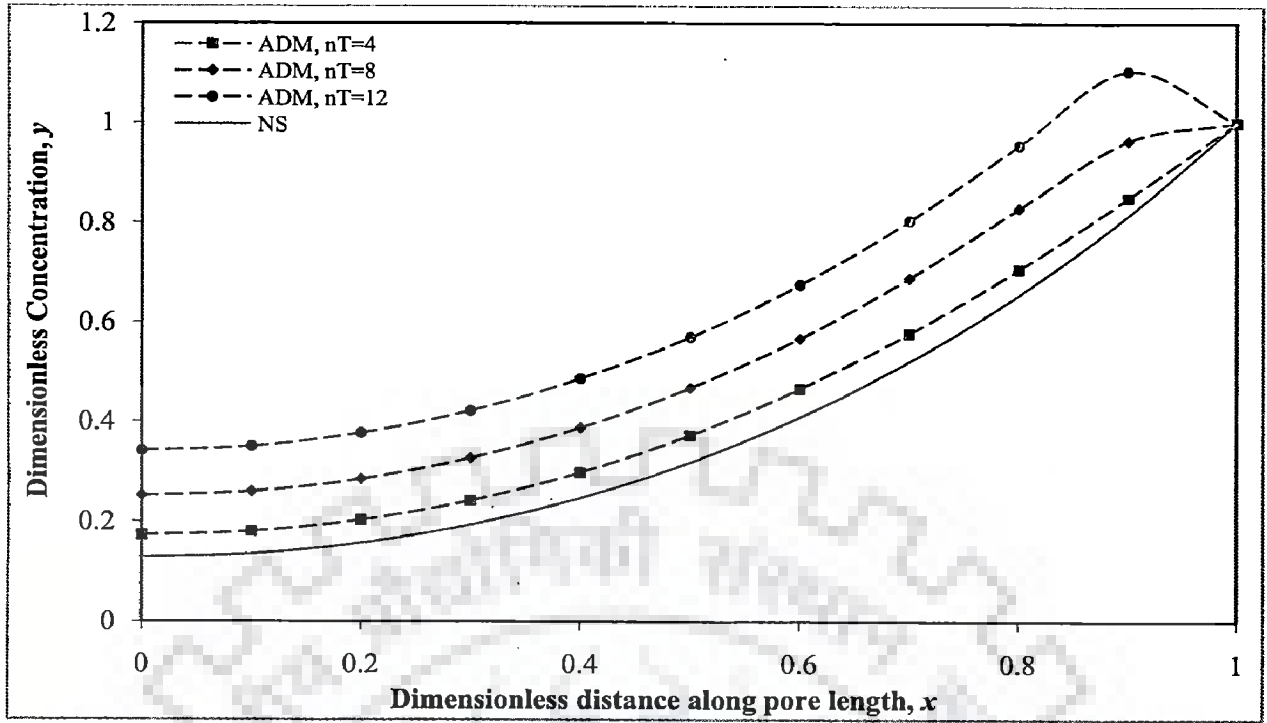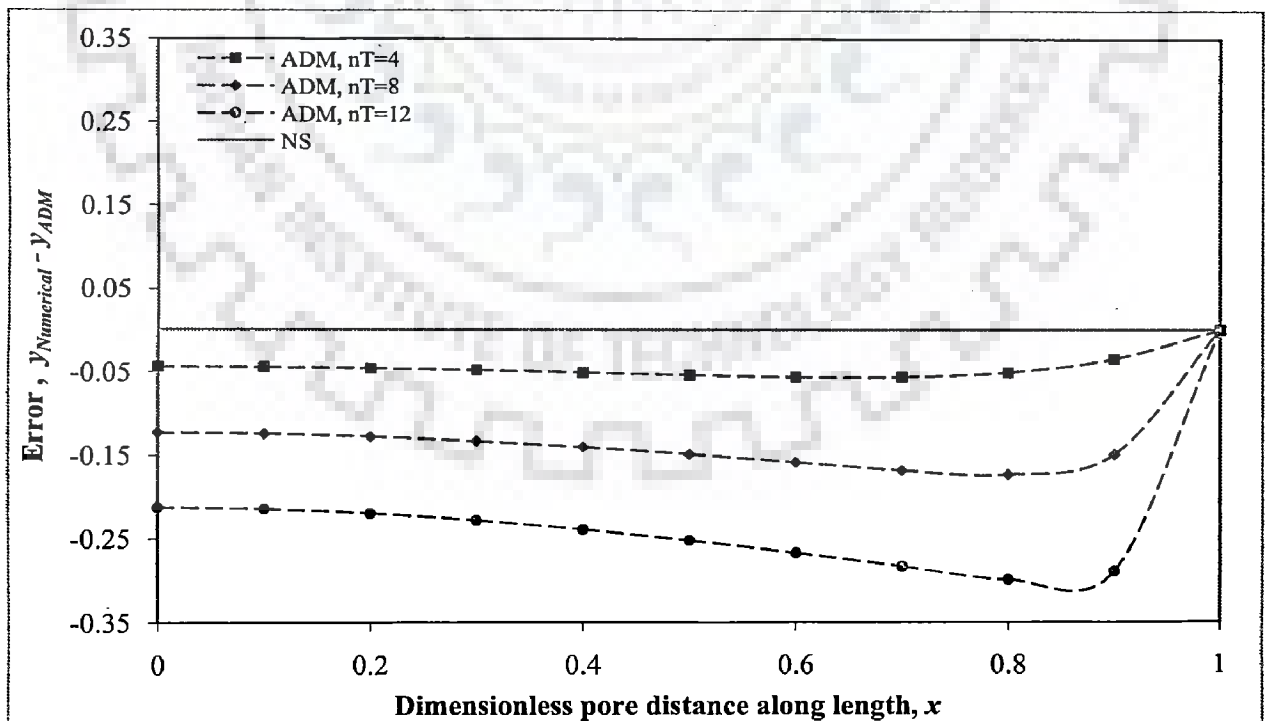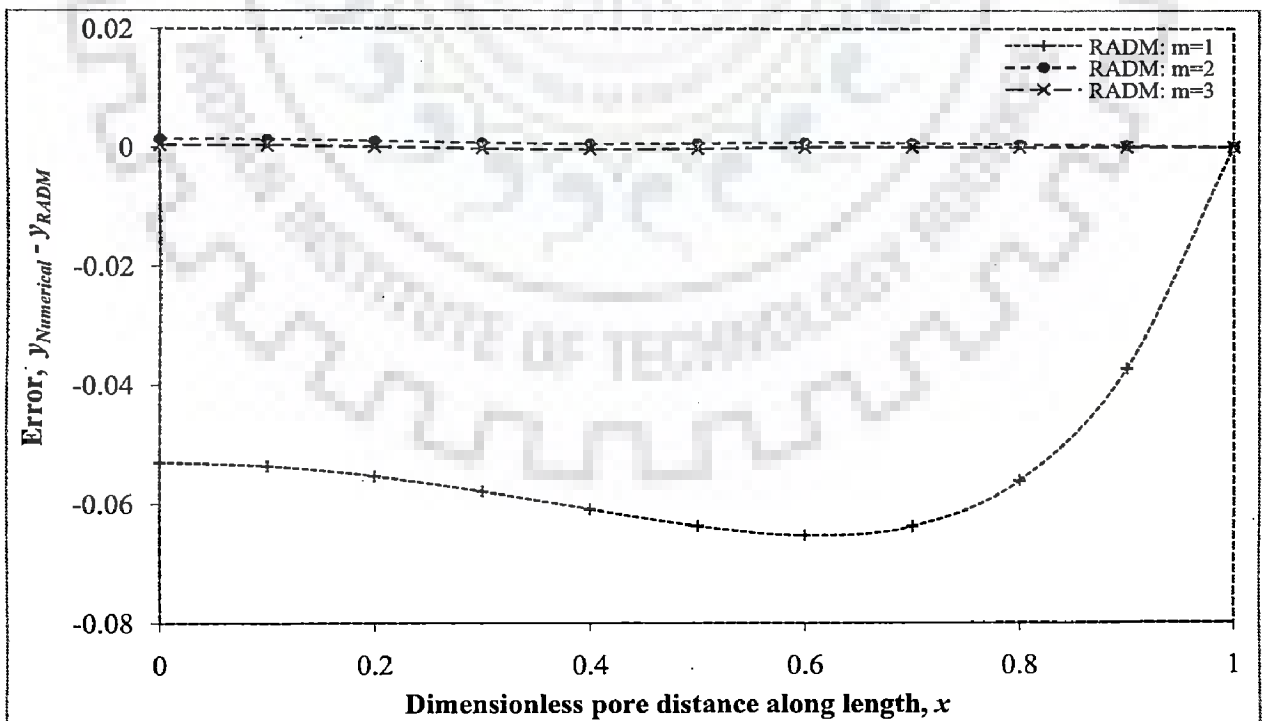

Figure 5.22: Error profiles [power-law kinetics: $n = 0.23$, $\phi = 2.6$; $x = 0$: pore end; $x = 1$: pore mouth]
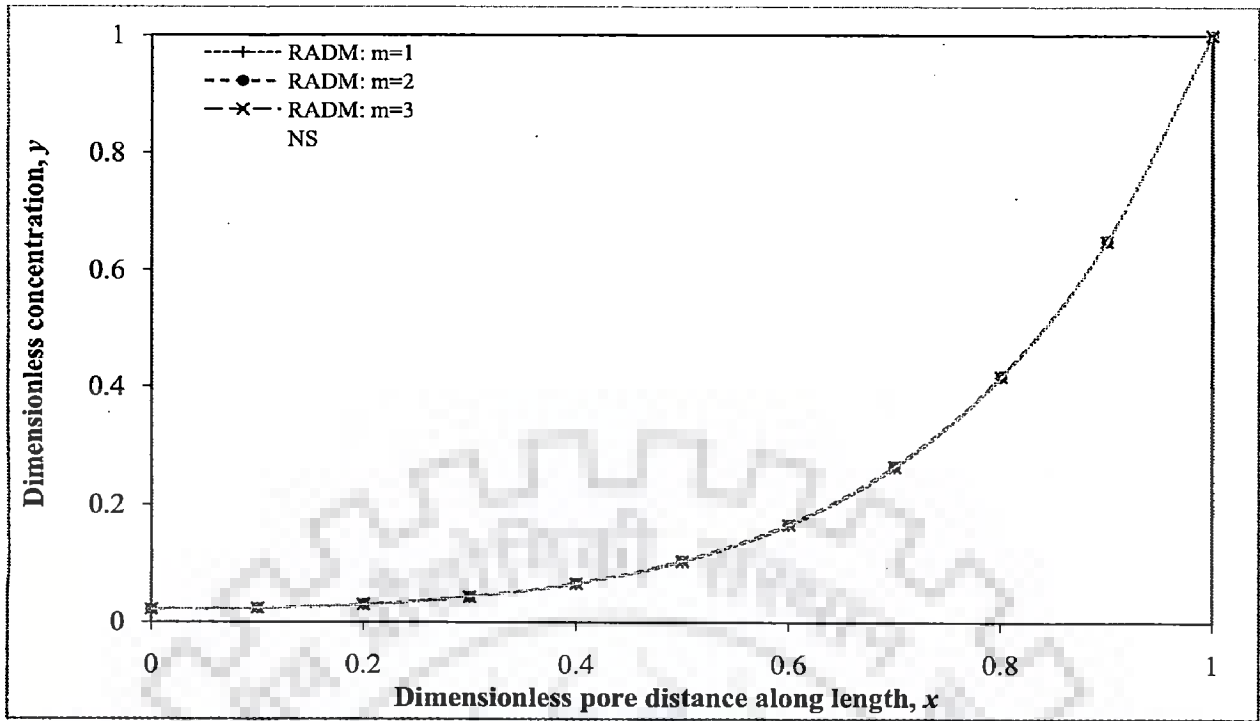
Figure 5.23: Dimensionless concentration profiles [power-law kinetics: $n = 0.78$, $\phi = 5$; $x = 0$: pore end; $x = 1$: pore mouth]
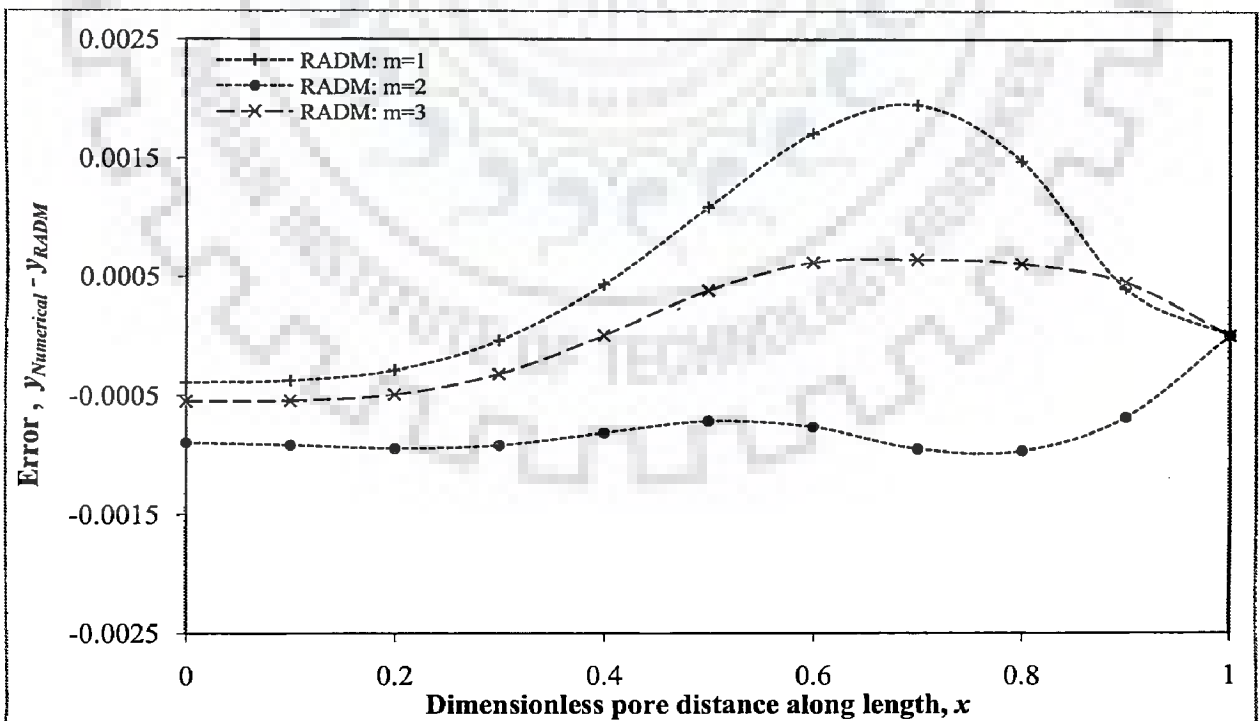
Figure 5.24: Error profiles [power-law kinetics: $n = 0.78$, $\phi = 5$; $x = 0$: pore end; $x = 1$: pore mouth]

restricted range of parameters' values, have been obtained by solving the Beattie-Bridgeman equation of state by using ADM and RADM. Limitations of these methods have also been illustrated and it is observed that the convergence of these two methods depends on several factors, namely canonical form of the equation, number of terms in the solution, and the range of parameters' values. In most of the cases, it is found that RADM outperforms ADM, but in exceptional cases ADM can converge, whilst RADM may diverge. Moreover, increasing the terms in both the methods does not always ensure the convergence. Nevertheless, in case of failure of ADM/RADM, other canonical forms of the equation should be employed.

(ii)   Friction Factor Equation

Approximate solutions of friction factor for the laminar and turbulent flow of Bingham fluids in smooth pipes have been obtained by using ADM and RADM. Reasonably accurate results are obtained by using these solutions. For turbulent flow, the RADM solution [$n_T = 5$, $m = 1$] exhibits a constant error of 0.005%, a smaller value as compared to other available correlations. Similarly for laminar flow, the error in the predictions of RADM solution [$n_T = 2$, $m = 2$] has been found to be within 5.2%. Nonetheless, the accuracy of these solutions can be increased further by taking into account more terms or by increasing the number of iteration in RADM. It is also observed that the number of iterations [m] in RADM has a more pronounced effect on the quality of results as compared to the number of terms [n_T].

(iii)   Reaction-Diffusion Process in a Porous Catalyst Slab

Approximate solutions of the concentration profile and effectiveness factor have been obtained by using ADM and RADM for power-law and Langmuir-Hinshelwood kinetics. It is shown that for reaction order $n < 1$ [$n \neq 0$] and for relatively higher values of Thiele modulus [$\phi \geq 2$], the present ADM solutions and the ADM solutions of Sun et al. (2004) both diverge. It is also shown that the approximate solution of Gottifredi and Gonzo (2005), though accurately predicts effectiveness factor, does not give satisfactory concentration profile especially near the pore end. On the other hand, the RADM

solutions are obtained without generating higher Adomian polynomials, and are in close agreement with the numerically obtained solutions. Moreover, the accuracy of RADM solutions can be increased by increasing the number of terms in the solution and/or by increasing the number of iteration in RADM.

(iv)   Reaction-Diffusion Process in a Porous Spherical Catalyst

Approximate solutions of the concentration profile and effectiveness factor have been obtained by using ADM and RADM for the power-law kinetics. Here also, it is shown that the presently obtained ADM solutions as well as the ADM solutions of Shi-Bin et al. (2003) both fail to give correct results for reaction order $n < 1$ [$n \neq 0$] for relatively higher values of Thiele modulus [$\phi \geq 2$]. However, this constraint can be rectified by using RADM.

NOMENCLATURE

Abbreviations

AS   analytical solution

ADM   Adomian decomposition method

APS   approximate solution

RADM   restarted Adomian decomposition method

NS   numerical solution

Notations

a_i, b_i [-]   constants

A_i [-] i^{th} Adomian polynomial

C_i [-] i^{th} constant of integration

C_A [mol.m^{-3}]   concentration of reactant A in catalyst pores

C_{AS} [mol.m^{-3}]   concentration of reactant A at the pore mouth

C_1, C_2 [-]   constants of integration

D [m]   pipe diameter

D_e [m^2.s^{-1}]   effective diffusivity of reactant inside the pore

f [-]   Fanning friction factor

f_D [-]   Darcy or Moody friction factor $[= 4f]$

$\mathbb{F}[y(x)]$ [-]   differential operators in an ODE [Eq. (5.9)]

$g(x)$ [-]   non-homogeneous term in ODE

He [-]   Hedstrom number $\left(= \dfrac{\tau_0 \rho D^2}{\mu_B{}^2} \right)$

i [-]   index variable

k_n [mol^{1-n}.m^{3n-3}s^{-1}]   rate constant for n^{th} order power-law kinetics

K [-]   dimensionless constant in Langmuir-Hinshelwood kinetics

K_1 [-]   constant term $\left(= \dfrac{16}{Re} + \dfrac{16He}{6Re^2} \right)$

293

K_2	[-]	constant term $\left(= -\dfrac{16He^4}{3Re^8}\right)$
L	[m]	pore length
$L[.]$	[-]	auxiliary linear operator
$L^{-1}[.]$	[-]	inverse operator of $L[.]$
m	[-]	number of iterations in RADM
n_1	[-]	number of OPs used in the approximation of nonlinearity [Eq. (5.71)]
n_2	[-]	number of OPs used in the approximation of ADM solution [Eq. (5.72)]
n_T	[-]	number of terms considered in ADM/RADM
$N(y)$	[-]	linear/nonlinear function of y
P	[atm]	pressure of gas
$P_i(x)$, $P_i(y)$	[-]	i^{th} Shifted-Legendre's polynomial
$-r_A$	[mol.m^{-3}.s^{-1}]	reaction rate of species A
$-r_{AS}$	[mol.m^{-3}.s^{-1}]	reaction rate of species A at the catalyst surface
$-r_y$	[-]	dimensionless reaction rate $\left(= \dfrac{(-r_A)}{(-r_{AS})}\right)$
r	[m]	radial distance
$\mathbb{R}[.]$	[-]	remainder of the linear operator
Re	[-]	Bingham Reynolds number $\left(= \dfrac{\rho \hat{v} D}{\mu_B}\right)$
Re_c	[-]	critical Reynolds number
t	[s]	time
$\hat{v}$	[m.s^{-1}]	average velocity of the fluid
V	[ℓ]	volume of gas
V_{ADM}	[ℓ]	volume of gas obtained by using ADM
V_{RADM}	[ℓ]	volume of gas obtained by using RADM
$V_{Numerical}$	[ℓ]	volume of gas obtained by numerical method
x	[m]	distance along pore length

$y^{(m)}$	[-]	solution of AE obtained after m^{th} iteration of RADM
y_i	[-]	i^{th} term in ADM solution
y_{ADM}	[-]	solution obtained by using ADM
y_{RADM}	[-]	solution obtained by using RADM

Greek letters

α	$[\ell]$	parameter in Beattie-Bridgeman equation of state
β	$[\text{atm. } \ell^2]$	constant in Beattie-Bridgeman equation of state
γ	$[\text{atm. } \ell^3]$	constant in Beattie-Bridgeman equation of state
δ	$[\text{atm. } \ell^4]$	constant in Beattie-Bridgeman equation of state
ε	[m]	pipe absolute roughness
μ_B	$[\text{kg.m}^{-1}.\text{s}^{-1}]$	viscosity of Bingham fluid
ρ	$[\text{kg.m}^{-3}]$	density of Bingham fluid
τ_0	$[\text{kg.m}^{-1}.\text{s}^{-2}]$	yield stress of Bingham fluid
λ	[-]	hypothetical parameter $[\lambda \in [0,1]]$
η	[-]	catalyst effectiveness factor: slab $\left(= \frac{1}{\phi^2} \frac{dy}{dx}\Big\vert_{x=1} \right)$, sphere $\left(= \frac{3}{\phi^2} \frac{dy}{dx}\Big\vert_{x=1} \right)$
ϕ	[-]	Thiele modulus: slab $\left(= \sqrt{\frac{(-r_{AS})L^2}{D_e C_{AS}}} \right)$, sphere $\left(= \sqrt{\frac{(-r_{AS})R^2}{D_e C_{AS}}} \right)$

Section 5.1

Notations

C_0	[-]	constant in canonical form of AE [Eq. (5.3)]
$F_0(y)$	[-]	function in canonical form of AE [Eq. (5.3)]
n	[-]	order of highest linear differential operator $L[.]$
x	[-]	independent variable
$y(x)$	[-]	dependent variable

Section 5.2

Notations

C_0, C_m	[-]	constants in the canonical form of AE at m^{th} iteration of RADM [Eqs. (5.23a)-(5.23c)]
$F_0(y), F_m(y)$	[-]	functions in the canonical form of AE at m^{th} iteration of RADM [Eqs. (5.23b)-(5.23c)]
n	[-]	order of highest linear differential operator $L[.]$
x	[-]	independent variable
$y(x)$	[-]	dependent variable

Section 5.3

Notations

A_0	[atm. ℓ^2]	parameter in Beattie-Bridgeman equation of state
b	[ℓ]	parameter in Beattie-Bridgeman equation of state
B_0	[mol.ℓ]	parameter in Beattie-Bridgeman equation of state
c	[mol.K. ℓ]	parameter in Beattie-Bridgeman equation of state
C_0	[-]	constant in canonical form of AE [Eqs. (5.33), (5.35), (5.37)]
$F_0(y)$	[-]	function in canonical form of AE [Eqs. (5.33), (5.35), (5.37)]
R	[atm.ℓ.K^{-1}.mol^{-1}]	universal gas constant [= 0.08206]
T	[K]	temperature of gas
y	[-]	variable

Section 5.4

Notations

A, B, C	[-]	constants defined in Eqs. (5.42b) and (5.42d)
C_0, C_m	[-]	constants in the canonical form of AE at m^{th} iteration of RADM
$F_0(y), F_m(y)$	[-]	functions in the canonical form of AE at m^{th} iteration of RADM
T	[-]	constant term in Eq. (5.56)

y [-]   variable

Section 5.5

Notations

n	[-]	reaction order
x	[-]	dimensionless distance along pore length $\left(=\dfrac{x'}{L}\right)$
y	[-]	dimensionless concentration $\left(=\dfrac{C_A}{C_{AS}}\right)$

Section 5.6

Notations

n	[-]	reaction order
R	[m]	radius of spherical catalyst
x	[-]	dimensionless distance along pore length $\left(=\dfrac{r}{R}\right)$
y	[-]	dimensionless concentration $\left(=\dfrac{C_A}{C_{AS}}\right)$

REACTION–DIFFUSION PROCESS AND TUBULAR CHEMICAL REACTOR – APPROXIMATE SOLUTIONS BY OHAM

6.0 INTRODUCTION

This chapter demonstrates the development of approximate solutions of the model equations of reaction-diffusion process taking place inside a porous spherical catalyst and a tubular chemical reactor modelled by the axial dispersion model. The model equation of reaction-diffusion process is used in evaluating the concentration profile and effectiveness factor, whereas, the model equation of real tubular reactor is concerned with the concentration profile existing in the reactor. Under steady state these model equations are represented by second order ODEs constituting BVPs.

In the literature, several researchers have solved these model equations by using various numerical/approximate methods, e.g. finite difference method, weighted residual method, perturbation method, ADM. However, to the best of our knowledge, application of some recent approximate methods, e.g. HAM, OHAM, for obtaining the solutions of these equations are unavailable.

For obtaining the approximate solutions of these model equations, a recently developed approximate method, namely OHAM has been employed; OHAM is basically an efficient variant of another approximate method, namely HAM. For evaluating its efficacy, the obtained results have been compared with the numerical results as well as with those obtained by using the available approximate solutions. For the sake of completeness, the descriptions of HAM and OHAM along with their methodologies have been presented in sections 6.1 and 6.2, respectively. In order to demonstrate the procedure of OHAM, two illustrations selected from literature have also been solved in section 6.2.

6.1 HOMOTOPY ANALYSIS METHOD [HAM]

Homotopy analysis method, first developed by Liao in early nineties, is basically a powerful tool for finding the approximate solutions of different types of non-linear equations (Liao, 1997; Liao, 2003). The basic concept of HAM has been derived from topology and its primary aim is to break the original difficult nonlinear equation into a set of infinite linear equations, which can subsequently be solved in an orderly fashion. The solutions of these linear equations are then combined to get the HAM solution [solution obtained by using HAM] in the form of series. The main advantages of HAM are that it can be applied to any type of nonlinearity, and unlike the perturbation method or the δ-decomposition method, it does not require the presence of small or large parameters (Liao, 2003). Moreover, for a certain choice of auxiliary quantities defined later, the working of HAM reduces to those of other approximate methods, e.g. ADM, HPM and δ-decomposition method (Liao, 2003; Allan, 2007). Hence, in some sense, HAM can also be regarded as a generalization of these approximate tools. Besides, computer implementation of HAM in available symbolic soft computing tools, e.g. MATHEMATICA, MAPLE, is also convenient.

A brief description of the HAM is presented below and other details of this method can be found in the original works of Liao (2003, 2009a, 2009b).

6.1.1 Selection of Auxiliary Quantities and Construction of Zero Order Deformation Equation

As suggested by Liao (2003), the first step in HAM is to choose the auxiliary quantities [parameters/functions/operators] corresponding to the given nonlinear equation and to form the related zero order deformation equation. For example, we consider the following operator form of a nonlinear ODE constituting a BVP:

$$N[y(x)] = 0 \quad \text{with} \quad B\left[y(x), \frac{dy(x)}{dx}\right] = 0 \tag{6.1}$$

where $N[.]$ represents the operator form of the nonlinear ODE and $B[.]$ is the associated boundary operator.

Now corresponding to Eq. (6.1), the following homotopy, also called zero order deformation equation, is constructed:

$$(1-\lambda)L[\psi(x,\lambda)-y_0(x)] \;=\; \lambda h H(x) N[\psi(x,\lambda)] \tag{6.2}$$

where $\lambda \in [0,1]$ is a hypothetical embedding parameter and h $[\neq 0]$ is an auxiliary parameter [also called convergence control parameter]. $H(x)$ $[\neq 0]$ is an auxiliary function and is added so as to ensure that in the later operations, the rule of coefficient of ergodicity is not violated. Rule of coefficient of ergodicity requires that the coefficients of all the component functions of the final HAM solution can be modified so as to ensure the completeness of the set of component functions (Liao, 2003). $L[.]$ is an auxiliary linear operator with the conditions that the order of this operator is same as that of the highest order operator in Eq. (6.1) and $L[0]=0$. $y_0(x)$ is the initial guess and in general contains unknown constants. These constants are found by using the associated ICs / BCs. $\psi(x,\lambda)$ is the unknown function.

It can be observed in Eq. (6.2) that as the parameter λ varies from 0 to 1, the unknown function $\psi(x,\lambda)$ varies from the initial guess $y_0(x)$ to the solution $y(x)$ of the original equation, as shown below:

$$\lim_{\lambda \to 0}\psi(x,\lambda) \;\to\; y_0(x) \tag{6.3a}$$

$$\lim_{\lambda \to 1}\psi(x,\lambda) \;\to\; y(x) \tag{6.3b}$$

6.1.2 Formulation of Higher Order Deformation Equation

After selecting the relevant auxiliary quantities and forming the zero order deformation equation, the next step is to construct the higher order deformation equation, which basically represents a family of easily solvable linear equations. For constructing the higher order deformation equation, the unknown function $\psi(x,\lambda)$ is expanded around $\lambda = 0$ by using Taylor series method and the following series is obtained:

$$\psi(x,\lambda) = \psi(x,0) + \sum_{m=1}^{\infty} \frac{1}{m!} \frac{\partial^m \psi(x,\lambda)}{\partial \lambda^m}\bigg|_{\lambda=0} \lambda^m \qquad (6.4a)$$

or

$$\psi(x,\lambda) = y_0(x) + \sum_{m=1}^{\infty} y_m(x)\lambda^m \qquad (6.4b)$$

where $y_m(x)$ $\left(= \frac{1}{m!} \frac{\partial^m \psi(x,\lambda)}{\partial \lambda^m}\bigg|_{\lambda=0} \right)$ is the yet unknown m^{th} term [or the component function] of the HAM solution and can be found as described below. The higher m^{th} order deformation equation [$m \geq 1$] is constructed by substituting Eq. (6.4b) in the zero order deformation equation, i.e. Eq. (6.2), and differentiating the resultant equation m times with respect to λ, and evaluating it at $\lambda = 0$. Thus obtained m^{th} order deformation equation yields m^{th} term of the HAM solution, i.e. $y_m(x)$. By m times differentiating the Eq. (6.2) with respect to λ, and letting $\lambda = 0$, and by also considering the Eq. (6.4b), one obtains the following m^{th} order deformation equation:

$$L[y_m(x) - \chi_m y_{m-1}(x)] = hH(x)R_m[\vec{y}_{m-1}(x), x] \qquad (6.5a)$$

where the vector $\vec{y}_{m-1}(x)$ denotes the following set of component functions:

$$\vec{y}_{m-1}(x) = \{y_0(x), y_1(x), ..., y_{m-1}(x)\} \quad \text{and}$$

$$R_m[\vec{y}_{m-1}(x), x] = \frac{1}{(m-1)!} \frac{\partial^{m-1} N[\vec{y}_{m-1}(x,\lambda)]}{\partial \lambda^{m-1}}\bigg|_{\lambda=0} \qquad (6.5b)$$

$$\text{with } \chi_m = \begin{cases} 0, & m=1 \\ 1, & m \geq 2 \end{cases} \qquad (6.5c)$$

The Eq. (6.5a) can also be written in the form of following recursive relation.

$$y_m(x) = \chi_m y_{m-1}(x) + hL^{-1}[H(x)R_m[\vec{y}_{m-1}(x), x]]; \quad m \geq 1 \qquad (6.6)$$

where $L^{-1}[.]$ denotes the inverse of the linear operator $L[.]$; for example, for a first order derivative operator $[L[.] = \frac{d}{dx}[.]]$, one has $L^{-1}[.] = \int_0^x [.]dx$ and so on. However,

302

care should be taken in choosing the proper definition of $L^{-1}[.]$ as the convergence of HAM solution strongly depends on it (Liao, 2003).

From the above recurrent relation, the following family of linear equations is found for different values of m [$m \geq 1$]:

$$y_1(x) = hL^{-1}[H(x)R_1[y_0(x), x]] \qquad (6.7a)$$

$$y_2(x) = y_1(x) + hL^{-1}[H(x)R_2[y_0(x), y_1(x), x]] \qquad (6.7b)$$

$$y_3(x) = y_2(x) + hL^{-1}[H(x)R_3[y_0(x), y_1(x), y_2(x), x]] \qquad (6.7c)$$

$$\dots$$

$$y_m(x) = y_{m-1}(x) + hL^{-1}[H(x)R_m[y_0(x), y_1(x), \dots, y_{m-1}(x), x]] \qquad (6.7m)$$

... and so on.

6.1.3   Final Solution

Using Eqs. (6.3b), (6.4b) and (6.7a)-(6.7m), the HAM solution for a pre-specified number of terms [say n_T] is obtained in the following form:

$$\psi(x,1) = y(x) \approx y_{HAM}(x) = y_0(x) + \sum_{m=1}^{n_T-1} y_m(x) \qquad (6.8)$$

It has been shown by Liao (2003) that if the auxiliary linear operator, auxiliary parameter, auxiliary function and initial guess are chosen properly then the above HAM solution will converge to one of the solutions of Eq. (6.1). It should also be noted that if one substitutes $H(x) = 1$ and $h = -1$ in Eq. (6.5), and the definitions of $L[.]$, $L^{-1}[.]$ and y_0 are kept same, then the Eq. (6.5) reduces to the one obtained by using ADM.

Normally, $H(x)$, L and $y_0(x)$ are chosen before the HAM is applied, however, the value of h is found only after the HAM solution is available. Therefore, by varying h, the convergence of the so found HAM solution can be monitored. In classical HAM, the value of h is basically selected from the valid region of the so-

called h-curve (Liao, 2003). The h-curve is obtained by plotting the values of the function or its derivatives at known locations [usually at the boundary of the domain of interest] against the different values of h [plots of $y_{HAM}(x)$, $\dfrac{dy_{HAM}(x)}{dx}$ or $\dfrac{d^2 y_{HAM}(x)}{dx^2}$ against h at some x belonging to the region of interest], and the valid region is that part of the h-curve, where these values of the function or its derivatives do not vary with h. However, in most of the situations the valid region for h in the h-curve is flat, and thus, many values of h exist which may be selected. Consequently, an uncertainty arises in choosing the correct value of h. To avoid this ambiguity in the selection of h, we have adopted an effective variant of HAM, namely OHAM (Liao, 2010). The main steps of OHAM are described in the following section.

6.2   OPTIMAL HOMOTOPY ANALYSIS METHOD [OHAM]

The key steps involved in OHAM (Liao, 2010) are the same as those in HAM, however, OHAM differs with HAM in the selection of h. In OHAM, h is found by minimizing the sum of square of residual errors of the resultant HAM solution. The residual error is found by substituting the HAM solution in the original Eq. (6.1), as given below:

Residual error at $x = N\big[y_{HAM}(x,h)\big]$

And, the sum of square of residual errors can be found by the following formula:

$$\Re = \int_0^1 \big(N[y_{HAM}(x,h)]\big)^2 dx$$

$$= \int_0^1 \left(N\left[\sum_{m=0}^{n_T-1} y_m(x,h)\right]\right)^2 dx \tag{6.9a}$$

Since, the analytical integration of the above series may be quite cumbersome, hence the following simple but efficient approximation of Eq. (6.9a) has been employed:

$$\Re \approx \sum_{i=1}^{M} \big(N[y_{HAM}(x_i,h)]\big)^2 \Delta x$$

304

$$= \sum_{i=1}^{M} \left(N\left[\sum_{m=0}^{n_T-1} y_m(x_i,h) \right] \right)^2 \Delta x \tag{6.9b}$$

where Δx represents the equispaced interval in the concerned region. Now, for the minimum value of $\mathfrak{R}$, $\dfrac{\partial \mathfrak{R}}{\partial h} = 0$, and one obtains the following equation:

$$\frac{\partial \mathfrak{R}}{\partial h} \approx \frac{\partial}{\partial h} \sum_{i=1}^{M} \left(N\left[\sum_{m=0}^{n_T-1} y_m(x_i,h) \right] \right)^2 \Delta x$$

$$= \frac{\partial}{\partial h} \sum_{i=1}^{M} \left(N\left[\sum_{m=0}^{n_T-1} y_m(x_i,h) \right] \right)^2 = 0 \tag{6.9c}$$

Eq. (6.9c) is basically an algebraic equation in h and by solving it, one obtains the optimum value of h. By substituting this value of h in Eq. (6.8), the final approximate OHAM solution can be constructed, as shown below:

$$y_{OHAM}(x) = y_0(x) + \sum_{m=1}^{n_T-1} y_m(x,h) \Bigg|_{h\,optimum} \tag{6.10}$$

6.2.1 Stepwise Procedure of OHAM

The algorithm of OHAM is depicted in Fig. 6.1 and the steps involved are summarized below:

(i) For a given nonlinear equation, the auxiliary quantities and the initial guess $[H(x), L[.]$ and $y_0(x)]$ are selected and the corresponding zero order deformation equation, i.e. Eq. (6.2), is constructed.

(ii) From the zero order deformation equation, higher order deformation equation, i.e. Eq. (6.6), is formed.

(iii) Using higher order deformation equation, the higher terms of the HAM solution $[y_m(x), 1 \le m \le n_T - 1]$ are found iteratively.

(iv)   After finding $y_m(x)$, $y_{HAM}(x)$ is found by summing all the terms as shown in Eq. (6.8).

$$y_{HAM}(x) = y_0(x) + \sum_{m=1}^{n_T-1} y_m(x)$$

(v)   One should note that constants of integration $[C_i\,\text{s}]$ and the convergence control parameter $[h]$ are still unknown in $y_{HAM}(x)$. The unknown constants of integration are found from the associated conditions, whereas, the optimum value of h is found by minimizing the sum of square of residual errors. The substitution of these quantities back in the HAM solution gives the OHAM solution, i.e.

$$y_{OHAM}(x) = y_{HAM}(x,h)\big|_{h\,optimum}$$

To increase the accuracy, one can increase the terms in OHAM solution, otherwise, one may restart with step (i), i.e. by making a different choices of the auxiliary quantities. Liao (2003) has solved several examples by using HAM and presents some guidelines for the proper selection of these auxiliary quantities. Use of OHAM has been made clear by solving the following two illustrations.

6.2.2   Illustrations

In this subsection, two ODEs have been solved by using OHAM. These two ODEs constitute singular BVPs and appear in various engineering applications. In literature, these two equations have recently been solved by Kumar and Singh (2010) by using a modified version of ADM, namely modified Adomian decomposition method [MADM]. MADM is basically similar to the ADM, however, these researchers have incorporated the usual operator proposed by Wazwaz (2005).

6.2.2.1 Illustration 6.1: Linear Singular BVP

The following linear second order ODE constituting a singular BVP has been taken from Kanth and Aruna (2008) and Kumar and Singh (2010).
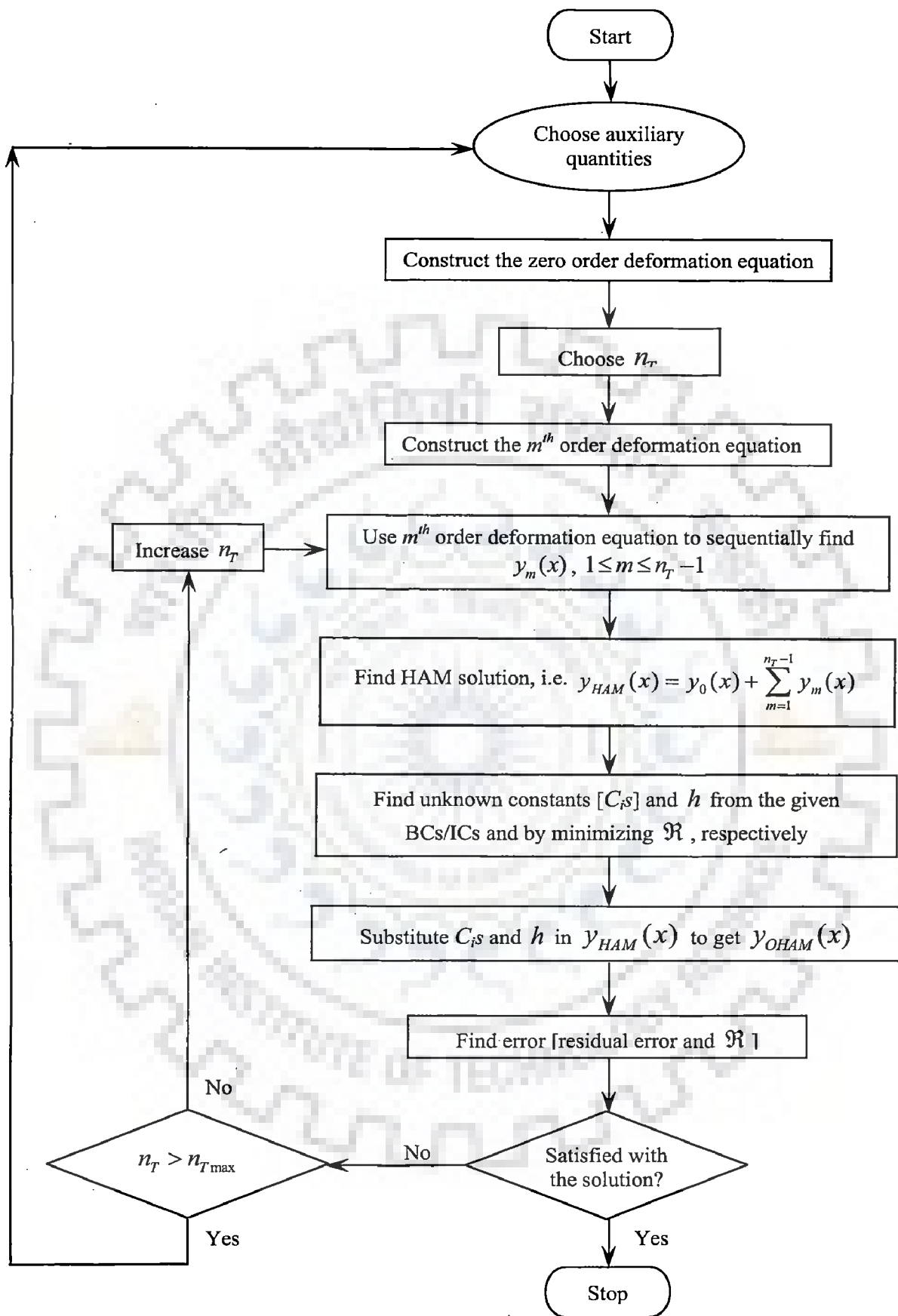
Figure 6.1: **Flow chart of OHAM**

$$\frac{d^2y}{dx^2} + \frac{1}{x}\frac{dy}{dx} + y = 4 - 9x + x^2 - x^3 \tag{6.11a}$$

BC I: $y = 0$ \qquad at $x = 1$ \hfill (6.11b)

BC II: $y = 0$ \qquad at $x = 0$ \hfill (6.11c)

For obtaining the OHAM solution of Eqs. (6.11a)-(6.11c), first the following auxiliary quantities are chosen:

$$N[y] = \frac{d^2y}{dx^2} + \frac{1}{x}\frac{dy}{dx} + y - 4 + 9x - x^2 + x^3, \; L[.] = \frac{1}{x}\frac{d}{dx}\left(x\frac{d[.]}{dx}\right) \text{ or}$$

$$L^{-1}[.] = \int_0^x \frac{1}{x}\int x\,[.]\,dx\,dx, \; H(x) = 1, \; y_0(x) = C_2$$

Thereafter, by using the above auxiliary quantities and with the help of the procedure given in subsection 6.1.1, the following zero order deformation equation, corresponding to Eq. (6.11a), is constructed:

$$(1-\lambda)L[\psi(x,\lambda) - y_0(x)] = \lambda h H(x)N[\psi(x,\lambda)] \tag{6.12a}$$

Similarly, as per the description given in subsection 6.1.2, the following m^{th} order deformation equation is obtained from Eq. (6.12a).

$$L[y_m(x) - \chi_m y_{m-1}(x)] = h H(x) R_m[\vec{y}_{m-1}(x), x] \tag{6.12b}$$

From Eq. (6.12b), the following recursive relation can be obtained for finding $y_m s$:

$$y_m(x) = \chi_m y_{m-1}(x) + h\int_0^x \frac{1}{x}\int x\left(R_m[\vec{y}_{m-1}, x] - (1-\chi_m)(4 - 9x + x^2 - x^3)\right)dx\,dx \tag{6.12c}$$

Now, with the aid of the auxiliary quantities and by iteratively using Eq. (6.12c), the following expressions for $y_m s$ are obtained. It should, however, be noted that if one substitutes $h = -1$ in Eq. (6.12c), then this equation yields the same iterative steps as were deduced by Kumar and Singh (2010) by using MADM. However, we have observed that for this value of h, the sum of square of residual error is not minimum for the obtained solution.

$$y_0(x) = C_2$$

$$y_1(x) = \left(-1 + \frac{C_2}{4}\right)hx^2 + hx^3 - \frac{hx^4}{16} + \frac{hx^5}{25}$$

$$y_2(x) = \frac{1}{4}(-4h + C_2h - 4h^2 + C_2h^2)x^2 + (h + h^2)x^3 + \frac{1}{64}(-4h - 8h^2 + C_2h^2)x^4$$

$$+ \frac{1}{25}(h + 2h^2)x^5 - \frac{1}{576}h^2x^6 + \frac{1}{1225}h^2x^7$$

$$y_3(x) = \frac{1}{4}(-4h + C_2h - 8h^2 + 2C_2h^2 - 4h^3 + C_2h^3)x^2 + (h + 2h^2 + h^3)x^3$$

$$+ \frac{1}{32}(-2h - 8h^2 + C_2h^2 - 6h^3 + C_2h^3)x^4 + \frac{1}{25}(h + 4h^2 + 3h^3)x^5$$

$$+ \frac{1}{2304}(-8h^2 - 12h^3 + C_2h^3)x^6 + \frac{1}{1225}(2h^2 + 3h^3)x^7 - \frac{1}{36864}h^3x^8 + \frac{1}{99225}h^3x^9$$

$$y_4(x) = \frac{1}{4}(-4h + C_2h - 12h^2 + 3C_2h^2 - 12h^3 + 3C_2h^3 - 4h^4 + C_2h^4)x^2$$

$$+ (h + 3h^2 + 3h^3 + h^4)x^3 + \frac{1}{64}(-4h - 24h^2 + 3C_2h^2 - 36h^3 + 6C_2h^3 - 16h^4 + 3C_2h^4)x^4$$

$$+ \frac{1}{25}(h + 6h^2 + 9h^3 + 4h^4)x^5 + \frac{1}{768}(-4h^2 - 12h^3 + C_2h^3 - 8h^4 + C_2h^4)x^6$$

$$+ \frac{3}{1225}(h^2 + 3h^3 + 2h^4)x^7 + \frac{1}{147456}(-12h^3 - 16h^4 + C_2h^4)x^8$$

$$+ \frac{1}{99225}(3h^3 + 4h^4)x^9 - \frac{1}{3686400}h^4x^{10} + \frac{1}{12006225}h^4x^{11}$$

$$y_5(x) = \frac{1}{4}(-4h + C_2h - 16h^2 + 4C_2h^2 - 24h^3 + 6C_2h^3 - 16h^4 + 4C_2h^4 - 4h^5 + C_2h^5)x^2$$

$$+ (h + 4h^2 + 6h^3 + 4h^4 + h^5)x^3$$

$$+\frac{1}{16}(-h-8h^2+C_2h^2-18h^3+3C_2h^3-16h^4+3C_2h^4-5h^5+C_2h^5)x^4$$

$$+\frac{1}{25}(h+8h^2+18h^3+16h^4+5h^5)x^5$$

$$+\frac{1}{1152}(-8h^2-36h^3+3C_2h^3-48h^4+6C_2h^4-20h^5+3C_2h^5)x^6$$

$$+\frac{2}{1225}(2h^2+9h^3+12h^4+5h^5)x^7$$

$$+\frac{1}{36864}(-6h^3-16h^4+C_2h^4-10h^5+C_2h^5)x^8$$

$$+\frac{2}{99225}(3h^3+8h^4+5h^5)x^9+\frac{1}{14745600}(-16h^4-20h^5+C_2h^5)x^{10}$$

$$+\frac{1}{12006225}(4h^4+5h^5)x^{11}-\frac{1}{530841600}h^5x^{12}+\frac{1}{20290520025}h^5x^{13}$$

Finally, the following six terms [$n_T=6$] OHAM solution is found.

$$y_{OHAM}=\sum_{i=0}^{5}y_i(x)$$

$$=C_2+$$

$$\frac{1}{4}\left(-20h+5C_2h-40h^2+10C_2h^2-40h^3+10C_2h^3-20h^4+5C_2h^4-4h^5+C_2h^5\right)x^2$$

$$+\left(5h+10h^2+10h^3+5h^4+h^5\right)x^3$$

$$+\frac{1}{64}\left(-20h-80h^2+10C_2h^2-120h^3+20C_2h^3-80h^4+15C_2h^4-20h^5+4C_2h^5\right)x^4$$

$$+\frac{1}{5}\left(h+4h^2+6h^3+4h^4+h^5\right)x^5$$

$$+\frac{1}{2304}\left(-40h^2-120h^3+10C_2h^3-120h^4+15C_2h^4-40h^5+6C_2h^5\right)x^6$$

$$+\frac{2}{245}\left(h^2+3h^3+3h^4+h^5\right)x^7+\frac{1}{147456}\left(-40h^3-80h^4+5C_2h^4-40h^5+4C_2h^5\right)x^8$$

$$+\frac{2}{19845}\left(3h^3+2h^4+h^5\right)x^9+\frac{1}{14745600}\left(-20h^4-20h^5+C_2h^5\right)x^{10}$$

$$+\frac{1}{2401245}\left(h^4+h^5\right)x^{11}-\frac{1}{530841600}h^5x^{12}+\frac{1}{2029052025}h^5x^{13} \qquad (6.13)$$

C_2 is found from the associated BC I, whereas, h is found by minimizing $\mathfrak{R}$ [Eq. (6.9c)]. It can be noticed that for this choice of initial guess y_0 and auxiliary quantities, the BC II is satisfied automatically. For $n_T=6$, the values of C_2 and h as obtained by OHAM are given below, which correspond to the minimum value of $\mathfrak{R}$.

$$C_2=2.139446\times10^{-10} \text{ and } h=-0.996758$$

Corresponding to the above values of C_2 and h, the six terms OHAM solution [Eq. (6.13)] is given below:

$$y_{OHAM} = 2.13945\times10^{-10} + x^2 - x^3 + 3.7759\times10^{-11} x^4 - 2.20264\times10^{-11} x^5$$

$$-5.87919\times10^{-10} x^6 + 2.76398\times10^{-10} x^7 + 2.82376\times10^{-9} x^8 - 1.04908\times10^{-9} x^9$$

$$-4.34067\times10^{-9} x^{10} +1.33276\times10^{-9} x^{11} +1.85346\times10^{-9} x^{12}$$

$$-4.84903\times10^{-10} x^{13} \qquad (6.14)$$

It is quite interesting to note that for $h=-1$ and $C_2=0$, the Eq. (6.13) reduces to the same expression as was found by Kumar and Singh (2010) by using MADM. The MADM solution [$n_T=6$] is given below:

$$y_{OHAM}(C_2=0,h=-1) = x^2 - x^3 + \frac{x^{12}}{530841600} - \frac{x^{13}}{2029052025} = y_{MADM} \qquad (6.15)$$

For the purpose of comparison, Kumar and Singh (2010) have also given the analytical solution of Eqs. (6.11a)-(6.11c), and we below reproduce the same analytical solution:

$$y_{Analytical} = x^2 - x^3 \tag{6.16}$$

For several values of n_T [= 6, 7, 8], the OHAM results are presented in Fig. 6.2 and Table 6.1 along with the MADM results [$n_T = 6$] as well as the results obtained by using the analytical solution. It can be seen from Fig. 6.2 and Table 6.1 that the results obtained by using above six terms OHAM solution, i.e. Eq. (6.14), agree well with those obtained from the six terms MADM solution, i.e. Eq. (6.15). Besides, these results are also quite close to those obtained from analytical solution, i.e. Eq. (6.16).

Fig. 6.3 shows the absolute error profiles of the OHAM and MADM solutions [$\left| y_{Analytical} - y_{OHAM} \right|$ and $\left| y_{Analytical} - y_{MADM} \right|$] on a Log_{10} scale. From this figure, it is clear that the error in MADM solution increases monotonically as one moves from $x = 0$ to $x = 1$, whereas, for OHAM solution it almost remains constant in most of the region and decreases sharply near $x = 1$. Besides, by increasing the number of terms in OHAM solution the error can be reduced. Hence, for a pre-specified maximum permissible error in the solution, one can choose the number of terms in OHAM solution.

Fig. 6.4 shows the residual error profiles of the OHAM solutions [$n_T = 6, 7, 8$], and the MADM solution [$n_T = 6$], and also indicates their respective sum of square of residual errors. It can be seen that the residual error and the sum of square of residual errors of OHAM solution are less than those of MADM solution for the same number of terms [$n_T = 6$]. As expected, the residual error profiles of the OHAM solutions approach to zero as the number of terms are increased.

6.2.2.2 Illustration 6.2: Nonlinear Singular BVP

The second equation considered by Kumar and Singh (2010) relates to the thermal explosion, and is as follows:

$$\frac{d^2y}{dx^2} + \frac{1}{x}\frac{dy}{dx} + ve^y = 0 \tag{6.17a}$$

BC I: $y = 0$ at $x = 1$ $\tag{6.17b}$

313

Table 6.1: Results of illustration 6.1 obtained by using analytical, MADM and OHAM solutions [linear singular BVP]

x	Analytical solution (Kumar and Singh, 2010)	Solution				Absolute Error			
		OHAM			MADM $[n_T=6]$ Kumar and Singh, (2010)	OHAM			MADM $[n_T=6]$ Kumar and Singh, (2010)
		$n_T=6$ $C_2=2.14E\text{-}10$ $h=-0.996758$	$n_T=7$ $C_2=-6.95E\text{-}13$ $h=-0.997953$	$n_T=8$ $C_2=1.79E\text{-}15$ $h=-0.998597$		$n_T=6$	$n_T=7$	$n_T=8$	
0	0.000000	0.000000	0.000000	0.000000	-	2.14E-10	6.95E-13	1.79E-15	-
0.1	0.009000	0.009000	0.009000	0.009000	0.009000	2.13E-10	6.93E-13	1.79E-15	1.8E-21
0.2	0.032000	0.032000	0.032000	0.032000	0.032000	2.12E-10	6.88E-13	1.79E-15	7.3E-18
0.3	0.063000	0.063000	0.063000	0.063000	0.063000	2.09E-10	6.79E-13	1.78E-15	9.2E-16
0.4	0.096000	0.096000	0.096000	0.096000	0.096000	2.05E-10	6.67E-13	1.76E-15	2.8E-14
0.5	0.125000	0.125000	0.125000	0.125000	0.125000	2.01E-10	6.52E-13	1.74E-15	3.9E-13
0.6	0.144000	0.144000	0.144000	0.144000	0.144000	1.97E-10	6.35E-13	1.70E-15	3.4E-12
0.7	0.147000	0.147000	0.147000	0.147000	0.147000	1.92E-10	6.19E-13	1.67E-15	2.1E-11
0.8	0.128000	0.128000	0.128000	0.128000	0.128000	1.74E-10	5.81E-13	1.61E-15	1.0E-10
0.9	0.081000	0.081000	0.081000	0.081000	0.081000	1.16E-10	4.20E-13	1.27E-15	4.1E-10
1	0.000000	0.000000	0.000000	0.000000	0.000000	3.33E-16	5.59E-17	8.99E-17	1.4E-09
$\Re$		6×10^{-18}	1×10^{-22}	1×10^{-27}	2×10^{-15}		-		-

Figure 6.2: Solutions of illustration 6.1 [linear singular BVP]

Figure 6.3: Absolute error profiles on Log_{10} scale for the solutions of illustration 6.1 [linear singular BVP]

Figure 6.4: Residual error profiles for the solutions of illustration 6.1 [linear singular BVP]

BC II: $y' = 0$ at $x = 0$ (6.17c)

Relevant auxiliary quantities are: $N[y] = \dfrac{d^2y}{dx^2} + \dfrac{1}{x}\dfrac{dy}{dx} + ve^y$, $L[.] = \dfrac{1}{x}\dfrac{d}{dx}\left(x\dfrac{d[.]}{dx}\right)$ or

$L^{-1}[.] = \displaystyle\int_0^x \dfrac{1}{x}\int x\,[.]\,dx\,dx$, $H(x) = 1$ and $y_0(x) = C_2$.

The corresponding zero and m^{th} order deformation equations are given by:

$$(1-\lambda)L[\psi(x,\lambda) - y_0(x)] = \lambda h H(x) N[\psi(x,\lambda)] \tag{6.18a}$$

$$L[y_m(x) - \chi_m y_{m-1}(x)] = h H(x) R_m[\vec{y}_{m-1}(x), x]; \quad m \geq 1 \tag{6.18b}$$

A slight rearrangement of Eq. (6.18b), along with the use of inverse operator L^{-1}, yields the following recursive relation:

$$y_m(x) = \chi_m y_{m-1}(x) + h\int_0^x \dfrac{1}{x}\int x R_m[\vec{y}_{m-1}, x]\,dx\,dx \tag{6.18c}$$

Using the above auxiliary quantities, the Eq. (6.18c) is evaluated iteratively, and the following expressions for $y_i s$ are obtained:

$$y_0(x) = C_2$$

$$y_1(x) = \dfrac{1}{4}e^{C_2}vhx^2$$

$$y_2(x) = \dfrac{1}{4}e^{C_2}(h + h^2)vx^2 + \dfrac{1}{64}e^{2C_2}h^2v^2x^4$$

$$y_3(x) = \dfrac{1}{4}e^{C_2}h(1+h)^2vx^2 + \dfrac{1}{32}e^{2C_2}h^2(1+h)v^2x^4 + \dfrac{1}{768}e^{3C_2}h^3v^3x^6$$

And the four terms $[n_T = 4]$ OHAM solution is given by:

$$y_{OHAM} = \sum_{i=0}^3 y_i(x)$$

$$= C_2 + \dfrac{3}{4}ve^{C_2}hx^2 + \dfrac{3}{4}ve^{C_2}h^2x^2 + \dfrac{1}{4}ve^{C_2}h^3x^2 + \dfrac{3}{64}v^2e^{2C_2}h^2x^4 + \dfrac{1}{32}v^2e^{2C_2}h^3x^4$$

$$+\frac{1}{768}v^3 e^{3C_2}h^3 x^6 \qquad (6.19)$$

For $v=1$ the unknown C_2 and h are found by using BC I [Eq. (6.17b)] and by minimizing $\Re$ [Eq. (6.9c)], respectively, and are given as: $C_2 = 0.316503$ and $h = -0.875052$. It should be noted that the BC II [Eq. (6.17c)] is satisfied automatically. Now the four terms OHAM solution can be found by substituting these values of C_2 and h in Eq. (6.19), and is given by:

$$y_{OHAM} = 0.316503 - 0.342411\, x^2 + 0.0281626\, x^4 - 0.0022548\, x^6 \qquad (6.20)$$

It can again be verified that by substituting $C_2 = a$ (Kumar and Singh, 2010) and $h = -1$, one obtains the following expression, which is identical to the one obtained by Kumar and Singh (2010) by using MADM:

$$y_{OHAM}(C_2 = a, h = -1) = a - \frac{1}{4}ve^a x^2 + \frac{1}{64}v^2 e^{2a}x^4 - \frac{1}{768}v^3 e^{3a}x^6 = y_{MADM} \qquad (6.21)$$

The values of a and v given by Kumar and Singh (2010) are: $a = 0.317234$ and $v = 1$. For the purpose of comparison. Kumar and Singh (2010) have also given the following analytical solution of this equation:

$$y_{Analytical} = 2Log\left[\frac{1 + \frac{1}{2}\left(8 - 2v - \sqrt{(8-2v)^2 - 4v^2}\right)}{1 + \frac{1}{2}\left(8 - 2v - \sqrt{(8-2v)^2 - 4v^2}\right)x^2}\right] \qquad (6.22)$$

The results obtained by using the above solutions have been shown in Figs. 6.5 - 6.7 and Table 6.2. Fig. 6.5 and Table 6.2 compare the results obtained by using the OHAM solutions [$n_T = 4$, 5, 6] with those obtained from the MADM solution [$n_T = 4$] and the analytical solution [Eq. (6.22)]. It is clear from Fig. 6.5 and Table 6.2 that a close agreement exists between the results obtained by using these three solutions.

The absolute error profiles, depicted in Fig. 6.6, shows that the OHAM solution exhibits lesser error in comparison to the MADM solution for the same number of terms. Moreover, the residual error profiles of these two solutions and their respective sum of square of residual error, shown in Fig. 6.7, are also smaller for the OHAM
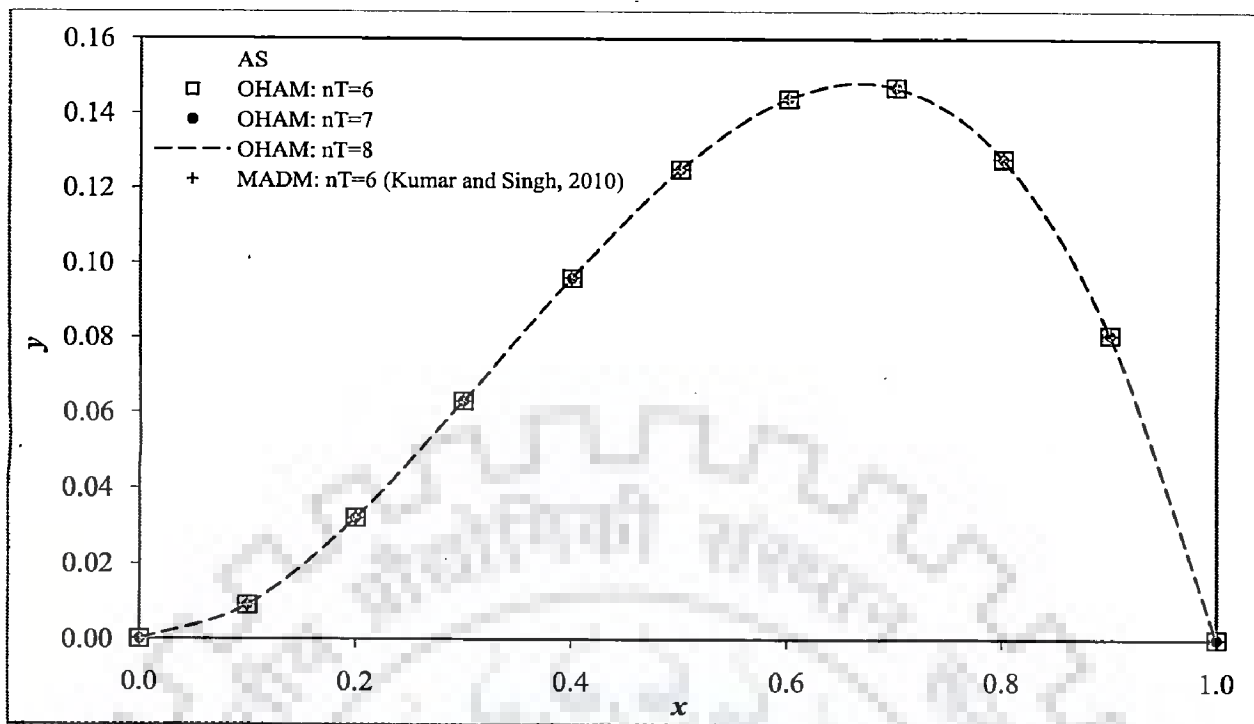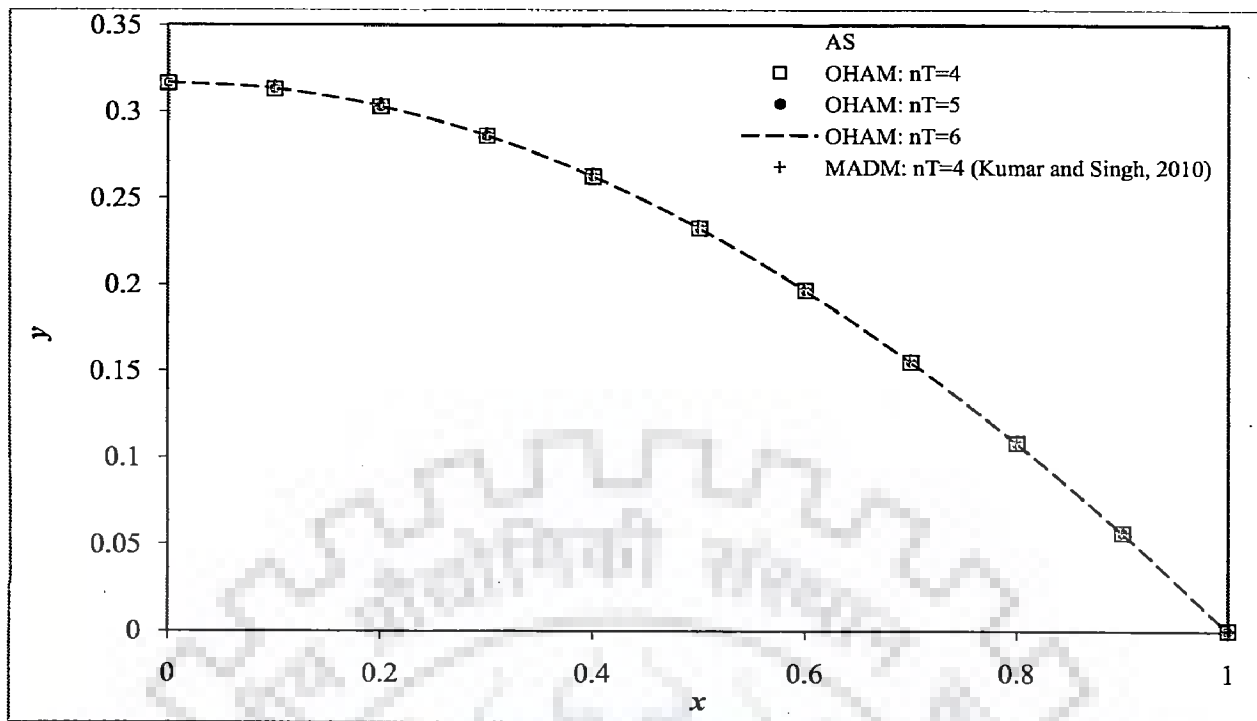
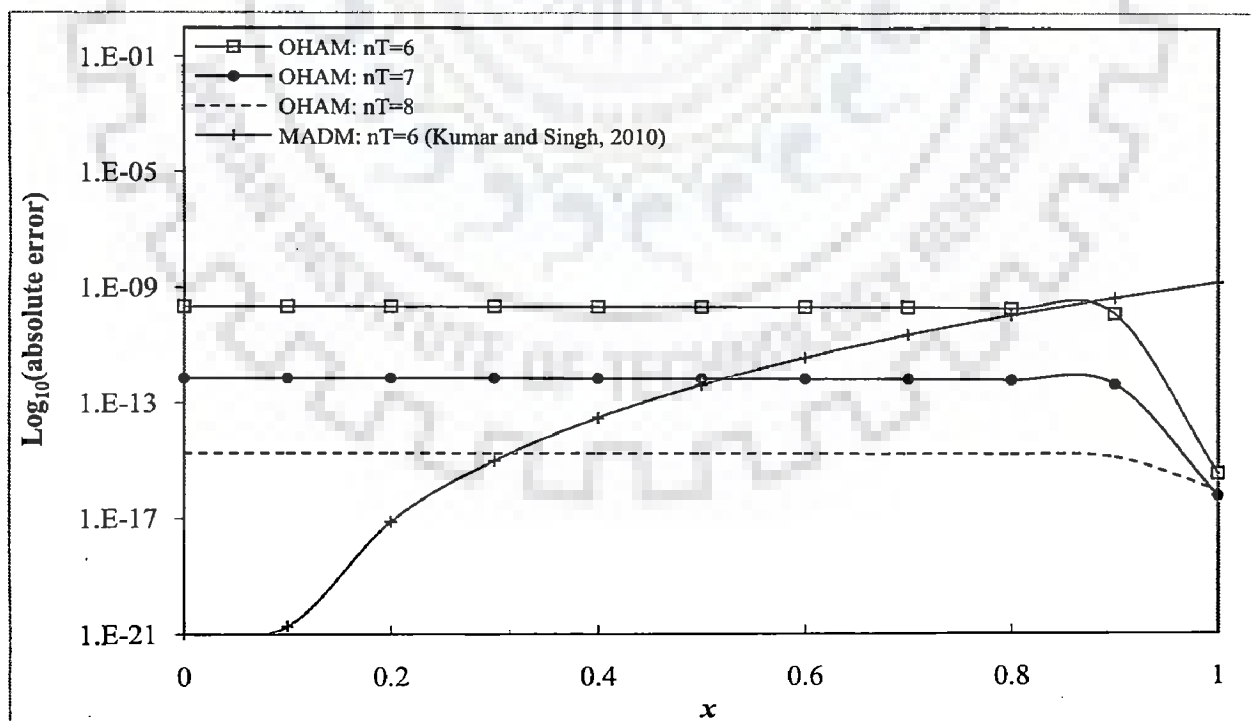**Figure 6.5:** Solutions of illustration 6.2 [nonlinear singular BVP]
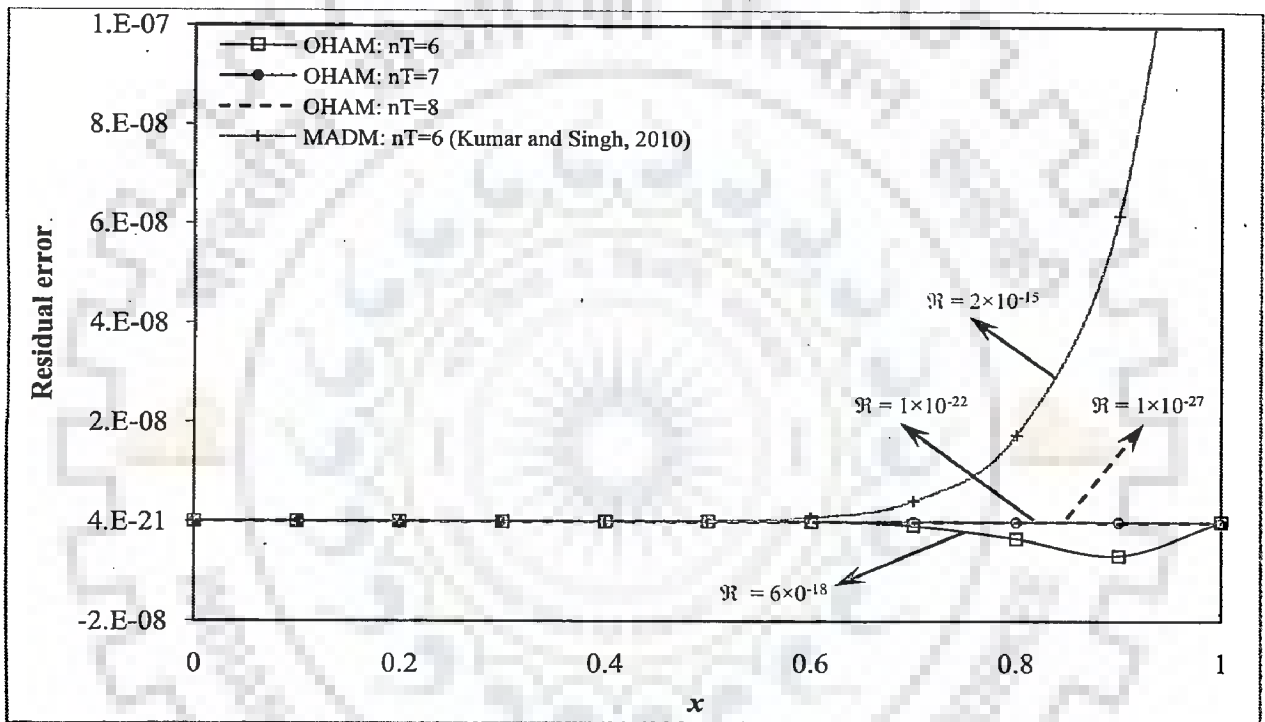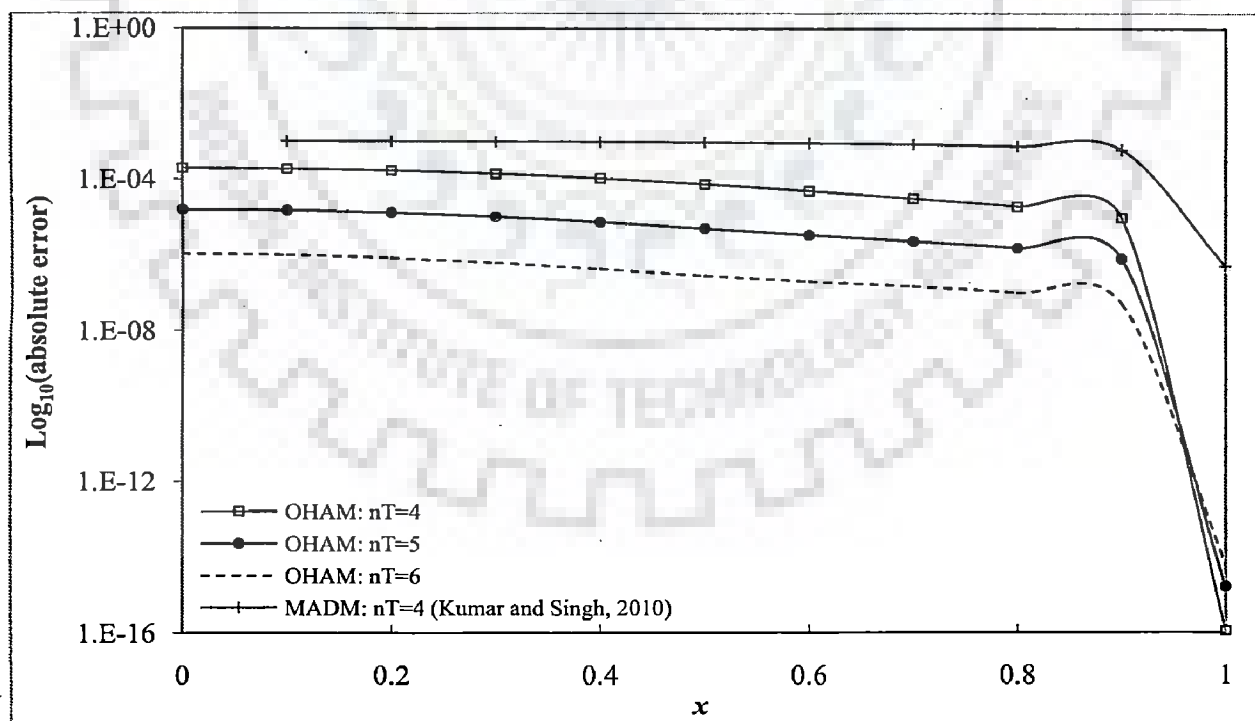

Figure 6.6: Absolute error profiles on Log_{10} scale for the solutions of illustration 6.2 [nonlinear singular BVP]

321
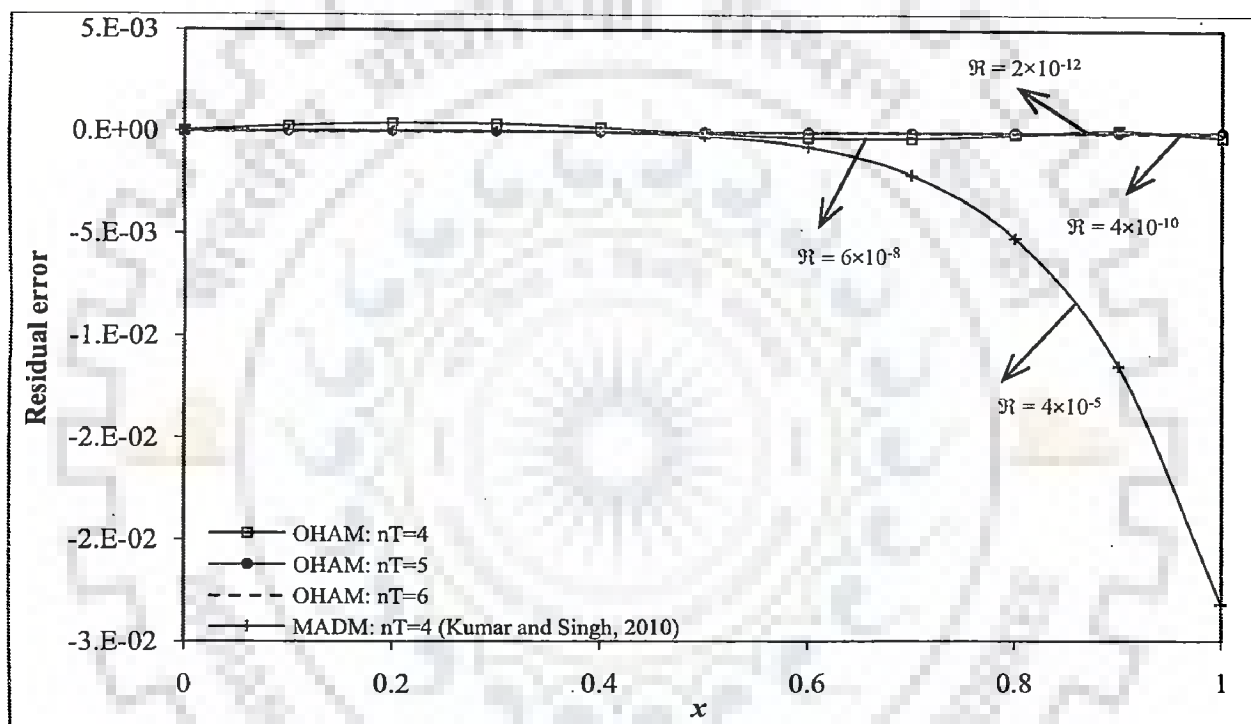
Figure 6.7: **Residual error profiles for the solutions of illustration 6.2 [nonlinear singular BVP]**

Table 6.2: Results of illustration 6.2 obtained by using analytical, MADM and OHAM solutions [nonlinear singular BVP]

x	Analytical solution (Kumar and Singh, 2010)	Solution				Absolute Error			
		OHAM			MADM [$n_T=4$] (Kumar and Singh, 2010)	OHAM			MADM [$n_T=4$] (Kumar and Singh, 2010)
		$n_T=4$ $C_2=0.316503$ $h=-0.875052$	$n_T=5$ $C_2=0.316679$ $h=-0.880623$	$n_T=6$ $C_2=0.316693$ $h=-0.887595$		$n_T=4$	$n_T=5$	$n_T=6$	
0.0	0.316694	0.316503	0.316679	0.316693	-	1.913E-04	1.525E-05	1.051E-06	-
0.1	0.313266	0.313082	0.313251	0.313265	0.314246	1.841E-04	1.452E-05	9.875E-07	9.80E-04
0.2	0.303015	0.302852	0.303003	0.303015	0.303986	1.639E-04	1.253E-05	8.218E-07	9.71E-04
0.3	0.286047	0.285913	0.286037	0.286047	0.287001	1.347E-04	9.827E-06	6.111E-07	9.54E-04
0.4	0.262531	0.262429	0.262524	0.262531	0.263462	1.021E-04	7.063E-06	4.182E-07	9.31E-04
0.5	0.232697	0.232625	0.232692	0.232697	0.233598	7.150E-05	4.779E-06	2.801E-07	9.01E-04
0.6	0.196827	0.196780	0.196824	0.196827	0.197689	4.698E-05	3.195E-06	1.970E-07	8.62E-04
0.7	0.155248	0.155218	0.155246	0.155248	0.156056	2.980E-05	2.194E-06	1.445E-07	8.08E-04
0.8	0.108323	0.108304	0.108321	0.108323	0.109045	1.833E-05	1.464E-06	9.852E-08	7.22E-04
0.9	0.056439	0.056429	0.056438	0.056439	0.057015	9.150E-06	7.577E-07	5.004E-08	5.76E-04
1.0	0.000000	0.000000	0.000000	0.000000	0.000000	0.000E+00	0.000E+00	0.000E+00	4.78E-07
$\Re$		6×10^{-8}	4×10^{-10}	2×10^{-12}	4×10^{-5}				-

325

solution as compared to the MADM solution for the same number of terms.

Hence, for both the illustrations, the solutions obtained by using OHAM are of better quality as compared to those of MADM. This is because: the OHAM (Liao, 2010) is based on a more general and versatile scheme of HAM, and is more advantageous in comparison to the MADM (Kumar and Singh, 2010), which is based on ADM. One should note that in the presented OHAM, we have employed the same inverse operator as was proposed by Wazwaz (2005) and used by Kumar and Singh (2010).

It should also be noted that Kumar and Singh (2010) have also presented another algorithm, in which the operator proposed by Wazwaz (2005) was replaced by a new operator, called new proposed operator [NPO]. However, we could not compare the OHAM results with those obtained by applying the [NPO], since no expressions or tabulated values of NPO solutions were given in the paper by Kumar and Singh (2010). Besides, the MATHEMATICA routine presented by Kumar and Singh (2010) was based on MADM only.

6.3 REACTION-DIFFUSION PROCESS IN A POROUS SPHERICAL CATALYST

In this section, the model equation of reaction-diffusion process occurring in a porous spherical catalyst has been solved by using OHAM, and the approximate solutions of dimensionless concentration profile and effectiveness factor have been obtained. These solutions have been found for two types of reaction kinetics: (i) power-law kinetics, which frequently arises in various heterogeneous chemical reactions, and (ii) Michaelis-Menten kinetics, which is often encountered in biochemical reactions. The obtained OHAM results have been compared with the numerically obtained results as well as those obtained by using other approximate methods (Kumar and Singh, 2010; Li et al., 2004). It should be noted that the same model equation has previously been solved by using ADM and RADM in section 5.6 of Chapter V.

6.3.1 Model Equation

The steady-state model equation of this process is described by a second order ODE constituting a singular BVP, and is given below:

$$D_e\left(\frac{d^2C_A}{dr^2}+\frac{2}{r}\frac{dC_A}{dr}\right) = (-r_A) \tag{6.23a}$$

BC I: $C_A = C_{AS}$ at $r = R$ [pore mouth]

(6.23b)

BC II: $\dfrac{dC_A}{dr}=0$ at $r = 0$ [pore end] $\tag{6.23c}$

6.3.2 Solutions and Discussion: Concentration Profile and Effectiveness Factor

6.3.2.1 Solution by OHAM: Power-law kinetics

Introducing the following dimensionless variables:

$$y=\frac{C_A}{C_{AS}}, \quad x=\frac{r}{R}, \quad \phi=\sqrt{\frac{(-r_{AS})R^2}{D_eC_{AS}}}=\sqrt{\frac{k_nC_{AS}^{n-1}R^2}{D_e}},$$

where ϕ denotes the Thiele modulus, the Eqs. (6.23a) - (6.23c) can be reduced to the following dimensionless forms:

$$\frac{d^2y}{dx^2}+\frac{2}{x}\frac{dy}{dx}-\phi^2 y^n = 0 \tag{6.24a}$$

BC I: $y=1$ at $x=1$ [pore mouth] $\tag{6.24b}$

BC II: $\dfrac{dy}{dx}=0$ at $x=0$ [pore end] $\tag{6.24c}$

Corresponding to the above equations, the following auxiliary quantities are defined:

$$N[y] = \frac{d^2y}{dx^2}+\frac{2}{x}\frac{dy}{dx}-\phi^2 y^n, \quad L[.]=\frac{1}{x^2}\frac{d}{dx}\left(x^2\frac{d[.]}{dx}\right) \text{ or } L^{-1}[.]=\int_0^x\frac{1}{x^2}\int x^2\,[.]\,dx\,dx,$$

$$H(x) = 1, \; y_0(x) = C_2$$

Thereafter, the following zero order deformation equation is formed:

$$(1-\lambda)L[\psi(x,\lambda) - y_0(x)] \;=\; \lambda h H(x) N[\psi(x,\lambda)] \tag{6.25a}$$

From the above zero order deformation equation, the following m^{th} order deformation equation is obtained:

$$L[y_m(x) - \chi_m y_{m-1}(x)] = h H(x) R_m[\vec{y}_{m-1}(x), x] \tag{6.25b}$$

The above equation results in the following iterative scheme for finding higher y_m s:

$$y_m(x) = \chi_m y_{m-1}(x) + h \int_0^x \frac{1}{x^2} \int x^2 R_m[\vec{y}_{m-1}, x] \, dx \, dx \tag{6.25c}$$

For the above defined auxiliary quantities, the sequential use of Eq. (6.25c) yields the following parts of the OHAM solution:

$$y_0 = C_2$$

$$y_1 = -\frac{1}{6} C_2^n h \phi^2 x^2$$

$$y_2 = -\frac{1}{6} C_2^n (h + h^2) \phi^2 x^2 + \frac{1}{120} C_2^{2n-1} n h^2 \phi^4 x^4$$

$$y_2 = -\frac{1}{6} C_2^n h (1+h)^2 \phi^2 x^2 + \frac{1}{60} C_2^{2n-1} n (1+h) h^2 \phi^4 x^4 - \frac{1}{15120} C_2^{3n-2} n (8n-5) h^3 \phi^6 x^6$$

$$y_4 = -\frac{1}{6} C_2^n h (1+h)^3 \phi^2 x^2 + \frac{1}{40} C_2^{2n-1} n (1+h)^2 h^2 \phi^4 x^4 - \frac{1}{5040} C_2^{3n-2} n (8n-5)(1+h) h^3 \phi^6 x^6$$

$$+ \frac{1}{3265920} C_2^{4n-3} n (70 - 183n + 122n^2) h^4 \phi^8 x^8$$

$$y_5 = -\frac{1}{6} C_2^n h (1+h)^4 \phi^2 x^2 + \frac{1}{30} C_2^{2n-1} n (1+h)^3 h^2 \phi^4 x^4 - \frac{1}{2520} C_2^{3n-2} n (8n-5)(1+h)^2 h^3 \phi^6 x^6$$

$$+ \frac{1}{816480} C_2^{4n-3} n (70 - 183n + 122n^2)(1+h) h^4 \phi^8 x^8$$

$$-\frac{1}{1796256000}C_2^{5n-4}n(-3150+10805n-12642n^2+5032n^3)h^5\phi^{10}x^{10}$$

Ultimately, the following six terms [$n_T = 6$] OHAM solution is found.

$$y_{OHAM} = C_2 - \frac{\phi^2 C_2^n}{6}(5h+10h^2+10h^3+5h^4+h^5)x^2$$

$$+\frac{n\phi^4 C_2^{2n-1}}{120}h^2(10+20h+15h^2+4h^3)x^4 - \frac{n(8n-5)\phi^6 C_2^{3n-2}}{15120}h^3(10+15h+6h^2)x^6$$

$$+\frac{n(70-183n+122n^2)\phi^8 C_2^{4n-3}}{3265920}h^4(5+4h)x^8$$

$$+\frac{n(3150-10805n+12642n^2-5032n^3)\phi^{10}C_2^{5n-4}}{1796256000}h^5 x^{10} \qquad (6.26)$$

For a particular value of n and ϕ, the values of C_2 and h can be found from BC I [Eq. (6.24b)] and Eq. (6.9c), respectively [BC II is satisfied automatically]. Substituting back the so found values of C_2 and h in Eq. (6.26), the six terms OHAM solution for the selected values of n and ϕ is obtained. For example, one finds $C_2 = 0.475958$ and $h = -0.886421$ for $n = 0.5$ and $\phi = 2$, and the following six terms OHAM solution is found by substituting these values in Eq. (6.26).

$$y_{OHAM} = 0.475958+0.459923\,x^2+0.066616\,x^4-0.003030\,x^6+0.000665x^8$$

$$-0.000133x^{10} \qquad (6.27)$$

As described earlier, one can also obtain the six terms [$n_T = 6$] MADM solution by substituting $h = -1$ in the above obtained six terms OHAM solution, i.e. Eq. (6.26), and the following six terms MADM solution is obtained:

$$y_{MADM} = C_2 + \frac{\phi^2 C_2^n}{6}x^2 + \frac{n\phi^4 C_2^{2n-1}}{120}x^4 + \frac{n(8n-5)\phi^6 C_2^{3n-2}}{15120}x^6$$

$$+\frac{n(70-183n+122n^2)\phi^8 C_2^{4n-3}}{3265920}x^8$$

$$-\frac{n(3150-10805n+12642n^2-5032n^3)\phi^{10}C_2^{5n-4}}{1796256000}x^{10} \qquad (6.28)$$

C_2 can be found by satisfying the BC I, and for $n = 0.5$ and $\phi = 2$, one finds $C_2 = 0.475967$. Substituting this value of C_2 in Eq. (6.28), the following six terms MADM solution is obtained:

$$y_{MADM} = 0.475967 + 0.459936\, x^2 + 0.066667\, x^4 - 0.003068\, x^6 + 0.000741x^8$$

$$-0.000242x^{10} \qquad (6.29)$$

In a similar fashion, the OHAM and MADM solutions have been found for various values of n and ϕ [$n = 0.5$, $\phi = 2$; $n = 2$, $\phi = 5$; $n = 1.5$, $\phi = 5$], and the corresponding dimensionless concentration profiles have been shown in Fig. 6.8 along with numerically obtained profiles. It is obvious from Fig. 6.8 that the concentration profiles obtained from OHAM agree well with those of MADM and numerical method. For the same values of n and ϕ, Table 6.3 compares the values of dimensionless concentration obtained by using OHAM and numerical method. it is clear from this table that and the OHAM results are quite close to the numerical results and the error in OHAM results decreases as the number of terms are increased.

In Fig. 6.9, a comparison between the OHAM and MADM solutions has been made by portraying the absolute error profiles of the OHAM solutions $\left[|y_{Numerical} - y_{OHAM}|\right]$ and the MADM solutions $\left[|y_{Numerical} - y_{MADM}|\right]$ for $n = 0.5$ and $\phi = 2$. It can be observed in Fig. 6.9 that the errors in OHAM solutions are less than the corresponding MADM solutions. Similar conclusions can also be drawn from Fig. 6.10, where residual error profiles of the OHAM and MADM solutions have been plotted. A discussion regarding the convergence of OHAM solutions [$n = 0.5$, $\phi = 2$; $n = 2$, $\phi = 5$] has also been presented in Appendix C1.

A similar comparison can also be made between the OHAM solution and the available analytical solution for first order kinetics [$n=1$]. For first order kinetics, the analytical solution is given by the following equation (Fogler, 1992):

$$y_{Analytical} = \frac{sinh[\phi x]}{x\, sinh[\phi]} \qquad (6.30)$$

330
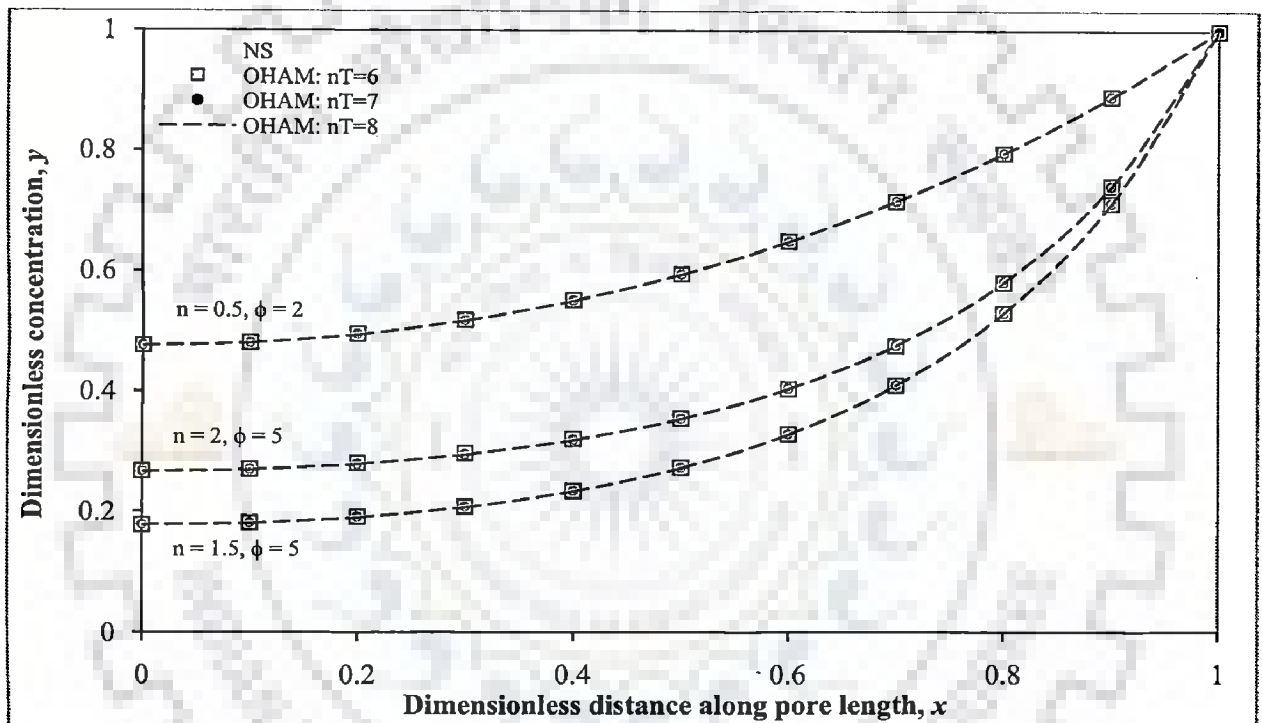
Figure 6.8: Dimensionless concentration profiles [power-law kinetics: $n = 0.5$, $\phi = 2$; $n = 2$, $\phi = 5$; $n = 1.5$, $\phi = 5$; $x = 1$: pore mouth; $x = 0$: pore end]

Table 6.3: **Results of reaction-diffusion problem obtained by numerical and OHAM solutions**

x	Numerical	Method OHAM			Absolute Error OHAM		
		$n_T = 6$	$n_T = 7$	$n_T = 8$	$n_T = 6$	$n_T = 7$	$n_T = 8$
		$n = 0.5, \phi = 2$			-	-	-
		$C_2 =$ 0.475958	$C_2 =$ 0.475934	$C_2 =$ 0.475925	-	-	-
		$h =$ -0.886421	$h =$ -0.859331	$h =$ -0.849534	-	-	-
0	0.475922	0.475958	0.475934	0.475925	3.617E-05	1.205E-05	3.229E-06
0.1	0.480528	0.480564	0.480540	0.480531	3.606E-05	1.188E-05	3.040E-06
0.2	0.494426	0.494461	0.494437	0.494428	3.547E-05	1.115E-05	2.284E-06
0.3	0.517853	0.517889	0.517864	0.517855	3.565E-05	1.118E-05	2.332E-06
0.4	0.551204	0.551239	0.551215	0.551206	3.520E-05	1.076E-05	2.044E-06
0.5	0.595023	0.595058	0.595033	0.595025	3.450E-05	1.046E-05	2.072E-06
0.6	0.650000	0.650033	0.650010	0.650002	3.284E-05	9.785E-06	2.053E-06
0.7	0.716964	0.716993	0.716972	0.716965	2.902E-05	7.850B-06	1.230E-06
0.8	0.796874	0.796898	0.796880	0.796875	2.385E-05	5.901E-06	9.937E-07
0.9	0.890818	0.890832	0.890820	0.890818	1.446E-05	2.237E-06	2.836E-07
1	1.000000	1.000000	1.000000	1.000000	0.000E+00	0.000E+00	0.000E+00
		$n = 2, \phi = 5$			-	-	-
x	Numerical	$C_2 =$ 0.266592	$C_2 =$ 0.266718	$C_2 =$ 0.266661	-	-	-
		$h =$ -1.678745	$h =$ -1.604982	$h =$ -1.577324	-	-	-
0	0.266680	0.266592	0.266718	0.266661	8.818E-05	3.758E-05	1.948E-05
0.1	0.269663	0.269968	0.269570	0.269699	3.048E-04	9.305E-05	3.600E-05
0.2	0.278857	0.280000	0.278517	0.278986	1.143E-03	3.397E-04	1.294E-04
0.3	0.295038	0.296696	0.294626	0.295168	1.658E-03	4.120E-04	1.297E-04
0.4	0.319666	0.320915	0.319491	0.319676	1.250E-03	1.741E-04	1.086E-05
0.5	0.355184	0.355218	0.355376	0.355073	3.442E-05	1.923E-04	1.108E-04
0.6	0.405602	0.404466	0.405962	0.405481	1.136E-03	3.601E-04	1.208E-04
0.7	0.477604	0.476255	0.477829	0.477555	1.349E-03	2.254E-04	4.901E-05
0.8	0.582792	0.582182	0.582820	0.582792	6.102E-04	2.755E-05	1.059E-08
0.9	0.742585	0.742605	0.742559	0.742594	1.950E-05	2.674E-05	8.487E-06
1	1.000000	1.000000	1.000000	1.000000	0.000E+00	0.000E+00	0.000E+00
		$n = 1.5, \phi = 5$			-	-	-
x	Numerical	$C_2 =$ 0.177480	$C_2 =$ 0.177548	$C_2 =$ 0.177509	-	-	-
		$h =$ -1.370805	$h =$ -1.369793	$h =$ -1.285938	-	-	-
0	0.177518	0.177480	0.177548	0.177509	3.735E-05	3.031E-05	8.402E-06
0.1	0.180659	0.180639	0.180683	0.180651	1.951E-05	2.432E-05	8.351E-06
0.2	0.190387	0.190391	0.190406	0.190378	4.686E-06	1.898E-05	8.941E-06
0.3	0.207669	0.207650	0.207703	0.207658	1.921E-05	3.381E-05	1.123E-05
0.4	0.234322	0.234223	0.234386	0.234308	9.884E-05	6.386E-05	1.398E-05
0.5	0.273373	0.273213	0.273451	0.273358	1.604E-04	7.724E-05	1.577E-05
0.6	0.329733	0.329621	0.329789	0.329714	1.121E-04	5.669E-05	1.841E-05
0.7	0.411407	0.411428	0.411444	0.411383	2.009E-05	3.684E-05	2.404E-05
0.8	0.531771	0.531822	0.531831	0.531743	5.089E-05	5.998E-05	2.888E-05
0.9	0.713977	0.713888	0.714051	0.713950	8.909E-05	7.440E-05	2.638E-05
1	1.000000	1.000000	1.000000	1.000000	0.000E+00	0.000E+00	0.000E+00

For $n=1$, the following six terms OHAM solution is obtained by using Eq. (6.26):

$$y_{OHAM} = C_2 - \frac{C_2\phi^2}{6}(5h + 10h^2 + 10h^3 + 5h^4 + h^5)x^2 + \frac{C_2\phi^4}{120}(10h^2 + 20h^3 + 15h^4 + 4h^5)x^4$$

$$- \frac{C_2\phi^6}{5040}(10h^3 + 15h^4 + 6h^5)x^6 + \frac{C_2\phi^8}{362880}(5h^4 + 4h^5)x^8 - \frac{C_2\phi^{10}h^5}{39916800}x^{10}$$

$$(6.31)$$

where C_2 is found by using BC I and is given below:

$$C_2 = 39916800\left(\begin{array}{l} 39916800 - 33264000h\phi^2 + 3326400h^2\phi^2(\phi^2 - 20) \\ -79200h^3\phi^2(840 - 84\phi^2 + \phi^4) + 550h^4\phi^2(-60480 + 9072\phi^2 - 216\phi^4 + \phi^6) \\ -h^5\phi^2(6652800 - 1330560\phi^2 + 47520\phi^4 - 440\phi^6 + \phi^8) \end{array}\right)^{-1}$$

Substituting the above obtained value of C_2 in Eq. (6.31), one finds the six terms OHAM solution for $n=1$. Although not shown, it can be verified that up to $\phi = 10$ the so obtained six terms OHAM solution possesses less than 2% error when compared with Eq. (6.30). However, for higher values of ϕ, more terms are need in OHAM solution.

It is also worthy to compare the OHAM and MADM solutions of effectiveness factor $[\eta]$. For a spherical porous catalyst, the effectiveness factor $[\eta]$ is given by the following dimensionless equation:

$$\eta = \frac{3}{\phi^2}\frac{dy}{dx}\bigg|_{x=1} \qquad (6.32)$$

Using Eqs. (6.26) and (6.32), the following six terms OHAM solution of η has been obtained:

$$\cdot\eta_{OHAM} = \frac{h}{59875200}\left(\begin{array}{l} -59875200C_2^n(5 + 10h + 10h^2 + 5h^3 + h^4) \\ +5987520C_2^{2n-1}h(10 + 20h + 15h^2 + 4h^3)n\phi^2 \\ -71280C_2^{3n-2}h^2(10 + 15h + 6h^2)n(8n - 5)\phi^4 \\ +440C_2^{4n-3}h^3(5 + 4h)n(70 - 183n + 122n^2)\phi^6 \\ -C_2^{5n-4}h^4n(-3150 + 10805n - 12642n^2 + 5032n^3)\phi^8 \end{array}\right) \qquad (6.33)$$

334
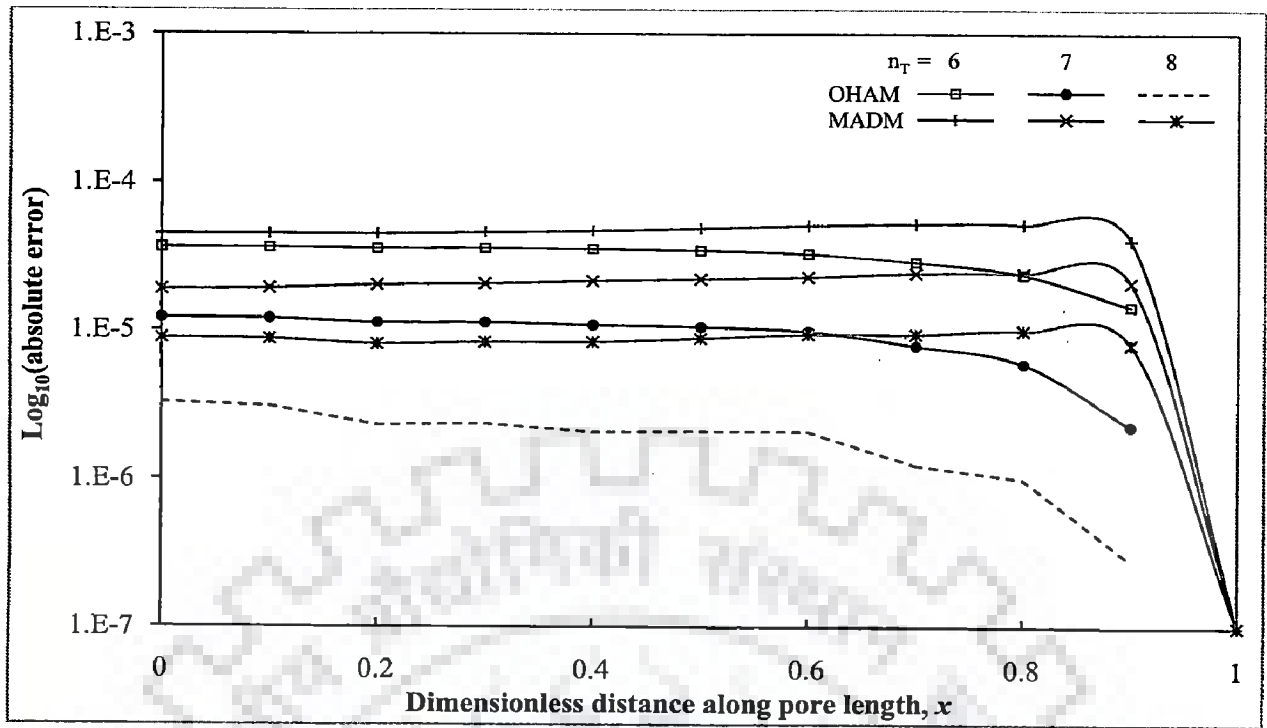
Figure 6.9: Absolute error profiles on Log_{10} scale [power-law kinetics: $n = 0.5$, $\phi = 2$; $x = 1$: pore mouth; $x = 0$: pore end]
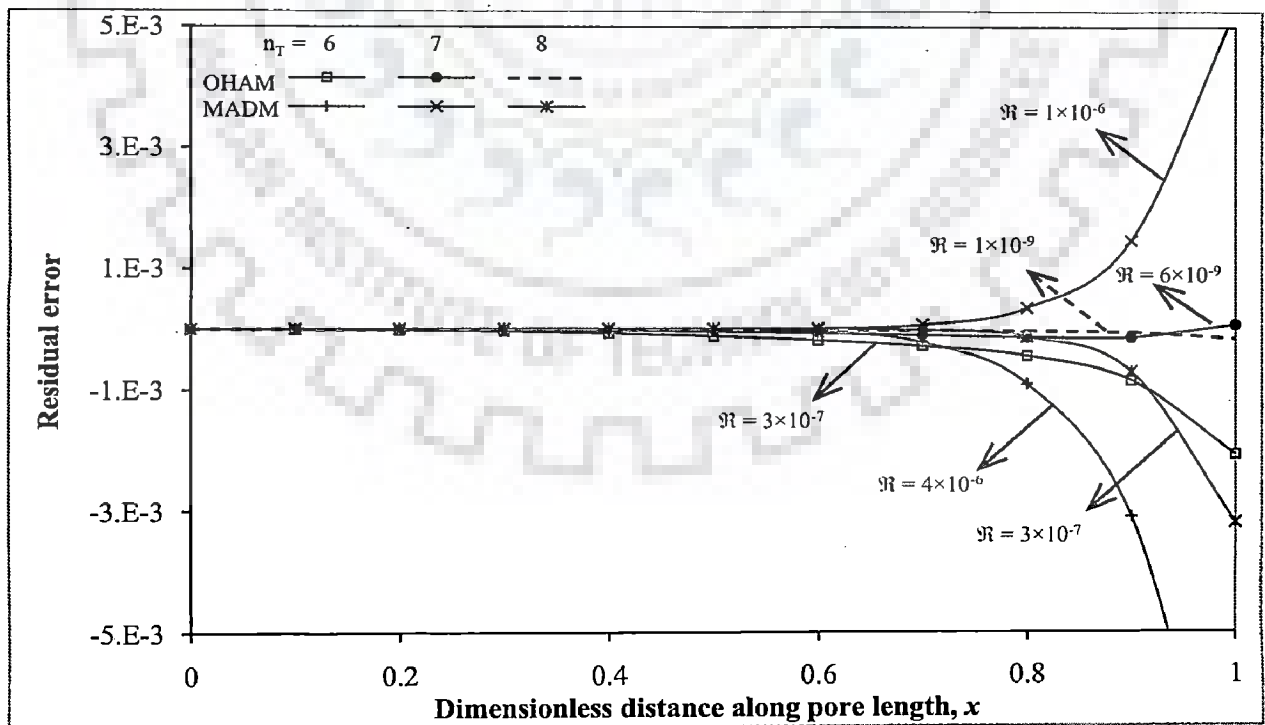
Figure 6.10: Residual error profiles [power-law kinetics: $n = 0.5$, $\phi = 2$; $x = 1$: pore mouth; $x = 0$: pore end]

Table 6.4: **Effectiveness factor [η] obtained by numerical, MADM and OHAM solutions**

n	ϕ	Method	Effectiveness Factor [η]				% Error $= (\eta_{Numerical}- \eta)/\eta_{Numerical}\times100$		
				$n_T=6$	$n_T=7$	$n_T=8$	$n_T=6$	$n_T=7$	$n_T=8$
0.5	2	Numerical	0.879268	-			-		
		OHAM	-	0.879096	0.879235	0.879249	0.020	0.004	0.002
		MADM	-	0.878729	0.879528	0.87912	0.061	0.030	0.017
1	5	Numerical	0.480055	-			-		
		OHAM	-	0.480276	0.480074	0.480056	0.046	0.004	0.000
		MADM	-	0.477087	0.479632	0.480009	0.618	0.088	0.010
1.5	5	Numerical	0.431958	-			-		
		OHAM	-	0.432273	0.431827	0.432001	0.073	0.030	0.010
		MADM	-	0.411137	0.422693	0.428071	4.820	2.145	0.900
2	5	Numerical	0.397233	-			-		
		OHAM	-	0.396996	0.397272	0.397192	0.060	0.010	0.010
		MADM	-	0.362854	0.377795	0.38654	8.655	4.893	2.692

By substituting $h=-1$ in Eq. (6.33), the following MADM solution of η is obtained:

$$\eta_{MADM} = \frac{1}{59875200}\begin{pmatrix} 59875200C_2^n + 5987520C_2^{2n-1}n\phi^2 \\ +71280C_2^{3n-2}n(8n-5)\phi^4 \\ +440C_2^{4n-3}n(70-183n+122n^2)\phi^6 \\ +C_2^{5n-4}n(-3150+10805n-12642n^2+5032n^3)\phi^8 \end{pmatrix} \quad (6.34)$$

For different values of n and ϕ, Table 6.4 shows the values of η obtained by using OHAM, MADM and the numerical method. It is clear that the OHAM predictions are better than those of MADM. Besides, the error decreases as one increases the terms in OHAM.

6.3.2.2 Solution by OHAM: Michaelis-Menten kinetics

In this subsection, the same model equation [Eqs. (6.23a)-(6.23c)] has been solved by using OHAM, however, the reaction rate is now given by the Michaelis-

Menten kinetics $\left[(-r_A) = r_m C_A / (K_m + C_A)\right]$ (Li et al., 2004). This model equation relates to the design of a biocatalytic reactor and is of interest to the biochemical engineers.

Using the previously introduced dimensionless variables, in addition to the following dimensionless variables,

$$\phi = \sqrt{\frac{(-r_{AS})R^2}{D_e C_{AS}}} = \sqrt{\frac{r_m R^2}{D_e K_m (1+\beta)}}, \quad \beta = \frac{C_{AS}}{K_m}$$

the Eqs. (6.23a)-(6.23c) attain the following dimensionless forms:

$$\frac{d^2 y}{dx^2} + \frac{2}{x}\frac{dy}{dx} - \phi^2 \frac{(1+\beta)y}{(1+\beta y)} = 0 \tag{6.35a}$$

BC I: $y = 1$ at $x = 1$ [pore mouth] $\tag{6.35b}$

BC II: $\dfrac{dy}{dx} = 0$ at $x = 0$ [pore end] $\tag{6.35c}$

Corresponding auxiliary quantities are:

$$N[y] = \frac{d^2 y}{dx^2} + \frac{2}{x}\frac{dy}{dx} - \phi^2 \frac{(1+\beta)y}{(1+\beta y)}, \qquad H(x) = 1, \qquad y_0(x) = C_2,$$

$$L[.] = \frac{1}{x^2}\frac{d}{dx}\left(x^2 \frac{d[.]}{dx}\right) \text{ or } L^{-1}[.] = \int_0^x \frac{1}{x^2}\int x^2 [.] \, dx \, dx$$

The corresponding zero order and m^{th} order deformation equations are:

$$(1-\lambda)L[\psi(x,\lambda) - y_0(x)] = \lambda h H(x) N[\psi(x,\lambda)] \tag{6.36a}$$

$$L[y_m(x) - \chi_m y_{m-1}(x)] = h H(x) R_m[\bar{y}_{m-1}(x), x] \tag{6.36b}$$

Eq. (6.36b) delivers the following recursive relation:

$$y_m(x) = \chi_m y_{m-1}(x) + h \int_0^x \frac{1}{x^2}\int x^2 R_m[\bar{y}_{m-1}, x] \, dx \, dx \tag{6.37}$$

For the above defined auxiliary quantities, the Eq. (6.37) presents the following four terms [$n_T = 4$] of the OHAM solution:

$$y_0 = C_2$$

$$y_1 = -\frac{1+\beta}{6+6C_2\beta}C_2 h\phi^2 x^2$$

$$y_2 = -\frac{(1+\beta)}{6(1+C_2\beta)}C_2 h(1+h)\phi^2 x^2 + \frac{(1+\beta)^2}{120(1+C_2\beta)^3}C_2 h^2(1+h)\phi^4 x^4$$

$$y_3 = -\frac{(1+\beta)}{6(1+C_2\beta)}C_2 h(1+h)^2 \phi^2 x^2 + \frac{(1+\beta)^2}{60(1+C_2\beta)^3}C_2 h^2(1+h)\phi^4 x^4$$

$$+\frac{(1+\beta)^3(-3+10C_2\beta)}{15120(1+C_2\beta)^5}C_2 h^3 \phi^6 x^6$$

Consequently, the following OHAM solution [$n_T = 4$] can be obtained:

$$y_{OHAM} = C_2 - \frac{C_2 h(3+3h+h^2)(1+\beta)\phi^2}{6+6C_2\beta}x^2$$

$$+\frac{C_2 h^2(3+2h)(1+\beta)^2 \phi^4}{120(1+C_2\beta)^3}x^4 + \frac{C_2 h^3(-3+10C_2\beta)(1+\beta)^3 \phi^6}{15120(1+C_2\beta)^5}x^6 \qquad (6.38)$$

The unknown C_2 and h can be found from BC I and Eq. (6.9c), respectively. For example, for $\phi = 3$, $\beta = 1$, one finds $C_2 = 0.20511$ and $h = -0.77673$, and by substituting these values in Eq. (6.38) the following four terms OHAM solution is found.

$$y_{OHAM} = 0.205106 + 0.504909x^2 + 0.276144x^4 + 0.0138409x^6 \qquad (6.39)$$

In the same way, one can find the OHAM solutions for higher number of terms and for different values of ϕ and β. The results obtained from the so found OHAM solutions have been compared with the numerical results and with the results obtained from the approximate solution of Li et al. (2004). However, while comparing the results with those of Li et al. (2004), one should be aware that the dimensionless quantities defined by Li et al. (2004) are slightly different from the present definitions of dimensionless quantities, which have been taken from Gottifredi and Gonzo (2005). Basically, Li et al. (2004) have proposed the approximate solution in the form of a cubic polynomial. The

coefficients of this polynomial solution are found by satisfying the model equation [Eq. (6.35a)] and the allied BCs [Eqs. (6.35b)-(6.35c)]. However, one should note that their solution is specific to the Michaelis–Menten kinetics. As an example, by following their method, we obtain the following approximate solution of dimensionless concentration profile for $\phi = 3$ and $\beta = 1$:

$$y_{Li} = 0.106107 + 0.287786\ x^2 + 0.606107\ x^3 \qquad (6.40)$$

For several values of ϕ and β [$\phi = 3$, $\beta = 1$; $\phi = 3$, $\beta = 10$], the dimensionless concentration profiles computed by using the OHAM solutions, approximate solution of Li et al. (2004) and the numerical method are shown in Figs. 6.11 and 6.12. From these figures, it can be observed that the concentration profiles obtained by using OHAM match closely with the numerically obtained concentration profiles and are either equally good or are better than those obtained by using the approximate solution of Li et al (2004). The accuracy of OHAM solutions increases with the increase in number of terms. Figs. 6.13 and 6.14 show the residual error profiles of the OHAM solutions and the one obtained by using the approximate solution of Li et al. (2004). Here also, one observes that the residual error of OHAM solution decreases with the increase in number of terms. Although not shown in detail, a similar comparison between the OHAM solution and the approximate solution of Li et al. (2004) has also been performed for η. For different values of ϕ and β, the values of η obtained by using these two solutions have been shown in Table 6.5 along with the numerically obtained values. It is clear from this table that the values of η obtained by using OHAM solutions are close to the numerically obtained values, and the error in η predicted by the OHAM solutions decreases with the increase in number of terms. However, there is no such provision of reducing the error in the approximate solution of Li et al. (2004).

Table 6.5: **Effectiveness factor [η] obtained by numerical, Li et al. (2004) and OHAM solutions**

ϕ	β	Effectiveness Factor [η]				
		Numerical solution	Li et al. (2004)	OHAM		
				$n_T = 6$	$n_T = 8$	$n_T = 10$
3	1	0.7439	0.7980	0.7445	0.7441	0.7439·
3	10	0.8679	0.8216	0.7653	0.8253	0.8474
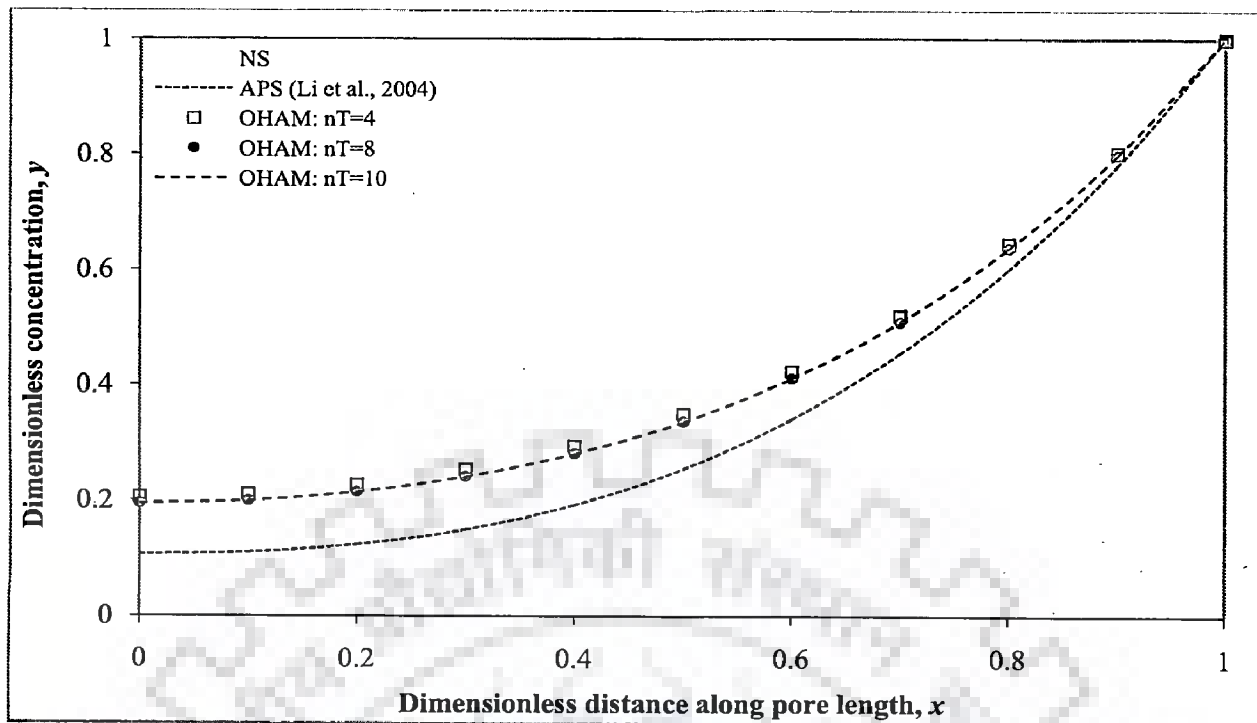
Figure 6.11: Dimensionless concentration profiles [Michaelis-Menten kinetics: ϕ = 3, β = 1; x = 1: pore mouth; x = 0: pore end]

Figure 6.12: Dimensionless concentration profiles [Michaelis-Menten kinetics: ϕ = 3, β = 10; x = 1: pore mouth; x = 0: pore end]

Figure 6.13: Residual error profiles [Michaelis-Menten kinetics: $\phi = 3$, $\beta = 1$; $x = 1$: pore mouth; $x = 0$: pore end]
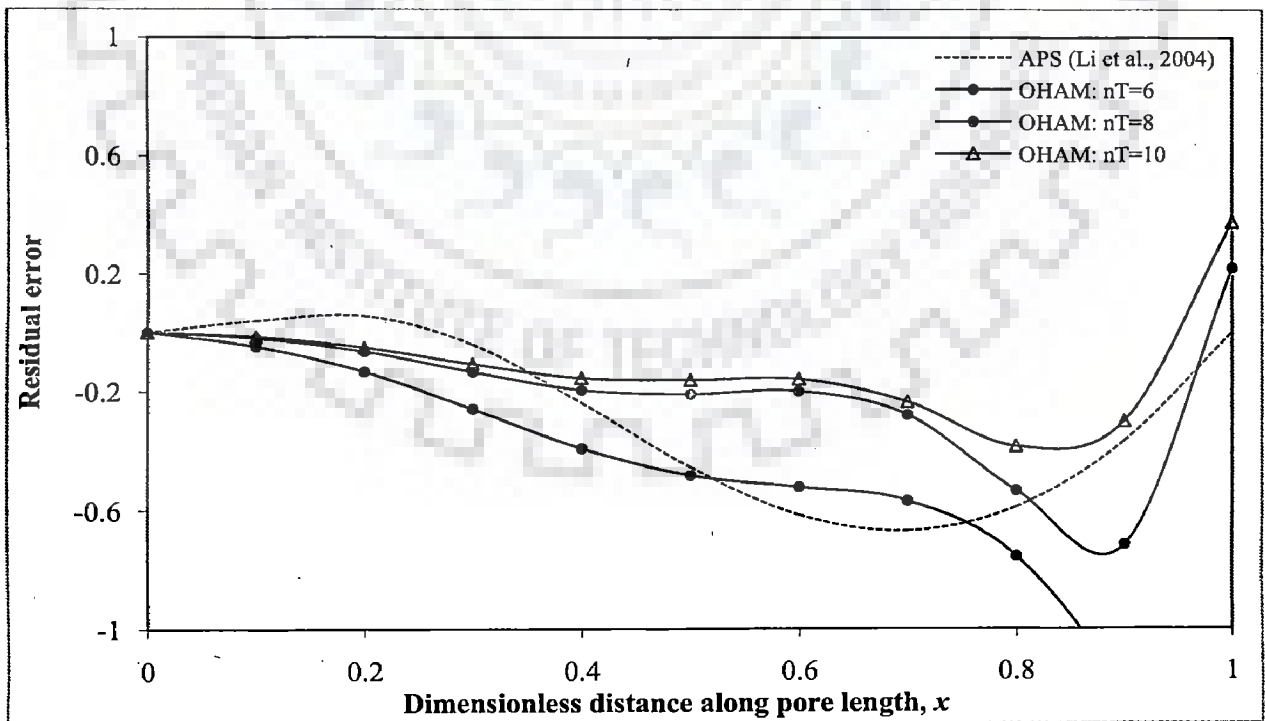
Figure 6.14: Residual error profiles [Michaelis-Menten kinetics: $\phi = 3$, $\beta = 10$; $x = 1$: pore mouth; $x = 0$: pore end]

6.4 TUBULAR CHEMICAL REACTOR

In this section, the axial dispersion model of a tubular chemical reactor supporting nonlinear kinetics has been solved by using OHAM. The obtained OHAM results have been compared with the numerical results as well as with those available in literature. Besides, utility of OHAM has been shown by capturing the dual solutions, which appear for non-monotonous reaction kinetics.

6.4.1 Model Equation

Consider a tubular chemical reactor in which a unimolecular reaction described by a nonlinear kinetics $(-r_A)$ is taking place. The reactor is assumed to operate under steady state and isothermal conditions. It is also assumed that the flow pattern existing in this reactor can be represented by the familiar axial dispersion model [Fig. 6.15 depicts the steady state convection-dispersion-reaction process in a tubular chemical reactor]. With these assumptions, the model equation of this reactor can easily be derived by applying the material balance for the reacting species [say A] over the control volume of the reactor. The so derived model equation is expressed by the following second order ODE constituting a BVP (Fogler, 1992; Levenspiel, 1999). The associated BCs at the inlet and outlet of the reactor are given by the famous Danckwerts BCs.

$$\underbrace{D_e \frac{d^2 C_A}{dZ^2}}_{\text{Dispersion term}} - \underbrace{U \frac{dC_A}{dZ}}_{\text{Convection term}} - \underbrace{(-r_A)}_{\text{Sink / Source term}} = 0 \tag{6.41a}$$

$$\text{BC I:} \quad UC_A - D_e \frac{dC_A}{dZ} = UC_{A0} \quad \text{at } Z = 0 \text{ [reactor inlet]} \tag{6.41b}$$

$$\text{BC II:} \quad \frac{dC_A}{dZ} = 0 \quad \text{at } Z = L \text{ [reactor outlet]} \tag{6.41c}$$

The above equations can be transformed into the following dimensionless form:

$$\underbrace{\frac{d^2 y}{dz^2}}_{\text{Dispersion term}} - \underbrace{Pe \frac{dy}{dz}}_{\text{Convection term}} - \underbrace{Pe\,Da\,f(y)}_{\text{Sink / Source term}} = 0 \tag{6.42a}$$

BC I: $\quad y - \dfrac{1}{Pe}\dfrac{dy}{dz} = 1 \qquad\qquad$ at $z = 0$ [reactor inlet] $\qquad\qquad$ (6.42b)

BC II: $\quad \dfrac{dy}{dz} = 0 \qquad\qquad\qquad$ at $z = 1$ [reactor outlet] $\qquad\qquad$ (6.42c)

where $y\left(=\dfrac{C_A}{C_{A0}}\right)$ is the dimensionless concentration, $z\left(=\dfrac{Z}{L}\right)$ is the dimensionless axial

distance, $Pe\left(=\dfrac{UL}{D_e}\right)$ and $Da\left(=\dfrac{(-r_{A0})L}{C_{A0}U}=\dfrac{(-r_{A0})\tau}{C_{A0}}\right)$ are the Péclet number and the

Damköhler number, respectively. $\tau\left(=\dfrac{L}{U}\right)$ is the residence time and $f(y)\left(=\dfrac{(-r_A)}{(-r_{A0})}\right)$ is

the dimensionless reaction rate.

6.4.2 Solutions and Discussion: Concentration Profile

For simplicity, the OHAM solutions of Eqs. (6.42a)-(6.42c) have been obtained for power-law kinetics $[f(y) = y^n]$, however, OHAM solutions for other forms of kinetics, e.g. Langmuir-Hinshelwood kinetics, can also be obtained in a similar fashion. Before applying OHAM to Eqs. (6.42a)-(6.42c), it is quite convenient to change the dimensionless axial coordinate z by $1-x$. As shown in later operations, this shifting of the coordinate [interchanging the locations of the reactor inlet/outlet] eases the computational efforts by directly evaluating one of the unknown constants appearing in the OHAM solution. With this modification, the Eqs. (6.42a)-(6.42c) attain the following forms for power-law kinetics:

$$\dfrac{d^2 y}{dx^2} + Pe\dfrac{dy}{dx} - Pe\,Da\,y^n = 0 \qquad\qquad (6.43a)$$

BC I: $\quad y + \dfrac{1}{Pe}\dfrac{dy}{dx} = 1 \qquad$ at $x = 1$ [reactor inlet] $\qquad\qquad$ (6.43b)

BC II: $\quad \dfrac{dy}{dx} = 0 \qquad\qquad\qquad$ at $x = 0$ [reactor outlet] $\qquad\qquad$ (6.43c)

346
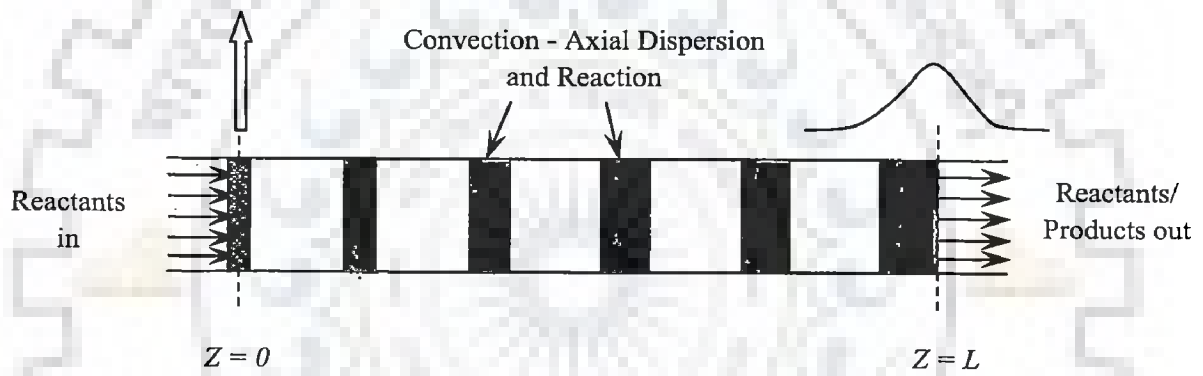
Figure 6.15: Convection, axial dispersion and chemical reaction in a tubular chemical reactor

6.4.2.1 Solution by OHAM

Corresponding to Eq. (6.43a), the following relations can be defined for auxiliary quantities:

$$N[y] = \frac{d^2 y}{dx^2} + Pe\frac{dy}{dx} - Pe\,Da\,y'' \tag{6.44a}$$

$$L[.] = \frac{d^2[.]}{dx^2} \text{ or } L^{-1}[.] = \int_0^x \int [.]dxdx \tag{6.44b}$$

$$H(x) = 1 \tag{6.44c}$$

$$y_0(x) = C_1 x + C_2 \tag{6.44d}$$

where C_1 and C_2 are the constants and can be determined by the related BCs.

Eventually, the following zero order deformation equation is obtained:

$$(1-\lambda)L[\psi(x,\lambda) - y_0(x)] = \lambda h \left(\frac{d^2\psi(x,\lambda)}{dx^2} + Pe\,\frac{d\psi(x,\lambda)}{dx} - Pe\,Da\,\psi(x,\lambda)'' \right) \tag{6.45}$$

Using Eq. (6.45), the higher m^{th} order deformation equation is derived, which after slight rearrangement yields the following recursive relation:

$$y_m(x) = \chi_m y_{m-1}(x)$$

$$+ hL^{-1}\left[\frac{1}{(m-1)!}\frac{\partial^{m-1}}{\partial\lambda^{m-1}}\left[\frac{d^2\psi(x,\lambda)}{dx^2} + Pe\frac{d\psi(x,\lambda)}{dx} - Pe\,Da\,\psi(x,\lambda)'' \right]\Big|_{\lambda=0} \right]$$

$$\text{for } m \geq 1 \tag{6.46}$$

Now with the chosen initial guess $y_0(x) = C_1 x + C_2$, one can easily evaluate higher $y_m s$ in a systematic manner by using Eq. (6.46). However, before finding higher $y_m s$, it is quite useful to analyze the BC II. It can be observed that the BC II requires one of the integration constant to be zero, i.e. $C_1 = 0$. Infact, this direct evaluation of one of the constants has only been possible due to the shifting of the axial coordinate,

i.e. z by $1-x$. Now with $C_1 = 0$ and by using Eq. (6.46) we get the following expressions for $y_m s$ [the detailed procedure for finding $y_m s$ for power-law as well as Langmuir-Hinshelwood kinetics has been presented in Appendix C2].

$$y_0(x) = C_2$$

$$y_1(x) = -\frac{h}{2} C_2^n Pe\, Da\, x^2$$

$$y_2(x) = -\frac{h}{2}(1+h)C_2^n Pe\, Da\, x^2 - \frac{h^2}{6} C_2^n Pe^2\, Da\, x^3 + \frac{h^2}{24} nC_2^{2n-1} Pe^2\, Da^2\, x^4$$

$$y_3(x) = -\frac{h}{2}(1+h)^2 C_2^n Pe\, Da\, x^2 - \frac{h^2}{3}(1+h)C_2^n Pe^2\, Da\, x^3$$

$$+\frac{1}{24} h^2 C_2^n (2C_2^{n-1} Dan + 2C_2^{n-1} Dahn - hPe)Pe^2 Da\, x^4 + \frac{h^3}{60} nC_2^{2n-1} Pe^3\, Da^2\, x^5$$

$$-\frac{h^3}{720} n(4n-3)C_2^{3n-2} Pe^3\, Da^3\, x^6$$

$$y_4(x) = -\frac{h}{2}(1+h)^3 C_2^n Pe\, Da\, x^2 - \frac{h^2}{2}(1+h)^2 C_2^n Pe^2\, Da\, x^3$$

$$+\frac{h^2}{8}(1+h)(C_2^n Dan + C_2^n hPe - C_2 hPe)C_2^{n-1} Pe^2\, Da\, x^4$$

$$+\frac{1}{120} C_2^{n-1} Dah^3 Pe^3 (6C_2^n Dan + 6C_2^n Dahn - C_2 hPe) x^5$$

$$-\frac{1}{240} C_2^{2n-2} Da^2 h^3 nPe^3 (-3C_2^n Da - 3C_2^n Dah + 4C_2^n Dan + 4C_2^n Dahn - C_2 hPe) x^6$$

$$-\frac{1}{5040} C_2^{3n-2} Da^3 h^4 nPe^4 (16n-13)x^7 + \frac{1}{40320} C_2^{4n-3} Da^4 h^4 nPe^4 (30-63n+34n^2)x^8$$

After simplification, the five terms [$n_T = 5$] OHAM solution is given by:

$$\psi(x,1) = y(x) \approx y_{OHAM}(x)$$

350

$$= y_0(x) + \sum_{m=1}^{4} y_m(x)$$

$$= C_2 - \frac{h}{2}(4 + 6h + 4h^2 + h^3)C_2^n Pe\,Da\,x^2 - \frac{h^2}{6}(6 + 8h + 3h^2)C_2^n Pe^2 Da\,x^3$$

$$+ \frac{h^2}{24}(6C_2^{n-1}Dan + 8C_2^{n-1}Dahn + 3C_2^{n-1}Dah^2 n - 4hPe - 3h^2 Pe)C_2^n Pe^2 Da\,x^4$$

$$- \frac{h^3}{120}(-8C_2^{n-1}Dan - 6C_2^{n-1}Dahn + hPe)C_2^n Pe^3 Da\,x^5$$

$$+ \frac{h^3}{720}(12C_2^{n-1}Da + 9C_2^{n-1}Dah - 16C_2^{n-1}Dan - 12C_2^{n-1}Dahn + 3hPe)nC_2^{2n-1}Pe^3 Da^2 x^6$$

$$- \frac{h^4}{5040}(-13 + 16n)nC_2^{3n-2}Pe^4 Da^3 x^7 + \frac{h^4}{40320}(30 - 63n + 34n^2)nC_2^{4n-3}Pe^4 Da^4 x^8$$

$$(6.47)$$

The unknown C_2 is found by forcing y_{OHAM} to satisfy the yet unutilized BC I, i.e. Eq. (6.43b), as shown below:

$$\frac{1}{Pe}\frac{dy_{OHAM}(1)}{dx} + y_{OHAM}(1) = 1 \qquad (6.48)$$

And, the optimum value of h is found by using Eq. (6.9c).

For the given values of the parameters $[n, Pe$ and $Da]$, the Eqs. (6.48) and (6.9c) are solved simultaneously so as to obtain the values of C_2 and h, which in turn are substituted back in Eq. (6.47) to get the OHAM solution of dimensionless concentration. One should note that for finding the HAM solution, all the Eqs. (6.44) - (6.48) remain valid, however, h is found from the valid region in h-curve instead of Eq. (6.9c).

For some of the parameters' values considered by several researchers, the dimensionless concentration profiles obtained by using the OHAM solutions have been plotted in Figs. 6.16 - 6.27 along with the numerically obtained profiles. Numerical profiles have been found in two different ways, viz. by implementing the inbuilt command of MATHEMATICA, i.e. "NDSolve" and by applying the orthogonal

collocation [OC] method. The orthogonal collocation method is used, since in some situations the command "NDSolve" does not respond properly and rather breaks down. From the Figs. 6.16 - 6.27, it is clear that a close harmony exists between the OHAM solutions and their numerical counterparts. It can also be observed that the accuracy of the OHAM solutions increases with the increase in number of terms.

For examining the effects of Danckwerts BCs, the concentration profiles with or without them have been plotted in Fig. 6.27 for the parameters' values given in Rao et al. (1981). It can be observed that the Danckwerts BCs cause a sudden drop in concentration at the inlet of the reactor and thereby decreases the whole concentration profile. The difference between the concentration profiles corresponding to the two different set of BCs decreases as one moves towards the exit of the reactor. Here also, the OHAM solutions match well with the numerical solutions. Corresponding to these concentration profiles, Fig. 6.28 shows the residual error profiles of the five points collocation solution and the OHAM solutions, and also indicates the respective sum of square of residual errors. From this figure, it can be seen that there is no appreciable difference between the residual profiles, obtained with or without Danckwerts BCs, which signifies the same level of accuracy for these two situations. However, it can be seen that the sum of square of residual errors of OHAM solution decreases with the increase in number of terms, and for $n_T = 8$ and 10, the sum of square of residual errors of OHAM solutions are less than that of the five points collocation solution. The same observations can also be drawn from Fig. 6.29, where the profiles of absolute percentage error have been plotted for five points collocation solution and OHAM solutions. The absolute percentage error has been found by using the following equation:

$$\text{Absolute percentage error at } x = \frac{\left| y_{Numerical} - y_{Calculated} \right|}{y_{Numerical}} \times 100$$

This also substantiates the accurate predictions of OHAM results. Although not shown, these observations have also been found to be true for other obtained profiles [Figs. 6.16-6.27]. In Appendix C3, convergence of the OHAM solutions has also been discussed by using various other approaches.
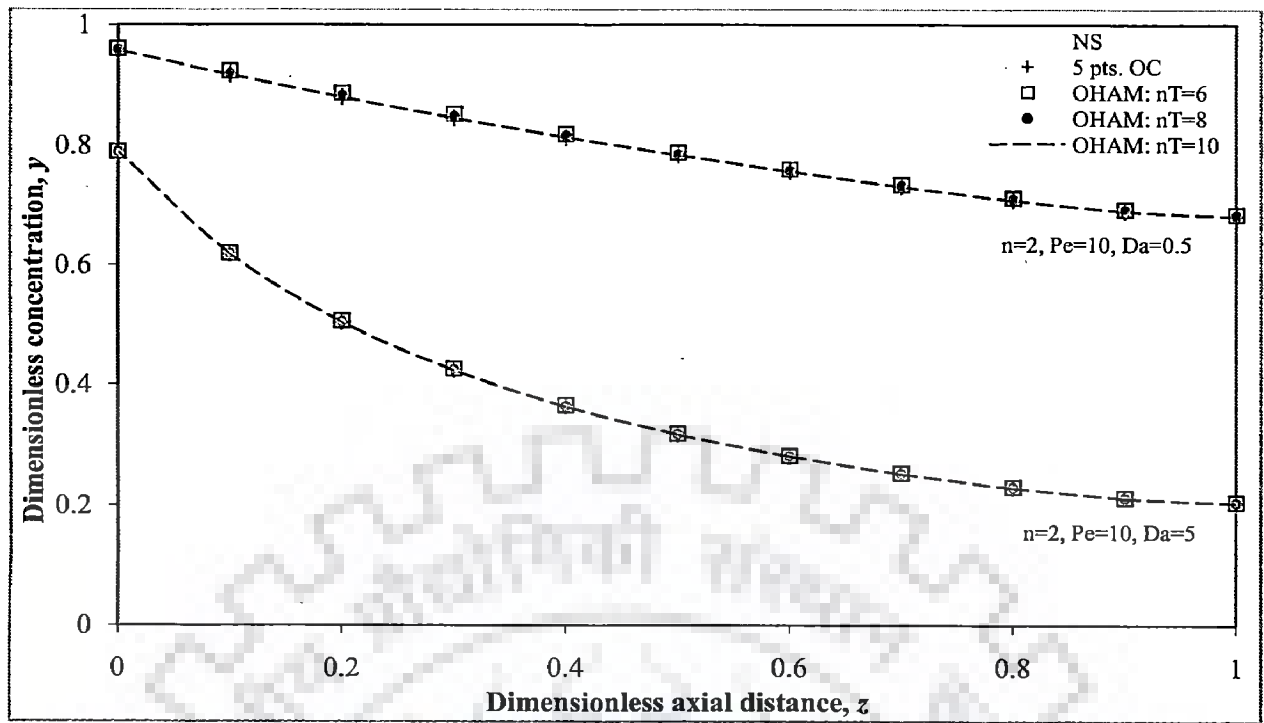
Figure 6.16: Dimensionless concentration profiles for the parameter values given in Freeman and Houghton (1966) [power-law kinetics: $n = 2$, $Pe = 10$, $Da = 0.5$; $n = 2$, $Pe = 10$, $Da = 5$]
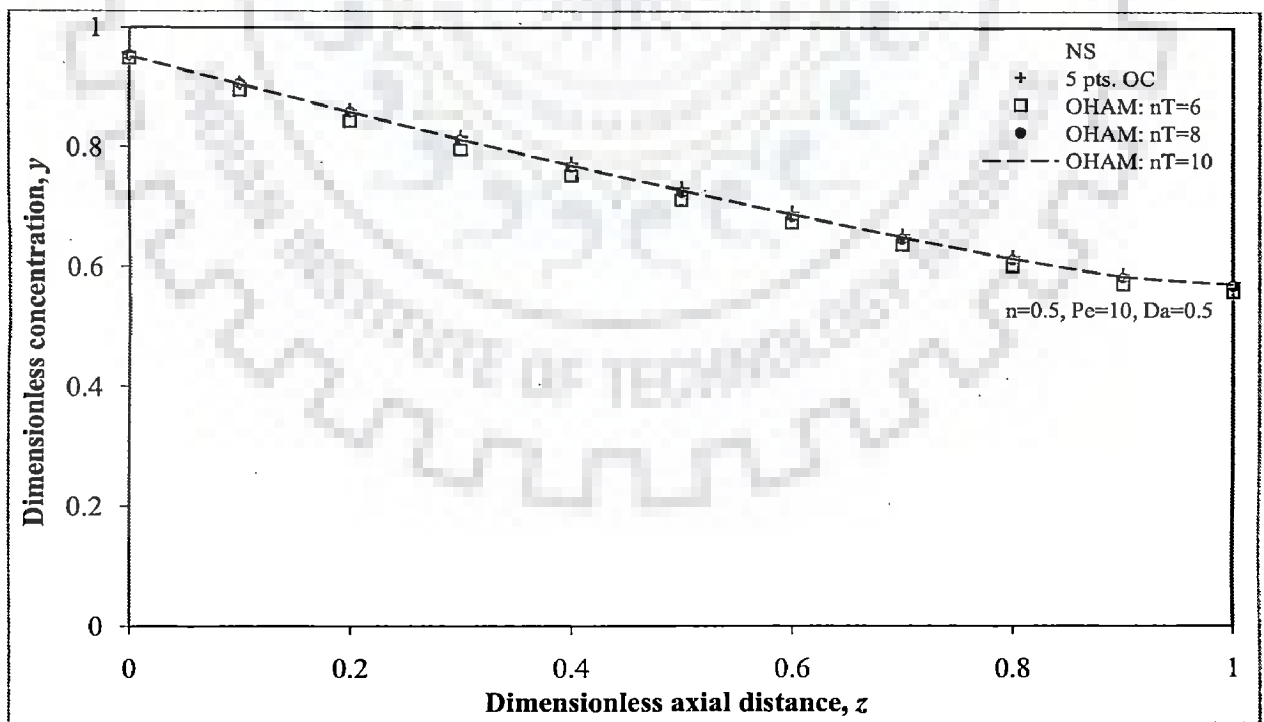
Figure 6.17: Dimensionless concentration profiles for the parameter values given in Freeman and Houghton (1966) [power-law kinetics: $n = 0.5$, $Pe = 10$, $Da = 0.5$]

353
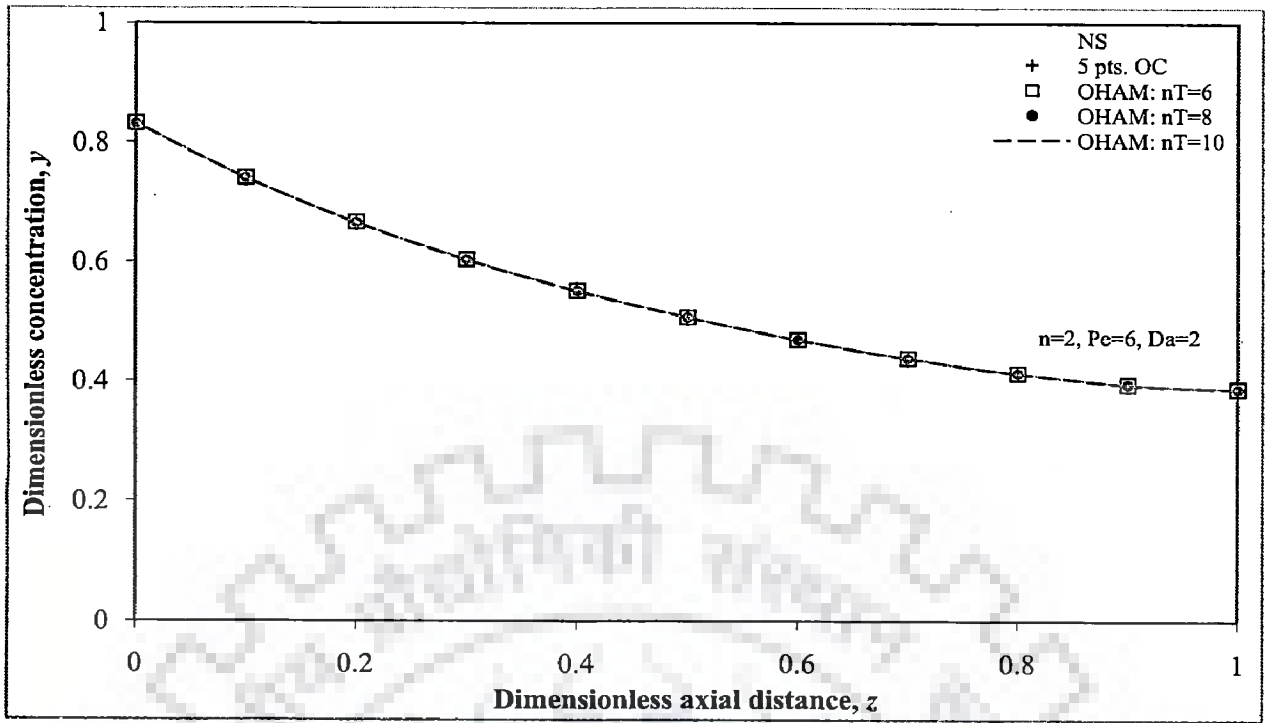
Figure 6.18: Dimensionless concentration profiles for the parameter values given in Lee (1966) [power-law kinetics: $n = 2$, $Pe = 6$, $Da = 2$]
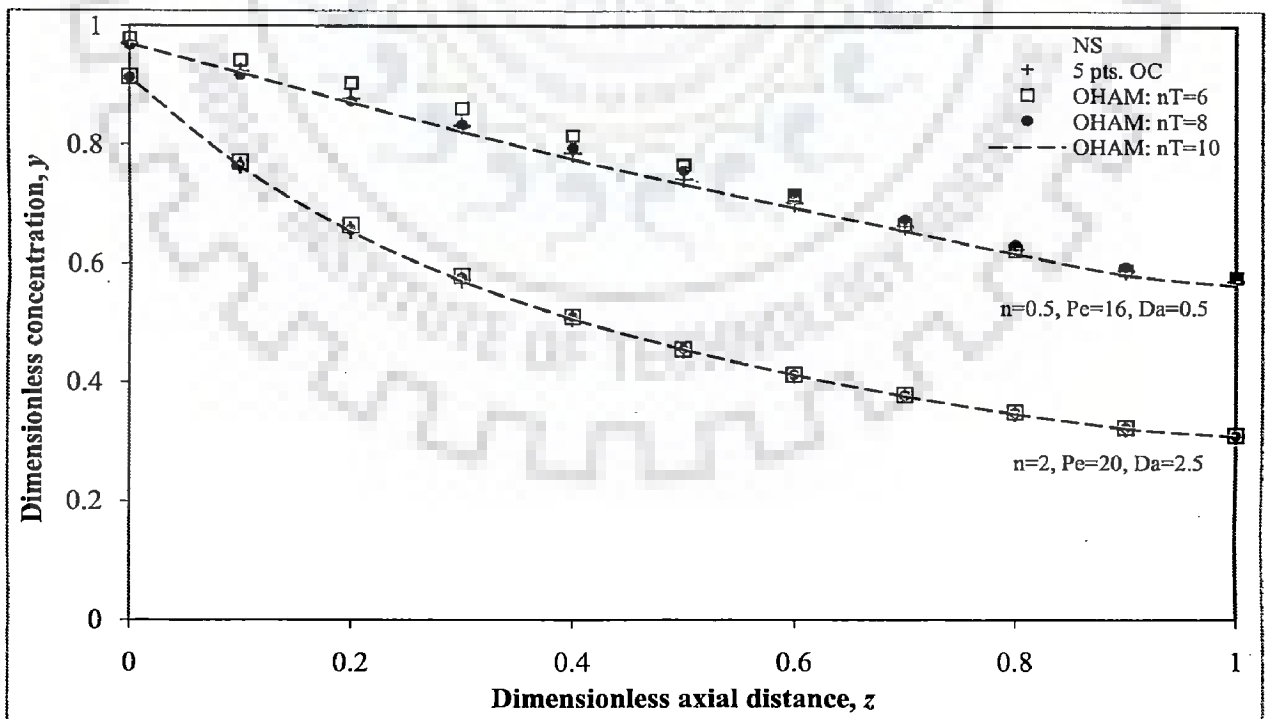
Figure 6.19: Dimensionless concentration profiles for the parameter values given in Burghardt and Zaleski (1968) [power-law kinetics: $n = 0.5$, $Pe = 16$, $Da = 0.5$; $n = 2$, $Pe = 20$, $Da = 2.5$]
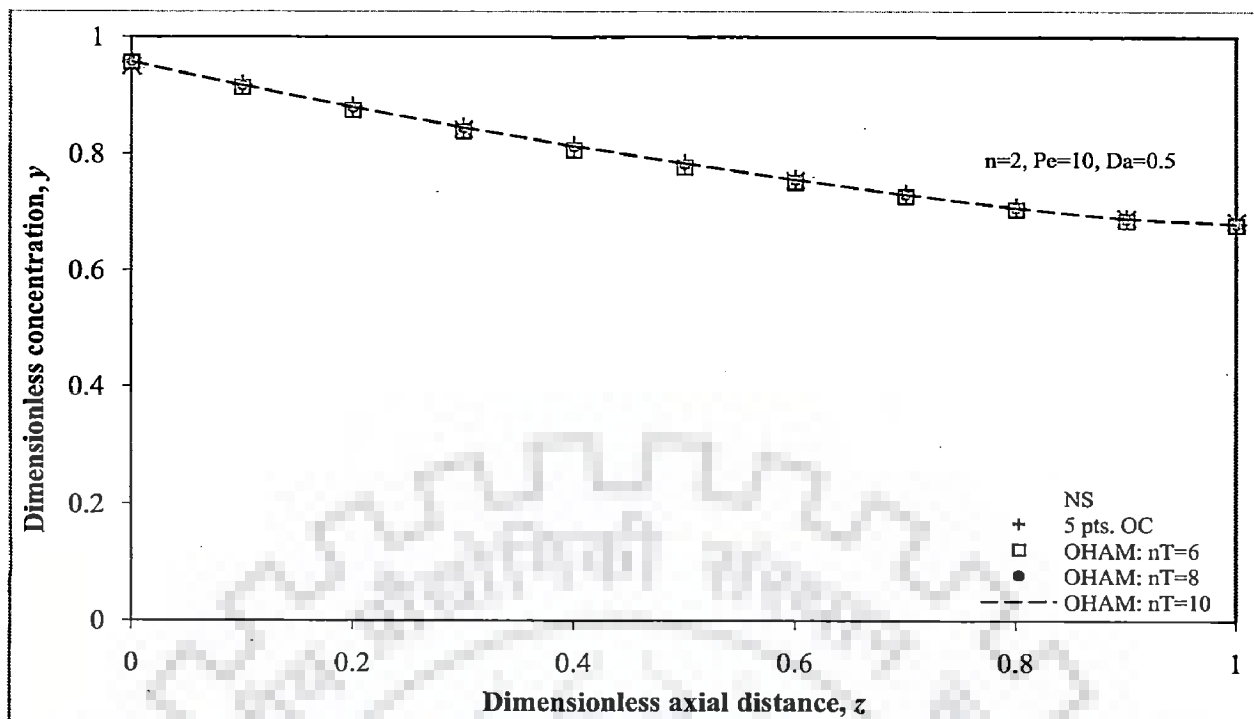
Figure 6.20: Dimensionless concentration profiles for the parameter values given in Wissler (1969) [power-law kinetics: $n = 2$, $Pe = 10$, $Da = 0.5$]
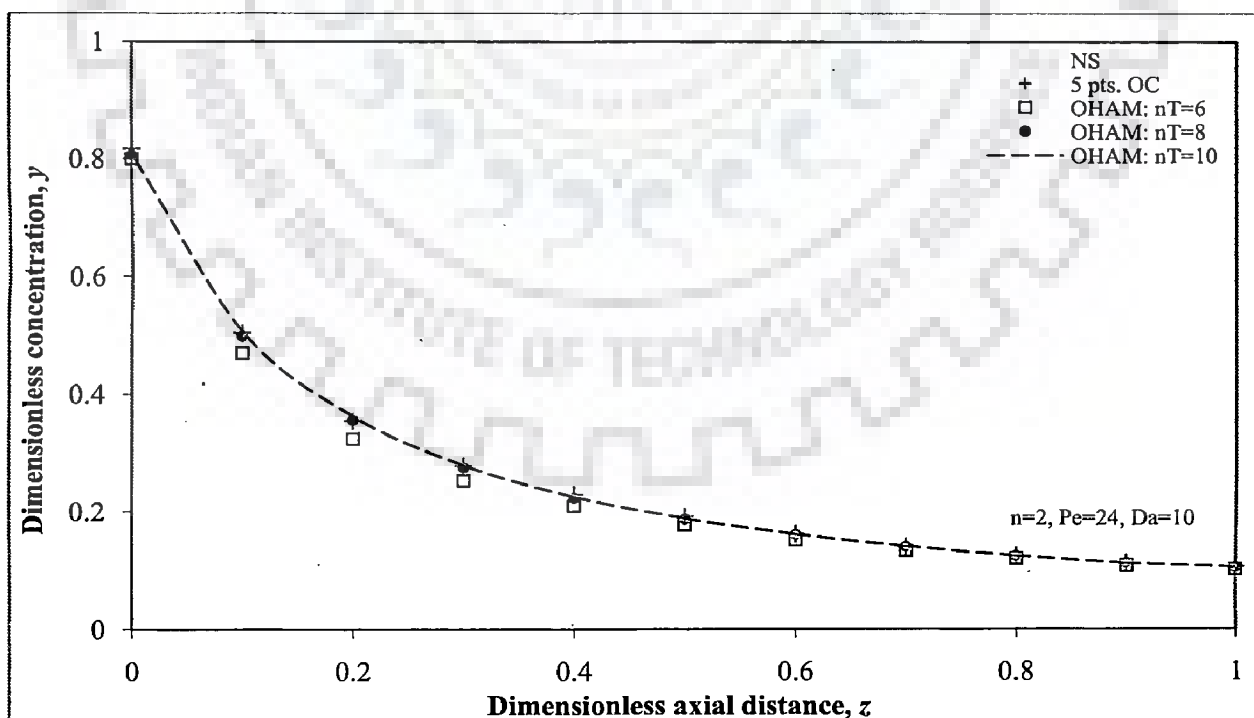
Figure 6.21: Dimensionless concentration profiles for the parameter values given in Wan and Zeigler (1970) [power-law kinetics: $n = 2$, $Pe = 24$, $Da = 10$]

357
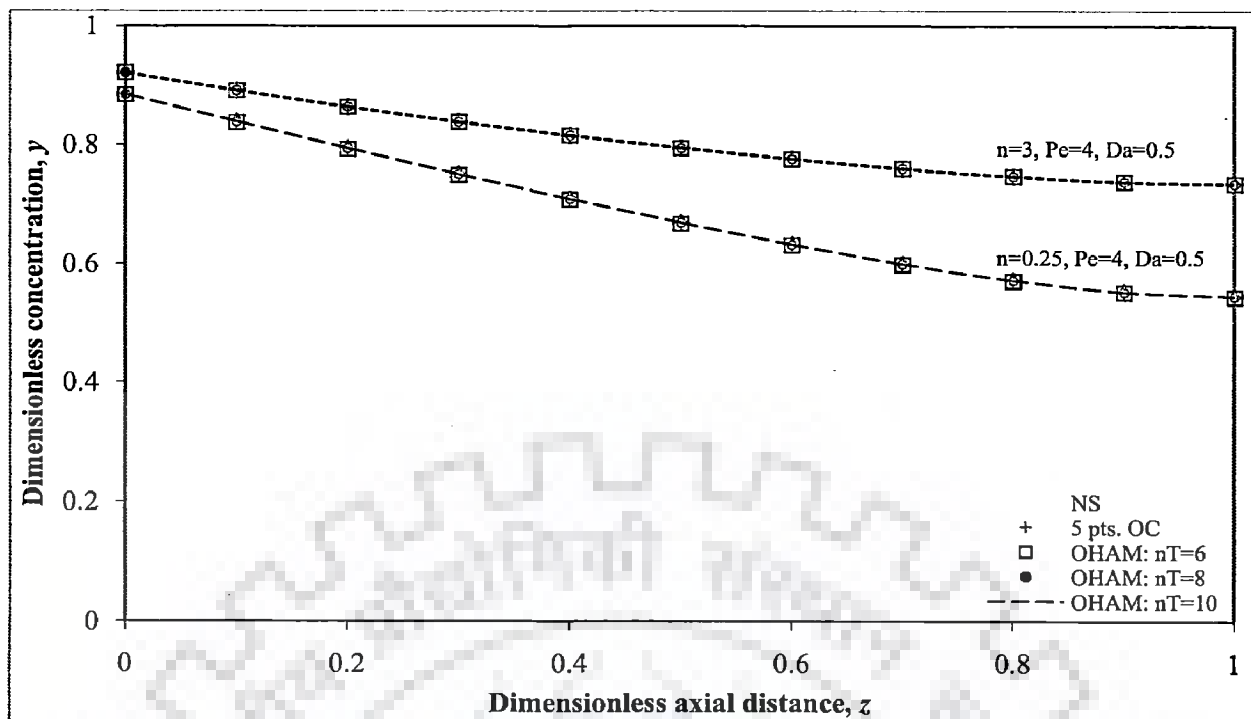
Figure 6.22: Dimensionless concentration profiles for the parameter values given in Fan et al. (1971) [power-law kinetics: $n = 3$, $Pe = 4$, $Da = 0.5$; $n = 0.25$, $Pe = 4$, $Da = 0.5$]
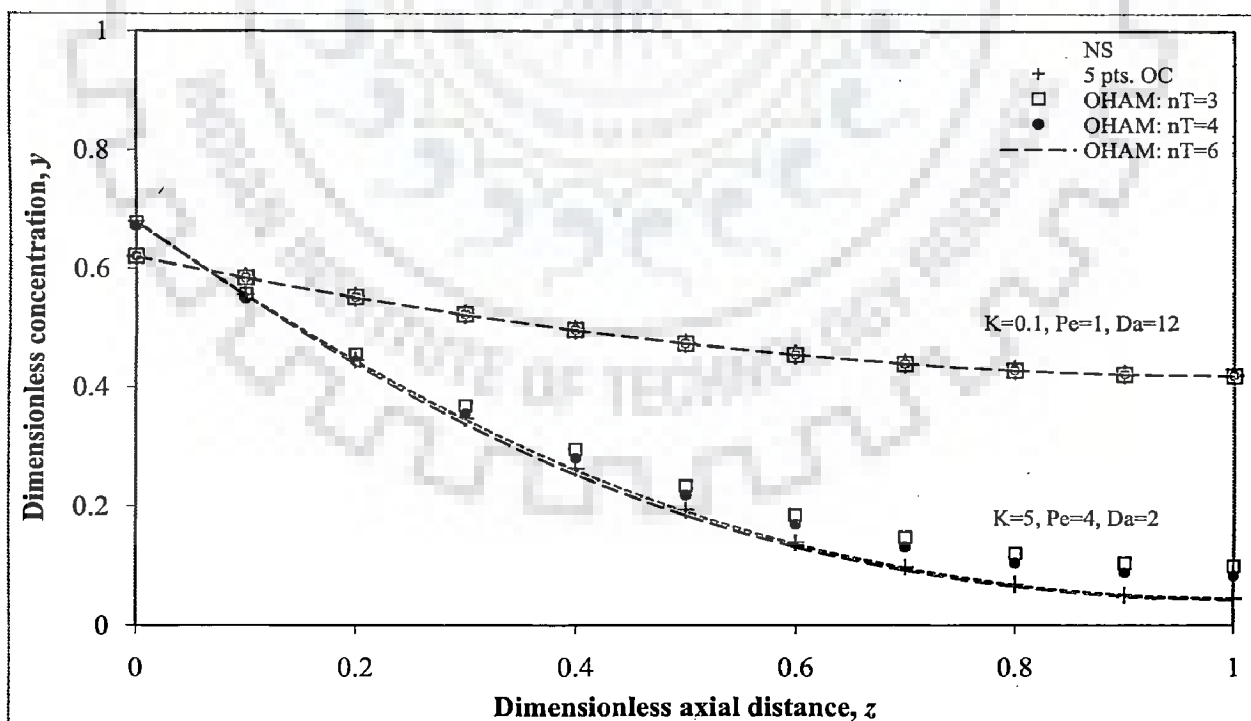
Figure 6.23: Dimensionless concentration profiles for the parameter values given in Fan et al. (1971) [Langmuir-Hinshelwood kinetics: $K = 0.1$, $Pe = 1$, $Da = 12.5$; $K = 5$, $Pe = 4$, $Da = 2$]
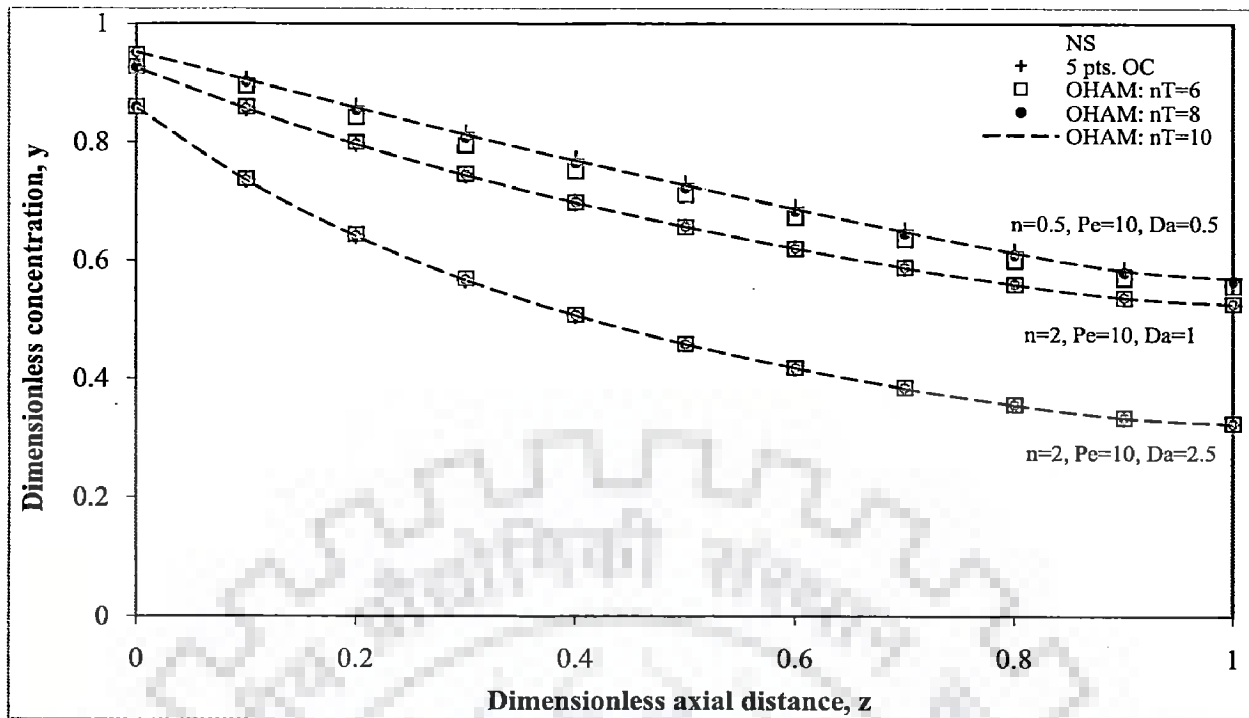
Figure 6.24: Dimensionless concentration profiles for the parameter values given in Shah and Paraskos (1975) [power-law kinetics: $n = 0.5$, $Pe = 10$, $Da = 0.5$; $n = 2$, $Pe = 10$, $Da = 1$; $n = 2$, $Pe = 10$, $Da = 2.5$]
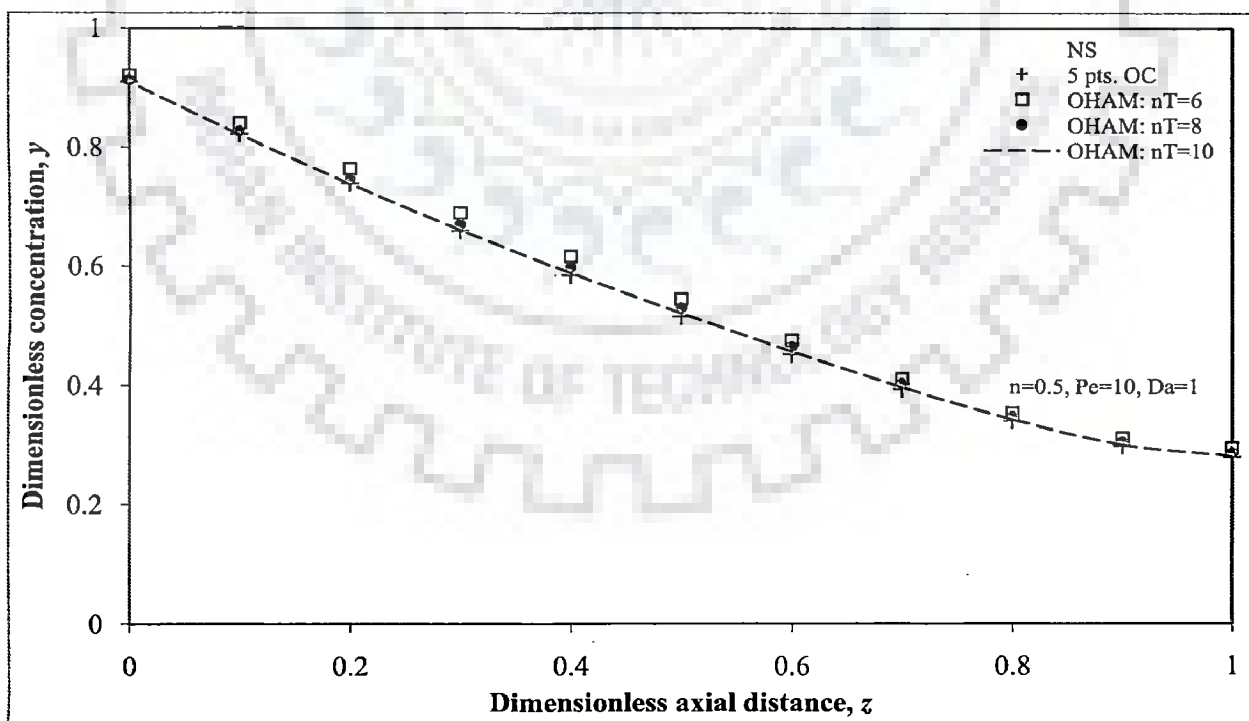
Figure 6.25: Dimensionless concentration profiles for the parameter values given in Marek and Stuchl (1975) [power-law kinetics: $n = 0.5$, $Pe = 10$, $Da = 1$]

361
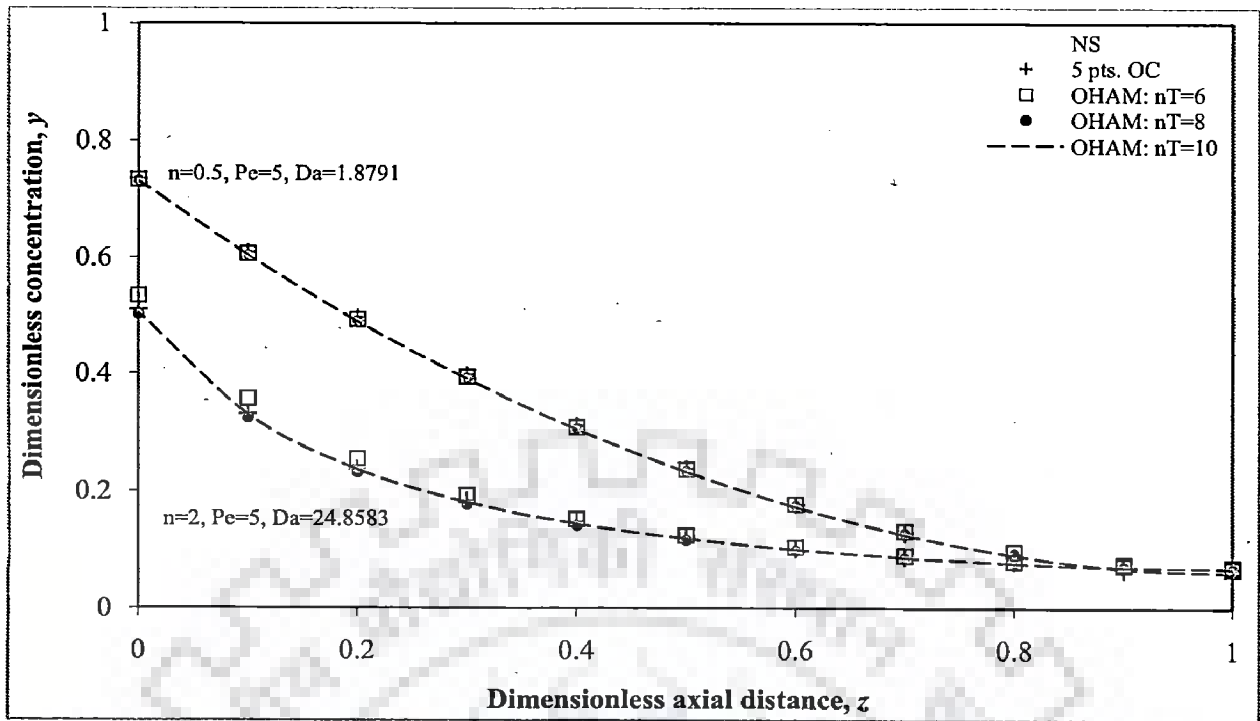
Figure 6.26: Dimensionless concentration profiles for the parameter values given in Kubicek and Hlavacek (1983) [power-law kinetics: $n = 0.5$, $Pe = 5$, $Da = 1.8791$; $n = 2$, $Pe = 5$, $Da = 24.8583$]
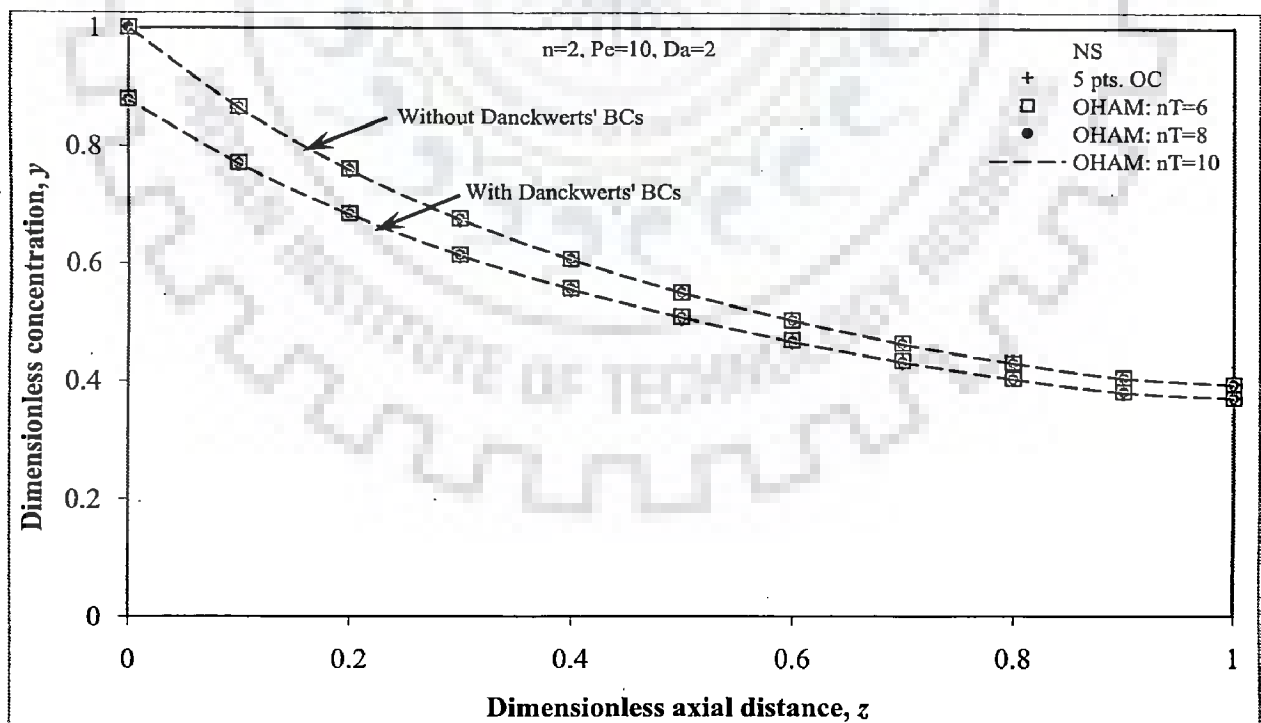
Figure 6.27: Dimensionless concentration profiles for the parameter values given in Rao et al. (1981) [power-law kinetics: $n = 2$, $Pe = 10$, $Da = 2$]
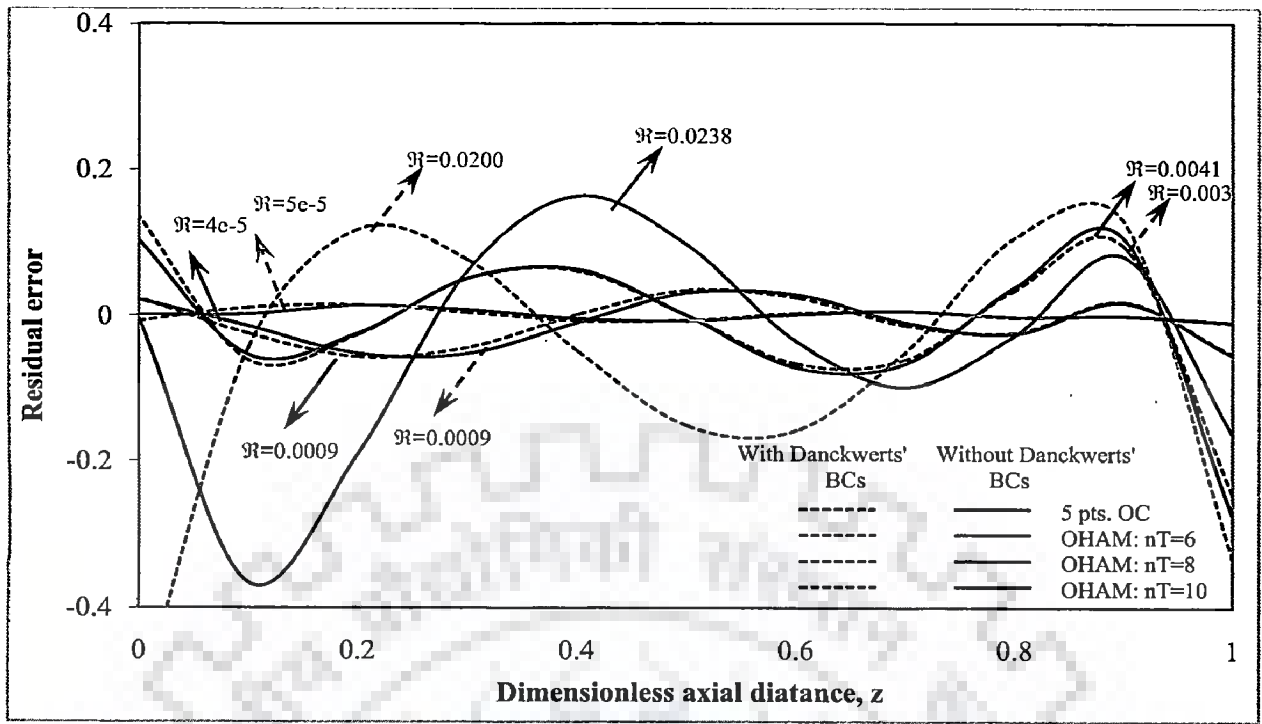
Figure 6.28: Residual error profiles for the parameter values given in Rao et al. (1981) [power-law kinetics: $n = 2$, $Pe = 10$, $Da = 2$]
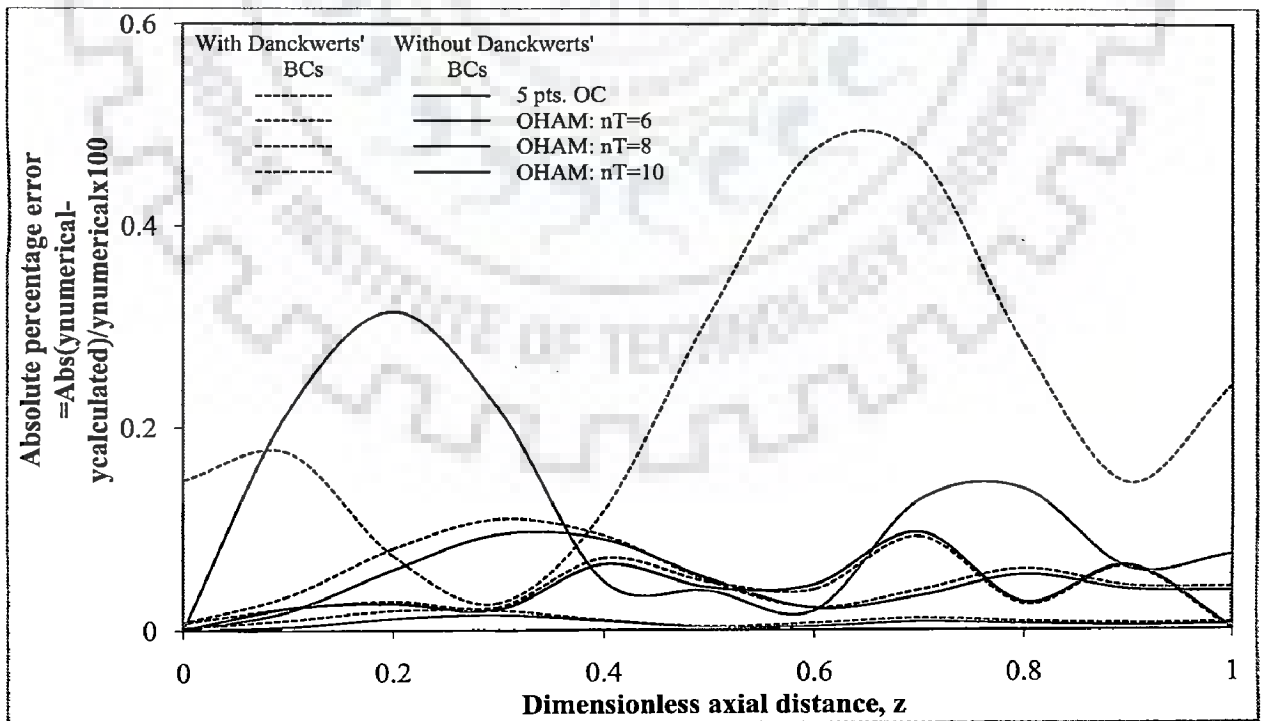
Figure 6.29: Absolute percentage error profiles for the parameter values given in Rao et al. (1981) [power-law kinetics: $n = 2$, $Pe = 10$, $Da = 2$]

(i) Exit concentration

Sometimes, one is interested only in the exit concentration and fortunately, exit concentration can easily be found by substituting $x=0$ in OHAM solution, i.e. Eq. (6.19), and is given by:

$$y(0) \approx y_{OHAM}(0) = C_2 \qquad (6.49a)$$

It should, however, be noted that for different n_T the value of C_2 will differ slightly. This is because, for different n_T the OHAM will have different solutions, which while satisfying BC I, give rise to somewhat different values of C_2. But as expected, the value of C_2 approaches to the true value as the terms in OHAM solutions are increased.

(ii) Inlet concentration

Like the exit concentration, the entrance concentration can also be found from the OHAM solution by substituting $x=1$. For $n_T = 5$, the inlet concentration is given below:

$$y(1) \approx y_{OHAM}(1)$$

$$= C_2 - 2C_2^n DaPeh - \frac{1}{4}(C_2^{n-1}DaPe(12C_2 + 4C_2Pe - C_2^n DanPe))h^2$$

$$- \frac{1}{180}\Big(C_2^{n-2}DaPe(360C_2^2 + 240C_2^2 Pe - 60C_2^{n+1}DanPe + 30C_2^2 Pe^2 - 12C_2^{n+1}DanPe^2$$

$$-3C_2^{2n}Da^2nPe^2 + 4C_2^{2n}Da^2n^2Pe^2)\Big)h^3 + \frac{1}{40320}\Big(-20160C_2^n DaPe - 20160C_2^n DaPe^2$$

$$+ 5040C_2^{2n-1}Da^2nPe^2 - 5040C_2^n DaPe^3 + 2016C_2^{2n-1}Da^2nPe^3 + 504C_2^{3n-2}Da^3nPe^3$$

$$- 672C_2^{3n-2}Da^3n^2Pe^3 - 336C_2^n DaPe^4 + 168C_2^{2n-1}Da^2nPe^4 + 104C_2^{3n-2}Da^3nPe^4$$

$$+ 30C_2^{4n-3}Da^4nPe^4 - 128C_2^{3n-2}Da^3n^2Pe^4 - 63C_2^{4n-3}Da^4n^2Pe^4 + 34C_2^{4n-3}Da^4n^3Pe^4\Big)h^4$$

$$(6.49b)$$

For some of the parameters' values, Table 6.6 compares the inlet/outlet concentrations predicted by the OHAM solutions with those obtained by using the orthogonal collocation solutions as well as with those available in literature. A reasonably close match is found between these values; the accuracy of OHAM solutions can be increased by considering more terms.

(iii)   Comparison between the OHAM solution and the analytical solution for first order and zero order kinetics

It is also worthwhile to compare the OHAM solution with the available analytical solution for first order kinetics $[n=1]$. The analytical solution of Eqs. (6.43a)–(6.43c) [axial coordinate reversed] for the first order reaction is given by (Fogler, 1992):

$$y_{Analytical} = e^{\frac{Pe(1-x)}{2}} \frac{qcosh\left[\frac{qx}{2}\right] + Pe\,sinh\left[\frac{qx}{2}\right]}{qcosh\left[\frac{q}{2}\right] + (Pe+2Da)sinh\left[\frac{q}{2}\right]} \qquad (6.50)$$

where $q = \sqrt{Pe}\sqrt{Pe+4Da}$. The Taylor series expansion of the above solution around $x=0$, $Pe=0$ and $Da=0$ is given by the following series:

$$y_{Analytical} \approx 1 - Da + Da^2 - Da^3 - \frac{Da^2 Pe}{6} + \frac{Da^3 Pe}{3} + \frac{Da^2 Pe^2}{24} - \frac{11Da^3 Pe^2}{120} - \frac{Da^2 Pe^3}{120} +$$

$$\frac{7Da^3 Pe^3}{360} + \frac{DaPex^2}{2} - \frac{Da^2 Pex^2}{2} + \frac{Da^3 Pex^2}{2} - \frac{Da^3 Pe^2 x^2}{12} + \frac{Da^3 Pe^3 x^2}{48} -$$

$$\frac{DaPe^2 x^3}{6} + \frac{Da^2 Pe^2 x^3}{6} - \frac{Da^3 Pe^2 x^3}{6} + \frac{Da^3 Pe^3 x^3}{36} + ... \qquad (6.51)$$

Now, if one substitutes $h=-1$ in the five terms OHAM solution [Eq. (6.47)], the following series is obtained:

$$y_{OHAM} = C_2 + \frac{C_2 DaPe}{2}x^2 - \frac{C_2 DaPe^2}{6}x^3 + \frac{C_2 Da^2 Pe^2}{24}x^4 + \frac{C_2 DaPe^3}{24}x^4 - \frac{C_2 Da^2 Pe^3}{60}x^5 -$$

$$\frac{C_2 DaPe^4}{120}x^5 + \frac{C_2 Da^3 Pe^3}{720}x^6 + \frac{C_2 Da^2 Pe^4}{240}x^6 - \frac{C_2 Da^3 Pe^4}{1680}x^7 + \frac{C_2 Da^4 Pe^4}{40320}x^8$$

Table 6.6: Comparative summary of inlet/outlet reactant concentration obtained by different methods

Entrance [x=1]/Exit [x=0] Concentration	Parameters' Values n, Pe, Da	Five points collocation solution	Method (Reference)	OHAM		
				$n_T = 6$	$n_T = 8$	$n_T = 10$
			Perturbation method (Burghardt and Zaleski, 1968)			
y(0)	2; 20, 2.5	0.3076	0.307	0.3087	0.3082	0.3077
y(0)	0.5, 16, 0.5	0.5686	0.569	0.5747	0.5765	0.5621
			Numerical method (Wan and Ziegler, 1970)			
y(0)	2, 24, 10	0.1048	0.1048	0.1006	0.1043	0.1050
			Collocation method (Fan et al., 1971)			
y(0)	0.25, 4, 0.5	0.5463	0.5463	0.5445	0.5458	0.5462
y(1)		0.8846	0.8846	0.8833	0.8843	0.8846
y(0)	3, 4, 0.5	0.7351	0.7351	0.7349	0.7351	0.7351
y(1)		0.9211	0.9211	0.9209	0.9211	0.9211
			Perturbation method (Ray et al., 1972)			
y(0)	1, 50, 10	0.00019	0.00019	0.00019	0.00019	0.00019
			Perturbation method (Marek and Stuchl, 1975)			
y(0)	0.5, 10, 1	0.2779	0.2763	0.2922	0.2852	0.2803
			Collocation method (Shah and Paraskos, 1975)			
y(0)	2, 10, 1	0.5272	0.5115	0.5275	0.5276	0.5271
y(0)	2, 10, 2.5	0.3244	0.2791	0.3249	0.3245	0.3244
y(0)	0.5, 10, 0.5	0.5717	0.5739	0.5566	0.5665	0.5698
			Collocation method with quasi-linearization (Rao et al., 1981)			
y(0)	2, 10, 2	0.3705	0.3675	0.3714	0.3707	0.3705
y(1)		0.8775	0.8787	0.8788	0.8775	0.8774

where C_2 is found from the BC I and is given by:

$$C_2 = \left(\frac{1}{40320} \left(\begin{array}{l} 40320 + 40320 Da + 6720 Da^2 Pe - 1680 Da^2 Pe^2 + 336 Da^3 Pe^2 \\ +336 Da^2 Pe^3 - 112 Da^3 Pe^3 + 8 Da^4 Pe^3 - 336 DaPe^4 + 168 Da^2 Pe^4 \\ -24 Da^3 Pe^4 + Da^4 Pe^4 \end{array} \right) \right)^{-1}$$

Substituting the value of C_2 in y_{OHAM} and expanding the resultant around $x = 0$, $Pe = 0$ and $Da = 0$ by using the Taylor series method, one obtains the following expansion:

$$y_{OHAM} \approx 1 - Da + Da^2 - Da^3 - \frac{Da^2 Pe}{6} + \frac{Da^3 Pe}{3} + \frac{Da^2 Pe^2}{24} - \frac{11 Da^3 Pe^2}{120} - \frac{Da^2 Pe^3}{120} +$$

$$\frac{7 Da^3 Pe^3}{360} + \frac{DaPex^2}{2} - \frac{Da^2 Pex^2}{2} + \frac{Da^3 Pex^2}{2} - \frac{Da^3 Pe^2 x^2}{12} + \frac{Da^3 Pe^3 x^2}{48} -$$

$$\frac{DaPe^2 x^3}{6} + \frac{Da^2 Pe^2 x^3}{6} - \frac{Da^3 Pe^2 x^3}{6} + \frac{Da^3 Pe^3 x^3}{36} + \dots \qquad (6.52)$$

It is clearly evident that both the series expansions, i.e. Eqs. (6.51) and (6.52), match well and thus proves the validity of OHAM solution. Fig. 6.30 shows the dimensionless concentration profile obtained by using OHAM and numerical method for the parameters' values given in Ray et al. (1972), i.e. $n = 1$, $Pe = 50$ and $Da = 10$. A close agreement is observed between the OHAM solutions and those obtained by numerical method.

The above discussion is also true for the zero order kinetics $[n = 0]$. For zero order kinetics, the analytical solution of Eqs. (6.43a) - (6.43c) is given by:

$$y_{Analytical} = \frac{Da\left(e^{-Pex} - 1\right) + Pe + Pe Da(x - 1)}{Pe} \qquad (6.53)$$

Expanding the above solution around $x = 0$, $Pe = 0$ and $Da = 0$ by using Taylor series method, one finds the following series expansion:

$$y_{Analytical} \approx 1 - Da + \frac{DaPe}{2} x^2 - \frac{DaPe^2}{6} x^3 + \frac{DaPe^3}{24} x^4 - \frac{DaPe^4}{120} x^5 + \frac{DaPe^5}{720} x^6 + \dots$$

$$(6.54)$$

For $n_T = 10$ and $h = -1$, the OHAM solution is found by following the same steps as were followed for first order kinetics [the relevant steps are shown in Appendix C2]. The Taylor series expansion of y_{OHAM} around $x = 0$, $Pe = 0$ and $Da = 0$ is given below, which is exactly the same as the one obtained for the analytical solution. Thus, the correctness of OHAM solution is verified again.

$$y_{OHAM} \approx 1 - Da + \frac{DaPe}{2} x^2 - \frac{DaPe^2}{6} x^3 + \frac{DaPe^3}{24} x^4 - \frac{DaPe^4}{120} x^5 + \frac{DaPe^5}{720} x^6 + \ldots$$

(6.55)

Fig. 6.31 shows the dimensionless concentration profile obtained by OHAM for $n = 0$, $Pe = 10$ and $Da = 4$ along with the numerically obtained profiles; here also a close conformity is observed. It should be noted that for zero order reaction, the reactant concentration can become zero prior to the exit of the reactor, and therefore, the above solution expressions [Eqs. (6.53)-(6.55)] become invalid. However, in such situations, one can obtain the analytical and OHAM solutions by employing the following BCs, in addition to the BC I:

BC II: $\dfrac{dy}{dx} = 0$ at $x = \delta$ [at some position inside the reactor]

BC III: $y = 0$ at $x = \delta$ [at some position inside the reactor]

where δ [$0 \le \delta < 1$] is a position in the reactor where reactant vanishes [$y = 0$] and can be found by using the additional BC III.

(iv) Dual solutions by OHAM: negative order kinetics

The utility of OHAM is also illustrated by capturing the multiple solutions exhibited by the axial dispersion model of a tubular chemical reactor sustaining a negative order reaction. Such rate expressions generally appear in the higher concentration ranges of the dual site kinetics of Langmuir-Hinshelwood type occurring on a catalytic surface. For example, the catalytic dehydrogenation of alcohols over zeolite for the production of olefins, and the oxidation of carbon monoxide over Pt catalyst is given by (Elnashaie and Abashar, 1990):

371

$$-r_A = \frac{kC_A}{(1+K_A C_A)^2} \quad \text{and} \quad -r_A = \frac{kC_A C_B}{(1+K_A C_A)^2}$$

For higher values of C_B and $K_A C_A$, the above rate expressions reduce to a negative reaction order kinetics [$n=-1$] and because of this non-monotonic reaction rate, the possibility of more than one solution exists. For a simple situation of unit effectiveness factor, and for the stated limiting situation of higher C_B and higher $K_A C_A$ in the above kinetics, the Eq. (6.43a) becomes:

$$\frac{d^2 y}{dx^2} + Pe \frac{dy}{dx} - Pe\,Da\,y^{-1} = 0 \qquad (6.56)$$

The concerned BCs [Eqs. (6.43b) and (6.43c)] remain the same. It can be numerically examined that for some region of the parameter space, the above equation exhibits (i) single solution (ii) dual solutions, and (iii) no solution. The single or dual solutions can also be found with the help of shooting or the weighted residual methods (Villadsen and Michelsen, 1978; Finlayson, 1980; Kubicek and Hlavacek, 1983). Here we have obtained the dual solutions, existing for some of the parameters' values, by using OHAM. However, before finding the dual solutions of Eq. (6.56), we first analyze the two extreme situations displayed by the axial dispersion model of a tubular chemical reactor. These situations are represented by the two ideal reactors namely PFR [plug flow reactor] and CSTR [continuous stirred tank reactor]. It can also be noted that the model equations of these two ideal reactors incorporate only one of the parameters [Da] since, the degree of mixing, described in axial dispersion model by the remaining parameter [Pe], lies at the extreme border lines, i.e. no mixing [$Pe=\infty$ for PFR] and maximum mixing [$Pe=0$ for CSTR].

(a) Plug flow reactor [$Pe=\infty$]

The model equation of a PFR can directly be deduced from the axial dispersion model equation of a tubular chemical reactor by substituting $Pe=\infty$ and for negative order kinetics [$n=-1$], it is given by the following dimensionless equation. It should, however, be noted that in the following equation, the axial coordinate is reversed so that the consistency is maintained for comparing the solution with that of axial dispersion
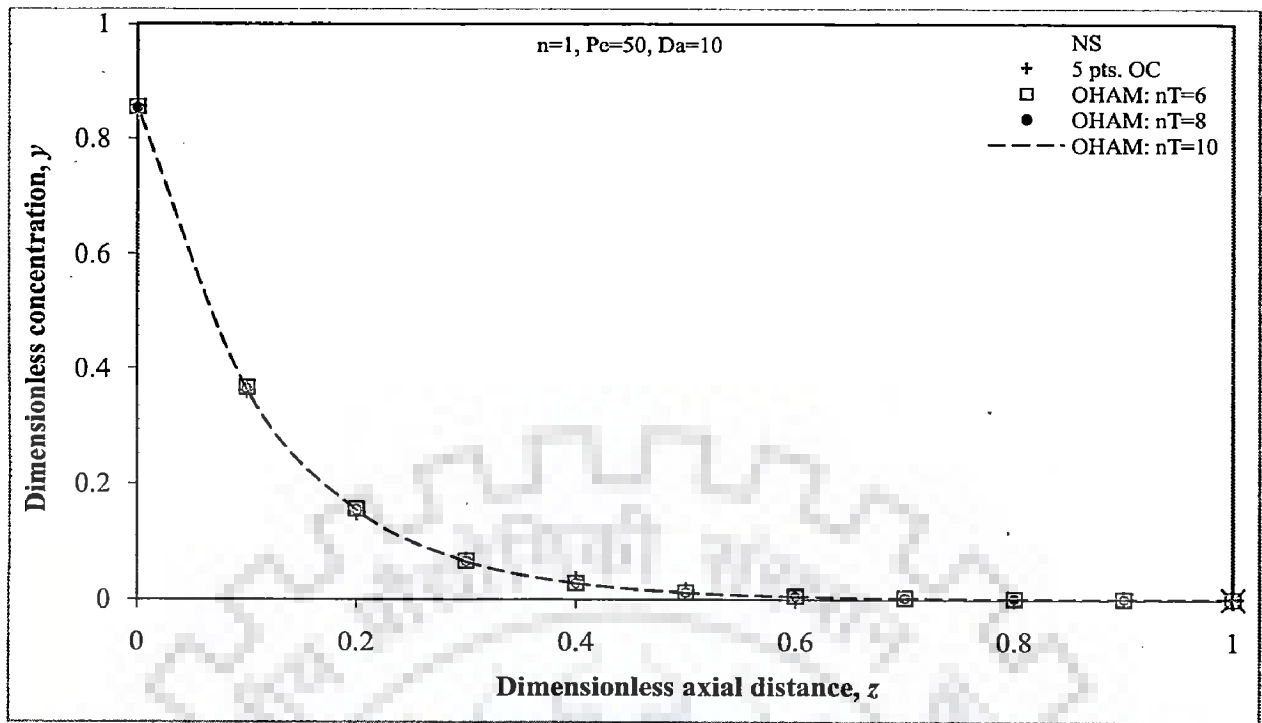
Figure 6.30: Dimensionless concentration profiles for the parameter values given in Ray et al. (1972) [first order kinetics: $Pe = 50$, $Da = 10$]
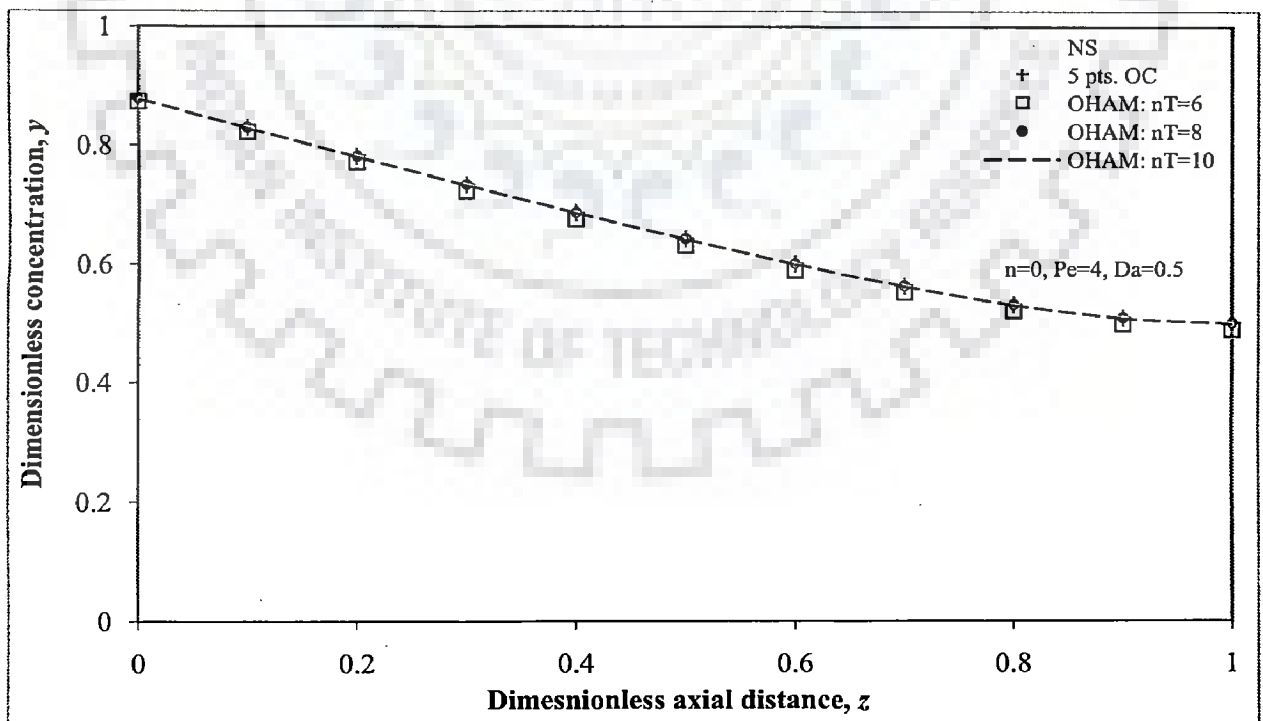
Figure 6.31: Dimensionless concentration profiles [zero order kinetics: $Pe = 4$, $Da = 0.5$]

model of a tubular chemical reactor. The discussion that follows will not be effected by the shifting of coordinates.

$$\frac{dy}{dx} - Da\, y^{-1} = 0; \quad y(1) = 1 \text{ and } x \in [0,1] \tag{6.57}$$

The Eq. (6.57) is amenable to the following analytical solution:

$$y = \sqrt{1 - 2Da + 2Da\, x} \qquad \text{with } x \in [0,1] \tag{6.58}$$

From the above equation, it can be seen that the real and single solution exists for $0 \le Da \le 0.5$ only, and for $Da > 0.5$ no physically realistic solution will exist.

(b)   Ideal CSTR [$Pe = 0$]

For $n = -1$, the model equation of an ideal CSTR is given by the following dimensionless equation:

$$1 - y = Da\, y^{-1} \tag{6.59}$$

Unlike PFR, the above equation bears following two analytical solutions:

$$y = \frac{1 - \sqrt{1 - 4Da}}{2} \tag{6.60a}$$

and

$$y = \frac{1 - \sqrt{1 + 4Da}}{2} \tag{6.60b}$$

It can be easily verified that for $Da < 0.25$ two real solutions exist, for $Da = 0.25$ only single solution exists, whereas, for $Da > 0.25$ no real solution exists.

(c)   Axial dispersion model [$0 < Pe < \infty$]

Since, the predictions of axial dispersion model lie between the above two limiting cases, hence, for some of the values of parameters, the axial dispersion model

may yield single, dual or no solutions for $n = -1$. The above results of two ideal reactors lead to the following conclusions for axial dispersion model:

- Irrespective of the value of Pe, no real solution can be found for $Da > 0.5$.

- For an ideal CSTR [$Pe = 0$], dual solutions can be found for $Da < 0.25$.

- For axial dispersion model, there is every likelihood of multiple solutions for Pe close to zero [for smaller Pe]. However, as Pe is increased, then at some value of Pe, dual solutions would converge into one, and thus would yield single solution thereafter. The boundary of Pe that decides the existence of single or dual solutions in the region $0 < Da < 0.25$, depends on the value of Da.

(d)   Dual solutions by OHAM

Basically, the same steps of OHAM are followed that were followed earlier while finding the single solution and thus the same solution expression corresponding to the Eq. (6.47) is obtained. However, now two different sets of C_2 and h are obtained while solving the Eqs. (6.48) and (6.9c), which in turn give rise to the dual solutions. For example, by solving the Eqs. (6.48) and (6.9c) for $n = -1$, $Pe = 1/5$ and $Da = 1/5$, the five terms OHAM solution [Eqs. (6.47)] yield the following two sets of C_2 and h:

$$C_2 = 0.238931, h = -0.822218 \text{ and } C_2 = 0.728762, h = -0.968018$$

The corresponding dual solutions [five terms OHAM solutions] are:

First solution [$C_2 = 0.238931, h = -0.822218$]

$$y_{OHAM} = 0.238931 + 0.083623x^2 - 0.005472x^3 - 0.004554x^4$$

$$+ 0.000328x^5 + 0.000672x^6 - 0.000043x^7 - 0.000083x^8 \quad (6.61a)$$

Second solution [$C_2 = 0.728762, h = -0.968018$]
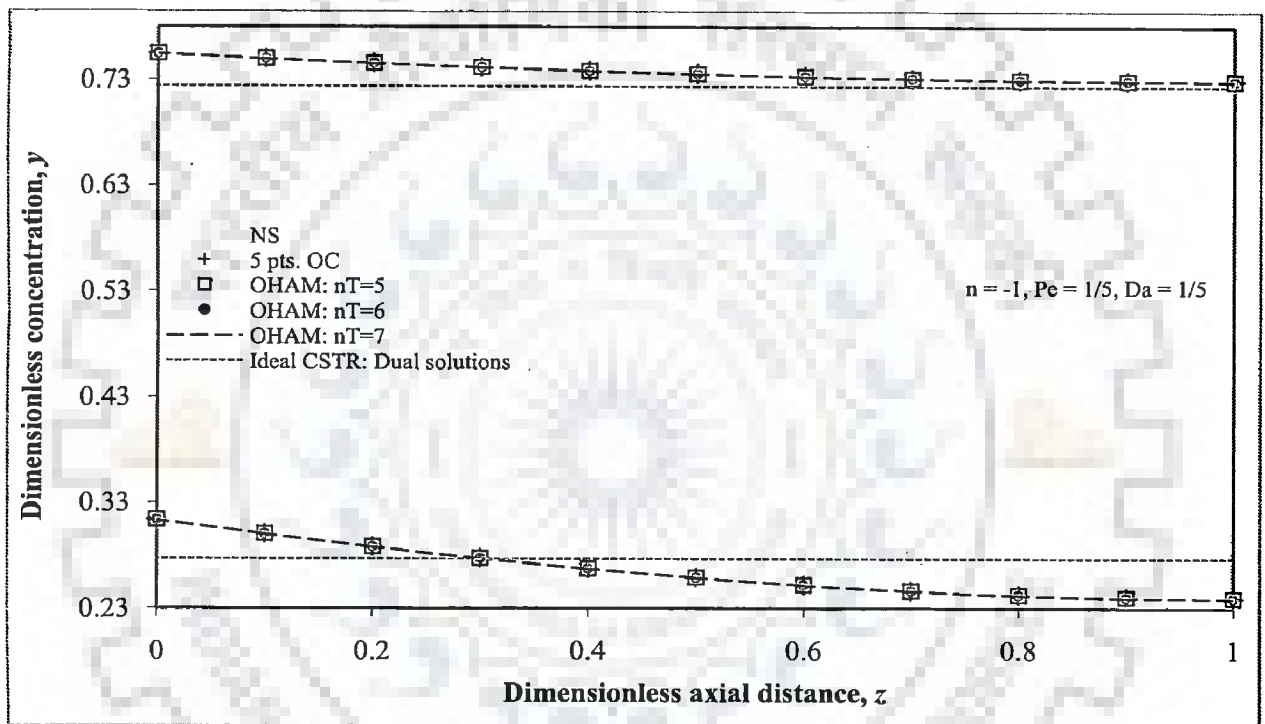
Figure 6.32: Dimensionless dual concentration profiles [non-monotonic power-law kinetics: $n = -1$, $Pe = 0.2$, $Da = 0.2$]
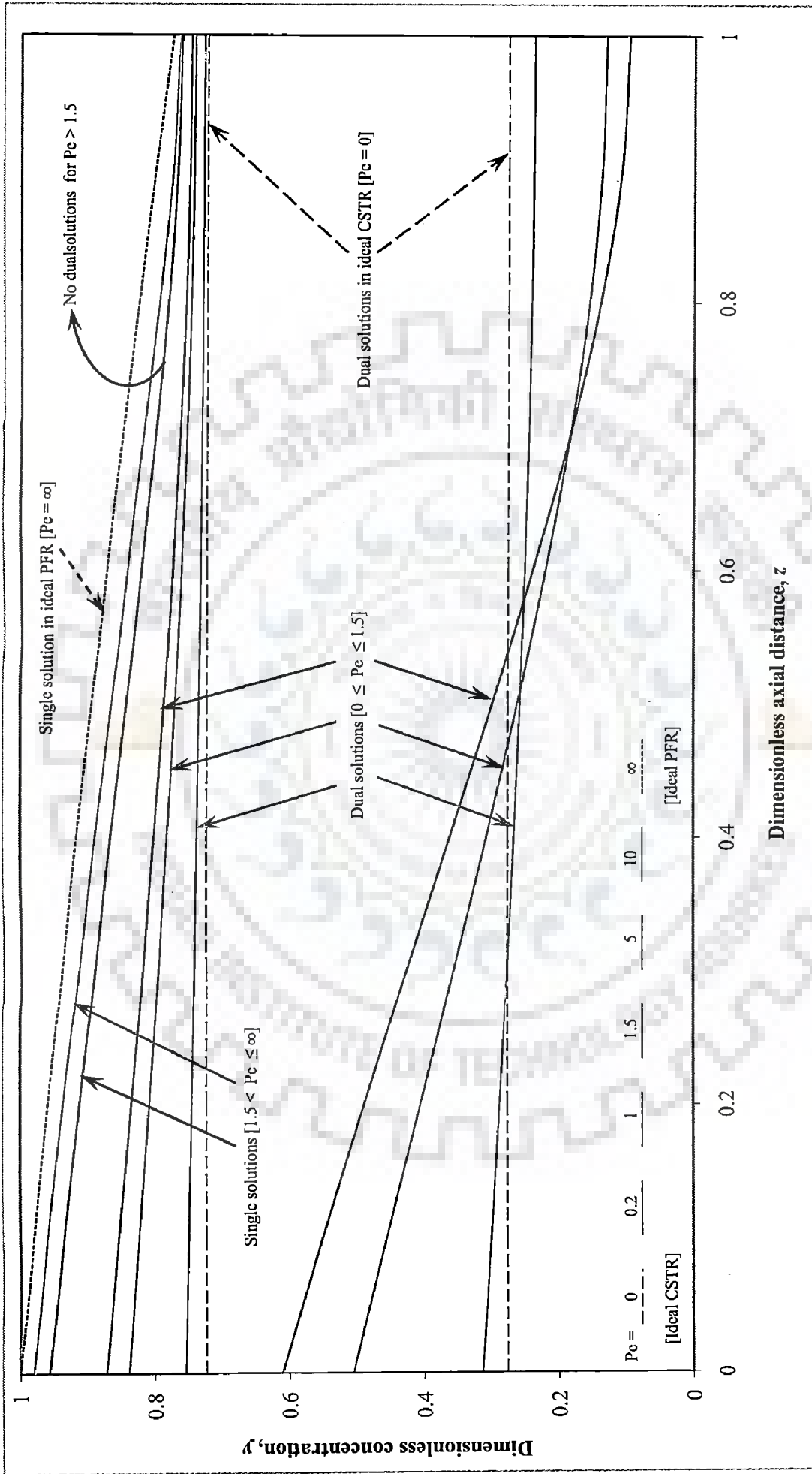
Figure 6.33: Dimensionless single and dual concentration profiles for various values of *Pe* [non-monotonic power-law kinetics: *n* = -1, *Da* = 1/5]

379

$$y_{OHAM} = 0.728762 + 0.027444x^2 - 0.001829x^3 - 0.000081x^4$$

$$+ 0.000010x^5 + 0.000002x^6 - 0.0000003x^7 - 0.00000006x^8 \quad (6.61\text{b})$$

Similarly, the OHAM solutions can be obtained for higher number of terms, and Fig. 6.32 shows the dimensionless concentration profiles obtained by using the OHAM solutions [$n_T = 5, 6, 7$], five points collocation solution and the numerical method. It can be seen that a close agreement exist between these profiles, which validates the OHAM solutions.

For several values of Pe and for $n = -1$ and $Da = 1/5$, the dimensionless concentration profiles have also been obtained by using OHAM and are shown in Fig. 6.33, along with the concentration profiles existing in a PFR [single solution] and in a CSTR [dual solutions]. It can be observed that for this value of Da [= 1/5], the dual solutions exist for $0 \leq Pe \leq 1.5$, whereas, single solutions prevail for $Pe > 1.5$.

6.5   CONCLUDING REMARKS

An efficient variant of HAM, namely OHAM, has been applied to solve the model equations of reaction-diffusion process and tubular chemical reactor, and the conclusions pertaining to them are summarized below.

(i)   Reaction-Diffusion Process in a Porous Spherical Catalyst

Approximate solutions of the concentration profile and effectiveness factor have been obtained by using OHAM for two types of kinetics, i.e. power-law kinetics and Michaelis-Menten kinetics. The results obtained by using the OHAM solution match well with the numerical results, and are found to have lesser error as compared to those obtained by using the MADM solution of Kumar and Singh (2010) and the approximate solution of Li et al. (2004). Besides, it is also shown that MADM is a special case of OHAM, and unlike the OHAM solutions, the MADM solutions do not correspond to the minimum value of sum of square of residual errors. Likewise, the approximate solution of Li et al. (2004) is specific to the Michaelis-Menten kinetics and there is no provision in the solution for improving its accuracy. In contrast to this, the OHAM is found to be

applicable to other forms of kinetics and the accuracy of the OHAM solution can be increased by considering more terms.

(ii) Tubular Chemical Reactor

Approximate solutions of the concentration profile have been found by using OHAM. The obtained OHAM results have been found to match well with the numerical results as well as those available in literature. Utility of OHAM has been demonstrated by capturing the multiple solutions, which appear for some of the parameters' range in case of non-monotonic reaction rates.
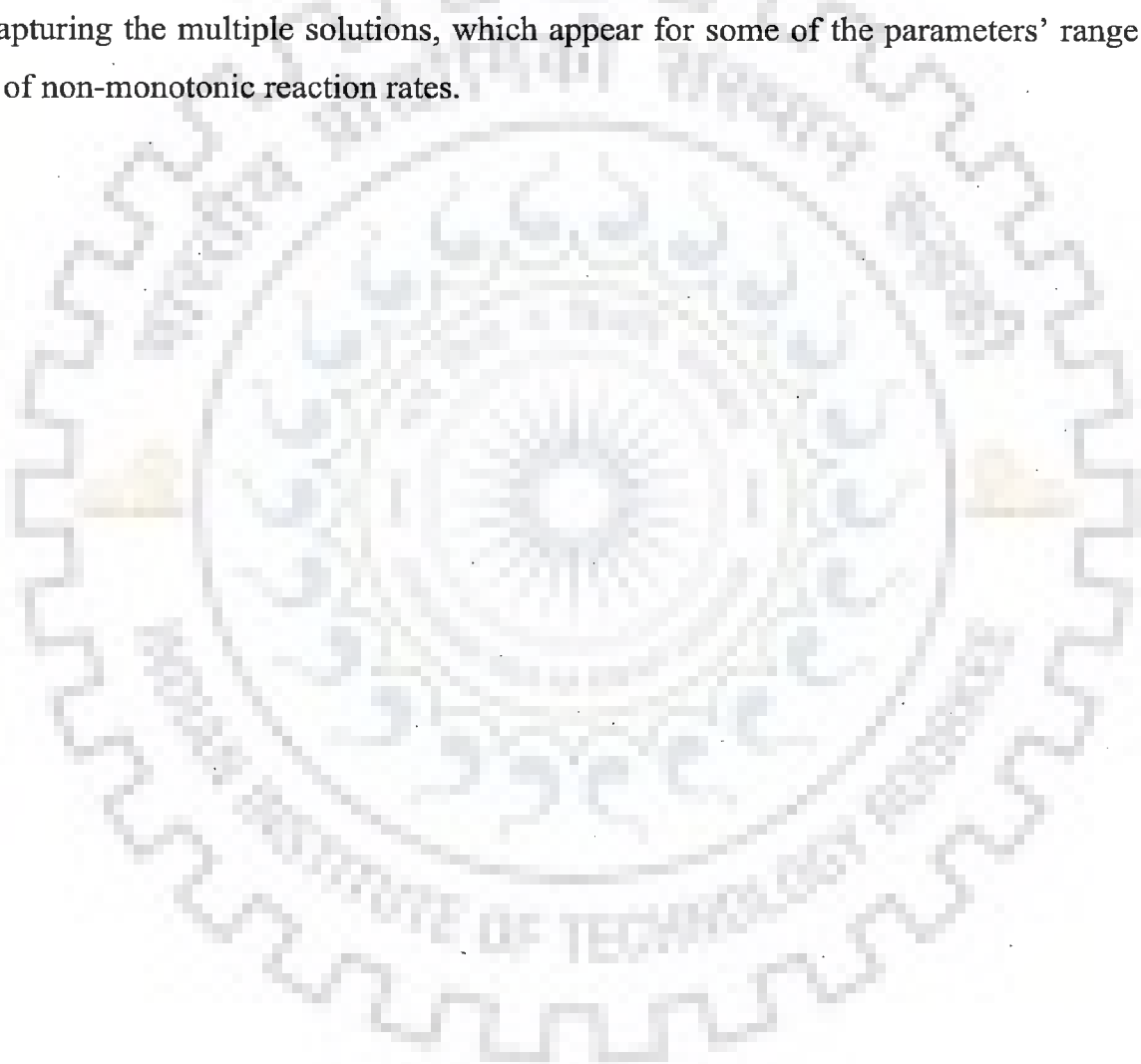
NOMENCLATURE

Abbreviations

AS   analytical solution

APS   approximate solution

HAM   homotopy analysis method

MADM   modified Adomian decomposition method

NS   numerical solution

OHAM   optimal homotopy analysis method

5 pts. OC   five points orthogonal collocation

Notations

a	[-]	constant considered by Kumar and Singh (2010)
$B[y]$	[-]	operator form of the BC [Eq.(6.1)]
$C_1, C_2 .....C_i$	[-]	constants in initial guess
Da	[-]	Damköhler number $\left(= \dfrac{(-r_{A0})L}{C_{A0}U} = \dfrac{(-r_{A0})\tau}{C_{A0}} \right)$
e	[-]	exponential function
$f(y)$	[-]	dimensionless reaction rate $\left(= \dfrac{(-r_A)}{(-r_{A0})} \right)$
h	[-]	auxiliary [convergence control] parameter in HAM/ OHAM
$h_{optimum}$	[-]	optimum value of h found by using Eq. (6.9c)
$H(x)$	[-]	auxiliary function in HAM/OHAM
i	[-]	index variable
k	[s⁻¹]; [m³.mol⁻¹.s⁻¹]	rate constant(s) used in Langmuir-Hinshelwood kinetics (Elnashaie and Abashar, 1990)
k_n	[mol¹⁻ⁿ.m³ⁿ⁻³.s⁻¹]	rate constant for n^{th} order power-law kinetics
K	[-]	dimensionless constant in Langmuir-Hinshelwood kinetics (Fan et al., 1971)
K_A	[m³.mol⁻¹]	constant in Langmuir-Hinshelwood kinetics

		(Elnashaie and Abashar, 1990)
K_m	[mol.m^{-3}]	parameter in Michaelis-Menten kinetics
L	[m]	length of the reactor
$L[.]$	[-]	auxiliary linear operator
$L^{-1}[.]$	[-]	inverse operator of $L[.]$
m	[-]	index variable
M	[-]	number of intervals
n	[-]	reaction order
n_T	[-]	number of terms in HAM/OHAM solution
n_{Tmax}	[-]	maximum number of terms in HAM/OHAM solution
$N[y]$	[-]	nonlinear operator form of the equation
Pe	[-]	Péclet number $\left(= \dfrac{UL}{D_e} \right)$
q	[-]	constant in Eq. (6.50) [$= \sqrt{Pe}\sqrt{Pe+4Da}$]
$-r_A$	[mol.m^{-3}.s^{-1}]	reaction rate of species A
$-r_{A0}$	[mol.m^{-3}.s^{-1}]	reaction rate of species A at concentration C_{A0}
$-r_{AS}$	[mol.m^{-3}.s^{-1}]	reaction rate of species A at the catalyst surface
r_m	[mol.m^{-3}.s^{-1}]	parameter in Michaelis-Menten kinetics
r	[m]	radial distance
R	[m]	radius of the spherical catalyst
$\mathfrak{R}$	[-]	sum of square of residual errors
$R_m[\vec{y}_{m-1}, x]$	[-]	term given by Eq. (6.5b) $\left(= \dfrac{1}{(m-1)!} \dfrac{\partial^{m-1} N[\vec{y}_{m-1}(x,\lambda)]}{\partial \lambda^{m-1}} \bigg|_{\lambda=0} \right)$
U	[m.s^{-1}]	bulk velocity
Δx	[-]	equispaced interval length
$y_0(x)$	[-]	initial guess in HAM/OHAM solutions
$y_m(x)$	[-]	m^{th} term in HAM/OHAM solutions
y_{MADM}	[-]	MADM solution

384

y_{HAM}	[-]	HAM solution
y_{OHAM}	[-]	OHAM solution
$y_{Analytical}$	[-]	analytical solution
$y_{Calculated}$	[-]	solution calculated by OHAM or by five points collocation method
$y_{Numerical}$	[-]	numerical solution
y_{Li}	[-]	solution obtained by the method of Li et al. (2004)
z	[-]	dimensionless axial distance from the reactor inlet $\left(=\dfrac{Z}{L} = 1-x \right)$
Z	[m]	axial distance from the reactor inlet

Greek letters

β	[-]	dimensionless parameter in Michaelis-Menten kinetics $\left(=\dfrac{C_{AS}}{K_m} \right)$
δ	[-]	dimensionless axial distance where concentration is zero for zero order reaction $[\, 0 \le \delta < 1\,]$
η	[-]	catalyst effectiveness factor for spherical catalyst $\left(=\dfrac{3}{\phi^2}\dfrac{dy}{dx}\Big|_{x=1} \right)$
λ	[-]	hypothetical parameter $[\,\lambda \in [0,1]\,]$
ν	[-]	constant in Eq. (6.17a)
τ	[s]	space time of $\left(=\dfrac{L}{U} \right)$
ϕ	[-]	Thiele Modulus for spherical catalyst $\left(=\sqrt{\dfrac{(-r_{AS})R^2}{D_e C_{AS}}} \right)$
χ_m	[-]	constant $= \begin{cases} 0, & m \le 1 \\ 1, & m \ge 2 \end{cases}$
$\psi(x,\lambda)$	[-]	unknown function such that $\psi(x,1) = y(x)$ and

385

$$\psi(x,0) = y_0(x)$$

Sections 6.1 and 6.2

Notations

x	[-]	independent variable
$y(x)$	[-]	dependent variable

Section 6.3

Notations

C_A	[mol.m^{-3}]	concentration of species A inside the catalyst pores
C_{AS}	[mol.m^{-3}]	concentration of species A at the catalyst surface
D_e	[m^2.s^{-1}]	effective diffusivity of reactant inside the pore
x	[-]	independent variable; dimensionless distance along pore length $\left(= \dfrac{r}{R} \right)$
$y(x)$	[-]	dependent variable; dimensionless concentration $\left(= \dfrac{C_A}{C_{AS}} \right)$

Section 6.4

Notations

C_A, C_B	[mol.m^{-3}]	concentration of species A and B, respectively
C_{A0}	[mol.m^{-3}]	inlet concentration of species A
D_e	[m^2.s^{-1}]	dispersion coefficient
x	[-]	dimensionless axial distance from the reactor outlet $[=1-z]$
$y(x)$	[-]	dimensionless concentration $\left(= \dfrac{C_A}{C_{A0}} \right)$

CONCLUSIONS AND RECOMMENDATIONS

7.1   CONCLUSIONS

The main conclusions of the present research work are summarized in following three categories:

[A]   Process Models solved by Analytical Methods

Analytical solutions have been obtained for the models of the following chemical engineering processes/systems:

(i)   Transient convective cooling of a lumped body

(ii)   Transient convective-radiative cooling of a lumped body

(iii)   Steady state heat conduction in a metallic rod

(iv)   Steady state radiative heat transfer from a rectangular fin

(v)   Steady state convective heat transfer from a rectangular fin

(vi)   Rotary kiln model for solid bed depth profile

(vii)   Poiseuille and Couette-Poiseuille flow of a third grade fluid between two parallel plates

The obtained analytical solutions have been successfully validated with the corresponding numerical solutions. For all of the above processes/systems, the limitations of corresponding available approximate solutions have also been shown by comparing them with the presently derived analytical solutions. For the model equations of transient convective-radiative cooling of a lumped body and the rotary kiln, the practical utilities of the corresponding analytical solutions have also been demonstrated by simulating the respective experimental studies. Besides, the criteria of existence,

uniqueness/multiplicity and stability of the analytical solutions, obtained for the process of steady state convective heat transfer from a rectangular fin, have also been discussed.

[B]   Process Models solved by Approximate Methods [ADM and RADM]

Approximate solutions have been obtained by using ADM and one of its variants, namely RADM, for the models of the following chemical engineering processes/systems.

(i)   Thermodynamic equation of state [Beattie-Bridgeman equation of state]

(ii)   Friction factor equation for the flow of Bingham fluids in smooth pipes

(iii)   Reaction-diffusion process inside a porous catalyst slab

(iv)   Reaction-diffusion process inside a porous catalyst sphere

While solving the thermodynamic equation of state, advantages and limitations of ADM and RADM have been illustrated, and guidelines have been proposed to avoid the failure of these methods. For friction factor equation, the RADM solutions have been found to be more accurate as compared to the ADM solutions and the available correlations. For reaction-diffusion processes, the limitations present in the ADM as well as in other available approximate solutions have been discussed and rectified by using RADM, which yield accurate results and is also applicable to the other forms of kinetics.

[C]   Process Models solved by Approximate Method [OHAM]

Approximate solutions have been obtained by using an effective variant of HAM, namely OHAM, for the models of the following chemical engineering process / system.

(i)   Reaction-diffusion process inside a porous catalyst sphere

(ii)   Tubular chemical reactor

The OHAM solutions obtained for the above models have been successfully verified with the respective numerical solutions. For the reaction-diffusion process, advantages of the OHAM solutions over existing approximate solutions have also been highlighted. For the tubular chemical reactor, the utility of OHAM has been demonstrated by capturing the multiple solutions, which arise for some of the parameters' range in case of non-monotonic reaction kinetics.

It is our view that the analytical and approximate solutions of selected process models, obtained in the present thesis, will be useful in many ways, i.e. for simulating experimental studies and for the estimation of parameters. Use of techniques and methods adopted for solving AEs and ODEs can also be made to other process models. We feel that if such an attempt is made it would certainly prove to be advantageous in terms of better understanding of the process and also in ease of obtaining solutions.

7.2   RECOMMENDATIONS

Research is an ongoing process and the completion of a research project opens many other avenues for future endeavors. The completion of this research work has led to an understanding of following points which require further investigation:

(i)   Beside the two familiar analytical methods used in the present work [separation of variables in conjunction with the partial fraction decomposition method and the derivative substitution method], other existing analytical methods can be employed for solving the nonlinear model equations. One such powerful analytical method is Lie's symmetry method, which transforms nonlinear equations into simpler linear/nonlinear equations. To the best of our knowledge, the potential of this method has not been fully realized in chemical engineering and it can be a promising tool for analytically solving some of the yet unsolved nonlinear model equations arising in chemical engineering.

(ii)   Other existing approximate methods, e.g. variational iteration method [VIM], as well as the variants of ADM and HAM with Padé approximation may also be employed to solve nonlinear model equations arising in chemical and allied engineering sciences.

(iii)   Use of some of the approximate methods, namely ADM, HAM and VIM, may also be made to improve the existing numerical methods, as was carried out by Abbasbandy (2003), Abbasbandy et al. (2007), and Motsa et al. (2010).

(iv)   In the present work, analytical/approximate solutions of models described by PDEs have not been attempted. It is our view that the solution of nonlinear PDE models of process systems by these methods and their variants would offer lot of challenges and opportunities, but it would certainly be a rich and rewarding experience.

REFERENCES

[1]   Abbaoui, K., Cherruault, Y., 1994. Convergence of Adomian's method applied to nonlinear equations. *Math. Comput. Model.* 20, 69-73.

[2]   Abbaoui, K., Cherruault, Y., 1995. New ideas for proving convergence of decomposition method. *Comput. Math. Appl.* 29, 103-108.

[3]   Abbaoui, K., Cherruault, Y., Ndour, M., 1995. The decomposition method applied to differential systems. *Kybernetes* 24, 32-40.

[4]   Abbas, Z., Wang, Y., Hayat, T., Oberlack, M., 2008. Hydromagnetic flow in a viscoelastic fluid due to the oscillatory stretching surface. *Int. J. Non-Linear Mech.*, 43, 783-793.

[5]   Abbas, Z., Wang, Y., Hayat, T., Oberlack, M., 2010. Mixed convection in the stagnation-point flow of a Maxwell fluid towards a vertical stretching surface. *Nonlinear Anal.: Real World Appl.* 11, 3218-3228.

[6]   Abbasbandy, S., 2003. Improving Newton-Raphson method for nonlinear equations by modified Adomian decomposition method. *Appl. Math. Comput.* 145, 887-893.

[7]   Abbasbandy, S., 2006a. The application of homotopy analysis method to nonlinear equations arising in heat transfer. *Phys. Lett. A* 360, 109-113.

[8]   Abbasbandy, S., 2006b. Modified homotopy perturbation method for nonlinear equations and comparison with Adomian decomposition method. *Appl. Math. Comput.* 172, 431-438.

[9]   Abbasbandy, S., Tan, Y., Liao, S.J., 2007. Newton-Homotopy analysis method for nonlinear equations. *Appl. Math. Comput.* 188, 1794-1800.

[10] Abbasbandy, S., 2008. Approximate solution for the nonlinear model of diffusion and reaction in porous catalysts by means of the homotopy analysis method. *Chem. Eng. J.* 136 (2-3), 144-150.

[11] Abbasbandy, S., Magyari, E., Shivanian, E., 2009. The homotopy analysis method for multiple solutions of nonlinear boundary value problems. *Commun. Nonlinear Sci. Num. Simul.* 14, 3530-3536.

[12] Abbasbandy, S., Shivanian, E., 2010. Exact analytical solution of a nonlinear equation arising in heat transfer, *Phys. Lett. A* 374, 567-574.

[13] Abbasbandy, S., Shivanian, E., Vajravelu, K., 2011. Mathematical properties of *h*-curve in the frame work of the homotopy analysis method. *Commun. Nonlinear Sci. Num. Simul.* 16, 4268–4275.

[14] Abdelwahid, F., 2003. A mathematical model of Adomian polynomials. *Appl. Math. Comput.* 141, 447-453.

[15] Abouzeid, A.Z.M., Fuerstenau, D.W., Sastry, K.V.S., 1980. Transport behavior of particulate solids in rotary drums: scale-up of residence time distribution using the axial dispersion model. *Powder Tech.* 27, 241-250.

[16] Abramowitz, M., Stegun, I., 1964. Handbook of Mathematical Functions. First ed., Dover, New York.

[17] Adomian, G., 1986. Nonlinear Stochastic Operator Equations. Academic Press Inc., New York.

[18] Adomian, G., Rach, R., Meyers, R., 1991. Numerical algorithms and decomposition. *Comp. Math. Applic.* 22, 57-61.

[19] Adomian, G., 1994. Solving Frontier Problems of Physics: The Decomposition Method. Kluwer Academic Pub., Dordrecht.

[20] Adomian, G., Rach, R., 1994. Modified decomposition solution of linear and nonlinear boundary value problems. *Nonlinear Anal. Theory Methods Appl.*, 23, 615-619.

[21] Akyildiz, F.T., Bellout, H., Vajravelu, K., 2004. Exact solutions of nonlinear differential equations arising in third grade fluid flows, *Int. J. Nonlinear Mech.* 39, 1571-1578.

[22] Ali N., Wang Y., Hayat T., Oberlack M., 2009a. Slip effects on the peristaltic flow of a third grade fluid in a circular cylindrical tube, *ASME J. Appl. Mech.*, 76, 011006-1–10.

[23] Ali, N., Wang, Y., Hayat, T., Oberlack, M., 2009b. Numerical solution of peristaltic transport of an Oldroyd 8-constant fluid in a circular cylindrical tube. *Canad. J. Phys.*, 87, 1047-1058.

[24] Alizadeh, E., Farhadi, M., Sedighi, K., Ebrahimi-Kebria, H.R., Ghafourian, A. 2009. Solution of the Falkner–Skan equation for wedge by Adomian decomposition method. *Commun. Nonlinear Sci. Numer. Simul.*, 14, 724-733.

[25] Allan, F.M., 2007. Derivation of Adomian decomposition method using the homotopy analysis method. *Appl. Math. Comput.* 190, 6-14.

[26] Aminataei, A, Hosseini, S.S., 2007. The comparison of the stability of Adomian decomposition method with numerical methods of equation solution. *Appl. Math. Comput.* 186, 665-669.

[27] Andrianov, I.V., Olevskii, V.I., Tokarzewski, S., 1998. A modified Adomian's decomposition method. *J. Appl. Math. Mech.*, 62, 309-314.

[28] Annamalai, K., Puri, I.K. 2002. Advanced Thermodynamics Engineering. CRC Press, Boca Raton, Florida.

393

[29] Aris, R., 1956. On the dispersion of a solute in fluid flowing through a tube. *Proc. Royal Society A* 235, 67-77.

[30] Aris, R., 1975. Mathematical Theory of Diffusion and Reaction in Permeable Catalyst, Vol. I & II. Clarendon Press, Oxford.

[31] Aslanov, A., Abu-alshaikh, I., 2008. Further developments to the decomposition method for solving singular initial-value problems. *Math. Comp. Model.* 48, 700-711.

[32] Ayub, M., Rasheed, A., Hayat, T., 2003. Exact flow of a third grade fluid past a porous plate using homotopy analysis method. *Int. J. Eng. Sci.* 41, 2091-2103.

[33] Aziz, A., Benzies, J. Y., 1976. Application of perturbation techniques to heat-transfer problems with variable thermal properties. *Int. J. Heat Mass Tr.* 19, 271-276.

[34] Babolain, E., Biazar, J., 2002a. On the order of the convergence of Adomian method. *Appl. Math. Comput.* 130, 383-387.

[35] Babolain, E., Biazar, J., 2002b. Solution of nonlinear equations by modified Adomian decomposition method. *Appl. Math. Comput.* 132, 167-172.

[36] Babolian, E., Javadi, Sh., 2003. Restarted Adomian method for algebraic equations. *Appl. Math. Comput.* 146, 533-541.

[37] Babolian, E., Biazar, J., Vahidi, A.R., 2004a. Solution of a system of nonlinear equations by Adomian decomposition method. *Appl. Math. Comput.* 150, 847-854.

[38] Babolian, E., Javadi. S., Sadeghi, H., 2004b. Restarted Adomian method for integral equations. *Appl. Math. Comput.* 153, 353-359.

[39]   Babolian, E., Goghary, H. S., Javadi, Sh., Ghasemi, M., 2005. Restarted
        Adomian method for nonlinear differential equations. *Int. J. Comput. Math.* 82,
        97–102.

[40]   Babu, B.V., 2004. Process Plant Simulation. Oxford University Press, New
        Delhi.

[41]   Babu, B.V., Angira, R., 2005. Optimal design of an auto-thermal ammonia
        synthesis reactor. *Comp. Chem. Eng.*, 29, 1041-1045.

[42]   Babu, B.V., Chakole, P.G., Mubeen, J. H. S., 2005. Multiobjective differential
        evolution (MODE) for optimization of adiabatic styrene reactor. *Chem. Eng.
        Sci.*, 60, 4822-4837.

[43]   Babu, B.V., Shah, K. J., Rao, V. G., 2007. Lateral mixing in trickle bed reactors.
        Chem. Eng. Sci., 62 (24), 7053-7059.

[44]   Basto, M., Semiao, V. Calheiros, F.L. 2006. A new iterative method to compute
        nonlinear equations. *Appl. Math. Comput.* 173, 468-483.

[45]   Bataineh, A.S., Noorani, M.S.M., Hashim, I., 2009. Homotopy analysis method
        for singular IVPs of Emden–Fowler type. *Commun. Nonlinear Sci. Numer.
        Simul.* 14, 1121-1131.

[46]   Bejan, A., Kraus, A.D., 2003. Heat Transfer Handbook. First ed., John Wiley &
        Sons, Inc., Hoboken, New Jersey.

[47]   Bellout, H., Nečas, J., Rajagopal, K.R., 1999. On the existence and uniqueness
        of flows of multipolar fluids of grade 3 and their stability. *Int. J. Eng. Sci.* 37,
        75-96.

[48]   Biazar, J., Babolian, E., Kember, G., Nouri, A., Islam, R., 2003a. An alternate
        algorithm for computing Adomian polynomials in special cases. *Appl. Math.
        Comput.* 138, 523-529.

[49] Biazar, J., Tango, M., Babolian, E., Islam, R., 2003b. Solution of the kinetic modeling of lactic acid fermentation using Adomian decomposition method. *Appl. Math. Comput.* 144, 433–439.

[50] Biazar, J., Babolian, E., Islam, R., 2004. Solution of the system of ordinary differential equations by Adomian decomposition method. *Appl. Math. Comput.* 147, 713-719.

[51] Bird, R.B., Armstrong, R.C., Hassager, O., 1987. Dynamics of Polymeric Liquids, Vol. 1, Fluid Mechanics. Second ed., Wiley, New York.

[52] Bird, R.B., Stewart, W.E., Lightfoot, E.N., 2002. Transport Phenomena. Second ed. John Wiley & Sons, Inc., New York.

[53] Bischoff, K.B., Levenspiel, O., 1962a. Fluid dispersion-generalization and comparison of mathematical models-I: generalization of models. *Chem. Eng. Sci.*, 17, 245-255.

[54] Bischoff, K.B., Levenspiel, O., 1962b. Fluid dispersion-generalization and comparison of mathematical models-II: comparison of models. *Chem. Eng. Sci.*, 17, 257-264.

[55] Bralts, V.F., Kelly, S.F., Shayya, W.H., Segerlind, L.J., 1993. Finite element analysis of microirrigation hydraulics using a virtual emitter system. *Trans. Am. Soc. Agric. Eng.* 36, 717-725.

[56] Burghardt, A, Zaleski, T., 1968. Longitudinal dispersion at small and large Peclet numbers in chemical flow reactors. *Chem. Eng. Sci.*, 23, 575-591.

[57] Campo, A., Blotter, J., 2000. Experimental and numerical evaluation of the unsteady cooling ball bearings in atmospheric air: dual influence of nonlinear natural convection and surface radiation. *Exp. Therm. Fluid Sci.*, 23, 105-114.

[58]   Casasús, L., Al-Hayani, W., 2002. The decomposition method for ordinary differential equations with discontinuities. *Appl. Math. Comput.* 131, 245-251.

[59]   Chang, Min-Hsing, 2005. A decomposition solution for fins with temperature-dependent surface heat flux. *Int. J. Heat Mass Tr.* 48, 1819-1824.

[60]   Chen, N.H., 1979. An explicit equation for friction factor in pipe. *Ind. Eng. Chem. Fundam.* 18, 296-297.

[61]   Cheng, J., Liao, S.J., Mohapatra, R.N., Vajravelu, K., 2008. Series solutions of nano boundary layer flows by means of the homotopy analysis method. *J. Math. Anal. Appl.* 343, 233–245.

[62]   Cherruault, Y., Adomian, G., Abbaoui, K., Rach, R., 1995. Further remarks on convergence of decomposition method. *Int. J. Bio-Med. Comput.* 38, 89-93.

[63]   Choi, H.W., Shin, J.G., 2003. Symbolic implementation of the algorithm for calculating Adomian polynomials. *Appl. Math. Comput.* 146, 257-271.

[64]   Chowdhury, M.S.H., Hashim, I., 2008. Analytical solutions to heat transfer equations by homotopy-perturbation method revisited. *Phys. Lett. A* 372, 1240-1243.

[65]   Chowdhury, M.S.H., Hashim, I., 2009. Solutions of Emden–Fowler equations by homotopy-perturbation method. *Nonlinear Anal.: Real World Appl.* 10, 104–115.

[66]   Chun, C., 2006. A new iterative method for solving nonlinear equations. *Appl. Math. Comput.* 178, 415-422.

[67]   Churchill, S.W., 1977. Friction factor equation spans all fluid-flow regimes, *Chem. Eng.* 84, 91-92.

[68] Colebrook, C.F., 1939. Turbulent flow in pipes with particular reference to the transition region between the smooth and rough pipe laws. *J. Inst. Civil Eng.* 11, 133-156.

[69] Cortés, C., Campo, A., Arauzo, I., 2003. Reflections on lumped models of unsteady heat conduction in simple bodies. *Int. J. Therm. Sci.*, 42, 921-930.

[70] Danckwerts, P.V., 1953. Continuous flow systems: distribution of residence times. *Chem. Eng. Sci.*, 2, 1-13.

[71] Deckwer, W.D., Mählmann, E.A., 1976. Boundary conditions of liquid phase reactors with axial dispersion. *The Chem. Eng. J.* 11, 19-25.

[72] Dennis, J.E., Schnabel, R.B., 1983. Numerical Methods for Unconstrained Optimization and Nonlinear Equations. Prentice-Hall, Englewood Cliffs, New Jersey.

[73] Dinarvand, S., Rashidi. M.M., 2010. A reliable treatment of a homotopy analysis method for two-dimensional viscous flow in a rectangular domain bounded by two moving porous walls. *Nonlinear Anal.: Real World Appl.* 11, 1502–1512.

[74] Domairry, G., Nadim, N., 2008. Assessment of homotopy analysis method and homotopy perturbation method in nonlinear heat transfer equation. *Int. Commun. Heat Mass Tr.* 35, 93-102.

[75] Dul'kin, I.N., Garas'ko, G.I., 2002. Analytical solutions of 1-D heat conduction problem for a single fin with temperature dependent heat transfer coefficient-I closed-form inverse solution, *Int. J. Heat Mass Tr.* 45, 1895-1903.

[76] Elnashaie, S.S.E.H., Abashar, M.E., 1990. The implication of non-monotonic kinetics on the design of catalytic reactors. *Chem. Eng. Sci.*, 45, 2964-2967.

[77] El-Sayed, S.M., 2002. The modified decomposition method for solving nonlinear algebraic equations. *Appl. Math. Comput.* 132, 589-597.

398

[78] Fan, L.T., Bailie, R.C., 1960. Axial diffusion in isothermal tubular flow reactors. *Chem. Eng. Sci.*, 13, 63-68.

[79] Fan, L.T., Chen, G.K.C., Erickson, L.E., 1971. Efficiency and utility of collocation methods in solving the performance equations of flow chemical reactors with axial dispersion. *Chem. Eng. Sci.* 26, 379-387.

[80] Fan, L.T., Fan, L.S., 1979. Simulation of catalytic fluidized bed reactors by a transient axial dispersion model with invariant physical properties and nonlinear chemical reactions. *Chem. Eng. Sci.* 34, 171-179.

[81] Ferguson, N.B., Finlayson, B.A., 1970. Transient chemical reaction analysis by orthogonal collocation. *The Chem. Eng. J.* 1, 327-336.

[82] Finlayson, B.A., 1980. Nonlinear Analysis in Chemical Engineering. Mc Graw-Hill, New York.

[83] Finlayson, B.A., 2006. Introduction to Chemical Engineering Computing: John Wiley & Sons, Inc., New Jersey.

[84] Fogler, H.S., 1992. Elements of Chemical Reaction Engineering. Second ed., Prentice-Hall, New Jersey.

[85] Fosdick, R.L., Rajagopal, K.R., 1980. Thermodynamics and stability of fluids of third grade. *Proc. R. Soc. London A* 339, 351-377.

[86] Freeman, L.B., Houghton, G., 1966. Singular perturbations of nonlinear boundary value problems arising in chemical flow reactors. *Chem. Eng. Sci.* 21, 1011-1024.

[87] Gabet, L., 1994. The theoretical foundation of the Adomian method. *Comput. Math. Appl.* 27, 41-52.

[88]   Ganji, D.D., 2006. The application of He's homotopy perturbation method to nonlinear equations arising in heat transfer. *Phys. Lett. A* 355, 337-341.

[89]   Ganji, D.D., Hosseini, M. J., Shayegh, J., 2007. Some nonlinear heat transfer equations solved by three approximate methods. *Int. Commun. Heat Mass Tr.* 34, 1003-1016.

[90]   Ghosh, S., Roy, A., Roy, D., 2007. An adaptation of Adomian decomposition for numeric–analytic integration of strongly nonlinear and chaotic oscillators. *Comput. Methods Appl. Mech. Eng.* 196, 1133–1153.

[91]   Golberg, M.A., 1999. A note on the decomposition method for operator equations. *Appl. Math. Comput.* 106, 215-220.

[92]   Gorder, R.A.V., Vajravelu, K., 2009. On the selection of auxiliary functions, operators, and convergence control parameters in the application of the homotopy analysis method to nonlinear differential equations: A general approach. *Commun. Nonlinear Sci. Numer. Simul.* 14, 4078–4089.

[93]   Gottifredi, J.C., Gonzo, E.E., 2005. Approximate expression for the effectiveness factor estimation and a simple numerical method for concentration profile calculation in porous catalyst. *Chem. Eng. J.* 109, 83-87.

[94]   Goudar, C.T., Sonnad, J.R., 2003. Explicit friction factor correlation for turbulent flow in smooth pipes. *Ind. Eng. Chem. Res.* 42, 2878-2880.

[95]   Govier, G.W., Aziz, K. 1972. The Flow of Complex Mixtures in Pipes. R.E. Krieger Pub. Co., Malabar, FL.

[96]   Gujarathi, A. M., B. V. Babu, 2009. Optimization of adiabatic styrene reactor: a hybrid multi-objective differential evolution (H–MODE) approach. *Ind. Eng. Chem. Res.*, 48, 11115-11132.

[97]   Gujarathi, A. M., B. V. Babu, 2010. Multi-objective optimization of industrial styrene reactor: adiabatic and pseudo-isothermal operation. *Chem. Eng. Sci.*, 65, 2009-2026.

[98]   Gunn, D.J., 1993. On axial dispersion in fixed beds. *Chem. Eng. Process.* 32, 333-338.

[99]   Gunn, D.J., 2004. An analysis of convective dispersion and reaction in the fixed-bed reactor. *Int. J. Heat Mass Tr.* 47, 2861-2875.

[100] Gupta, S. K., Singh, H., Sahgal, P. N., 1986. Gas absorption in laminar falling film with a finite gas phase resistances. *Ind. Chem. Eng.* 29 (2), 3-8.

[101] Gupta, S.K., 1995. Numerical Methods for Engineers. New Age International Publishers Ltd., New Delhi.

[102] Hanks, R.W., Pratt, D.R., 1967. On the flow of Bingham plastic slurries in pipes and between parallel plates, *Soc. Petrol. Eng. J.*, 342-346.

[103] Hasan, Y.Q., Zhu, L.M., 2009. Solving singular boundary value problems of higher-order ordinary differential equations by modified Adomian decomposition method. *Commun. Nonlinear Sci. Numer. Simul.* 14, 2592-2596.

[104] Haswani, R., Gupta, S. K., Kumar, A., 1995. Semianalytical solution of isothermal nylon 6 polymerization in batch reactors. *Polym. Eng. Sci.*, 35, 1231-1240.

[105] Hayat, T., Javed, T., Sajid, M., 2007. Analytic solution for rotating flow and heat transfer analysis of a third-grade fluid. *Acta Mech.* 191, 219–229.

[106] Hayat, T., Ellahi, R., Mahomed, F.M., 2008. Exact solutions for thin film flow of a third grade fluid down an inclined plane. *Chaos Solitons Fractals* 38, 1336-1341.

[107] Hayat, T., Mustafa, M., Asghar. S., 2010. Unsteady flow with heat and mass transfer of a third grade fluid over a stretching surface in the presence of chemical reaction. *Nonlinear Anal.: Real World Appl.* 11, 3186–3197.

[108] He, J.H., 2004. Comparison of homotopy perturbation method and homotopy analysis method. *Appl. Math. Comput.* 156, 527–539.

[109] Hillier, J. R., Ting, D. L., Kopplin, L., Koch, M., Gupta, S. K., 2002. Determining the flow characteristics of a power law liquid. *Chem. Eng. Edu.*, 36, 304-309.

[110] Himmelblau, D.M., Bischoff. K.B., 1967. Process Analysis and Simulation. John Wiley & Sons, Inc., New York.

[111] Holmquist, S.M., 2007. An Examination of the Effectiveness of the Adomian Decomposition Method in Fluid Dynamic Applications. Ph.D. Thesis, Department of Mathematics, University of Central Florida, Florida, US.

[112] Hosseini, M.M., 2006. Adomian decomposition method with Chebyshev polynomials. *Appl. Math. Comput.* 175, 1685-1693.

[113] Hosseini, M.M., Nasabzadeh, H., 2006. On the convergence of Adomian decomposition method. *Appl. Math. Comput.* 182, 536–543.

[114] Hosseini, M.M., Nasabzadeh, H., 2007. Modified Adomian decomposition method for specific second order ordinary differential equations. *Appl. Math. Comput.* 186, 117-123.

[115] Hsu, J.T., Dranoff, J.S., 1986. On initial condition problems for reactor dispersion model. *Chem. Eng. Sci.* 41, 1930-1934.

[116] Idrees, M., Islam, S., Haq, S., Islam, S., 2010. Application of the optimal homotopy asymptotic method to squeezing flow. *Comp. Math. Appl.* 59, 3858-3866.

[117] Inc, M., Ergut, M., Cherruault, Y., 2005. A different approach for solving singular two-point boundary value problems. *Kybernetes* 34, 934–940.

[118] Iqbal, S., Javed, A., 2011. Application of optimal homotopy asymptotic method for the analytic solution of singular Lane–Emden type equation. *Appl. Math. Comput.* 217, 7753–7761.

[119] Jafari, H., Daftardar-Gejji, V., 2006. Revised Adomian decomposition method for solving a system of nonlinear equations. *Appl. Math. Comput.* 175, 1-7.

[120] Jang, B., 2008. Two-point boundary value problems by the extended Adomian decomposition method. *J. Comp. Appl. Math.* 219, 253-262.

[121] Jiao, Y.C., Yamamoto, Y., Dang, C., Hao, Y., 2002. An after treatment technique for improving the accuracy of Adomian decomposition method. *Comput. Math. Appl.*, *43*, 783-798.

[122] Jiao, Y.C., Dang, C., Yamamoto, Y., 2008. An extension of the decomposition method for solving nonlinear equations and its convergence. *Comput. Math. Appl.* 55, 760-775.

[123] Kanth, A.S.V.R., Aruna, K., 2008. Solution of singular two-point boundary value problems using differential transformation method. *Phys. Lett. A* 372, 4671-4673.

[124] Kaya, D., El-Sayed, S.M., 2004. Adomian's decomposition method applied to systems of nonlinear algebraic equations. *Appl. Math. Comput.* 154, 487-493.

[125] Kaya, D., 2004. A reliable method for the numerical solution of the kinetics problems. *Appl. Math. Comput.* 156, 261-270.

[126] Keady, G., 1998. Colebrook-White formula for pipe flows, ASCE J. Hydraul. Eng. 124, 96-97.

[127] Kechil, S.A., Hashim, I., 2007. Non-perturbative solution of free-convection boundary-layer equation by Adomian decomposition method. *Phys. Lett. A. 363*, 110-114.

[128] Kim, D.H., Lee, J., 2004. A robust iterative method of computing effectiveness factors in porous catalysts. *Chem. Eng. Sci.* 59, 2253-2263.

[129] Kim, D.H., Lee, J., 2006. A simple formula for estimation of the effectiveness factor in porous catalysts. *AIChE J.* 52, 3631-3635.

[130] Kramers, H., Croockewit, P., 1952. The passage of granular solids through inclined rotary kilns. *Chem. Eng. Sci.* 1, 259-265.

[131] Kraus, A.D., Aziz, A., Welty, J., 2001. Extended Surface Heat Transfer. First ed., John Wiley & Sons, Inc., New York.

[132] Kreyszig, E., 2001. Advanced Engineering Mathematics. Eight ed., John Wiley & Sons, Inc., New York.

[133] Kubicek, M., Hlavacek, V., 1983. Numerical Solution of Nonlinear Boundary Value Problems with Applications. Prentice-Hall Inc., New Jersey.

[134] Kumar, M., Singh, N., 2009. A collection of computational techniques for solving singular boundary-value problems. *Adv. Eng. Soft.* 40, 288-297.

[135] Kumar, M., Singh, N., 2010. Modified Adomian decomposition method and computer implementation for solving singular boundary value problems arising in various physical problems. *Comp. Chem. Eng.* 34, 1750-1760.

[136] Kupiec, K., Komorowicz, T., 2010. Simplified model of transient radiative cooling of spherical body, *Int. J. Therm. Sci.*, 49, 1175-1182.

[137] Layeni, O.P., 2008. Remark on modifications of Adomian decomposition method. *Appl. Math. Comput.* 197, 167-171.

[138] Lebas, E., Hanrot, F., Ablitzer, D., Houzelot, J.L., 1995. Experimental study of residence time, particle movement and bed depth profile in rotary kiln. *The Canad. J. Chem. Eng.* 73, 173-180.

[139] Lee, E.S., 1966. Quasi-linearization, nonlinear boundary value problems and optimization. *Chem. Eng. Sci.*, 21, 183-194.

[140] Lesnic, D., Heggs, P.J., 2004. A decomposition method for power-law fin type problems, *Int. Commun. Heat Mass Tr.* 31, 673-682.

[141] Lesnic, D., 2007. A nonlinear reaction–diffusion process using the Adomian decomposition method. *Int. Commun. Heat Mass Tr.* 34, 129–135.

[142] Levenspiel, O., 1999. Chemical Reaction Engineering. Third ed., John Wiley & Sons, Inc., New York.

[143] Li, J.-L., 2009. Adomian's decomposition method and homotopy perturbation method in solving nonlinear equations. *J. Comput. Appl. Math.*, 228, 168-173.

[144] Li, X., Chen, X.D., Chen. N., 2004. A third order approximate solution of the reaction-diffusion process in an immobilized bio-catalyst particle. *Biochem. Eng. J.* 17, 65-69.

[145] Liao, H.T., Shiau, C.Y., 2000. Analytical solution to an axial dispersion model for the fixed bed adsorber. *AIChE J.* 46, 1168-1176.

[146] Liao, S.J., 1995. An approximate solution technique which does not depend upon small parameters: a special example. *Int. J. Nonlinear Mech.* 30, 371-380.

[147] Liao, S.J., 1997. Numerically solving non-linear problems by the homotopy analysis method. *Comp. Mech.* 20, 530-540.

[148] Liao, S.J., 2003. Beyond Perturbation: An Introduction to the Homotopy Analysis Method. Chapman & Hall/CRC Press, Boca Raton.

[149] Liao, S.J., Pop, I., 2004. Explicit analytic solution for similarity boundary layer equations. *Int. J. Heat Mass Tr.* 47, 75–85.

[150] Liao, S.J., 2005. Comparison between the homotopy analysis method and homotopy perturbation method. *Appl. Math. Comput.* 169, 1186–1194.

[151] Liao, S.J., Su, J., Chwang, A.T., 2006. Series solutions for a nonlinear model of combined convective and radiative cooling of a spherical body, *Int. J. Heat Mass Tr.* 49, 2437–2445.

[152] Liao, S.J., 2009a. Notes on the homotopy analysis method: some definitions and theorems. *Commun. Nonlinear Sci. Numer. Simul.* 14, 983-997.

[153] Liao, S.J., 2009b. A general approach to get series solution of non-similarity boundary-layer flows. *Commun. Nonlinear Sci. Numer. Simul.* 14, 2144-2159.

[154] Liao, S.J., 2010. An optimal homotopy analysis approach for strongly nonlinear differential equations. *Commun. Nonlinear Sci. Numer. Simul.* 15, 2003-2016.

[155] Liu, Y., 2009. Adomian decomposition method with orthogonal polynomials: Legendre polynomials. *Math. Comput. Model.* 49, 1268-1273.

[156] Liu, X.Y., Zhang, J., Specht, E., Shi, Y.C., Herz, F., 2009. Analytical solution for the axial solid transport in rotary kilns, *Chem. Eng. Sci.* 64, 428-431.

[157] Liu, C.S., 2010. The essence of the homotopy analysis method. *Appl. Math. Comput.* 216, 1299-1303.

[158] Liu, C.S., 2011. The essence of the generalized Taylor theorem as the foundation of the homotopy analysis method. *Commun. Nonlinear Sci. Numer. Simul.* 16, 1254-1262.

[159] Lu, J., 2007. Variational iteration method for solving two-point boundary value problems. *J. Comp. Appl. Math.* 207, 92–95.

[160] Magyari, E., 2008. Exact analytical solution of a nonlinear reaction-diffusion model in porous catalysts. *Chem. Eng. J.* 143, 167-171.

[161] Magyari, E., 2010. Exact analytical solutions of diffusion reaction in spherical porous catalyst. *Chem. Eng. J.* 158, 266–270.

[162] Mahmood, A.S., Casasús, L., Al-Hayani, W., 2005. The decomposition method for stiff systems of ordinary differential equations. *Appl. Math. Comput.* 167, 964-975.

[163] Majhi, S.N., Nair, V.R., 1994. Pulsatile flow of third grade fluids under body acceleration-modelling blood flow. *Int. J. Eng. Sci.* 32, 839-846.

[164] Manadilli, G. 1997. Replace implicit equations with sigmoidal functions. *Chem. Eng.* 104, 129-132.

[165] Marek, M., Stuchl, I., 1975. Approximate relations for description of heat and mass transfer effects in reacting systems. *Chem. Eng. Sci.* 30, 555-562.

[166] Marinca, V., Herişanu, N., 2008. Application of optimal homotopy asymptotic method for solving nonlinear equations arising in heat transfer. *Int. Commun. Heat Mass Tr.* 35, 710-715.

[167] Marinca, V., Herişanu, N., Nemeş, I., 2008. Optimal homotopy asymptotic method with application to thin film flow. *Central Europ. J. Phys.* 6, 648-653.

[168] Mehdizadeh, A., Oberlack, M., 2010. Analytical and numerical investigations of laminar and turbulent Poiseuille–Ekman flow at different rotation rates. *Phys. Fluids*, 22, 105104-1-11.

[169] Mehta, B.N., Aris, R., 1971. Communications on the theory of diffusion and reaction - VII The isothermal p^{th} order reaction. *Chem. Eng. Sci.*, 26, 1699-1712.

[170] Mickley H.S., Sherwood, T.S., Reed, C.E., 1957. Applied Mathematics in Chemical Engineering. Second ed., McGraw-Hill, New York.

[171] Mittal, R.C., Nigam, R., 2008. Solution of a class of singular boundary value problems. *Numer. Algor.*, 47, 169–179.

[172] Mo, L.-F., 2007. Variational approach to reaction–diffusion process. *Phys. Lett. A* 368, 263–265.

[173] Modest, M.F., 2003. Radiative Heat Transfer. Second ed., Academic Press, New York.

[174] Moitsheki, R.J., Hayat, T., Malik, M.Y., Mahomeda, F.M., 2010a. Symmetry analysis for the nonlinear model of diffusion and reaction in porous catalysts. *Nonlinear Anal.: Real World Appl.* 11, 3031–3036.

[175] Moitsheki, R.J., Hayat, T., Malik, M.Y., 2010b. Some exact solutions of the fin problem with a power law temperature-dependent thermal conductivity. *Nonlinear Anal.: Real World Appl.* 11, 3287-3294.

[176] More, A.A., 2006. Analytical solutions for the Colebrook and White equation and for pressure drop in ideal gas flow in pipes. *Chem. Eng. Sci.* 61, 5515-5519.

[177] Motsa, S.S., Sibanda, P., Shateyi, S., 2010. A new spectral-homotopy analysis method for solving a nonlinear second order BVP. *Commun. Nonlinear Sci. Numer. Simul.* 15, 2293-2302.

[178] Nayfeh, A.H., 1981. Introduction to Perturbation Techniques. John Wiley & Sons, Inc., New York.

[179] Nelson, P., 1988. Adomian's method of decomposition: critical review and examples of failure. *J. Comput. Appl. Math.* 23, 389-393.

[180] Nigam, R., 2009. Solution of Some Differential Equations by Adomian Decomposition Method. Ph.D. Thesis, Department of Mathematics, Indian Institute of Technology Roorkee, Roorkee, India.

[181] Niu, Z., Wang, C., 2010. A one-step optimal homotopy analysis method for nonlinear differential equations. *Commun. Nonlinear Sci. Numer. Simul.* 15, 2026-2036.

[182] Odibat, Z.M., 2010. A study on the convergence of homotopy analysis method. *Appl. Math. Comput.* 217, 782-789.

[183] Oldroyd, J.G., 1950. On the formulation of rheological equations of state. *Proc. R. Soc. London A* 200, 523-541.

[184] Parand, K., Dehghan, M., Rezaei, A.R., Ghaderi, S.M., 2010. An approximation algorithm for the solution of the nonlinear Lane–Emden type equations arising in astrophysics using Hermite functions collocation method. *Comp. Phys. Commun.* 181, 1096-1108.

[185] Parang, M., Crocker, D.S., Haynes, B.D., 1990. Perturbation solution for spherical and cylindrical solidification by combined convective and radiative cooling. *Int. J. Heat Fluid Flow*, 11, 142-148.

[186] Passerini, A., Patria, M.C. 2000. Existence, uniqueness and stability of steady flows of second and third grade fluids in an unbounded "pipe-like" domain. *Int. J. Nonlinear Mech.* 35, 1081-1103.

[187] Patria, M.C., 1989. Stability questions for a third-grade fluid in exterior domains. *Int. J. Nonlinear Mech.*, 24, 451-457.

[188] Pushpavanam, S., Narayanan, R., 1988. Uniqueness conditions for steady solutions in the case of m-th order reactions: non isothermal pellets with variable transport coefficients. *Chem. Eng. Sci.*, 43 (2), 394-396.

[189] Pushpavanam, S., 1998. Mathematical Methods in Chemical Engineering. Prentice Hall of India Pvt. Ltd., New Delhi.

[190] Rach, R., Adomian, G., Meyers, R.E., 1992. A modified decomposition. *Comput. Math. Appl.* 23, 17-23.

[191] Rach, R.C. 2008. A new definition of the Adomian polynomials, *Kybernetes* 37, 910-955.

[192] Raina, G. K., Wanchoo, R. K., 1984. Direct contact heat transfer with phase change: theoretical expression for instantaneous velocity of a two-phase bubble. *Int. Commun. Heat Mass Tr.*, 11, 227-237.

[193] Rajabi, A., Ganji, D.D., Taherian, H., 2007. Application of homotopy perturbation method in nonlinear heat conduction and convection equations. *Phys. Lett. A*, 360, 570-573.

[194] Rajagopal, K.R., 1980. On the stability of third grade fluids. *Arch. Mech.* 32, 867-875.

[195] Rajagopal, K.R., Sciubba, E., 1984. Pulsating Poiseuille flow of a non-Newtonian fluid. *Math. Comp. Simul.* 26, 276-288.

[196] Rahman, M., 1974. Some aspects of perturbation solutions arising in non-isothermal tubular chemical flow reactors. *Chem. Eng. Sci.* 29, 2169-2176.

[197] Ramos, J.I., 2008. Series approach to the Lane–Emden equation and comparison with the homotopy perturbation method. *Chaos Solitons Fractals* 38, 400–408.

[198] Ramos, J.I., 2009. Piecewise-adaptive decomposition methods. *Chaos Solitons Fractals* 40, 1623-1636.

[199] Rao, K.C., Prabhu, S.S., Mehta, S.C., 1981. Finite element collocation solution of tubular and packed bed reactor two point boundary value problems. *Chem. Eng. Sci.* 36, 987-992.

[200] Ray, W.H., Marek, M., Elnashaie, S., 1972. The effect of heat and mass dispersion on tubular reactor performance. *Chem. Eng. Sci.* 27, 1527-1536.

[201] Repaci, A., 1990. Nonlinear dynamical systems: on the accuracy method Adomian's decomposition method. *Appl. Math. Lett.* 3, 35-39.

[202] Rice, R.G., Do, D.D., 1995. Applied Mathematics and Modeling for Chemical Engineers. John Wiley & Sons, Inc., New York.

[203] Rivlin, R.S., Ericksen, J.L. 1955. Stress-deformation relations for isotropic materials. *J. Rational Mech. Anal.* 4, 323-425.

[204] Rodrigues, A.E., Lu, Z.P., Lopes, J.C.B., Dias, M.M., Silva, A.M., 1994. The effect of intraparticle convection on conversion in heterogeneous isothermal fixed-bed reactors with large-pore catalysts for first-order reactions. *The Chem. Eng. J. the Biochem. Eng. J.* 54, 41-50.

[205] Roetzel, W., Lee, D., 1993. Experimental investigation of leakage in shell-and-tube heat exchangers with segmental baffles. *Int. J. Heat Mass Tr.* 36, 15, 3765-3771.

[206] Roetzel, W., Das, S.K., Luo, X., 1994. Measurement of the heat transfer coefficient in plate heat exchangers using a temperature oscillation technique. *Int. J. Heat Mass Tr.*, 37, Suppl. I. 325-331.

[207] Roetzel, W., Balzereit F., 1997. Determination of axial dispersion coefficients in plate heat exchangers using residence time measurements. Revue Générale de Thermique, 36, 8, 635-644.

[208] Roetzel, W., Balzereit, F., 2000. Axial dispersion in shell-and-tube heat exchangers. *Int. J. Therm. Sci.* 39, 1028–1038.

[209] Romeo, E., Royo, C., Monzón, A. 2002. Improved explicit equations for estimation of the friction factor in rough and smooth pipes. *Chem. Eng. J.* 86, 369-374.

[210] Sablani, S.S., Shayya, W.H., Kacimov, A. 2003. Explicit calculation of the friction factor in pipeline flow of Bingham plastic fluids: a neural network approach. *Chem. Eng. Sci.* 58, 99-106.

[211] Sadat, H., Dubus, N., Dez, V. L., Tatibouët, J.M., Barrault, J., 2010. A simple model for transient temperature rise and fall in a dielectric barrier discharge reactor after ignition and shut down, *J. Electrostatics*, 68, 27–30.

[212] Saeman, W.C., 1951. Passage of solids through rotary kilns: factors affecting time of passage. *Chem. Eng. Prog.* 47, 508-514.

[213] Sai, P.S.T., Surender, G.D., Damodaran, A.D., Suresh, V., Philip, Z.G., Sankaran, K., 1990. Residence time distribution and material flow studies in a rotary kiln. *Metal. Trans. B*, 21B, 1005-1011.

[214] Sajid, M., Hayat, T., 2008a. Comparison of HAM and HPM methods in nonlinear heat conduction and convection equations. *Nonlinear Anal.: Real World Appl.* 9, 2296-2301.

[215] Sajid, M., Hayat, T. 2008b. The application of homotopy analysis method to thin film flows of a third grade fluid. *Chaos Solitons Fractals* 38, 506-515.

[216] Sakin, M., Ertekin, F.K., Llicali, C., 2009. Convection and radiation combined surface heat transfer coefficient in baking ovens, *J. Food Eng.*, 94, 344-349.

[217] Sanchez, F., Abbaoui, K., Cherruault, Y., 2000. Beyond the thin-sheet approximation: Adomian's decomposition. *Optics Commun.*, *173*, 397-401.

[218] Scott, D.M., Davidson, J.F., Lim, S.-Y., Spurling, R.J., 2008. Flow of granular material through an inclined, rotating cylinder fitted with dam. *Powder Tech.* 182, 466-473.

[219] Sen, A.K., Trinh, S., 1986. An exact solution for the rate of heat transfer from a rectangular fin governed by a power law type temperature dependence. *ASME J. Heat Tr.* 108, 457-459.

[220] Sen, A.K., 1988. An application of the Adomian decomposition method to the transient behaviour of model biochemical reaction. *J. Math. Anal. Appl.* 131, 232-245.

[221] Seng, V., Abbaoui, K., Cherruault, Y., 1996. Adomian's polynomials for nonlinear operators. *Math. Comput. Model.* 24, 59-65.

[222] Serghides, T.K., 1984. Estimate friction factor accurately. *Chem. Eng.* 91, 63-64.

[223] Shah, Y.T., Paraskos, J.A., 1975. Approximate solutions to single and two phase axial dispersion problems in isothermal tubular flow reactors. *Chem. Eng. Sci.* 30, 465-471.

[224] Shateyi, S., Motsa, S.S., Sibanda, P., 2010. Homotopy analysis of heat and mass transfer boundary layer flow through a non-porous generation. *The Canad. J. Chem. Eng.* 9999, 1-8.

[225] Shi-Bin, L., Sun, Y.P., Scott, K., 2003. Analytic solution of diffusion-reaction in spherical porous catalyst. *Chem. Eng. Tech.* 26, 87-95.

[226] Siddiqui, A.M., Mahmood, R. Ghori, Q.K., 2008a. Homotopy perturbation method for thin film flow of a third grade fluid down an inclined plane. *Chaos Solitons Fractals* 35, 140-147.

[227] Siddiqui, A.M., Zeb, A., Ghori, Q.K., Benharbit, A.M., 2008b. Homotopy perturbation method for heat transfer flow of a third grade fluid between parallel plates. *Chaos Solitons Fractals* 36, 182-192.

[228] Siddiqui, A.M., Hameed, M., Siddiqui, B.M., Ghori, Q.K. 2010. Use of Adomian decomposition method in the study of parallel plate flow of a third grade fluid. *Commun. Nonlinear Sci. Numer. Simul.* 15, 2388-2399.

[229] Siegel, R., Howell, J.R., 1992. Thermal Radiation Heat Transfer. Fourth ed., Taylor and Francis, New York.

[230] Smith, J.M., Van Ness, H.C., Abbott, M.M., 2003. Introduction to Chemical Engineering Thermodynamics, Sixth ed., McGraw-Hill, New York.

[231] Sporleder, F., Dorao, C.A., Jakobsen, H.A., 2010. Simulation of chemical reactors using the least-squares spectral element method. *Chem. Eng. Sci.* 65, 5146-5159.

[232] Spurling, R.J., 2000. Granular Flow in an Inclined Rotating Cylinder: Steady State and Transients. Ph.D. Thesis, Department of Chemical Engineering, University of Cambridge, UK.

[233] Spurling, R.J., Davidson, J.F., Scott, D.M., 2001. The transient response of granular flows in an inclined rotating cylinder. *Trans. IChemE.* 79, 51-61.

[234] Su, J., 2004. Improved lumped models for transient radiative cooling of a spherical body. *Int. Commun. Heat Mass Tr.* 31, 85-94.

[235] Sudah, O.S., Chester, A.W., Kowalski, J.A., Beeckman, J.W., Muzzio, F.J., 2002. Quantitative characterization of mixing processes in rotary calciners. *Powder Tech.* 126, 166-173.

[236] Sullivan, J.D., Maier, C.G., Ralston, O.C., 1927. Passage of solid particles through rotary cylindrical kilns. U.S. Bureau of Mines, Technical Papers 384, 1-42.

[237] Sun, Y.-P., Liu, S., Scott, K., 2004. Approximate solution for the nonlinear model of diffusion and reaction in porous catalysts by means of the homotopy analysis method. *Chem. Eng. J.* 102, 1-10.

[238] Sun, Y.P., Scott, K., 2004. An analysis of the influence of mass transfer on porous electrode performance. *Chem. Eng. J.* 102, 83–91.

[239] Sunden, B., Heggs, P.J. (Eds.), 2000. Recent Advances in Analysis of Heat Transfer for Fin Type Surfaces. WIT Press, Southampton, Boston.

[240] Sweet, E., 2009. Analytical and Numerical Solutions of Differential Equations arising in Fluid Flow and Heat Transfer. Ph.D. Thesis, Department of Mathematics, University of Central Florida, Florida, US.

[241] Tan, X., Li, K., 2000. Investigation of novel membrane reactors for removal of dissolved oxygen from water. *Chem. Eng. Sci.* 55, 1213-1224.

[242] Tan, Z., Su, G., Su, J., 2009. Improved lumped models for combined convective and radiative cooling of a wall. *Appl. Therm. Eng.*, 29, 2439–2443.

[243] Tari, H., Ganji, D.D., Babazadeh, H. 2007. The application of He's variational iteration method to nonlinear equations arising in heat transfer, *Phys. Lett. A* 363, 213–217.

[244] Taylor, G.I., 1953. Dispersion of soluble matter in solvent flowing through a tube. *Proc. Royal Soc. A* 219, 186-203.

[245] Theodoropoulou, A., Adomaitis, R. A., Zafiriou, E., 1998. Model reduction for optimization of rapid thermal chemical vapor deposition systems, *IEEE Trans. Semicond. Manuf.*, 11, 85-98.

[246] Thiele, E. W., 1939. Relation between catalytic activity and size of particle, *Ind. Eng. Chem.* 31, 916-920.

[247] Tien, W., Chen, C., 2009. Adomian decomposition method by Legendre polynomials. *Chaos Solitons Fractals.* 39, 2093-2101.

[248] Turian, R.M., 1973. Solutions of problems in chemical flow reactors by perturbation methods. *Chem. Eng. Sci.* 28, 2021-2031.

[249] Turkyilmazoglu, M. 2010. A note on the homotopy analysis method. *Appl. Math. Lett.* 23, 1226–1230.

[250] Turkyilmazoglu, M., 2011. Some issues on HPM and HAM methods: A convergence scheme. *Math. Comp. Model.* 53, 1929–1936.

[251] Vajravelu, K., Cannon, J.R., Rollins, D., Leto, J., 2002. On solutions of some nonlinear differential equations arising in third grade fluid flows, *Int. J. Eng. Sci.* 40, 1791-1805.

[252] Valdes-Parada, F.J., Sales-Cruz, M., Ochoa-Tapia, J.A., Alvarez-Ramirez, J., 2008. On Green's function methods to solve nonlinear reaction-diffusion systems. *Comp. Chem. Eng.* 32, 503-511.

[253] Varma, A., Morbidelli, M., 1997. Mathematical Methods in Chemical Engineering. Oxford University Press, New York.

[254] Venkatarangan, S.N., Rajalakshmi, K., 1995. Modification of Adomian deomposition method to solve equations containing radicals. *Comput. Math. Appl.*, 29, 75-80.

[255] Villadsen, J, Michelsen, M.L., 1978. Solution of Differential Equation Models by Polynomial Approximation. Prentice-Hall Inc., New Jersey.

[256] Wan, C.G., Ziegler, E.N., 1970. On the axial dispersion approximation for laminar flow reactors. *Chem. Eng. Sci.* 25, 723-727.

[257] Wanchoo, R. K., Sharma, S. K., Bansal, R., 1996. Rheological parameters of some water soluble polymers. *J. Polym. Mat.,* 13, 49-55.

[258] Wanchoo, R. K., Narula, M., Thakur, A., 2007a. Miscibility studies on some water soluble polymer-polymer blends. *J. Polym. Mat.,* 24, 57-64.

[259] Wanchoo, R. K., Kaur, N., Bansal, A., Thakur, A., 2007b. RTD in trickle bed reactors: experimental study, *Chem. Eng. Commun.,* 194:11, 1503-1515.

[260] Wanchoo, R. K., Thakur, A., Sweta., 2008. Viscometric and rheological behaviour of Chitosan-Hydrophilic polymer blends. *J. Chem. Biochem. Eng.,* 22, 15-24.

[261] Wang, Shu-Qiang, He, J.H., 2008. Variational iteration method for a nonlinear reaction-diffusion process. *Int. J. Chem. Reac. Eng.* 6, Article A37.

[262] Wang, Y., Ali, N., Hayat, T., Oberlack, M., 2011. Peristaltic motion of a magnetohydrodynamic micropolar fluid in a tube. *Appl. Math. Model.,* 35, 3737-3750.

[263] Wang, Qi. 2011. The optimal homotopy-analysis method for Kawahara equation. *Nonlinear Anal.: Real World Appl.* 12, 1555-1561.

[264] Wazwaz, A.M., 1998. A comparison between Adomian decomposition method and Taylor series method in the series solutions. *Appl. Math. Comput.* 97, 37-44.

[265] Wazwaz, A.M., 2000a. Approximate solutions to boundary value problems of higher order by the decomposition method. *Comput. Math. Appl.* 40, 679-691.

[266] Wazwaz, A.M., 2000b. A new algorithm for calculating Adomian polynomials for nonlinear operators. *Appl. Math. Comput.* 111, 53-69.

[267] Wazwaz, A.M., 2002. A new method for solving singular initial value problems in the second-order ordinary differential equations. *Appl. Math. Comput.* 128, 45–57.

[268] Wazwaz, A.M., 2005. Adomian decomposition method for a reliable treatment of the Emden–Fowler equation. *Appl. Math. Comput.* 161, 543–560.

[269] Wehner, J.F., Wilhelm, R.H., 1956. Boundary conditions of flow reactor. *Chem. Eng. Sci.* 6, 89-93.

[270] Wheeler, A., 1955. Reaction rate and selectivity in catalyst pores, *Catalysis* 2, 105-165.

[271] Wissler, E.H., 1969. On the asymptotic behaviour of a tubular reactor in the limit of small axial diffusivity. *Chem. Eng. Sci.* 24, 829-832.

[272] Xu. H., Liao, S.J., 2008. Dual solutions of boundary layer flow over an upstream moving plate. *Commun. Nonlinear Sci. Numer. Simul.*, 13, 350-358.

[273] Yeh, R.H., Liaw, S.P., 1990. An exact solution for thermal characteristics of fins with power-law heat transfer coefficient. *Int. Commun. Heat Mass Tr.* 17, 317-330.

[274] Zain, O.S., Kumar, S., 1996. Simulation of multiple effect evaporator for concentrating caustic soda solution - computational aspects. *J. ChE. Eng. Japan* 29, 889-893.

[275] Zhu, H., Shu, H., Ding, M., 2010. Numerical solutions of partial differential equations by discrete homotopy analysis method. *Appl. Math. Comput.* 216, 3592–3605.

[276] Zigrang, D.J., Sylvester, N.D., 1982. Explicit approximations to the Colebrooks friction factor. *AIChE J.* 28, 514-515.

Transient convective-radiative cooling of a lumped body

Roots of the quartic equation $\dfrac{Bi_c}{N_{rc}}(\theta_{av} - \theta_a) + (\theta_{av}^4 - \theta_a^4) = 0$ are given as follows:

$$r_1 = \theta_a$$

$$r_2 = \frac{1}{3}\left(-\theta_a - \frac{16^{1/3}e_1\theta_a^2}{\gamma^{1/3}} + \frac{\gamma^{1/3}}{2^{1/3}e_1}\right)$$

$$r_3 = \frac{1}{3}\left(-\theta_a + \frac{2^{1/3}\left(1+i\sqrt{3}\right)e_1\theta_a^2}{\gamma^{1/3}} - \frac{\left(1-i\sqrt{3}\right)\gamma^{1/3}}{16^{1/3}e_1}\right)$$

$$r_4 = \frac{1}{3}\left(-\theta_a + \frac{2^{1/3}\left(1-i\sqrt{3}\right)e_1\theta_a^2}{\gamma^{1/3}} - \frac{\left(1+i\sqrt{3}\right)\gamma^{1/3}}{16^{1/3}e_1}\right)$$

where $\gamma = (-27e_1^2 - 20e_1^3\theta_a^3 + 3\sqrt{3}\sqrt{27e_1^4 + 40e_1^5\theta_a^3 + 16e_1^6\theta_a^6})$ and $e_1 = \dfrac{N_{rc}}{Bi_c}$. Following

points can be noted down regarding the properties of the roots:

(i) First root is known a priory and is having a real positive value, i.e. $r_1 = \theta_a (>0)$.

(ii) Second root is negative and real [say r_2] whereas, the third and fourth roots [r_3 and r_4] are complex conjugates.

(iii) No root is repeated [multiplicity of all the roots is one].

Transient convective-radiative cooling of a lumped body

Constants A_1, B_1, C_1 and D_1 appeared in Eqs. (3.20)-(3.22) due to the partial fraction decomposition in Eq. (3.19) are given as follows:

$$A_1 = \frac{1}{(r_1 - r_2)\left((r_1^2 - (r_3 + r_4)r_1 + r_3 r_4)\right)} = \frac{1}{(r_1 - r_2)\left((r_1 - a)^2 + b^2\right)}$$

$$B_1 = \frac{1}{(r_2 - r_1)\left((r_2^2 - (r_3 + r_4)r_2 + r_3 r_4)\right)} = \frac{1}{(r_2 - r_1)\left((r_2 - a)^2 + b^2\right)}$$

$$C_1 = \frac{r_1 + r_2 - r_3 - r_4}{(r_3 - r_1)(r_3 - r_2)(r_1 - r_4)(r_2 - r_4)} = \frac{r_1 + r_2 - 2a}{\left((r_1 - a)^2 + b^2\right)\left((r_2 - a)^2 + b^2\right)}$$

$$D_1 = \frac{r_1 r_2 - r_1 r_3 - r_2 r_3 + r_3^2 - r_1 r_4 - r_2 r_4 + r_3 r_4 + r_4^2}{(r_3 - r_1)(r_3 - r_2)(r_1 - r_4)(r_2 - r_4)} = \frac{r_1 r_2 - 2(r_1 + r_2)a + 3a^2 - b^2}{\left((r_1 - a)^2 + b^2\right)\left((r_2 - a)^2 + b^2\right)}$$

Steady state heat conduction in a metallic rod

Here, we show that the same analytical solutions [Eqs. (3.39a) and (3.39b)] can also be obtained by using the derivative substitution method. This method is generally helpful whenever the independent variable ξ is absent in the concerned equation and has been successfully applied to solve various nonlinear ODEs (Rice and Do, 1995). In this method, it is assumed that the solution exhibits an implicit form, i.e. $f(\theta) = \xi$. In other words, the derivative θ' is a function of θ only, i.e. $\theta' = p(\theta)$. Therefore,

$\theta'' = \dfrac{1}{2}\dfrac{d\left(p(\theta)^2\right)}{d\theta}$, where $p(\theta)$ is an unknown function of θ, only.

Now, replacing θ' and θ'' in Eq. (3.36a) by the above respective relations, one obtains:

$$(1+\beta\theta)\frac{d\left(p(\theta)^2\right)}{d\theta}+2\beta p(\theta)^2 = 0 \tag{A3.1}$$

Substituting $p(\theta)^2 = y$ and after little manipulation, the above equation reduces to the following first order linear ODE:

$$(1+\beta\theta)y'+2\beta y=0 \tag{A3.2}$$

where $y'=\dfrac{dy}{d\theta}$. Now, solving the above first order linear ODE by using the integrating factor method, one finds:

$$y=\frac{C_1}{(1+\beta\theta)^2} \tag{A3.3}$$

where C_1 is a [positive] constant of integration. Using the relation $p^2 = (\theta')^2 = y$, one obtains:

$$p(\theta) = \frac{d\theta}{d\xi} = \frac{\sqrt{C_1}}{(1 + \beta\theta)} \tag{A3.4}$$

Positive sign before the radical sign has been considered to reflect the true situation. Integrating the Eq. (A3.4) once more, one finds the expression for θ [it should be noted that the equation below is similar to the Eq. (3.38)]:

$$\left(\theta + \beta\frac{\theta^2}{2}\right) = \sqrt{C_1}\,\xi + C_2 \tag{A3.5}$$

where C_2 is another constant of integration. $C_1\left[=\left(1 + \frac{\beta}{2}\right)^2\right]$ and $C_2[=0]$ have been evaluated from the associated BCs. Substituting these values in Eq. (A3.5), and solving the resultant equation for θ, one arrives at the following two solutions, which are exactly same as those given by Eqs. (3.39a) and (3.39b).

$$\theta = \frac{-1 + \sqrt{1 + 2\beta\xi + \beta^2\xi}}{\beta} \tag{A3.6a}$$

[also Eq. (3.39a)]

$$\theta = \frac{-1 - \sqrt{1 + 2\beta\xi + \beta^2\xi}}{\beta} \tag{A3.6b}$$

[also Eq. (3.39a)]

The second solution is not physically viable and is discarded.

Steady state convective heat transfer from a rectangular fin

Case 1(b): $\beta + n = -2$ & $\beta = n = -1$

(i)   Temperature profile

For this case, the Eq. (3.59) reduces into the following linear form [it should be noted that the following equation is independent of n and β]:

$$y' - 2\theta^{-1}y - 2N^2\theta = 0 \qquad (A4.1)$$

Now, by applying the integrating factor method together with BC I, the Eq. (A4.1) can be solved analytically, and the following solution is obtained:

$$y(\theta) = \left(\frac{d\theta}{d\xi}\right)^2 = 2N^2\theta^2 ln\left[\theta\big/\theta_0\right] \qquad (A4.2)$$

Simplifying the above equation and integrating it between the limits $\theta = \theta_0$ at $\xi = 0$ to θ at ξ, one finds the following integral:

$$\int_{\theta_0}^{\theta} \frac{d\theta}{\sqrt{2N^2\theta^2 ln\left[\theta\big/\theta_0\right]}} = \int_0^{\xi} d\xi \qquad (A4.3)$$

Evaluation of the above integral yields the following relation for θ:

$$\theta = \theta_0 Exp\left(\frac{N^2\xi^2}{2}\right) \qquad (A4.4)$$

[also Eq. (3.68)]

The unknown θ_0 is evaluated by using the BC II, i.e. $\theta(1) = 1$, and is given by:

$$\theta_0 = Exp\left(-N^2\big/2\right) \qquad (A4.5)$$

[also Eq. (3.69)]

Case 2(a): $\beta + n \neq -2$ & $\beta = n \neq -1$

(i)   Temperature profile

For this case, the Eq. (3.59) reduce to:

$$y' + 2n\theta^{-1}y - 2N^2\theta = 0 \qquad\qquad (A4.6)$$

Solution of the above equation can be obtained by applying the integrating factor method and is given by:

$$y = \left(\frac{d\theta}{d\xi}\right)^2 = \theta^{-2n}\left(C_1 + \frac{N^2\theta^{2+2n}}{(1+n)}\right) \qquad\qquad (A4.7)$$

where $C_1\left[= -\frac{N^2\theta_0^{2+2n}}{(1+n)}\right]$ is the constant of integration, and has been found by using the

BC I. Placing C_1 in Eq. (A4.7), one finds:

$$y = \left(\frac{d\theta}{d\xi}\right)^2 = \frac{N^2}{(1+n)}\theta^{-2n}\left(\theta^{2+2n} - \theta_0^{2+2n}\right) \qquad\qquad (A4.8)$$

Integration of the above Eq. (A4.8) between the limits $\theta = \theta_0$ at $\xi = 0$ to θ at ξ, yields the following integral:

$$\int_{\theta_0}^{\theta} \frac{\theta^n d\theta}{\sqrt{\frac{N^2}{(1+n)}\left(\theta^{2+2n} - \theta_0^{2+2n}\right)}} = \int_0^{\xi} d\xi \qquad\qquad (A4.9)$$

Evaluation of the above integral gives the following result:

$$\frac{\theta_0^{1+n}\sqrt{1-\theta^{2+2n}\theta_0^{-2-2n}}\ sin^{-1}\left[\theta^{1+n}\theta_0^{-1-n}\right]}{\sqrt{(1+n)N^2}\sqrt{\theta^{2+2n} - \theta_0^{2+2n}}} + \frac{\sqrt{(1+n)}\pi\theta_0^n}{2\sqrt{-\frac{(1+n)}{\theta_0}}\sqrt{(1+n)N^2\theta_0^{1+2n}}} = \xi \quad (A4.10)$$

After little mathematical alterations, the cumbersome expression in Eq. (A4.10) can be simplified to attain the following more convenient form of θ:

$$sin^{-1}\left[\theta^{1+n}\theta_0^{-1-n}\right] = \frac{\pi}{2} - i\sqrt{(1+n)N^2}\ \xi \qquad\qquad (A4.11)$$

426

where $i = \sqrt{-1}$. With some more rearrangements, the above expression can further be simplified into the following form:

$$\theta = \theta_0 \left(\cosh[N\sqrt{1+n}\,\xi] \right)^{\frac{1}{1+n}}$$

(A4.12)

[also Eq. (3.71)]

The unknown θ_0 in above Eq. (A4.12), can be found by satisfying the remaining BC II, i.e. $\theta(1) = 1$, and is given by the following equation:

$$\theta_0 = \left(\cosh[N\sqrt{1+n}] \right)^{\frac{-1}{1+n}}$$

(A4.13)

[also Eq. (3.72)]

Substituting the expression of θ_0 in Eq. (A4.12), the following explicit analytical solution of the dimensionless temperature is obtained:

$$\theta = \left(\frac{\cosh[N\sqrt{1+n}\,\xi]}{\cosh[N\sqrt{1+n}]} \right)^{\frac{1}{1+n}}$$

(A4.14)

Case 2(b): $\beta + n \neq -2$ & $\beta \neq n$ & $2\beta + n \neq -3$

(i)   *Temperature profile*

For this choice of β and n, Eq. (3.59) stays unaltered in its most general and original form, and is reproduced below:

$$y' + 2\beta\theta^{-1}y - 2N^2\theta^{1+n-\beta} = 0$$

(A4.15)

Solution of the above linear equation is found by using the integrating factor method and with the help of BC I, and is given by:

$$y = \left(\frac{d\theta}{d\xi} \right)^2 = \frac{2N^2}{2+n+\beta}\theta^{-2\beta}\left(\theta^{2+n+\beta} - \theta_0^{2+n+\beta} \right)$$

(A4.16)

On integrating the Eq. (A4.16) between the limits $\theta = \theta_0$ at $\xi = 0$ to θ at ξ, one finds the following integral:

427

$$\int_{\theta_0}^{\theta} \frac{\theta^\beta \, d\theta}{\sqrt{\dfrac{2N^2}{2+n+\beta}\left(\theta^{2+n+\beta} - \theta_0^{2+n+\beta}\right)}} = \int_0^{\xi} d\xi \qquad (A4.17)$$

After solving the above integral, the following analytical solution of θ is obtained:

$$\frac{\theta^{1+\beta}\sqrt{1 - \dfrac{\theta^{2+n+\beta}}{\theta_0^{2+n+\beta}}} HG_2F_1\left[\dfrac{1+\beta}{2+n+\beta}, \dfrac{1}{2}, \dfrac{3+n+2\beta}{2+n+\beta}, \dfrac{\theta^{2+n+\beta}}{\theta_0^{2+n+\beta}}\right]}{(1+\beta)\sqrt{\dfrac{2N^2(\theta^{2+n+\beta} - \theta_0^{2+n+\beta})}{2+n+\beta}}}$$

$$-\frac{\sqrt{-\pi(2+n+\beta)}\,\theta_0^{1+\beta}\,\Gamma\left[\dfrac{3+n+2\beta}{2+n+\beta}\right]}{(1+\beta)\sqrt{2N^2\theta_0^{2+n+\beta}}\,\Gamma\left[\dfrac{4+n+3\beta}{4+2n+2\beta}\right]} = \xi \qquad (A4.18)$$

[also Eq. (3.75)]

where $\Gamma[z]$ and $HG_2F_1[a,b,c,z]$ are the well known Gamma and the Gauss' Hypergeometric functions, respectively [Eqs. (3.51a) and (3.51b), respectively]. The unknown θ_0 in Eq. (A4.18) is obtained in a usual manner as shown below, i.e. by satisfying the remaining BC II [$\theta(1) = 1$].

$$\frac{\sqrt{1 - \dfrac{1}{\theta_0^{2+n+\beta}}} HG_2F_1\left[\dfrac{1+\beta}{2+n+\beta}, \dfrac{1}{2}, \dfrac{3+n+2\beta}{2+n+\beta}, \dfrac{1}{\theta_0^{2+n+\beta}}\right]}{(1+\beta)\sqrt{\dfrac{2N^2(1 - \theta_0^{2+n+\beta})}{2+n+\beta}}}$$

$$-\frac{\sqrt{-\pi(2+n+\beta)}\,\theta_0^{1+\beta}\,\Gamma\left[\dfrac{3+n+2\beta}{2+n+\beta}\right]}{(1+\beta)\sqrt{2N^2\theta_0^{2+n+\beta}}\,\Gamma\left[\dfrac{4+n+3\beta}{4+2n+2\beta}\right]} = 1 \qquad (A4.19)$$

[also Eq. (3.76)]

Thus obtained value of θ_0 is placed back in Eq. (A4.18) to get the analytical solution of dimensionless temperature θ.

Case 2(c): $\beta + n \neq -2$ & $\beta \neq n$ & $2\beta + n = -3$

(i) **Temperature profile**

For the values of β and n pertaining to this case, the Eq. (3.59) becomes:

$$y' - (3+n)\theta^{-1}y - 2N^2\theta^{\frac{(5+3n)}{2}} = 0 \qquad (A4.20)$$

The solution of the above equation can be found by using the integrating factor method and BC I, and is found to be:

$$y = \left(\frac{d\theta}{d\xi}\right)^2 = \frac{4N^2}{1+n}\theta^{\frac{(3+n)}{2}}\left(\theta^{\frac{1+n}{2}} - \theta_0^{\frac{1+n}{2}}\right) \qquad (A4.21)$$

Integration of Eq. (A4.21) between limits $\theta = \theta_0$ at $\xi = 0$ to θ at ξ, yields the following integral equation:

$$\int_{\theta_0}^{\theta} \frac{d\theta}{\sqrt{\frac{4N^2}{1+n}\theta^{\frac{(3+n)}{2}}\left(\theta^{\frac{1+n}{2}} - \theta_0^{\frac{1+n}{2}}\right)}} = \int_0^{\xi} d\xi \qquad (A4.22)$$

By solving the above integral, one obtains the following analytical solution of θ for this case:

$$-\frac{\sqrt{\frac{\left(\theta^{\frac{(1+n)}{2}} - \theta_0^{\frac{(1+n)}{2}}\right)}{1+n}}\left(-\sqrt{1-\left(\frac{\theta_0}{\theta}\right)^{\frac{(1+n)}{2}}} + sin^{-1}\left[\left(\frac{\theta_0}{\theta}\right)^{\frac{(1+n)}{4}}\right]\right)}{N(\theta\theta_0)^{\frac{(1+n)}{2}}\sqrt{\left(1-\left(\frac{\theta_0}{\theta}\right)^{\frac{(1+n)}{2}}\right)}} + \frac{\pi\theta_0^{-(1+n)}\sqrt{\theta_0^{\frac{(-1+n)}{2}}}}{2N\sqrt{\frac{(1+n)}{\theta_0}}} = \xi$$

$$\qquad (A4.23)$$
$$\text{[also Eq. (3.79)]}$$

Using BC II, the unknown θ_0 is evaluated by the following equation and its subsequent substitution into Eq. (A4.23) yields the temperature profile.

$$-\frac{\sqrt{\dfrac{\left(1-\theta_0^{\frac{(1+n)}{2}}\right)}{1+n}}\left(-\sqrt{1-\theta_0^{\frac{(1+n)}{2}}}+\sin^{-1}\left[\theta_0^{\frac{(1+n)}{4}}\right]\right)}{N\theta_0^{\frac{(1+n)}{2}}\sqrt{\left(1-\theta_0^{\frac{(1+n)}{2}}\right)}}+\frac{\pi\theta_0^{-(1+n)}\sqrt{\theta_0^{\frac{(-1+n)}{2}}}}{2N\sqrt{\dfrac{(1+n)}{\theta_0}}}=1 \qquad \text{(A4.24)}$$

[also Eq. (3.80)]

Fluid flow process

Model Equations for the Flow of Third Grade Fluid between Two Parallel Plates

For the sake of completeness, the derivation of Eqs. (4.17), (4.19a)-(4.19c) and (4.40a)-(4.40c) has been taken from the works of Siddiqui et al. (2008b) [Siddiqui, A.M., Zeb, A., Ghori, Q.K., Benharbit, A.M., 2008. Homotopy perturbation method for heat transfer flow of a third grade fluid between parallel plates. *Chaos Solitons Fractals* 36, 182-192], and is reproduced below.

Basic conservation equations

The fundamental laws of the conservation of mass and conservation of momentum for an incompressible fluid are given below:

$$\nabla . u = 0 \tag{B1.1}$$

$$\rho \frac{Du}{Dt} = \rho f + \nabla . \tau \tag{B1.2}$$

where u is the velocity field, f is body force, τ is the stress tensor, ρ is the constant density of the fluid and $\frac{D}{Dt}$ is the material derivative [substantial derivative].

Constitutive equation for a third grade fluid

The constitutive equation for a third grade fluid is

$$\tau = -pI + \mu A_1 + \alpha_1 A_2 + \alpha_2 A_1^2 + \beta_1 A_3 + \beta_2 (A_1 A_2 + A_2 A_1) + \beta_3 (tr A_2) A_1$$

$$\tag{B1.3}$$

where p is the fluid pressure, μ is the coefficient of viscosity, α_i and β_i are the material constants [material moduli (Rivlin and Ericksen, 1955)], A_1, A_2, A_3 are the

kinematic tensors (Rajagopal and Sciubba, 1984) defined by

$$A_1 = L^T + L \qquad (B1.4)$$

$$A_n = \frac{DA_{n-1}}{Dt} + A_{n-1}L + L^T A_{n-1}, \quad n = 2, 3 \qquad (B1.5)$$

where L is gradient of u $[= \nabla u]$.

Model equation for Couette-Poiseuille flow

Consider the steady flow of a third grade fluid between two infinite parallel plates, which are at a distance $2h$ apart [Fig. 4.9]. The lower and upper plates are, respectively, located in the planes $x = -h$ and $x = h$ of an orthogonal coordinate system with y-axis in the direction of flow. The velocity field is assumed to be of the form:

$$u = [0, u(x, y, z), 0]; \quad u(x, y, z) = u(x) \qquad (B1.6)$$

We consider that the lower plate is stationary and the fluid motion is driven by the movement of upper plate moving with a constant velocity a as well as by the constant pressure gradient. With these assumptions, the continuity equation is satisfied identically, and the momentum equation [Eq. (B1.2)] yields

$$\mu \frac{\partial^2 u}{\partial x^2} + 6(\beta_2 + \beta_3)\left(\frac{\partial u}{\partial x}\right)^2 \frac{\partial^2 u}{\partial x^2} = \frac{\partial \hat{p}}{\partial y} \qquad (B1.7)$$

$$\frac{\partial \hat{p}}{\partial x} = \frac{\partial \hat{p}}{\partial z} = 0 \qquad (B1.8)$$

Thus $\hat{p}$ [generalized pressure] is a function of y alone and is given by

$$\hat{p} = p - (2\alpha_1 + \alpha_2)\left(\frac{du}{dx}\right)^2 \qquad (B1.9)$$

Further, from Eqs. (B1.7) and (B1.8) we find that

$$\frac{\partial \hat{p}}{\partial y} = \text{constant} = \frac{d\hat{p}}{dy}. \qquad (B1.10)$$

Fluid flow process

Derivation of the Solutions for Case 2(b) and Case 2(c)

Case 2(b): Couette-Poiseuille flow with upper plate moving in positive y direction with a high velocity [a>0 and large]

In this situation, the maximum velocity of the fluid [U_0], due to the higher plate velocity, will be same as that of the moving plate, and throughout the region $-1 \leq X \leq 1$, the velocity gradient will be positive [$U' > 0$]. In other words, the location X^*, where $U' = 0$, will lie outside the region of interest, i.e. $X^* > 1$. However, in the region of interest [$-1 \leq X \leq 1$], the location of the maximum velocity will lie at the moving plate, i.e. at $X = 1$. Hence, one can replace $X^* > 1$ with $X^* = 1$, and U_0 with A. As a result, one need not to evaluate the values of X^* and U_0 in such situations. To obtain the solution for this situation, the same methodology as followed in subsection 4.2.2.2, has also been adopted here, and one can initiate again with Eq. (4.41), while retaining the positive sign for the slope, i.e.

$$U' = \frac{dU}{dX} = +\sqrt{\frac{-1 + \sqrt{1 + 12\beta(C_1 - 2U)}}{6\beta}} \qquad \text{for } -1 \leq X \leq 1 \qquad \text{(B2.1)}$$

where C_1 is the constant of integration. After slight rearrangement and the subsequent integration of the above equation, the following implicit analytical solution of U is obtained.

$$-\frac{\sqrt{-1 + \sqrt{1 + 12\beta(C_1 - 2U)}}\left(2 + \sqrt{1 + 12\beta(C_1 - 2U)}\right)}{3\sqrt{6\beta}} = X + C_2 \qquad \text{(B2.2)}$$

where C_2 is the second constant of integration. To find the unknown C_1 and C_2, the Eq. (B2.2) is forced to satisfy the associated BCs, i.e. Eqs. (4.40b) and (4.40c). In doing so, the following coupled equations are obtained:

$$-\frac{\sqrt{-1+\sqrt{1+12\beta C_1}}\left(2+\sqrt{1+12\beta C_1}\right)}{3\sqrt{6\beta}}=-1+C_2 \tag{B2.3a}$$

$$-\frac{\sqrt{-1+\sqrt{1+12\beta(C_1-2A)}}\left(2+\sqrt{1+12\beta(C_1-2A)}\right)}{3\sqrt{6\beta}}=1+C_2 \tag{B2.3b}$$

C_1 can also be obtained by using the following equation, which has been obtained by adding the Eqs. (B2.3a) and (B2.3b).

$$-\sqrt{-1+\sqrt{1+12\beta(C_1-2A)}}\left(2+\sqrt{1+12\beta(C_1-2A)}\right)$$

$$+\sqrt{-1+\sqrt{1+12\beta C_1}}\left(2+\sqrt{1+12\beta C_1}\right) = 6\sqrt{6\beta} \tag{B2.3c}$$

[also Eq. (4.51)]

For the given β and A [>0], the values of C_1 and C_2 can be obtained by solving the above coupled equations. Once C_1 and C_2 are known, the velocity profile U can be obtained from Eq. (B2.2). However, instead of using the implicit analytical solution, i.e. Eq. (B2.2), we have used the following explicit analytical solution of U, which has been derived by analytically solving Eq. (B2.2) for U.

$$U=\frac{1-T^2+12C_1\beta}{24\beta} \tag{B2.4}$$

[also Eq. (4.50)]

where $T=-1+\dfrac{3(2)^{1/3}}{\left(K_3+\sqrt{-2916+K_3^2}\right)^{1/3}}+\dfrac{\left(K_3+\sqrt{-2916+K_3^2}\right)^{1/3}}{3(2)^{1/3}}$,

$K_1=-3\sqrt{6\beta}$, $K_2=\sqrt{-1+\sqrt{1+12C_1\beta}}\left(2+\sqrt{1+12C_1\beta}\right)$ and

$K_3=54+27K_1^2+54K_1K_2+27K_2^2+54K_1^2X+54K_1K_2X+27K_1^2X^2$.

435

Case 2(c): Couette-Poiseuille Flow with Upper Plate Moving in Negative y Direction with a High Velocity [$A < 0$ and $|A|$ is Large]

For this subcase, the fluid moves with the upper plate in a negative y direction, therefore the maximum *positive* velocity of the fluid will be same as that of the stationary plate, i.e. 0, and throughout the concerned region [$-1 \leq X \leq 1$], the velocity gradient will be negative, i.e. $U' < 0$. Alternatively, the location X^*, where $\frac{dU}{dX} = 0$, will be positioned outside the concerned region, i.e. $X^* < -1$. However, for a realistic situation the location of the maximum velocity will lie at the stationary plate. This implies that $X^* < -1$ should be replaced with $X^* = -1$, and U_0 with 0. Here also, one starts with Eq. (4.41), however, now the negative sign for U' is retained, i.e.

$$U' = \frac{dU}{dX} = -\sqrt{\frac{-1+\sqrt{1+12\beta(C_1 - 2U)}}{6\beta}} \quad \text{for } -1 \leq X \leq 1 \tag{B2.5}$$

where C_1 is the constant of integration. Solution of the above equation yields the following implicit analytical solution of U :

$$\frac{\sqrt{-1+\sqrt{1+12\beta(C_1 - 2U)}}\left(2+\sqrt{1+12\beta(C_1 - 2U)}\right)}{3\sqrt{6\beta}} = X + C_2 \tag{B2.6}$$

where C_2 is another constants of integration. To find the unknown C_1 and C_2, Eq. (B2.6) is forced to satisfy the related BCs, i.e. Eqs. (4.40b) and (4.40c), and the following coupled equations are found:

$$\frac{\sqrt{-1+\sqrt{1+12\beta C_1}}\left(2+\sqrt{1+12\beta C_1}\right)}{3\sqrt{6\beta}} = -1 + C_2 \tag{B2.7a}$$

$$\frac{\sqrt{-1+\sqrt{1+12\beta(C_1 - 2A)}}\left(2+\sqrt{1+12\beta(C_1 - 2A)}\right)}{3\sqrt{6\beta}} = 1 + C_2 \tag{B2.7b}$$

The unknown C_1 can be found from the following equation:

436

$$\sqrt{-1+\sqrt{1+12\beta(C_1-2A)}}\left(2+\sqrt{1+12\beta(C_1-2A)}\right)$$

$$-\sqrt{-1+\sqrt{1+12\beta C_1}}\left(2+\sqrt{1+12\beta C_1}\right) \;=\; 6\sqrt{6\beta} \qquad \text{(B2.7c)}$$

[also Eq. (4.54)]

For the given values of β and A, the values of C_1 and C_2 are found by solving the above equations and can either be substituted in the implicit analytical solution, i.e. Eq. (B2.6) or in the following explicit analytical solution, i.e. Eq. (B2.8), to get the desired velocity profile U. The following explicit analytical solution of U is obtained by analytically solving the Eq. (B2.6).

$$U = \frac{1-T^2+12C_1\beta}{24\beta} \qquad \text{(B2.8)}$$

[also Eq. (4.53)]

where $T = -1 + \dfrac{3(2)^{1/3}}{\left(K_3+\sqrt{-2916+K_3^2}\right)^{1/3}} + \dfrac{\left(K_3+\sqrt{-2916+K_3^2}\right)^{1/3}}{3(2)^{1/3}}$,

$K_1 = -3\sqrt{6\beta}$, $K_2 = \sqrt{-1+\sqrt{1+12C_1\beta}}\left(2+\sqrt{1+12C_1\beta}\right)$ and

$K_3 = 54+27K_1^2 - 54K_1K_2 + 27K_2^2 + 54K_1^2X - 54K_1K_2X + 27K_1^2X^2$

437

Reaction-diffusion inside a porous spherical catalyst

Convergence Analysis of OHAM Solutions

For the model equation of reaction-diffusion process inside a porous spherical catalyst, the classical h-curves (Liao, 2003) for establishing the convergence region have been plotted in Figs. C1.1 and C1.2 for $n = 0.5$, $\phi = 2$ and $n = 2$, $\phi = 5$, respectively. In these h-curves, the flat region, where the values of variable and its derivatives remain constant, offers the proper values of h. It can be noted that as the number of terms in the OHAM solutions is increased the region of convergence widens. However, as is visible from these two figures the flat region covers a wide range of h, and hence the visual selection of proper value of h becomes difficult. In place of this, the plots of sum of square of residual errors, shown in Figs. C1.3 and C1.4, offer a somewhat better choice for the selection of proper values of h [the sum of square of residual errors approaches zero as h approaches optimum value]. Here also, the convergence region for h widens, as one increases the terms in OHAM solution. The best value of h [$= h_{optimum}$], which corresponds to the minimum value of sum of square of residual errors of the OHAM solution, can be found from these figures, i.e. Figs. C1.3 and C1.4. Alternatively, one can also use Eq. (6.9c). Since, Eq. (6.9c) directly evaluates $h_{optimum}$ it is better to employ this equation instead of finding $h_{optimum}$ from these curves.

Another way of judging the convergence of OHAM solutions is by using the ratio test theorem (Kreyszig, 2001). The theorem states: *if a series* $y_1 + y_2 + y_3 + ...$ *with* $y_n \neq 0$ [$n = 1,2,3,...$] *has the property that for every* n *greater than some* N , $\left| \dfrac{y_n}{y_{n-1}} \right| \leq q < 1$ *for* $n > N$ [*where q<1 is fixed*], *then this series converges absolutely. On the other hand, if for every* $n > N$, $\left| \dfrac{y_n}{y_{n-1}} \right| \geq 1$, *then this series diverges.*

For the same values of parameters [$n = 0.5$, $\phi = 2$; $n = 2$, $\phi = 5$], Figs. C1.5 and C1.6 show the plots of absolute ratios of terms in different OHAM solutions. The OHAM

solutions with different number of terms depict a similar trend, i.e. the absolute ratios of terms in finite OHAM series $\left(= \left| y_n \big/ y_{n-1} \right| \right)$ first decreases, then increases and then finally decreases monotonically. It is hoped that the same trend will also be observed for larger terms [approaching infinite] in OHAM solution. Therefore, there will exist a value of N, after which $\left| \dfrac{y_n}{y_{n-1}} \right| < 1$. Hence, from the above theorem the OHAM solution with very large number of terms [approaching infinite, $n_T \to \infty$] will also be convergent. Since, the sum of square of residual errors approaches zero as one increases the terms, this convergent OHAM series solution [very large number of terms, $n_T \to \infty$] will be the desired solution of the concerned equation.

Beside these curves, the ratio [absolute] of the last two terms of different OHAM solutions have also been drawn in Figs. C1.7 and C1.8. These figures show that this ratio decreases with the increase in number of terms in OHAM solution and is less than unity.
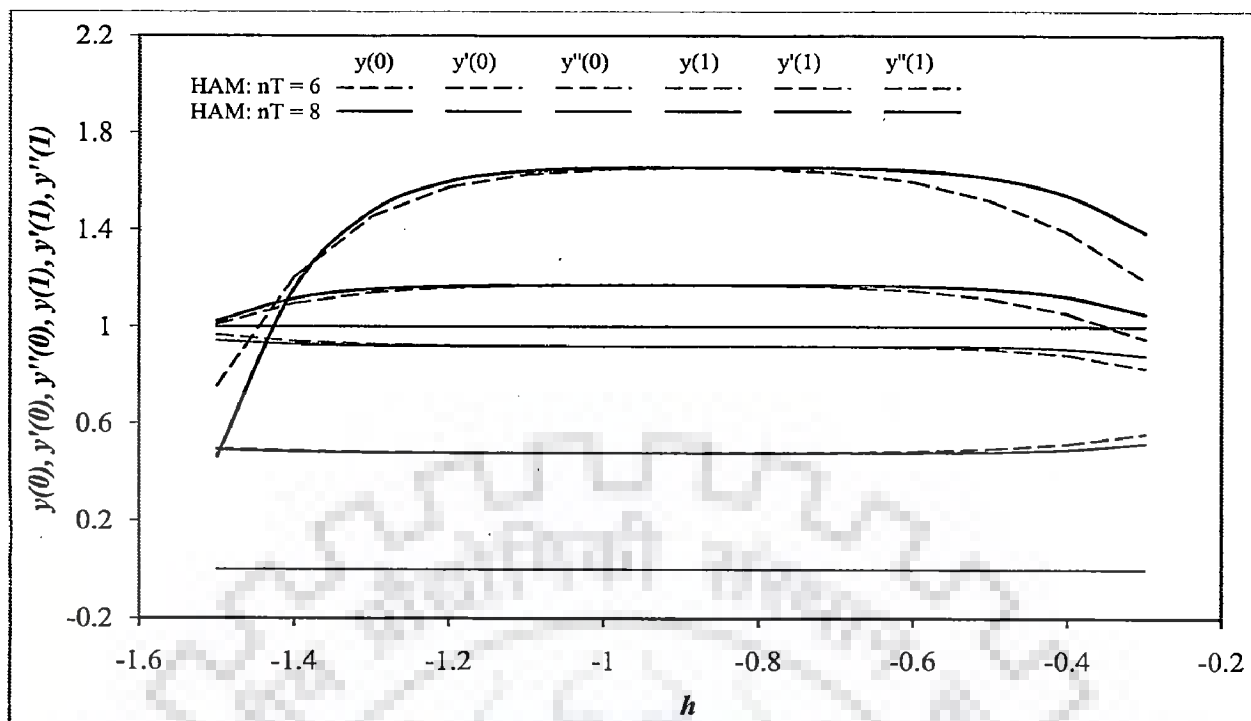
Figure C1.1: Classical h-curves [power-law kinetics: $n = 0.5$, $\phi = 2$]
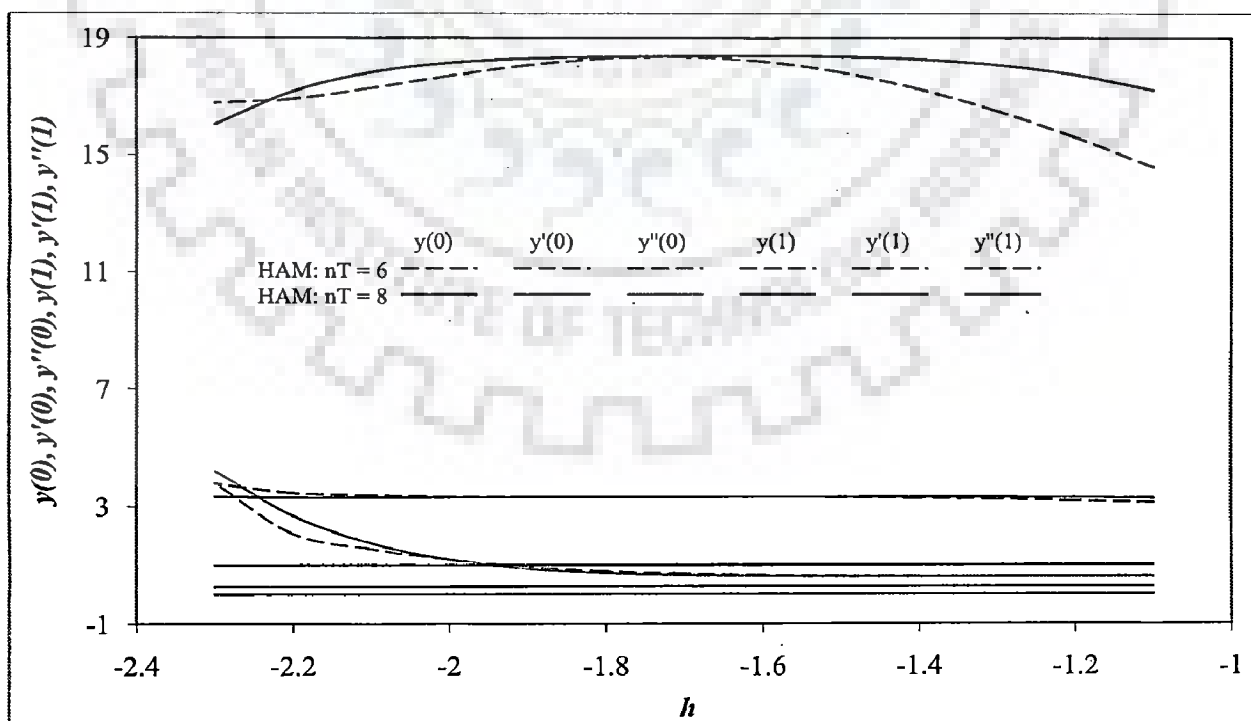
Figure C1.2: Classical h-curves [power-law kinetics: $n = 2$, $\phi = 5$]

441
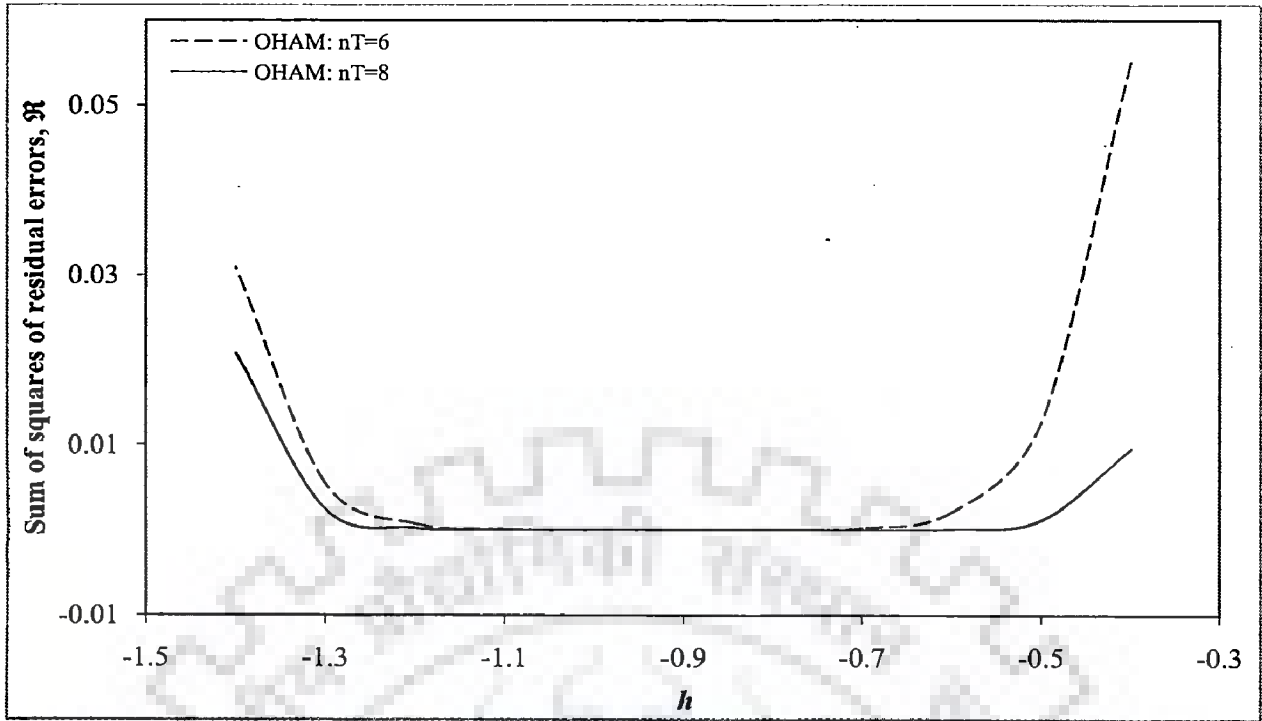
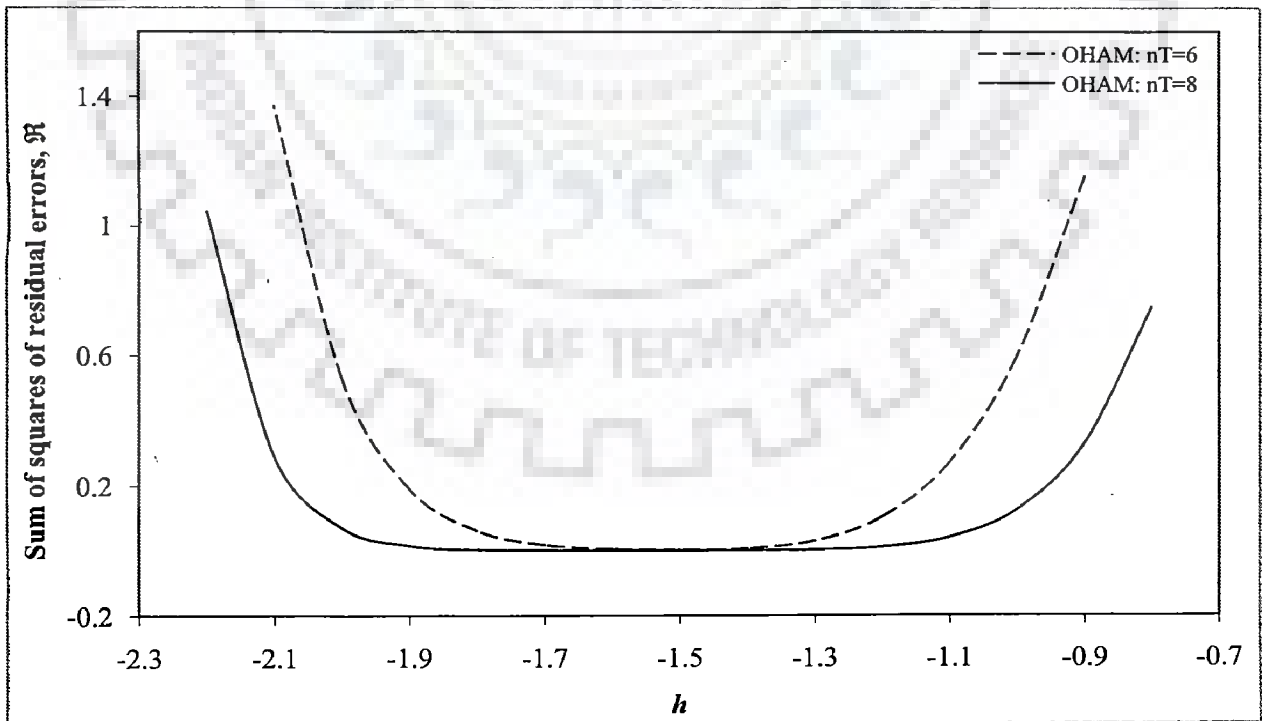**Figure C1.3:** Variation of sum of square of residual errors with h [power-law kinetics: $n = 0.5$, $\phi = 2$]

Figure C1.4: Variation of sum of square of residual errors with h [power-law kinetics: $n = 2$, $\phi = 5$]
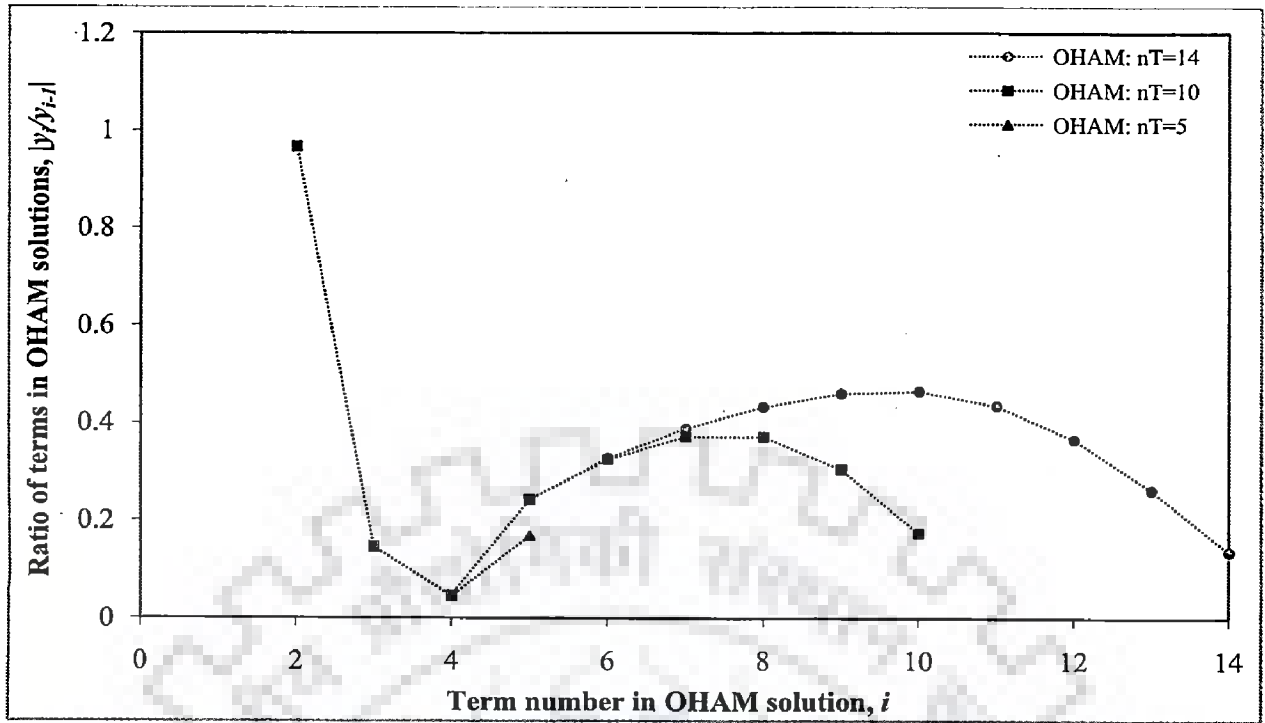
443

Figure C1.5: Variation of the absolute values of ratio of consecutive terms [= $|y_i/y_{i-1}|$, $2 \leq i \leq n_T$] with term number for different OHAM solutions [power-law kinetics: $n = 0.5$, $\phi = 2$]
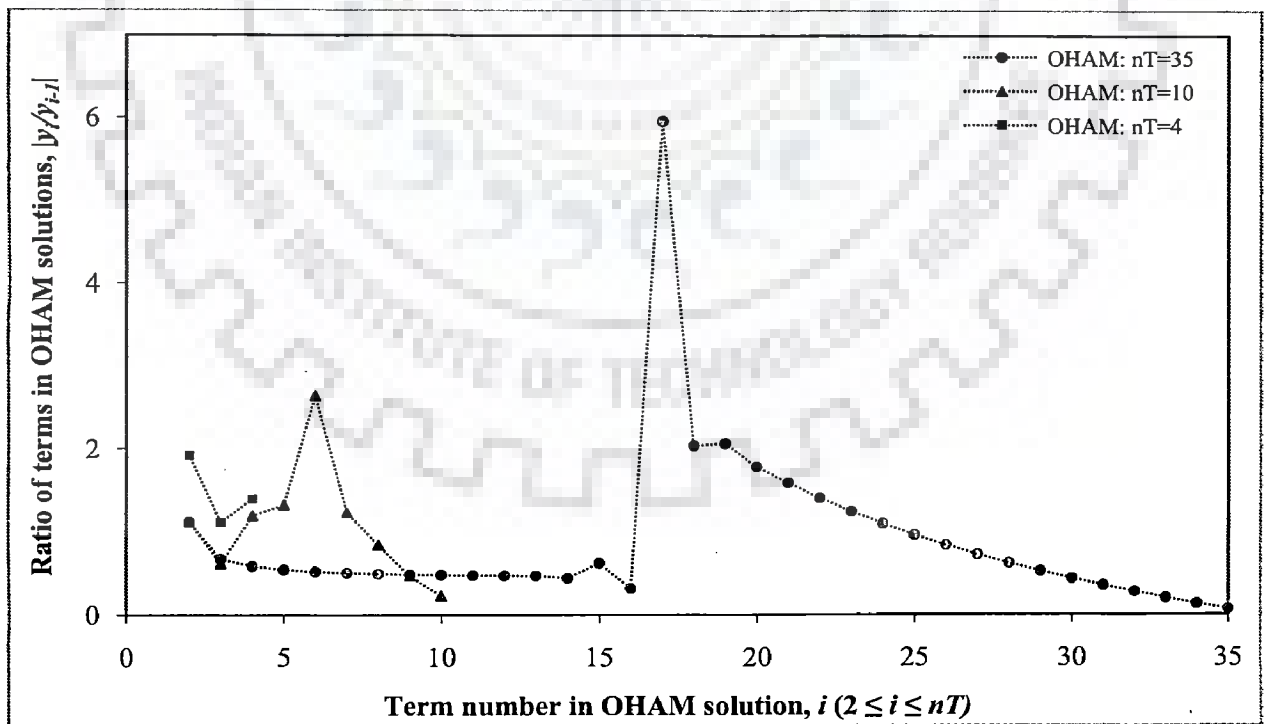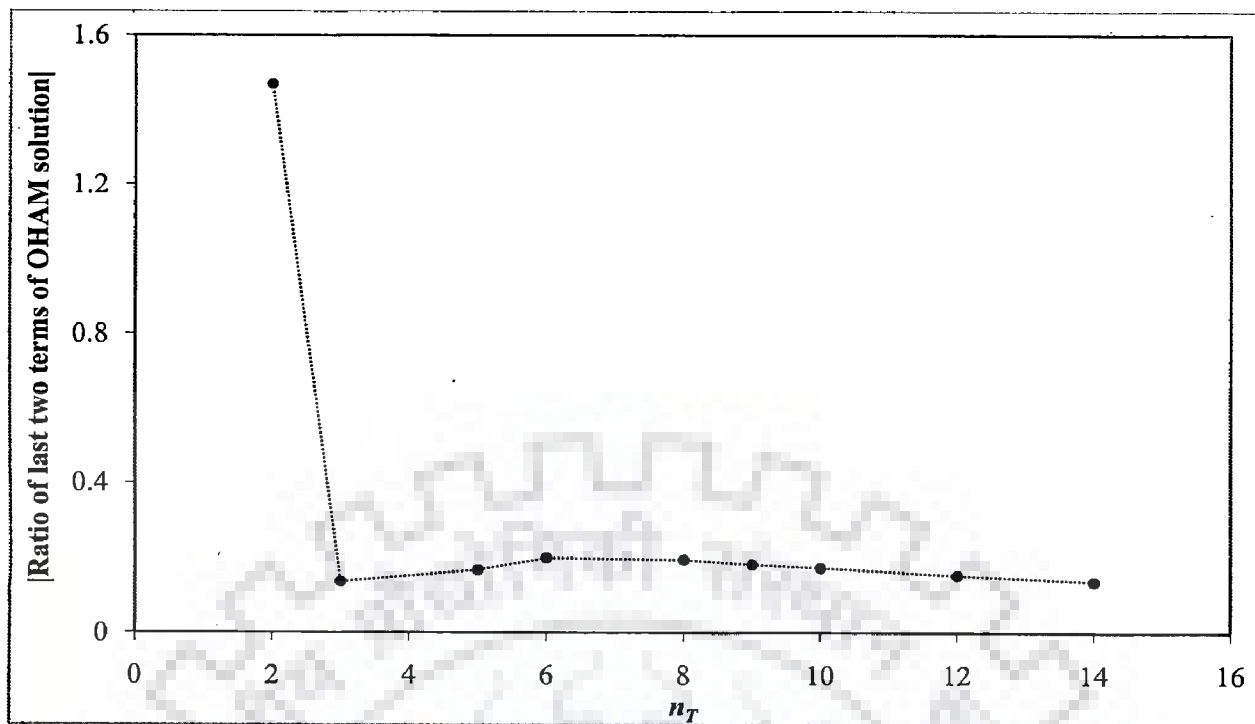

Figure C1.6: Variation of the absolute values of ratio of consecutive terms [= $|y_i/y_{i-1}|$, $2 \leq i \leq n_T$] with term number for different OHAM solutions [power-law kinetics: $n = 2$, $\phi = 5$]

Figure C1.7: Variation of the ratio [absolute] of last two terms of OHAM solutions with n_T [power-law kinetics: $n = 0.5$, $\phi = 2$]
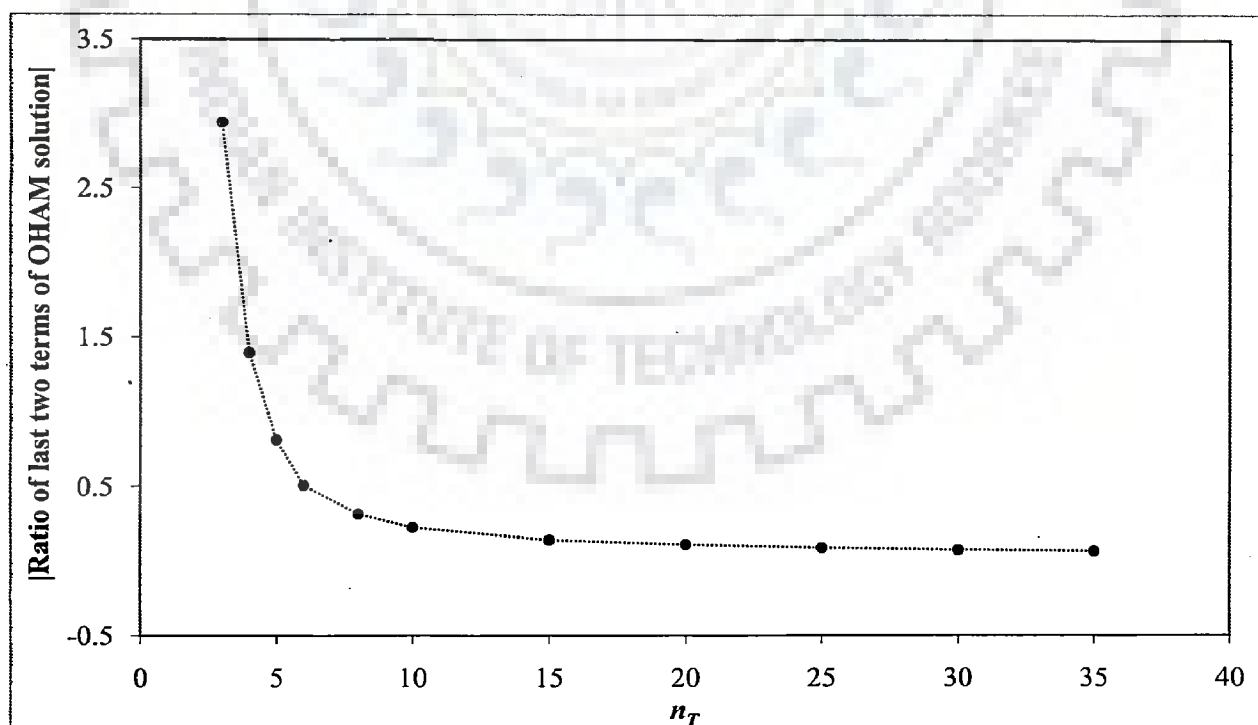
Figure C1.8: Variation of the ratio [absolute] of last two terms of OHAM solutions with n_T [power-law kinetics: $n = 2$, $\phi = 5$]

Axial dispersion model of a tubular chemical reactor

OHAM Solution for Power-Law Kinetics [$n \neq 0$]

After substituting $\lambda = 0$ in Eq. (6.46) the following m^{th} order deformation equation is obtained for power-law kinetics [$f(y) = y^n$]:

$$y_m(x) = \chi_m y_{m-1}(x) + hL^{-1}\left[\frac{d^2 y_{m-1}(x)}{dx^2}\right] + hPeL^{-1}\left[\frac{dy_{m-1}(x)}{dx}\right]$$

$$- hPe\,DaL^{-1}\left[A_{m-1}(y_0, y_1, ..., y_{m-1})\right] \qquad \text{for } m \geq 1 \qquad (C2.1)$$

The terms in the right most square brackets are the so called Adomian polynomials [$A_{m-1}(y_0, y_1, ..., y_{m-1})$] corresponding to the nonlinearity $\psi(x, \lambda)^n$ and have been obtained by expanding the nonlinear term around $\lambda = 0$ and equating the coefficients of same power of λ with those of Adomian series, i.e.

$$\psi(x, \lambda)^n = \sum_0^\infty \frac{1}{m!}\frac{\partial^m\left[\psi(x, \lambda)^n\right]}{\partial\lambda^m}\Bigg|_{\lambda=0} \lambda^m = \sum_0^\infty A_m(y_0, y_1, ..., y_m)\lambda^m \qquad (C2.2)$$

where $A_m(y_0, y_1, ..., y_m) = \frac{1}{m!}\frac{\partial^m\left[\psi(x, \lambda)^n\right]}{\partial\lambda^m}\Bigg|_{\lambda=0}$

However, $\psi(x, \lambda) = y = \sum_0^\infty y_m\lambda^m$ $\qquad (C2.3)$

where $y_m = \frac{1}{m!}\frac{\partial^m y}{\partial\lambda^m}\Bigg|_{\lambda=0}$

Hence, $\psi(x, \lambda)^n = y^n = \left(\sum_{m=0}^\infty y_m\lambda^m\right)^n = \sum_{m=0}^\infty A_m(y_0, y_1, ..., y_m)\lambda^m \qquad (C2.4)$

In this way one finds the relations between A_m and $y_0, y_1, ..., y_m$. Now, evaluating and simplifying the Eq. (C2.1), the following relations for y_ms are obtained.

$$y_1(x) = hL^{-1}\left[\frac{d^2 y_0(x)}{dx^2}\right] + hPeL^{-1}\left[\frac{dy_0(x)}{dx}\right] - hPe\,DaL^{-1}\left[\underbrace{y_0(x)^n}_{A_0}\right] \qquad \text{(C2.5a)}$$

$$y_2(x) = y_1(x) + hL^{-1}\left[\frac{d^2 y_1(x)}{dx^2}\right] + hPeL^{-1}\left[\frac{dy_1(x)}{dx}\right] - hPe\,DaL^{-1}\left[\underbrace{ny_0(x)^{n-1}y_1(x)}_{A_1}\right]$$

$$\text{(C2.5b)}$$

$$y_3(x) = y_2(x) + hL^{-1}\left[\frac{d^2 y_2(x)}{dx^2}\right] + hPeL^{-1}\left[\frac{dy_2(x)}{dx}\right]$$

$$-hPe\,DaL^{-1}\left[\underbrace{(n-1)n/2\,y_0(x)^{n-2}y_1(x)^2 + ny_0(x)^{n-1}y_2(x)}_{A_2}\right] \qquad \text{(C2.5c)}$$

$$y_4(x) = y_3(x) + hL^{-1}\left[\frac{d^2 y_3(x)}{dx^2}\right] + hPeL^{-1}\left[\frac{dy_3(x)}{dx}\right] - hPe\,DaL^{-1}$$

$$\left[\underbrace{(n-2)(n-1)n/6\,y_0(x)^{n-3}y_1(x)^3 + (n-1)ny_0(x)^{n-2}y_1(x)y_2(x) + ny_0(x)^{n-1}y_3(x)}_{A_3}\right]$$

$$\text{(C2.5d)}$$

… and so on.

As already mentioned, the above approach of finding the Adomian polynomials can conveniently be extended for any type of nonlinearity. For zero order and Langmuir-Hinshelwood kinetics the OHAM solutions are obtained as follows.

OHAM Solution for Zero Order Kinetics [$n = 0$]

Following deformation equations are obtained for zero order kinetics [$f(y) = 1$].

$$y_1(x) = hL^{-1}\left[\frac{d^2 y_0(x)}{dx^2}\right] + hPeL^{-1}\left[\frac{dy_0(x)}{dx}\right] - hPe\,DaL^{-1}[A_0(x)] \qquad \text{for} \quad m=1$$

$$\text{(C2.6a)}$$

$$y_m(x) = \chi_m y_{m-1}(x) + hL^{-1}\left[\frac{d^2 y_{m-1}(x)}{dx^2}\right] + hPeL^{-1}\left[\frac{dy_{m-1}(x)}{dx}\right] \qquad \text{for} \quad m \geq 2$$

$$\text{(C2.6b)}$$

It should be noted that the Adomian polynomials for zero order kinetics are given as:

$$A_m(x) = \begin{cases} 1 & m = 0 \\ 0 & m \geq 1 \end{cases} \tag{C2.7}$$

Using the above relations one finds the following relations for y_ms for $n_T = 10$ and $h = -1$.

$$y_0 = C_2, \qquad y_1 = \frac{DaPe}{2}x^2, \qquad y_2 = -\frac{DaPe^2}{6}x^3, \qquad y_3 = \frac{DaPe^3}{24}x^4,$$

$$y_4 = -\frac{DaPe^4}{120}x^5, \qquad y_5 = \frac{DaPe^5}{720}x^6, \qquad y_6 = -\frac{DaPe^6}{5040}x^7, \qquad y_7 = \frac{DaPe^7}{40320}x^8,$$

$$y_8 = -\frac{DaPe^8}{362880}x^9, \qquad y_9 = \frac{DaPe^9}{3628800}x^{10}$$

Eventually, the OHAM solution is given by the following series.

$$y_{OHAM} = C_2 + \frac{DaPe}{2}x^2 - \frac{DaPe^2}{6}x^3 + \frac{DaPe^3}{24}x^4 - \frac{DaPe^4}{120}x^5 + \frac{DaPe^5}{720}x^6$$

$$- \frac{DaPe^6}{5040}x^7 + \frac{DaPe^7}{40320}x^8 - \frac{DaPe^8}{362880}x^9 + \frac{DaPe^9}{3628800}x^{10} \tag{C2.8}$$

where $C_2 \left(= \dfrac{3628800(1-Da) - DaPe^9}{3628800} \right)$ has been found from the BC I. Substituting C_2

in y_{OHAM} and computing the six terms Taylor series expansion around $x = 0$, $Pe = 0$

and $Da = 0$ the resultant yields the following series expansion, i.e.

$$y_{OHAM} \approx 1 - Da + \frac{DaPe}{2}x^2 - \frac{DaPe^2}{6}x^3 + \frac{DaPe^3}{24}x^4 - \frac{DaPe^4}{120}x^5 + \frac{DaPe^5}{720}x^6 + \dots \tag{C2.9}$$

OHAM Solution for Langmuir-Hinshelwood Kinetics

Following deformation equations are obtained for Langmuir-Hinshelwood

kinetics (Fan et al., 1971) $\left(f(y) = \dfrac{Ky}{(1+Ky)} \right)$.

$$y_1(x) = hL^{-1}\left[\frac{d^2 y_0(x)}{dx^2}\right] + hPeL^{-1}\left[\frac{dy_0(x)}{dx}\right] - hPe\,DaL^{-1}\left[\underbrace{\frac{Ky_0(x)}{1+Ky_0(x)}}_{A_0}\right] \quad \text{(C2.10a)}$$

$$y_2(x) = y_1(x) + hL^{-1}\left[\frac{d^2 y_1(x)}{dx^2}\right] + hPeL^{-1}\left[\frac{dy_1(x)}{dx}\right] - hPe\,DaL^{-1}\left[\underbrace{\frac{Ky_1(x)}{(1+Ky_0(x))^2}}_{A_1}\right]$$

$$\text{(C2.10b)}$$

$$y_3(x) = y_2(x) + hL^{-1}\left[\frac{d^2 y_2(x)}{dx^2}\right] + hPeL^{-1}\left[\frac{dy_2(x)}{dx}\right]$$

$$- hPe\,DaL^{-1}\left[\underbrace{\frac{-K^2 y_1(x)^2 + Ky_2(x) + K^2 y_0(x)y_2(x)}{(1+Ky_0(x))^3}}_{A_2}\right] \quad \text{(C2.10c)}$$

$$y_4(x) = y_3(x) + hL^{-1}\left[\frac{d^2 y_3(x)}{dx^2}\right] + hPeL^{-1}\left[\frac{dy_3(x)}{dx}\right] - hPe\,DaL^{-1}$$

$$\left[\underbrace{\frac{K^3 y_1(x)^3 - 2K^2 y_1(x)y_2(x) - 2K^3 y_0(x)y_1(x)y_2(x) + Ky_3(x) + 2K^2 y_0(x)y_3(x) + K^3 y_0(x)^2 y_3(x)}{(1+Ky_0(x))^4}}_{A_3}\right]$$

$$\text{(C2.10d)}$$

452

Axial dispersion model of a tubular chemical reactor

Convergence Analysis of OHAM Solutions

The classical h-curves for the axial dispersion model equation of a tubular chemical reactor for the data of Rao et al. (1981), i.e. $n = 2$, $Pe = 10$, $Da = 2$, have been drawn in Fig. C3.1. Similarly, plots of sum of square of residual errors against h have also been drawn in Fig. C3.2. One notes that it is difficult to pick the proper value of parameter h, i.e. $h_{optimum}$, from the h-curve [Fig. C3.1], since larger flat regions exist for all the h-curves. On the other hand, the plots of sum of square of residual errors provide a relatively better option for the selection of $h_{optimum}$, and near $h_{optimum}$ the sum of square of residual errors approaches zero. Moreover, in this figure, the flat region widens with the increase in number of terms in OHAM solution, whereas there is no effect of number of terms in classical h-curves [Fig. C3.1]. Like the model equation of reaction-diffusion process in a porous spherical catalyst [Appendix C1], here also one can select $h_{optimum}$ from Fig. C3.2 or employ Eq. (6.9c).

In Figs. C3.3 and C3.4, the absolute ratios of terms in different OHAM solutions, i.e. $\left| \dfrac{y_n}{y_{n-1}} \right|$ for $n \in [2, n_T]$, and the ratio [absolute] of the last two terms of different OHAM solutions have been shown, respectively. It is visible in Fig. C3.3 that all the curves [corresponding to different OHAM solutions] eventually approach zero. Similarly, in Fig. C3.4 the ratio [absolute] of last two terms also decreases for the different OHAM solutions. Hence, from the ratio test theorem and subsequent discussion presented in Appendix C1, the convergence of OHAM solution is established. This fact has also been discussed in subsection 6.4.2.1 with the help of Figs. 6.28 and 6.29, where residual and absolute error profiles of the OHAM solutions were drawn.

In the same way, the plots of classical h-curves and the sum of square of residual errors for dual solutions [$n = -1$, $Pe = 0.2$, $Da = 0.2$] have been drawn in Figs. C3.5 and
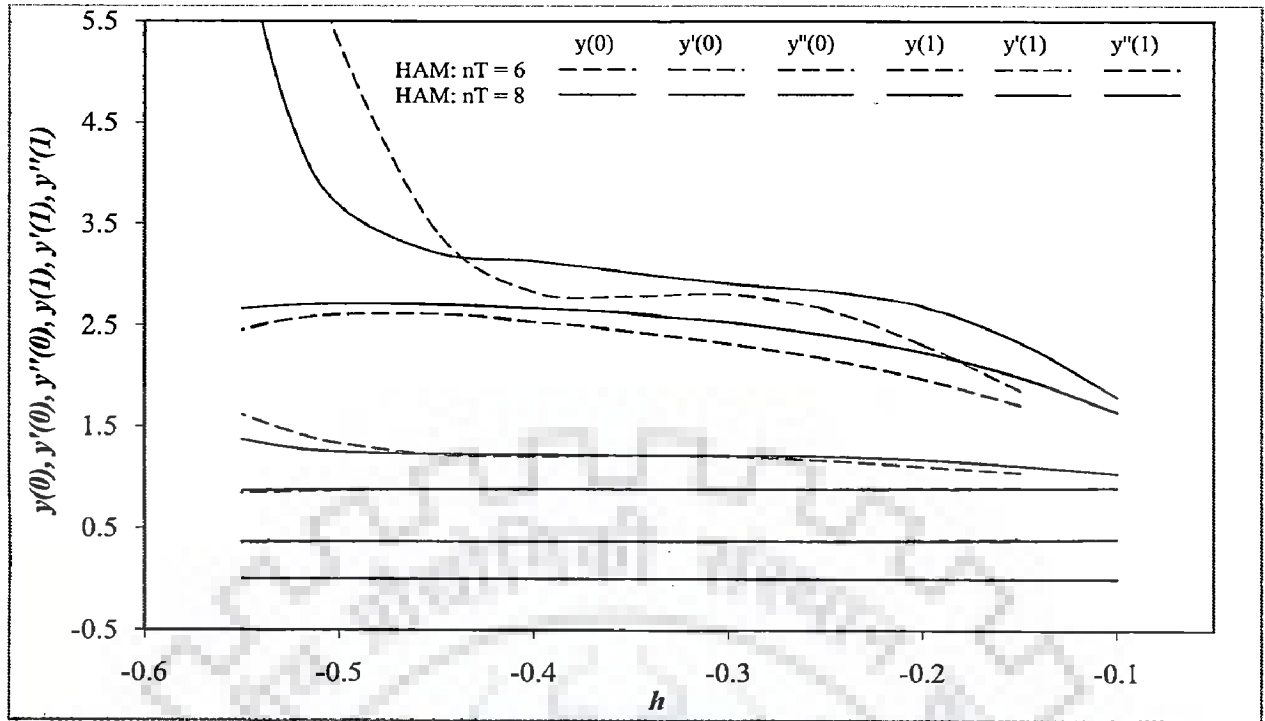
Figure C3.1: Classical h-curves for the parameter values given in Rao et al. (1981) [power-law kinetics: $n = 2$, $Pe = 10$, $Da = 2$]
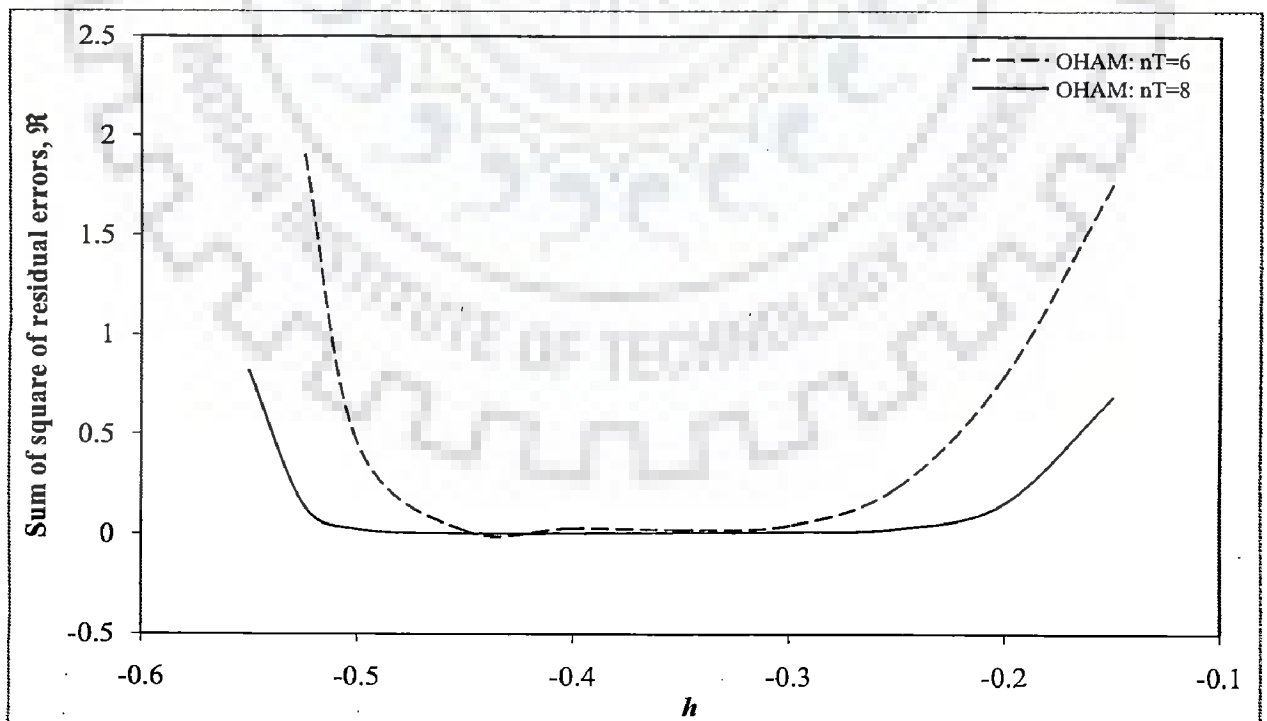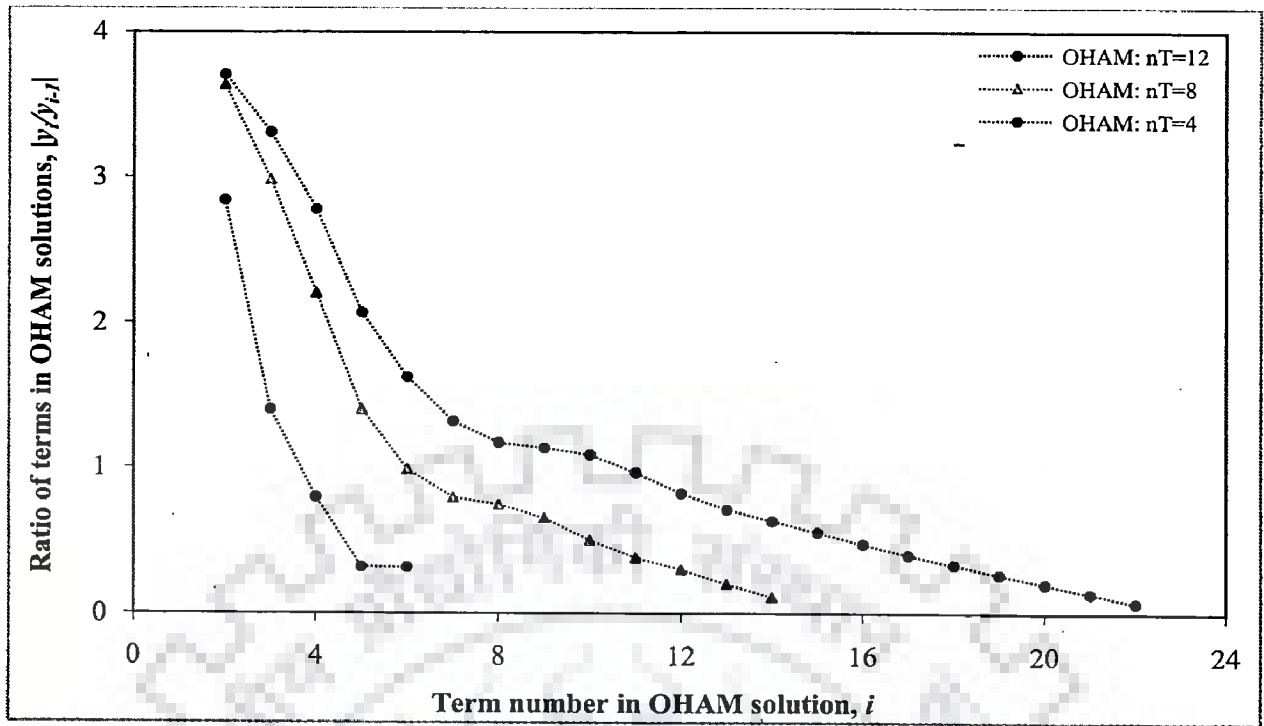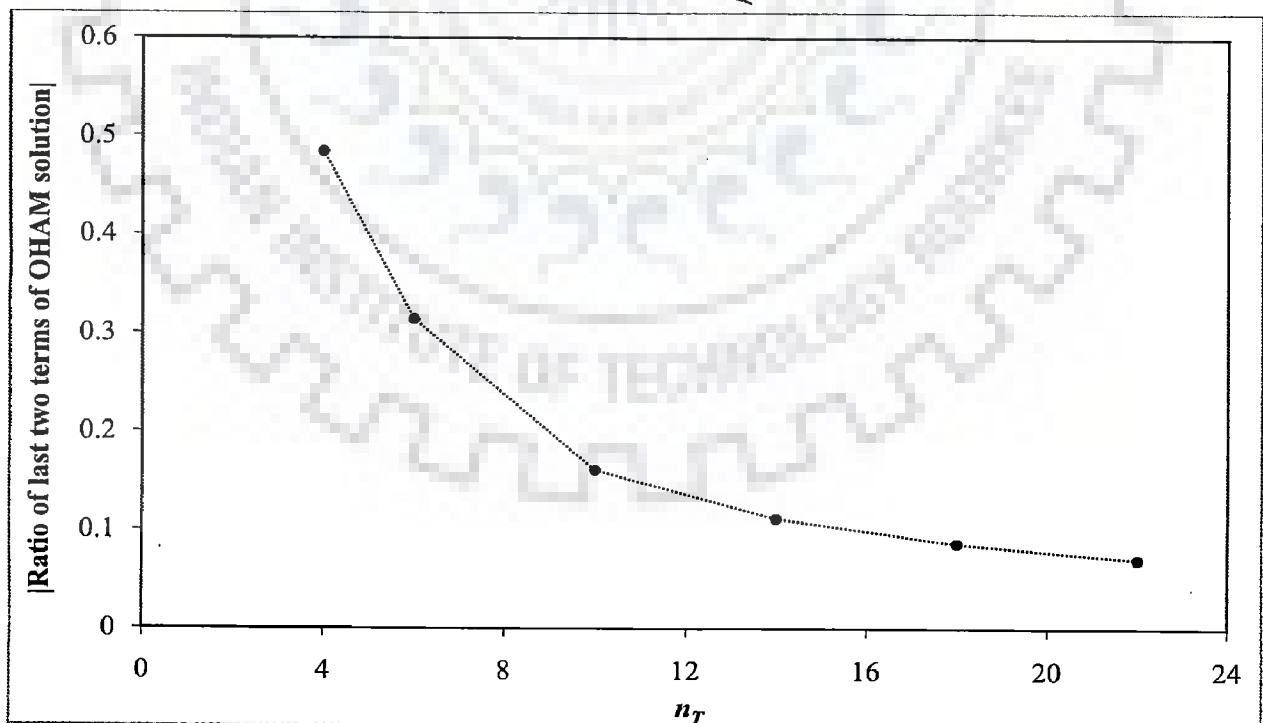

Figure C3.2: Variation of the sum of square of residual errors with h for the parameter values given in Rao et al. (1981) [power-law kinetics: $n = 2$, $Pe = 10$, $Da = 2$]

Figure C3.3: Variation of the absolute values of ratio of consecutive terms [= $|y_i/y_{i-1}|$, $2 \leq i \leq n_T$] with term number for different OHAM solutions for the parameter values given in Rao et al. (1981) [power-law kinetics: $n = 2$, $Pe = 10$, $Da = 2$]

Figure C3.4: Variation of the ratio [absolute] of last two terms of OHAM solutions with n_T for the parameter values given in Rao et al. (1981) [power-law kinetics: $n = 2$, $Pe = 10$, $Da = 2$]
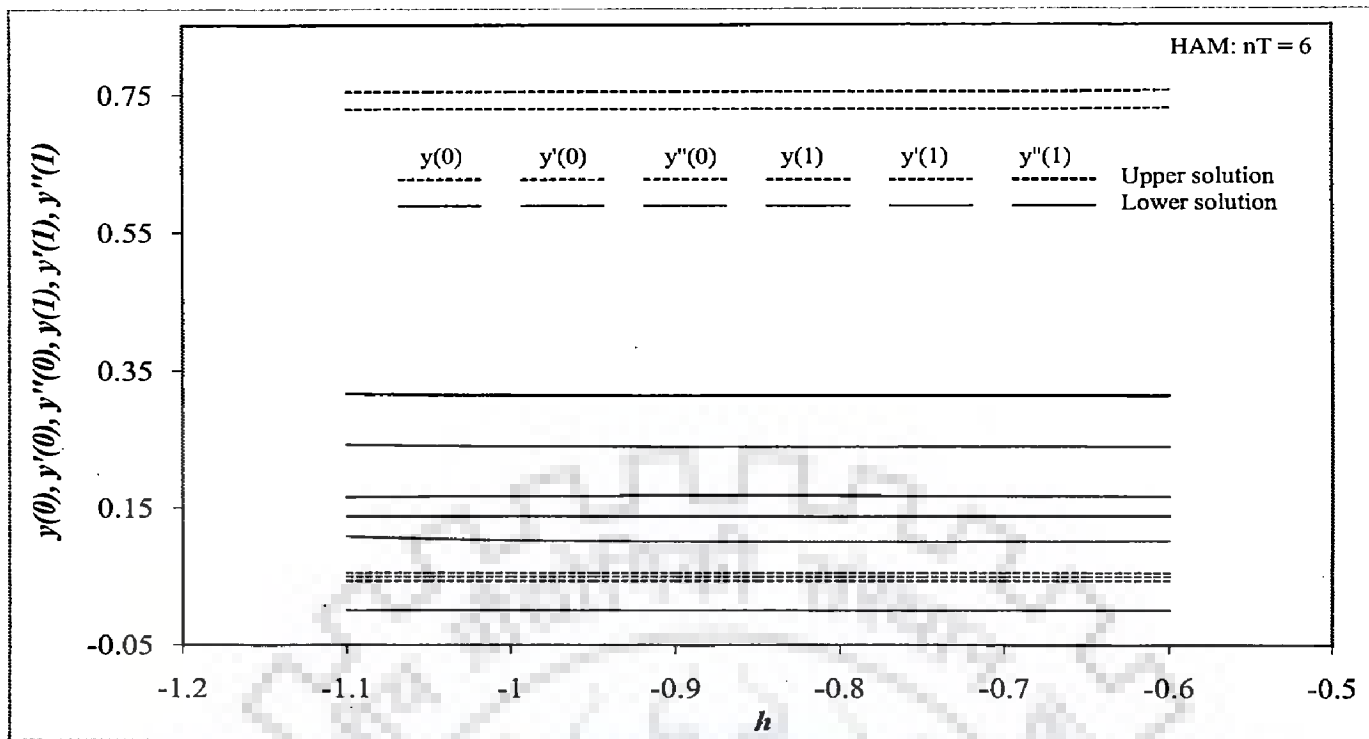
457

Figure C3.5: Classical *h*-curves for dual solutions [power-law kinetics: $n = -1$, $Pe = 1/5$, $Da = 1/5$]
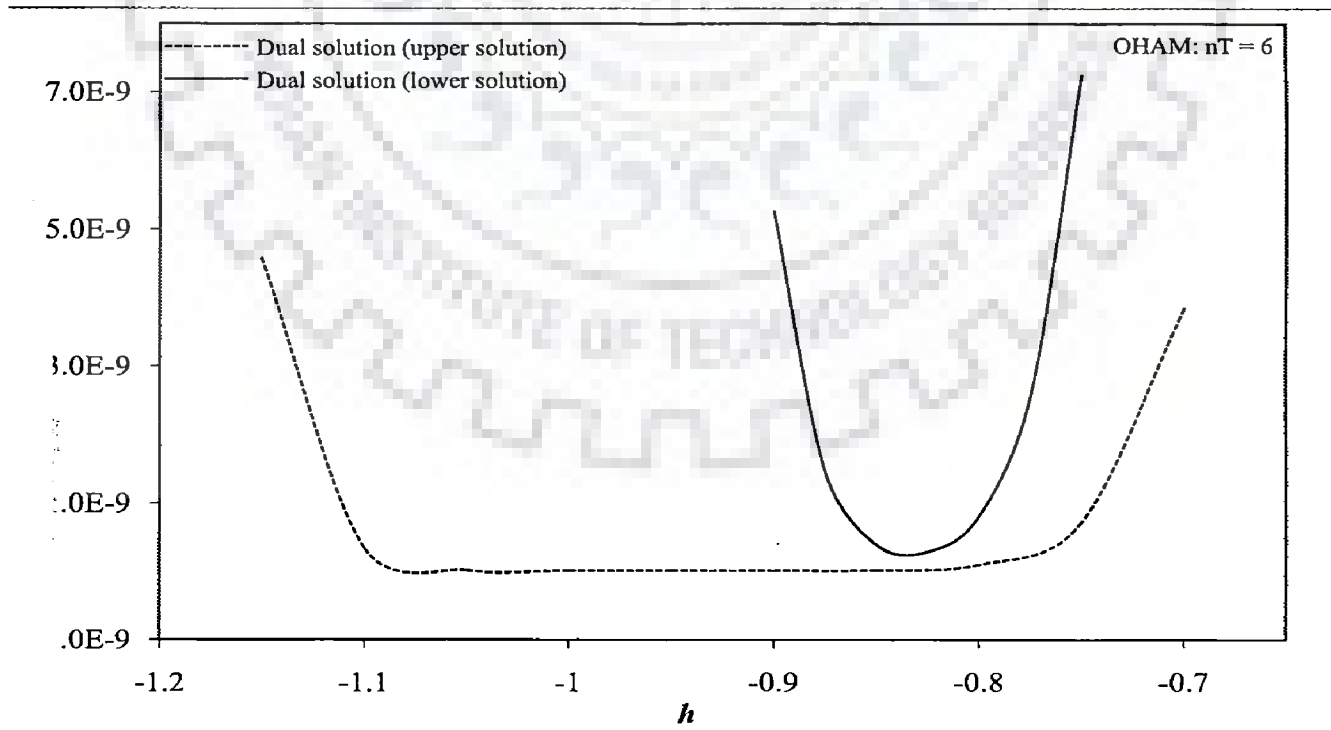

Figure C3.6: Variation of sum of square of residual errors with *h* for dual solutions [power-law kinetics: $n = -1$, $Pe = 1/5$, $Da = 1/5$]